Investigation of the Role of Autophagy in Breast Cancer Progression

By

Charlett Giuliani

Submitted in fulfilment of the requirements for the degree of
Doctor of Philosophy



Institute for Health and Sport
Victoria University

2022

Declaration

Doctor of Philosophy Declaration

"I, Charlett Giuliani, declare that the PhD thesis entitled Investigation of the Role of Autophagy in Breast Cancer Progression is no more than 80,000 words in length including quotes and exclusive of tables, figures, appendices, bibliography, references and footnotes. This thesis contains no material that has been submitted previously, in whole or in part, for the award of any other academic degree or diploma. Except where otherwise indicated, this thesis is my own work. I have conducted my research in alignment with the Australian Code for the Responsible Conduct of Research and Victoria University's Higher Degree by Research Policy and Procedures"

Ethics Declaration

"All research procedures reported in the thesis were approved by the Institutional Biosafety Committee (IBC application numbers VIBC13-04 and VIBC 18-04)."

Signature



Date 25/02/2022

Abstract

Autophagy is a degradation process that removes proteins and organelles and culminates at the lysosome to degrade its "cargo". The three types of autophagy are macro, micro and chaperone-mediated autophagy. Macroautophagy is an indiscriminate degradation pathway that degrades defunct organelles and protein aggregates into recyclable components for reuse in metabolism and replenishes amino acid reserves. Its activity is shown to be minimal at basal levels within the cell and more commonly associated with an intracellular stressors such as nutrient deprivation, hypoxia and amino acid deficits. However, it also responds to extracellular insults such as chemotherapeutics and radiation. It was generalised as a survival mechanism that maintains cellular homeostasis by removing cellular debris that could lead to genotoxicity and or cell death. Therefore, it was surprising that this protective mechanism would be upregulated in the context of cancer. It has been agreed that its role is contradictory and has also been shown to be context-specific. The current dogma suggests macroautophagy prevents carcinogenesis in the non-transformed cell, but once the cell has transformed, it provides support and even facilitates chemoresistance. The exact mechanisms of this activity have been examined in this study in relation to mutant RAS. Initial gene array data collected from MCF10A transformed with $HRAS^{V12}$ resulted in the upregulation of approximately 60 macroautophagy-related genes. Macroautophagy was examined in a panel of breast cell lines with different RAS expressions such as mutant, null and activated wild type. This panel included normal mammary epithelial cell MCF10A with ectopic expression of $HRAS^{V12}$, RAS mutant breast cancer cell lines HS578T and MDA-MB-231 and a model of RAS activation in MDA-MB-468 breast cancer cell lines through EGF treatment. It was found that the expression of the crucial macroautophagy marker LC3-II was increased at basal levels for all transformed cell lines, and with extracellular stress induction, there was an increase in the LC3-II marker as expected except in those breast cancer cell lines with mutant RAS where expression did not alter.

Further functional analysis of autophagic flux determined that autophagic activity was present at the basal level. When the RAS mutant breast cancer cell lines

underwent autophagic induction, this activity was suppressed, suggesting that in the context of these RAS perturbations, mutant cell lines cannot respond to “normal” induction ques to activate autophagy. This reliance on autophagy in these more aggressive cell lines was reflected in the patient, demonstrating that high expression of the LC3 isoform LC3B correlates explicitly to poor prognosis. Interestingly this was in contrast to the LC3A and LC3C isoforms, with their increased expression correlating to a better prognosis, suggesting that the LC3B isoform is associated with a pathologic form of autophagy.

Several autophagic inhibitors were utilised to examine the importance of autophagy in cancer survival and growth to extrapolate the significance of this role of macroautophagy in further supporting mutant RAS. Given that macroautophagy is a stepwise process, it has numerous points where it can “potentially” be inhibited, and this is still an area of ongoing development. Two stages of the process that can be inhibited are at the initial stages through the inhibition of PI3KC3/VPS34, of which three drugs were examined, and the final stage of the autophagic process, which was inhibited at the lysosome using the VTPase inhibitor Bafilomycin A1. All transformed cell lines were sensitive to growth inhibition and cell viability compared to the control non-transformed mammary epithelial cell line with high sensitivity to 3Ma-IV of the VPS34 inhibitors and an even higher sensitivity to Bafilomycin A1. These results highlight the importance of autophagy to oncogenic cell lines and the significance of the lysosome.

The lysosome, as previously mentioned, is a hub for all three autophagic processes, so the scope of the study was broadened to include chaperone-mediated autophagy, which has known crosstalk with macroautophagy. Chaperoned-mediated autophagy (CMA) differs from macroautophagy because it discriminates and targets specific proteins for degradation. The key effector of chaperone-mediated autophagy is Lamp2A, which resides on the lysosome. This study has shown that Lamp2A is expressed in all RAS mutant breast cell lines but demonstrated a clear trend based on molecular subtypes, which was observed to be significantly upregulated in the triple-negative subtypes. The biological relevance of this increase in chaperone-mediated autophagy was examined with the development of a doxycycline inducible-shRNA against Lamp2A specifically. The functional studies examined the viability and metastatic potential in three oncogenic triple-negative subtypes and one normal. The

results demonstrated that chaperone-mediated autophagy activity has a pivotal role in the three oncogenic triple-negative subtypes cell lines compared to one normal, with all biological aspects significantly impacted by the knockdown of Lamp2A. This research has demonstrated the importance of chaperone-mediated autophagy and postulates that it targets specific substrates, directly regulating the cancer cell's ability to proliferate, migrate, invade and colonise.

In summary, this research has demonstrated that macroautophagy supports RAS activity in the context of mutation and exposes itself as a viable biomarker for combination treatment with autophagic inhibitors. In concert with these findings, chaperone-mediated autophagy has also revealed itself to be a fundamental regulator in the metastatic phenotype. There are no viable treatment options to inhibit chaperone-mediated autophagy, but the development of these is warranted. Chaperone-mediated autophagy has also revealed itself as a significant potential treatment target not only for breast cancer but also for metastatic disease

Table of Contents

Declaration i

Abstract ii

Table of Contents v

List of Figures xiii

List of Tables xx

List of Abbreviations xxi

Acknowledgements xxiv

Chapter 1: Literature Review 1

1.1 Breast Cancer – The current landscape 1

1.2 Breast Cancer Biology - an overview 2

1.2.1 Carcinogenesis 2

1.2.2 Intrinsic breast cancer subtypes 3

1.3 Breast cancer and RAS - unlikely allies 8

1.4 Breast cancer metastasis - how this moves the story 10

1.5 Autophagy - what we know to date 15

1.6 Microautophagy- the smallest of them all 17

1.7 Macroautophagy-the indiscriminaTE member 18

1.7.1 Canonical Pathway 20

1.7.2 Non-Canonical Pathways 23

1.8 Autophagy - friend, foe or both? 24

1.9 Autophagy and breast cancer - current findings and contradictions 25

1.10 Autophagy and Metastasis-Is There a connection 28

1.10.1 Epithelial to Mesenchymal transition and Autophagy 29

1.11 RAS and Autophagy - Is there a relationship? 30

1.12 Chaperone-Mediated Autophagy - what is known 32
1.13 Chaperone-Mediated Autophagy - where does it fit in the cancer story? 38
1.14 Autophagic Regulation - the current state 40
1.15 Autophagic Activators 41
1.15.1 Rapamycin 41
1.16 Autophagic Inhibitors 42
1.16.1 PI3KC3 Inhibitors 43
1.16.2 3-Methyladenine (3Ma) 43
1.16.3 SAR-405 44
1.16.4 VPS34-INI 45
1.16.5 Lysosomal Inhibitors 45
1.16.6 Bafilomycin A1 46
1.16.7 Chloroquine 47
1.17 Conclusion 48
1.18 Project Rationale & Objectives 49
1.18.1 Rationale 49
1.18.2 Objectives 50
Chapter 2: Material and Methods 51
2.1 MOLECULAR CLONING 51
2.1.1 Bacterial cell cultures 51
2.1.2 Bacteria transformation 51
2.2 CELL CULTURE AND CELL LINES. 59
2.2.2 Compounds 60
2.3 IN VITRO EXPERIMENTATION 61
2.3.1 Three-dimensional acini formation 61
2.3.2 Xcelligence RTCA DP System 61
2.3.3 Real-Time Cell Analysis of cytotoxicity induced by autophagic inhibition 62
2.3.4 Cell viability 62

2.3.5 Epithelial to Mesenchymal Transition (EMT) 62
2.3.6 Autophagic Flux assay 63
2.3.7 Wound healing assay 63
2.3.8 Anchorage-dependent clonogenic survival and growth assay 63
2.3.9 Microchemotaxis Migration Assay 64
2.3.10 Invasion Outgrowth Assay 64
2.3.11 Immunofluorescence of adherent cells 65
2.3.12 Staining of MCF-10A acini 65
2.3.13 Western Blot Analysis and Antibodies 66
2.3.14 Lysosome Enrichment 66
2.3.15 Microarray analysis 67
2.3.16 Statistical analysis. 67
2.4 MATERIALS 68
2.4.1 Plasmid constructs utilised in this study 68
2.4.2 Cell culture reagents and chemotherapeutics 70
2.4.3 In vitro Experimentation Reagents 71
2.4.4 Commercial Kits 72
Antibodies 72
2.4.5 General consumables 73
Chapter 3: THE IMPACT OF RAS ON MACROAUTOPHAGY IN THE CONTEXT OF BREAST CANCER CELL PLASTICITY. 74
3.1 INTRODUCTION 74
3.2 Hypothesis and Aims 78
3.3 RESULTS 79
3.3.1 Increased expression of LC3-II to LC3-I ratio under basal conditions in Triple-Negative Basal B subtypes with RAS Mutation. 79
3.3.2 LC3B expression increases in the presence of RAS mutation in the breast cancer cell lines 82

3.3.3 The ectopic expression of the $HRAS^{V12}$ mutation in the mammary epithelial cell line MCF10A models leads to oncogenic transformation. 84

3.3.4 MCF10A $HRAS^{V12}$ acini upregulate autophagy and autophagy-related genes. 88

3.3.5 Autophagic markers LC3 show increased expression and activity in the $HRAS^{V12}$ transformed MCF10A compared to the non-transformed MCF10A. 90

3.3.6 The $HRAS^{V12}$transformation increased P62 expression at basal conditions compared to MCF10A control cells. 94

3.3.7 The expression of $HRAS^{V12}$ alters LC3 isoforms and orthologue turnover rate. 96

3.3.8 EGF induced morphological changes to indicate the epithelial to mesenchymal transition in breast cancer cell line MDA-MB-468. 97

3.3.9 The expression of autophagic markers increased during RAS activation in the EMT breast cancer model. 99

3.3.10 The turnover rates of P62 suggest that during the epithelial to mesenchymal transition, its role shifts NRF2 and KEAP1 pathways. 101

3.3.11 The expression profile of LC3 isoforms and orthologues does not change but enhances with the addition of EGF. 102

3.3.12 Increased expression of LC3-II to LC3-I ratio under basal conditions in TNBC subtypes with RAS Mutation. 104

3.3.13 LC3-II levels and turnover are significantly different between breast cancer subtypes 106

3.3.14 Autophagic flux becomes dysregulated in the more aggressive phenotypes in response to nutrient stress. 108

3.3.15 RAS mutant induced autophagic activity is independent of the autophagy canonical pathway 113

3.3.16 The HRAS mutation in Hs578T results in differential expression of autophagic marker LC3 isoforms and orthologue 116

3.3.17 The MDA-MB-231 displays a preferential expression of LC3 isoforms and orthologues. 119

3.3.18 The LC3 isoforms inpatient data set indicate a difference in prognosis dependent on the level of the LC3 isoform and orthologue expressed. 122

3.4 DISCUSSION 127

3.4.1 Autophagy and associated gene upregulation in a model of transformation..... 127

3.4.2 Increased autophagic activity sensitises RAS-transformed cells 131

3.4.3 Increased dependence on autophagy in breast cancer progression 133

3.4.4 RAS activation is an oncogenic driver rather than RAS mutation in breast cancer 134

3.4.5 RAS activation increases autophagic activity 136

3.5 CONCLUSION 138

Chapter 4: IDENTIFICATION OF A RELATIONSHIP BETWEEN AUTOPHAGY AND RAS IN BREAST CANCER PROGRESSION..... 139

4.1 INTRODUCTION..... 139

4.2 Hypothesis and Aims 143

4.3 RESULTS 144

4.3.1 The expression of $HRAS^{V12}$ in MCF10A increased their sensitivity to 3Ma-IV..... 144

4.3.2 Breast cancer progression through RAS activation sensitises the MDA-MB-468 breast cancer cell line to treatment with VPS34 inhibitor 3Ma-IV. 147

4.3.3 Breast cancer cells demonstrate increased sensitivity to treatment with 3Ma-IV compared to other VPS34 inhibitors. 150

4.3.4 The expression of $HRAS^{V12}$ improved the efficacy of VPS34 inhibitor SAR-405. 153

4.3.5 VPS34 inhibitor SAR-405 increased cell viability in MDA-MB-468, which was lessened by the addition of EGF. 156

4.3.6 The VPS34 inhibitor SAR-405 shows a differential response in breast cancer cell lines. 158

4.3.7 The expression of HRASV12 increased sensitivity to treatment with the VPS34 inhibitor VPS34-INI. 161

4.3.8 The presence of EGF with breast cancer cell line MDA-MB-468 increased insensitivity to treatment with VPS34 inhibitor VPS34-INI. 163

4.3.9 Response to VPS34-INI is reduced with increases in dose concentration in all breast cancer cell lines. 165

4.3.10 The presence of $HRAS^{V12}$ significantly increased sensitivity to vacuolar H+ ATPase (V-ATPase) inhibition with Bafilomycin A1 treatment. 170

4.3.11 The presence of EGF with breast cancer cell line MDA-MB-468 did not change the sensitivity to treatment with vacuolar H+ ATPase (V-ATPase) inhibitor Bafilomycin A1. 172

4.3.12 Lysosomal inhibition demonstrated efficacy in all breast cancer cell lines but significantly increased in the triple-negative subtype. 174

4.4 DISCUSSION 177

4.4.1 The VPS34 inhibitor's treatment efficacy was more influential in the transformed cells than normal counterparts. 177

4.4.2 VPS34 inhibition is an efficacious treatment to target the aggressive breast cancer phenotype. 179

4.4.3 VPS34 inhibitors as a potential dual-target for RAS and autophagy in breast cancer 181

4.4.4 The lysosomal inhibitor showed improved efficacy in all subtypes compared to the control. 182

4.4.5 Bafilomycin A1 highlights the potential of lysosome inhibition for breast cancer treatment. 183

4.5 CONCLUSION 185

Chapter 5: THE ROLE OF CHAPERONE-MEDIATED AUTOPHAGY IN THE DEVELOPMENT AND PROGRESSION OF BREAST CANCER 186

5.1 INTRODUCTION 186

5.2 HYPOTHESIS AND AIMS 189

5.3 RESULTS 190

5.3.1 Lamp2A expression is increased in more aggressive breast cancer phenotypes. 190

5.3.2 Lamp2A expression does not correlate with the presence of a RAS mutation. 195

5.3.3 The loss of Lamp2A in breast cell line MCF10A confers no significant biological effect. 198

5.3.4 Knockdown of Lamp2A showed no functional importance to the MCF10A breast cell line 204

5.3.5 The knockdown of Lamp2A in the basal breast cancer cell line MDA-MB-468 resulted in biological changes. 211

5.3.6 The addition of EGF in the MDA-MB-468 with Lamp2A knockdown enhances the biological effects observed. 217

5.3.7 The knockdown of Lamp2A in the breast cancer cell line Hs578T resulted in biological changes 221

5.3.8 The knockdown of Lamp2A in the MDA-MB-231 breast cancer cell line has a biological impact 228

5.3.9 Removal of Lamp2A impaired the functional activity of the breast cancer cell line MDA-MB-231 233

5.4 DISCUSSION 243

5.4.1 The breast cell subtype demonstrates a correlation with CMA but not mutant RAS 243

5.4.2 CMA inhibition was shown to have no functional implications in regular mammary epithelial compared to a carcinogenic counterpart. 245

5.4.3 CMA dependence increases as cells transition from basal to mesenchymal phenotype. 246

5.4.4 EGFR activation sensitives cells to the knockdown of Lamp2A 248

5.4.5 CMA reduction was demonstrated to impede the more aggressive phenotype's functionality significantly. 249

5.4.6 Lamp2A roles beyond that of crucial effector molecule for CMA 251

5.5 CONCLUSION 253

Chapter 6: FINAL DISCUSSION 255

6.1 Introduction 255

6.2 Summary of findings of this study 256

6.2.1 RAS is reliant on macroautophagy in breast cancer cell lines. 256

6.2.2 Inhibition of macroautophagy in RAS active breast cancer cell lines..... 257

6.2.3 Chaperone-mediated autophagy in breast cancer cell progression..... 260

6.3 Targetability of autophagy in breast cancer treatment 262

6.4 Future directions..... 267

6.5 Conclusion..... 268

REFERENCES 269

APPENDIX I 316

APPENDIX II 317

APPENDIX III 320

APPENDIX IV 321

APPENDIX V 322

APPENDIX VI 326

APPENDIX VII 327

List of Figures

Figure 1-1 Breast cancer intrinsic/molecular subtypes 7

Figure 1-2 Metastatic breast cancer 13

Figure 1-3 Types of Autophagy 16

Figure 1-4 Schematic overview of macroautophagy 19

Figure 1-5 Autophagy Canonical Pathway 22

Figure 1-6 Chaperone-Mediated Autophagy 37

Figure 2-1 Schematic of the Tripz vector map (A) and Tripz restriction sites(B)..... 56

Figure 3-1 Schematic representation of rationale for the cell lines of this study 77

Figure 3-2 Increased autophagosome formation observed in basal breast cancer cell lines compared to luminal subtypes 81

Figure 3-3 The distinct LC3 family member expression in RAS breast cell line panel 83

Figure 3-4 The $HRAS^{V12}$ induces an aggressive and invasive phenotype during acini development. 85

Figure 3-5 Downregulation of epithelial marker E-cadherin by the ectopic expression of $HRAS^{V12}$ in the mammary epithelial cell line 87

Figure 3-6 Gene analysis of MCF10A $HRAS^{V12}$ increases many autophagic-related genes. 89

Figure 3-7 Oncogenic transformation with $HRAS^{V12}$ induces autophagosome formation at the basal state 91

Figure 3-8 Schematic of expected LC3-II levels 92

Figure 3-9 The ectopic expression of $HRAS^{V12}$ upregulates autophagic activity. 93

Figure 3-10 P62 expression and phosphorylation specific to autophagy were increased in the $HRAS^{V12}$ expressing cell line 95

Figure 3-11 The expression of LC3 isoforms and autophagic markers are similar between MCF10A and MCF10A HRAS^{V12} in response to activation and inhibition. 96

Figure 3-12 The inclusion of epidermal growth factor (EGF) cause MDA-MB-468 cells to transition from epithelial to mesenchymal phenotype. 97

Figure 3-13 Epithelial marker E-cadherin decrease, and mesenchymal marker vimentin increase to EGF addition. 98

Figure 3-14 Autophagic marker LC3 increase in a dose-dependent response to EGF addition. 100

Figure 3-15 P62 turnover rates vary between MDA-MB-468 and MDA-MB-468 with EGF at basal state and autophagic activation. 101

Figure 3-16 The expression of LC3 isoforms and orthologue increased with the inclusion of EGF. 103

Figure 3-17 Morphological differences between luminal and triple-negative breast cancer subtypes. 105

Figure 3-18 LC3-II turnover is decreased in the more aggressive breast cancer phenotypes 107

Figure 3-19 Autophagic flux of T47D breast cancer cell line 109

Figure 3-20 Autophagic flux of HS578T breast cancer cell line 111

Figure 3-21 Autophagic flux of MDA-MB-231 breast cancer cell line 112

Figure 3-22 Autophagy “Canonical” pathway 113

Figure 3-23 Canonical pathway regulators decrease in basal subtypes compared to luminal A. 115

Figure 3-24 LC3 Fluorescence in Hs578T breast cancer cell line 118

Figure 3-25 There is differential expression of autophagic markers in response to activation and inhibition. 118

Figure 3-26 LC3 Fluorescence in MDA-MB-231 breast cancer cell line 121

Figure 3-27 There is an unusual expression pattern of LC3 isoforms irrespective of activation or inhibition. 121

Figure 3-28 The LC3 isoforms confer different overall survival prognoses in breast cancer patients 123

Figure 3-29 The LC3 isoforms have a differential effect on relapse-free survival in breast cancer patients 123

Figure 3-30 Significant differences in the prognosis probability between the LC3 isoforms in breast cancer patients 124

Figure 3-31 The LC3 isoforms and their gene ratio expression significantly correlate with patient relapse-free survival in breast cancer as a whole.... 125

Figure 4-1 Schematic of VPS34's role in the context of the autophagic process... 142

Figure 4-2 The original 3-Methyladenine (3Ma) is limited clinically by its reduced solubility and cell permeability. 145

Figure 4-3 The expression of $HRAS^{V12}$ sensitises MCF10A cells to 3Ma-IV treatment 146

Figure 4-4 The presence of EGF sensitives the breast cancer cell line MDA-MB-468 to treatment with 3Ma-IV. 148

Figure 4-5 The presence of EGF sensitives the breast cancer cell line MDA-MB-468 to treatment with 3Ma-IV utilising Alamar Blue. 149

Figure 4-6 Increased sensitivity of advanced breast cancer cell lines to 3Ma-IV. .. 151

Figure 4-7 Increased sensitivity to 3Ma-IV in the TNBC breast cancer cell lines .. 152

Figure 4-8 The expression $HRAS^{V12}$ reduces the efficacy of SAR-405 treatment in the breast cell line MCF10A 154

Figure 4-9 Real-time analysis of the MCF10A transformed with $HRAS^{V12}$ responds to SAR-405 by increasing cellular impedance. 155

Figure 4-10 The presence of EGF increases the efficacy of the VPS34 inhibitor SAR-405 treatment. 157

Figure 4-11 The breast cancer cell lines had altered cell viability in responses to treatment with SAR-405. 159

Figure 4-12 The breast cancer cell lines had contrasting responses to treatment with SAR-405. 160

Figure 4-13 Transformation MCF10A with $HRAS^{V12}$ responds differently to VPS34-INI treatment. 162

Figure 4-14 The presence of EGF ceases treatment efficacy with VPS34 inhibitor VPS34-INI. 164

Figure 4-15 Limited dose-response to VPS34-INI treatment in breast cancer cell lines 166

Figure 4-16 Real-time analysis demonstrates negligible response to VPS34-INI in breast cancer cell lines 167

Figure 4-17 Schematic diagram of activity of Bafilomycin A1 on the autophagic process. 169

Figure 4-18 The presence of $HRAS^{V12}$ increases sensitivity to Bafilomycin A1 171

Figure 4-19 The treatment with Bafilomycin A1 is as equally effective with or without the presence of EGF 173

Figure 4-20 Bafilomycin A1 treatment efficacy is improved in the aggressive phenotype 175

Figure 5-1 Schematic of substrate processing by chaperone-mediated autophagy . 187

Figure 5-2 Schematic of substrate processing by chaperone-mediated autophagy. 188

Figure 5-3 Lamp2A and Lamp2B are differential expressed in molecular subtypes 193

Figure 5-4 CMA regulators are expressed in the lysosomal enrichment of oncogenic subtypes. 194

Figure 5-5 The expression of lamp 2A increased in the breast cancer cell line compared to breast cell lines 197

Figure 5-6 Lamp2A knockdown was observed in the MCF10A breast cell line..... 199

Figure 5-7 The MCF10A cellular morphology was unchanged by the knockdown of Lamp2A 200

Figure 5-8 MCF10A morphology does not change with Lamp2A knockdown. 201

Figure 5-9 The lysosomal enrichment of MCF10A with Lamp2A KD shows differences in known CMA substrates 203

Figure 5-10 The cell viability of MCF10A cells did not change 24 hours after knockdown 205

Figure 5-11 The wound healing capacity of MCF10A was unchanged by Lamp2A KD 207

Figure 5-12 Schematic representation of the colony-forming experimental design 208

Figure 5-13 The removal of Lamp2A after colony formation did not affect growth. 209

Figure 5-14 The knockdown of Lamp2A did not affect colony formation in the MCF10A breast cell line. 209

Figure 5-15 The knockdown of Lamp2A did not alter the MCF10A acini formation. 210

Figure 5-16 Lamp2A is knockdown in the MDA-MB-468 breast cancer cell line. 212

Figure 5-17 The breast cancer cell line MDA-MB-468 displays a reduction in cell numbers with Lamp2A KD. 213

Figure 5-18 The MDA-MB-468 breast cancer cell line displays minimal differences with Lamp2A KD. 214

Figure 5-19 The knockdown of Lamp2A significantly decreases cell viability in the MDA-MB-468 breast cancer cell line. 215

Figure 5-20 The invasive potential of MDA-MB-468 breast cancer cell line by the reduction of Lamp2A 216

Figure 5-21 EGF does not prevent the decrease in cell viability with Lamp2A KD in the MDA-MB-468 breast cancer cell line. 218

Figure 5-22 The addition of EGF with Lamp2A knockdown leads to increased cell death in the MDA-MB-468 cell line. 219

Figure 5-23 The presence of EGF further reduced colony formation in MDA-MB-468 with Lamp2A KD. 220

Figure 5-24 Lamp2A knockdown is confirmed in the Hs578T breast cancer cell line. 222

Figure 5-25 The breast cancer cell line Hs578T displays confirmation of Lamp2A KD. 223

Figure 5-26 The Hs578T breast cancer cells display no changes to CMA substrates with Lamp2A knockdown. 224

Figure 5-27 The knockdown of Lamp2A reduces cell viability in the Hs578T breast cancer cell line. 225

Figure 5-28 The Hs578T breast cancer cell lines colony growth was not altered by Lamp2A knockdown. 227

Figure 5-29 The knockdown of Lamp2A decreased the colony-forming capacity of the Hs578T breast cancer cell line 227

Figure 5-30 The MDA-MB-231 breast cancer cell line was successfully transduced with Lamp2A knockdown 229

Figure 5-31 MDA-MB-231 breast cancer cell line high tRFP confirms Lamp2AshRNA expression. 230

Figure 5-32 The knockdown of Lamp2A reduces MDA-MB-231 breast cancer cell numbers. 230

Figure 5-33 The removal of Lamp2A in the MDA-MB-231 breast cancer cell line does not affect CMA substrates. 231

Figure 5-34 The knockdown of Lamp2A in the MDA-MB-231 breast cancer cell line resulted in a decrease in cell viability compared to the control ... 232

Figure 5-35 The MDA-MB-231 breast cancer cell line had a decreased rate of wound healing with Lamp2A knockdown. 234

Figure 5-36 The knockdown of Lamp2A impeded migration in the MDA-MB-231 breast cancer cell line. 236

Figure 5-37 The colony growth was impaired by Lamp2A knockdown in MDA-MB-231 breast cancer cell lines..... 237

Figure 5-38 MDA-MB-231 breast cancer cells could not form colonies with the knockdown of Lamp2A. 238

Figure 5-39 The addition of EGF does not reverse the colony growth inhibition observed in MDA-MB-231 with Lamp2A knockdown..... 239

Figure 5-40 The MDA-MB-231 cell line displays altered invasive growth with the knockdown of Lamp2A. 241

Figure 6-1 Autophagy in metastatic breast cancer..... 268

List of Tables

Table 2-1 LAMP 2A shRNAmir sequences 55

Table 2-2 Table of mir30 primers 55

Table 3-1. Summary of findings 126

Table 4-1 VPS34 Inhibitors specificity and mechanism of action (M.O.A) 141

Table 4-2 Increased autophagic activity sensitises RAS active cells to VPS34 inhibition 168

Table 4-3 Increased autophagic activity sensitises RAS cells to lysosomal inhibition 176

Table 5-1 Summary of findings 242

Table 6-1 Summary of findings for chapter 3 and chapter 4 259

Table 6-2 Summary of findings chapter 5 261

List of Abbreviations

3MaIV	3-methyl-6-(3-methylpiperidin-1-yl)-3H-purine
AMBRA1	Autophagy And Beclin 1 Regulator 1
AMPK	AMP-activated protein kinase
Apaf-1	Apoptotic protease activating factor 1
ATCC	American Type Culture Collection
Atg12	Autophagy-related 12
Atg14L	Atg14-like protein
Atg16L1	Autophagy-related 16 like 1
Atg4	Autophagy-related gene 4
Atg5	Autophagy related 5
Atg7	Autophagy Related 7
Atg9	Autophagy-related 9
ATM	Ataxia-telangectasia mutated protein
ATP	Adenosine triphospate
BAD	Bcl-2-associated death promoter
BAG3	Bcl2-associated athanogene 3
BAX	Bcl-2 associated X
BCA	Bicinchoninic acid
Bcl-2	B-cell lymphoma 2
Bcl-xL	B-cell lymphoma-extra large
BECN1	Beclin 1
BSA	Bovine serum albumin
CQ	Chloroquine
ctrl	Control
DAPI	4’6-diamidino-2-phenylindole
DEPTOR	DEP domain-containing mTOR-interacting protein
DMEM	Dulbecco’s modified Eagle Medium
DMEM/F12	Dulbecco’s modified Eagle Medium / Ham’s nutrient mixture F12
DMSO	Dimethyl sulfoxide
DNA	Dioxyribonucleic acid
Dox	Doxycycline
ECM	Extracellular matrix
EDTA	Ethylenediaminetetraacetic acid
eEF1A	Elongation factor 1A
EGF	Epidermal growth factor
EGFP	Enhanced green fluorescence protein
EGFR	Epidermal growth factor receptor
EMT	Epithelial to Mesenchymal Transition
ER	Estrogen receptor
Erk	Extra cellular-regulated kinase

FbCM	Fibroblast conditioned media
FBS	Fetal Bovine Serum
FGF	Fibroblast growth factor
FIP200	FAK family kinase-interacting protein of 200 kDa
GAPs	GTPase activating proteins
GAPDH	Glyceraldehyde-3-Phosphate Dehydrogenase
HDAC6	Histone deacetylase
HIF-1α	Hypoxia inducible factor 1α
HK II	Hexokinase II
HSC70/HSPA8	Heat shock cognate 71 kDa protein
IC_{50}	Inhibitory concentration-50
IGF	insulin-like growth factor
JNK	c-jun N-terminal kinase
KEAP1	Kelch-like ECH-associated protein 1
LC3	Microtubule-associated protein 1A/1B-light chain 3
LDH	Lactate dehydrogenase
MAP	Mitogen-activated protein
MAPK	MAP kinase
Mdm2	Human murine double minute 2 protein
MEFs	Mouse embryonic fibroblasts
MEK	MAPk-activated protein kinase
MHC	Major histocompatibility complex
mLST8	Mammalian lethal with SEC13 protein 8
MMP	Matrix metalloproteinase
MOI	Multiple of infection
mRNA	Messenger RNA
MTOR	Mammalian target of rapamycin
MTORC1	is composed of mTOR, Raptor, mLST8 , PRAS40 and DEPTOR
NBR1	Autophagy cargo receptor
NF-κB	Nuclear factor kappa-B
NRF2	Nuclear factor-erythroid factor 2-related factor 2
OD	optical density
P62/SQSTM1	Ubiquitin-binding protein p62 /Sequestosome-1
PARP	Poly(ADP-ribose) polymeRASe
PBS	Phosphate bufferred saline
PCM	Phase-contrast microscopy
PCR	polymerase chain reaction
PE	Phosphatidylethanolamine
PI3K	Phosphoinositide 3-Kinase
PI3KC1	Phosphoinositide 3-Kinase Class I
PI3KC2	Phosphoinositide 3-Kinase Class II
PI3KC3	Phosphoinositide 3-Kinase Class III
PK M2	Pyruvate Kinase (Isoforms referred to as M1 and M2)
PMSF	phenylmethanesulfonyl fluoride
PR	Progesterone receptor

PRAS40	Proline-rich Akt substrate of 40 kDa
pRB	Retinoblastoma protein
PTEN	Phosphatase and tensin homolog
REN	Renilla shRNAmir control
RIP	Receptor Interacting Protein
RNAi	RNA interference
RNAP II	RNA PolymeRASe II
ROI	region of interest
ROS	Reactive oxygen species
rpm	revolutions per minute
RT	Room temperature
RT-qPCR	Real-time quantitative PCR
RUBCN	Beclin-1 associated RUN domain containing protein/Rubicon Autophagy Regulator
scr.	scrambled shRNAmir control
SD	Standard deviation
SDS-PAGE	Sodium dodecyl sulfate-polyacrylamide gel electrophoresis
shRNA	Short haripin RNA
shRNAi	short haripin RNA interference
Sirt1	Sirtuin-1
SOS	Son of Sevenless
STAT	Signal transducer and activator of transcription
SUMO	Small ubiquitin related modifier
TBST	Tris buffered saline-tween
TF	Transcription factor
TNBC	Triple negative breast cancers
TNF-α	Tumour necrosis factor α
TRAP1	Tumour necrosis factor receptor associated protein
TRE	Tetracycline response element
tRFP	Turbo red fluorescent protein
ULK1	UNC-51-like kinase -1
ULK2	UNC-51-like kinase -2
UPR	Unfolded protein response
UV	Ultra-violet
UVRAG	ultraviolet irradiation resistance-associated gene
VEGF	Vascular endothelial growth factor
VPS15/p150	Vacuolar Protein Sorting 15
VPS34	Vacuolar Protein Sorting 34

Acknowledgements

My passion for research has kept me committed to this journey during the highs and lows, but this achievement reflects the team of those around me. Firstly, I have been humbled and inspired by my supervisor Professor John Price. He has fuelled my passion for research and has inspired me to follow his lead into the research field, to him and his postdoc (Chau and Sarrabeth) for providing me with the practical skills to fulfil my PhD. Also, he has been of great support and compassion during the unforeseen circumstances and obstacles that have arisen during my long journey to the end, so thank you. Then to my extended family, the Price lab and surrogate lab members who have made the darkest days brighter through their friendship and support (Joe, Tabitha, Asha, Natasha, Canh-Vinh, Das, Dean, Lauren and Val).

To my background supporters, my family, firstly my parents Jenny and Mick, for their sideline cheering endless motivation and encouragement. My sister Jazz, you have gone above and beyond; not only have you read through and edited this entire thesis, but you have also been my sounding board when I need it. I could never thank you enough. To my husband, Tim, thank you for everything. I honestly would not have been able to do this without your love and support. Although I am sure when I said I wanted to make a career change, you did not expect me to fall in love with something other than you as I have for research. To my children and now grandchildren (David, Robi, Joanne, Stefan, Kane, Chyna, Atticus, Thena and Indiana.) I hope I have proved to you all that you can have dreams and achieve them at any time in life you need to believe in yourself and work hard.

Finally, I dedicate this in loving memory of my daughter CoCo, I was so blessed to have you in my life, and I promise to honour your memory by continuing to pursue research in the plight to make life better for one person.

Chapter 1: Literature Review

1.1 BREAST CANCER – THE CURRENT LANDSCAPE

Breast cancer is the second most common cause of death among women; it is estimated that 1 in 7 women will be diagnosed with breast cancer, and an estimated 3102 women will die from breast cancer in Australia in 2021 [1]. Furthermore, breast cancer is currently the most commonly diagnosed cancer in persons of all ages in Australia, with an incident rate of 67.8 per 100,000, ranking above prostate and skin cancer [1]. The development of metastatic breast cancer occurs in approximately 10% of patients who have been diagnosed with localised and regional diseases. The burden of disease is defined as the loss of life earlier than expected and the loss of healthy years due to disease and disability. Breast cancer ranked as the top and second to lung cancer in years lost to cancer or 'years of disability' [2]. The five-year relative survival rate has increased significantly over the last 60 years, from 25% to 100% with stage I, 94.6% at stage II, 80.6% at stage III and a rapid decline to 32% at stage IV [1, 2]. These statistics are notable as approximately 5% of women are diagnosed at stage IV, and approximately 10% of patients who have been diagnosed with localised and regional diseases will develop metastatic breast cancer [1]. The breast cancer incidence rate has also increased and is forecast to continue to rise in the future [1]. This increase in diagnosis at the earlier stages of breast cancer development has resulted in a decline in cancer-related deaths. Current data from the Australian Institute of Health and Welfare (AIHW) has shown that 80% of breast cancer diagnoses were at stages I and II [1, 2]. This apparent increase in incidence may reflect the improvements in the sensitivity and population-based screening for breast cancer and, therefore, the associated rise in diagnosis. Enhanced community awareness of the problem, leading to increased numbers of women being screened, has subsequently contributed to the effectiveness of current breast cancer foundations and breast cancer screening initiatives. Collectively the improved survival rates at these earlier stages are reflective of, earlier diagnosis, which has led to more treatment options and combined with the improvement in available therapies for patients.

The financial cost of breast cancer to the Australian national health care system was more than $1,056 million per annum in 2020 and is predicted to increase. Other developed countries replicate these Australian figures; however, the survival rate in poorer countries is impacted by a lack of infrastructure to support early prevention programs, and, as a result, breast cancer survival rates are significantly decreased, for example, to 60% in India and 44% in Africa. These reduced survival rates in lower socioeconomic countries are of genuine concern as breast cancer is the most prevalent cancer globally and, in 2020, resulting in 685,000 deaths [3]. As many of these deaths are preventable, the World Health Organisation has started the Global Breast Cancer Initiative, a program to reduce breast cancer deaths by 2.5% per annum from 2020 to 2040, equating to a total of 2.5 million deaths prevented [4-8]. The patient statistics indicate that the need for research in breast cancer, particularly metastatic disease, is still very much warranted as the number of patients with breast cancer continues to rise with our ageing population.

1.2 BREAST CANCER BIOLOGY - AN OVERVIEW

1.2.1 Carcinogenesis

Breast cancer development is associated with several risk factors, including age. For example, people over 55 years are at higher risk. Females are one hundred times more likely to develop breast cancer than males and are twice as likely to get breast cancer if she has a female relative of the first degree that has been affected [9-13]. Other risk factors include obesity, a long menstruation life cycle due to beginning menarche before 12 years old and late menopause after 55 [14-16]. Excessive consumption of alcohol, extended use of hormone replacement therapy for more than 15 years, contraceptive pill use and not having children or breastfeeding, previous history of breast hyperplasia and exposure to chest radiation are other common risk factors [17-25]. In addition, breast cancer can be inherited and is associated with mutations, this group accounts for 10% of all breast cancers, and of those, 25% are related to BRCA1 and BRCA2 gene mutations [26-28]. Thus, due to one or several risk factors, mutations will occur in a cell. By simple

definition, breast cancer results from genetic mutations in cells within the mammary tissue. The cancers themselves are identified by the cell they arose from, so carcinomas arise from epithelial cells in the lobules or ducts [29, 30]. In contrast, sarcoma arises from the connective tissue compartment's stromal cells, including blood vessels and myofibroblasts [31, 32]. The pathological features further differentiate the cancer nomenclature. If the cancer is non-invasive, it is commonly referred to as 'in situ' because it has not moved beyond where it has arisen, whereas 'invasive' refers to the spread of cancer into neighbouring tissue and 'metastatic' refers to when the cancer cells have spread to secondary sites. Patient prognosis and treatment decisions will be guided by the intrinsic subtyping of the breast cancer and the TNM staging system. The TNM staging system is a clinical tool developed by the American Joint Committee on Cancer that enables clinicians to determine the patient cancer stage by tumour size (T), lymph node involvement (N) and metastasis (M) [33]. This system has been used for many decades, with the latest updates to the system made in 2018. Updates such as the inclusion of the intrinsic biomarkers ER, PR and HER2 as part of the evaluation process guide the cancer stage in conjunction with TNM [34, 35]. Breast physiology lends itself to being a transformation 'paradise' as it is an area of constant change and adaption, with changes observed in the breast during puberty, pregnancy and lactation. For these changes to occur, strong endocrine signals activate and maintain proliferation and growth pathways when the breast environment is victim to several genetic events resulting in genetic mutations. The consequence is activation of proto-oncogenes or the loss of tumour suppressor genes and usually a combination of both. These cells no longer have controls to regulate them, so they gain and accumulate attributes as defined by the 'hallmarks of cancer' to facilitate their survival and thrive [36].

1.2.2 Intrinsic breast cancer subtypes

Breast cancer results from numerous genetic mutations, and clinically breast cancer has been grouped and classified by its intrinsic molecular characteristics, which have since been used in combination with TNM staging [37] to predict prognosis and direct treatment strategies [38-42]. The ability to determine a patient's outcome based on cancer's molecular profile mean that these attributes can be targeted for treatment,

explaining why triple-negative has the worst prognosis, as it lacks the expression of these targets. The initial molecular characteristics used to define breast cancers subtypes are the presence or lack thereof of estrogen (ER), progesterone (PR) and human epidermal growth factor receptor 2 (HER2). The breast cancer subtypes as classified clinically are Luminal A (LA), which is positive for ER, and PR and HER2 negative, which has the best prognosis. The Luminal B (LB) subtype is ER-positive, PR positive or negative and HER2 positive and has an intermediate prognosis. The HER2 subtype is ER, PR negative, and HER2 positive and has a poor prognosis, and the final subtype is in the triple-negative (TNBC) subtype, which has the worst prognosis and is negative for all receptors [41, 42] (Figure 1.1). These subtypes have been further stratified to include 'Normal-like', which has the same PR, ER and HER2 status as LA, but its gene expression profile is the same as normal breast profile and has an intermediate prognosis, making it slightly better than LB. The triple-negative subtype has been further divided into basal-like and claudin-low (often called basal A and basal B, respectively). Although both are negative for receptor presence, basal-like is observed to express EGFR receptors, and the claudin-low subtype is as described low in claudin with increased mesenchymal features, particularly vimentin expression [43, 44]. These molecular characteristics have proven to be indicators of relapse-free survival, overall survival, recurrence, and guide treatment options for clinicians [45].

It was later determined that this TNBC stratification was limited due to the high heterogeneity of TNBC. As a collective, TNBC has a poorer survival rate and is more common in younger women, making its correct treatment important. The older stratification system provided the information required to choose the most appropriate treatments. With specific cluster analysis of the TNBC tumour sample, a new group of six TNBC's cellular subtypes were defined based on their particular gene expression signatures [46]. The six defined TNBC groups are: basal-like 1 (BL1), defined by upregulation of cell cycle, DNA repair and proliferation genes, and the basal-like 2 (BL2) group show an increase in growth receptor signalling pathways. The Immunomodulatory (I) group has increased gene expression of immune signalling pathways, and the mesenchymal-like (M) group demonstrate elevated cell motility and migration signalling. The mesenchymal stem-like (MSL) group has downregulation of proliferation markers but has an increase in stemness genes, and the luminal androgen receptor (LAR) group have an upregulation and activation of hormone receptor signalling.

There is still some conjecture regarding the current clinical and cellular TNBC subtyping, and much of the literature uses the subtyping interchangeably, with most retaining the old cellular subtyping of basal A and B, but there has been recent debate about the validity of basal B/claudin-low subtype [47]. The identification of heterogeneity suggests that the use of the old subtyping may not be as robust or clinically relevant as once considered. In combination with more recent studies, reclassifying the breast cancer cell into the six molecular subtypes indicate it will be more likely that the classification criteria for the TNBC subtyping will shift. Although there is still some debate on the current six subtypes and whether they could be refined to four, as described by Burstein et al. [48], who refined the groups after performing gene profiling into four groups. These four subtypes are luminal androgen receptors (LAR) with high androgen receptors and cell surface mucin. The Basal-like immunosuppressed (BLIS) subtype has a high VCTN1 immune (TCell) inhibitor expression. The Basal-like immune-activated (BLIA) subtype has increased the expression of cytokine and STAT signalling molecules. The final subtype is the mesenchymal (MES), which has an upregulation of PDGFRα and cKit receptors.

More recently, the Fudan University Shanghai Cancer Center (FUSCC) classification, as described by Liu et al., has defined TNBC subtypes with mRNA and included lncRNA [49]. The four subtypes defined by FUSCC are: immunomodulatory (IM) subtypes, which have an increased expression of immune and cytokine signalling genes; the luminal androgen receptor subtype (LAR) subtype has a high expression of androgen receptor genes; the mesenchymal-like subtype (MES) subtype, which has an upregulation of growth signalling pathways; and, the final subtype which has basal-like and immune-suppressed (BLIS), increased DNA repair and cell cycle genes in conjunction with suppression of immune signalling gene. The inclusion of the lncRNA is suggested to provide a more robust subtype grouping that could lead to definitive biomarkers [46], so it is hoped that there will be a decision about the grouping. The issue surrounding this shift is that the subtypes are based on mRNA expression and thus may not be reflective in immunohistochemical analysis. From a clinical perspective, gene expression profiling is currently not feasible, so either technology needs to advance to support personalised medicine in the clinic, or there need to be newly defined markers for these subtypes to be used for traditional immunohistochemical staining [50]. These changes in the subtypes have arisen from apparent discrepancies in the results of patients

based on the original basal A and basal B criteria. What has since been established is that the TNBC subtype is highly heterogeneous. As technology develops and the ability to examine gene and ontology profiles expands, we can identify the cellular populations within the TNBC. This exploration of the TNBC heterogeneity has led to the refinement of Lehman's grouping in Burstein's model 2 of each of Lehman's subtypes that are found within the one group. Liu's subtyping expanded further to show that all the Lehman's subtypes exist within a group but at different ratios, reflecting TNBC heterogeneity. To date, there is a need to find more specific biomarkers for the TNBC subtypes to group them by to accurately stratify patients and ultimately guide effective treatment [51-54].

In respect to the cell lines used in this study and comparing Lehman et al. subtypes to the original grouping, basal-like/basal A is equivalent to basal-like 1/BL1-MDA-MB-468 breast cancer cell lines, and claudin-low/basal B is equivalent to the mesenchymal stem-like/MSL -Hs578T and MDA-MB-231 breast cancer cell lines or mesenchymal-like/M-BT549 breast cancer cell lines. To date, in respect to FUSCC classification, only the following cell lines have been classified as the MDA-MB-231instead are IM, and the Hs578T instead are LAR [46, 49, 55]

Breast cancer biology is an ever-evolving field of knowledge that attempts to understand processes in play during transformation to oncogenesis and finally metastasis. After many decades of research, what has become apparent is that at each of the stages and subtypes is a different set of underlying processes and molecules at play, which varies again depending on the cell of origin. This complexity and heterogeneity have helped explain why treatment options have not applied to all breast cancers, as they are not alike. Therefore, it is necessary to understand the different mechanisms that underpin breast cancer progression, metastasis and heterogeneity. In addition, identifying more specific targets will aid in the development of new treatments, improve the efficacy of current treatments and seek to reduce adverse side effects associated with such treatments.

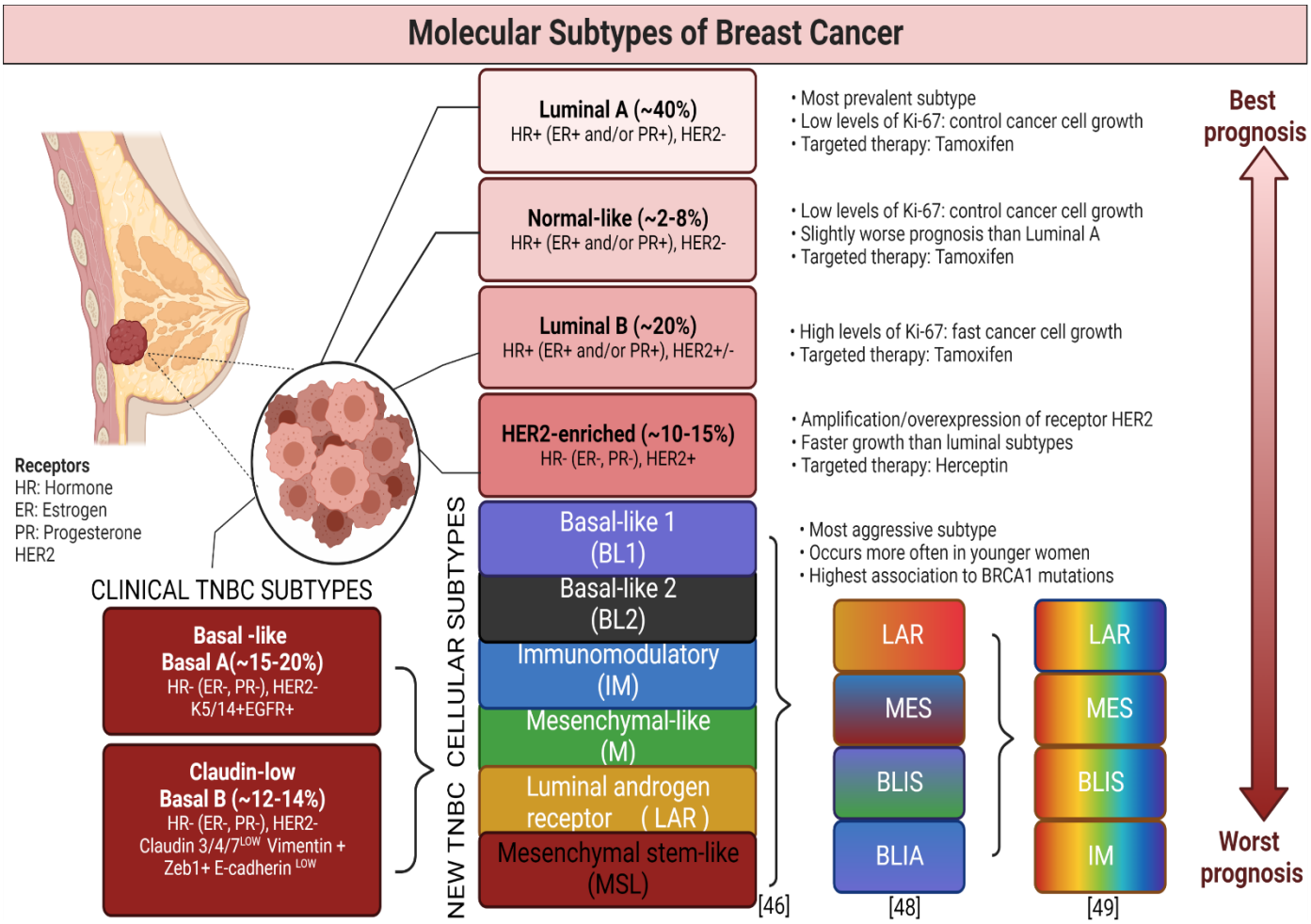


Figure 1-1 Breast cancer intrinsic/molecular subtypes

Breast cancer is divided into subtypes based on the presence or absence of defined biomarkers; Hormone receptors (HR) which include Progesterone (PR), Estrogen (ER) collectively, Human Epidermal growth factor receptor 2 (HER2), along with proliferation marker Ki-67, in conjunction with imaging techniques are used clinically to direct treatment strategies and estimate prognosis. As depicted above, the subtypes include: Luminal A, Normal-Like, Luminal B, HER2 and TNBC, ordered from best prognosis to worst prognosis due primarily to the fact that the expression HR and HER2 receptors have allowed for targeted treatment. The TNBC subtype continually evolves at a cellular level as specific biomarkers are determined. TNBC subtypes are Basal-like/TNBC and claudin-low/TNBC these are still clinically relevant. However, there is growing research into refining these TNBC subtypes further to reflect the heterogeneity of this group. So a model by Lehmann has identified six cellular subtypes [46]. Then Burstein refined this further, showing cellular subtypes that were combinations of Lehmann's [48] and finally the FUSSC classification that expanded the gene expression profiling further to include lncRNA, which has also identified four cellular subtypes; interestingly, these four subtypes are shown to have varying ratios of all six of Lehmann's subtypes [49].

Adapted from "Intrinsic and Molecular Subtypes of Breast Cancer" by BioRender.com (2021). Retrieved from https://app.biorender.com/biorender-templates

1.3 BREAST CANCER AND RAS - UNLIKELY ALLIES

Regardless of where it has originated, cancer development is made possible and expedited by the incidence of driver mutations referred to as proto-oncogenes that result in a gain of function, or alternatively by tumour suppressor genes, which result in loss of function or both gain and loss. These gain of function attributes are associated with genes that regulate and drive cell growth and proliferation. Whereas tumour suppressor genes restrict cell growth cell cycle regulation and drive apoptosis. Mutations can be derived somatically, arising in a single cell and passed to its progeny and only that cell lineage. In comparison, germline mutations arise in gametes and are present in all cells and can be inherited and passed on to offspring. Mutations in breast cancer and cancers generally are somatic variants, and germline variants are less common [56]. Furthermore, it was shown that these differences might be correlated with age as there was found to be a higher expression of cancer-related genes affected by germline mutations in a younger age group. In contrast to the germline mutations observed in a younger demographic, these same increases in cancer-related genes effects were due to somatic mutations in the older age group [57]. These findings support clinical data where most of the younger women affected by breast cancer have BRCA1/2 germline mutation, though it is important to note that a BRCA1/2 can also be somatic [58]. This oncogenic transformation has been the focus of much research and has led to the discovery of numerous genuine oncogenes. For example, oncogenes often observed in breast cancer include ErbB2/HER2, c-MYC, PIK3CA, Cyclin D1 and Cyclin E. Some of the tumour suppressors commonly observed are RB, TP53, and PTEN, but not limited to these [59, 60]. Examining these oncogenes and identifying new ones has indirectly yielded insights into cancer mechanisms where these oncogenes are pivotal [61, 62].

In addition, there has been the identification of cancers that are suspectable due to their driver mutation, so in this respect, much work has focused on several targeted treatments for this scenario. An example is the epidermal growth factor receptor (EGFR). Activation of this receptor leads to intracellular signalling for proliferation and differentiation and, therefore, EGFR mutation leads to uncontrolled cell proliferation. This type of mutation is a frequent driver in lung cancer development and progression [63]. This knowledge has led to targeted therapy toward EGFR. Furthermore, it was

observed to be a favourable treatment for chemoresistance of the non-EGFR mutant lung cancer cell. The rationale for targeting EGFR in non-EGF mutated cells is that it was observed that in lung cancer that it becomes resistant to frontline treatment by gaining EGFR mutations, and therefore the use of EGFR inhibitors in this context, combined with first-line treatment, improves efficacy [63]. However, EGFR inhibitors have yet to be proven efficacious in breast cancer treatment.

Another driver mutation is Rat sarcoma virus (RAS), which is a family of three genes that transcribe four proteins; Neuroblastoma RAS viral oncogene homolog (NRAS), Harvey rat sarcoma viral oncogene homolog (HRAS), Kirsten rat sarcoma viral oncogene homolog (KRAS), two isoforms KRAS4A and KRAS4B. Collectively all the RAS proteins function within the cell as a molecular switch responsible for activating many pathways involved in proliferation, cell cycle regulation and growth [64]. KRAS is a frequent driver mutation in pancreatic cancer, so theoretically, it should have responded to targeted treatment. To date, there is no specific treatment for RAS but rather targeting downstream effector pathways; however, most treatment responses have been obstructed by resistance [65, 66]. It has been suggested that a strategy to circumvent resistance is to simultaneously treat with multiple agents against different driver mutations [67, 68].

Curiously, breast cancer has limited mutations within the RAS oncogenes, including KRAS, HRAS and the NRAS isoforms. KRAS is observed more in breast cancer than HRAS, with NRAS being the least frequent. Although these incidences have been somewhat called into question, studies have shown there is a nominal frequency of KRAS mutations in TNBC as previously described [69]. Recently, the expression of mutant KRAS was shown to facilitate the epithelial cell differentiation to the mesenchymal claudin-low phenotype (TNBC) [70]. Furthermore, there is a recent suggestion that the presence of KRAS in TNBC is a favourable prognostic marker for breast cancer patients' overall survival and disease-free survival in all breast cancer and TNBC [71]. Moreover, the KRAS expression did not correlate with KRAS mutation and was observed equally in the high KRAS expression group compared to the low KRAS expression group; however, only the high KRAS conferred this survival advantage. This suggests that the upregulation of KRAS is independent of a mutation in breast cancer, and the effects are equal to or better than a mutation. Thus, the patient data confirms that RAS is not a driver mutation in breast cancer and is often hyperactive in many breast cancer cell lines resulting in the same upregulation as that seen with a KRAS mutation [72, 73]. However, this lack of

RAS mutation is not essential given that the RAS hyperactivation is an adequate substitute and possibly better as its presence is not as prominent but has the potential to be just as impactful if it increases to this level. In conclusion, patient data does suggest that treatments focused on downstream targets of RAS may be a therapeutic option in instances of RAS hyperactivation in breast cancer and therefore warrant further investigations [74].

1.4 BREAST CANCER METASTASIS - HOW THIS MOVES THE STORY

Breast cancer survival is more likely at lower grades, such as stages I through to stages III, but once breast cancer progresses to stage IV, it has spread to a distant site referred to as metastasis and survival rates and prognosis are abysmal at approximately 30% [1]. The rationale behind this decline is that metastatic disease is not receptive to most frontline chemotherapies and is further compounded by the consequence of the distant organ affected. The incidence of recurrence is correlated to breast cancer subtype, with HER2 and TNBC having the highest incidence of recurrence. HER2 was found to present with local recurrence, whereas TNBC was a regional recurrence. LA and LB subtypes returned after a protracted time frame [75]. Regarding breast cancer, the most common sites for organ tropism are observed to be bone, brain, liver and lungs. However, it is suggested that the subtypes can be associated with specific recurrence sites. It has been observed that overall, bone is the most common site of recurrence, particularly in the LB subtype, whereas visceral recurrence (including lung, liver, CNS, bone marrow and others) had the highest incidence in HER2 and TNBC, and nodal positivity was highest in TNBC and more commonly resulted in recurrence in CNS. Intriguingly there was an increase in visceral recurrence in the HER2 subtype in response to chemotherapy treatment higher than TNBC [76, 77]. It is worth noting that these findings were collected prior to the implementation of treatment with the adjuvant trastuzumab for the HER2 subtype. However, when more recent data was reviewed, there was a significant increase in relapse free-survival (RFS), although some noted adverse effects with specific frontline treatment, particularly anthracyclines. Still, this drug family has grown to include the newer generation of pertuzumab. However, 25% of patients still relapse and resistance is

a problem, so this is still very much an evolving landscape with many promising interventions being tried [78-83]. Cancer development is a stepwise process, with each additional mutation adding further attributes to benefit its survival and progression [84]. It is essential that each step is fulfilled for cancer that seeks to spread beyond its boundaries and progress to metastatic disease. At the fundamental level, the cancer cell must gain enough attributes to move from the primary tumour into adjacent tissue, and adaptations are required to move to a distant site [83].

An overview of the process (Figure 1-2) and the steps required for the metastatic process to occur highlights the attributes required by the cell to progress to a secondary site. In step one, the cancer cell disseminates, invading into local surroundings. This process requires the cell to make morphological changes to evade apoptotic cues in response to the breaking of epithelial junctions. Also, it needs to gain the ability to physically migrate and invade the surrounding tissues. The cell will gain these attributes by becoming undifferentiated and mesenchymal in the epithelial to mesenchymal transition. In step two, intravasation, cancer cells enter the blood and lymphatics vessels; this may be an existing nearby vessel or new vessels recruited to the tumour. In step three, cancer cells enter the lymphatic/blood circulation; of those that enter the vasculature, only a few will survive due to shearing force of the circulation fluid or destruction by an immune cell. The cancer cell has been shown to release factors that recruit platelets to aggregate around them to shield them, aid with extravasation by facilitating attachment to the endothelium, and release factors that aid cancer cell change and prepare the micro-environment [85, 86]. In step four, the cancer cell leaves the circulation via a process referred to as extravasation. As mentioned previously, this is facilitated by the platelet aggregation or emboli to allow for attachment or occlusion of the blood vessel at a distant site. The cancer cell will secrete factors to enable it to extravasate the endothelial layer. The aspect that is not clearly understood is that this appears not to be a random event where the cancer cells extravasate, as there is definite organ tropism for each cancer, with breast cancer having a higher propensity for metastases to the lung, bone, brain and liver. There is evidence that this is facilitated by chemokine signalling with chemokine receptor and ligand interaction for the cancer cell to find its specific metastatic site. In breast cancer, the chemokine receptor CXCR4 is highly expressed and migrates to its ligand CXCL12, which is highly expressed in bone marrow, brain, lung and liver [87]. In step five, the cancer cell arrives at the distant site, which has been prepared for its arrival, with

the primary site releasing growth factors and integrins on their own or integrins within exosomes to the distant site to prepare the area for colonisation by cancer cells, referred to as the pre-metastatic niche [88, 89]. Finally, the cancer cell will go on to form micrometastasis. The cell may become dormant at this stage, resulting in a latency period and may not proliferate until a later date of even ten years or more after initial seeding [90, 91]. Alternatively, the micrometastasis may continue to proliferate to form clinically detectable macrometastases (Figure 1-2). It is apparent from the metastatic process outlined that the primary cancer cell is starkly different to the cell that has been able to fulfil this process, which is why much research is focused on understanding the mechanisms involved. To aid the development of targeted treatment, the biggest obstacle to date is that therapies for the primary tumour have limited to no efficacy on its metastatic derivative and may even exacerbate its growth and survival [83, 92-97]. One of the most necessary adaptions is cellular plasticity, EMT, and conversely mesenchymal to epithelial transition (MET), which is a necessary process, given that most cancers arise from epithelial cells (Figure 1-2). As a result, the epithelial cancer cell can change to a mesenchymal phenotype. The mesenchymal adaptation allows the cell to invade and migrate, essential capabilities for the cell to move to a distant site. In reverse, once the cell arrives at the secondary site, it will undergo MET as this phenotype is more advantageous for colonisation as it requires adherence and tight gap junctions to reach its growth potential [98, 99].

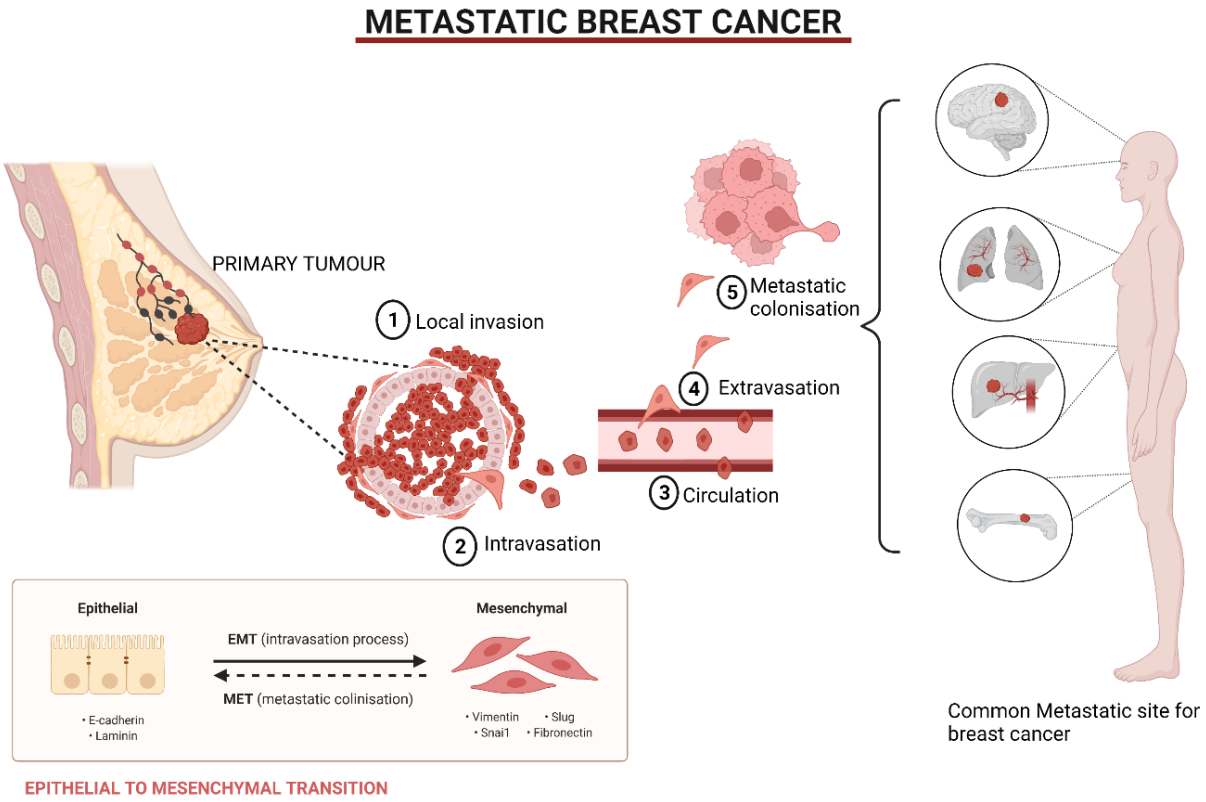


Figure 1-2 Metastatic breast cancer

The stepwise process of metastasis: Step 1- breast cancer cell begins to invade tissue; Step 2- breast cancer cell undergoes EMT to facilitate intravasation; Step 3- breast cancer cell enters systemic or lymphatic circulation to travel to a secondary site; Step 4- breast cancer cell extravasate the circulation to "pre-metastatic niche"; Step 5- breast cancer cell undergoes MET to develop into micro/macrometastases. Organ tropism of breast cancer is brain, lung, liver and bone.

Created with BioRender.com

Therefore, experimentally, invasion, migration and colonisation assays are used to study the major steps in metastasis; examples include wound healing, invasion outgrowth, colony formation and chemomigration assays. This thesis uses these and others for in vitro evaluation of metastatic cell attributes. In addition to these assays, numerous biomarkers can be examined, for example, in EMT biomarkers such as loss of E-cadherin and gain of vimentin, N-cadherin, with the reverse being an indicator of MET. In addition, changes to transcription factors that regulate these biomarker expressions, such as Zeb1, Snail and Slug, allow researchers to analyse a cell's capacity to fulfil the metastatic process or lack thereof.

The focus on identifying biomarkers of metastasis has been an area of ongoing focus. As a means of preventing or treating metastatic disease through personalized medicine, for example, the increased gene expression of interleukin -1β occurs in breast cancer that metastasises to the bone [100]. Pertinent to this thesis, a recent study comparing matched sample pairs from the patient's primary and metastatic sites examined the genetic profiles to identify novel markers for metastasis. One major pathway significantly altered was the autophagy pathway, which was significantly upregulated in the metastatic samples compared to the primary site [101]. Since nearly all breast cancer patients' deaths are attributed to metastasis, it highlights the importance of identifying these novel targets and pathways to improve survival outcomes.

1.5 AUTOPHAGY - WHAT WE KNOW TO DATE

Autophagy is a highly conserved process that translates to “self-eating” from Greek and represents a catabolic process where proteins, organelles, and other cellular components are degraded into recyclable units and released back into the cell. Currently, numerous forms of autophagy exist, including macroautophagy, which mediates the degradation of cellular components through the bulk engulfment of proteins, organelles, and macromolecules non-selectively. By forming the autophagosome around the “cargo”, it interacts and fuses with the lysosome, thus forming the autolysosome where the degradation occurs (Figure 1-3 and Figure 1-4). Furthermore, macroautophagy has specific variants dependent on the cargo, such as mitophagy, which is the select movement and degradation of the mitochondria. Ribophagy involves removing and degrading ribosomes, lipohagy is the removal of lipids and aggrephagy is the removal of aggregated proteins. Microautophagy involves selective proteins containing the KFERQ amino acid motif and or bulk degradation of protein and smaller molecules through endocytosis into endosomal multivesicular bodies that enter the lysosome or are secreted from the cell (Figure 1-3). Chaperone-mediated autophagy involves the selective targeting of proteins with a KFERQ amino acid motif, which is facilitated by the translocation of the protein across the lysosomal membrane (Figure 1-3 and Figure 1-6). With the identification of the various types of autophagy and the advancement of research within respective types, it is apparent that these processes have roles to play in many pathologies. So further understanding of the mechanisms underpinning their functions could lead to treatments for many pathological states [102-104].

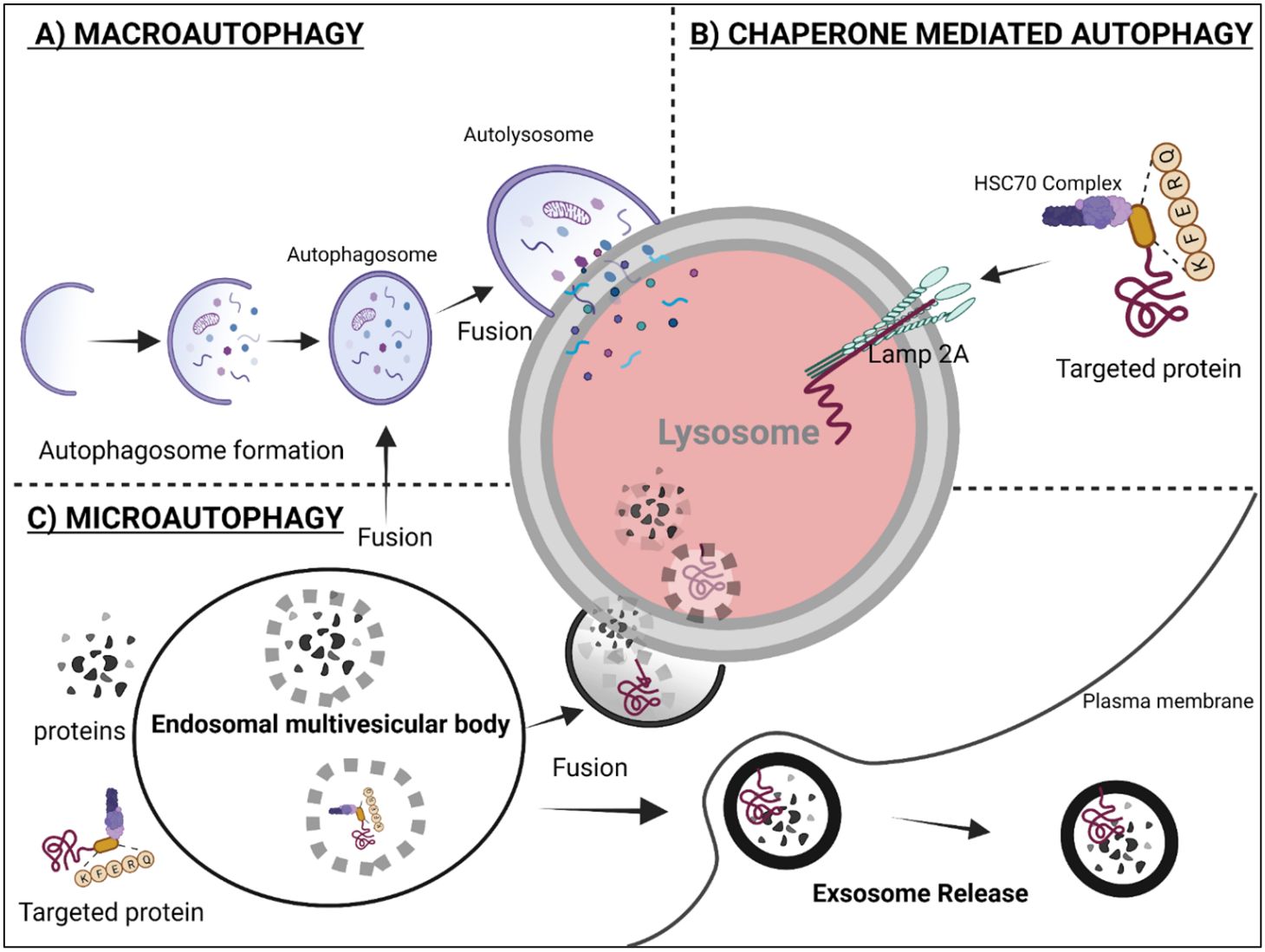


Figure 1-3 Types of Autophagy

Schematic overview of the different types of autophagy. **(A)** Macroautophagy is the bulk degradation of proteins and organelle indiscriminately with the formation of the autophagosome around the cargo, which fuses with the lysosome to enable cargo degradation. **(B)** CMA is the sequestering of proteins with a KFERQ motif targeted by HSC70 and its co-chaperones, whereby they deliver the protein to Lamp2A at the lysosome membrane, where it is unfolded and translocated into the lysosome for degradation. **(C)** Microautophagy involves the collection of indiscriminate proteins or targeted proteins with the KFERQ motif that HSC70 delivers, and its co-chaperones all are encapsulated in the MVB to be taken to the lysosome for degradation, secreted in endosomes at the plasma membrane or fuses with the autophagosome to form an amphisome and delivered to the lysosome for degradation. The net result of all processes except endososmal secretion is to provide recyclable molecules back into the cell.

1.6 MICROAUTOPHAGY- THE SMALLEST OF THEM ALL

Microautophagy was described in mammalian cells half a century ago, but its identification in yeast has been more recent within the last two decades and has been instrumental in providing much of the knowledge in this area [105-107]. This autophagy differs from the other types in that it can facilitate targeted and indiscriminate protein degradation and is specific to proteins and smaller molecules. Also, it involves the late endosomal system encapsulating its cargo to form an endosomal multivesicular body (MVB) formed by the endosomal sorting complexes required for transport (ESCRT). From here, there are a few routes the MVB can follow, including fusing with the lysosome to enable content degradation, or the MVB can fuse with the autophagosome to form an amphisome that is subsequently taken to the lysosomes. It is worth noting that these functions have more recently been termed endosomal-microautophagy (eMI) [108]. When the contents are secreted from the MVB in endosomes at the plasma membrane, this is an exocytosis function, specifically not an autophagic process [109, 110]. Microautophagy can also sequester proteins specifically with the assistance of HSC70 as the co-chaperone with the protein targeted by its KFERQ motif. Although, the similarity shared between microautophagy and chaperone-mediated autophagy (CMA) regarding protein targeting would suggest some redundancy between the processes. It has been observed that the two can be discriminated, as microautophagy does not require the molecule Lamp2A, which is needed for CMA. Moreover, initial studies have noted that microautophagy will also uptake aggregates and proteins that will not unfold upon entry, unlike CMA, where the proteins are unfolded and then pass across the lysosomal membrane. It was observed that the presence of the KFERQ motif alone was insufficient to target it to be sequestered by microautophagy, so it would indicate there are other requirements which will be identified as research in this area progresses [105, 108, 110]. The research into microautophagy is still limited, but it has been observed that it similarly responds to starvation as macroautophagy but is independent of MTORC1 inactivation. Its role in this context was to replenish essential macroautophagy components required for autophagic processing, such as receptor proteins P62 and NRB [111-113].

On the other hand, a similar study in yeast showed that MTORC1 inactivation was responsible for the activation of microautophagy, and in this context, it was observed to recycle vacuole proteins for degradation and, as such, is vital in vacuole biogenesis [114]. In addition, it was shown that microautophagy facilitates the secretion of GAPDH into the plasma membrane surface and extracellular matrix during starvation to capture iron. It is further suggested to be a means by which microautophagy rids the cell of toxic proteins [115]. Another recent observation suggests that CMA, microautophagy and exosome release are under the same regulators as their activity was found to be mutual to protect/maintain the cell's proteostasis. However, it should be noted that the microautophagy in focus was targeted, not indiscriminate [116]. There is some preliminary evidence to date that it presents a beneficial process in maintaining neuronal health and may prevent degeneration related to Alzheimer's disease [117]. However, as more research is still to be undertaken in microautophagy, the current landscape is likely to change.

1.7 MACROAUTOPHAGY-THE INDISCRIMINATE MEMBER

Macroautophagy (hereafter referred to as autophagy) is the most researched of all the autophagic processes. This has been aided by the fact that it is highly conserved between yeast and mammals. An indiscriminate degradation process involves de novo synthesis of a double-sided membrane called the phagophore that extends around its cargo to encapsulate it and form the autophagosome. The formation of the autophagosome makes it distinguishable from the other autophagic processes, although, to date, it is acknowledged to be involved in multiple pathophysiologies, including cancer, neurodegeneration [118-120], ageing [121-123], metabolic syndrome [124, 125], myopathies [126, 127], infectious disease [128-130], immunity [131-133], cardiomyopathies [134, 135], to name just a few. Its relationship to many of these disease states is related explicitly to its dysfunction. The current findings concerning cancer will be the focus of this chapter and will be discussed later. To understand its role in disease, the type of autophagic pathways being utilized and the molecular mechanisms involved in its activity need to be identified; currently, the activation pathways can be grouped as either canonical or non-canonical.

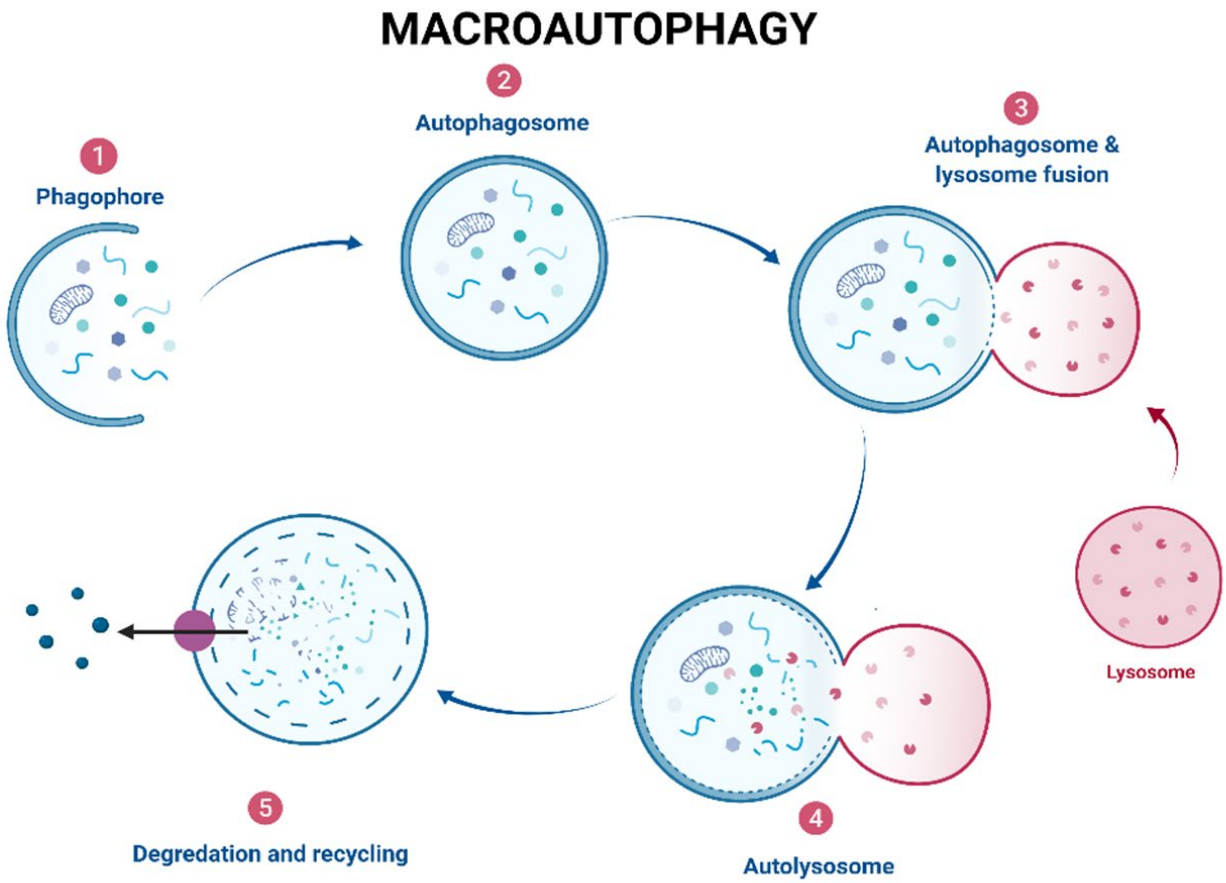


Figure 1-4 Schematic overview of macroautophagy

Schematic overview of the autophagic process excluding molecular mechanism: Phagophore develops around cargo **(1)** and fuses to form the autophagosome **(2)** the autophagosome and lysosome fuse **(3)** to form the autolysosome **(4)** facilitating cargo degradation and **(5)**recycled molecules released back into the cell.

1.7.1 Canonical Pathway

The fundamental role of autophagy is to maintain homeostasis within the cell by removing cytotoxic protein aggregates, defunct organelles and pathogens. In addition, it responds to nutrient deprivation by providing an alternate nutrient reservoir by degrading non-essential cellular contents. This 'normal' autophagic response is activated by autophagy-related proteins (ATG) in a hierarchical process called the canonical pathway. The canonical pathway begins with the development at the phagophore, also referred to as the phagophore assembly site (PAS), or omegasome, in yeast and mammalian systems, respectively. Although the membrane components of the phagophore have been suggested to be derived from numerous sources [136], including the endoplasmic reticulum–Golgi intermediate compartment (ERGIC) [137, 138], plasma membrane [139], endoplasmic reticulum (ER) [140], mitochondria -ER [141], endosome [142, 143] and ATG 9 recruitment [144], in reality, it is most likely a combination, and it varies depending on the cellular context [145].

The process is stepwise with the initial activation of the unc-51-like autophagy activating the kinase (ULK1/2) complex, which includes focal adhesion kinase family interacting protein of 200 kDa (FIP200 RB1CC1), autophagy-related protein 13 (ATG13), and autophagy-related protein 101(ATG101). The activity of this complex is inhibited by the mammalian target of rapamycin (MTORC1) or specifically MTOR complex1 through phosphorylation of ULK1/2. MTORC1 is involved in cell growth and proliferation, and its downstream targets are eukaryotic initiation factor (eIF), 4E-binding protein 1 (4EBP1) and ribosomal S6 protein kinase 1 (SK61). Its activity is sensitive to stress signals, particularly nutrient deprivation or chemical inhibition with rapamycin directly or indirectly via other molecules such as AMP-activated protein kinase alpha subunit (AMPKα) activation, which block MTORC1. All result in releasing the inhibitory effects of MTORC1 and facilitating autophagy activation through the ULK1/2 complex [146-149]. The activated ULK1/2 complex interacts with the phagophore and PI3K complex. Note that there is evidence of interaction between these complexes, and the phagophore is maintained by autophagy-related protein 9 (ATG 9). ATG9 is also responsible for all membrane trafficking to the growing autophagosome; furthermore, it has been observed that the activity of ATG9 is dependent on ULK1 and PI3K complexes [150-153]. The PI3K complex consists of beclin1 (BECN1), phosphatidylinositol 3-kinase catalytic

subunit type 3 (VPS34 or PI3KC3), vacuolar protein sorting 15 (VPS15) and autophagy-related protein 14 (ATG14). As a consequence of its activation, it recruits phosphatidylinositol 3-phosphate (PI3P) to enable the elongation of the autophagosome and allow binding to WD-repeat protein interacting with phosphoInositides (WIPI). This facilitates the recruitment of the autophagy-related 16-like gene (ATG16L) complex. The ubiquitin-like system forms the ATG16L complex, and the conjugation of autophagy-related protein 12 (ATG 12) to autophagy-related protein 14 (ATG 5) by autophagy-related protein 7 (ATG7) acts as E1. Then autophagy-related protein 10 (ATG10) acts as E2 releasing ATG7 and binding ATG5, facilitating ATG16L binding to form a complex recruited to the autophagosome. The other ubiquitin-like system in this process is Microtubule-associated protein 1A/1B-light chain 3 (LC3) is cleaved by autophagy-related protein 4 (ATG 4). It is lipidated with the conjugation of phosphatidylethanolamine (PE) by autophagy-related protein 3 (ATG 3) and ATG 7; the result is the formation of LC3-II. With the assistance of the ATG16L complex, LC3-II is attached to the luminal side of the autophagosomal membrane [154, 155]. LC3-II can interact and bind P62, which binds ubiquitin-tagged protein aggregates. The autophagosome completes its maturation and fuses closed. The removal of PI3P and ATGs from the outer surface coincides, but the exact mechanisms or relationship of this final step in maturation is yet to be elucidated in the mammalian system, but in yeast, it is facilitated by ATG4. Soluble N-ethylmaleimide-sensitive factor attachment protein receptors (SNAREs) and RAS-related protein in brain (RAB) are responsible for fusing the autophagosome to the lysosome. The regulation of this activity is shown to increase when UV radiation resistance-associated (UVRAG) binds the PI3K complex, or conversely, the binding of rubicon (RBCN) inhibits it [156-158]. The final step in the degradation process is the release of hydrolase enzymes from the lysosome into the autophagosome, where the contents are broken down to their constituents and then exported through the autolysosome membrane to the cytosol. Then the autolysosome is degraded with lysosomal components stored for the development of lysosomes at a later stage [159-165] (Figure 1-5).

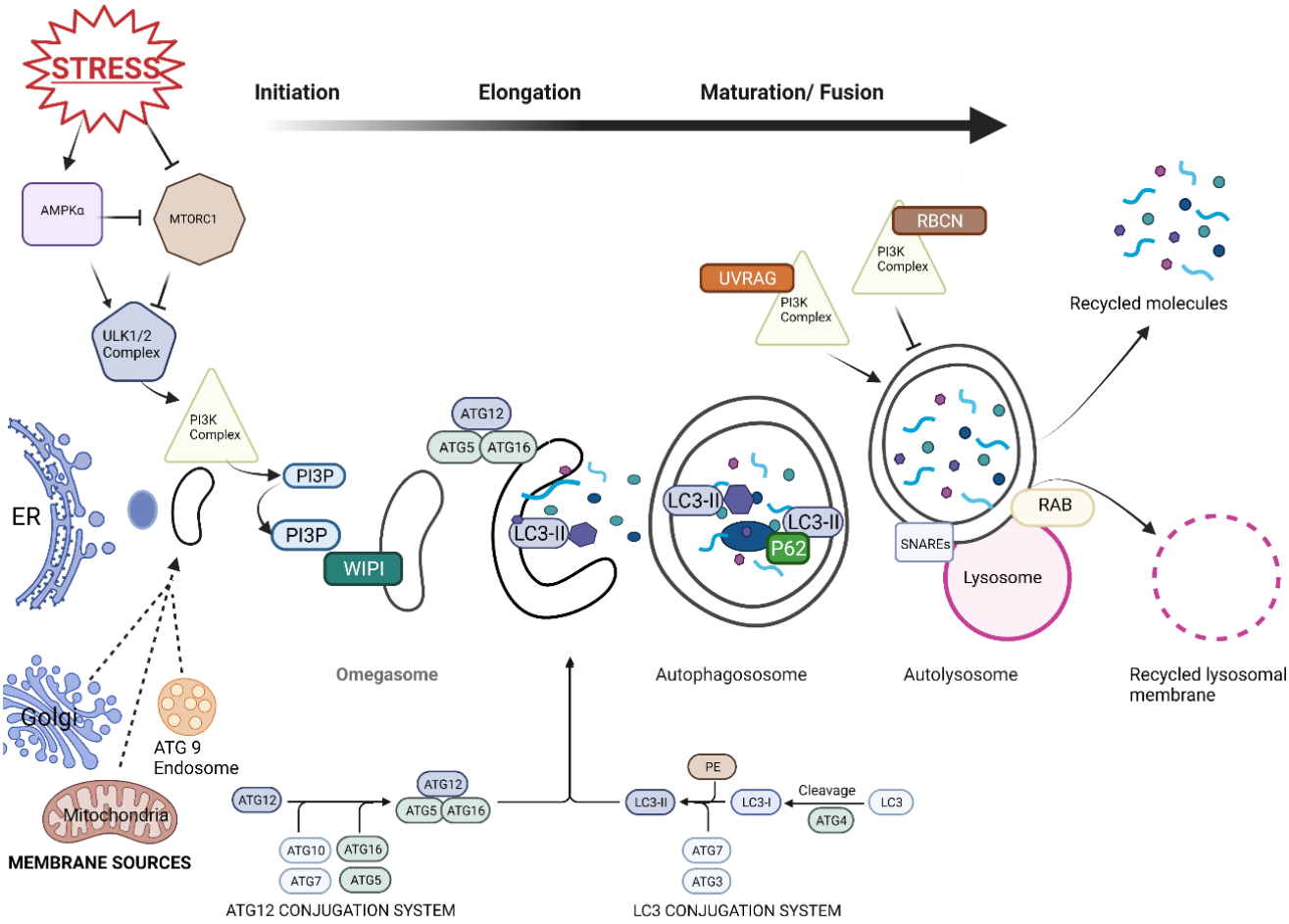


Figure 1-5 Autophagy Canonical Pathway

Schematic of the canonical pathway in autophagy is a stepwise process as detailed above: Stressors such as starvation induce AMPK to become activated, it can either inhibit MTOR complex I, which results in the release of its inhibition on ULK1/2 complex. Alternatively, AMPK can act directly on ULK1, and once ULK1 is actioned, it acts on the initiation complex. The initiation complex recruits PI3P to initiate and nucleate the phagophore, elongation and maturation are regulated by the ATG12 conjugation system, and the LC3 system involves the formation of LC3-II, which is the only ATG to be embedded in the membrane. P62 bound to protein aggregates can either bind LC3 or the autophagosome membrane. After the membrane closes to form the autophagosome, it fuses with the lysosome to form the autolysosome with the assistance of RAB and SNAREs. PI3 K complex bound by UVRAG can activate this fusion, or PI3K complex bound by RBCN can inhibit it. The contents of the autolysosome are degraded into their constituent molecules and released back into the cell to be recycled into metabolic substrates. The lysosomal membrane is also recycled into components for later lysosomal biogenesis.

Created with BioRender.com.

1.7.2 Non-Canonical Pathways

Canonical is the focus pathway in this thesis as it is relevant to treatments utilised within these studies. However, for clarity, non-canonical is defined as autophagic activity that does not require the hierarchical ATGs and other regulators such as BECN1 PI3K for initiation and or elongation. In respect to initiation stages, the activation of autophagy has been observed independent of BECN1 presence in the PI3K complex. This particular pathway has been shown to occur in response to various treatments such as resveratrol [166], Z18 [167], cobalt chloride-induced hypoxia [168] and staurosporine [169]. These are just a few studies that have identified BECN1-independent autophagy in different cellular contexts, though it would be interesting to determine if the common feature is the activity of these treatments with B-cell lymphoma-2 (BCL-2) family members, as this autophagy was found to cause cell death. Ulk1/2- independent autophagy therefore, the necessity for MTOR and or AMPKα is circumvented. This autophagic activity has been observed to occur in response to hypoxia [170], hyperosmotic stress [171] and ammonia generated through glucose deprivation [172]. Leading on from that study, there was evidence demonstrating that during glucose deprivation, FIP200 can interact with ATG16L without ULK1/2 [173]. Regarding the elongation stage of the autophagic process, ATG5/7 independent autophagy was observed in vivo and absent for LC3-II and shown to involve Rab9 for autophagosome-lysosome fusion [174]. In addition to these findings, it has been shown ATG5 independent activity is responsible for mitophagy [175]. More recently, ATG5 independent autophagy was responsible for the clearance of inactivated proteasomes [176]. At the very least, these findings demonstrate that autophagic activity occurs in the absence of traditional regulators. These ‘non-canonical’ activities have been observed in cells with the genetic loss of ATG5/7 but in the wild type too. This suggests that it may not be one or the other and that all are present and work collectively within the cell to meet its needs. This ability of autophagic activity to progress, albeit of core regulators, does highlight the complexity of autophagy and the problems that will arise or have as a treatable target.

1.8 AUTOPHAGY - FRIEND, FOE OR BOTH?

Autophagy has been shown to have paradoxical roles in cancer. This review focuses on autophagy in transformed cells, which has been identified to facilitate pro-survival mechanisms by facilitating resistance towards anticancer therapies and providing an alternative nutritional pathway within the tumour microenvironment, which often lacks sufficient nutrients due to decreased vascularization. However, on the other side of this paradox is the benefits of autophagy that should be highlighted. For example, it is shown to prevent oncogenic transformation by tumour protein P53 (TP53) due to an upregulation of transglutaminase 2 (TGM2)[177] . Further evidence shows that P62 regulates DNA damage repair between autophagy and P53. However, in pathologies, particular chromatin remodelling complexes are involved, and there was a reduction in P62, which condenses autophagy and increases the DNA damage leading to a senescent and ageing phenotype [178]. This link between DNA damage and autophagy was also observed in response to ionizing radiation, where DNA damage worsened when autophagy was inhibited. There was also an accumulation of reactive oxygen species (ROS), leading to increased cellular injury and death [179]. This loss of autophagy and increase in DNA damage would increase the potential of spontaneous mutations, which will lead to oncogenic transformation. There are extensive reviews on autophagy in inflammation and its beneficial role in immune survival [175] and a cytoprotective role in specific tissues in response to systemic infection [180]. Although these are not specific to cancer, there are well-defined links between the inflammatory process and oncogenesis, and these findings may lend insight to autophagy and cancer development.

Furthermore, a clear connection is identified in metabolism, particularly in obesity [181, 182] and endocrine signalling [183], which are all intimately linked to carcinogenesis when dysregulated. Autophagy has a significant role in cellular homeostasis from reducing DNA damage, maintaining metabolism, effective cellular signalling, immunity and protection against pathogens and inflammation. Consequently, it prevents mutational events and aberrant cell survival. This protective effect can all be associated with all attributes that need to be circumvented or suppressed for a cell to transform and attain the hallmark of cancer. Although it is protective in nature toward the non-transformed cell by preventing the aggregation of proteins, accumulation of defunct

organelles or damaged DNA and or mutated DNA can lead to oncogenic transformation [184-189].

1.9 AUTOPHAGY AND BREAST CANCER - CURRENT FINDINGS AND CONTRADICTIONS

A current area of interest in cancer therapeutics that has resurfaced is metronomic treatment, which is chemotherapy administered over an extended time at a low dose [190]. It has been witnessed that patients with hormone receptor (HR) positive breast cancer had an increased expression of autophagic and apoptotic markers in metronomic chemo-endocrine treatment. This correlated with improved responses to treatment compared to endocrine therapy on its own, although there were autophagic markers present but lacked functional studies [191]. As this paper was limited by its design in that it used tissue samples, which does not allow for the interpretation of autophagic activity, so the expression of LC3 and Beclin-1 observed may be related to suppression autophagy processing. Furthermore, these results may be counterintuitive as a meta-analysis, and systematic review of LC3B and BECN1 found LC3B was a poor prognostic marker, whereas BECN1 was an indicator of favourable prognosis [192]. Their mere presence in these patient samples warrants further investigation into the role of autophagy in this low dose regiment, as this suggests it may reduce its resistance effect or even heighten them.

BECN1 has significant roles in the canonical pathway, but interestingly it is found to have altered expression in cancer. Particularly in breast cancer, where BECN1 can have altered expression due to haploinsufficiency, and its loss is thought to drive oncogenesis [193, 194]. A recent description of the tumour suppressive role of BECN1 was attributed to its regulation of E-cadherin on the plasma membrane allowing for its epithelial functioning, so with the loss of BECN1, there is reduced E-cadherin localisation to the plasma membrane, consequently facilitating loss of E-cadherin function at the plasma membrane which is to limit cell growth and metastasis [195].

Autophagy's role in facilitating chemoresistance has been well documented in most treatment scenarios [196-201]. However, this landscape has changed depending on the context due to the heterogeneity of the tumour. The current premise is that a distinct

population of cells, the CSC cells is responsible for treatment resistance as well it is suggested to be accountable for metastatic spread. This population of cells are stem-like in that they have high expression of stemness markers CD44, ALDH1, CD24 and orCD133, and more that have been described in detail and are colloquially referred to as cancer stem cells (CSC)[202-204] In variation to this it should be noted that breast cancer stem cells are observed to express high CD44 and low CD24.

Earlier research has shown a clear relationship of chemoresistance facilitated by autophagy, and in accordance with this, current research has supported these findings and defined them further. Current research has shown that the CSC population is responsible for the chemoresistance and has shown high autophagy activity on which they appear to be dependent. Commonly, the general term hormone receptor (HR) is used to describe the presence or absence of ER and PR in cancer cells clinically. The role of autophagy has been demonstrated in a recent trial that focused on CSC in HR negative breast cancer patients receiving Reparixin, an inhibitor of C-X-C Motif Chemokine Receptor 1 (CXCR1), the receptor found overexpressed in breast cancer CSC's. The study evaluated autophagy as a measure of the tumour microenvironment and resistance, the level of P62 was found to decline, so it suggested that there are autophagic changes, but further experimentation is required to delineate what these are [205]. There was further evidence relating breast cancer with brain metastasis being facilitated by astrocytes secreting C-X-C Motif Chemokine Ligand 12 (CXCL12), resulting in the inhibition of KISS-1 Metastasis Suppressor (KISS1), an inhibitory regulator of autophagy. Its subsequent blockade by the astrocyte allows the circulating breast cancer cells to proliferate and form brain metastases [206].

The CSC's are an area of great interest at the moment as it has been shown that this group of the cell population facilitates metastasis and chemoresistance, particularly in breast cancer. This role of autophagy in CSC's was further explained to maintain stemness. Stemness is defined as the ability of the CSC to self-renew and produce differentiated progeny. Therefore, the CSC's potentially present a target in the battle to treat metastasis and prevent chemoresistance. These studies relating to autophagy and CSC have been guided by several earlier studies where the alteration of autophagic markers has significantly impacted CSC. For example, a paper by Maycotte et al. demonstrated that when ATG7 or BECN1 was knocked down in breast cancer cells, there was a subsequent reduction in the CSC population. The mechanism underpinning this

regulation of CSC by autophagy was found to be due to autophagic control of cytokine secretion, expressly interleukin 6 (IL6). It should also be noted that this was found to be context-dependent in nature [207]. These findings were in line with an earlier study where the BECN1 and autophagy were required for the survival of the CSC population[208]. This study did show there was an increased autophagic flux at basal and starvation-induced conditions within the CSC population [208]. Other studies have demonstrated this increased autophagic flux in the CSC population and using treatments that inhibit autophagic resulted in a more significant apoptotic effect on these populations. However, cell death was still present in the other population, not to the extent of the CSC's [209, 210].

Furthermore, a study of breast cancer CSC using RNAi screen found ATG4 essential in maintaining the CSC population and was further shown to facilitate tumourigenicity *in vivo* [211]. Also, there has been observed that cerebellar degeneration-related protein 1 transcript (CDR1) induces autophagy and regulation of autophagic genes in the CSC population [212]. It was also shown in another study that CSC tumorigenic potential was diminished with the reduction in autophagy through the removal of FIP200 and when combined with Signal Transducer And Activator Of Transcription 3 (STAT3) or Transforming growth factor-beta (TGF-β) inhibitors, induced CSC death and prevented cell growth [213]. It has been suggested that autophagy is activated in response to the extracellular matrix rigidity with increased firmness, and a concomitant increase in autophagy suggests that autophagy responds to the microenvironmental cues. These findings also show that the CSC's presence was abundant in the softer matrix, conflicting with the increased autophagy activation. Like numerous studies, the data indicate there is an increase in autophagosome formation but does not include the data to determine actual autophagic activity, which may reveal that although there may be increased LC3-II expression, there could be an overall suppression in activity [214].

The tumour micro-environment reveals itself as a significant regulator in maintaining stemness, and it has been demonstrated that cancer associated fibroblasts (CAF's) signalling to breast cancer to maintain stemness is facilitated by autophagy [215]. Furthermore, it was also revealed nutrient-deprived CSC upregulate autophagy and release factors to protect the tumour environment [216]. The breast cancer CSC area is promising and further emphasises the validity of autophagy as an adjuvant therapy in cancer treatment. However, it may not be only in the context of inhibition; it is

hypothesised that autophagic activation in the highly active autophagic cell will lead to lethality and may explain the finding of Rotterlin treatment which was observed to induce autophagy resulted in increased apoptosis in the CSC population [217]. Furthermore, this autophagic induction and cell death were also observed in breast cancer stem cells treated with resveratrol [218].

1.10 AUTOPHAGY AND METASTASIS-IS THERE A CONNECTION

The role of autophagy has been identified to have a role in breast cancer metastasis. In addition, the autophagic function has been attributed to its role as an alternative nutrient source, mainly when the cell is metastatic and or dormant. However, the current dogma surrounding metastatic growth is that it is not a linear model whereby the cell leaves the primary, moves to the secondary site and proliferates. Instead, the patient data and advances in research reflect an interrupted model whereby the metastatic cell undergoes a period of cellular dormancy. Dormancy in cancer cells collectively is still an area of active research. What is observed in these cells is that they are in a state of cell cycle arrest, yet they are not observed to be senescent and can re-activate from this state. Furthermore, when these types of cells gene expression profiles were examined, it was similar to the quiescence of stem cells [219-221]. A recent study of breast cancer dormancy found these dormant cells to be highly autophagic active, and these dormant cells demonstrated a higher metastatic burden than control cells. The autophagic mechanism underpinning this activity was independent of BECN1 and the non-canonical pathway involved along with ATG 7.

Moreover, the requirement for autophagy was related to increased turnover of mitochondria or specifically mitophagy and is speculated to protect the cell from toxic by-products of mitochondrial damage [222]. Similar results were observed in another study where increased metastasis and poor patient survival were facilitated by autophagy through ATG7 but regulated by circular RNA CircCDYL[223]. However, in contrast to these findings, it has been observed that the inhibition of autophagy resulted in increased metastasis due to the accumulation of neighbour to BRCA1 (NBR1) [224] . It is suggested that these observed differences may be a reflection of context or, as was eluded to by

Vera-Ramirez et al., where inhibition of autophagic activity was only effective at the time of seeding of dormant cells, it is speculated there is a temporal aspect to autophagy that needs to be explained to achieve better treatment efficacy [222]. Finally, concerning bone-specific breast cancer metastasis, autophagy was observed to increase its activity in a transcription factor Runx2 dependent manner, where it is proposed that autophagy facilitates the metabolic and osteolytic effects of Runx2 [225].

1.10.1 Epithelial to Mesenchymal transition and Autophagy

An essential attribute for a cancer cell to acquire is the transition from an epithelial to mesenchymal phenotype, allowing the cell properties that are required to invade and migrate. There is evidence to indicate autophagy has a role in this process. An earlier study has suggested that EMT results in a concomitant increase in autophagy and immune evasion [226]. The immune invasion was specific to CTL-mediated death and was directly attributed to autophagy or, more specifically, canonical autophagy [226]. In contrast, data reveals that the loss of autophagy results in the accumulation of P62, which can bind to Twist Family BHLH Transcription Factor 1 (TWIST1), which results in EMT and other tumourigenic changes [227]. In contradiction to the previous study from Qiang et al., Saxena et al. showed that TWIST1 is regulated by phosphorylated AMPKα and resulted in EMT, although this study did not examine autophagy specifically, the downstream effector of AMPKα is autophagy [228]. It is put forth that the accumulation of P62 prior may have been reflective of dysfunction rather than inhibited autophagic activity. Although both studies show TWIST1 is responsible for EMT activation, the other difference may also be due to the cellular contexts used. A similar study demonstrated that the inhibition of P62 specific autophagy by tripartite motif 59 (TRIM59), which then enabled the activity of programmed cell death protein 10 (PDCD10) and facilitated the transition to the mesenchymal phenotype through suppression of RAS homolog family member A (RhoA) and Rho-associated protein kinase (ROCK). It is of interest that P62 is not always involved in autophagy; its specific role is to bind ubiquitinated protein aggregates and deliver them to the autophagosomes. The downregulation of P62 does not indicate inhibition of autophagy and the data shows that with P62 loss, LC3 was present.

It is worth noting that P62 has other roles that would warrant investigation in this context [229].

In summary, autophagy has a role in breast cancer, particularly in facilitating metastatic potential, although it is also apparent that there are many contradictions regarding this. It is suggested that it may not be a case of one being correct over the other, but instead, all are valid, and the contradictions are a reflection of heterogeneity and that specific cell populations within the tumour may have reduced autophagic activity while others upregulate theirs in response to cellular needs. There are apparent conflicts in the literature and a strong suggestion that these variables may also be temporal and spatially regulated, which adds to the complexity and highlights an aspect that still requires more research to determine and explain. Research into these contradictions will be aided by further advances in the experimental methods available to examine and identify dormancy, heterogeneity and specific types of autophagy and their activity.

1.11 RAS AND AUTOPHAGY - IS THERE A RELATIONSHIP?

An area of particular interest relates to autophagy and its relationship with RAS, observed in RAS-driven cancers. It is shown that cell with activated RAS utilise autophagy to remove the increase in toxic by-products due to its hyperactivity when mutated in the context of cancer [230], also observed to regulate metabolism [231] and facilitate the secretion of tumourigenic supporting factors such as IL6 [232]. A preliminary study has suggested that autophagy can be involved in the degradation of RAS-GTPase, leading to some future insight into how autophagy regulates RAS pathways [233]. There are many cancer types where this co-dependence between RAS mutation and autophagy have been observed including in glioblastoma[234], renal cell [235], ovarian [236] and melanoma [237, 238]. Furthermore, in recent studies in RAS driven colorectal cancer, there is evidence to suggest the concomitant increase in autophagic activity with RAS. It was further determined to be regulated by the Wingless-related integration site (Wnt)β-catenin and AKT pathways which are also known to interact with each other through the Glycogen synthase kinase-3β (GSK3β) [239] . Although in KRAS specific mutations, MAP kinase kinase (MEK)/ extracellular signal-related kinase (ERK)

pathways were observed to regulate the autophagic activity, suggesting disparities between the autophagic induction and the RAS isoform [240-242].

Lung cancer has also shown that autophagy supports KRAS as an alternate metabolic reservoir [243]. Similar findings have been observed in other studies showing KRAS mutations dependent on autophagy. However, it was recently proposed that copper binding with ULK1/2 is the mechanism involved in the activation of autophagy [244].

Intriguingly when there is an up-regulation of RAS by DEPPC1, it has an inhibitory effect on autophagic activity, but this was observed in mutant RAS [245]. For example, gastric cancers have been observed to facilitate dormancy and even can result in cell death through the endogenous RAS inhibitor RAS family member 3 (DIRAS3)[246] ; similar findings were observed in ovarian cancer but observed in family members DIRAS1 and DIRAS2 [247, 248]. Furthermore, autophagic induction was also observed with the RAS inhibitor Aplasia RAS homolog member I (ARHI) in glioblastoma [249]. These findings demonstrate how in one context, autophagy can act in a pathological manner when induced by RAS mutation, but when induced by RAS inhibition, it can be cytoprotective; this is put forth cautiously as dormancy may not be a positive result depending on the context.

The most highly researched cancer concerning autophagy and RAS mutation is pancreatic cancer and the KRAS mutation. Furthermore, despite some differences observed between mutations at different locations, the upregulation of autophagy and MEK/ERK is consistent [250]. Importantly, autophagic induced chemoresistance is a common feature of gemcitabine treatment in KRAS mutant lines. It is suggested that other mechanisms are responsible for this resistant activated autophagy through Vacuole Membrane Protein 1 (VMP1), but it is specific to the KRAS mutant cell line [251]. This relationship between RAS and autophagy in pancreatic cancer has been demonstrated in the recent bio-informatic analysis used to develop a prognosis predictor [252].

Much research has focused on targeting autophagy in the context where RAS driven cancers are being targeted by inhibitors of MEK/ERK, which have not been as efficacious as expected, ironically due to autophagic activity[253]. So, therefore, combining an autophagic inhibitor with these treatments has been an area of great interest and has shown promising results clinically. For example, MEK inhibitor trametinib combined with autophagic inhibitor hydroxychloroquine has proven efficacious in pancreatic cancer

[65, 254]. In contrast, a phase II trial with gemcitabine and nab-Paclitaxel with hydroxychloroquine showed no significant difference with or without hydroxychloroquine [255]. A recent preliminary study in breast cancer cell lines showed some efficacy, although the study did not use RAS mutant lines, and the basal line, which had the increased sensitivity (SUM190), had the lowest levels of RAS expression. However, this study was done in combination with Fluorouracil, and these results might also reflect the off-target effects of hydroxychloroquine as it is not a specific autophagic inhibitor[256]. It has since been shown in an MCF-10A model with HRAS mutation that chloroquine had a synergistic effect with HDAC inhibitors and had increased efficacy in the HRAS mutant cell compared to control [257]. It should be noted that a recent study used a combination siRNA platform to examine RAS pathway interactions. To establish an effective treatment strategy for KRAS mutation in colorectal and pancreatic cancers, then inhibiting v-RAF murine sarcoma viral oncogene homolog B1 (BRAF) or C-Raf Proto Oncogene Serine/Threonine Protein Kinase (CRAF) and ATG7 was predicted to be an effective cytotoxic combination with limited adverse effects [242].

The RAS mutation literature highlights the paradox of autophagic activity and the benefits of its inhibition, and the challenges. It has enormous potential in some treatment-refractory cancers such as pancreatic, lung and glioblastoma. However, many questions still need to be answered for autophagy to be targeted effectively in this context; firstly, does upregulation of RAS mimic the behaviour of oncogenic RAS, and if so, would cancers within this context be suited to autophagic inhibition? Secondly, what would be the repercussion if the protective autophagy is lost? Thirdly, wherein the autophagic process would inhibition be consistent and effective? These questions and many more require elucidation before the true potential of autophagic inhibition can be realised. This thesis seeks to address these questions.

1.12 CHAPERONE-MEDIATED AUTOPHAGY - WHAT IS KNOWN

Chaperone-mediated autophagy (CMA) is a specific type of autophagy responsible for the removal and degradation of targeted proteins. Unlike autophagy, which is not specific and is capable of engulfing larger molecules such as organelles, CMA shares

some commonalities with microautophagy, as shown in Figure 1-3 Microautophagy also utilises the HSC70 complex and KFERQ motif to target proteins; however, CMA requires Lamp2A to facilitate targeted proteins delivery directly into the lysosome where microautophagy does not [258, 259]. Lamp2 has three transcript variants: Lamp2A, Lamp2B and Lamp2C, which all vary at their cytosolic tail and transmembrane domain but retain homology at the luminal tail. Lamp2A is the only variant that can bind CMA substrate, so there are no redundancies between the variants [260]. (Figure 1-6)

The identification of CMA is a more recent discovery, and much is still to be learned regarding the molecular mechanisms involved. CMA still utilises the lysosome, but selected proteins are translocated across the lysosomal membrane. Chaperone-mediated autophagy aims not to degrade proteins and organelles indiscriminately as in macroautophagy; instead, it involves the degradation of molecules with a specific targeting motif of, which is speculated to account for approximately 40% of all proteins [258]. From a physiological perspective, CMA provides amino acid pools during exposure to stressors and is responsible for the cellular environment through its discriminative degradation of proteins such as enzymes, transcription factors and substrates. This function of CMA suggests that it maintains proteostasis but can potentially shape the cellular responses and features through protein regulation [261-263]. The KFERQ motif consists of a five invariable amino acid sequence (KFERQ) with the binding capacity resulting from the amino sequences is the most critical component of the motif, which must comprise glutamine (Q) at either the start or the end of the motif. Up to two positively charged amino acids such as arginine (R) and lysine (K), one negatively charged amino acids such as glutamic acid (E), aspartic acid (D) and one or two hydrophobic amino acids such as isoleucine (I), valine (V), leucine (L) or phenylalanine (F). Including numerous amino acids within each group shows the options for which amino acids can be substituted with other amino acids with the same properties, and hence the number of amino acid combinations could constitute a KFERQ motif. For example, lysine is positively charged and could be substituted for arginine, also positively charged [262, 264]. As research has developed in this area, it has become apparent that acetylation and phosphorylation of proteins can also result in the targeting motif, and this has expanded the possible proteins that are potential targets of CMA. Kirchner et al. have developed a KFERQ motif tool that allows researchers to search proteins with this software to identify if the KFERQ- motifs are present and denote if it is canonical or

result of post-translational modifications [264]. In contrast, a protein with a targeting motif is not targeted by CMA as the conformation of the protein may be such that HSC70 and its co-chaperones can not access it for binding. So, it is predicted that research relating to the CMA process will be propelled forward by this advancement, but it will still require experimentation to validate that a particular protein is a 'bona fide' target of CMA.

This motif of the substrate protein is bound by the heat shock-cognate 70 (hsc70) chaperone and its co-chaperones that include hsc70-interacting protein (HIP), hsc70-hsp90 organizing protein (HOP), Bcl2-associated athanogene 1 protein (BAG1), heat shock protein of 40 kDa (HSP40) and heat shock protein of 90 kDa (HSP90) [265, 266] . The role of these chaperones is that they facilitate binding of HSC70 with KFERQ motif, attachment, release and unfolding at the lysosomal membrane where the CMA substrate bound by HSC70 and co-chaperones is delivered. Here HSC70 aids the binding of the CMA substrate to the cytosolic tail of lysosome-associated membrane protein type 2A (Lamp2A) monomer, noting that the HSC70 bound substrate can only bind to Lamp2A as a monomer. However, upon binding to the substrate, Lamp2A forms a multimeric translocation complex as substrates can only be translocated into the lysosome via a multimeric Lamp2A complex. During the formation of this complex, the stability of Lamp2A is maintained by heat shock protein 90 (HSP90) located both at the luminal and cytosolic sides of the lysosome membrane [258, 267]. The role of HSP90 in this context has strengthened recently as the literature has shown CMA processing to be inhibited by HSP90 inhibitor 17AAG and geldanamycin [268, 269]. The targeted protein is unfolded and prepared for translocation during this assembly, and the exact mechanisms are yet to be elucidated [267, 270]. It has been shown that for a protein to be translocated across the lysosomal membrane via the Lamp2A complex, it requires the involvement of a lysosomal form of hsc70 (lys-hsc70)[271] . Hydrolase enzymes degrade the target protein upon entry into the lysosomal lumen.

The multimeric Lamp2A from the cytosol surface of the lysosome membrane is also stabilised by glial fibrillary acidic protein (GFAP), which stabilises HSC70 binding to Lamp2A and prevents disassociation. However, it is also present in its phosphorylated form pGFAP, bound by elongation factor 1α (EF1α). In the presence of Guanosine-5'-triphosphate (GTP), EF1α is released from pGFAP, which recruits non-phosphorylated GFAP from the Lamp2A complex initiating disassembly [272]. The negative regulation of

GFAP through its phosphorylation is AKT Serine/Threonine Kinase 1 (AKT1) dependent which is under the control of MTORC2 and results in the inhibition of Lamp2A multimerisation. Conversely, activation of Lamp2A multimeric formation is through pleckstrin homology domain, and leucine-rich repeat protein phosphatase 1 (PHLPP1), which inhibits AKT1, increasing GFAP (non-phosphorylated), and this increase stimulates Lamp2A multimerisation [258, 271, 273]. Disassembly of the multimeric Lamp2A complex is dependent on HSC70 [274]. After disassembly, there are numerous fates for Lamp2A. It can be retained as a monomer for further complex formation. If it has entered the lysosomal lumen, it can be reinserted back into the membrane and degraded by cathepsin A. Notably, Lamp2A is the rate-limiting factor in the CMA process, so it can regulate Lamp2A availability through renewal by *de novo* synthesis and or changes to Lamp2A half-life which are essential in times of need [275-278]. There is still limited research on the molecular mechanisms that activates CMA, although the retinoic acid receptor α(RARα) and calcineurin–nuclear factor of activated T cells (NFAT) have been identified as playing a role [279, 280]. More recently nuclear factor, erythroid derived 2, like 2 (NRF2) has been shown to regulate Lamp2A and thus CMA activity at basal and during oxidant stress conditions [281, 282].

Chaperone-mediated autophagy is known to be induced by stress, including starvation, ROS, hypoxia and toxicities (protein, genetic, chemical). However, it should be acknowledged that starvation-induced CMA is at a substantially later time-point than autophagy, four and 10 hours, respectively, and lasts longer, for up to three days. Crosstalk and or a co-operation between autophagy and chaperone-mediated autophagy have been postulated in the literature. Massey et al. observed that through the selective knockdown of CMA, there is a concomitant increase in macro autophagy. Even though protein degradation was sufficient to maintain the viability of cells during starvation conditions, these cells were found to be more susceptible to other stressors such as oxidation and ultraviolet light exposure [283]. Conversely, when autophagy was blocked, CMA was observed to be upregulated and rescue its function [284]. These findings suggest that although there are compensatory mechanisms in place, autophagy cannot wholly substitute the CMA role and its selective functions, although the opposite appears to be true in autophagy loss, this may relate to differences in the studies and contexts [283, 285]. Recently it has been identified that CMA degrades ULK1/2 showing a direct link between autophagy regulation by CMA [286].

Since CMA's discovery less than 30 years ago, it has been identified in ageing and disease. There was earlier identification of the Lamp2 gene total rather than transcript variants in Danon's disease. This disease is due to dysfunction of the Lamp2 gene, but it is suggested that the phenotype is reflective of Lamp2A loss, but Lamp2B is the predominant variant associated with this disease [287]. Similar to autophagy, CMA or, more specifically, Lamp2A, is observed to decline in the lysosomal membrane with ageing, resulting in cellular damage reflected by the ageing process and in this context, it is shown to be cytoprotective in function. Intriguingly studies have found that the rescue of Lamp2A rectifies the age-related changes explicitly observed in the retina and liver of animals of these studies [288, 289]. Nephropathies have also been associated with CMA either directly or indirectly. Nephropathies are a consequence of toxicity whereby the CMA process is overcome and accumulates toxic products [290]. For example, in diabetic-induced renal hypertrophy, CMA is downregulated and contributes to the pathology of renal hypertrophy [291].

The area of most interest and research has related to CMA's role in neurodegenerative diseases. Neurodegenerative diseases phenotypically relate to an accumulation of protein aggregates resulting in proteotoxicity. For example, in Alzheimer's disease, CMA is downregulated, and amyloid-beta precursor protein (APP) is a target of CMA. Through CMA loss, amyloid plaques develop, as does the disease pathogenesis [292]. Furthermore, it has been shown in a recent study that the phosphorylation of TAU protein prevents its targeting by CMA, resulting in the propagation of TAU proteins and disease pathology [293].In Parkinson's disease, there is a reduction in CMA activity, leading to increases in α-synuclein and the formation of Lewy bodies [294]. Research is currently seeking to activate CMA activity in many previously mentioned diseases. For example, a study identified humanin protein as activating CMA in neuronal cells and cardiomyocytes [269]. Although, in contrast, it has been shown in Huntington's disease that CMA is upregulated in response to autophagic inhibition, CMA is suggested to be inadequate to compensate for autophagy, and as such, the disease progresses [295]. A more recent area of active research is CMA in cancer, which has been of interest and will be focused on in more detail later in this chapter. The potential for CMA to be a significant regulator of the cellular phenotype has been highlighted in a paper demonstrating that CMA targeted protein regulation controls the pluripotency of embryonic stem cells [296]. However, this area of research into CMA and

its role in ageing and disease is still evolving, and there is still much to discover and understand.

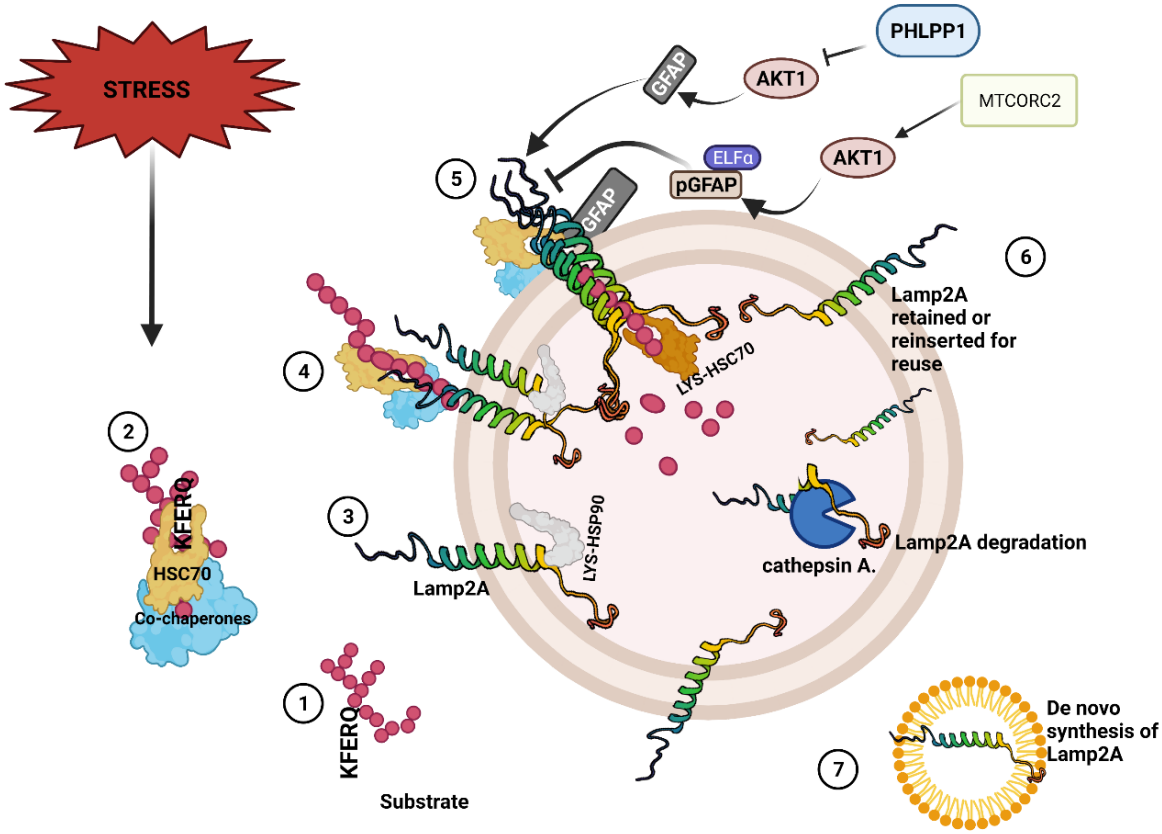


Figure 1-6 Chaperone-Mediated Autophagy

Chaperone-mediated autophagy process: **(1)** Stress results in a protein with the KFERQ motif to be targeted as CMA substrates. **(2)** HSC70 and co-chaperones bind KFERQ motif and deliver it to Lamp2A. **(3)** Lamp2A is located as a transmembrane protein at the lysosome. **(4)** HSC70 and substrate bind Lamp2A cytosolic tail causing the Lamp2A to multimerize with the assistance of lysosome HSP90, and unfolding of protein begins. **(5)**The multimeric Lamp2A complex is formed, allowing the unfolded protein to be translocated with the aid of lysosome HSC70. The Lamp2A complex is supported by not just HSC70 and co-chaperone but also GFAP.GFAP is phosphorylated by AKT1 who is activated by MTORC2 to form pGFAP, causing it to be bound by ELFα, inhibiting the function of GFAP. Alternatively, AKT1 inhibition by PHLPP1 releases GFAP to bind to Lamp2A, encouraging CMA activity.) **(6)** HSC70 and release of GFAP cause multimer disassembly, and Lamp2A monomer can be retained or re-inserted for later use or degraded by cathepsin A. **(7)** Lamp2A monomers are synthesised and enter the lysosomal membrane within lipid microdomains

Created with BioRender.com.

1.13 CHAPERONE-MEDIATED AUTOPHAGY - WHERE DOES IT FIT IN THE CANCER STORY?

Chaperone-mediated autophagy has only recently been examined in the context of cancer, with this area still evolving, as are the techniques to facilitate research growth [297]. Nevertheless, CMA presents itself as a pivotal regulator in cancer and is in line with other types of autophagy to have both cytoprotective and pathologic functions. An example of its cytoprotective role was observed in the targeted degradation of several of the mutant variants of P53, specifically mutations R248Q, R273H and R175H, which are often present in aggressive cancers. However, CMA did not target wild type P53, only the previously mentioned mutant forms. Acting as a cellular mechanism by which gain of function mutations of p53 can be removed from the cell with preferential maintenance of wild-type p53 to ensure cellular integrity [285].

Moreover, CMA was also observed to target oncogenic MYC and stability substate C330027C09Rik/KIAA1524/CIP2A (CIP2A), which, when removed, causes ubiquitination of MYC for degradation in the normal cell, preventing oncogenic transformation both direct and indirectly [298]. Resistance to tamoxifen treatment and the use of fulvestrant in the treatment of estrogen-positive breast cancer was shown to arise due to the prevention of targeted degradation of MORC family CW-type zinc finger 2 (MORC2), a usual CMA target. However, by its phosphorylation, it can no longer be bound by HSC70 and is suggested to be phosphorylated in response to treatment [299]. In addition, CMA has a role in maintaining the genomic stability of the cell through its regulation of cell cycle checkpoint kinase 1 (Chk1), consequently keeping DNA repair mechanisms constrained [300]. It has also recently been identified that CMA is involved in inducing ferroptosis through its removal of GPX4 [30]. The recent examination of ovarian, breast and lung cancer cell lines found various translation factors for proliferation and growth as CMA target substrates, such as eukaryotic translation initiation factor 4H (EIF4H) and more, found to upregulated in all cancers alike. This suggests a significant role in facilitating carcinogenesis and demonstrates a potential focus for treatment in this context, as these models may benefit from CMA activation [301]. Moreover, CMA has been shown to target pro-apoptotic factors such as BCL2 binding component 3 (BBC3) to maintain tumour cell survival [302]. In addition, recent data shows that translationally

controlled tumour protein (Tpt1/TCTP) is targeted by CMA when acetylated. Intriguingly, it is found to be upregulated in many cancers and increased CMA, suggesting deacetylation mechanisms in play that may be reducing CMA targeting of Tpt1/TCTP[303]. Furthermore, a study by Li et al. has shown that deacetylation of the tumour suppressor mammalian STE20-like kinase 1 (MST1) causes it to be targeted by CMA and suggested to be the reason why MST1 levels are reduced in breast cancer [304].

When CMA is commonly observed to be pathologic in its role, it is observed as upregulated, or at least its markers are. This upregulation was observed in colorectal cancer, where Lamp2A was increased in patient samples and replicated *in vitro* and *in vivo*. The removal of Lamp2A significantly reduced cell survival by inducing apoptosis and inhibiting cell proliferation, although exact mechanisms are yet to be elucidated [305]. In a study of non-small cell lung cancer, upregulation of Lamp2A was preferential in the aggressive phenotypes with invasive and survival capacity lost with knockdown of Lamp2A. It was also found to increase sensitivity to cisplatin treatment [306], where similar findings in human lung cancer xenografts were observed in an earlier study [307]. Moreover, oesophageal cancer showed decreased proliferation and cisplatin sensitivity with Lamp2A loss [308]. In gastric cancer, Lamp2A presented itself as a prognostic marker and facilitated cancer cell proliferation through the target substrate Rho Family GTPase 3 (RND3) [309] . Breast cancer patient samples were shown to have high expression of Lamp2A and *in vitro* studies found CMA activity to correlate with increased cell survival and its inhibition sensitised cells to doxorubicin treatment [310].

Furthermore, it was shown that Lamp2A levels correlated with breast cancer grade in patient samples. The cause of this correlation was described as a consequence of autophagy inhibition with the targeted degradation of ATG5 by CMA. The results indicate that there is still autophagic flux with or without Lamp2A. Therefore, it is suggested that lysosomal identification of ATG5 needs to be ascertained to confirm it as a bona fide target. Also, levels of the other ATG's associated with ATG5, such as ATG12, would be of interest to ascertain if this targeting occurs while bound in the ATG5-ATG12 complex or whilst it is on its own, which warrants further investigation [311]. In addition, research has shown that glioblastoma cells can signal to the surrounding pericytes to activate CMA to regulate immune suppression and protect the glioblastoma cells from immune destruction [312].

There has been direct evidence in a study by Lv et al. that CMA substrates regulation can support tumour growth. This study indicates that CMA targets the pyruvate kinase M2 isoform when it has been acetylated at lysine 305. This acetylation caused an accumulation of glycolytic substrates and NADH, which was shown to promote tumour growth, while CMA controlled this activity [313]. A study by Xia et al. demonstrates that the CMA target Hexokinase II (HKII) could be manipulated through the chemical activation of CMA, leading to its increased degradation by the inhibition of stress-induced autophagy resulting in CMA causing a metabolic crisis in leukemic cell and subsequent cell death [314, 315].

The literature to date, although not expansive, indicates that CMA has a significant role in cancer. It is shown to be anti-tumourigenic and pro-tumourigenic dependent on the cellular contexts, with the latter being the most important. Curiously, in respect to cancer, it is upregulated rather than downregulated, as observed in ageing and the many diseases mentioned earlier. However, there is still much to be learned and understood about why CMA is upregulated in the context of cancer, the essential proteins it regulates to support survival and metastatic potential, which are common attributes lost in the context of cancer. By answering these questions and the mechanism that controls CMA activity, this process would have greater potential as a therapeutic target.

1.14 AUTOPHAGIC REGULATION - THE CURRENT STATE

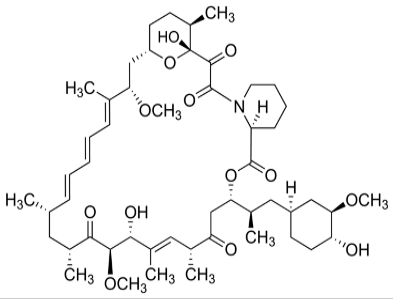
The current research has led to the discovery of some of the pathways that regulate autophagy and CMA, and as such, the substrates that induce and inhibit its activity have been identified. This understanding has allowed research to continue and result in the development of new targeted therapeutics or the repurposing of existing agents. There is some cross over in the activator and inhibitors between autophagy and CMA. Those that will be addressed are relevant to this study, and it should be noted that others have not been included in this review. Notably, autophagy and CMA can be activated indirectly by specific chemotherapeutic agents to facilitate resistance.

1.15 AUTOPHAGIC ACTIVATORS

Collectively autophagy and CMA are stress responses, and their role is to provide recyclable macromolecule and amino acids for use in metabolism and protein synthesis during times of deprivation. Therefore, the most well-described treatment to activate autophagy is nutritional deprivation, mainly starvation. Experimentally, this can include glucose withdrawal, amino acid deprivation, or non-supplemented growth media. Autophagic activity is observed in vitro to be induced by nutritional and amino acid deprivation within 3-4 hours and 10-12 hours for macroautophagy and CMA, respectively [316]. Hypoxia (0.5-1% Oxygen) is also observed to induce macroautophagy and CMA at 8hr and up to 24 hours [317, 318]. In addition, genotoxic damage, protein aggregates and oxidative stress will induce autophagy and CMA. There is currently little evidence regarding the chemical induction of CMA, although there is some evidence that HSP-90 inhibitor (geldanamycin) and antimetabolite (6-aminonicotinamide) can indirectly activate this pathway; however, results have not been consistent between cell types [268, 316]. A recent study suggests that PI3K class I inhibitors but not class III can also activate CMA [319].

In contrast, several pharmacological agents can induce autophagy by inhibiting negative or activating positive regulators within the canonical pathways. These have included AMPK activation through agents such as metformin, quercetin, and resveratrol. Alternatively, MTOR inhibition is the most commonly used experimentally rather than nutritional deprivation. Regarding this research, nutritional deprivation for CMA and autophagy and Rapamycin was included as another means to induce autophagy.

1.15.1 Rapamycin



Rapamycin

Rapamycin is an antifungal metabolite produced by Streptomyces Hygroscopicus which is a bacterium that resides in soil. It was observed that rapamycin binds to12-kDa FK506-binding protein (FKBP12) to form a complex that binds to MTORC1 and inhibits its activity. It has been shown to have activity against MTORC2 with

prolonged use but does have greater specificity for MTORC1 [320]. MTORC1 directly controls protein synthesis and regulates metabolic pathways, particularly glycolysis. Since identifying MTORC1, it has been demonstrated to play a significant role in numerous diseases such as neurodegenerative metabolic disease and cancer. In many cancers, MTORC1 is observed to be upregulated, and this is often a consequence of mutations or hyperactivation of upstream regulators AKT, PI3K and RAS or suppression of inhibitory regulators such as liver kinase B1 (LKB1), phosphatase and tensin homolog deleted on chromosome 10 (PTEN) and tuberous sclerosis proteins 1 and 2 (TSC1/2). Therefore, the potential for inhibiting MTORC1 with rapamycin was a promising cancer therapeutic; however, it was found not a feasible option due to solubility issues and kinetics. Since then, there has been the development of analogues with improved solubility and kinetics, which have included temsirolimus and everolimus; these analogues are approved by the Food and Drug Administration (FDA) in USA for treatment in angiomyolipomas, HER2-negative breast cancers, pancreatic neuroendocrine tumours, renal cell carcinomas and subependymal giant cell astrocytomas and are currently being, or have been tested, in numerous cancers in various clinical trials [321]. However, despite the promising improvement in the analogues for treatment use, their efficacy has been disappointing due to resistance, and off-target effects of MTORC1 inhibition has been problematic [322].Rapamycin inhibition of MTORC1 to induce autophagy in yeast and most mammalian cells has resulted in it being a staple in the laboratory as it is used extensively within the experimentation of autophagy. It is expected that researchers should use different methods to validate the presence of autophagy [316, 323].

1.16 AUTOPHAGIC INHIBITORS

The inhibition of autophagy and CMA has been a greater area of growth than activation as it is not as easy to control with simple environmental changes such as nutrition. It has become apparent that autophagy and CMA do upregulate in response to stressors, but they are still active at basal levels. As previously mentioned, only the drugs used in this thesis will be detailed, but it is worth noting that many inhibitors have been developed, and many more are being developed as both autophagy and CMA play a role in disease and present themselves as significantly targetable. Autophagic inhibitors have

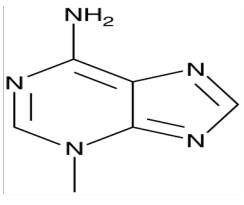
gained much attention, so several available inhibitors focus on developing molecules towards PI3KC3/VPS34, ULK1/2 and Bcl-2. Within these groups, there are many compounds that are being trialled in the adjuvant setting in various cancer types [324].

Currently, CMA does not have any specific inhibitors, but its activity can be halted by the genetic knockdown of Lamp2A or inhibiting lysosomal function. Similarly, autophagy can be halted with the VTPase inhibitor Bafilomycin A1, the weak bases Ammonium Chloride, Chloroquine and hydroxychloroquine.

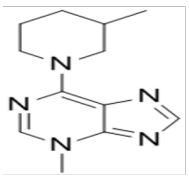
1.16.1 PI3KC3 Inhibitors

The PI3KC3 complex is an integral modulator of the canonical pathway in autophagy. There have been specific inhibitors developed to many of the molecules within the complex, but predominantly they have focused on PI3KC3, hereafter referred to as VPS34. There has been continual development of VPS34 inhibitors as they have been shown to have limited specificity for VPS34, and most have displayed activity against other PI3K family members. The PI3K family is divided into classes I, II and III, with numerous isoforms within classes I and II. PI3K class I isoforms form part of the AKT MTOR axis and regulate growth, metabolism, cellular movement and protein synthesis. PI3K class II isoforms are involved in endocytosis, mitosis and cell migration. The class III enzyme is involved in autophagy and extra vesicle trafficking and is the only nutrient sensor and PI3K that is conserved from yeast to mammals [325-327].

1.16.2 3-Methyladenine (3Ma)



3-Methyladenine (3Ma)



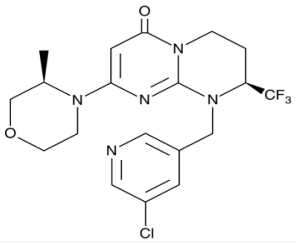
3Ma-IV

The most commonly used autophagic inhibitor over the last decade has been 3Ma. 3Ma inhibits VPS34 by binding to its ATP binding site, but this binding is conserved amongst some of the isoforms. Consequently, this particular agent is observed to have a binding affinity with P110γ, an isoform of the PI3K class I group, so its use will inhibit autophagy and block growth, survival and motility signalling. A study by Wu et al. showed that the autophagic activity of 3Ma was observed to have transient binding

to VPS34 whilst it binds constant with p110γ. Although the inhibitory concentration showed disparities between them with IC_{50} of 25μM for VPS34 and 60μM for p110γ. There are also temporal differences with VPS34 inhibition observed at forty-eight hours, whereas activity towards p110γ was from eight hours [328, 329]. Although later studies have shown autophagic inhibition beyond 24 hours, particularly in the context of cancer cells [330]. The dual activity has not been limited regarding potential clinical use as p110γ is often aberrantly expressed in most cancers, which may add to its efficacy. However, the problem has been its poor solubility, which has limited its use in many settings. As a result, Wu et al. has developed several 3Ma derivatives, of which compound 18 (3Ma-IV) is commercially available and used in this thesis. It was shown that there was improved solubility of 12.06 mg/ml to 62.58mg/ml in water for 3Ma compared to 3Ma-IV, respectively. Furthermore, the specificity has been improved with 3Ma-IV shown to have no inhibitory effects on PI3K class I or p110γ [331].

A few recent studies have proven to be efficacious in treating colorectal cancer cells in hypoxic conditions with 3Ma causing apoptosis [332]. Another has shown that treatment in head and neck cancers with reactivation of p53 and induction of tumour cell apoptosis (RITA). The treatment potential of RITA has been limited to date due to resistance which was overcome with the addition of 3Ma [333]. Curiously, both studies presented LC3 levels to represent autophagy but did not show any PI3K class I activity to ascertain if this pathway had a role. Concerning the newer derivative 3Ma-IV, it focused on 3Ma as the most effective at reducing cell viability across cell lines compared to 3Ma-IV, SAR-405 and lysosomal inhibitors. However, it was shown that 3Ma induced DNA damage resulting in subsequent cell death. It was also shown that 3Ma had a minimal inhibitory effect on PI3K class I downstream targets. In contrast, both 3Ma-IV and SAR405 had no effect on the PI3K class I targets [334].

1.16.3 SAR-405

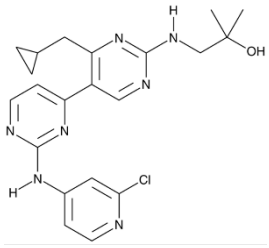


SAR-405

SAR-405 is a first in class ATP-competitive inhibitor of VPS34 and was identified through high throughput small molecule screening. Its activity is specific to VPS34 inhibiting autophagy and late endosome to lysosome trafficking [335, 336]. Curiously, it has been shown that SAR-405 IC_{50} significantly

decreases when an MTOR inhibitor induces autophagy. Therefore, a study into the combination of SAR-405 and MTOR inhibitor everolimus showed increased cytotoxicity in renal cancer cell lines [336, 337]. More recently, it has been shown to induce inflammation within the tumour and provide an environment for the successful use of immunotherapeutic agents in vivo in melanoma and colorectal cancer models [338]. There is evidence to show that SAR405 ameliorates radiotherapy-induced mitophagy and results in improved tumour refraction when radiotherapy is combined with SAR405 in head and neck cancer in vivo [339].

1.16.4 VPS34-INI



VPS34-INI

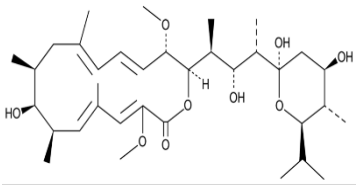
VPS34-INI is a specific and potent VPS34 inhibitor, and its mechanisms of action are suggested to be through its PtdIns(3)P-binding PX domain but are yet to be fully elucidated [340]. A recent study showed improved efficacy of Ceritinib with VPS34-INI in treating non-small cell lung cancer cells reduced cell survival. It was also suggested that VPS34-INI and SAR-405 offered more significant treatment potential due to their specificity [341]. Recently, VPS34-INI has been shown to have promising effects in Acute myeloid leukaemia (AML) cells, with increased cell death observed in response to treatment [342].

1.16.5 Lysosomal Inhibitors

The lysosome offers a broad spectrum effect compared to the PI3KC3 inhibitor as the lysosome does not just facilitate a degradation vessel for autophagy but includes CMA, microautophagy, immune signalling and endocytic pathways [343]. It is a critical centre for removing and supplying cellular contents to recyclable constituents. This process indirectly regulates all cellular processes within the cell. In the context of cancer, lysosomal biogenesis generally increases, so it offers an effective treatment option. However, the conundrum is how to target such a pivotal organelle as research advances? It is becoming apparent that not all lysosomes are alike, and that may present an opportunity to generate a more specific targeting option. The research into several lysosomal disorders has given greater insight into lysosomal functions and demonstrated

options to circumvent its loss, such as administering enzymes that can correct some loss of lysosomal function. The lysosomal inhibitors currently act to reduce the internal lysosomal acidity rendering them inactive. However, these agents work by either acting as weak bases or interfering with proton pumps, and as it suggests, these mechanisms of action are not very specific and often yield undesirable off-target effects [344-350].

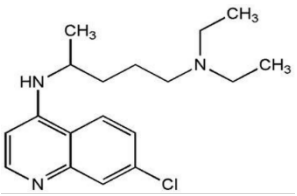
1.16.6 Bafilomycin A1



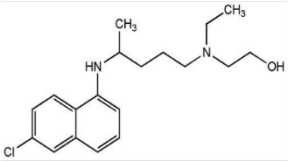
Bafilomycin A1

Bafilomycin A1, produced by Streptomyces griseus, is a macrolide antibiotic that inhibits the vacuolar H+ ATPase (V-ATPase). Bafilomycin A1 binds the V0 component of the VTPase pump, preventing its activity and inhibiting proton exchange. The loss of the proton pump prevents the maintenance of lysosomal luminal acidity and thus the activation of lysosomal enzymes and degradative functions [351]. Through this inhibition, autophagic processing is halted, and there has been evidence to suggest autophagosome and lysosome fusion is prevented and was proposed to be due to the lysosomal VTPase pumps. However, it has since been demonstrated that the changes in intracellular calcium concentrations prevent the lysosome autophagosome fusion, and the calcium dysregulation is due to off-target binding of other VTPase's [352]. It has also been shown to be a potassium carrier to mitochondria, resulting in mitochondrial swelling and dysfunction; this activity was observed at nanomolar concentrations [353]. It has been suggested that Bafilomycin A1 is not feasible due to toxicity, although interestingly, claims of toxicities have not been supported by data, and on the contrary, there are studies, at least in leukaemia, that have shown no toxicity in vivo [354, 355]. The toxicity is potentially related to the off-target effect mentioned previously, and there is evidence to suggest these would be reduced in a dose-dependent manner, and the efficacy has been proven at the lower doses in vivo for some cancer types [354, 356, 357].

1.16.7 Chloroquine



Chloroquine



Hydroxychloroquine

The most well recognised and clinically relevant autophagic inhibitor is chloroquine, or its less toxic derivative hydroxychloroquine. First discovered as an anti-malarial, it prevents the conversion of heme to haemozoin in protozoan infections [358]. They have a potent immunomodulatory effect resulting in a reduction of cytokine and inflammatory mediators, and it is commonly used to treat rheumatoid arthritis, systemic lupus erythematosus and several clotting disorders. In addition, they are lysosomotropic and accumulate with acidic vessels, particularly the lysosome, where their weak base formula reduces lysosome acidity and function, although the exact mechanism is yet to be elucidated. However, at high concentrations, they will cause the membrane of the lysosome to permeabilise and rupture, with the lysosomal contents being released into the cell, causing cell damage or death, which has been attributed to the retinopathy observed in patients. Other adverse effects reported are myopathy and cardiovascular cytotoxicity and arrhythmias, though retinopathy is the most predominant, with medical guidelines of the prescribed dose to limit this [359-361]. The exact mechanism on how these agents block autophagy was recently highlighted by Mauthe et al., who observed that autophagosome-lysosome fusion was inhibited by treatment with chloroquine and hydroxychloroquine. This blocked fusion was attributed to the observed autophagic failure rather than direct changes in the lysosomal. It was further suggested to be caused by Golgi and endoplasmic reticulum (ER) stress. So it is worth noting that the stress observed with the ER and Golgi may be attributed to some of the clinical results rather than just autophagic inhibition [362]. Most of the current clinically relevant trials and use of an inhibitor to block autophagy for cancer treatment involve using hydroxychloroquine. A systematic review and meta-analysis of all cancer trials that have been undertaken using chloroquine or hydroxychloroquine for cancer treatment were then analysed to determine efficacy. The review assessed the use combined with gemcitabine, doxorubicin, radiation, temozolomide and single therapy with hydroxychloroquine. Cancers included were glioblastoma, non-Hodgkin's lymphoma, pancreatic, metastatic non-small cell lung cancer and metastatic breast cancer. The meta-analysis demonstrated that the overall response rate was significantly higher with the inclusion of hydroxychloroquine or chloroquine than without [363].

1.17 CONCLUSION

The literature highlights autophagy and CMA as areas of importance in the context of cancer. However, this has been complicated by the paradoxical role of autophagy in that it can be both anti-tumorigenic and pro-tumourigenic, and while autophagy research has advanced significantly, many questions are still to be answered. Until there is an insight into the regulatory mechanisms, particularly in cancer, to explain why autophagy becomes pathologic, the development of effective treatments which target its activity will be limited. The initial treatment options have shown promise but have been limited by off-target effects and a lack of specificity. This thesis aims to contribute to the body of knowledge of autophagy and CMA in breast cancer and breast cancer progression to eventually aid the development of better-targeted treatments towards autophagy and CMA.

1.18 PROJECT RATIONALE & OBJECTIVES

1.18.1 Rationale

The literature, as discussed previously, has shown autophagy to provide a supportive role to oncogenic RAS. The observations to date have led researchers to focus on this as a targetable weakness. However, the research has primarily focused on RAS-driven cancers such as pancreatic and non-small cell lung cancer. In addition, the research has shown the inhibition of autophagy to increase first-line treatment efficacy and attenuate chemoresistance, which has been demonstrated in vitro, in vivo and clinically. However, this has not been investigated in breast cancer as it is not recognised as a predominantly RAS-driven cancer. Nevertheless, it can present with RAS mutations, although it is more common to have an upregulation of RAS activity in the absence of oncogenic mutations, particularly in the metastatic phenotype. This gap in the literature led to the investigation of autophagic activity in the presence of oncogenic RAS and or RAS activity to delineate if breast cancer is dependent on autophagy in the context of RAS (Chapter 3).

As highlighted in the literature review, there have been great expectations of using an autophagic inhibitor to treat cancer, but these have been fraught with inconsistencies and disappointments. This quandary has led to an influx of autophagic inhibitors, but there is evidence lacking for their feasibility. To determine if breast cancer would be responsive to targeted treatment with an autophagic inhibitor was undertaken, and drugs for the same target were compared and contrasted to determine feasibility within varying breast cancer cell contexts. (Chapter 4)

Autophagy is not alone in the degradation pathway to the lysosome. It is a hub for microautophagy and CMA. Furthermore, evidence suggests there is crosstalk between at least autophagy and CMA, which is suggested to help overcome any losses of either pathway. Therefore, to effectively target autophagy, the role of CMA needs to be understood and vice versa. This study set out to define the role of CMA in breast cells and breast cancer cell lines and identify a potential role in breast cancer progression. (Chapter 5)

1.18.2 Objectives

The underlying hypothesis of this research is:

"Autophagy has an integral role in breast cancer cell biology concerning its survival, proliferation, metastatic potential and is sensitive to its inhibition".

The specific aims of this study are:

-To examine the presence of autophagy in breast cancer subtypes and progression (Chapter 3)

-To explore the relationship between autophagy and RAS in breast cancer cells (Chapter 3)

-To investigate the sensitivity of breast cancer cell lines to the chemical inhibition of autophagy (Chapter 4)

-To compare the efficacy of PI3K inhibitors in breast cancer cells (Chapter 4)

-Examine CMA in breast cancer progression (Chapter 5)

-To determine the functional importance of CMA in breast cancer cells (Chapter 5)

Chapter 2: Material and Methods

2.1 MOLECULAR CLONING

2.1.1 Bacterial cell cultures

Bacterial cells were cultured for cloning or plasmid DNA generation in Terrific Broth (T.B.) (1.2% tryptone, 2.4% yeast extract, 0.5% glycerol and 10% TB-B) or Luria Broth (L.B.) (1% tryptone, 0.5% yeast extract and 1% NaCl). The suspended bacterial cells were grown in appropriate broth at 37°C on an orbital shaker at 225 revolutions per minute (rpm). Colony selection was undertaken by culturing bacterial colonies on L.B. agar plates (1% tryptone, 0.5% yeast extract, 1% NaCl and 2% agar) in an incubator at 37°C. As prescribed, antibiotics were included in growth media, most commonly ampicillin (100µg/mL) and zeocin (25µg/mL). All broths and agar were sterilised in the autoclave for 20 minutes at 121°C before use.

2.1.2 Bacteria transformation

2.1.2.1 Preparation of competent E.Coli

Preparing chemically competent *Escherichia coli (E.Coli)* cells was performed as described in detail by Nakata *et al.* and Liu *et al.* (1997 and 2018) [364, 365]. *E. coli* cells DH5α were made competent by chemical methods as briefly described below. Firstly, the DH5α were thawed, streaked onto L.B. agar plates and grown with plates inverted in an incubator at 37°C until colonies formed. Next, colonies were used to inoculate 5ml of L.B. and incubated overnight at 225rpm. Then 1mL of this was added to 99mL of fresh L.B. and grown at 37°C for approximately 2-3 hours or until OD 0.4-0.6 was reached. Cells were then incubated on ice for 20 minutes and centrifuged (4°C) at 4000 rpm for 10 minutes to pellet cells. Cells were then resuspended in 20mL of ice-cold 100mM $CaCl_2$ and incubated on ice for 30 minutes, after which they were centrifuged (4°C) at 4000rpm for 10 minutes, and the pellet resuspended in 5mL of an ice-cold storage solution

(100mM $CaCl_2$ and 15% glycerol). Finally, the competent bacterial stock was aliquoted into cryotubes at 100µL volumes for later use and stored at -80°C for three months.

2.1.2.2 Plasmid transformation

Competent DH5α *E.Coli* cells (as described above) were thawed on ice, and up to 100ng of plasmid was added to 100µL of cells. This was incubated on ice for 30 minutes and then heat shocked by placing into a water bath at 42°C for precisely 45 seconds and immediately cooled on ice for 2 minutes. An addition of 200µL of L.B. or T.B. was added to cells to dilute, and the resulting dilution was shaken at 225rpm on an orbital shaker for 1 hour at 37°C. Then 100µL of the transformed cell dilution was added to L.B. agar plates with the prescribed selection antibiotic (ampicillin at100µg/mL and zeocin at 25µg/mL). The bacterial culture plates were inverted and incubated overnight. Control plates were included with all experiments, which contained L.B. agar plates with no antibiotic.

2.1.2.3 Bacterial glycerol stock

Bacterial colonies were selected and inoculated into a 5mL tube with L.B. and incubated at 37°C in an orbital shaker at 225 rpm overnight. Glycerol stock was made with 800µL of bacterial culture grown in L.B. overnight and 200µL of glycerol (sterile). The glycerol and bacterial culture were gently mixed with vortex or pipette (1000mL) and placed into cryotubes and stored at -80°C as per IBC guidelines in a secure box within the freezer.

2.1.2.4 Plasmid Extraction

Crude extraction was performed to confirm the presence of the plasmid of interest in transformed colonies. Ten colonies were collected and cultured overnight (as described in 2.3.1.) in 5mL of L.B. on an orbital shaker at 225 rpm. Cells were pelleted by centrifugation (4°C) at 4000 rpm for 7 minutes. The pellet was then resuspended in the P1 buffer (50mM Tris HCl pH 8.0, 10mM EDTA, and100µg/ml RNase A). Then, cells were lysed with 250µL of P2 buffer (200nM NaOH, 1% SDS), and the tube was inverted five times before a 5 minute incubation at room temperature (R.T.). To stop lysis, P3 buffer (3M KOAc, pH 5.5) was added and gently mixed with the pipette. Next, the sample was centrifuged at 14000 rpm for 10 minutes to remove cell membrane and debris, following this, approximately 700µL of supernatant was extracted and transferred to a new microcentrifuge tube. After adding 490µL of isopropanol, the tube was inverted several times before centrifugation (4°C) at 14000 rpm for 30 minutes. The supernatant was removed, leaving the plasmid DNA pellet, which was washed with 70% ethanol and

centrifuged at 13000 rpm for 10 minutes. Ethanol was removed, and the pellet was left to dry at R.T. before being resuspended in T.E. buffer (10mM Tris-Cl, pH 8.0).

For large-scale extraction of Plasmid DNA for mammalian cell transfection or DNA sequencing and plasmid validation, the commercially available Plasmid Midiprep kit (Invitrogen, California, USA) (cat. K210004) and Plasmid Miniprep kit (Qiagen, California, USA) (cat.27104) were used as per manufacturer's instructions.

2.1.2.5 Restriction enzyme digestion

When restriction digestion was performed for diagnostic purposes, 1µg of DNA was used in a 10µL reaction. For molecular cloning protocols, 10-15µg of DNA was digested in a 50µL reaction. All enzyme restriction digestion reactions included enzymes buffers from NEB (New England Biolabs, Massachusetts, USA), bovine serum albumin (BSA), and DNA. Double digestion was performed with buffers of 100% efficiency and was determined using the NEB online tool platform. All restriction enzyme digestion protocols were determined online and followed as per the manufacturer's instructions. The resultant DNA samples underwent agarose electrophoresis as described in 2.3.7.

2.1.2.6 Ligation reaction

The ligation reactions were performed as prescribed by NEB protocols. In brief, a 10µL reaction with T4 DNA ligase, buffer, plasmid backbone and DNA of interest was inserted at a 1:3 molar ratio respectively and incubated at R.T. for 30 minutes. Following that, 4-5µL was used to transform competent *E.Coli*. for amplification for plasmid selection.

2.1.2.7 Agarose gel electrophoresis

The agarose gel was made at 1% for DNA larger than 500 base pairs and up to 2% for anything less than 500 base pairs. The agarose was combined with TAE buffer (40 mM tris-acetate, 1 mM EDTA, pH 8.3) and heated until dissolved with the addition of Syrbr Safe (1µL/mL) for DNA visualisation. Gels were then poured and left to set at room temperature. Agarose gels were loaded with DNA samples, which were mixed with 6X loading dye, and an appropriate DNA ladder was included for size estimation. The gel was electrophoresed at110V for 50 minutes and covered to protect from light. The DNA bands were observed and captured using the U.V. illuminator in the Fusion F.X. (Vilber Lourmat, SAS, France). When DNA was required for further cloning, fragments were cut out using a U.V. transmitter and cutting pipette. This gel section could also allow further

DNA purification when processed using a DNA gel extraction kit (Qiagen, California, USA) (cat.28704) as the manufacturer's protocol prescribes.

2.1.2.8 DNA sequencing

To confirm the identity of shRNAmir within the Tripz Plasmid DNA, the Plasmid DNA from two clones resulting in a total of 10 samples was collected. DNA was extracted as described in 2.3.2.5 using a Qiagen miniprep kit (cat.27104), and DNA purity and weight were validated by agarose gel electrophoresis[366]. Samples were aliquoted in 20µL volumes at a concentration of 300-450ng along with 50µL of Tripz primers at 5µM as required by Micromon (Monash University, Clayton, Australia) sanger sequencing.

2.1.2.9 Generation of retroviral vectors targeting Lamp2A

The Lamp2A knockdown model developed constructs with shRNAmir directed towards Lamp2A. The protocol was similar to that outlined by Paddison *et al*. and others [367-370]. In brief, the DSIR platform was used (http://biodev.extra.cea.fr/DSIR/DSIR.html) to design a 21-mer siRNA sequence to Lamp2A with an algorithm described in detail by Vert *et al*. [371]. The top five rated Lamp2A siRNA sequences determined by the DSIR program were chosen for further development. The siRNA sequences were entered into the Cold Springs Harbour online platform (http://katahdin.cshl.org//siRNA/RNAi.cgi?type=shRNA) to design a 97-mer shRNA oligonucleotide as detailed in table 2.1. These oligo sequences were sent to Sigma Aldrich (Sigma Aldrich, Missouri, USA). to synthesise the required sequences. On arrival, they were amplified with mir30 primers, as detailed in Table 2.2. The mir30 forward and reverse primers contained restriction sites for XHOI and MLUI, respectively. The restriction sites were then used to ligate the Lamp2A shRNA into the Tripz vector backbone (open biosystems, Heidelberg, Germany) (Fig.2.1). All five constructs were transformed into competent *E.Coli* as described in 2.3.2.2 and cultured. Finally, the plasmid DNA was extracted and sent for DNA sequencing as described in 2.1.2.8. Two of the shRNAmirs chosen to be used were shRNAmir2 with the highest knockdown efficiency and shRNAmir5 as a non-targeting control. As an additional negative control, the study used a Tripz-shRNA-Renilla, previously developed by the lab, which targeted renilla lucifeRASe.

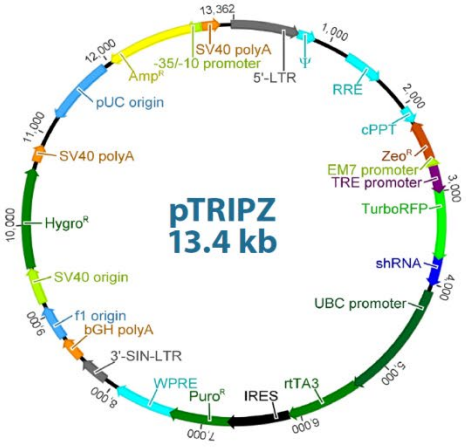
Table 2-1 LAMP 2A shRNAmir sequences

Construct	Hairpin shRNAmir Sequence (sense, mir loop, antisense)	Target site on Lamp2A mRNA Accession. no. NM_002294.3
TRIPZ-LAMP2A-shRNAmir (1)	TGCTGTTGACAGTGAGCGCGGTGTTCTGTTTCAATGTATATAGTGAAGCCACAGATGTATATACATTGAAACAGAACACCATGCCTACTGCCTCGGA	992-1120
TRIPZ-LAMP2A-shRNAmir (2)	TGCTGTTGACAGTGAGCGCGCAGTGCAGATGACGACAACTTAGTGAAGCCACAGATGTAAGTTGTCGTCATCTGCACTGCATGCCTACTGCCTCGGA	1088-1207
TRIPZ-LAMP2A-shRNAmir (3)	TGCTGTTGACAGTGAGCGCGCATGAAGTTAGTACCTCAAGTAGTGAAGCCACAGATGTACTTGAGGTACTAACTTCATGCTTGCCTACTGCCTCGGA	859-966
TRIPZ-LAMP2A-shRNAmir (4)	TGCTGTTGACAGTGAGCGCGCATAAAGTTCATTAAATAAATAGTGAAGCCACAGATGTATTTATTTAATGAACTTTATGCATGCCTACTGCCTCGGA	137-278
TRIPZ-LAMP2A-shRNAmir (5)	TGCTGTTGACAGTGAGCGAAGTTGAATGAAGTAGAGAATGTAGTGAAGCCACAGATGTACATTCTCTACTTCATTCAACTGTGCCTACTGCCTCGGA	638-793

Table 2-2 Table of mir30 primers

HUMAN 5'-miR30-XHOI-F	FORWARD	5'-CAGAAGGCTCGAGAAGGTATATGCTGTTGACAGTGAGCG-3'
HUMAN 3'-miR30-MLUI-F	REVERSE	5'-CTAAAGTAGCCCCTTACGCGTTCGAGGCAGTAGGCA-3'

A



B

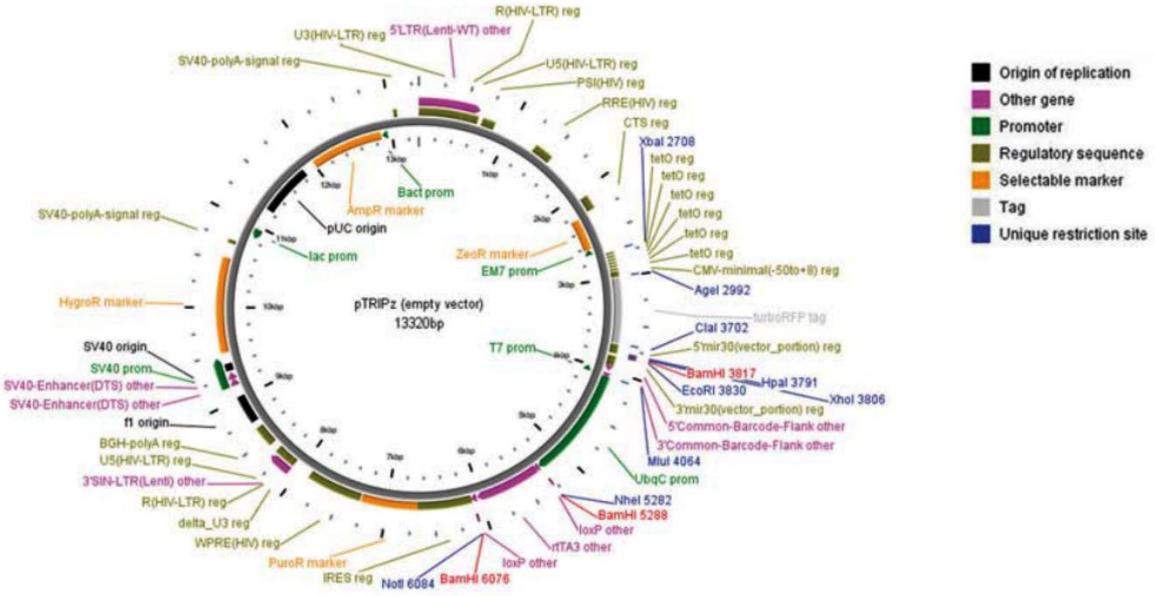


Figure 2-1 Schematic of the Tripz vector map (A) and Tripz restriction sites(B)

2.1.2.1 Generation of stable cell lines expressing inducible Lamp 2A knockdown

Generation of the stably transfected lentivirus cell lines was carried out using the Tripz vector with Lamp2A shRNAmirs cloned in this study (as described in 2.3.2.10), although the Tripz vector itself was developed by Prof. Hannon whilst at Cold Spring Harbour Laboratory (CSHL) in conjunction with Prof. Elledge from Harvard [372, 373]. The protocol was similar to that detailed in the technical manual for Inducible Dharmacon™ TRIPZ™ Lentiviral shRNA (note that Dharmacon now owns the previously detailed open biosystems).In brief, the virus production was carried out using the HEK293T cell line. First, cells were plated at 5.5×10^6 cells in growth media as described in 2.3.2 in a 100mm culture plate. Cells were then incubated at 37 °C with 5% CO_2 overnight, and 2 hours before transfection, media was changed with growth media minus antibiotic/antimycotic. Finally, the lentivirus particle was produced with the addition of Plasmid DNA (Lamp2A) with 3rd generation packaging system pMDLg/pRRE, pMD2.g and pRSV-REV at a ratio of 4 (plasmid DNA); 2 (packaging pMDLg/pRRE); 1(envelope pMD2.g); 1 (pRSV-REV).

Lipofectamine LTX with PLUS transfection reagents (Invitrogen, California, USA) were used to facilitate plasmid transfection of the HEK293T according to the manufacturer's protocol using the above-described ratios. The transfection mixture was added dropwise with the plate gently rocked to evenly disperse the complexes. After 16 hours, transfection media was removed and replaced with harvesting media. Harvesting media (culture media with reduced [2%] or serum-free and no antibiotic/antimycotic) was left for 48 hours and then removed. The virus media was filtered with a 0.45um filter before being used for transduction or stored at -80°C for later use.

A serial titration of virus particles was undertaken with a fivefold dilution of the stock virus. First, it was added to HEK293T in a 24-well plate for 4 hours, and then the virus titration mix was removed and replaced with growth media with 1µg/ml of doxycycline and the cells were returned to the incubator for 72 hours; after which the well was examined under the fluorescent microscope for positive RFP cells which were counted and used to determine the Transducing units per millilitre (T.U./mL). These numbers were used in the following formula to determine TurboRFP positive colonies counted × dilution factor × 40 = T.U./mL.

Transduction of human cells and human breast cancer cell lines required them to be seeded at 1.5 – 2 $x10^6$ cells in a 25cm flask one day before infection. The following day,

media was replaced with fresh media, including the correct volume of virus particles to obtain an MOI = 0.3. Polybrene (hexadimethrine bromide) was also included in the media at a concentration of 5-10 µg/ml depending on the cell line to increase transduction efficiency. The cells were incubated in transduction media for 24 hours before adding new media for a 24-hour recovery period before puromycin selection. Puromycin was added at a concentration between 2-4 µg/ml as predetermined by a puromycin kill curve determined for each cell line. The puromycin media was refreshed and maintained on the cells for 10-15 days. After selection, cells were grown and underwent cryopreservation. In conjunction to this, 1 X 10^5 cells were plated in six-well plates and treated with a doxycycline titration for 72 hours to capture images of positive RFP cells before cell lysate collection and western blot analysis to confirm knockdown of the protein of interest (Lamp2A) and the optimal doxycycline concentration to be used.

2.1.2.1 Generation of cells stably expressing HRAS^{V12}

MCF10A cells expressing mCherry (control) or HRAS^{V12} retroviruses produced from MSCV-mCherry and MSCV HRAS^{V12} mCherry retroviral vectors, respectively (kindly provided by Dr. Patrick Humbert, Peter McCallum Cancer Center and La Trobe University, Victoria, Australia) [374]. These vectors were used to stably transfect the MCF10A cell line previously in the lab by Dr. Chau Nguyen to produce MCF10A mCherry and MCF10A HRAS^{V12} cells. Briefly, the virus infection was performed in the presence of 10µg/ml polybrene, and the cells were sorted twice by FACS to select for those expressing mCherry (specific detail are described in the paper by Nyguen et al.[375] . In addition, western blot analysis was performed to confirm the ectopic expression of HRAS^{V12} and validated again for these experiments.

2.2 CELL CULTURE AND CELL LINES.

The human immortalised mammary epithelial cell line MCF-10A and human cancer cell lines T47D, ZR-75-1, MDA-MB-361, MCF-7, SKBr3, MDA-MB-453, BT-474, MDA-MB-468, BT549, Hs578T and MDA-MB-231 were obtained from American Type Culture Collection (ATCC; Manassas, VA, USA). All cells were grown in cell culture-approved humidified incubators set at 37°C at 5% CO_2, with regular decontamination and all water pans filled with sterile water treated by reverse osmosis (R.O.) and disinfectant such as Incuwater-Clean at 1 in 100 dilutions (VWR, Tingalpa, Australia).

MCF-10A were cultured and maintained as described by Debnath *et al.*, in growth media containing Dulbecco's Modified Eagle Medium/Nutrient Mixture F-12 (DMEM/F12) supplemented with 25% horse serum, 20ng/ml epidermal growth factor (EGF), 10µg/ml insulin human recombinant, 100ng/ml cholera toxin, 0.5µg/ml hydrocortisone and 1% antibiotic/antimycotic)[376]. Cells were rinsed with versine (sterile) twice, and then 2ml of Trypsin (hereafter referred to by trade name Tryple) was added and rolled over the cells briefly before removing 1.5ml of triple to leave a thin coat over the cells. Cells were placed in the incubator for approximately 15 minutes or until rounding; all cells were lifted by mechanical agitation. Resuspension media was added (DMEM/F12, 20% horse serum and 1% antibiotic/antimycotic) at 10mL for a 75cm flask. The cell suspension was pipetted into a 15ml tube and centrifuged at 1200rpm for 5 minutes. Resuspension media was discarded, and the cell pellet was resuspended in growth media and seeded at the required density.

HEK293T, ZR-75-1, MDA-MB-361, MDA-MB-453, BT-474, MDA-MB-468, BT549, Hs578t and MDA-MB-231 cell lines were maintained in Dulbecco's Modified Eagle's Medium (DMEM) (Life Technologies, Grand Island, NY, USA) containing 10% fetal bovine serum (FBS; Thermo Fisher Scientific, Rockford, IL, USA), 1% antibiotic/antimycotic (Life Technologies). T47D, BT549 cell lines were maintained in Roswell Park Memorial Institute (RPMI) containing 10% fetal bovine serum (FBS; Thermo Fisher Scientific, Rockford, IL, USA), antibiotic/antimycotic (Life Technologies). MCF-7 were grown in DMEM containing 10µg/ml insulin human recombinant, 10% FBS and 1% antibiotic/antimycotic. The SKBr3 cell line was cultured in McCoys 5A modified medium (Life Technologies, Grand Island, NY, USA) in addition to 10% FBS and 1% antibiotic/antimycotic. All cells were lifted per the same

method, culture media removed, and the flask rinsed twice with PBS (sterile); then Tryple was added at 1ml for 75cm flack, 500µl for 25cm flask and 2ml for 175cm flask. The flask was returned to the incubator for 2-3 minutes or until cells had rounded up and lifted upon mechanical agitation. Respective cultured media was added to the flask to neutralise Tryple, and cells were diluted at the appropriate rate and plated into the new flask.

Cell culture assay media also included Hanks' Balanced Salt Solution containing 6 mmol/L glucose (HBBS//starvation medium) (Life technologies). Serum-free media is any culture media described above minus the serum such as FBS. Fibroblast conditioned media (FbCM) is collected from Fibroblast cells grown to near confluence and rinsed before adding fresh DMEM with 10% FBS. After 48 hours, culture media is collected and centrifuged at 15000 rpm for 20 minutes. The supernatant (FbCM) is aliquoted and stored at -80°C.

All cell lines were never passaged beyond passage ten, and all tested negative for mycoplasma infection. Mycoplasma testing was undertaken regularly using the Lonza myco alert as prescribed by the manufacturer (MycoAlert; Lonza, Basel, Switzerland).

2.2.1.1 Cryopreservation of cell lines

The cells were lifted at approximately 70-80% confluence, as detailed above 2.3.2, and the cell resuspension was centrifuged at 1500rpm for 5 minutes. Next, cells were resuspended in freezing media that had been kept on ice. The MCF10A cell line freezing media consisted of 70% growth media, 20% horse serum and 10% DMSO, while all other cell line freezing media consisted of 90% FBS and 10% DMSO. After cells were resuspended in freezing media, they were aliquoted as 1ml volumes into cryotubes, which were adequately labelled and then placed on ice for 5 minutes. Afterwards, the cryotubes were placed in the freezing container (Mr. Frosty™, Thermo Scientific) for temporary storage at -80°C for no longer than eight weeks before being relocated to long-term liquid nitrogen storage.

2.2.1.2 Cell morphology observations

Cells were examined regularly under the microscope during treatments and before collection. Images were taken using bright field and phase contrast at 40X and 100X magnification on the Olympus IX81inverted fluorescent Microscope.

2.2.2 Compounds

Rapamycin, 3-methyl-6-(3-methylpiperidin-1-yl)-3H-purine (3MaIV), vacuolar protein Sorting 34 Inhibitor- SAR405 (VPS-SAR405), vacuolar protein Sorting 34

Inhibitor – IN1 (VPS-INI) and Bafilomycin A1 were all obtained from Millipore Sigma (Burlington, Massachusetts, United States). Chloroquine was obtained from Enzo life sciences (C/O: United BioResearch Products, Dural, Australia). All compounds were reconstituted at the highest concentration with DMSO, then aliquoted and stored along with the same DMSO used for reconstitution to be used as a vehicle control.

2.3 IN VITRO EXPERIMENTATION

2.3.1 Three-dimensional acini formation

MCF10A cells were grown in 3-D on a basement membrane matrix (referred to as trade mark name Geltrex; note this product has replaced Cultrex) culture by an overlay method, as described previously [376]. Geltrex LDEV-Free Reduced Growth Factor Basement Membrane Matrix (Thermo Fisher Scientific) was thawed on ice, and 80µl was added to each well of an eight-well chamber glass slide (Millipore, Massachusetts, USA) and spread evenly. The geltrex was solidified by incubating at 37°C for 20 minutes. MCF10A cells were grown to 70% confluence, lifted and then resuspended in assay media (DMEM/F12 supplemented with 2% horse serum, 10µg/ml insulin from bovine pancreas, 5µl/ml hydrocortisone and 1% antibiotic/antimycotic) at 25,000 cells/ml. The cell suspension was mixed with stock assay media containing 10ng/ml EGF and 4% Geltrex at a 1:1 ratio to obtain cells in final assay media containing 5ng/ml EGF and 2% Geltrex. The mixture (400µl/5,000 cells) was added on top of the solidified Geltrex layer in each well of the chamber slide. Cells were grown in a 5% CO_2 humidified incubator at 37°C for 14 days. Assay media containing 5ng/ml EGF and 2% Geltrex was replenished every four days.

2.3.2 Xcelligence RTCA DP System

The Xcelligence RTCA DP system is a real-time analyser used to determine the cell index based on cellular impedance. Impedance is the resistance to electrical conduction between the electrodes within the well plate, which is converted by the systems software (RTCA software) to a representative cell index [377-379]. The cell's adherence to the well surface directly impacts the conductivity between the electrodes; thus, an increase in cell number within the well will correlate with an increase in cell index.

2.3.3 Real-Time Cell Analysis of cytotoxicity induced by autophagic inhibition

The Xcelligence RTCA DP system (Agilent Technologies, California, USA) was used for real-time analysis of the cytotoxic effect of autophagic inhibition on mammary epithelial cell line MCF10A MCF10A+HRAS^{V12} and breast cancer cell lines T47D, Hs578T, MDA-MB-231, MDA-MB-468 and MDA-MB-468 +EGF (50ng/ml). The following treatments were administered in independent experiments and repeated in triplicate for the following drugs, at a 10-fold dilution of 3MaIV from 0.15 M to 15 mM, VPS-SAR405 from 100 pM to 10 μM and VPS-INI from 25 pM to 250 nM with vehicle controls added. This analysis was performed with cell lines that were seeded at a density to reach confluence at 24 hours in 150 μL of complete growth medium per well in a 16 or 96-well E-plate (OLS; Bremen, Germany) before the addition of the previously mentioned compounds, which were refreshed every 24 hours for 100 hours[380]. Data analysis was performed using the RTCA Software v2.0 to calculate the half-maximal inhibitory concentration (IC_{50}) for 72 hours of treatment.

2.3.4 Cell viability

The Alamar blue reagent (Thermo Fisher Scientific) was utilised as described by the manufacturer to determine cell viability for drug treatments and proliferation for genetically modified cell lines. Cells were seeded at a density for cytotoxicity to result in 90% -100% confluence the following day. Cells were treated at concentrations as mentioned in 2.3.2.3 with the inclusion of vehicle control, no treatment and media alone with no cells. The treatment was removed after 24 hours and replaced with media containing Alamar blue for 1 hour, at which time the Alamar blue media was pipetted into an opaque plate for fluorescent reading in the Varioskan Flash (Thermo Fisher Scientific) at Excitation/Emission of 560/590 nm. The seeding density for Alamar blue experiments were established by performing a cell number titration for each cell line of 10000-80000 cells generating a proliferation curve, and the seeding number was determined to best achieve cell viability for 96 hours. The cells were seeded at this determined number after 24 hours, and media was replaced with either growth media plus doxycycline at 1μg/ml or growth media alone. Finally, Alamar blue was applied after 72 hours and readings were performed after 1 hour.

2.3.5 Epithelial to Mesenchymal Transition (EMT)

The EGF treatment was carried out as described previously [381, 382]. EMT was induced by adding the EGF ligand to the growth media of the MDA-MB-468 cell line.

EMT was specifically achieved by growing the cells as a monolayer, then serum-starving them for 24 hours before being treated with 50 ng/mL EGF in DMEM supplemented with 10% FBS (Bio-Strategy, Melbourne, Victoria, Australia) for 72 hours, unless otherwise specified.

2.3.6 Autophagic Flux assay

Cells were grown to semi-confluence before the addition of treatments which included serum starvation for 4 hours, refreshing complete media and the additional inclusion of the positive control rapamycin (4μM) and negative controls of chloroquine (5μM) or 3-methyladenine (3-MA) (3mM) for 5 hours within each respective media. CYTO-ID® Autophagy Detection kit (Enzo Life Sciences, Inc.) was used according to the manufacturer's protocol. Briefly, cells were stained with CYTO-ID for 1 hour at 37°C in the dark and treated with the agents above. Next, cells were grown in the monolayer to 60-70% confluency, lifted by Tryple and resuspended in 1X PBS at approximately $1x10^7$ cells/ml before being subjected to the fluorescence analysis using a FACS DIVA (B.D., California, USA). Data was analysed using Weasel software V3.2.1 (Frank Battye, Australia). Autophagic flux was determined using Δ Mean fluorescent intensity (MFI) Cyto-ID = MFI Cyto-ID (+CQ) - MFI Cyto-ID (-C.Q.).

2.3.7 Wound healing assay

The Xcelligence RTCA MP 96 well plate system (Agilent Technologies, California, USA) along with AccuWound® 96 scratch tool (cat.380601420) performed wound healing. The protocol was followed as detailed by the manufacturer. In summary, cells were seeded in 96 well plates at a density to reach 100% confluence within 24 hours. When confluence was reached, and cell index had plateaued on the RTCA software, the plate was removed, and the scratch tool was used to make a wound. The wound was generated where the electrodes are positioned, so the impedance signal is removed by the scratch resulting in loss of cell index. However, it returns as the cells move to fill the gap and adhere to the surface of the electrodes generating an impedance signal. This signal is continuously monitored and recorded by the RTCA software until or if the wound is healed.

2.3.8 Anchorage-dependent clonogenic survival and growth assay

The anchorage-dependent survival and growth assay was carried out as described by Kattan *et al.*[383] . In short, cells were seeded at a low density (100-200 cells per well) and at a high density (1000 cells well plate) and cultured until colonies had formed (10-12

days) with media refreshed every 2-3 days. At completion, colonies were fixed with methanol and stained with Diff-Quick dyes (Fronine Lab Supplies, New South Wales, Australia), Quickdip I for 1 minute and Quick dip II for 2 minutes. The inducible cell lines underwent a "pre-treatment" where doxycycline was added at 1µg/ml for 72 hours before seeding with doxycycline administration maintained during the colony-forming period. There was also the inclusion of a "post-treatment", whereby cells were seeded as described above, but doxycycline was only added at 1µg/ml 24 hours after seeding, after which doxycycline was maintained for the duration of colony formation. After staining, the plates were allowed to dry and then scanned with the Epsom dual-lens photo scanner (V700 Photo, Epsom). The images were then analysed by the colony-counting macro and or manually using FIJI (software National Institutes of Health (NIH) Bethesda, Maryland, USA).

2.3.9 Microchemotaxis Migration Assay

The migration assay was undertaken in the Xcelligence RTCA DP system with the RTCA CIM Plates (Agilent technologies cat. 5665825001). RTCA system and CIM plates were prepared and run per manufacturers protocol and described by Bird *et al*. and Limame *et al*. [384, 385]. The inducible cell lines were pre-treated with doxycycline for 72 hours before the assay, and 24 hours prior, the media was changed to 0.1% BSA with no serum. The cells were also pretreated with Mitomycin C at 10µg/ml to prevent proliferation prior to preparation, and all other reagents were followed as described by Kouspou and Price [386]. Briefly, cells were lifted non-enzymatically with versene and resuspended at $5x10^5$ cells/ml to $2x10^6$ cells/ml for highly migratory and least migratory cells, respectively. The CIM plate's bottom chamber was filled with fibroblast conditioned media (FbCM) with 0.1% BSA, and as a negative control, base growth media with 0.1% BSA was included. The cells were loaded into the CIM plate, and the RTCA software performed continuous readings (15-minute intervals) for 24 hours. The data was analysed using the RTCA software and setting the cut-off time across all cell lines as consistently 4-5 hours.

2.3.10 Invasion Outgrowth Assay

The invasion outgrowth assay was performed as previously described [387]. The overlay method was utilized as this was the most consistent method for the studied cell lines. The eight chamber slides from Merck Millipore (Millicell™ EZ Slides cat. PEZGS0816) were used with Geltrex™ LDEV-Free Reduced Growth Factor Basement Membrane Matrix (Thermo Fisher Scientific cat. A1413202), which was used to coat the bottom of the wells and allowed to set at 37°C for 30 minutes. Cells were lifted and

resuspended in Geltrex™ at a concentration of 4 x10^5 cells/ml, this suspension was overlayed onto the set Geltrex™. The Geltrex™ cell suspension containing the cells was allowed to set for 30 minutes at 37°C before growth media was added and replenished as required. (Note that the doxycycline-inducible cell lines were treated with dox after seeding.) The outgrowths were imaged with each media change for 10-12 days with the Olympus IX81inverted fluorescent Microscope at 100X and 40X magnification with a bright field filter.

2.3.11 Immunofluorescence of adherent cells

Cells were cultured in chamber slides for 24 hours, washed thrice with Phosphate-buffered saline (PBS), and then fixed using 4% paraformaldehyde in PBS at room temperature (R.T.) for 25 minutes, followed by three washes of PBS. Next, cells were incubated for 30 minutes in permeabilisation/blocking solution (0.2% powdered skim milk, 0.1M Glycine, 1% BSA, 1% BSA in PBS) and rinsed with PBS three times. Next, cells were incubated with primary antibody diluted in dilution buffer (filtered 0.1% BSA in PBS) overnight at 4°C. Cells were washed with washing buffer (0.001% tween and PBS) and incubated with secondary antibody diluted in dilution buffer for 1 hr at R.T. followed by three washes in washing buffer. Chamber slides were dried and mounted on a coverslip (22mmX 60mm) using Fluoromount-G (Life technologies) mounting media. Cells were imaged on a Nikon C1 confocal microscope with x40 or x60 magnification. Images analysis and processing used FIJI software [388].

2.3.12 Staining of MCF-10A acini

The MCF10A acini were grown in the ibidi chamber slide with the coverslip bottom glass at 1.5 H (Lochhamer Schlag, Gräfelfing, Germany) (cat.80807) for improved imaging. The acini were stained for viable cells with Hoechst (Thermo Fisher Scientific) (cat.33342); this was performed in living cells as prescribed by the manufacturer. In short, the Hoechst powder was dissolved to make a 10mg/ml stock solution, media was removed, and Hoechst solution diluted in PBS at 1 in 200 was added for 30 minutes before removal and replaced with fresh assay media as described in 2.3.2.2. Images were taken with the Nikon C1 confocal microscope with the 60x objective, and images were taken on a single plane or as Z-stacking sections. In addition, ethidium bromide was utilised for cell death analysis as described by Debnath *et al*. [376]. In brief, the media from the acini was removed and washed with PBS, and then ethidium bromide (1μM) in PBS was added and incubated for 30 minutes. Images were then captured with the Nikon

C1 confocal microscope with the rhodamine channel with the 60X objectives in both single plane and Z stacking.

2.3.13 Western Blot Analysis and Antibodies

Cell were lysed at 4 °C in RIPA buffer (50 mM Tris-HCl pH 8.0, 150 mM NaCl, 0.5% sodium deoxycholate, 0.1% SDS, 0.5% Triton X-100, freshly supplemented with phosphatase and protease inhibitor cocktail 2 (Sigma Aldrich). According to the manufacturer's protocol, cell lysate concentration was determined using Pierce™ BCA Protein Assay Kit (Thermo Fisher Scientific cat. 23227). The cell lysate was used at a concentration of 15µg; this was mixed with laemmli buffer and heated at 95 °C for 10 min. The whole-cell lysate was loaded in the Novex NuPAGE 4-12% Bis-Tris (Invitrogen) and then transferred on 0.45 µm PVDF membranes using the iBlot 2 Dry Blotting System (Thermo Fisher Scientific) on setting P0. Membrane blocking was performed with 3% skim milk in TBS-tween for 1 hr at R.T. Membranes were incubated with primary antibodies overnight at 4 °C, washed, and then incubated with secondary antibodies for 1hr at R.T. Detection was performed with chemiluminescence method as prescribed by the manufacturer in the Fusion F.X. (Vilber Lourmat, SAS, France). Data analysis was performed with the Fusion-Capt Advance software. All primary and secondary antibodies are listed below with the supplier and dilution.

2.3.14 Lysosome Enrichment

The lysosome enrichment protocol was developed for this study but is modified from Hao *et al.* and several other studies [301, 389, 390]. Cells were cultured to achieve a cell number of 5-10 $x10^{7,}$ which were lifted and centrifuged at 600 g/rcf (G-force /Relative Centrifugal Force) for 5 minutes, then washed twice with cells PBS. The pellet was resuspended in 1 ml of lysis buffer (0.25M sucrose1 mM EDTA,20 mM HEPES-NaOH, pH 7.4) for 10 minutes on ice. The cell suspension was then sonicated with a probe sonicator (Bandelin Sonoplus HD 2200) at 3x 10% (duty cycle-percentage of power during pulse rate) at 1x75% (duty cycle) for 15 seconds, and the sequence was repeated twice in the cold room. A 50µl sample was taken and treated as per 2.3.2.2 as the whole lysate (W.L.) comparison. The remainder of the sample was centrifuged at 1000 g/rcf at 4°C for 5 minutes, then the supernatant was removed to a new tube and centrifuged at 5000g/rcf at 4°C for 5 minutes. The supernatant was transferred to an ultracentrifuge tube and placed in the Thermo Scientific ultracentrifuge (Sorvall MTX 150) at 20000 g/rcf for 30 minutes at 4°C. A sucrose gradient was made with iodixanol

made of equal parts of OptiPrepTM (Sigma Aldrich cat. D1556) and OptiPrepTM diluent (0.25 M sucrose, 2 mM EDTA, 40 mM HEPES-NaOH, pH 7.4). An iodixanol gradient of 15%, 17%, 20%, 23%, 27% and 30% was made with iodixanol and lysis buffer. The gradients were overlayed with 30% up to 15% in the ultracentrifuge tube. The 15% gradient was used to resuspend the pellet before being overlayed. The gradients were placed in the ultracentrifuge and spun at 150000g/rcf at 4°C for 3 hours. After completion, the lysosome fraction within the first 1ml was removed or alternatively was collected in fractions of 500µl, diluted with 3ml of lysis buffer, and centrifuged in ultraltracentrifudge for 30 minutes at 100000g/rcf at 4°C. The pellet was resuspended in 50µl RIPA buffer for western blot analysis (as per 2.3.2.2) and stored at -80°C.

2.3.15 Microarray analysis

The result were previously generated within the Price lab, and a list of differentially expressed genes were provided from these experiments. Briefly, total RNA was extracted from acini formed by the MCF10A and MCF10A $HRAS^{V12}$ cell lines using an RNA extraction kit (Qiagen, California, USA), with the Geltrex being dissolved in RLT buffer (Qiagen cat. no. 79216). RNA was diluted to 50ng/µl and submitted to Agilent Technologies (The Ramaciotti Center, New South Wales, Australia) for microarray processing.

2.3.16 Statistical analysis.

Results are shown as mean ± standard deviation (S.D.) and the number of biological replicates in figures (n=). Graphs were created, and statistical analysis was performed using GraphPad Prism (v7.0). All the tests were performed using either a t-test or one-way ANOVA with Tukey's post hoc test or two-way ANOVA with Sidak's post hoc test. P-values less than 0.05 were considered significant, with specific p values indicated in graph figures.

2.4 MATERIALS

2.4.1 Plasmid constructs utilised in this study

PLASMIDS	SOURCE
MSCV Ha-RAS^{V12} mCherry	Patrick Humbert, Peter MacCallum Cancer Centre, Victoria, Australia
MSCV mCherry	Patrick Humbert, Peter MacCallum Cancer Centre, Victoria, Australia
pTRIPZ-Renilla	Dr Chau Nguyen and Dr Ben Lang
pTRIPZ-Lamp2AshRNAmir(1)	This study
pTRIPZ- Lamp2AshRNAmir(2)	This study
pTRIPZ-Lamp2AshRNAmir(3)	This study
pTRIPZ-Lamp2AshRNAmir(4)	This study
pTRIPZ-Lamp2AshRNAmir(5)	This study
pMDLg/pRRE	Addgene (12251)
pMD2.g	Addgene (12259)
pRSV-REV	Addgene (12253)

2.4.1.1 Cloning primers

Name	Direction	Primer Sequence
HUMAN 5'-miR30-XHOI-F	FORWARD	5'-CAGAAGGCTCGAGAAGGTATATGCTGTTGACAGTGAGCG-3'
HUMAN 3'-miR30-MLUI-F	REVERSE	5'-CTAAAGTAGCCCCTTACGCGTTCGAGGCAGTAGGCA-3'

2.4.1.2 Cloning reagents

Reagent	Catalogue No.	Supplier
10mM dNTP	F-506L	Thermo Fisher Scientific
1kb DNA ladder	G5711	Promega
Ampicillin	A-2804	Merck
Bacto Yeast Extract	212750	BD Bioscience
BactoTryptone (Pancreatic Digest of Casein)	211705	BD Bioscience
Gel loading dye(6X) 4ml	B7021S	New England Biolabs
High-grade DNA agarose	BIO-41026	Bioline
LB Agar	71752-5	Merck
Phusion Hot Start Flex DNA	M0535S	New England Biolabs
Phusion® High-Fidelity	M0531S	New England Biolabs
Restriction Enzymes; AvrII, BamHI, BglII, EcoRI, HindIII, KpnI, MluI, NdeI, SacI, XhoI		New England Biolabs
Sybr safe DNA gel stain	S33102	Thermo Fisher Scientific
T4 DNA Ligase	M0202	New England Biolabs
T4 DNA polymeRASe	M0203S	New England Biolabs
Zeocin	R25001	Thermo Fisher Scientific

2.4.2 Cell culture reagents and chemotherapeutics

Reagent	Catalogue No.	Supplier
Alamar Blue	DAL1025	Thermo Fisher Scientific
Ammonium Chloride for molecular biology	A9434	Merck
Antibiotic-Antimycotic (100X)	15240062	Thermo Fisher Scientific
Autophagy Inhibitor IV, Cpd18 - Calbiochem	505980	Merck
Bafilomycin A1	196000	Merck
DMEM, high glucose, GlutaMAX™ Supplement, HEPES	10564029 (BOX)	Thermo Fisher Scientific
DMEM/F12 + glutamax	10565-018	Thermo Fisher Scientific
DMSO (Dimethyl Sulfoxide)	D2438	Merck
Doxycycline hydrochloride	D3447	Merck
Epidermal Growth Factor EGF Human Rec.	BDAA354052	Bio Strategy
FBS GAMMA IRRAD AUSTRALIAN	10101145	Thermo Fisher Scientific
HBSS (X10)calcium magnesium	14065056	Thermo Fisher Scientific
Hexadimethrine bromide	H9268	Merck
Insulin, Recombinant Human ZN	12585014	Thermo Fisher Scientific
McCoys 5A media	16600-082	Thermo Fisher Scientific
Mitomycin C from Streptomyces caespitosus	M4287	Merck
Nunc™ Biobanking and Cell Culture Cryogenic Tubes (450pcs)	377267PK	Thermo Fisher Scientific
Nunc™ EasYDish™, 100mm / 17mm Case 150	150464	Thermo Fisher Scientific
Puromycin cell culture	P8833	Merck
Rapamycin	553210	Merck
RPMI	11875119	Thermo Fisher Scientific
RPMI medium 1640	11875-093	Thermo Fisher Scientific
Sodium Pyruvate (100 mM)	11360070	Thermo Fisher Scientific
Tryple express	12604013	Thermo Fisher Scientific
VPS34 Inhibitor, SAR405	533063	Merck
VPS34 Inhibitor, VPS34-IN1 - CAS 1383716-33-3 - Calbiochem	532628	Merck
Wortmannin ready-made solution	W3144	Merck

2.4.3 In vitro Experimentation Reagents

Reagent	Catalogue No.	Supplier
Coverslips for microscope slides 22mmX22mm	Z692271	Merck
ETHYLENE GLYCOL-BIS(2-AMINOETHYLETHER)-N,N,N',N'-TETR ACETIC ACID	E3889	Merck
Geltrex™ LDEV-Free, hESC-Qualified, Reduced Growth Factor Basement Membrane Matrix	A1413302	Thermo Fisher Scientific
Iblot PVDF transfer stacks	IB24001	Thermo Fisher Scientific
iBlot™ 2 Transfer Stacks, PVDF, mini	IB24002	Thermo Fisher Scientific
Novex™ Sharp Pre-stained Protein Standard	LC5800	Thermo Fisher Scientific
NUPAGE 4-12% Bis-Tris Gel 1.0mm 15-well	NP0336BOX	Thermo Fisher Scientific
NUPAGE antioxidant	NP0005	Thermo Fisher Scientific
NuPAGE MES SDS Running Buffer	NP0002	Thermo Fisher Scientific
NuPAGE Sample Reducing Agent	NP0004	Thermo Fisher Scientific
NuPAGE™ 4 to 12%, Bis-Tris, 1.0 mm, Midi Protein Gel, 20-well	WG1402BOX	Thermo Fisher Scientific
NuPAGE™ 4 to 12%, Bis-Tris, 1.0 mm, Midi Protein Gel, 12-well	NP0322BOX	Thermo Fisher Scientific
NuPAGE™ 4 to 12%, Bis-Tris, 1.5 mm, Mini Protein Gel, 10-well	NP0335BOX	Thermo Fisher Scientific
NuPAGE™ LDS Sample Buffer (4X)	NP0007	Thermo Fisher Scientific
OptiPrep™ Density Gradient Medium	D1556	Merck
Restore™ PLUS Western Blot Stripping Buffer	46430	Thermo Fisher Scientific
SuperSignal™ West Pico PLUS Chemiluminescent Substrate	34580	Thermo Fisher Scientific
Tween 20 cell cultures tested	P2287	Merck
Vector VECTA SHIELD Hard set	VEH1400	Abacus ALS

2.4.4 Commercial Kits

Name of product	Catalogue No.	Supplier
BCA Protein Assay Kit	23227	Thermo Fisher Scientific
Cyto-ID Autophagy	ENZ-51031-0050	United biosearch
PureLink™ HiPure Plasmid Midiprep Kit	K210004	Thermo Fisher Scientific
QIAprep Spin Miniprep Kit	27104	Qiagen
QIAquick DNA Gel Extraction Kit	28704	Qiagen

Antibodies

Antibody	Dilution	Catalogue No.	Supplier
Anti-HSPA8/ Hsc70 Clone N69 Mouse mAb	1:1000	MABE1120	Merck
Anti-Lamp2A antibody Rabbit mAb	1:1000	125068	Abcam
Anti-Lamp-2b antibody Rabbit mAb	1:2000	ab18529	Abcam
Apoptosis antibody sampler kit Rabbit mAb	1:1000	9915S	Cell signalling
Autophagy antibody sampler kit Rabbit mAb	1:1000	4445S	Cell signalling
Autophagy Induction (ULK1 Complex) Antibody Sampler Kit Rabbit mAb	1:1000	46486	Cell signalling
beta-Actin (8H10D10) Mouse mAb	1:5000	3700S	Cell signalling
E-Cadherin (24E10) Rabbit mAb	1:1000	3195S	Cell signalling
GABARAP (E1J4E) Rabbit mAb	1:1000	13733	Cell signalling
GABARAPL1 (D5R9Y) XP® Rabbit mAb	1:1000	26632	Cell signalling
GABARAPL2 (D1W9T) Rabbit mAb	1:1000	14256	Cell signalling
Glycolysis Antibody Sampler Kit Rabbit mAb	1:1000	8337	Cell signalling
KEAP1 Rabbit mAb	1:1000	8047T	Cell signalling
LAMP-1 Rabbit mAb	1:1000	9091s	Cell signalling
LAMP-2 Rabbit mAb	1:1000	49067s	Cell signalling
Lamp2A Rabbit mAb	1:1000	ab18528	Abcam
LC3A Rabbit mAb	1:1000	4599s	Cell signalling
LC3A/B (D3U4C) XP	1:1000	12741S	Cell signalling
Rabbit mAb	1:1000		Cell signalling
LC3B Rabbit mAb		3868s	
LC3C Rabbit mAb	1:1000	14736s	Cell signalling
Loading control cell signalling sampler kit Rabbit mAb	1:5000	5142	Cell signalling
N-Cadherin Rabbit mAb	1:1000	13116S	Cell signalling

Novus HSP70/HSC 70 antibody Mouse mAb	1:1000	NOVNB1202788	Novus
NRF2 Rabbit mAb	1:1000	12721T	Cell signalling
Phospho-SQSTM1/P62 (Ser349) (E7M1A) Rabbit mAb	1:1000	16177	Cell signalling
Phospho-SQSTM1/P62 (Ser403) (D8D6T) Rabbit mAb	1:1000	39786	Cell signalling
PI3 Kinase Class III (D4E2) Rabbit mAb	1:1000	3358S	Cell signalling
SQSTM1/P62 (D5L7G) Mouse mAb	1:1000	88588	Cell signalling
Vimentin Rabbit mAb	1:1000	57415	Cell signalling

Antibody	Dilution	Catalogue No.	Supplier
Goat Anti-Rabbit IgG, (H+L), Peroxidase conjugated	1:10000	G-21234	Thermo Fisher Scientific
Goat anti-Mouse IgG (H+L) secondary	1:10000	31430	Thermo Fisher Scientific

2.4.5 General consumables

Reagent	Catalogue No.	Supplier
2-propanol	I9516	Merck
Acetic acid	695092	Merck
Di-sodium Hydrogen Phosphate	71643	Merck
Ethanol	443611	Merck
Glycerol	G5516	Merck
Glycine	50046	Merck
L-Ascorbic Acid 2-Phosphate	A8960	Merck
Methanol	34860	Merck
Paraformaldehyde	158127	Merck
Potassium Phosphate	P9791	Merck
Sodium Chloride (NaCl)	S5886	Merck
Sodium Deoxycholate	D6750	Merck
Sucrose	S0389	Merck
Triton (X100)	93443	Merck
Trizma	T1503	Merck

Chapter 3: THE IMPACT OF RAS ON MACROAUTOPHAGY IN THE CONTEXT OF BREAST CANCER CELL PLASTICITY.

3.1 INTRODUCTION

Macroautophagy (hereafter referred to as autophagy) is a cellular process for the degradation of organelles, macromolecules, and proteins, generating by-products that contribute to the maintenance of amino acid pools and metabolic substrates in cells in response to numerous stressors [391]. As such, autophagy is a known survival mechanism in the context of the basal state of a cell; however, the expanding literature on autophagy has shown that this activity can be frequently ambiguous in pathological states. For example, research has shown that autophagy prevents cancer initiation by removing aggregates and defunct organelles, which maintains genetic stability [392]. However, during cancer development and the progression towards metastasis, autophagy is thought to facilitate oncogenic changes and supports nutritional requirements in the challenging micro-environment of the tumour [393]. Thus, more research into the autophagic mechanism is needed to elucidate its role in cancer and provide information explaining these ambiguities. To this end, this study focused on the role autophagy has in the progression of breast cancer.

Briefly, the process of autophagy involves the development of a membrane that surrounds the cargo to form the autophagosome, after which the autophagosome fuses to the lysosome, forming the autolysosome. The release of hydrolytic enzymes results in the degradation of the cargo to simple molecules, which are then recycled back into the cell for use.

RAS mutations occur in 30% of all cancers, and much research has focused on these RAS mutations as drivers of transformation. Three RAS genes encode four isoforms referred to as KRAS (which has two splice variants, KRAS4A and KRAS4B; HRAS and NRAS, all are similar, only differing at the c-terminus in the hypervariable region [394].

Their oncogenic potential is tumour-specific, with KRAS mutations more common in lung, pancreatic and colon cancer. In contrast, NRAS is more frequent in leukaemia, with HRAS being more commonly associated with hepatic, colorectal, head and neck cancers [64, 395]. Interestingly, RAS mutations occur in less than 1% of breast cancers; however, hyperactivation of RAS is present in 50% of breast cancer [72, 396], particularly in breast cancers with increased EGFR and HER2 receptor signalling found in the luminal B and basal molecular subtypes [397]. The current dogma is that this hyperactivation facilitates the aggressive phenotypes of these subtypes, particularly during the epithelial to mesenchymal transition (EMT) [73, 398].

Currently, no literature has examined the role of autophagy concerning RAS activity in breast cancer. However, recent research has highlighted the importance of this relationship in a small number of other cancers, including a clinical trial in pancreatic cancer [399-401]. A particular focus has been on targeting the KRAS mutation in combination with autophagy inhibition which has shown promising results in adjuvant treatments combining an autophagic inhibitor with trametinib [65]. Findings have shown that inhibition of MEK1/2, a downstream effector of the RAS-RAF-ERK axis, with trametinib induces autophagy which compromises drug efficacy. However, its combination with the autophagic inhibitor hydroxychloroquine significantly improved treatment response [65].

Although literature differs on the reasons for this dependency upon autophagy in various KRAS mutated cancers, particularly in pancreatic cancer, it is suggested that the primary role is to provide and maintain metabolic nutrients. However, reports do differ on the specific target substrates such as arginine [402], glycolytic substrates [403] and those related to oxidative metabolism [404].

This study has utilised a panel of breast cancer lines to represent a cancer progression continuum, with the least to most aggressive phenotypes, a primary screening tool in breast cancer research [55, 405]. This panel includes each of the molecular subtypes Luminal A (LA) (T47D), luminal B (LB) (BT474), HER 2 (H2) (SKBr3), basal A (TNA) (MDA-MB-468) and basal B (TNB) (Hs578T & MDA-MB-231) [55, 406]. This study examines the relationship between autophagic activity and RAS in the context of human breast cancer progression. Specifically, examining the role of autophagy in various RAS contexts, including RAS transformation, tumourigenesis maintained by RAS mutations and RAS activation in established breast cancer cell lines. [55, 405] . The study

has put together a RAS progression panel (Figure 3-1) with the rationale, and the names of the cell lines included are as follows.

The role of RAS transformation and its effects on autophagy in breast cancer required an *in vitro* model development. Therefore, this study has utilised the mammary epithelial cell line MCF10A (immortalised) [376, 407, 408] transduced with $HRAS^{V12,}$ resulting in a transformation model used for this study [409]. In addition, the role of autophagy regarding RAS activation was also examined in the MDA-MB-468 breast cancer cell line as these cells have high expression levels of EGF receptors, resulting in increased RAS signalling. Moreover, in this model, the addition of EGF increases RAS activity to cause hyperactivation of RAS signalling and its downstream targets [410-412]. Consequently, the cell line undergoes an epithelial to mesenchymal transition and displays a more aggressive phenotype with increased plasticity [382, 413].

In addition, endogenous $HRAS^{G12}$ and $KRAS^{G13}$ mutations in the breast cancer cell lines Hs578T and MDA-MB-231 [414, 415] were used to examine the role of autophagy within these RAS mutation contexts of breast cancer cell lines that, as a consequence, are the most aggressive and both classify as the Triple-negative basal B (TNB) or phenotypically mesenchymal. Finally, the T47D cell line was included to provide a control, lacking any RAS mutation or aberrant activation and is the least aggressive of the breast cancer cell lines. All three cell lines possess mutant p53 and express wild-type BRCA1 [416](Figure 3-1).

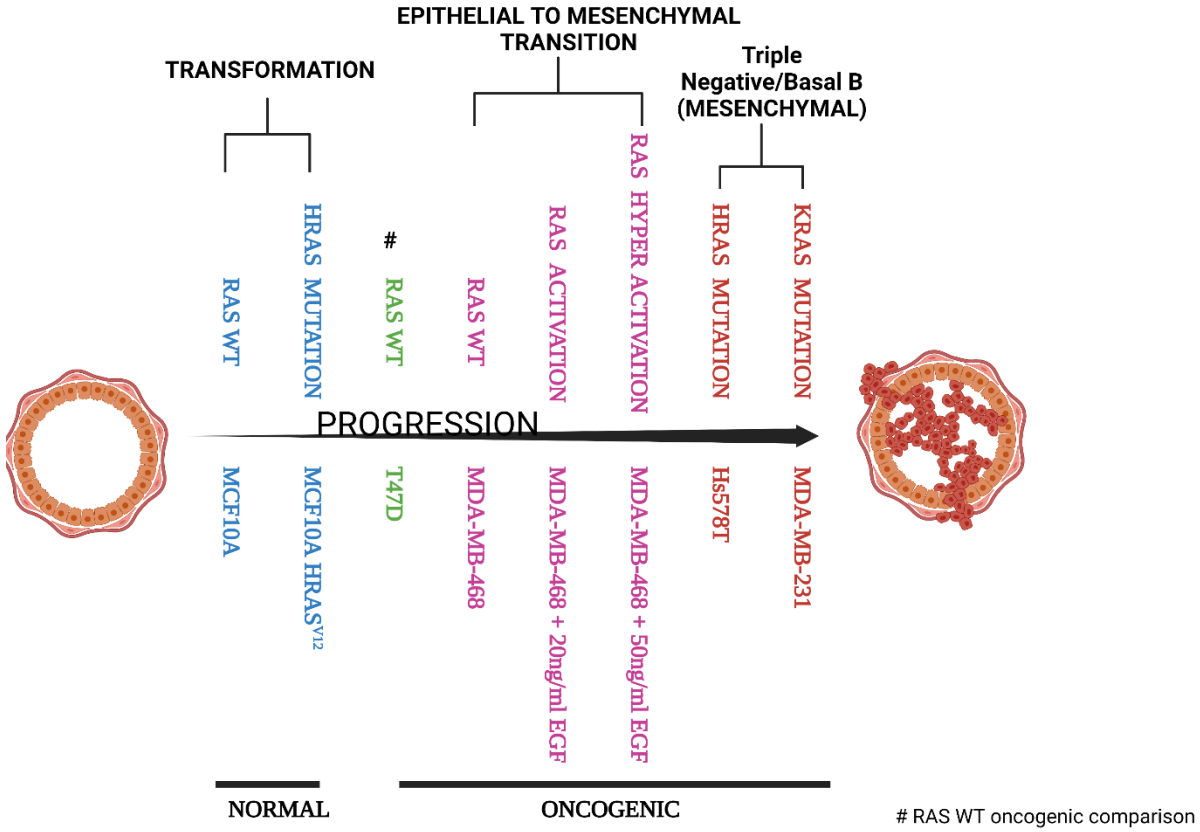


Figure 3-1 Schematic representation of rationale for the cell lines of this study

The schematic describes the cell lines, including their RAS status. For example, its order from the normal cell line MCF-10A with WT RAS transformed MCF10A with $HRAS^{V12}$ mutation to oncogenic cell lines in order of aggressiveness T47D with WT RAS, MDA-MB-468 with WT RAS, then a RAS activation model of MDA-MB-468 with EGF the inclusion of 20ng/ml of EGF for RAS activation, then 50ng/ml defined as RAS hyperactivation, Hs578T cell line has HRAS mutation, and MDA-MB-231 cell line has KRAS mutation.

Created with BioRender.com

3.2 HYPOTHESIS AND AIMS

Hypothesis:
"Autophagy has a regulatory role in facilitating and maintaining breast cancer progression in conjunction with RAS".

The aims of this chapter are:
-To determine if autophagy activity is altered by the presence of a RAS mutation in the MCF-10A model of transformation (non-transformed MCF10A cells and MCF10A cells transformed with H-RAS^{V12})
- To examine the presence of autophagic markers and functional activity in a panel of progressive breast cancer cell lines.

- To investigate the role of autophagy and its activity during the epithelial to mesenchymal transition of breast cancer cell line MDA-MB-468 as a model of RAS activity.

3.3 RESULTS

3.3.1 Increased expression of LC3-II to LC3-I ratio under basal conditions in Triple-Negative Basal B subtypes with RAS Mutation.

A panel of breast cancer cell lines was investigated for autophagic activity in relation to breast cancer progression. The breast cancer cell lines utilised in the panel represent differing breast cancer phenotypes. Breast cancer has been divided into molecular subtypes, which are genotypically and phenotypically different. The subtypes included in this study were T47D, a luminal A (referred to as LA) subtype, characterised by the expression of estrogen (ER) and progesterone (PR) receptors. BT-474 cell line represented the Luminal B (referred to as LB) subtype, which presents with estrogen and or progesterone receptors plus the presence of human epidermal growth factor receptor 2 (HER2), while SKBr3 cell line is a HER2 (are referred to as H2) subtype, only expressing amplified HER2 receptors.

The final two subtypes are triple-negative subtypes. The MDA-MB-468 represents the basal-like morphology (referred to as TNA) which is negative for HER2, PR and ER receptors but overexpress EGFR. Finally, the Hs578T and MDA-MB-231 cell lines are also characterised as triple-negative, not expressing ER, PR or HER2 receptors, however, they differ from TNA due to their distinct mesenchymal morphology and low claudin levels, constituting another subgroup referred to as TNB [417-419].

As depicted in the micrograph images in Figure 3-2 A, there is a distinct morphological difference between the subtypes related to their molecular characteristics. For example, the least aggressive cell line, T47D, is an epithelial type characterised by the cuboidal shape. However, as the cell lines progress, they lose their epithelial characteristics and display a mesenchymal morphology which is more spindle-like morphology is most identifiable in the triple-negative subtype mesenchymal (TNB).

Protein lysate was isolated from each breast cancer cell line and analysed by western blot from the least to the most aggressive phenotype (i.e. LA, LB, H2, TNA, TNB). To determine the presence of autophagic activity, or more accurately, autophagosome formation, the level of expression of the autophagic marker LC3 in its precursor (LC3-I) and active (LC3-II) forms (note the antibody targets all LC3 isoforms)

by western blot analysis was performed (Figure 3-2). The LC3-II to LC3-I ratio was determined to reveal the presence and level of autophagosome formation in all cell lines, which were grouped into their respective molecular sub-types (Figure 3-2). Since autophagy is induced by particularly such as nutritional deprivation and hypoxia. All experiments were controlled for this by culturing cells under normoxic conditions and adding fresh media four hours before lysate collection.

In Figure 3-2 there was observed to be a significant increase in the ratio of LC3-II to LC3-I in the basal B (TNB) subtype, which included the Hs578T and MDA-MB-231 cell lines, compared to the luminal A (LA) subtype, which included the T47D cell line, indicating a rise in elongation and maturation of the autophagosome in the more aggressive phenotypes. These findings suggested an increase in autophagic activity and were of interest when the cell lines were examined further; it was observed that these increases correlated with the presence of RAS mutation. The Hs578T breast cancer cell line carries $HRAS^{G12}$ mutation, and the MDA-MB-231 breast cancer cell line carries $KRAS^{G13}$ mutation suggesting there may be a relationship between autophagy and mutant RAS in this context and warranted further investigation

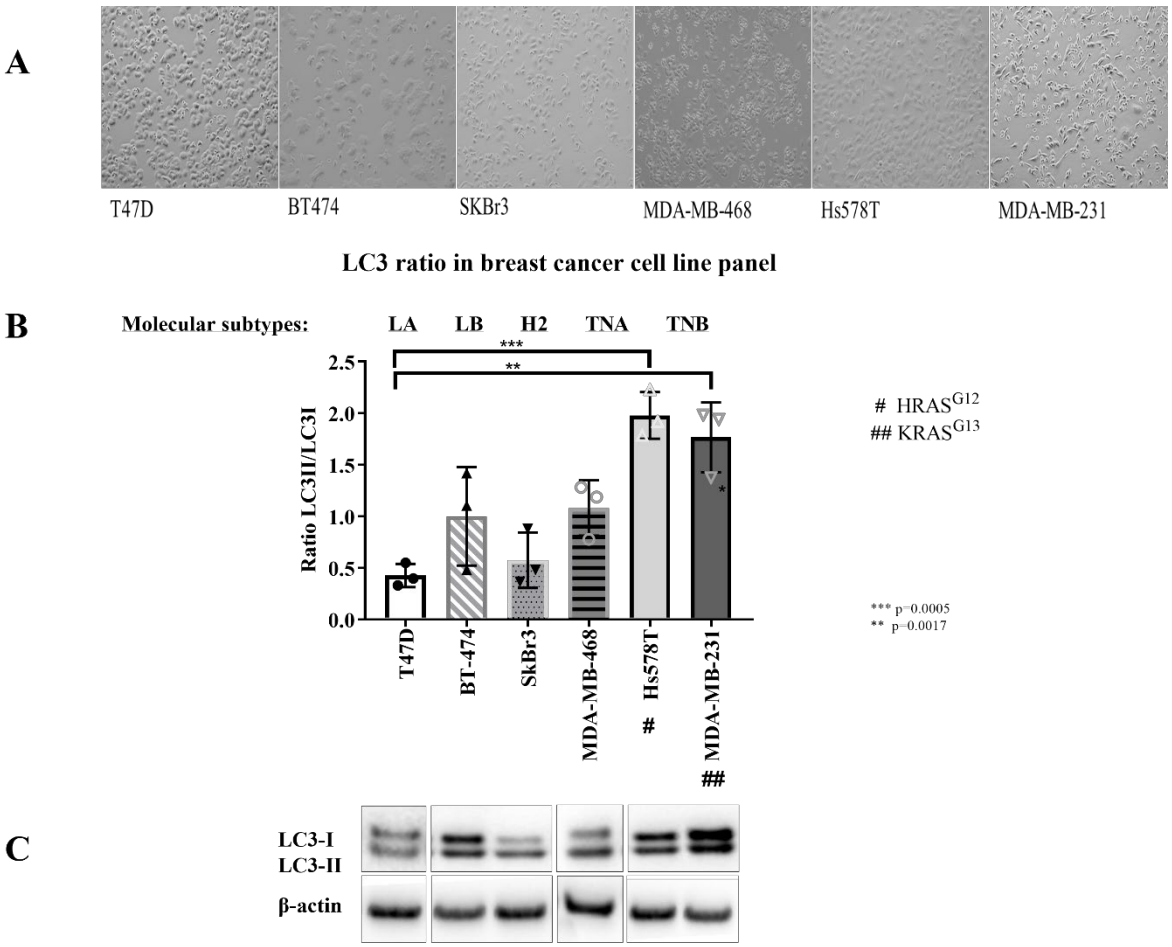


Figure 3-2 Increased autophagosome formation observed in basal breast cancer cell lines compared to luminal subtypes

(A) Micrograph images were taken with a phase-contrast filter at X100 magnification of the breast cancer cell lines to represent the cellular morphology of T47D (LA), BT474 (LB), SkBr3(H2), MDA-MB-468 (TNA), Hs578T and MDA-MB-231(TNB). **(B)** Densitometry revealed that autophagosome formation is present in all breast cancer cell lines as indicated by the LC3-I to LC3-II ratio. This ratio was significantly increased in the breast cancer cells within the triple-negative subtypes compared to the lesser aggressive subtypes, suggesting an upregulated formation in this phenotype. The hash symbol # indicates a RAS mutation. Molecular subtypes; Luminal A (LA), luminal B (LB), HER2 (H2), triple-negative/basal A (TNA) and triple-negative/basal B (TNB). **(C)** Representative western blot with LC3 A/B antibody (n=3, ±SD, $p<0.05$ ANOVA and Tukey's post hoc test ***p=0.0005 and **p=0.0017)

3.3.2 LC3B expression increases in the presence of RAS mutation in the breast cancer cell lines

The protein lysate was isolated from each cell line within the RAS progression breast cell line panel and analysed by western blot grouped by cellular subtypes (i.e. LA, TNA and TNB). The protein for this experiment was collected together to examine the panel as a whole and is not the same as the lysate collection for further experiments. This experiment collectively allows for a reliable overview of the RAS models and gives insight into differences and trends.

To determine the presence of the critical autophagic marker and indicator of autophagosome formation, LC3 was examined to gain a clearer picture of LC3 in this context; the LC3 isoforms A, B and C (note C was absent, so data not included) and LC3 family orthologues gabarap1 and gabarap2 (Figure 3-3). The results indicate that the LC3A isoform was lowly expressed in nearly all cell lines except for the MDA-MB-468, but of interest, this expression decreased with the addition of EGF and RAS activation (Figure 3-3B). The LC3B isoform was the most highly expressed of all the LC3 family members; it appears to increase with RAS, although it was highly expressed in the T47D (Figure 3-3C). The orthologue gabarap1 was highly expressed in MDA-MB-468, and this expression increased dose-dependently with EGF addition, and it was significantly decreased in both the TNB cell lines Hs578T and MDA-MB-231 (Figure 3-3D). Gabarap 2 displayed similarly low expression levels in all cell lines except the MDA-MB-468, increasing the maximum EGF addition (Figure 3-3F).

The study will examine each component of the RAS progression panel separately; therefore, RAS transformation with $HRAS^{V12}$ with the MCF10A model, epithelial to mesenchymal transition with RAS activation in the MDA-MB-468 model and RAS mutation in breast cancer cell lines Hs78T and MDA-MB-231 (includes T47D as RAS WT control). The rationale is that it will enable a more thorough investigation into understanding and determining a linkage between RAS and autophagy.

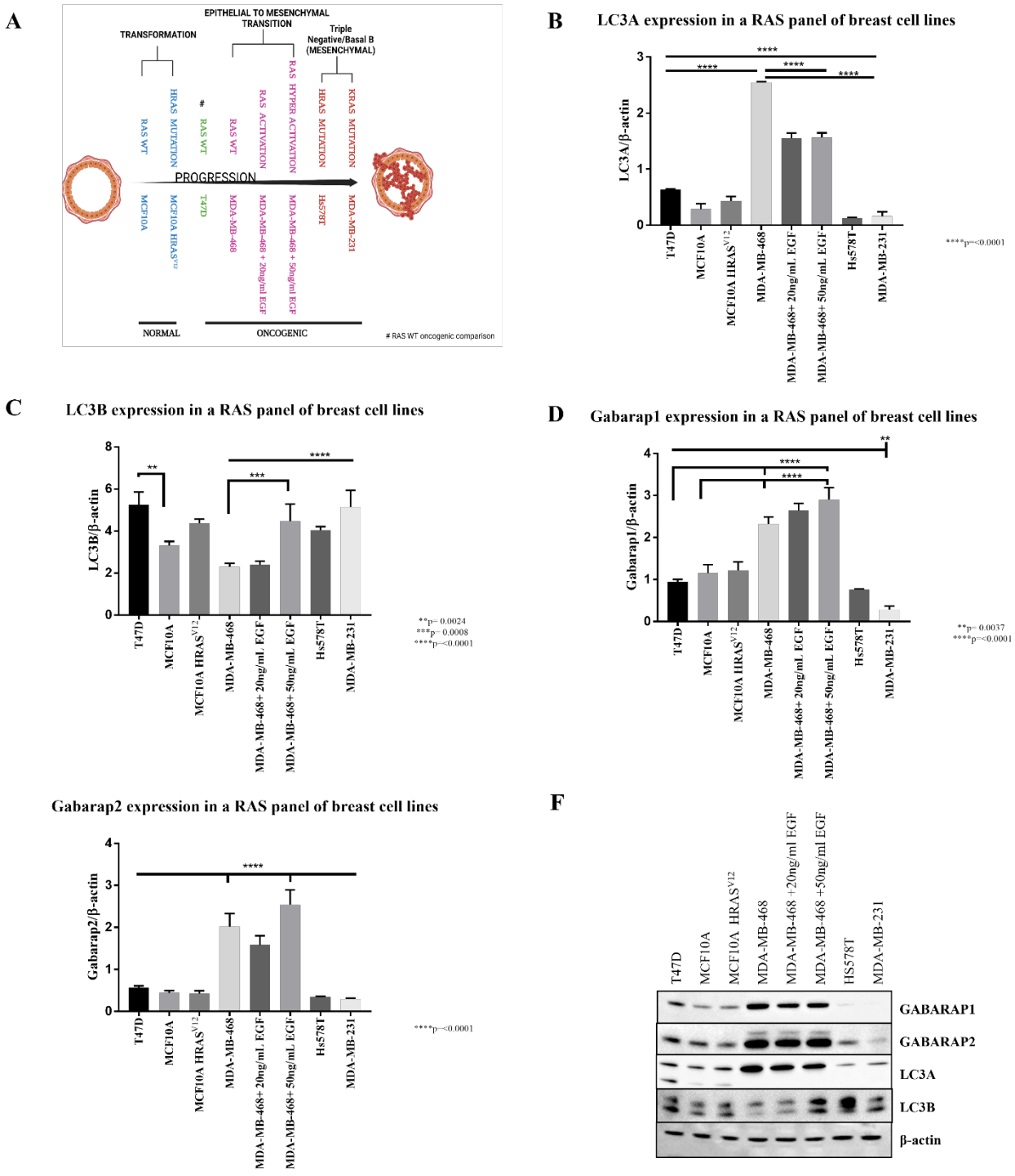


Figure 3-3 The distinct LC3 family member expression in RAS breast cell line panel

(A) schematic of the cell lines included and RAS status of the RAS breast cell line panel**. (B)** The normalised expression of LC3 isoform LC3A. (****p=<0.0001) **(C)** The normalised expression of LC3 isoform LC3B.(**p=0.0024,***p=0.0008 ****p=<0.0001) **(D)** The normalised expression of LC3 orthologue gabarap1(**p=0.0037, ****p=<0.0001) **(E)** The normalised expression of LC3 orthologue gabarap2.(****p=0.0001) (F). Representative immunoblot image. (n=3, ±SD, p<0.05 ANOVA and Tukey's post hoc test)

3.3.3 The ectopic expression of the HRAS^{V12} mutation in the mammary epithelial cell line MCF10A models leads to oncogenic transformation.

To investigate the previous findings further and begin to explore the role of a RAS mutation in relation to autophagy, an in vitro model of transformation was utilised. This model was developed using the immortalised mammary epithelial cell line MCF10A transduced with HRAS^{V12}. To validate the model, cell morphology was examined in a 2D (APPENDIX II) and 3D (Figure 3-4) environment for fundamental morphological changes expected with oncogenic transformation. The introduction of the HRAS mutation should, as previously shown by other groups [409, 420], result in the transition of the cells from one of cuboidal and organised to mesenchymal and disorganised in appearance (refer to Appendix II for additional images). Furthermore, the cells were grown in a 3-dimensional environment using an extracellular matrix (Geltrex^{TM}) to form acini structures. These acini will follow an established development pattern to include sphere formation over days four to eight. From day eight, the inner cell mass begins to undergo apoptosis to form a hollow lumen by day 12, similar to the functional acini structures found within the terminal ducts of the breast [376]. In Figure 3-4, the initial images were taken on day four with phase-contrast microscopy and clearly illustrated acini formation in both the MCF10A and MCF10A HRAS^{V12} but what can be observed and highlighted by the white arrow is the protrusion and projections from the spheres, which were found to be smaller than the MCF10A control counterparts. The acini were grown over 12 days, and their media was refreshed every four days or as required. It was evident that both cell lines initially formed the spherical structures notably smaller in the HRAS^{V12} compared to control, but by day six, there was a definite shift in the appearance of the structures with the control cell lines forming acini while the HRAS^{V12} grew and merged to form large masses of cells. The ethidium bromide images in Figure 3-4 B are from day ten, and it can be seen that the inner cell mass has been removed by cell death but is only apparent on the luminal surface, as expected in the MCF10A control cells (Refer to Appendix II for further Hoechst and lower magnification images).

In contrast, the inclusion of HRAS^{V12} resulted in limited cell death within the inner mass; with a large number of viable cells found residing within the core of these masses (Appendix II), so it appears to be increasing the size of the disorganised masses of cells

until beyond day 12 when these structures have covered the entire surface of the Geltrex^{TM}.

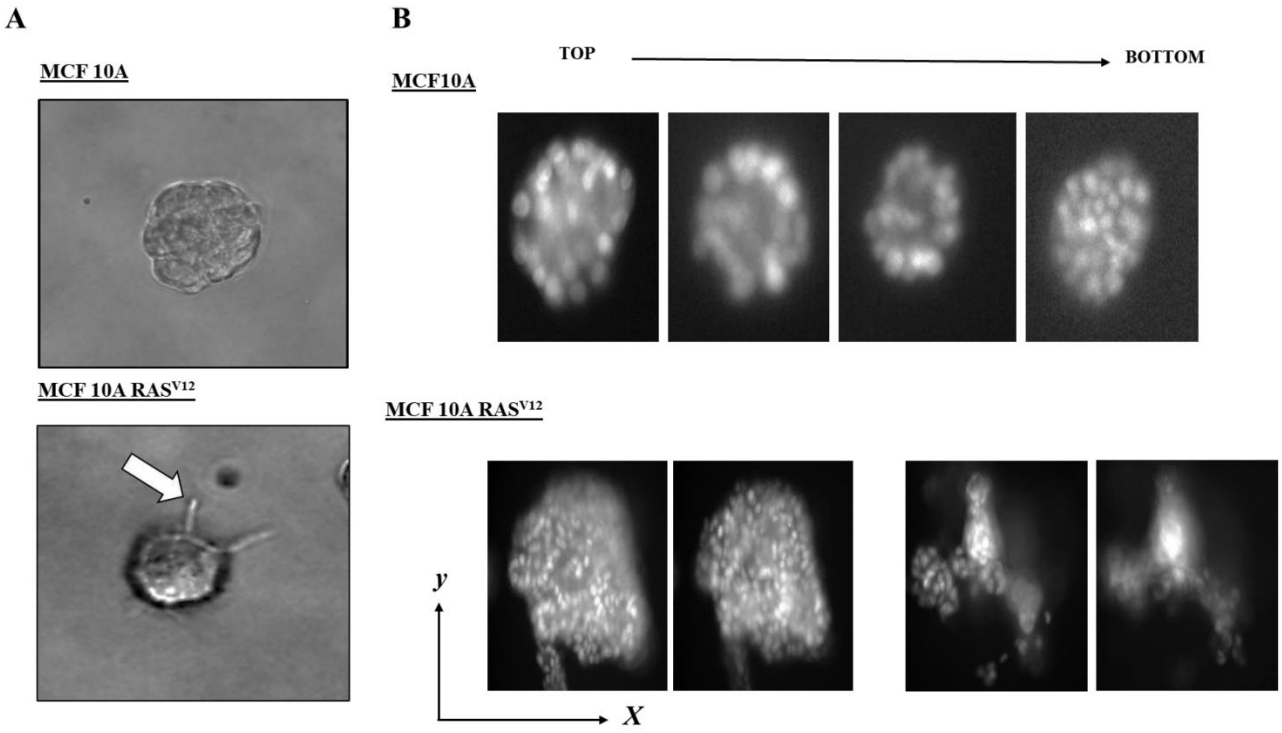


Figure 3-4 The HRAS^{V12} induces an aggressive and invasive phenotype during acini development.

(A) When cultured in a 3-D reconstituted basement membrane (Geltrex), the MCF10A non-transformed and HRAS^{V12} transformed control cells formed organised acini structures observed under a microscope with a bright field filter. Ectopic expression of HRAS in the non-transformed cells did not affect the acini structures. In contrast, HRAS^{V12} transformed MCF10A cells exhibited highly disorganised invasive growth observed under a bright-field microscope, with significantly increased acini projections. **(B)** Serial sections of acini structures on the z-axis stained with ethidium bromide revealed that the non-transformed control cells formed acini with a hollow lumen. In contrast, acini created by HRAS^{V12} transformed have a filled lumen and disorganised growth (n=3).

The changes observed in Figure 3-4 were supported by the protein expression changes observed in Figure 3-5. The inclusion of $HRAS^{V12}$ resulted in the downregulation of epithelial marker E-cadherin, a crucial regulator of the cuboidal epithelial shape and cell-to-cell adherence. The loss of E-cadherin facilitates the epithelial structure's collapse and the upregulation of the migratory regulators, such as N-cadherin. The increased N-cadherin expression enables the cells to transition into a migratory phenotype and no longer be bound by epithelial constraints (Figure 3-5C).

As expected, the ectopic expression of the oncogenic $HRAS^{V12}$ in the "normal" (immortalised) mammary epithelial had given rise to phenotypic changes that will enhance its survival. These include the reduction in the critical regulators of the epithelial cell as these attributes do not lend themselves to invasiveness. This model highlights the simple genetic changes that initiate transformation from "normal" to cancer, which by definition, is the ability to migrate beyond their site of origin, and this is achieved by the cells ability to move as in the context of breast cancer.

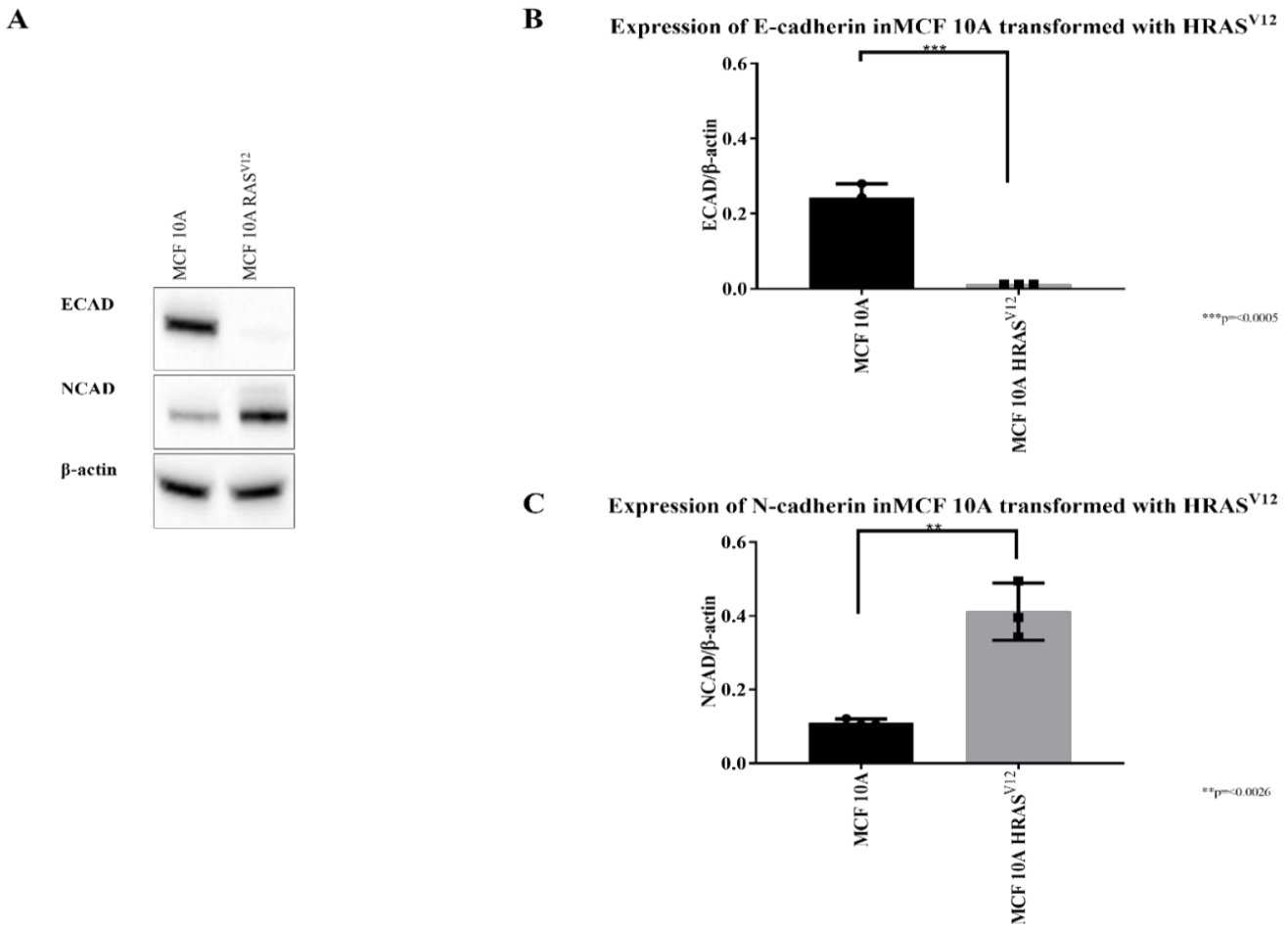


Figure 3-5 Downregulation of epithelial marker E-cadherin by the ectopic expression of $HRAS^{V12}$ in the mammary epithelial cell line

(A) The ectopic expression of $HRAS^{V12}$ alters cellular phenotype from epithelial to mesenchymal, with the down regulation of epithelial marker E-cadherin and up-regulation of the mesenchymal marker N-cadherin. **(B)** The decrease in E-cadherin expression was significantly lower in the MCF10A $HRAS^{V12}$ compared to control (***p=0.0004) **(C)** Significant increase in N-cadherin expression in the MCF10A $HRAS^{V12}$ compared to control (**p=0.0026) (n=3, ±SD, $p<0.05$ t-test)

3.3.4 MCF10A HRAS^{V12} acini upregulate autophagy and autophagy-related genes.

Microarray analysis was carried out to determine if the ectopic expression of HRAS^{V12} resulted in changes in the mRNA expression of autophagic genes during oncogenic transformation. The MCF10A and MCF10A HRAS^{V12} cell lines were grown in three-dimensional cell culture in Figure 3-4 to form acini and collected on day 12. The acini underwent RNA extraction and subsequent gene array analysis. The array was conducted with all samples collected in triplicate using three different RNA samples for each sample, with the significant difference for each gene determined by combining the data from the three arrays. It should be noted that all experimentation for this was performed previously in the lab by Dr Chau Nguyen.

For this study, the results were interrogated for autophagic and autophagic related genes from the upregulation group of at least two-fold increase between MCF10A control and MCF10A HRAS^{V12} groups. The list of autophagic genes identified included 55, as listed in Figure 3-6, and HRAS (highlighted yellow) was included as a reference gene to bring the total of genes represented in Figure 3-6 56 genes. The gene array supports a genetic landscape of increased autophagic activity in response to the ectopic expression of HRAS$^{V12.}$

The gene array identifies an upregulation in autophagic pathways, and this increase is a consequence of the inclusion of HRAS^{V12}. Suggesting the HRAS^{V12} requires autophagy to facilitate the oncogenic transformation compared to the “normal” counterpart. It should be emphasised that the gene changes observed (Figure 3-6) may not confer these same changes at a protein level and will be examined further to understand the implications of these significant genetic changes.

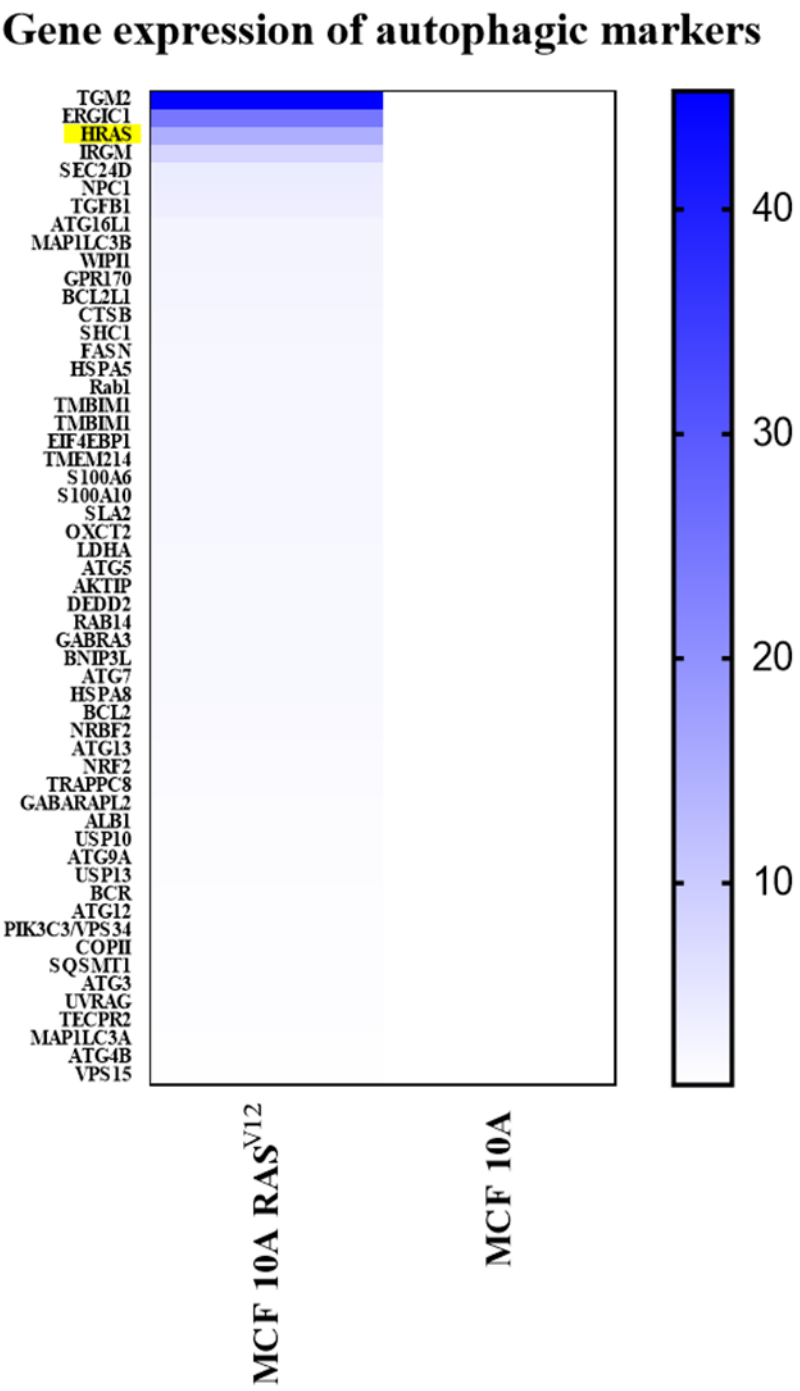


Figure 3-6 Gene analysis of MCF10A HRAS^{V12} increases many autophagic-related genes.

Gene expression microarray analysis revealed that a total of 56 autophagy or autophagy-related genes to be upregulated in HRAS^{V12} transformed cells compared to non-transformed control. HRAS highlighted in yellow is a reference gene of expression levels for comparison to other included genes

3.3.5 Autophagic markers LC3 show increased expression and activity in the $HRAS^{V12}$ transformed MCF10A compared to the non-transformed MCF10A.

To explore the importance of $HRAS^{V12}$ mutation in the regulation of autophagy, protein lysate from MCF10A and MCF10A $HRAS^{V12}$ was collected and analysed by western blot. The analysis focused on vital autophagic markers LC3-I and LC3-II. To determine the presence of autophagic activity, or more accurately, autophagosome formation, the level of expression of the autophagic marker LC3 in its precursor (LC3-I) and active (LC3-II) forms (note the antibody targets all LC3 isoforms) by western blot analysis was performed as depicted in Figure 3-7. The ratio of LC3-II to LC3-I was determined to reveal the presence and level of autophagosome formation in cell lines (Figure 3-7 A and B). Ectopic expression of $HRAS^{V12}$ results in the presence of LC3-II, which is the conjugated form of LC3-I that occurs in response to phagophore formation and is suggested to be responsible for its maturation to the autophagosome [421-423]. This experiment controls for environmental stress by culturing cells under normoxic conditions and adding fresh media four hours before lysate collection to prevent nutrient deprivation. This measurable LC3-II to LC3-I ratio was only exhibited in the mutated cell line during basal condition; the same was not observed in the control cell line suggesting a stress environment requiring autophagic activity, which was not observed in the MCF10A control cells. To validate these findings, the same experiment was performed with the inclusion of starvation media to induce autophagy, as demonstrated in Figure 3-7 B. The starvation media is Hanks buffered salt solution with minimal glucose and serum added as described in Chapter 2. The starvation media is applied for four hours before cell lysate collection is performed, as this is the well-established time point required to induce autophagy (specifically macroautophagy) [424]. The result from the starved samples displayed the presence of LC3-II to LC3-I in both the $HRAS^{V12}$ and control cell lines. Interestingly, the ratio was similar for both cell lines but as expected in increased levels in $HRAS^{V12}$ in basal compared to starved conditions.

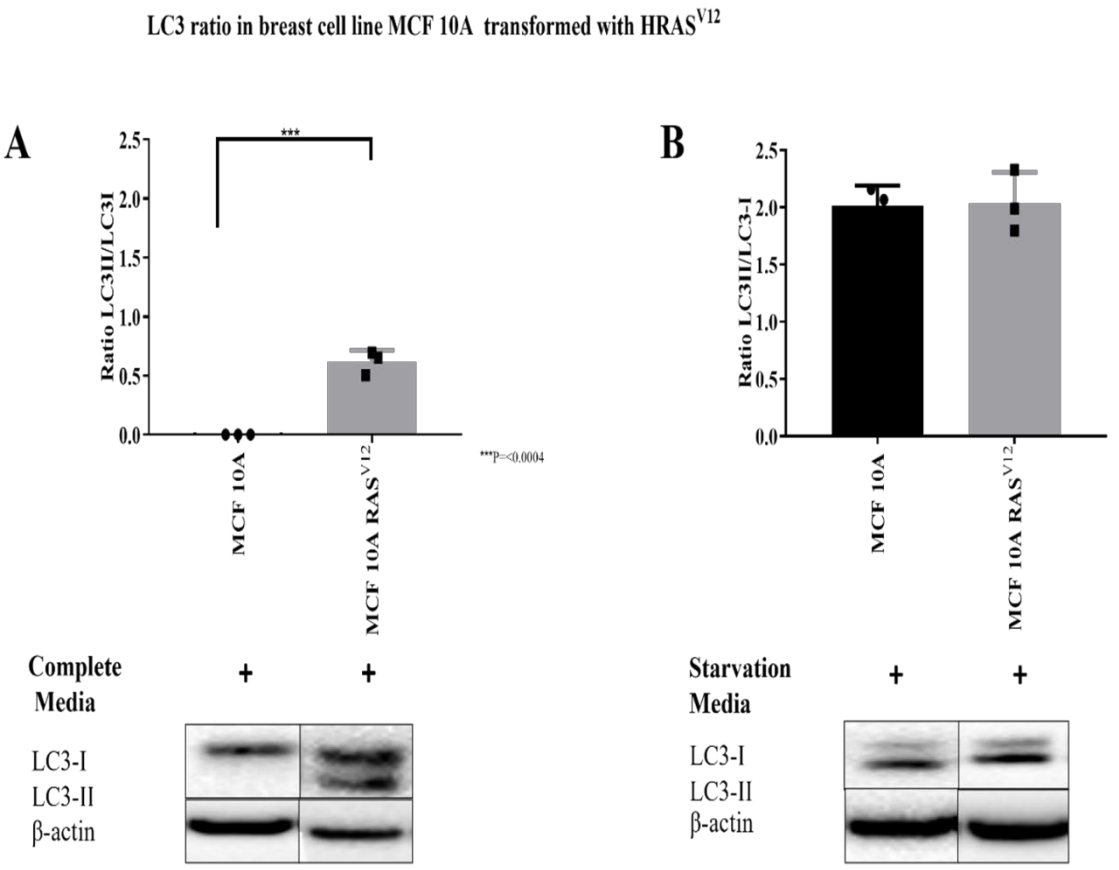


Figure 3-7 Oncogenic transformation with HRAS^{V12} induces autophagosome formation at the basal state

(A) Western blot analysis revealed that autophagosome formation was only present in the MCF10A with ectopic expression of HRAS^{V12} as indicated by the LC3-I to LC3-II ratio (***p=0.0004) **(B)** The addition of nutrient deprivation through the use of starvation media identified LC3-I and LC3-II presence in both MCF10A and MCF10A HRAS^{V12} (n=3, ±SD, $p<0.05$ t-test)

To clarify the expected observations of LC3-II levels in different environmental conditions, a schematic representation has been included in Figure 3-8. As presented in Figure 3-8, under basal state, there should be an equilibrium between LC3-I and LC3-II. The inclusion of stressors, particularly nutritional deprivation and hypoxia, will lead to an increase in levels of LC3-II. Hence, all experiments are controlled by culturing cells under normoxic conditions and adding fresh media four hours before lysate collection to prevent nutrient deprivation. Furthermore, LC3-II/autophagy activity can be explicitly identified by including a lysosomal inhibitor such as Bafilomycin A1 (or Chloroquine or Ammonia Chloride) to the cell culture to prevent fusion of the lysosome and autophagosome. The consequence is that it prevents degradation of LC3-II located on the luminal side of the autophagosome membrane allowing the rate at which LC3-II is being processed to be measured to determine its turnover indicating functionality

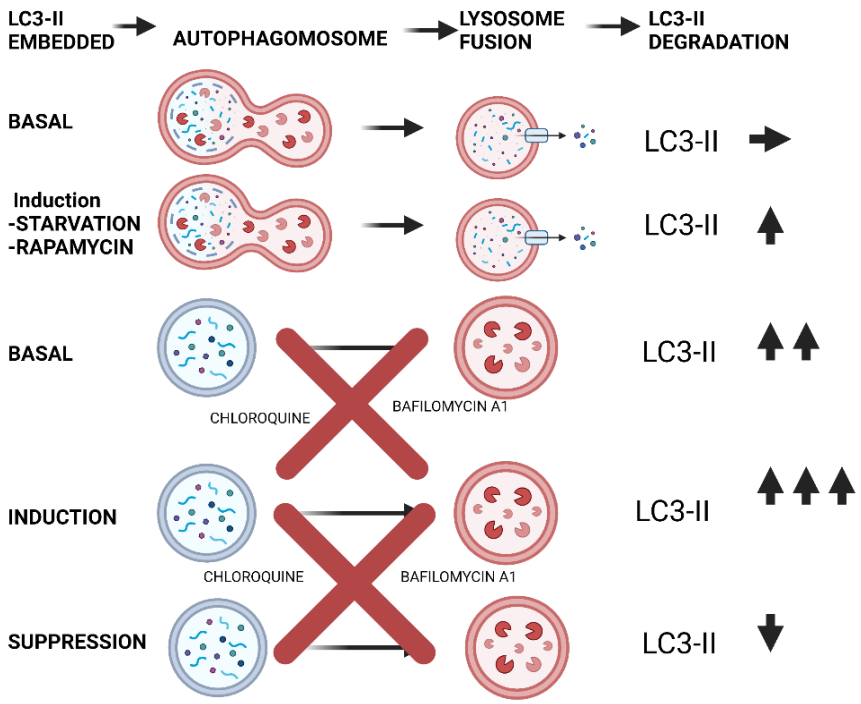


Figure 3-8 Schematic of expected LC3-II levels

Schematic diagram explaining LC3-II turnover, which in standard autophagy processing LC3-II is decreased after the autophagosome and lysosome fuse. Thus, blocking the lysosome with inhibitors, such as Chloroquine or Bafilomycin A1, will result in increased levels of LC3-II under basal conditions and increase further when autophagy has been induced. However, if autophagy is suppressed due to dysregulation, then the level of LC3-II will not increase.(It is worth noting all turnover experiments is this thesis utilise antibodies that probe for all LC3 isoforms.

Created with BioRender.com

Further investigations were undertaken to examine autophagic activity in the MCF10A model; this time, autophagy was induced using rapamycin. In Figure 3-9, the turnover of LC3-II is examined as a measure of activity and is measured by blocking the lysosome to prevent LC3-II degradation. The difference between the level of LC3-II levels with and without lysosome inhibition is calculated to establish the turnover rate. Therefore, it is expected that the LC3-II levels will increase compared to the LC3-II levels without the inhibitor, and they should increase further with an autophagic activator such as Rapamycin. The data in Figure 3-9 clearly shows this activity is significantly increased during basal conditions in $HRAS^{V12}$ and is further increased with activation. These results (Figure 3-6 to Figure 3-9) suggest that autophagy fulfils some requirements for transformation under the control of RAS signalling, proposed to be nutrition, aggregate degradation, defunct organelle removal, or a combination of all.

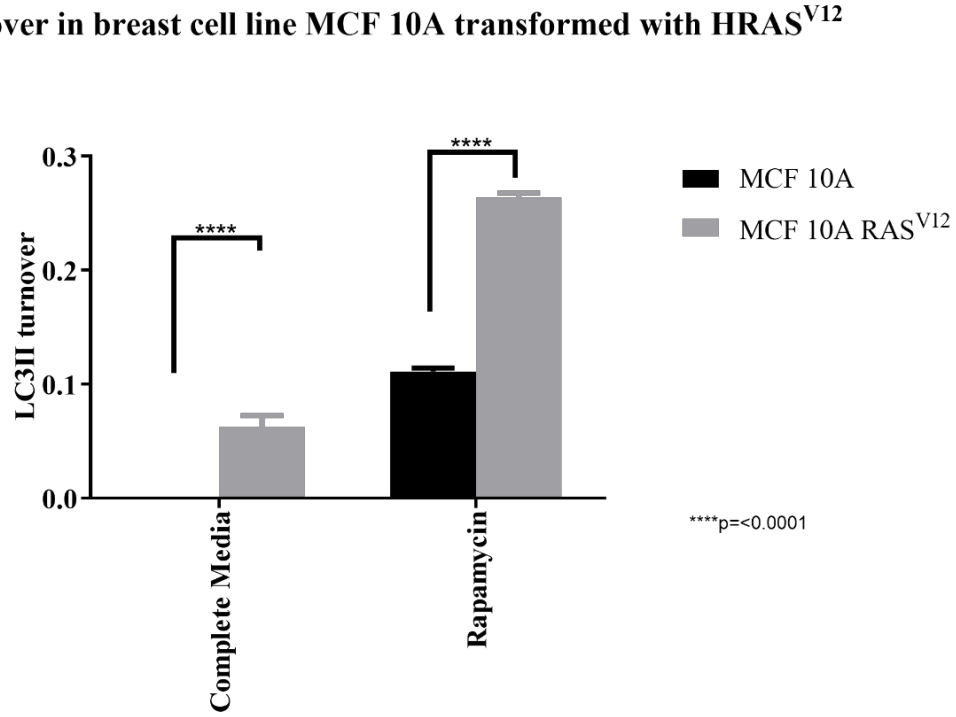


Figure 3-9 The ectopic expression of $HRAS^{V12}$ upregulates autophagic activity.

The expression of $HRAS^{V12}$ significantly correlated with an increase in LC3 turnover (refer above) in both basal conditions and during autophagic induction with rapamycin (10nM) and Bafilomycin A1 (25nM) for lysosomal inhibition (****p=<0.0001) (n=3, ±SD, p<0.05 ANOVA and Sidak's post hoc test)

3.3.6 The HRAS^{V12}transformation increased P62 expression at basal conditions compared to MCF10A control cells.

To identify if these observed increases in autophagic processing resulted from the specific type of cargo, such as aggrephagy, which targets and removes an accumulation of protein aggregates. P62/SQSMT1was examined as it is a critical molecule in aggrephagy; it is a ubiquitinated protein that binds to protein aggregates, allowing for interaction between LC3-II and P62/SQSMT1 and protein aggregate. This interaction with LC3-II facilitates protein aggregate's targeted inclusion into the phagophore membrane by binding with LC3-II within the inner membrane [425]. It should be noted that P62/SQSMT1 has roles in the Nrf-2-Keap-1 pathway, where P62/SQSMT1 is shown to stabilise Nrf-2 through its inactivation of Keap-1; as a consequence, Nrf-2 can be translocated to the nucleus where it initiates the transcription of genes to protect the cell from oxidative or electrophilic stress [426]. However, a specific phosphorylation site on P62 indicates its autophagic activity at serine 403 [427]. The changes observed in P62/SQSMT1 lysate from the MCF10A model were probed for phosphorylation site serine 349, which is specific to the Nrf2-Keap-1 axis. When probed by western blot, no band was present at this phosphorylation site, so this data was not included. Figure 3-10 A shows an increase in phosphorylation site serine 403 when HRAS^{V12} is included; change is observed in both treatment conditions, complete media, and starvation. We examined this P62/SQSMT1 expression further with treatment to induce autophagic, with P62/SQSMT1 known to be increased in starvation conditions, particularly in the “normal” cellular context (Figure 3-10B).

Interestingly, the actual turnover rates were much higher in the MCF10A than in MCF10A HRAS^{V12,} but when an activator (rapamycin at 10nM) and a lysosomal blocker (Bafilomycin A1 at 25nM) were added, there were equal amounts of P62/SQSMT1 expressed between groups. It suggests that even though there is an increase, there is not an equal proportion of degradation with the inclusion of HRAS^{V12}; it is proposed that either the autophagic process can not keep up with demand, given that it is a rate-limiting process. However, alternatively, the abundance of P62/SQSMT1 could result from P62 binding to Keap-1 independent of phosphorylation site 349 as there were no changes in Nrf-2 or Keap-1 observed (data not shown). Recent evidence suggests that the P62 and

Keap-1 interaction is degraded via autophagy, so this significant increase in P62 may reflect that it is active in autophagy and Nrf-2 stabilisation in parallel.

In conclusion, although P62/SQSMT1 specific to autophagy/aggrephagy is found to increase, these levels did not correlate with a simultaneous increase in the turnover rate of P62. It indicates no concomitant increase in autophagic activity to meet this demand irrespective of the increases in P62 at an mRNA and protein expression level. It was found to decrease compared to control; whether this is due to rate limiting mechanisms or subsequent interactions with the Nrf-2-Keap-1 is yet to be established

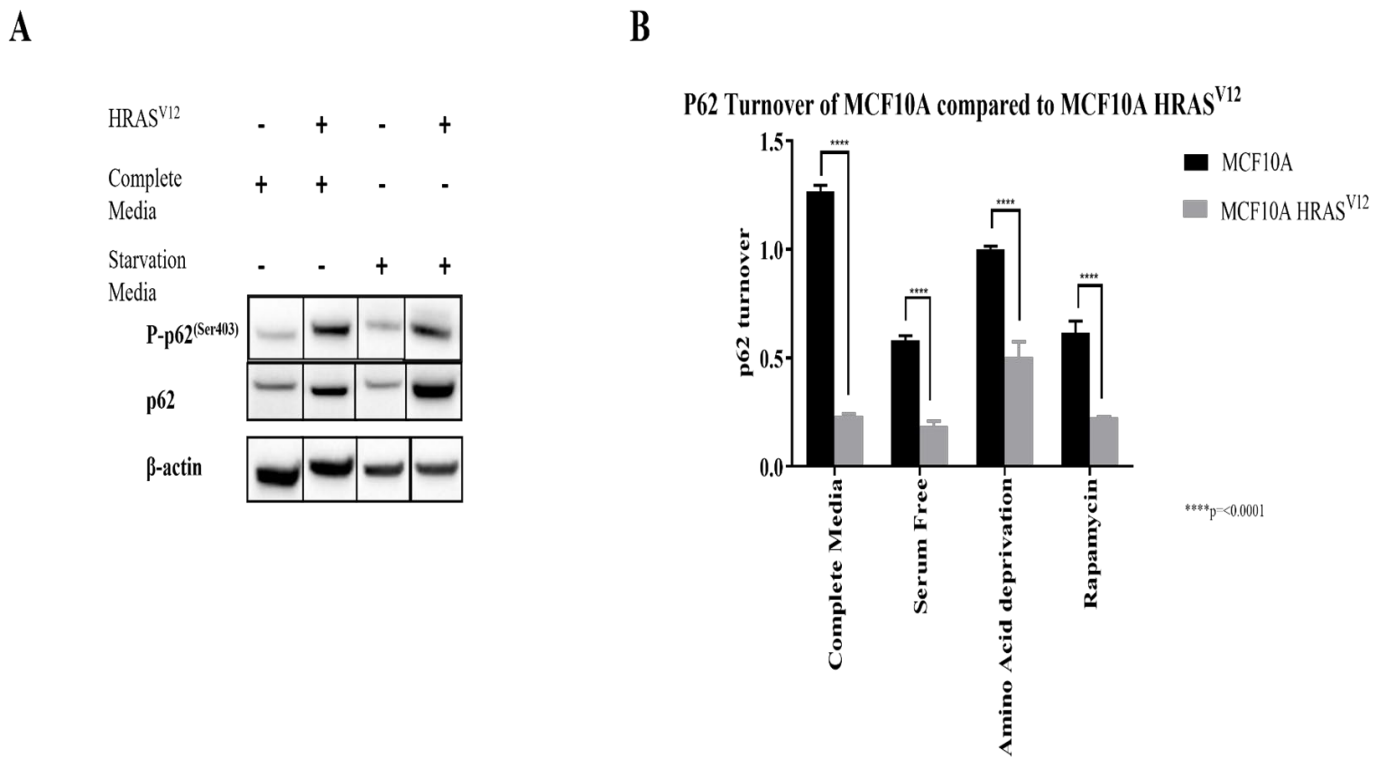


Figure 3-10 P62 expression and phosphorylation specific to autophagy were increased in the HRAS^{V12} expressing cell line

(A) Ectopic expression of HRAS^{V12} upregulated levels of phosphorylated P62 and total P62. In contrast, non-transformed control had no impact on the whole and phosphorylated and overall levels of this protein (n=3). **(B)** Ectopic expression of HRAS^{V12} significantly decreased the turnover rates of P62 in the transformed cells in all treatment conditions compared to the non-transformed control except during blockade of P62 breakdown. (****p=<0.0001) (n=3, ±SD, $p<0.05$ ANOVA and Sidak's post hoc test)

3.3.7 The expression of HRAS^{V12} alters LC3 isoforms and orthologue turnover rate.

The MCF10A model was further exposed to autophagic activators including rapamycin, amino acid deprivation, starvation and autophagic activity was halted with Bafilomycin A1. The protein lysate was collected from the MCF10A and the MCF10A HRAS^{V12} and probed for the LC3 isoforms LC3 A, B and C, orthologues Gabarap1, P62 and phosphorylation site p-P62$^{ser\ 403}$ and ATG16L (Figure 3-11). The rationale for examining these markers is to validate the gene array findings, which were reflected. Interestingly, the expression was constant in both groups regardless of treatment, except in the amino acid deprivation, which decreased consistently in all three replicates (Figure 3-11B). It is speculated that the increased presence of ATG16L is required to facilitate the lipidation of LC3-I to LC3-II. It is worth noting that LC3C did not result in bands for either group, so data was not included.

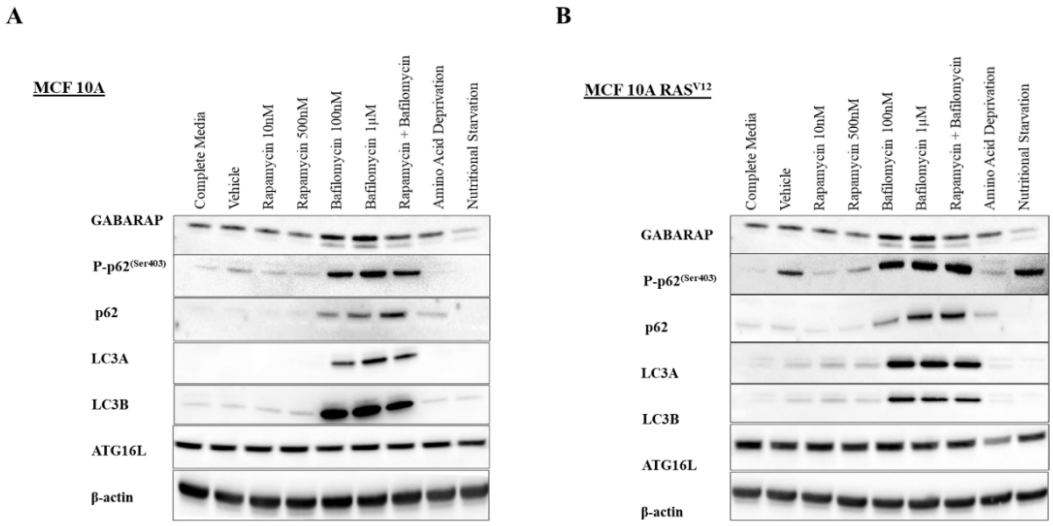


Figure 3-11 The expression of LC3 isoforms and autophagic markers are similar between MCF10A and MCF10A HRAS^{V12} in response to activation and inhibition.

(A) Western blot analysis revealed that non-transformed cells increased levels of LC3 in both its precursor form LC3-I (upper band) and conjugated active form LC3-II (lower band). LC3B-II with Bafilomycin treatment in a dose-dependent manner, with LC3B-I present during all other conditions. **(B)** Cells transformed by HRAS^{V12} showed increased levels of LC3A-II (II=bottom band), ATG16L and phosphorylated P62. Also, ectopic expression of HRAS^{V12} expressed both bands I and II in both the isoforms, LC3A and LC3B, in all treatment conditions (n=3).

3.3.8 EGF induced morphological changes to indicate the epithelial to mesenchymal transition in breast cancer cell line MDA-MB-468.

The relationship between autophagy and RAS activation was examined, rather than mutant RAS, as RAS hyperactivation rather than mutation is more commonly observed in breast cancer. An in *vitro* model was utilised, including the basal cell line MDA-MB-468. The MDA-MB-468 has an upregulated EGFR receptor expression due to an amplification [428]. The downstream target in response to the activation of the EGFR receptor via the binding of EGF is the RAS-MAPK axis [429, 430]. Therefore, the MDA-MB-468 cell line in the presence of the EGF ligand stimulates RAS hyperactivation and facilitates the transition from an epithelial to mesenchymal phenotype. The epithelial to mesenchymal transition (EMT) confers survival advantages to the cancer cell by allowing dedifferentiation to a phenotype that enables plasticity, migratory and invasive attributes which aides survival and metastasis [431, 432]. These morphological changes can visually assess the model's validity, as per Figure 3-12. The cells display a distinct cellular change from a cuboidal to spindle-like morphology with the addition of EGF.

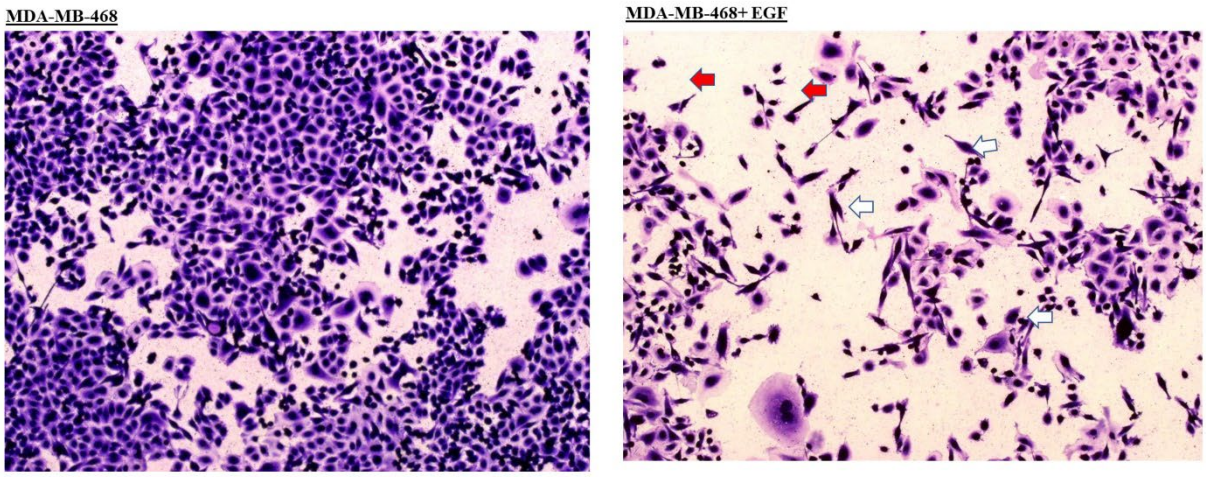


Figure 3-12 The inclusion of epidermal growth factor (EGF) cause MDA-MB-468 cells to transition from epithelial to mesenchymal phenotype.

The addition of 50ng/ml EGF ligand to the culture media of the MDA-MB-468 cell line results in a transition of cellular morphology from an epithelial to mesenchymal phenotype. The image shows the appearance of the spindle-like morphology as represented by the arrows (white) and the rounded morphology of the cells with increased plasticity represented by the arrows (red) (n=3).

These observed morphological changes are due to the loss of the epithelial marker E-cadherin (ECAD) and a synchronised upregulation of mesenchymal markers vimentin (Figure 3-13 A-C). The epithelial marker ECAD decreases in a response dose-dependently to EGF addition (Figure 3-13 B). Conversely, the mesenchymal marker vimentin increases dose-dependently to EGF addition (Figure 3-13 C). The results have shown that the MDA-MB-468 model transitions from an epithelial to mesenchymal phenotype in response to EGF inclusion, as shown by others [433, 434].

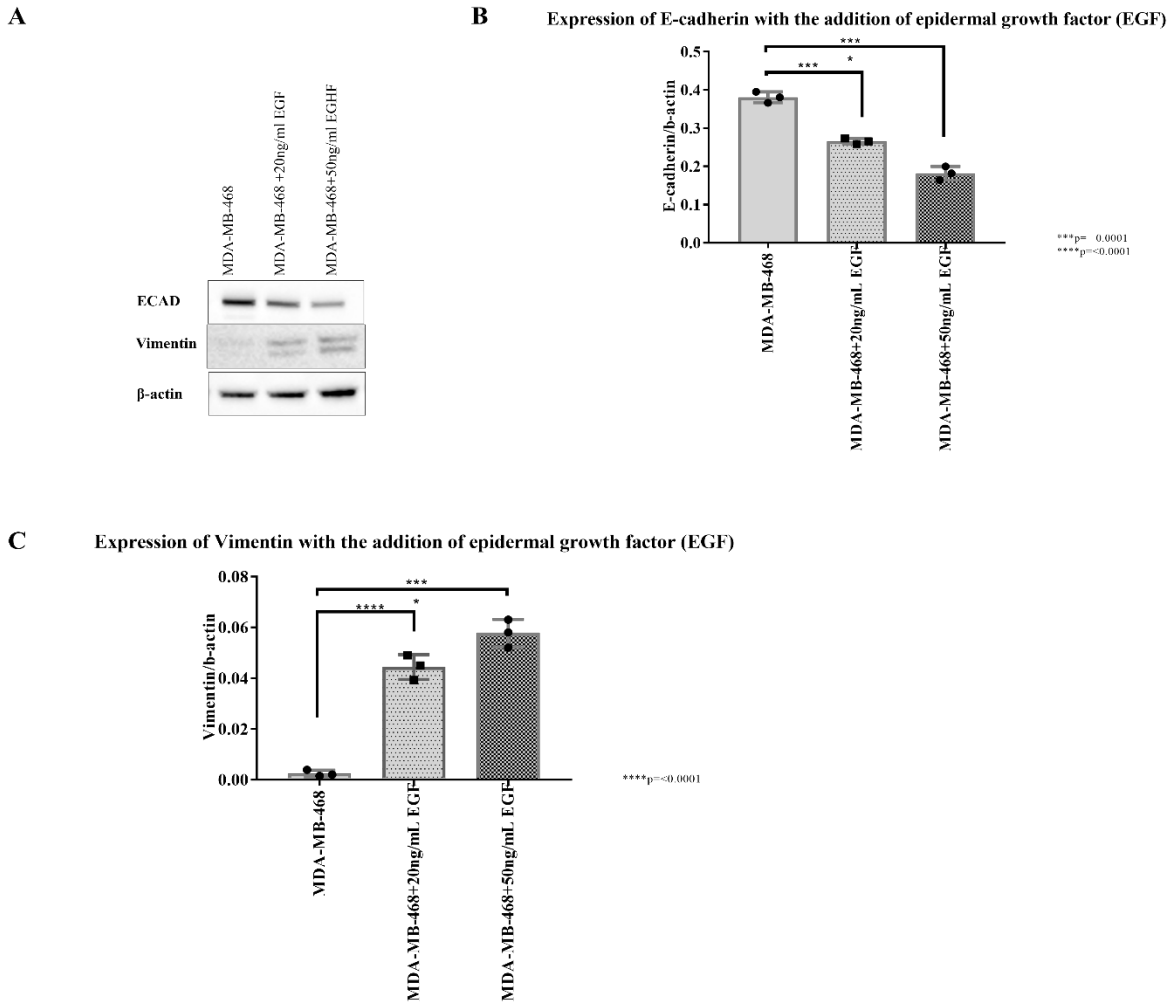


Figure 3-13 Epithelial marker E-cadherin decrease, and mesenchymal marker vimentin increase to EGF addition.

(A) In response to epidermal growth factor (EGF), the MDA-MB-468 cell line downregulates the epithelial marker E-cadherin and upregulates mesenchymal marker vimentin (***p=0.0001, ****p=<0.0001) **(B).** The protein expression levels of E-cadherin are significantly reduced in a dose-dependent response to EGF (****p=<0.0001)**(C).** The expression of vimentin was significantly increased dose-dependently to EGF addition (n=3, ±SD, $p<0.05$ ANOVA and Tukey's post hoc test)

3.3.9 The expression of autophagic markers increased during RAS activation in the EMT breast cancer model.

RAS activation was studied to determine its effects on autophagy markers and autophagic function. The MDA-MB-468 breast cancer cell line was exposed to EGF, activating RAS and facilitating the changes required to undergo the epithelial to mesenchymal transition. Figure 3-14 A shows that Gabarap1 expression decreased in response to EGF. In contrast, there remained no change in the expression of the Gabarap2 in response to the addition of EGF. Furthermore, although no change in the Gabarap2 isoform was observed in response to EGF, its expression level was maintained in all treatment groups (Figure 3-14A).

Interestingly the expression of LC3B increased dose-dependently to EGF expression in both the lipidated form LC3-II and precursor form LC3-I, suggesting an increase in autophagosome formation. Furthermore, this increase in expression of LC3-II was shown to increase the rate of LC3 turnover, indicating that this increase in protein expression is reciprocated in autophagic functionality (Figure 3-14B). However, the expression of the LC3A isoform reduced its expression as the dose of EGF increased (Figure 3-14A).

The turnover rate of LC3-II, which indicates autophagic flux, was observed to increase with EGF treatment. However, the turnover rate of the MDA-MB-468 +EGF was reduced by adding rapamycin, suggesting that the activity is at capacity and inclusion of the autophagic activator results in dysfunction rather than an increase in autophagic activity (Figure 3-14 B). In comparison, the MDA-MB-468 cell line without EGF presented the expected response; a slight increase in turnover rate was observed with the inclusion of rapamycin (Figure 3-14 B). Thus, the results revealed increased autophagic activity and marker expression in response to EGF. Given that EGF is responsible for RAS activation, it is proposed that RAS may rely on autophagy for its activity.

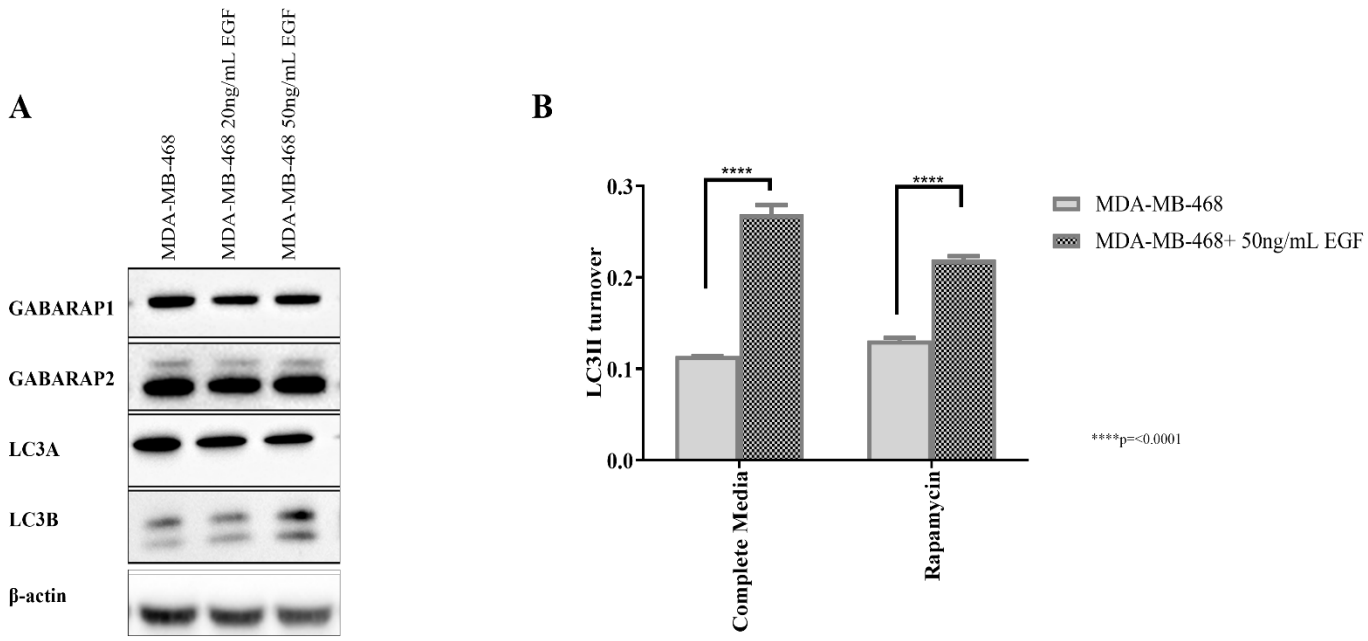


Figure 3-14 Autophagic marker LC3 increase in a dose-dependent response to EGF addition.

(A) The LC3 isoform expression differed in response to EGF; the LC3A isoform decreases, whereas the LC3B isoform increases; in contrast, the orthologues Gabarap are not changed or decline their expression **(B)** The LC3 turnover (refer to Figure 3-8) rates increase with the addition of EGF and are indicative of increased autophagic activity (treatments rapamycin 10nM and bafilomycin A1 25nM)(****p=<0.0001) (n=3, ±SD, $p<0.05$ ANOVA and Sidaks post hoc test)

3.3.10 The turnover rates of P62 suggest that during the epithelial to mesenchymal transition, its role shifts NRF2 and KEAP1 pathways.

To determine if aggrephagy contributed to the increased autophagic activity observed in the MDA-MB-468 breast cancer cell model. The cells were exposed to treatments to activate autophagy with the chemical inducer rapamycin and to block the autophagic process at the lysosome with the agent Bafilomycin A1. The cell lysate collected after treatment was probed for P62, from which the turnover rate was calculated. At basal levels, the rate of P62 turnover was equivalent in both the MDA-MB-468 cell line and the MDA-MB-468 cell line with EGF (Figure 3-15). Thus, indicating the addition of EGF in complete media does not change the rate at which P62 is utilised and suggests that the role is conserved. Furthermore, rapamycin's treatment resulting in a decline in turnover rate is similar to those observed in the MCF10A $HRAS^{V12}$ model (Figure 3-10). Therefore, there was no evidence to conclude that these changes were reflected in the NRF2 pathway as expected. In this context, it indicates a potential change in the loss of P62-induced autophagy in response to rapamycin (10nM).

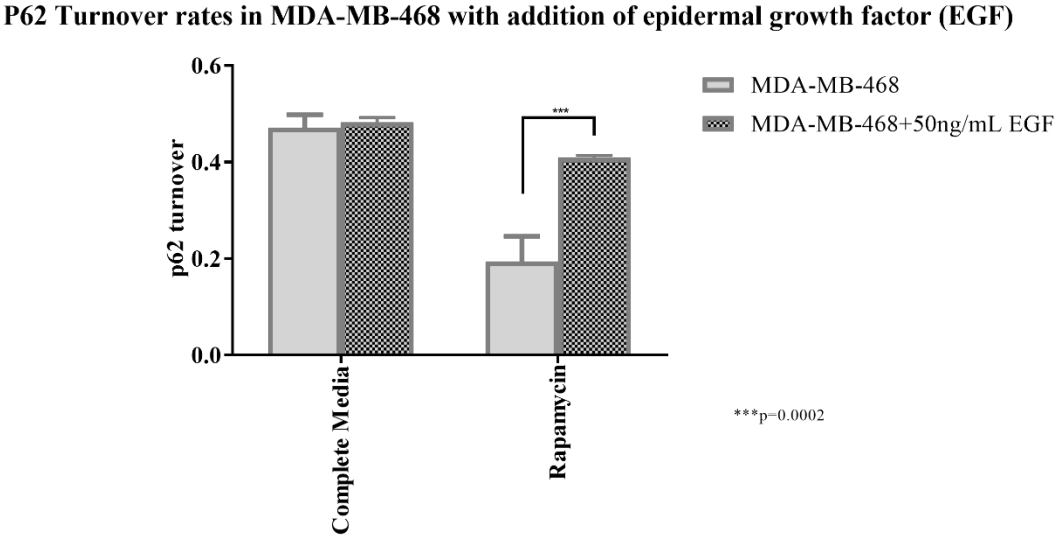


Figure 3-15 P62 turnover rates vary between MDA-MB-468 and MDA-MB-468 with EGF at basal state and autophagic activation.

The turnover rate of P62 is similar at basal conditions but decreases in response to rapamycin treatment, with a significant difference between groups with the inclusion of EGF increasing the turnover rate compared to control. However, there are less total P62 in the MDA-MB-468 plus EGF in this pathway compared to control (***p=0.0002) (n=3, ±SD, $p<0.05$ ANOVA and Sidak's post hoc test)(Rap=10nM & Baf25nM)

3.3.11 The expression profile of LC3 isoforms and orthologues does not change but enhances with the addition of EGF.

The expression profile of LC3 isoforms and orthologues was examined in the MDA-MB-468 and MDA-MB-468 with EGF breast cancer cell lines to determine the effects of RAS activation upon LC3 family members (Figure 3-16). The cell lines were exposed to treatment with chemical agents Bafilomycin A1 and rapamycin, an autophagic inhibitor and activator, respectively. The biological autophagic inducers, amino acid deprivation, nutritional starvation for comparison at basal conditions, and vehicle control were also included. After treatment, cell lysate was collected and probed for various autophagic markers.

The expression level of the LC3 orthologue Gabarap was similar between MDA-MB-468 and MDA-MB-468 with EGF; there was a decline in expression in response to all concentrations of rapamycin (Figure 3-16). These changes were also observed in the nutritional starvation group, which is expected given that the pathway and mechanism involved in activating autophagy are the same. P62 exhibits variations between the groups with higher levels in the MDA-MB-468 with EGF, and the expression is consistent across all treatments with a slight decrease with rapamycin and a slight increase with Bafilomycin A1 (Figure 3-16). The expression of LC3A was only observed in the Bafilomycin A1 treatment in the MDA-MB-468 cell line; in contrast, there was LC3A present in more treatments in the MDA-MB-468 with EGF. These findings are similar to those observed in the MCF10A RAS (Figure 3-11), with a higher expression of LC3A isoform, suggesting LC3A expression may be correlated with RAS activity. LC3B is more prevalent than any of the LC3 isoforms in both groups; however, the presence of LC3B is observed in all rapamycin treatments in the MDA-MB-468 with EGF not observed in the MDA-MB-468 cell line group (Figure 3-16).

Interestingly there is a lack of expression in amino acid deprivation and nutrient starvation in the MDA-MB-468 with EGF similar to MCF10A RAS (Figure 3-11), further supporting the hypothesis that RAS increases basal levels to such that upon biological induction, this activity becomes defunct due to maximal capacity being exceeded

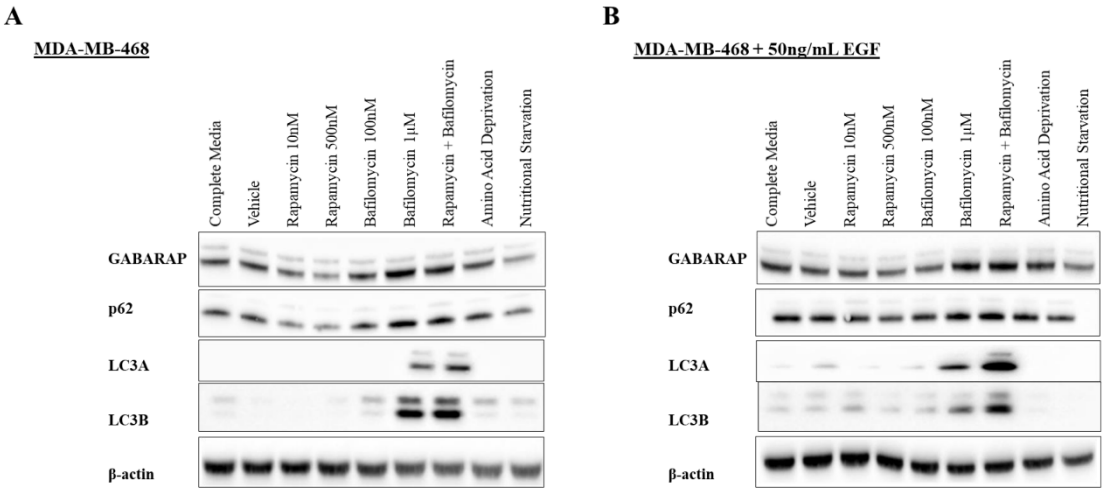


Figure 3-16 The expression of LC3 isoforms and orthologue increased with the inclusion of EGF.

(A) Western blot analysis revealed that MDA-MB-468 cells increased levels of LC3B-II and LC3A-II with Bafilomycin A1 treatment in a dose-dependent manner. Note LC3 has two forms its precursor form LC3-I (upper band) and conjugated active form LC3-II (lower band). **(B)** With the addition of EGF, cells increased levels of LC3B-II in all conditions except for amino acid deprivation and nutritional starvation. Also, LC3A-II was expressed similarly to LC3B (n=3).

3.3.12 Increased expression of LC3-II to LC3-I ratio under basal conditions in TNBC subtypes with RAS Mutation.

To investigate autophagic activity concerning RAS mutations in breast cancer cells line. This section of the chapter will primarily focus on the oncogenic cell lines T47D (LA), Hs578T (TNB) and MDA-MB-231 (TNB) from the previously illustrated RAS progression panel (Figure 3-1).

In the micrograph images in Figure 3-17, the morphology of the T47D cell line is cuboidal and presents an epithelial structure growing together and adherent. Conversely, the Hs578T and MDA-MB-231 cells present a spindle-like morphology; they lack cellular connections and demonstrate independent growth. These were further verified by western blot analysis (refer to APPENDIX II). In addition, the proliferation rate is observed to be slower in the T47D than in the Hs578T and MDA-MB-231

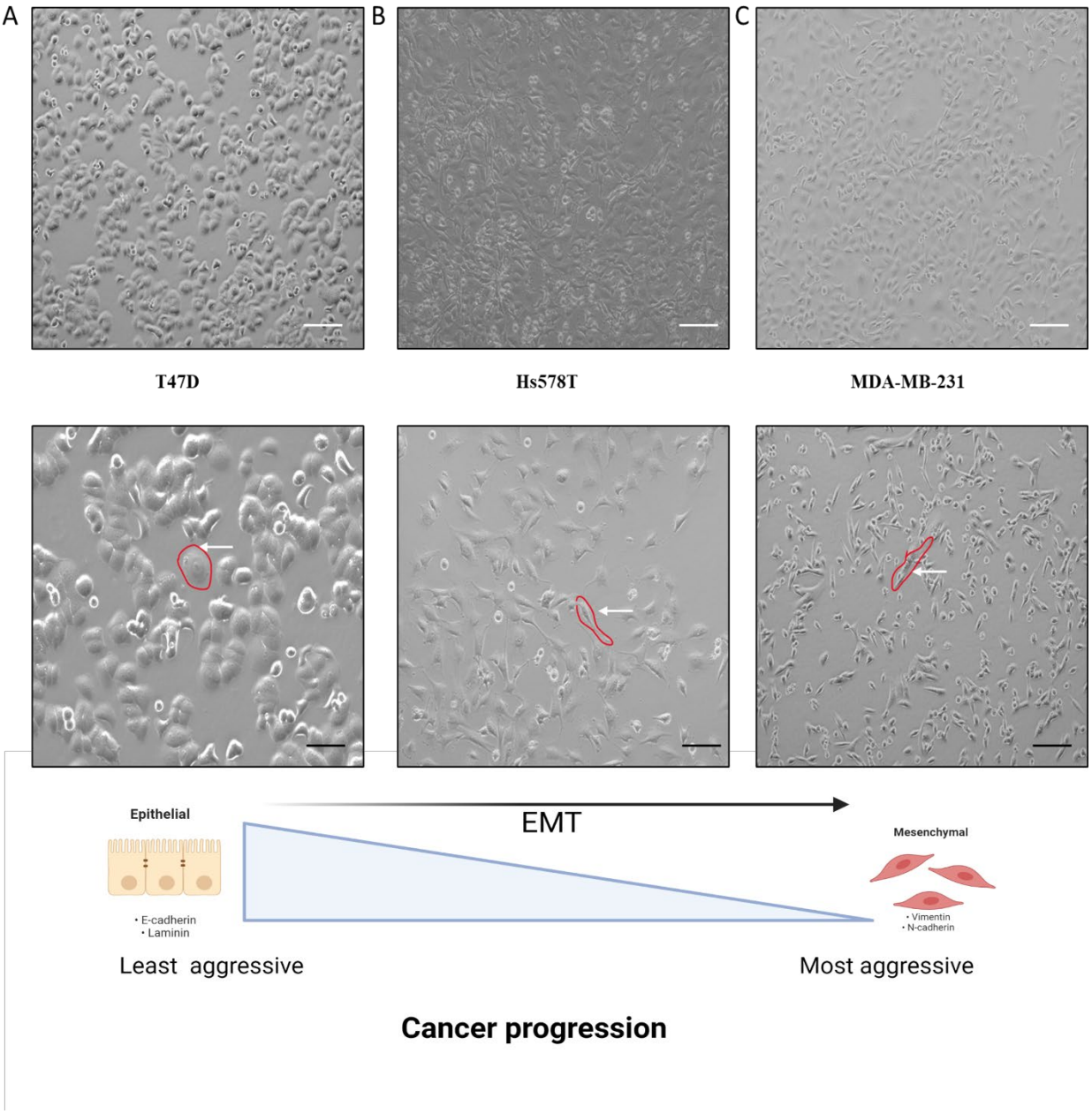


Figure 3-17 Morphological differences between luminal and triple-negative breast cancer subtypes.

Micrograph images were taken with a phase-contrast filter of the breast cancer cell lines to represent the cellular morphology of T47D (LA), Hs578T (TNB) and MDA-MB-231 (TNB), red outline and arrow highlighting the distinct cellular shape and features. The T47D cell line features an epithelial phenotype; in contrast, as the breast cancer cell progresses, it presents a distinct mesenchymal phenotype. Which has been described in the schematic demonstrating the morphological changes from epithelial to mesenchymal (EMT) and how these parallel with a more aggressive phenotype Images taken at X100 and X200 magnification (white scale bar= 100µm and black scale bar= 50 µm)

3.3.13 LC3-II levels and turnover are significantly different between breast cancer subtypes

As mentioned earlier, the study narrowed its focus to the oncogenic cell lines T47D, Hs578T and MDA-MB-231. As displayed in earlier data (Figure 3-2 and Figure 3-3), there was a significant increase in LC3-II in the basal B (TNB) subtypes, with RAS mutation, which included the Hs578T and MDA-MB-231 cell lines, compared to luminal A (LA) subtype, with RAS WT which was included the T47D cell line. Indicating a rise in elongation and maturation of the autophagosome in the more aggressive phenotypes

This part of the study will examine this further, and as shown in Figure 3-18, the ratio of LC3-II to LC3-I was significantly higher in the Hs578T and MDA-MB-468 cell lines compared to T47D. This increase of LC3-II suggests increased autophagosome formation but does not indicate activity. So next, the turnover rate was examined to determine autophagic processing. As mentioned, this is assessed using the lysosomal inhibitor Bafilomycin A1 to prevent LC3-II degradation. Therefore, it is expected that the LC3-II levels will increase compared to the LC3-II levels without the inhibitor, and they should increase further when an autophagic activator such as rapamycin is utilised. The results show a decrease in turnover rate in both the TNB cell lines with the RAS mutation; this was observed in both conditions, although the MDA-MB-231 turnover rate increased slightly with rapamycin treatment. The T47D cell line reflects expected results (Figure 3-18 B). It suggests that both the TNB cell lines with the mutant RAS suppress autophagic processing in the early or later stages. Curiously, rapamycin did not restore the turnover rate suggesting in at least the case of the MDA-MB-231 cell line that the suppression may be at the earlier stages as rapamycin acts on MTOR providing initiation support.

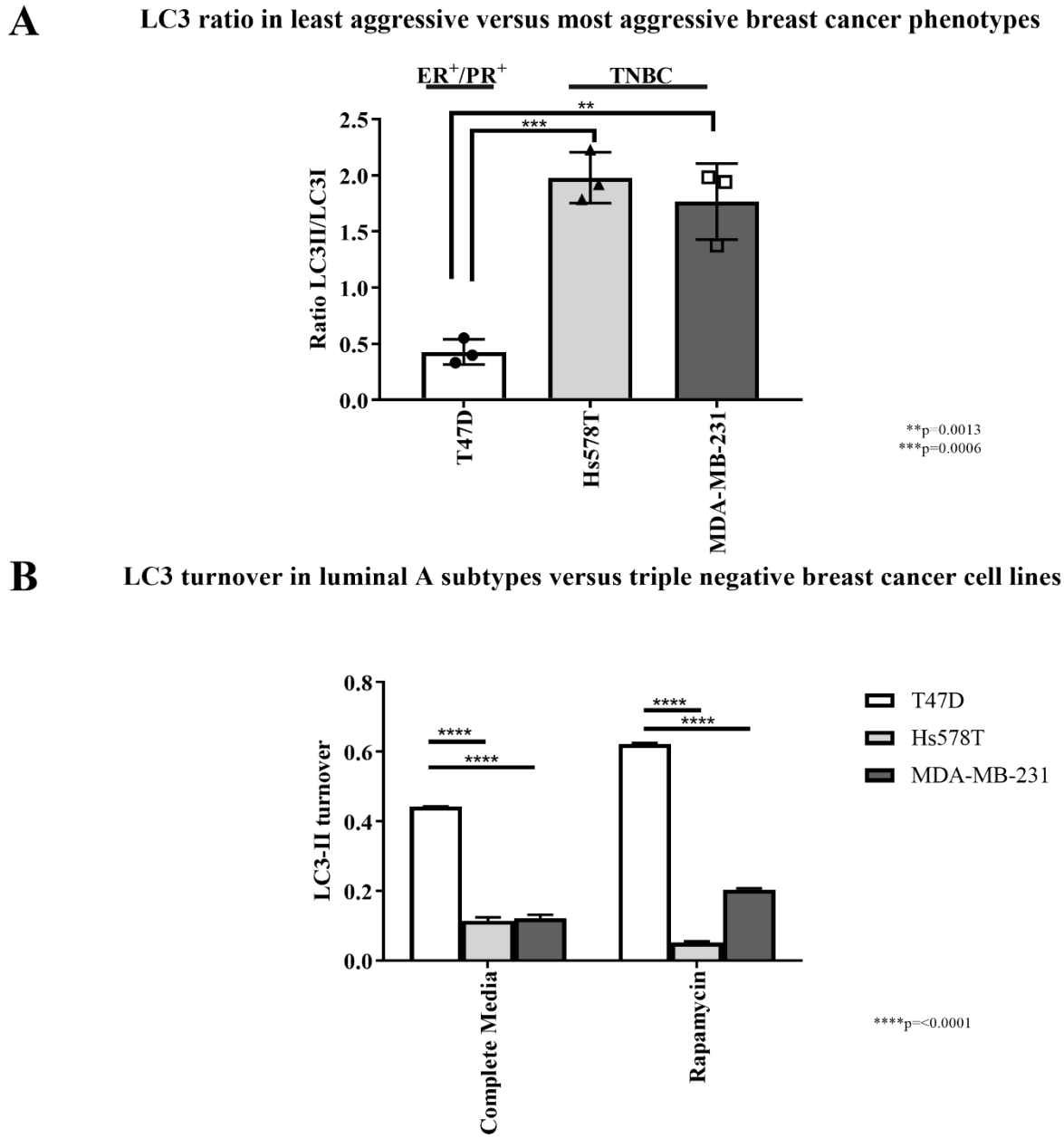


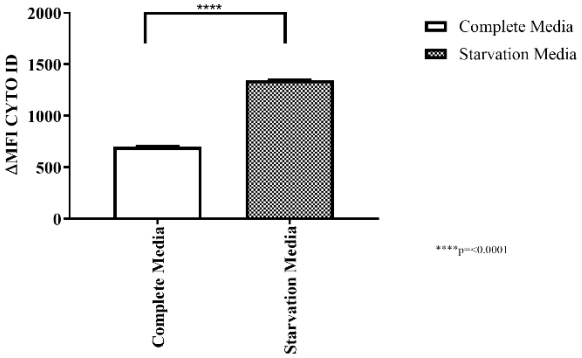
Figure 3-18 LC3-II turnover is decreased in the more aggressive breast cancer phenotypes

(A) The ratio of LC3-II active form compared to LC3-I, the precursor, significantly increased in the triple-negative (TNB) compared to the luminal A (LA) subtype. Indicating there is an increase in autophagosome formation. (**p=0.0013, ***p=0.0006) **(B)** The LC3-II turnover (refer to Figure 3-8) rates significantly decrease in the triple-negative subtypes at basal conditions and with rapamycin (10nM) treatment as an autophagic activator and bafilomycin A1(25nM) as a lysosomal inhibitor (****p=<0.0001) (n=3, ±SD, p<0.05 ANOVA and Sidak's post hoc test)

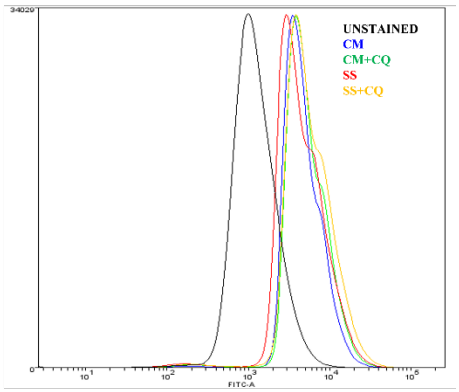
3.3.14 Autophagic flux becomes dysregulated in the more aggressive phenotypes in response to nutrient stress.

To further examine autophagic functionality or autophagic processing, the autophagic flux was measured in T47D, Hs578T and MDA-MB-231 oncogenic cell lines. To measure this, an amphiphilic tracer dye targeted to LC3-II examines autophagic activity in intact cells in real-time through flow cytometry, as described in Chapter 2. Autophagic flux is measured by the mean fluorescent intensity (MFI) of cells with numerous treatment conditions with or without the lysosomal inhibitor chloroquine (CQ at 5μM). As previously described, adding chloroquine to cells inhibits the lysosome, thus preventing the degradation of LC3-II, resulting in an overall increased fluorescent intensity. The difference between the two samples, i.e. with or without chloroquine, determines fluxation, also referred to as the delta mean fluorescence intensity (ΔMFI). As observed in Figure 3-19, the T47D breast cancer cells displayed an active autophagic process with a positive autophagic flux at basal levels, and this was observed to increase under starvation conditions as expected. At the same time, the fluorescent intensity increased with chloroquine treatment which is also expected as LC3-II can not be degraded (Figure 3-19).

A



B



C

T47D	
CONDITION	**MEAN FLUORESCENT INTENSITY (MFI)**
UNSTAINED	1493
COMPLETE MEDIA (CM)	5476
COMPLETE MEDIA + CHLOROQUINE (CQ)	6177
STARVATION MEDIA (SS)	5533
STARVATION MEDIA+ CHLOROQUINE(CQ)	6879

D

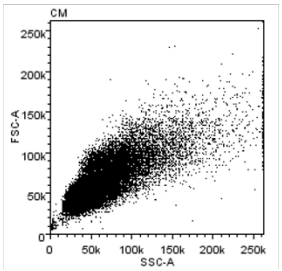
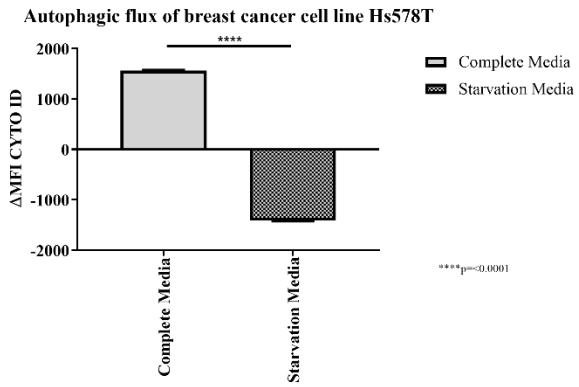


Figure 3-19 Autophagic flux of T47D breast cancer cell line

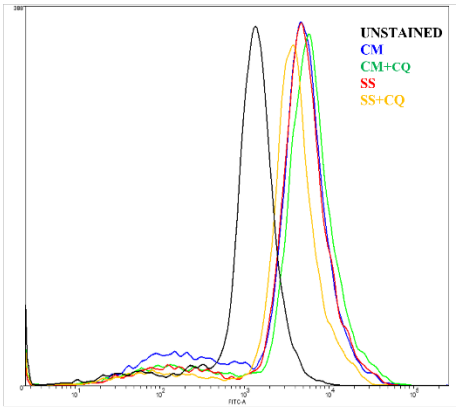
Autophagic flux in luminal A subtype is determined with an amphiphilic tracer dye used in the flow cytometry platform to measure mean fluorescent intensity (MFI). To establish flux, a ΔMFI was calculated (ΔMFI=MFI(+CQ)-MFI(-CQ)). **(A)** ΔMFI of T47Dbreast cancer cell line under basal and starvation conditions (****p=<0.0001) **(B)** Representative FACS plot of all treatment conditions **(C)** Mean fluorescent intensity readings for all conditions with and without lysosomal inhibitor (CQ) for the T47D cell line. **(D)**. Representative forward and side scatter dot plot for T47D breast cancer cell line(n=3, ±SD, p<0.05 t-test)

As with the T47D cells, the Hs578T (Figure 3-20) and MDA-MB-231 (Figure 3-21) breast cancer cell lines exhibited a positive difference in fluorescent intensity at basal conditions representative of functioning autophagy which also further increased with the addition of chloroquine (Figure 3-20 C Figure 3-21 C). However, exposure of these cells to stress, in this instance, nutritional deprivation, resulted in a suppression of autophagic flux (Figure 3-20 A and Figure 3-21 A). The fluorescent intensity levels of the cells show that autophagic activity is unexpectedly lower in these cell types during starvation. Moreover, adding chloroquine (CQ) reduced the mean intensity further during starvation, implying that autophagic flux is suppressed. The reasons suggested could be the result of an increase in production of LC3-II beyond the rate at which it can be degraded, but if we look at basal conditions, the intensity is higher, so this theory does not hold unless LC3-II is being utilised elsewhere or degraded via other mechanisms or in these conditions, the cleavage of LC3-I to LC3-II is halted. Alternatively, it may reflect a lysosomal dysfunction or treatment response to CQ, particularly in the Hs578T cell line (Figure 3-20). However, the MDA-MB-231 cell line specifically displayed a reduction in mean intensity with or without CQ, suggesting that the capacity for autophagic processing can not be maintained with the standard autophagic induction ques such as starvation in this cellular context. This disturbance to autophagic function may be because the capacity of the autophagic process is already at the maximal rate.

A



B



C

Hs578T	
CONDITION	**MEAN FLUORESCENT INTENSITY (MFI)**
UNSTAINED	1489
COMPLETE MEDIA (CM)	5595
COMPLETE MEDIA + CHLOROQUINE (CQ)	7161
STARVATION MEDIA (SS)	6058
STARVATION MEDIA+ CHLOROQUINE(CQ)	4642

D

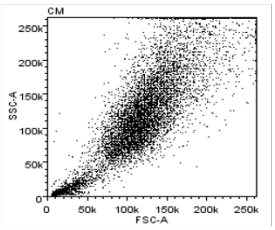
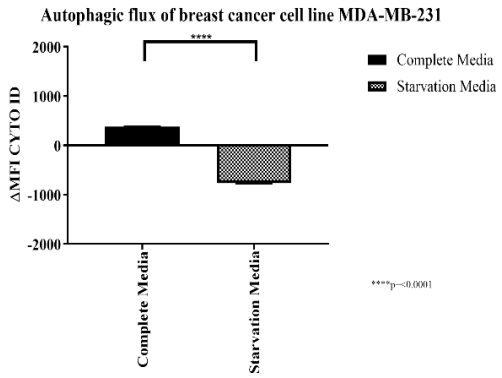


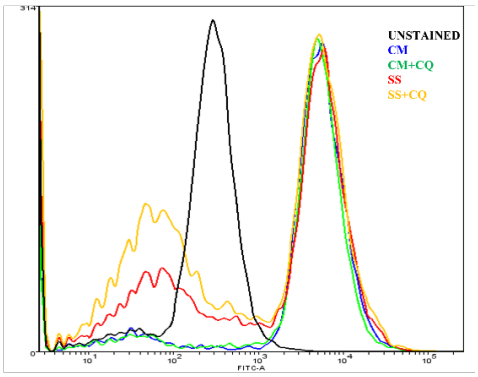
Figure 3-20 Autophagic flux of HS578T breast cancer cell line

Autophagic flux in the triple-negative subtype is determined with an amphiphilic tracer dye used in the flow cytometry platform to measure mean fluorescent intensity (MFI). To establish flux, a ΔMFI was calculated (ΔMFI=MFI(+CQ)-MFI(-CQ)). **(A)** ΔMFI of Hs578T breast cancer cell line under basal and starvation conditions (****p=<0.0001) **(B)** Representative FACS plot of all treatment conditions **(C)** Mean fluorescent intensity readings for all conditions with and without lysosomal inhibitor (CQ) for the Hs578T cell line. **(D).** Representative forward and side scatter dot plot for Hs578T breast cancer cell line (n=3, ±SD, p<0.05 t-test)

A



B



C

MDA-MB-231	
CONDITION	**MEAN FLUORESCENT INTENSITY (MFI)**
UNSTAINED	320
COMPLETE MEDIA (CM)	6200
COMPLETE MEDIA + CHLOROQUINE (CQ)	6579
STARVATION MEDIA (SS)	4650
STARVATION MEDIA+ CHLOROQUINE(CQ)	3880

D

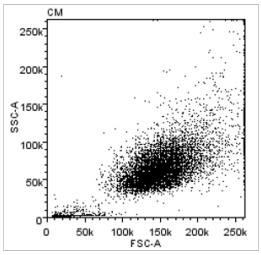


Figure 3-21 Autophagic flux of MDA-MB-231 breast cancer cell line

Autophagic flux in the triple-negative subtype is determined with an amphiphilic tracer dye used in the flow cytometry platform to measure mean fluorescent intensity (MFI). To establish flux, a ΔMFI was calculated (ΔMFI=MFI(+CQ)-MFI(-CQ)). **(A)** ΔMFI of MDA-MB-231breast cancer cell line under basal and starvation conditions (****p=<0.0001) **(B)** Representative FACS plot of all treatment conditions **(C)** Mean fluorescent intensity readings for all conditions with and without lysosomal inhibitor (CQ) for the MDA-MB-231cell line. **(D).** Representative forward and side scatter dot plot for MDA-MB-231breast cancer cell line (n=3, ±SD, p<0.05 t-test).

3.3.15 RAS mutant induced autophagic activity is independent of the autophagy canonical pathway.

To explore the possible molecular pathway utilised to activate autophagy in the context of RAS mutations, breast cancer cell lines were examined for the presence of essential molecules from the canonical pathway. The autophagy canonical pathway is a stepwise process of initiation, nucleation, elongation, maturation, degradation of cargo for recycling by the cell as illustrated below in Figure 3-22 and described in detail in chapter 1.

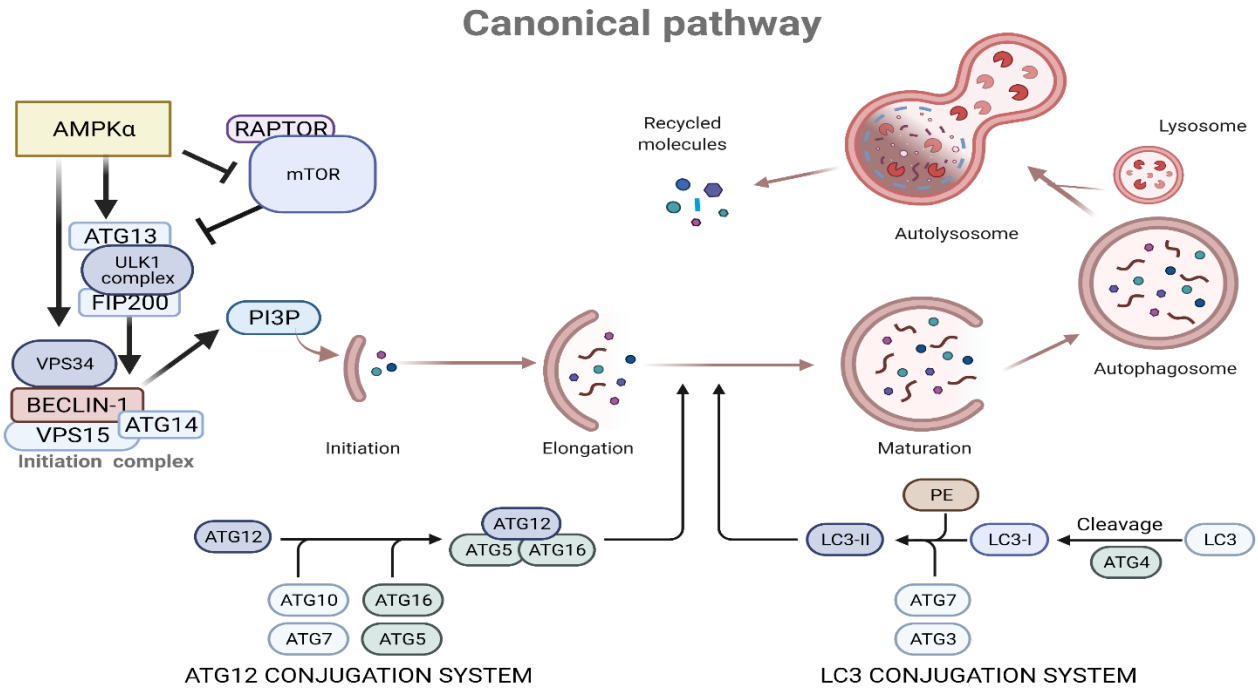


Figure 3-22 Autophagy "Canonical" pathway

Schematic of the canonical pathway in autophagy where stressors such as starvation induce the stepwise process detailed above; AMPK in activated blocking mTOR complex I, ULK1 complex is actioned to act on the initiation complex, or it can be acted on directly by AMPK. The initiation complex recruits PI3P to initiate and nucleate the phagophore, elongation and maturation is regulated by the ATG12 conjugation system, and the LC3 system involves the formation of LC3-II, which is the only ATG to be embedded in the membrane. After which the membrane closes to form the autophagosome, it fuses with the lysosome to form the autolysosome, where contents are degraded into their constituent molecules and released back into the cell to be recycled into metabolic substrates.

Created with BioRender.com

The canonical pathway has well-defined molecules that regulate these steps during this process. Therefore, many of these molecules involved in the canonical pathway were examined by western blot analysis (Figure 3-23A) and quantified by densitometry (Figure 3-23 B). Note that all lysate was collected from cell lines at basal conditions and culture media replenished 4 hours prior to collection.

The data revealed that the T47D cell line had expressed higher levels of the initiation molecules Raptor, ULK 1 as expected if the canonical pathway was utilised. However, in the RAS mutant cell lines, Hs578T and MDA-MB-231 are expressed at a lower level. Furthermore, at the nucleation step, the expression of Beclin-1 is higher in T47D than in Hs578T and MDA-MB-231, although haploinsufficiency of Beclin-1 is common in breast cancer and may account for these decreases. However, the elongation and maturation stage found in ATG7 similarly demonstrated a decline in the MDA-MB-231 cell line compared to T47D and Hs578T, which may reflect a KRAS-specific alteration.

Furthermore, the ATG12, ATG5, ATG 12-5 complex and ATG 16 molecules increased in the RAS mutated cell lines. Corresponding to increases seen in LC3-II, the primary role of these ATGs is to facilitate lipidation of LC3 with the cleavage and addition of a phosphatidylethanolamine (PE) to LC3-I to form LC3-II. There is also evidence to suggest that these ATGs are responsible for the tethering of the phagophore membrane [435], which may explain the increase of LC3 lipidation alone but would also result in ATG 7 having shown the same trend. Collectively, the data from the regulatory molecules (Figure 3-23) suggests that the activation of autophagy is independent of the canonical pathway in the TNBC cell lines.

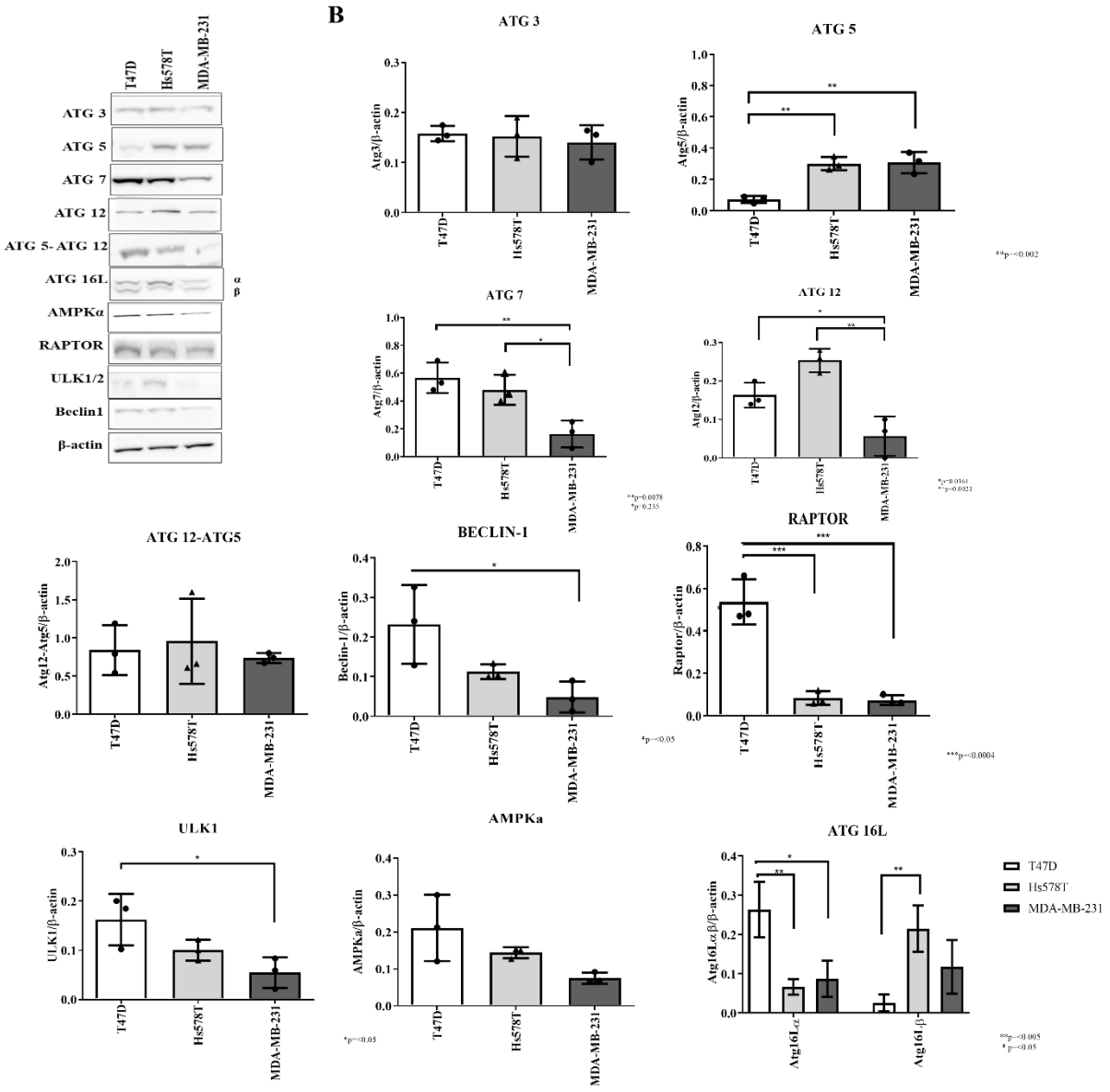


Figure 3-23 Canonical pathway regulators decrease in basal subtypes compared to luminal A.

(A) Western blot images of the canonical pathway molecules display differences in the luminal A cell line T47D compared to basal B cell lines Hs578T and MDA-MB-231 at basal conditions (note basal condition media is refreshed 4 hours before protein lysate collection). **(B)** The densitometry analysis of expression intensity compared to loading control demonstrated that the difference observed in the immunoblot was significant between the sub-types (n=3, ±SD, $p<0.05$ ANOVA and Tukey's post hoc test)

3.3.16 The HRAS mutation in Hs578T results in differential expression of autophagic marker LC3 isoforms and orthologue.

The presence of autophagosome was examined with Cyto ID^{TM} with the FITC filter in the Hs578T breast cancer cell line. These distinct punctae are visible in complete media conditions (Figure 3-24); however, these punctae are not as evident in other treatment groups. The other notable feature is that the addition of 3-methyladenine (3Ma), a PI3KC3/VPS34 inhibitor, was cytotoxic in this setting. Changes in the cell morphology were demonstrated, such as retraction of the cytoplasm and cell membrane indicative of cellular distress and apoptosis. Signs of cellular distress were also noted in cells treated with rapamycin, with definite morphological changes, and the cells are usually large and spindle-like in morphology when untreated (refer to Appendix III). The chloroquine group maintained their regular appearance, but the fluorescent intensity increased, which was expected since CQ is lysosomotropic.

The western blot analysis explored the protein expression of autophagic markers intimately involved in the autophagosome membrane and are activity indicators (Figure 3-25). The results show the Hs578T cell line at basal conditions and in response to treatments including autophagic activators, rapamycin, nutrient deprivation and the autophagic inhibitor chloroquine. Furthermore, the exposure time for treatments was extended compared to the images; treatments were only administered for four hours, whereas the cell lysate was collected at time points up to 24 hours. The lysate was probed for key autophagic markers, including P62 and its autophagic specific site ser403, all LC3 isoforms LC3A, LC3B, LC3C and finally LC3 orthologue Gabarap (Figure 3-25). The data shows an increase in phosphorylated P62 with the addition of 3-methyladenine, likely due to its action on VPS34. The expression of Gabarap was consistently present and slightly increased at 24 hours but was present irrespective of conditions. The LC3 isoform's appearance was unexpected, with the expression of LC3A-I and LC3A-II being higher than LC3B. The LC3B was only expressed as LC3B-II, its active form rather than precursor LC3B-I in all treatments. LC3C was only present as a single band at approximately 14 KD, found to increase at the four-hour time point with the inclusion of chloroquine within complete or nutrient-deprived media, suggesting that it is involved in or within the autophagosome and suggesting why it was not observed in other westerns as it appears to only be present at this earlier time point (Figure 3-25). The variations

observed by the LC3 isoforms may indicate an off-target effect arising with chloroquine and rapamycin after four hours that were identified compared to other lysosomal inhibitors, notably Bafilomycin A1in further studies of this cell line. (chapter 4)

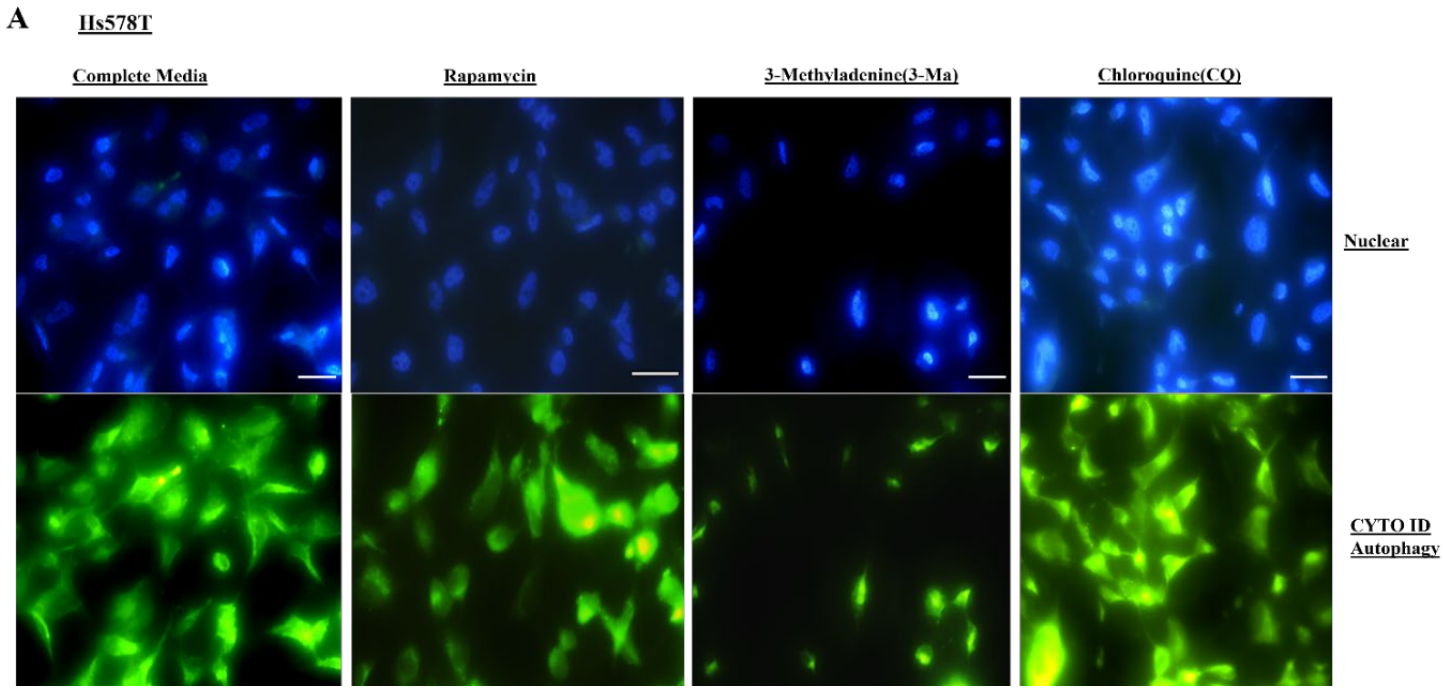


Figure 3-24 LC3 Fluorescence in Hs578T breast cancer cell line

(A) The expression of LC3 appeared punctate and diffuse in all conditions, mainly basal; its appearance declined upon treatment with autophagic activator rapamycin. There was significant cell loss in the 3-methyladenine (3Ma) group. (Scale bar- 100µM)

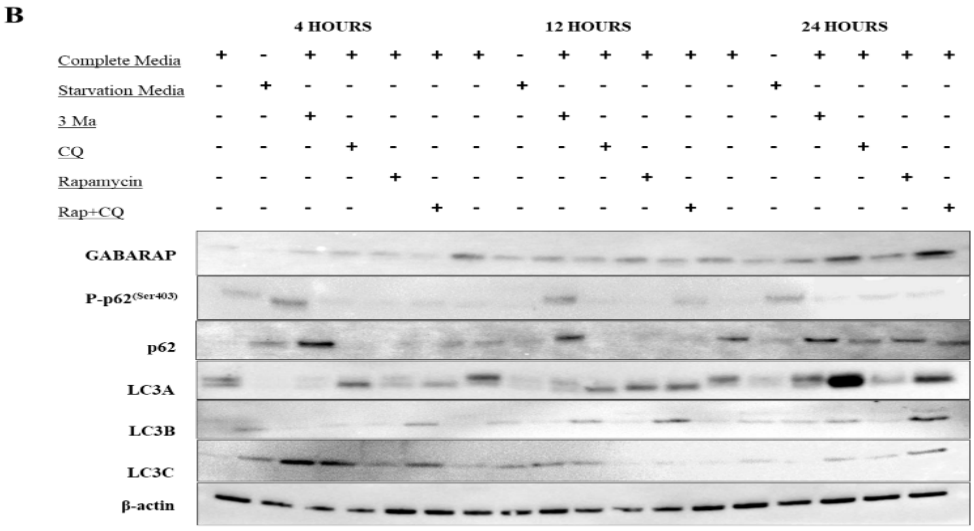


Figure 3-25 There is differential expression of autophagic markers in response to activation and inhibition.

(B) Western blot of protein expression under the same conditions but with time intervals; this LC3 expression is different amongst the isoforms and orthologues. (n=3)

3.3.17 The MDA-MB-231 displays a preferential expression of LC3 isoforms and orthologues.

The effects of KRAS mutation on autophagy, particularly the LC3 isoforms and orthologues, were examined using the MDA-MB-231 breast cancer cell line containing a $KRAS^{G13}$ mutation. The localisation of autophagosomes and autolysosomes was visualised with fluorescent probes (Cyto ID®) using confocal microscopy; the cells presented with a distinct punctate pattern described by others [436-438]. The punctate was observed within the cytoplasm of the cells, and it was notably higher density in complete media, chloroquine and rapamycin treatment groups. (Figure 3-26 A) The punctate appearance is reduced in the 3Ma group and has a different expression pattern it appears to aggregate, suggesting that the inhibition initially causes the autophagic vacuoles to aggregate. Treatment with chloroquine resulted in cellular swelling and indicated the importance of lysosomal degradation in maintaining homeostasis in this cell line (Figure 3-26 A). Although this study is cautious that LC3 punctate may not be reflective of autophagic activity as once determined and as was demonstrated by Runwal et al. [439] (Refer to APPENDIX III for phase-contrast images)

Next, the cell lysate was collected from the MDA-MB-231 cells that had been treated with numerous chemical modulators of autophagy to elicit initiation or/and inhibition of its activity, overset timepoints; four hours, 12 hours and 24 hours. The protein expression of crucial autophagic markers and their isoform were analysed. The analysis found that the expression of P62 was not exceptionally high but peaked during the 12-hour time point irrespective of treatment, which may indicate a rise in aggrephagy that is dependent on time rather than treatment (Figure 3-27B). Furthermore, the LC3A isoform was only expressed in its active form (LC3A-II) at low levels compared to LC3B, which was highly expressed in its precursor and active forms LC3B-I and LC3B-II, respectively.

Similarly, LC3C was expressed at low levels and as a single band at around 14 KD as was also observed in the Hs578T cell line, suggesting the expression of this isoform is not related to autophagic activity as it would be expected to be lipidated and if so, it would be detected at the higher molecular weight. Interestingly, LC3B-II was present with 3Ma treatment at all time points suggesting that LC3B is still being processed even though the initiation complex has been inhibited. Furthermore, the expression increases

and variation in Gabarap closely mimics the expression pattern of LC3B, suggesting that these proteins are intimately linked in this cellular context. Thus, the data in the KRAS context shows that crucial autophagic markers are not acting as expected in the context of a normal cell, suggesting that these changes are a consequence of RAS and that autophagic molecules, mainly LC3, may be downstream targets RAS.

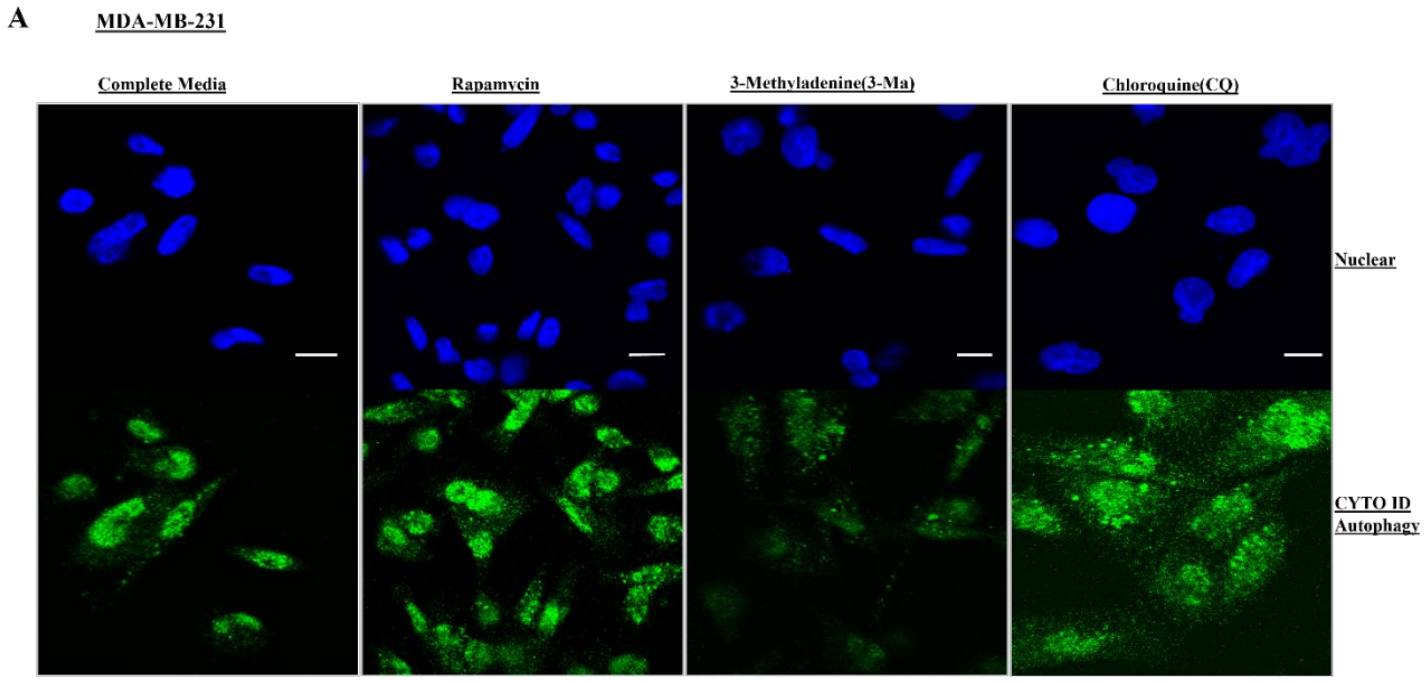


Figure 3-26 LC3 Fluorescence in MDA-MB-231 breast cancer cell line

(A) The expression of LC3 had a distinct punctate appearance that was diffuse within the cytoplasm in complete media and rapamycin groups. With the addition of 3-methyladenine (3Ma) and chloroquine (CQ), the cells have significantly swelled due to treatment, also dense perinuclear staining in the chloroquine group(Scale bar- 100µM)

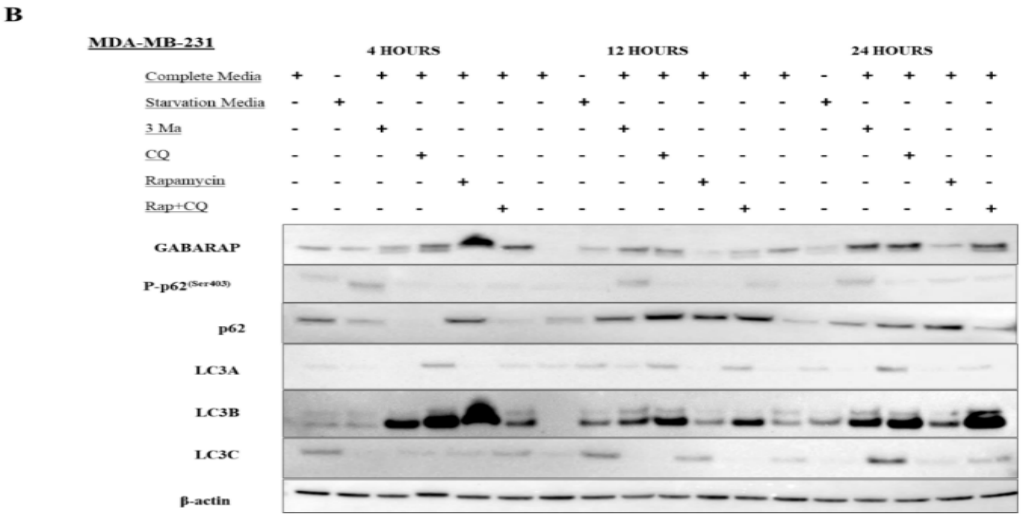


Figure 3-27 There is an unusual expression pattern of LC3 isoforms irrespective of activation or inhibition.

(B) Western blot of protein expression under the same conditions but with time intervals, this LC3 expression is different amongst the isoforms favouring LC3B. (n=3)

3.3.18 The LC3 isoforms inpatient data set indicate a difference in prognosis dependent on the level of the LC3 isoform and orthologue expressed.

The publicly available Kaplan Meier plotter platform was utilised to investigate the correlation between autophagic marker expression and patient outcomes. It has 6,234 samples (breast) available, and analysis is performed with gene chip technology [440, 441]. The data set was interrogated for overall survival (Figure 3-28), relapse-free survival (Figure 3-29) and distant metastasis-free survival (Figure 3-30) in breast cancer patients as a whole for each of the LC3 isoforms. In addition, the prognoses associated with each isoform were examined, and a hazard ratio (HR) for each was indicated. A hazard ratio of greater than one means that the marker is associated with a poor prognosis, and a ratio of less than one means it is associated with a good prognosis. It is important to note that the risk estimate is based on increases in expression; therefore, the hazard ratio is always based on increased expression of the gene of interest. The categories tested were overall survival (OS) which refers to the time a patient survives after their cancer diagnosis. Relapse-free survival (RFS) is the time taken before the sign and symptoms of that cancer remerge after primary cancer treatment has ceased. Distant metastasis-free survival (DMFS) is classified as the period from diagnosis or treatment of cancer to its spread to a secondary site.

Results from overall survival analysis identified significantly different outcomes between LC3B and LC3A and LC3C isoforms, where higher expression of LC3B is associated with poor prognosis compared to higher expression of LC3A and LC3B results in better prognosis, respectively (Figure 3-28 A-C). However, in all remaining survival analysis groups, relapse-free survival (Figure 3-29 A-C) and distant metastasis-free survival (Figure 3-30 A-C), the same significant trend was observed: an increased expression of LC3B was a poorer prognostic indicator. Alternatively, LC3A and LC3C were highly expressed and correlated with better outcomes in breast cancer patients (A-C).

Overall Survival (OS)

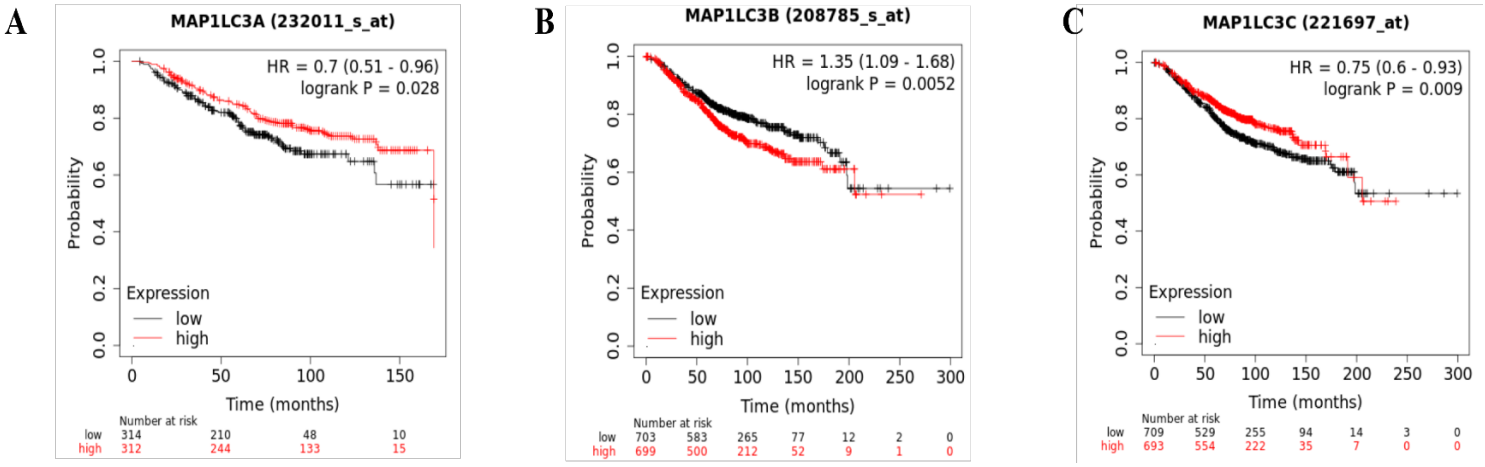


Figure 3-28 The LC3 isoforms confer different overall survival prognoses in breast cancer patients

(A) High LC3A isoform significantly correlated with better OS **(B)** LC3B isoform expression correlates with high expression and poor OS **(C)**The LC3C isoform significantly correlates with high expression and better prognosis in OS

Relapse Free Survival (RFS)

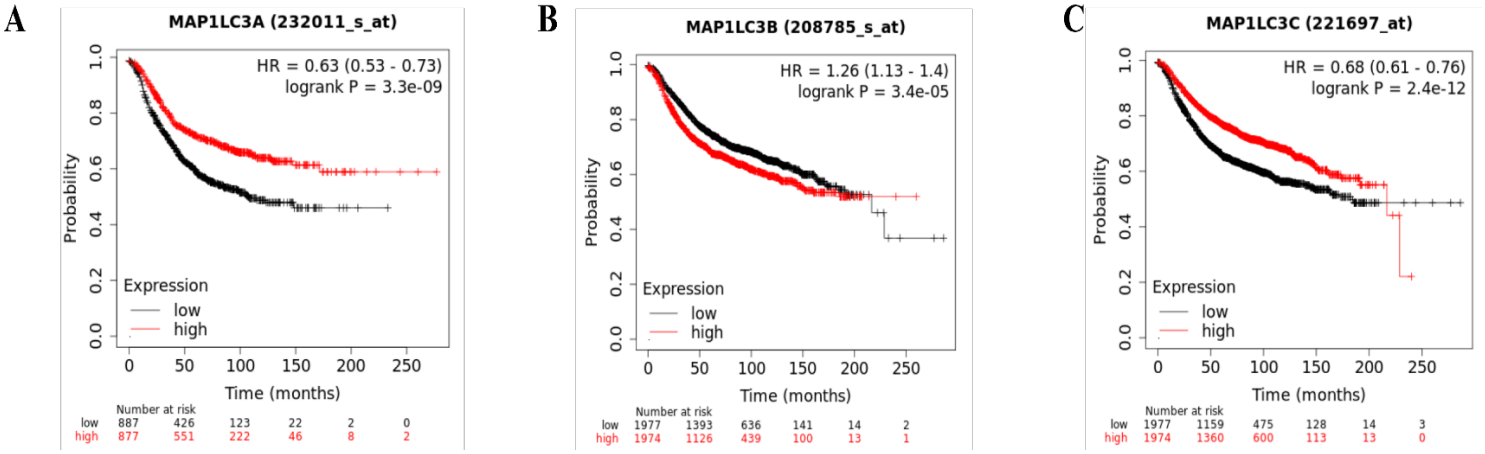


Figure 3-29 The LC3 isoforms have a differential effect on relapse-free survival in breast cancer patients

(A) The high expression of LC3A significantly correlates with improved RFS. **(B)** The high expression of LC3B significantly correlates with a poor prognostic marker of RFS **(C).** The LC3C isoform correlates with high expression and improved patient RFS.

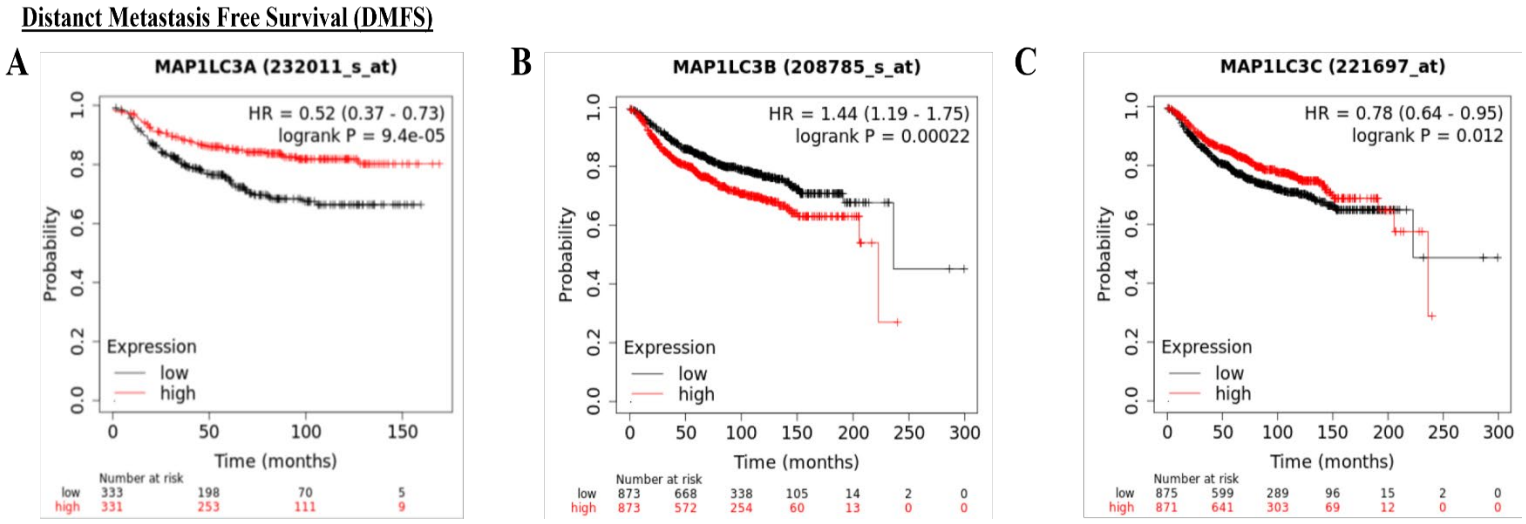


Figure 3-30 Significant differences in the prognosis probability between the LC3 isoforms in breast cancer patients

(A) High expression of LC3A significantly correlates with a decrease in the probability of DMFS. **(B)** LC3B high expression correlates as a poor prognostic marker for DMFS. **(C)** High expression of LC3C was an excellent prognostic marker for DMFS.

To further interrogate these analyses, the ratio of two isoform genes is examined as prognostic markers (Figure 3-31). As previously suggested in Figure 3-29 and Figure 3-30, there are different prognostic values between the isoforms or LC3B with LC3A and LC3C. The LC3 isoforms were then analysed as a ratio, and it was observed that an increase in LC3B expression compared to LC3A Or LC3C resulted in a significantly poorer prognosis (Figure 3-31 A-B). When the inverse was analysed, thus higher expression of LC3Aand LC3C than LC3B, there was a significantly better prognosis in relapse-free survival for breast cancer patients (Figure 3-31 C-D). The patient data from the LC3 orthologues, Gabarap, GabarapL1 and GabarapL2, had no significant correlation with patient outcomes individually; however, they all significantly correlated as a ratio of LC3B with lower expression resulting in poor prognosis. (Appendix IV)

The patient data set identifies a substantial prognostic value in the LC3 isoforms and highlights a feasible target, given that all isoforms conserve the autophagic domain. Therefore, the possibility of inhibiting LC3B would remove the deleterious outcomes and increase the expression of positive prognostic markers LC3A and or LC3C.

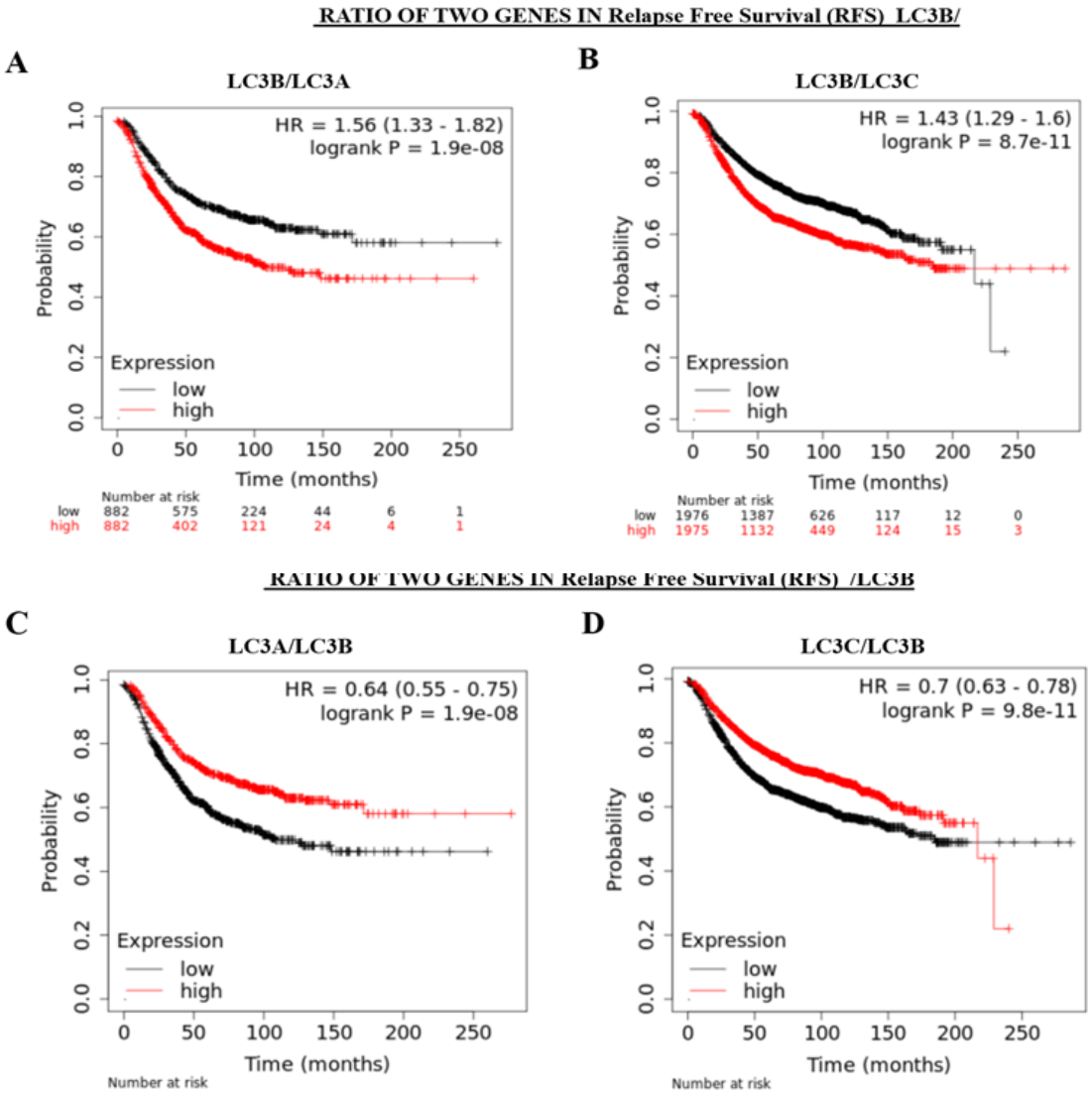


Figure 3-31 The LC3 isoforms and their gene ratio expression significantly correlate with patient relapse-free survival in breast cancer as a whole.

(A) The increased gene ratio between LC3B to LC3A presented as a significantly poor prognostic marker in RFS **(B)** The increased expression of gene ratio between LC3B to LC3C presented as a significantly poor prognostic marker in RFS. **(C)** The inverse gene ratio between LC3A to LC3B presented high expression and better OS **(D).** The inverse gene ratio between LC3C to LC3B presented as high expression and better OS.

Table 3-1. Summary of findings

Cell line	LC3-II turnover		Autophagic Flux		P62 turnover	
CONDITION	BASAL	INDUCED	BASAL	INDUCED	BASAL	INDUCED
MCF10A	→	↑	N/A	N/A	↑	↓
MCF10A HRAS^{V12}	↑	↑	N/A	N/A	↑	↓
T47D	↑	↑	+	+	N/A	N/A
MDA-MB-468	↑	→	N/A	N/A	↑	↓
MDA-MB-468 + EGF	↑	↓	N/A	N/A	↑	↓
HS578T	↑	↓	+	×	N/A	N/A
MDA-MB-231	↑	↑	+	×	N/A	N/A

LEGEND : ↑ INCREASE ↓ DECREASE → UNCHANGED

\+ POSITIVE FLUX × BLOCKED/SURPRESSED FLUX

3.4 DISCUSSION

Autophagy has been identified as having opposing roles in cancer, whereby it has a preventable function at the early stages of the disease. However, as the disease progress, the role of autophagy switches in favour of supporting cancer survival and progression. The role of autophagy in RAS-active cancers is relatively unknown. This study presented work that has demonstrated that autophagy activity increases, suggesting a correlation with heightened RAS activation as displayed in various breast cancer cell lines and models. The concomitant increase in basal levels of autophagy to ectopic expression of $HRAS^{V12}$ in the MCF10A cell line was most significant, which is suggested to have a role in these phenotypes to maintain tumorigenesis and facilitate cancer progression. Furthermore, it highlights the context-dependent role of mutant RAS on autophagy to maintain this aggressive phenotype in breast cancer.

3.4.1 Autophagy and associated gene upregulation in a model of transformation

The current literature acknowledges the correlation between increased autophagy and cancer progression, but the mechanisms under which this is regulated are still unknown. Based on the initial results from this study, it became apparent that apart from the breast cancer cell lines with increased autophagy being from the more aggressive subtype, they shared another critical feature: the presence of a RAS mutation. Therefore, it was hypothesised based on the data from the initial studies that there may be a relationship between autophagy and RAS.

The potential mechanistic role of RAS on autophagy was investigated with an *in vitro* model, which our lab previously developed. It utilised the immortalised mammary epithelial cell line MCF10A transduced to ectopically express $HRAS^{V12}$. This model and its parental counterpart were grown in 3D culture to form acini, after which the acini were collected for gene array analysis. The data analysis compared MCF10A (parental) versus MCF10A $HRAS^{V12}$ (parental+ $HRAS^{V12}$) (hereafter referred to as $HRAS^{V12}$) there was a significant increase in at least 50 associated autophagic genes. Furthermore, there were increases found in many LC3(ATG8) group family members, specifically in ATG4,

ATG5, ATG7, ATG9, ATG12, ATG13 and ATG16L. ATGs are crucial in the many facets of the autophagic process, including autophagic induction, phagophore recruitment, elongation, autophagosome closure and particularly in the lipidation of LC3 with PE [159].

The top ten upregulated genes compared to control cells, apart from HRAS (it should be noted there was a fifteen-fold increase in HRAS compared to control), include transglutaminase 2 (TGM2) there was a forty-five-fold increase. This gene has been shown to activate autophagy via the NF-κB pathway in the context of breast primary cell (HMEC), mantle cell lymphoma and cystic fibrosis [442-444]. Although variations between findings by Yeo et al. [442] illustrate this autophagic paradox wherein their setting, autophagy is suggested to protect against transformation; however, here, we observe autophagic genes being increased in response to $HRAS^{V12}$ transformation suggesting its activity is integral in facilitating its progression, as will be examined in more detail further. Endoplasmic reticulum-golgi intermediate compartment (ERGIC1) had a twenty-four-fold increase, and this gene is suggested to provide a membrane for autophagosomal biogenesis [445, 446]. Immunity-related GTPase family M protein (IRGM) was upregulated eightfold, and this gene has been shown to govern core autophagic machinery through IFN-Y and ATG16L, which was also found in this array to be upregulated [447, 448]. The COPII-cargo adaptor complex (SEC24D) was increased four-fold, which is proposed to facilitate ATG9 binding when phosphorylated on COPII, and this interaction is shown to determine the number of autophagosomes [449, 450]. NPC intracellular cholesterol transporter 1 (NPC1) is increased four-fold, and this gene is shown to be involved in the fusion between the autophagosome and lysosome and mutations. Furthermore, this gene has been found to result in autophagic flux dysfunction and lipid accumulation as it also has a vital role in lipid transport [451-455]. Transforming growth factor-beta 1 (TGFB1) was upregulated four-fold. It has been shown to induce autophagy and interact with LC3 within the autophagosome [456-459]. Autophagy-related 16-like 1 (ATG16L1) was increased by three-fold. ATG16L is involved in the ATG12 ubiquitin-like conjugation system, but recent studies have identified polymorphisms within this gene that correlated with cancer onset [460-462]. Finally, microtubule-associated protein 1 light chain 3 beta (LC3B) was upregulated threefold compared to controls. It is also worth noting that LC3A was also increased but only by 1.5 fold. As mentioned previously, LC3B is the central molecule to interact with

the autophagosomal membrane, and it is proposed that it facilitates membrane elongation, maturation, substrate interaction and general autophagosome biogenesis [463, 464]

The most considerable upregulation observed in the ATG family was of member ATG16L, which has an essential role in supporting and facilitating the conversion of LC3. It performs this by acting as the functional link between the ubiquitin-like enzymes ATG5 and ATG12, responsible for adding PE to LC3 to form LC3-II [465-467]. Alternatively, it is suggested that ATG16L interact with ULK1; however, in this context, the data showed downregulation of ULK1/2 gene expression, and protein expression level remained unchanged [467]. Several studies have specifically linked ATG16L activity to the LC3B isoform. However, in isolation, the binding region of ATG16L is targeted to the LC3B isoform specifically and may explain the preference of LC3B isoform over that of LC3A or LC3C isoform. This finding is significant given that LC3B is clinically a poor prognostic marker in breast cancer patients compared to the A and C isoform, respectively, which are positive prognostic markers [468, 469]. It was further shown by Lystad *et al.* (2019) that the ATG16L isoform α and β have distinct roles not only in the lipidation of LC3B and membrane recruitment in all autophagic mediated responses but in the recruitment of LC3B to the endosome membrane, specifically in the β isoform of ATG16L [469]. This distinct variation in function between the isoforms is noteworthy, although it was not distinguishable in the $HRAS^{V12}$which may relate to antibody specificity to the one used in the breast cancer cell lines (Fig.3.4), which showed a preference of the B isoform in the TNBC cell lines and a preference for the A in the LA cell line. Therefore, it would be essential to ascertain if an LC3B single membrane endosome is present in breast cancer and its role in this context. Although it was generally examined in this study, it would have been intriguing to determine if the ATG16L isoform preference is shifted upon the treatment with VPS34 inhibitors that were utilised and will be discussed in chapter 4 and whether that could account for the efficacy.

In the scope of this study, the upregulation observed in ATG16L compared to all other ATG's is suggested to be related to its role in LC3B lipidation, although the other components integral to this process, ATG 5 and ATG 12, were not found to increase. It is speculated that these molecules are readily available; therefore, the availability of ATG16L is the rate-limiting step in the process. So ATG16L expression must increase to meet the demand for autophagosome formation, particularly the insertion of LC3-II into the internal membrane of the autophagosome. This LC3-II interaction with the membrane

has a role in interacting with P62 and other cargo sequestering molecules and initiates the curvature and closure of the phagophore membrane to form the autophagosome. Furthermore, it would then be expected that the expression of ATG16L would mirror that of LC3-II expression. Therefore, it suggests there may be some other role for ATG16L or there is an accumulation of phagophores and an abundance of ATG16L bound to the outer membrane as previously observed by Fujita *et al.* and found to have an inhibitory effect on autophagy activity. However, the mechanism of this inhibition has yet to be determined [154].

Other notable genes upregulated in the switch to the oncogenic phenotype were P62/SQSTM1, LC3A and LC3B; these increases were also observed at the protein level. P62/SQSTM1 upregulation supports findings by Li *et al.* [470], where they observed that this increase correlated to the metastatic phenotype. These effects could be attenuated with its loss, although this group associates this suggested being a consequence of its new regulation of vimentin. However, surprisingly they had not assessed autophagic activity [471]. Interestingly, both LC3 isoforms were upregulated, although one and a half versus a three-fold increase in LC3A and LC3B, respectively. This result is surprising as all publicly available data sets show that high expression of LC3A correlates better than LC3B, which is a poor prognostic marker in breast cancer, but this data shows that both are available isoforms, although more of LC3B than LC3A. Thus, this difference is unlikely to translate to the clinical differences observed and suggests that although all three isoforms conserve the autophagic domain, there must be functional differences that are proposed to be related to other genetic drivers such as RAS but are yet to be elucidated. (Refer to Appendix IV for gene ratio of HRAS/KRAS with LC3B).

This genetic variety was explained in-depth in a study by Ellis *et al.* [472], which exposed a distinct difference in consequence of a mutation in the breast cancer subtypes when he compiled and compared all data from recent genome studies of breast cancer. He identified the basal-like genetic landscape to be very different from that of luminal cancer, with the basal-like being similar to other epidermis-derived cancers such as head, neck and lung. Of interest was the PI3KCA pathway, which has a broader genetic signature and alternative genetic pathways than luminal subtypes. However, this signature was not observed to confer activation in the basal subtypes, which could explain the presence of higher autophagic activity in the basal subtypes and may explain the

improved efficacy of treatment targeted to this PI3KCA pathway in the luminal subtypes [472-474].

3.4.2 Increased autophagic activity sensitises RAS-transformed cells

The $HRAS^{V12}$ model of transformation performed as shown by others; presented with a spindle-like morphology, lacked epithelial junctions and reduced E-cadherin expression [409]. In 3D culture, the cells formed acini structures as expected, but with the ectopic expression of $HRAS^{V12}$, the acinus lacked the presence of a lumen as was observed in control cells. They also lost their organised spherical formation displaying cellular disorganisation and the presence of protrusions as published by others [409, 475]. This model is clinically relevant as it replicates the mutation observed in the transformation process similar to that of the TNBC cell line Hs578T. However, the Hs578T cell line has progressed and has many other mutations in combination with RAS, so delineating the relationship between RAS and autophagic regulators, specifically the $HRAS^{V12}$ model, was also utilised.

The principal autophagic markers examined as an autophagic presence and function indicator is P62 and LC3 [476, 477]. P62 is a multifunctional protein that targets aggregates for degradation via autophagy and the NRF2-KEAP1 pathway. In autophagy, P62 is the interconnecting adaptor protein LC3-II and ubiquitinated proteins targeted for degradation and usually include protein aggregates, defunct mitochondria, peroxisomes and lysosomes [478]. P62 can bind to the ubiquitin chains such as K63 attached to targeted cargo and allows for P62 bound with the cargo to be translocated to bind the luminal aspect of the autophagosome membrane where it binds to LC3-II on for subsequent degradation. Conversely, it is also suggested that the cargo is bound to the P62 already bound to LC3-II on the autophagosome membrane. Irrespective of the order of the events, the result is that protein aggregates and defunct organelles are bound to P62 with or without the inclusion of a ubiquitin chain. They are recruited to autophagophore membrane due to the interaction between P62 and LC3-II, which may trigger the fusion or completion of autophagophore to the autophagosome [479, 480]. The autophagic relevant P62 phosphorylation site is serine 403; this was examined to determine if the P62 observed was correlated with its autophagic specific function. The results indicated a

significant increase in expression in the presence of $HRAS^{V12}$ compared to control, suggesting it is increased expression was in response to RAS or RAS activity.

However, P62 is also linked to the RAS pathway; to ascertain this, the phosphorylation sites serine 349 were also examined and not found present, suggesting that the observed increase was directly related to the autophagic activity rather than the autophagic activity than with the alternative pathway. To corroborate these findings, the specific components of that pathway were examined, KEAP1 and NRF-2, which were found to not change in this context [481]. Although recent literature suggests there is binding between KEAP1, P62 and protein aggregates resulting in KEAP 1 degradation and NRF-2 activation, we did not observe this at a protein level, but there was an upregulation in mRNA of NRF-2, but this model did lack mutant p53 which others have shown to facilitate this activity in breast cancer [482, 483].

One explanation for increases in P62 may be a reflection of dysregulation, as speculated earlier, because the capacity of activity has been reached at the basal state that any additional stress applied causes the process to break down, resulting in the accumulation of cargo its molecular components. This accumulation may occur in the cytoplasm or even within the autophagosome. However, due to a limited number of lysosomes, there is a decrease in the fusion between autophagosomes and lysosomes to facilitate the degradation, but the reality is it is probably a combination of both. Therefore, the components usually found translocated to and then within the autophagosome during autophagic activity, such as P62, are not being degraded, so their presence will increase. It is proposed that this increase in P62 within the cytoplasm may result in its interaction and heightened activity in its other roles such as NRF2- KEAP1 axis independent of the specific phosphorylation as it has a strong affinity for KEAP1 this would then affect the RAF-MEK-ERK pathway and confer an environment that favours metastatic development. Although it is a preposition, it warrants further investigation; particularly mechanistically, it suggests the potential efficacy of adjuvant treatment with RAF, MEK or VPS34 inhibitors feasibility in metastatic breast cancer [484].

The primary autophagic marker is LC3, of which there are three isoforms, and all conserve the autophagic domain [155, 464]. It has a precursor LC3-I, and its lipidated form LC3-II interacts directly with the inner side of the autophagosome membrane. LC3-II was expressed significantly higher in the $HRAS^{V12}$ cells than the “normal” counterpart at basal conditions, which reports the autophagosome formation. This autophagic activity

observed could be observed in the "normal" cell line with the addition of an autophagic inducer such as rapamycin. Interestingly the inclusion of rapamycin did not increase the LC3-II to LC3-I ratio levels further in the $HRAS^{V12}$ cells compared to control cells. However, the turnover rate of LC3-II indicative of autophagic activity was significantly higher in the $HRAS^{V12}$ cells suggesting the requirement of the autophagic process by RAS. However, the turnover rates were lower than one, reflecting the high levels of the LC3-II being expressed and suggesting that LC3 is being utilised somewhere other than the autophagosome, such as endosomes as previously described by Lystad *et al*. [469] .

3.4.3 Increased dependence on autophagy in breast cancer progression

Autophagy in the "normal" context has been mainly associated as a stress responder in that it recycles non-essential cellular components for alternative metabolic substrates in times of nutrient deprivation. However, this is a limited view of autophagy's role, and recent studies have shown that autophagy has many crucial physiological functions relating to development and disease prevention [485]. In cancer, the role of autophagy has not been clear as there is variation between cancer types and even cellular subtypes. Although many articles exploit the term "autophagy", there is still a lack of studies examining the disparities in cellular subtypes, at least the area of breast cancer. This study has identified variation in autophagy in the different breast cancer molecular subtypes as seen by the expression of LC3. With a chosen panel of breast cancer cell lines was, to include all the molecular subtypes to define any difference between the subtypes. There was a significant increase in autophagic expression from the luminal A (LA) to the triple-negative subtype (TNBC). These subtypes indicate a least to more aggressive phenotype, respectively (Fig.3.1). Clinically this progression in the breast cancer lines is correlated with poor prognosis, and the more advanced subtype TNBC tends to be treatment refractory [414, 486-488].

The significant difference observed between the LA and TNBC leads to further in-depth studies of these particular cancer cell lines. The T47D breast cancer cell line was representative of the LA sub-type. Hs578T and MDA-MB-231 breast cancer cell lines represent the TNBC subtypes. The rationale for including two cell lines from the TNBC is that they have two differing RAS mutations, HRAS and KRAS, respectively. The data

shows LC3 was expressed in both the precursor form LC3-I and the active form LC3-II across all subtypes. The results indicated a 3-fold increase in TNBC subtypes compared to the LA subtype at basal condition.

However, the ratio of LC3-II to LC3-I does not examine activity, so several methods were used to examine autophagic flux (Fig. 3.2 and Fig.3.3), which included LC3-II turnover and FACS analysis with LC3 amphiphilic tracer dye as prescribed by Klionsky *et al*. [489]. At basal conditions, it is expected that the treatment with rapamycin, amino acid deprivation and starvation media for a specified time, as described in Chapter 2, will induce autophagic activity [489]. Furthermore, the inclusion of Chloroquine and Bafilomycin A1 will inhibit lysosomal function, and as a consequence, the autophagic process will be halted. The results from this study support many studies with an upregulation of autophagic flux observed and commonly referred to as "dysregulation", with several studies associating it with breast cancer progression [206, 222, 223, 490-493]. The LA breast cancer cell line displayed expected results with autophagic flux increasing with the inclusion of autophagic inducers; in contrast, the TNBC breast cancer cells demonstrated a high autophagic flux at basal conditions. However, the addition of starvation media resulted in dysfunction and suppression of flux. It is proposed that given autophagy is a rate-limiting that in the TNBC cell lines are already at maximal capacity, so the induction of autophagy in these cells exhausts the capacity to respond to typical induction ques. These findings extend the current knowledge of autophagic activity, particularly concerning variations between the sub-types and the arrest of its activity in the TNBC cell lines. These results emphasise the importance of autophagic presence in this aggressive phenotype and agree with others who recognise autophagy for its targetable potential [496].

3.4.4 RAS activation is an oncogenic driver rather than RAS mutation in breast cancer

Breast cancer is not commonly recognised for the presence of RAS mutation, as it only occurs in 1% of breast cancer cases. However, approximately 50% of breast cancer have increased RAS irrespective of the RAS mutation. One reason for this increase in RAS activity is proposed to be due to a reduction or removal of NF1. NF1 is one of the RAS GTPase Activating Proteins (RAS GAPs); it has a role in the hydrolysis of the GTP

active form to its inactive GDP form, which acts as the on-off switch for RAS activity [497]. These RAS GAPs are classified as tumour suppressors due to their regulatory role in proto-oncogenes such as RAS [473]. A decrease in NF1 is observed in many breast cancer subtypes, but a complete loss is observed in the TNBC cell line MDA-MB-231; its loss is suggested to facilitate their resistance to treatment via MAPK and RAS [498]. This study supported these findings and found a reduction in NF1, but interestingly in this model, the NF1 loss results from $HRAS^{V12}$ expression, which suggests that the increase in $HRAS^{V12}$ itself can actively reduce the expression of NF1. It may also result in the hyperactivation of the other RAS isoforms to further exacerbate oncogenic potential. It has been suggested that some possible indirect mechanisms responsible for NF1 loss are gene silencing or even through degradation pathways. However, the latter indicates protein expression, which was not examined in this study but would warrant further investigation into autophagy as a possible degradation pathway [473, 497-502].

Other molecules have been associated with the indirect hyperactivation of RAS apart from NF1. They include Disabled homolog 2-interacting protein (DAB21P) and RAS protein activator like 2 (RASAL2). A recent study found silencing either of RASL2 and DAB12P or in concert as observed in Luminal B breast cancer subtype, and this combination developed into a more aggressive phenotype. The combined effect of the loss was shown to activate multiple RAS isoforms and increase activation of downstream targets such as ERK AKT, but there was an increase in the NF-κB pathway specifically related to DAB21P loss [396]. Simarlily to this study, there was a decrease in this gene array of DAB21P in the $HRAS^{V12}$ cell line compared to the control. Therefore, in a model where HRAS mutation has been expressed, the genetic landscape is further altered to support RAS activation, and it would have been interesting to examine the RAS isoforms and the downstream targets to determine what is the consequence mechanistically of this excessive activation or conversely, are the targets of their silencing altered in the context of a RAS mutation.

Interestingly in contradiction to the previous studies, RASAL2 was not observed to be down-regulated in the gene array of the $HRAS^{V12}$ compared to control, as was seen with NF1 and DAB21P. Suggesting that this model is more reliant on the activation of NF-κB pathways; this pathway plays an essential and distinct role in EMT and metastasis, which explains this requirement. DAB2IP has a more suppressive role on RAS and NF-κB pathways than RASAL2, which only influences the RAS pathway. The variation in

the results probably relates to the context; the studies using different subtypes in the previous study examined cells null for RAS mutation. The lack of RAS mutation in this context, the DAB2IP act as a co-activator shown to occur with RASAL2 in luminal B breast cancers to activate RAS rather than a signal enhancer where RAS mutation is present.

3.4.5 RAS activation increases autophagic activity

The initial data identifies a relationship between RAS mutations and increased autophagic activity at the basal state that becomes defunct upon typical initiation cues. The question remaining was whether this increase in autophagy is specific to the RAS mutation examined in the $HRAS^{V12}$and breast cancer cell lines Hs578T, or is it KRAS mutation also found in the MDA-MB-231? The preliminary data of the breast cancer panel of cell lines suggested not the latter. Although some cell lines do not carry a RAS mutation, they are known to have increased RAS activity. Furthermore, they were observed to present with an increased expression in autophagic markers. An example of this would be the basal cell line MDA-MB-468. These cells have increased RAS activity due to their overexpression of EGFR receptors, so to increase the RAS activation to a hyperactive state as expected *in vivo* due to increased signal transduction due to extracellular ligands, including EGF. Recapitulating the *in vivo* environment was achieved by adding EGF to the media of the MDA-MB-468 cell line at various concentrations. This increase in RAS activity within the breast cancer cell line MDA-MB-468 with the addition of EGF has been shown by previous studies to be a consequence of SOS [410].

As a consequence of the addition of EGF, the cells begin to transition from an epithelial to mesenchymal phenotype, as others have previously published [503, 504]. During this transition, the cellular morphology exhibits observable changes, such as the change from the epithelial cells with a cuboidal shape to the mesenchymal cells with a spindle-like appearance. These cellular transformations are enabled by decreasing and increasing a distinct regulatory protein, as observed in this study [505-508].

The stimulation of RAS with EGF resulted in a concomitant increase in autophagy markers which were found to be increased dose-dependently with EGF. This finding further supports the hypothesis that RAS is reliant or at the very least has a relationship

with autophagy. Furthermore, the increase in LC3 turnover rate increased with EGF, indicating the formation of the autophagosome and activity, which alludes to a potential regulatory role of RAS in the activation of autophagy via some mechanism yet to be exposed.

Interestingly the P62 rate was increased in the EGF model compared to the control when exposed to rapamycin. However, there was a significant difference between the groups when there was the inclusion of rapamycin and Bafilomycin A1. This difference may imply that all available P62 is not being used in the autophagic process and instead is being circumvented to other roles, at least in response to EGF and rapamycin. Alternatively, as mentioned previously, is it due to increased accumulation of P62, leading to an increased probability of binding to Keap1? Alternatively, even the accumulation of aggregates may be occurring but may not be accounted for due to the timepoint limitations of this study, as aggregate degradation can take more than 20 hours [509-511]. The accumulation in P62 with amino acid deprivation was observed at a protein expression level, and there was a subsequent loss in LC3A and LC3B, specifically in the EGF model. These observations indicate that autophagic activity is lost during amino acid deprivation and supports findings by Villar *et al*. [512], who they found that the accrual of P62 during amino acid deprivation led to the activation of caspase 8 and apoptosis. However, using MTORC inhibitors such as rapamycin prevents this process and is suggested to explain the lack of efficacy with MTORC inhibition in cancer as it prevents this apoptotic process by activating autophagy and protecting the cell [512]. Also of interest were the results for LC3 orthologue Gabarap1 expression decreased in response to EGF, which may be related to its suggested role as a tumour suppressor that was observed to be reduced in breast cancer with lower histological grade [513-515]

The increased autophagic activity due to RAS activation may result from increased protein degradation. It is speculated that due to an influx in aggregates as the cell removes proteins that are detrimental to its survival and allows for the enhancement of those in favour of growth and adaption, suggesting that the upregulation of autophagic molecules may be more directed and targeted in the context of the cancer cell. A recent study has shown that 47 cancer cell lines with KRAS mutation also increased autophagic-specific molecules [516]. This evidence has since guided the rationale for several clinical trials in pancreatic cancers with KRAS mutation and the adjuvant use of chloroquine to inhibit this dependence on autophagy and has shown promising results to date [399].

3.5 CONCLUSION

This study focuses on autophagic activity at a basal state, comparing and contrasting this activity in the differing breast cancer molecular subtypes. Although a correlation between RAS and autophagy was identified through this exploration, there was observed to be a concomitant increase in autophagic activity with RAS activation. This relationship between autophagy and RAS may assist in explaining the contradictory roles of autophagy observed in the context of cancer. It is proposed that there is a breast cancer paradigm where the phenotype progress to that of metastasis, and in doing so, it utilises either hyperactivated or mutated RAS, which is sustained or facilitated by autophagy. It is further suggested that this linkage between RAS and autophagy is of reliance, therefore exposing autophagy as the "Achilles' heel" of the metastatic phenotype.

Chapter 4: IDENTIFICATION OF A RELATIONSHIP BETWEEN AUTOPHAGY AND RAS IN BREAST CANCER PROGRESSION

4.1 INTRODUCTION

Autophagy is a critical survival mechanism responding to numerous metabolic stressors such as amino acid and nutritional deprivation. In response, it facilitates the degradation of non-essential cellular molecules and recycles them into reusable metabolic substrates to replenish deficits. It maintains cellular homeostasis by degrading cellular aggregates, defunct organelles, and proteins, ironically resulting in cell death or mutations. This study postulates that in the context of breast cancer, autophagy underpins and supports advanced cancer and the metastatic phenotype acting as a “non-oncogenic addiction” for the metastatic cancer cell, consistent with what has been observed for other cancer types [517, 518].

Furthermore, the cancer cell's reliance on autophagy has been shown by White et al. to correlate with RAS mutations, specifically, KRAS-driven lung cancer, where autophagy is activated to reduce oxidative stress and maintain metabolic homeostasis [519]. In addition, a study by Lee et al., who also utilised the MCF10A transformation model with mutant KRAS, demonstrated the role of autophagy in malignant transformation [401]. However, most studies have focused on mutant RAS-driven cancers such as pancreatic and colorectal cancer, mainly focused on multiple KRAS mutations, which have demonstrated a direct relationship between autophagy and KRAS oncogenic survival. To translate these findings to the clinical setting and provide potential improved treatments and outcomes for patients, current clinical trials, including first-line chemotherapy combined with the autophagic inhibitor hydroxychloroquine, have demonstrated treatment responses in a patient with stage IV pancreatic cancer [65]. The only limitation with this study is that

hydroxychloroquine is not a very specific autophagic inhibitor, and thus results may also reflect non-specific off-target effects.

Although breast cancer is not predominantly a mutant RAS driven cancer, although some breast cancer cell lines do harbour HRAS and KRAS mutations (e.g. Hs578T and MDA-MB-231cell lines, respectively), a large proportion of breast cancers do have hyperactivated RAS pathways that are equivalent to their RAS mutant counterparts [72].

In chapter 3, increased autophagic markers with HRAS mutation also correlate with an aggressive breast cancer cell phenotype, consistent with what has been found in other cancer types [222, 393, 520-523]. To extend these findings and those of chapter 3 further to determine whether the increases observed in autophagic activity is essential in the survival and maintenance of this phenotype and facilitate its progression to metastatic disease. Within this chapter, the study sought to examine cell viability and IC_{50} measures of a series of autophagic inhibitors. This study was performed in the breast cancer cell line and models utilised in Chapter 3 to determine the reliance of the more aggressive breast cancer phenotypes on autophagic activity. If demonstrated, this would provide additional evidence that autophagy is a promising future target in the treatment against aggressive breast cancer and metastatic breast cancer disease, which has been proposed for other untreatable cancers, including pancreatic [65, 524].

Autophagic inhibitor research is an area of active research that is rapidly developing; currently, most available agents target the initiation complex to prevent early autophagosome formation through inhibition of PI3K, mTOR, ULK1/2 or BECN1[525-528]. However, drugs have also been developed that target the later stages of the autophagic process, such as the inhibition of lysosomal function resulting in the blockage of autophagic flux [65, 356, 529].

This study examines the blockage of early autophagosome formation by inhibiting PI3K class III (hereafter referred to as VPS34). PI3K is a family of enzymes of which there are three classes, with classes I and II having many members, class III one member and a PI3K-like enzyme referred to as class IV [530]. Consequently, many drugs are active on more than one of the classes as all the family members retain conserved motifs. In addition, the family members are distinguished by the inclusion of additional domains and their individual catalytic and regulatory protein interactions [531].

This study primarily examined several VPS34 inhibitors to account for the varying specificity between the drugs for other PI3K classes (Figure 4-1). The VPS34 inhibitors

examined in this study include SAR-405, which is highly specific for class III and binds to the ATP cleft of VPS34 but has no reported action on PI3K class I, class II or MTOR below 10μM [337, 532]. In addition, VPS34-INI - a highly specific VPS34 inhibitor that also has a limited effect on PI3K classes I and II [297, 340] was included in the study. In addition, initial results from 3-Methyladenine (3- Ma), but then the improved derivative referred to as 3Ma-IV, were also used within the study. The 3Ma-IV is a cell-permeable version of 3-Ma which binds to VPS34 and p110Y class I, but 3Ma-IV has been suggested to have improved specificity for VPS34(Table 4-1) [331, 533].

Advanced cancer cell reliance on autophagy was further substantiated by inhibiting the later steps in the autophagic process, specifically the autophagosome and lysosome fusion and lysosomal degradation processes. These are inhibited with Bafilomycin A1, an inhibitor of vacuolar H+ ATPase (V-ATPase) responsible for importing H+ protons to enable lysosomal acidification, facilitating its degradative actions. In addition, Bafilomycin A1 has also been shown to prevent autophagosome and lysosomal fusion through several other mechanisms, such as the interference with the calcium channel SERCA [351, 352].

Table 4-1 VPS34 Inhibitors specificity and mechanism of action (M.O.A)

			Other published downstream targets								
Drug Name	M.O.A	VPS34	p110δ	P110γ	PI3KC 2β	SGK3	MTOR	PI3KCI	PI3KC 2	Mitophagy (Inhibits)	KD
3Ma	Binding to the ATP binding site via hydrophobic interactions	+ Pan inhibitor	+	+	+			+ *60μM		Yes	
3Ma-IV	3Ma derivative with increased cell permability and solubility	++						+ *50μM			
SAR-405	First in class ATP competitive VPS34 inhibitor	++++ Specific inhibitor					+ *10μM	+ *10μM	+ *10μM		1.52 ± 0.77 nM (± s.d.)
VPS34-INI	Inhibits generation of PtdIns(3)P at endosomal membrane	++++ Specific inhibitor				+					

Legend= "+" indicates inhibitory effect. Increased inhibition is marked by a higher "+" designation

* Effect observed at these published concentration

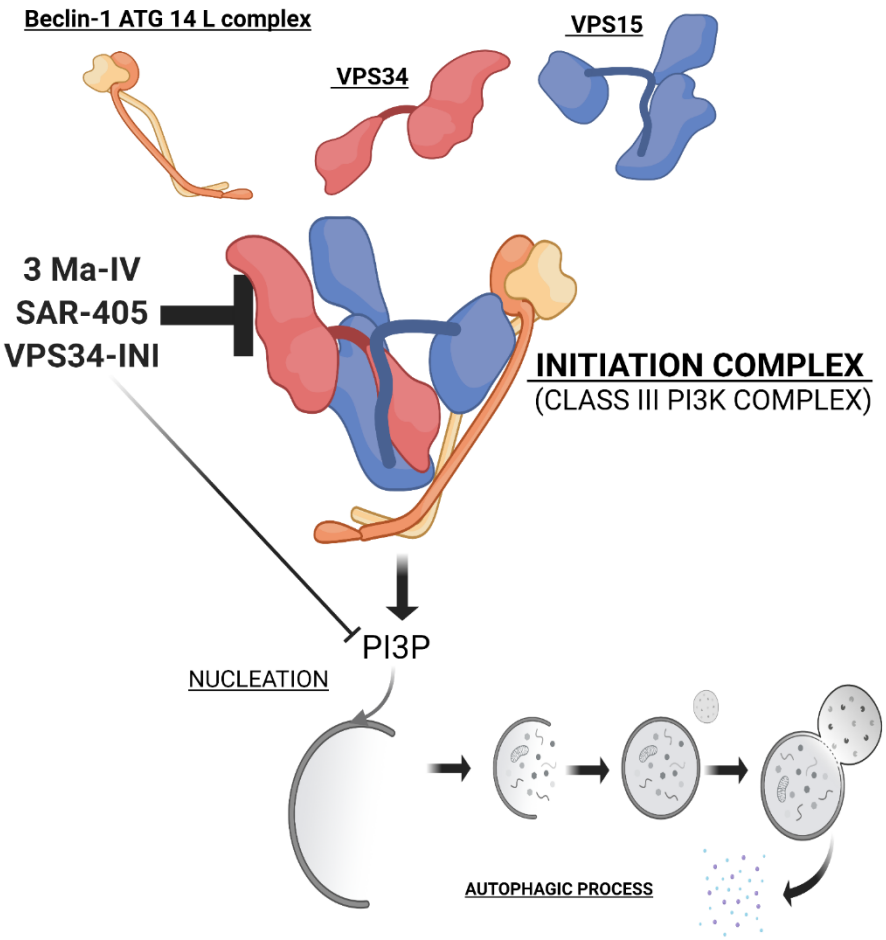


Figure 4-1 Schematic of VPS34's role in the context of the autophagic process

The autophagic process responds to various stressors upon which the "INITIATION COMPLEX" is activated and formed via the phosphorylation of VPS34 and Beclin-1. This activation of the initiation complex results in the recruitment of phosphatidylinositol-3-phosphate (PI3P) and the nucleation of the phagophore assembly site (PAS). Although 3Ma-IV, SAR-405 and VPS34-INI all target and inhibit VPS34, they have different mechanisms to block VPS34 activity, but the net result of the loss of PI3P

Created with BioRender.com

4.2 HYPOTHESIS AND AIMS

Hypothesis:
"Targeting autophagy is more effective in advanced RAS activated cells than in less advanced non-active cells."
The aims of this chapter are:
-To investigate the dependence of breast cancer cells upon autophagic activity through its inhibition.

- To examine the efficacy of autophagic inhibition at the initiation complex utilising several VPS34 inhibitors.

-To examine the difference in efficacy through autophagic inhibition at later stages of the autophagic process with the lysosomal inhibitor Bafilomycin A1.

-To determine if activated RAS breast cancer cells have an increased sensitivity to autophagic inhibition.

-To investigate the potential relationship of autophagy and RAS as a potential biomarker for treatment interventions utilising autophagic inhibitors.

4.3 RESULTS

4.3.1 The expression of HRAS^{V12} in MCF10A increased their sensitivity to 3Ma-IV.

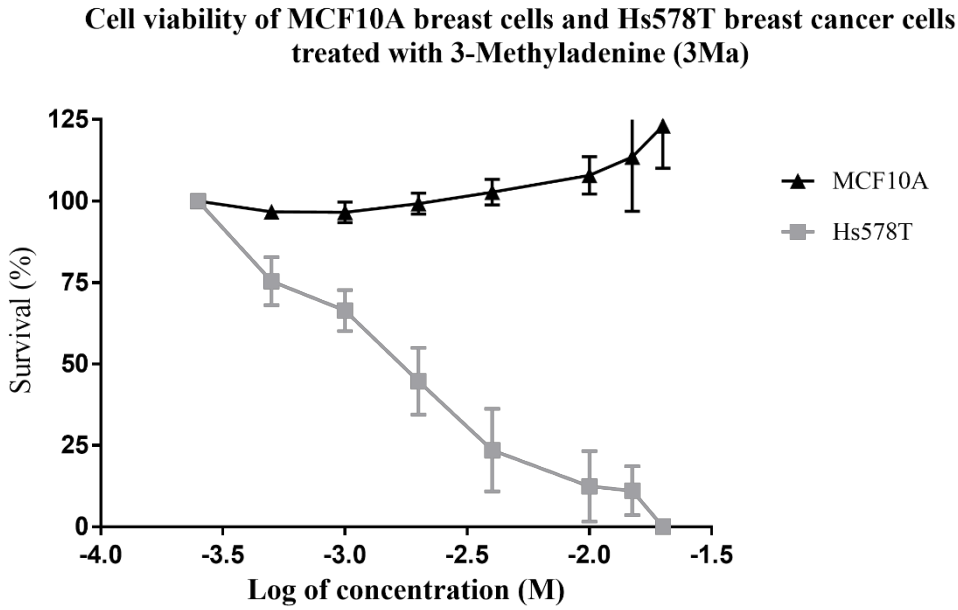
The initial experiments examined the efficacy of 3Ma, which, as displayed in Figure 4-2, there was no response in the MCF10A breast cells with increased sensitivity TNBC cell line Hs578T. However, solubility was a limiting factor, and the concentration range could not be extended beyond 20mM. There was a newly developed derivative that was a derivative 3Ma-IV was developed with improved solubility, so this was utilised in the study. There were similar increases in sensitivity in the triple-negative cell lines, Hs578T, compared to the MCF10A cell line observed with 3Ma-IV (Table 4-2), pointed toward the potential importance of RAS activity and the autophagic axis in breast cancer cell sensitivity to autophagic inhibition. The well-characterised MCF10A oncogenic HRAS^{V12} transformation model from Chapter 3 [375] was utilised to determine the correlation between transformation and autophagy, although, in this context, this was explicitly examined in relation to oncogenic (mutant) RAS.

The results in Figure 4-3 A demonstrate a reduction in the cell viability at all 3Ma-IV concentrations in the MCF10A HRAS^{V12} cell line. In contrast, there was an increase in cell viability at lower concentrations of 3Ma-IV treatment in the control MCF10A cells. The viability of the MCF10A cells was not impacted until the maximal concentration of 3Ma-IV was reached. The cell lines were seeded at confluence as described in Chapter 2, and the real-time analysis system (Xcelligence) was used to determine the cell index based on cellular impedance. The results clearly showed that the expression of HRAS^{V12} increased the sensitivity of the cells to 3Ma-IV by four logs compared to the MCF10A control cells (Figure 4-3 B and C). Interestingly, the sensitivity of the MCF10A HRAS^{V12} cells is similar to that observed in the Hs578T breast cancer cell line, which also possesses the same HRAS^{V12} mutation, further supporting these results.

These findings in the MCF10A HRAS^{V12} model indicate that the transformation of the normal breast to an oncogenic cell by RAS causes a dependence upon autophagy that can be exploited through autophagy inhibition. Therefore, it is suggested that this may

increase as the cell progresses further as recapitulated in the epithelial to mesenchymal transition as observed with the MDA-MB-468 breast cancer cell model.

A



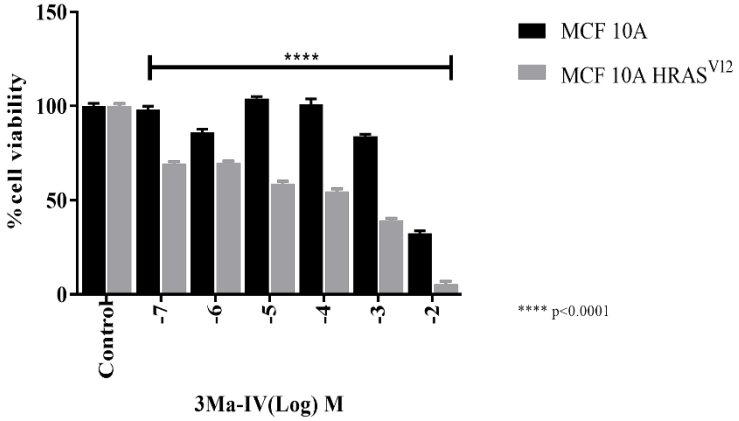
B

Cell line	IC_{50} (M)	P value
MCF10A	Not converged	
Hs578T	$1.668X10^{-3}$ M	<0.0003

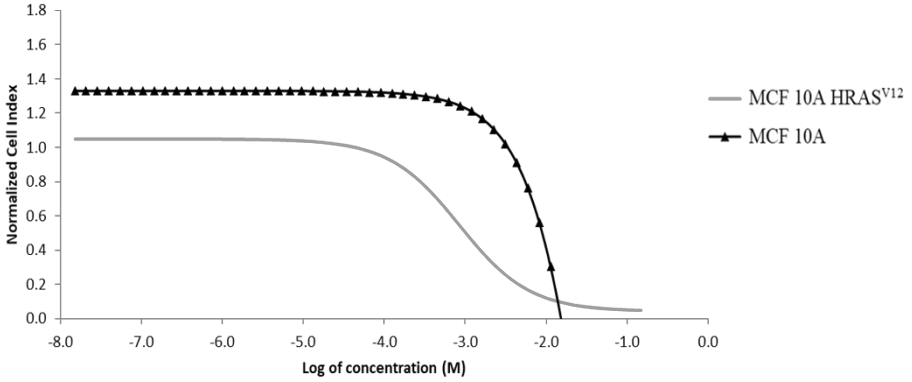
Figure 4-2 The original 3-Methyladenine (3Ma) is limited clinically by its reduced solubility and cell permeability.

(A) Alamar Blue analysis was utilised to determine the IC_{50} of MCF10A breast cell line versus Hs578T breast cancer cell lines treated with 3Ma for 72 hours **(B)** The IC_{50} values could be determined for the Hs578T cell line as determined by prism software with a statistical analysis comparing the cell lines. (n=4, ±SD, $p<0.05$ t-test)

A **Cell viability of breast cancer cell MCF 10A expressing HRAS^{V12} treated with 3Ma-IV**



B **Real time analysis of IC50 for 3Ma-IV treatment in MCF 10A HRAS^{V12} cell line**



C

Cell line	IC_{50} (M)	P value
MCF10A	0.88	
MCF10A HRAS^{V12}	8.7 X10^{-4}	<0.0001

Figure 4-3 The expression of HRAS^{V12} sensitises MCF10A cells to 3Ma-IV treatment

(A) An initial study for cell viability using Alamar Blue analysis at 24 hours timepoint.Significance was demonstrate between groups p<0.0001 **(B)** Real-time analysis of MCF10A and MCF10A HRAS^{V12} cells with increasing concentrations of 3Ma-IV were assessed using the Xcelligence system to determine their IC_{50} towards the drug. for 72 hours **(C)** The IC_{50} values for the cell lines as determined by RTCA software with a statistical analysis comparing the cell lines (n=4, ±SD, p<0.05 ANOVA and Sidak's post hoc test)

4.3.2 Breast cancer progression through RAS activation sensitises the MDA-MB-468 breast cancer cell line to treatment with VPS34 inhibitor 3Ma-IV.

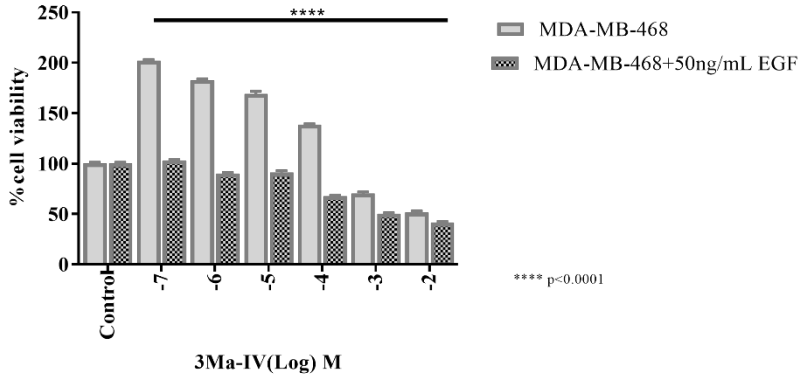
There is a limited incidence of RAS mutations in breast cancer, but hyperactivation of RAS signalling pathways is common and is perhaps why RAS mutation occurs less frequently in breast cancers. RAS activation was modelled with exogenous addition of the EGF ligand to stimulate the EGFR pathway upstream of RAS; a common signalling pathway, MDA-MB-468 cells, was utilised. The addition of EGF at 50ng/mL to these cells results in robust activation of the RAS pathway due to the high expression of EGF receptors (EGFR) in these cells. Furthermore, EGF treatment results in the MDA-MB-468 cell line undergoing an epithelial-mesenchymal transition (EMT), indicative of a more advanced phenotype.

Initially, the Xcelligence system was employed to determine IC_{50}; however, this was not used for the remaining drug treatments as cells exposed to EGF combined with the drug treatment led to many cells detaching transiently and re-attaching, leading to inconsistencies in the impedance readings with the Xcelligence system. Therefore, it was decided that apart from the treatment with 3Ma-IV, where this did not occur, and both methods could be used (Figure 4-4 and Figure 4-5), all the other drug treatments only utilised the Alamar Blue assay to determine IC_{50} results.

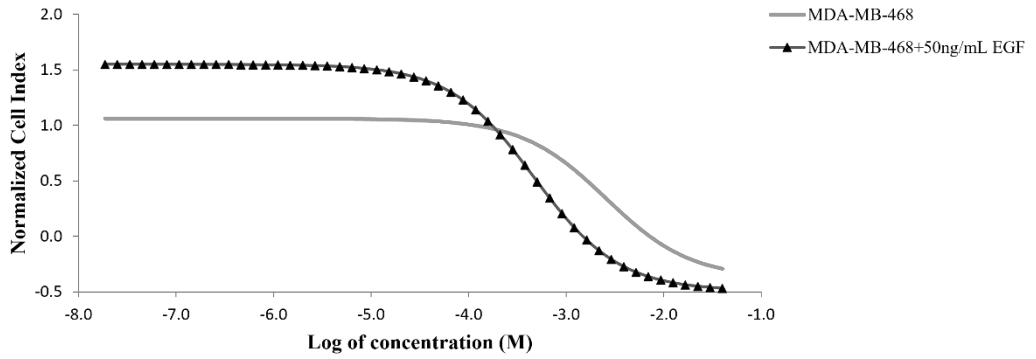
In addition, there was a dose-dependent increase in cytotoxicity in the response by MDA-MB-468 with EGF to 3Ma-IV treatment. Interestingly, the cell number significantly increased to greater than 100% in the lower concentration of 3Ma-IV in the parental cells (Figure 4-4A), with a decrease in viability observed at the two highest concentrations. These findings would indicate that blockade of the autophagic initiation complex in this cellular context is advantageous to cell viability, which would be of concern as the control cells are a triple-negative basal phenotype (TNA) breast cancer. However, these have not been reflected by the IC_{50} results, which suggests that these viability results are transient temporal response or there is anti-oxidant effects of the drug or induced within these concentrations, which others have shown to increase cell viability in Alamar blue assays [534] Figure 4-4 B and C represent the real-time analysis which reveals that the inclusion of EGF sensitises the MDA-MB-468 cell line to treatment with 3Ma-IV. The real-time system detected a log shift in treatment efficacy and was replicated and supported by

experiments performed with the Alamar Blue assay to determine IC_{50}, as seen in Figure 4-5.

A **Cell viability of breast cancer cell MDA-MB-468 in the presence of EGF treated with 3Ma-IV**



B **Real time analysis of IC50 for 3Ma-IV in MDA-MB-468 cell line in the presence of EGF**



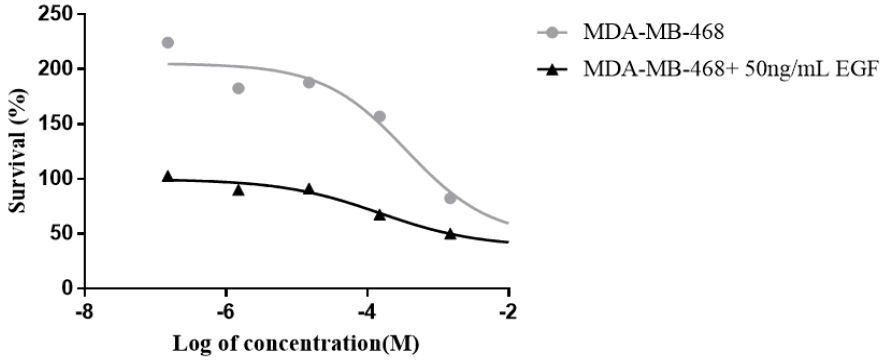
C

Cell line	IC_{50} (M)	P value
MDA-MB-468	$2.57.x10^{-3}$	
MDA-MB-468+50ng/mL EGF	$4.70 x10^{-4}$	<0.0001

Figure 4-4 The presence of EGF sensitives the breast cancer cell line MDA-MB-468 to treatment with 3Ma-IV.

(A) A cell viability study using the traditional Alamar Blue analysis at the at 24 hours timepoint. **(B)** Real-time analysis of breast cancer cell lines MDA-MB-468 in the presence of 50ng/mL EGF seeded in the Xcelligence system to determine the IC_{50} for the treatment with 3Ma-IV for 72 hours **(C).** The IC_{50} values of all cell lines as determined by RTCA software with a statistical analysis comparing the cell lines (n=4, ±SD, $p<0.05$ ANOVA and Sidak's post hoc test)

A **IC50 for 3Ma-IV in MDA-MB-468 cell line in the presence of EGF**



B

Cell line	IC50 (M)	P value
MDA-MB-468	3.58×10^{-3}	
MDA-MB-468+50ng/mL EGF	1.49×10^{-4}	0.00241

Figure 4-5 The presence of EGF sensitives the breast cancer cell line MDA-MB-468 to treatment with 3Ma-IV utilising Alamar Blue.

(A) Alamar Blue analysis was utilised to determine the IC_{50} of breast cancer cell lines MDA-MB-468 with 50ng/mL EGF treated with 3Ma-IV for 72 hours **(B)** The IC_{50} values of all cell lines as determined by graph pad prism software with a statistical analysis comparing the cell lines. (n=4, $p<0.05$ and t-test)

4.3.3 Breast cancer cells demonstrate increased sensitivity to treatment with 3Ma-IV compared to other VPS34 inhibitors.

To examine the dependence of the oncogenesis on autophagy, the breast cancer cell lines observed to have higher autophagic markers and RAS mutations\ from chapter 3 were utilised in this study which included the Hs578T and MDA-MB-231 breast cancer cell lines as a comparison the least aggressive breast cancer cell line the T47D which possess wild type RAS

The treatment of 3Ma-IV in the cell lines underwent preliminary examination using a traditional endpoint assay for viability with Alamar Blue (Figure 4-6). The viability assay demonstrated significantly enhanced sensitivity to the drug in the TNBC cell lines versus the luminal subtypes.

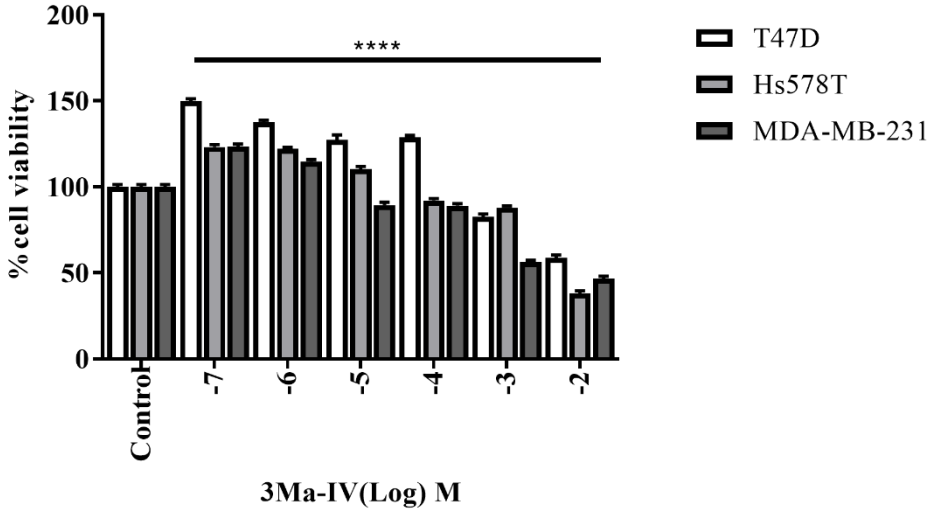
The viability study from Figure 4-6 led to further real-time analysis of the 3Ma-IV treatment to establish an $IC_{50,}$ and it allows for real-time visualisation of cellular response over time and can determine a suitable timepoint or strategy for treatment.

The breast cancer cells were seeded at confluence and treated in the Xcelligence for beyond 72 hours. The IC_{50} determined by the RTCA software on the Xcelligence system at 72 hours of treatment in Figure 4-7A and B shows the treatment with 3Ma-IV is more efficacious in the more advanced phenotypes. In addition, there was a log shift in sensitivity in the triple-negative breast cancer subtype B (TNB), specifically the Hs578T and MDA-MB-231 cell lines, compared to the luminal subtype T47D cell line. Specifically, a further decrease in the IC_{50} between the TNBC subtypes showed that MDA-MB-231 had a higher sensitivity than the Hs578T cell line.

Although there is improved viability compared to the real-time analysis, this may be due to the experimental design differences as with cell viability, is a single end timepoint being 24 hours. In contrast, the real-time system takes a continuous reading every 15 minutes for an extended period beyond the 24-hour time point. However, the real-time system did show the transient increases observed at some of the lower concentrations in the cell viability results before their decline.

The treatment with 3Ma-IV (Figure 4-6 and Figure 4-7) indicates that the more aggressive phenotype (mesenchymal), particularly those with a RAS mutation or hyperactivation, such as the Hs578T, MDA-MB-231 breast cancer cell lines and MDA-MB-468 with EGF, are more sensitive to this autophagy inhibitor. These findings are further supported by the MCF10A $HRAS^{V12}$ model (Figure 4-3), indicating that activated RAS has a dependence upon autophagy that can be exploited through autophagy inhibition.

A **Cell viability of breast cancer cells treated with autophagy inhibitor (3Ma-IV)**



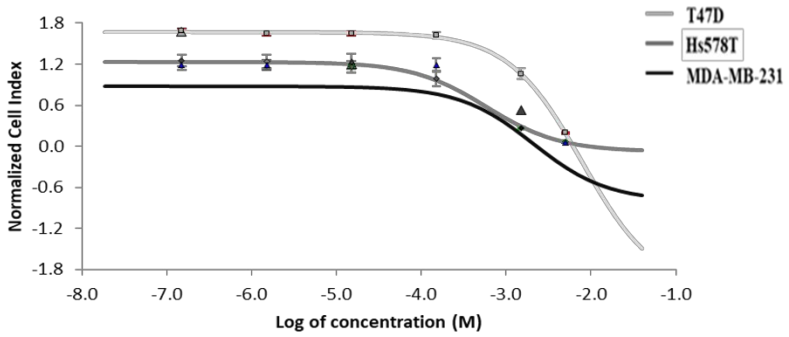
B

Cell line	Comparison	P value
T47D	Versus Hs578T Versus MDA-MB-231	<0.0001 <0.0001
Hs578T	Versus T47D Versus MDA-MB-231	<0.0001 <0.0001
MDA-MB-231	Versus T47D Versus Hs578T	<0.0001 <0.0001

Figure 4-6 Increased sensitivity of advanced breast cancer cell lines to 3Ma-IV.

(A) An initial cell viability study using the traditional Alamar Blue analysis at 24 hours. **(B)** Comparison of groups found significance between the following (n=4, ±SD, $p<0.05$ ANOVA and Sidak's post hoc test)

A **Real time analysis of IC50 for 3Ma-IV in breast cancer cell lines**



B

Cell line	IC_{50} (M)	Comparison	P value
T47D	7.81 $X10^{-3}$	Versus Hs578T Versus MDA-MB-231	<0.0001 <0.0001
Hs578T	5.85 $X10^{-4}$	Versus T47D Versus MDA-MB-231	<0.0001 0.0087
MDA-MB-231	2.09 $X10^{-4}$	Versus T47D Versus Hs578T	<0.0001 0.0087

Figure 4-7 Increased sensitivity to 3Ma-IV in the TNBC breast cancer cell lines

(A) Real-time analysis of breast cancer cell lines T47D, Hs578T and MDA-MB-231 in the Xcelligence system was used to determine the IC50 for the treatment with 3Ma-IV for 72 hours **(B)** The IC50 values of all cell lines as determined by RTCA software with a statistical analysis comparing the cell lines (n=4, ±SD, $p<0.05$ t-test)

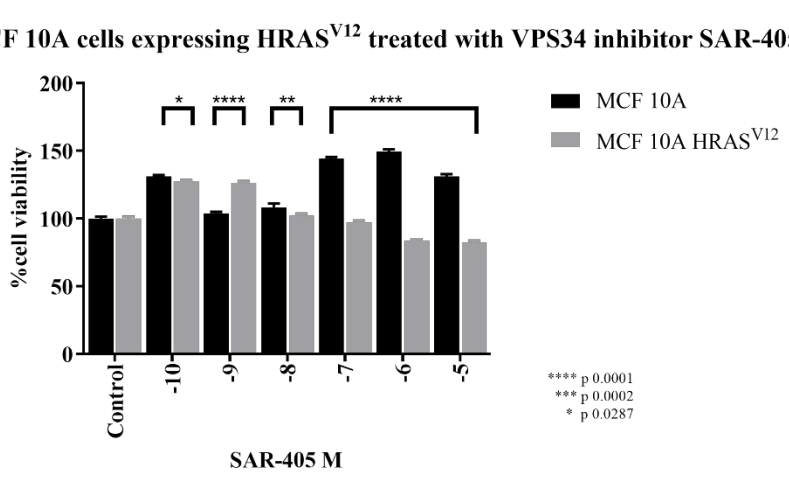
4.3.4 The expression of HRAS^{V12} improved the efficacy of VPS34 inhibitor SAR-405.

To understand the effects of VPS34 inhibition more thoroughly and due to the general lack of specificity between the PI3K classes, particularly 3Ma, which was known to have activity against PI3KC1, although the new derivative used in this study, 3Ma-IV has been suggested to have none [331]. Therefore, more specific inhibitors were utilised to delineate the efficacy of VPS34 inhibition, and the MCF10A HRAS^{V12} model was treated with the SAR-405 to examine its efficacy.

The results in Figure 4-8 strongly suggest that the increase in efficacy of SAR-405 can be attributed to the HRAS mutation or, more reasonably, its cellular effects. When treatment was examined in a viability assay, differences between the HRAS^{V12} and parental control (Figure 4-8), these differences were significant; however, the results were all with positive increases in viability, and the treatment with SAR-405 in the parental cells instigated a 50% spike in viability to 150%. This treatment response by the parental cells was responsible for the significance of the HRAS^{V12} cells, which maintained their viability at around 100%. This viability assay was utilised to determine the $IC_{50,}$ which could only be determined for the cell line expressing HRAS^{V12} compared to MCF10A, which was not converged, as shown in Figure 4-8 B. This increase in viability by the MCF10A cells may reflect an intermittent stress response or the action of SAR-405 may have a favourable impact on cell survival or even anti-oxidant effects of the treatment interfering with the assay.

To observe these results in real-time, the Xcelligence was utilised to analyse the cellular response to SAR-405 as shown in Figure 4-9, the cell line response graph, and treatment is administered where the black arrow is seen. Figure 4-9 A is of MCF10A, and there are minimal changes in response to treatment. However, the 10μM is decreasing the cell index, and future studies would warrant higher concentrations and longer timepoint, as the current concentration range was based on the literature but were different cellular contexts [535] In the demonstrated that the IC_{50} of the cells expressing HRAS^{V12} was increased, compared to MCF10A as shown in Figure 4-8.

A



B

Cell line	IC_{50} (M)	P value
MCF10A	Not converged	
MCF10A $HRAS^{V12}$	1.768 $X10^{-4}$	0.0482

Figure 4-8 The expression $HRAS^{V12}$ reduces the efficacy of SAR-405 treatment in the breast cell line MCF10A

(A)A study of the cell viability using the traditional Alamar Blue analysis at 24 hours time point **(B)** The IC50 values of cell lines that responded to treatment as determined by prism software with a statistical analysis comparing the cell lines (n=4, ±SD, $p<0.05$ ANOVA and Sidak's post hoc test)

To observe these results in real-time, the Xcelligence was utilised to analyse the cellular response to SAR-405 as shown in Figure 4-9, the cell line response graph, and treatment is administered where the black arrow is seen. Figure 4-9 A is of MCF10A, and there are minimal changes in treatment response, although the 10μM decreases the cell index slightly. Similarly, the HRASV12 did not demonstrate any dose-specific responses, but the red arrow indicated a significant peak in cell index, suggesting either a shape change such as rounding or an increase in adherence. Further studies to examine cell morphology and cytoskeleton proteins in response to treatment with SAR-405 would be of interest.

In summary, the mechanism of action of SAR-405 showed varied responses between the cell lines and delineating the cause of these variations would warrant further studies beyond the scope of this investigation. It would warrant higher concentrations and longer timepoint, as the current concentration range was based on the literature but were in different cellular contexts [535]

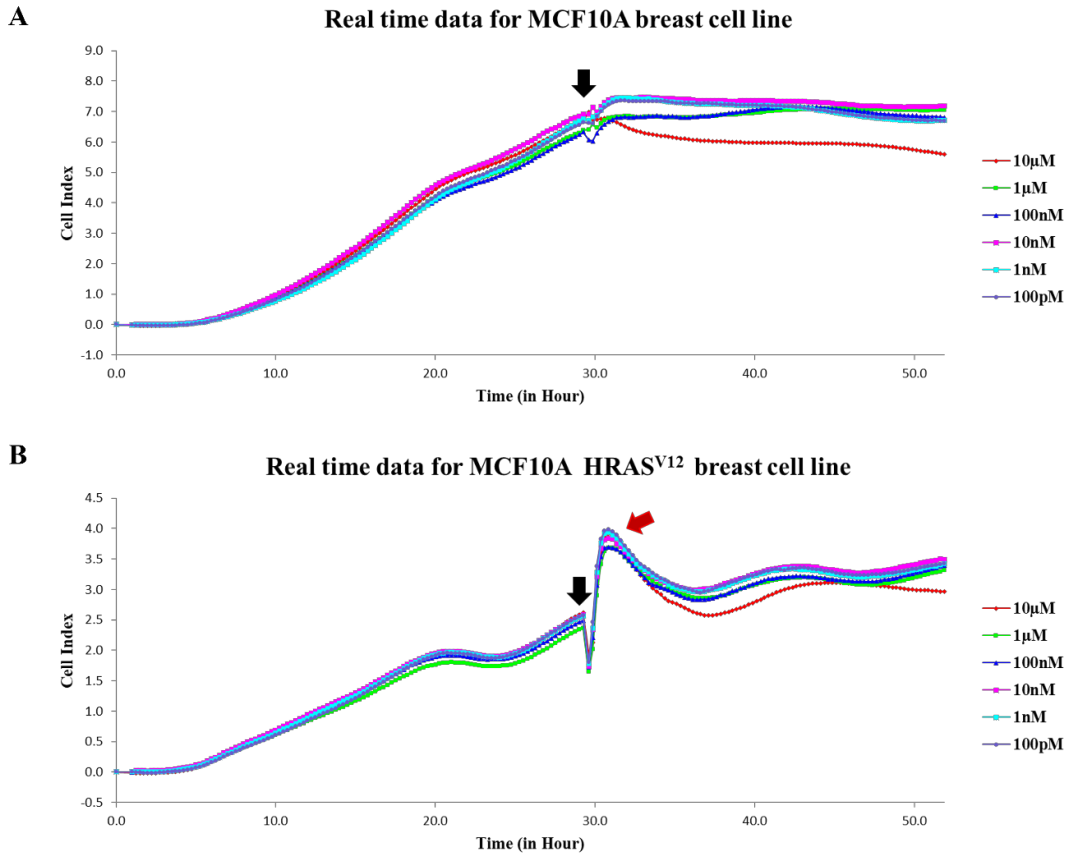


Figure 4-9 Real-time analysis of the MCF10A transformed with HRAS^{V12} responds to SAR-405 by increasing cellular impedance.

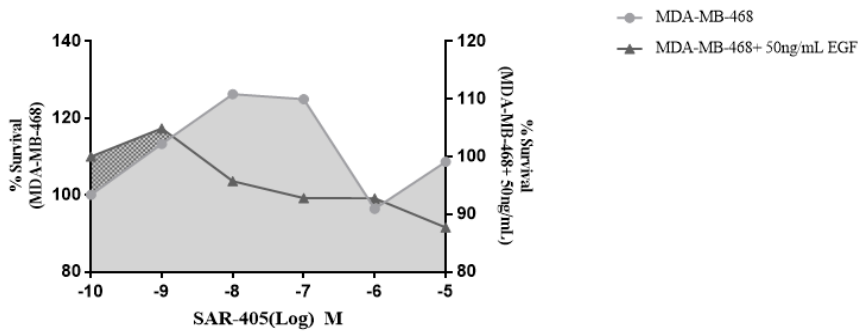
(A) Representative data from the real-time analysis of MCF10A breast cell lines demonstrate no response of cells to treatment with VPS34 inhibitor SAR-405 for 24 hours. (treatment addition indicated by the black arrow) **(B)** Real-time analysis data of the MCF10A transduced with HRAS^{V12} in the Xcelligence system indicates a cellular increase in impedance, as indicated by the red arrow. (n=4)

4.3.5 VPS34 inhibitor SAR-405 increased cell viability in MDA-MB-468, which was lessened by the addition of EGF.

The efficacy of targeting RAS-active breast cancer cells with VPS34 inhibitors was examined further by testing another VPS34 inhibitor, SAR-405. Due to the discovery of the population of cells that became particularly mesenchymal with a tendency to remain in suspension and only adhere to the surface transiently, the decision was made not to utilise the real-time system in the analysis of SAR-405 treatment. Instead, this study utilised the Alamar Blue assay, as depicted in Figure 4-8, to determine viability and IC_{50} over an extended time course (72 hours). However, the results indicate that the viability of the MDA-MB-468 and MDA-MB-468 with EGF was increased. While an IC_{50} could not be determined, an area under the curve could be determined. The AUC data increases with all values for each concentration and cell type being more than 80% (Figure 4-10A). When the AUC was determined using Prism software, with the baseline set at a control level of 100%, it was found that the parental cell viability was significantly increased compared to the addition of EGF (Figure 4-10 B).

Both cell lines increased their cell number in response to the treatment with SAR-405, similarly to the previous results where this trend was continued with the MCF10A cell line (Figure 4-8), suggesting there is a characteristic shared between these cell types that acquire them an insensitivity to the efficacy of SAR-405. The results demonstrate that SAR-405 treatment at the doses examined had minimal effect on cell viability. The treatment with SAR-405 may require multiple dosing or longer timepoints to determine its potential efficacy in future investigations.

A **AUC for the treatment of VPS34 inhibitor SAR-405 in breast cell line MDA-MB-468 with EGF**



B

Cell line	AUC (Base line set at 100)	P value
MDA-MB-468	66.85	
MDA-MB-468+50ng/mL EGF	27.44	<0.0001

C **Cell Viability of breast cancer cell MDA-MB-468 in the presence of EGF treated with VPS34 inhibitor SAR-405**

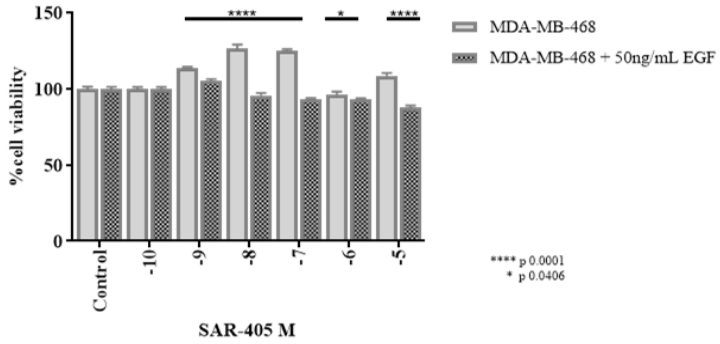


Figure 4-10 The presence of EGF increases the efficacy of the VPS34 inhibitor SAR-405 treatment.

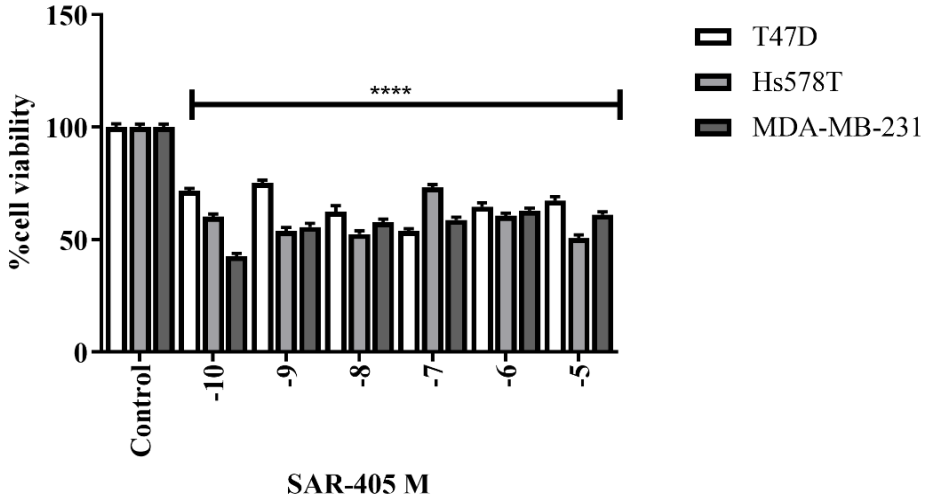
(A) Alamar Blue analysis was utilised to determine the AUC of breast cancer cell lines MDA-MB-468 in the presence of 50ng/mL EGF treated with VPS34 inhibitor SAR-405 **(B)** The AUC values of all cell lines as determined by prism software with a statistical analysis comparing the cell lines **(C)** Cell viability Alamar Blue analysis at 24 hours timepoint. (n=4, ±SD, $p<0.05$ ANOVA and Sidak's post hoc test)

4.3.6 The VPS34 inhibitor SAR-405 shows a differential response in breast cancer cell lines.

The breast cancer cell lines were subject to a preliminary viability test with Alamar Blue as the data demonstrates the Hs578T are dying in response to the treatment (Figure 4-11A and B). The Alamar Blue data shows a loss of viable cells in all subtypes, and the T47D declined somewhat dose-dependent, whilst the MDA-MB-231 responded with greater efficacy at lower concentrations. However, it should be noted that the cell viability did vary minimally in the T47D cell between the concentrations, almost a biphasic effect. The Hs578T cell line did not reach below 50% cell viability at any of the concentrations suggesting their sensitivity is lower than the other cell lines.

These findings highlight the complexity of the blanket approach to cancer treatment, as shown in the same cancer cell types, where treating five different cellular subtypes resulted in various drug efficacy. SAR-405 and 3Ma-IV are specific for VPS34 at these concentrations, given the differences in their effectiveness suggest that either 3Ma-IV or other activity on p110Y may be responsible for this or there is increased efficacy at the alternative binding sites.

A **Cell Viability of breast cancer cells treated with VPS34 inhibitor SAR-405**



B

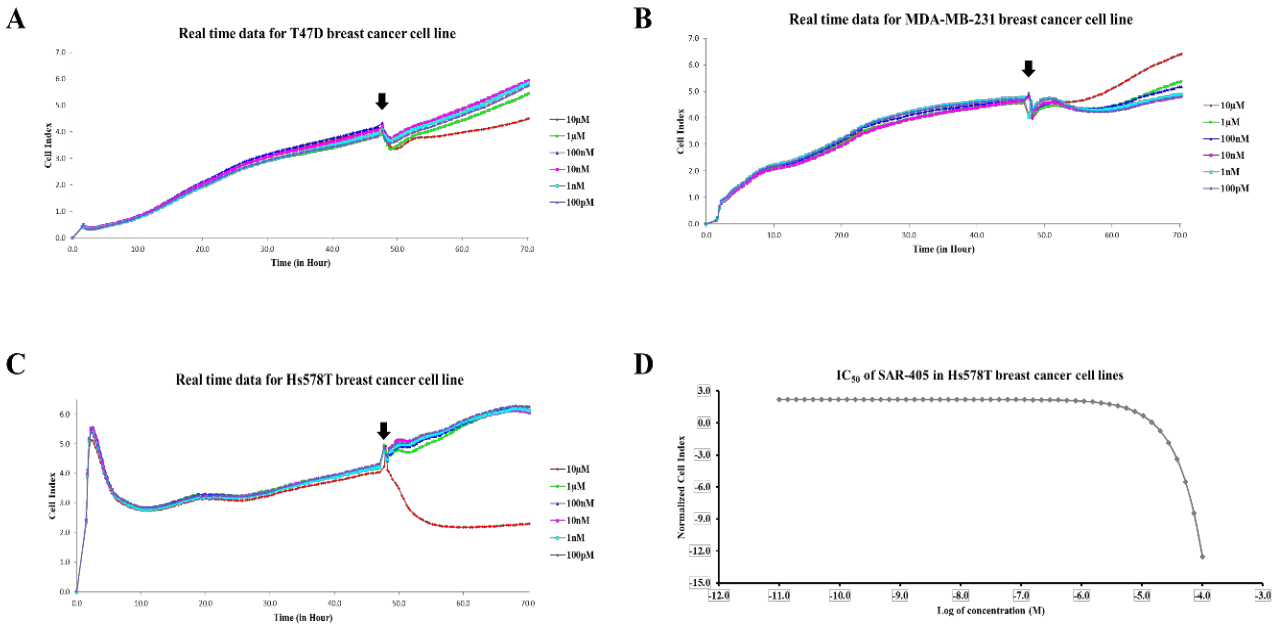
Cell line	Comparison	P value
T47D	Versus Hs578T Versus MDA-MB-231	<0.0001 <0.0001
Hs578T	Versus T47D Versus MDA-MB-231	<0.0001 0.0008
MDA-MB-231	Versus T47D Versus Hs578T	<0.0001 0.0008

Figure 4-11 The breast cancer cell lines had altered cell viability in responses to treatment with SAR-405.

(A) The cell viability using the traditional Alamar Blue analysis was examined in the breast cancer cell lines at 24 hours timepoint. **(B)** Significance determined between groups as tabled (n=4, ±SD, $p<0.05$ ANOVA and Sidak's post hoc test)

To investigate this variability further, the study treated the cells in the real-time analysis, showing contrast in the effect of SAR-405 in the cell lines tested. (Figure 4-12). There was a high differential between the T47D Hs578T and the MDA-MB-231 cells. The T47D slightly declined cell index at the highest concentration (Figure 4-12 A). In contrast, the MDA-MB-231 displayed an increase in cell index at the highest concentration, so it may be speculated that it reflects a morphological change. However, the only effect was observed in the Hs578T cell line, which responded to SAR-405 with an IC_{50} within the molar range, similar to the MCF10A $HRAS^{V12}$ in Figure 4-8, suggesting there may be a

shared response mechanism. The observed changes of the repurposed small molecule SAR-405 are interesting and suggest that this drug's effects may be cytostatic rather than cytotoxic.



Cell line	IC_{50} (M)
Hs578T	$1.21X10^{-5}$

Figure 4-12 The breast cancer cell lines had contrasting responses to treatment with SAR-405.

The Xcelligence system was used to collect real-time analysis of breast cancer cell lines in response to SAR-405 treatment **(A)** A representative data of the T47D breast cancer cell line real-time data show no effect on cell index after SAR-405 treatment (treatment addition indicated by the black arrow) **(B)** Representative data from the real-time analyser for the MDA-MB-231 breast cancer cell line show no effect to cell index after SAR-405 treatment. **(C)** A representative image of Hs578T breast cancer cells over 72 hours (48-hour growth phase and 24-hour treatment) demonstrated decreased cell index in response to SAR-405 treatment **(D).** The Xcelligence system was used to determine the IC_{50} for VPS34 inhibitor SAR-405 for 24 hours. The IC_{50} values for Hs578T cell lines as determined by RTCA software (n=4)

4.3.7 The expression of HRASV12 increased sensitivity to treatment with the VPS34 inhibitor VPS34-INI.

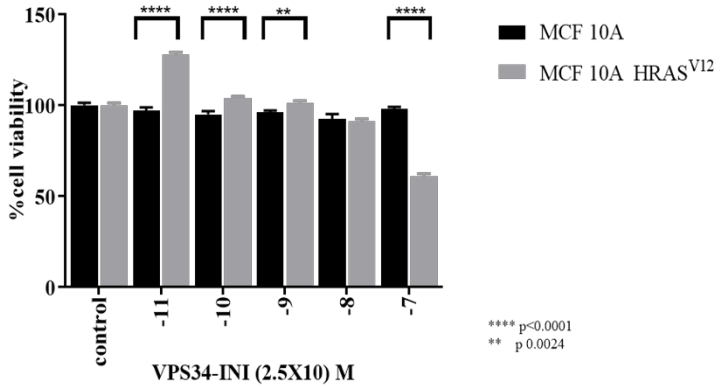
To further examine the importance of autophagy in breast cancer survival, the inhibition of the initiation complex with antagonism of VPS34 with various molecules was undertaken, and the last to be analysed was VPS34-INI.

Figure 4-13 shows that the sensitivity to treatment is higher in the $HRAS^{V12}$ cell line than in MCF10A parental. However, there is no disparity between the real-time analysis and Alamar Blue results even though the endpoint of Alamar Blue versus the continuous monitoring of the real-time system, allowing for an increase in sensitivity in the real-time analysis. It may also indicate that treatment improves over time or increasing concentration range further is all factors that need further examination.

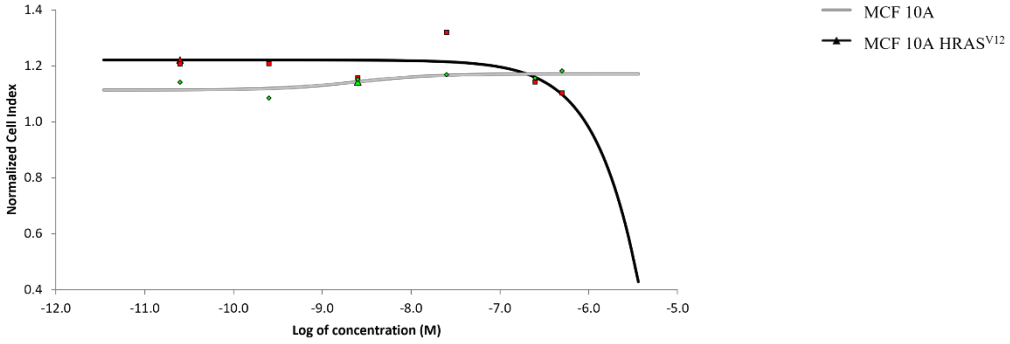
The real-time analysis supported the Alamar Blue result in that the MCF10A $HRAS^{V12}$ model treated with VPS34-INI, as shown in Figure 4-13A, resulted in a drug response, which was not observed in control MCF10A cells. This response appears specific to the transformed cell, where a typical drug response is exhibited with increased concentration and concomitant increase in cytotoxicity.

The efficacy of VPS34-INI was minimal, but it did reflect that of SAR-405, which targets ATP binding through a different mechanism. It does suggest that targeting VPS-34 specifically may need further adjustments in concentrations to be efficacious on its own and would warrant combination potentially with a frontline chemotherapeutic that elicits an autophagic response to determine its clinical efficacy.

A **Cell Viability of MCF 10A cells expressing HRAS^{V12} treated with VPS34 inhibitor VPS34-INI**



B **Real time analysis of IC50 for VPS34-INI treatment in MCF10A HRAS^{V12} cell lines**



C

Cell line	IC50 (M)	P value
MCF10A	Not converged	
MCF10A HRAS^{V12}	$2.4x10^{-5}$	0.0011

Figure 4-13 Transformation MCF10A with HRAS^{V12} responds differently to VPS34-INI treatment.

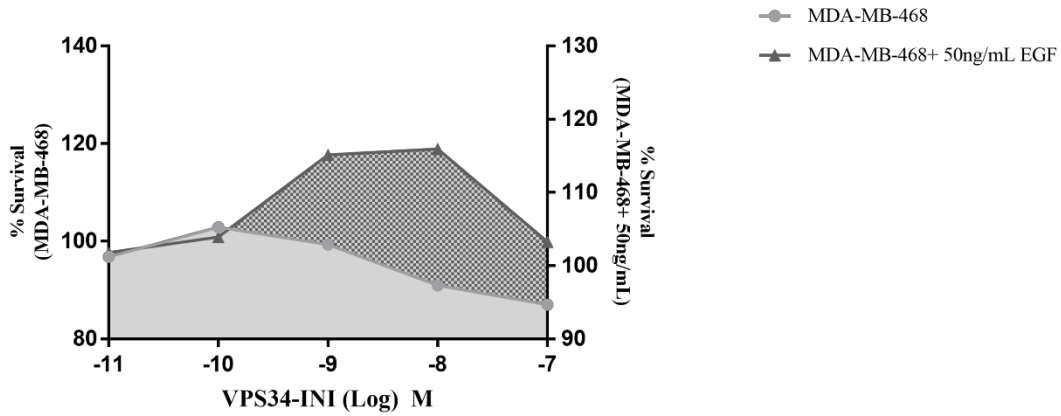
(A) A study of the cell viability using the traditional Alamar Blue analysis at the 24 hours timepoint. **(B)** Real-time analysis of MCF10A breast cell lines transduced with HRAS^{V12} in the Xcelligence system was used to determine the IC_{50} for the treatment with the VPS34 inhibitor VPS34-INI for 24 hours **(C).** The IC_{50} values of all cell lines as determined by RTCA software with a statistical analysis comparing the cell lines (n=4,±SD, $p<0.05$ ANOVA and Sidak's post hoc test)

4.3.8 The presence of EGF with breast cancer cell line MDA-MB-468 increased insensitivity to treatment with VPS34 inhibitor VPS34-INI.

The study included another VPS34 inhibitor to be tested, VPS34-INI, in the EMT model of RAS activation. As previously mentioned, in response to the EGF, the MDA-MB-468 cells generate a population of cells that lift and prefer to remain suspended and transiently adhere to the surface. This non-adherent cell population was observed to increase in treatment with both SAR-405 and VPS34-INI, excluding the real-time system, which uses adherence to determine the cell impedance (represented as a cell index). Similarly to the result observed earlier, using VPS34-INI resulted in no decrease in cell viability of greater than 20%. Therefore, the AUC was examined as depicted by the graph in Figure 4-14A. AUC was determined using Prism software with the baseline set at the control level of 100%. The result demonstrates that the presence of EGF significantly increased cell viability compared to the parental cell line.

The results in Figure 4-14 suggest that, at least initially, VPS34-INI increases cell number or proliferation, but there is a slight decline at the higher dose. Thus, suggesting the study should have potentially increased the drug concentration range to improve efficacy. Although at the time, this range was established in the current literature. The use of VPS34 inhibitors in the RAS active cellular context was limited by a lack of drug efficacy in this model, with 3Ma-IV the only inhibitor to result in cytotoxicity with an increase in sensitivity during RAS activation, as shown in Table 4-2. It would indicate that the effectiveness of 3Ma-IV is due to how it inhibits VPS34 or that it may be effective due to its non-specific effects. However, this has been shown to reduce and suggested to be absent in this derivative [331]. Given the consistency of 3Ma-IV throughout this study, it warrants further investigation.

A **AUC for the treatment of VPS34 inhibitor VPS34-INI in breast cell line MDA-MB-468 with EGF**



B

Cell line	AUC (Baseline set at 100)	P value
MDA-MB-468	18.61	
MDA-MB-468+50ng/mL EGF	37.49	0.0008

C **Cell Viability of breast cancer cell MDA-MB-468 in the presence of EGF treated with VPS34 inhibitor VPS34-INI**

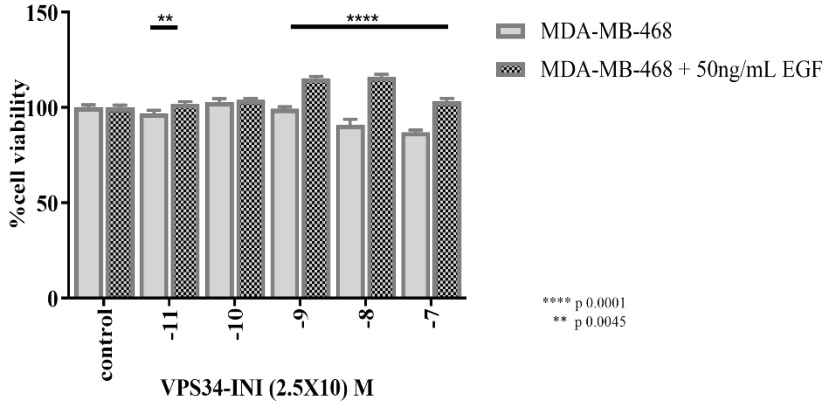


Figure 4-14 The presence of EGF ceases treatment efficacy with VPS34 inhibitor VPS34-INI.

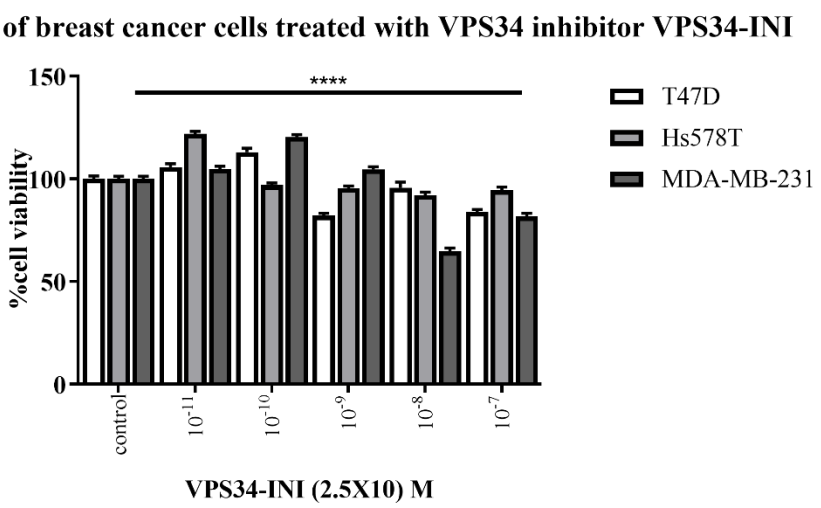
(A) Alamar Blue analysis was utilised to determine the AUC of breast cancer cell lines MDA-MB-468 in the presence of 50ng/mL EGF treated with VPS34 inhibitor VPS34-INI for 72 hours. **(B)** The AUC values of all cell lines as determined by prism software with a statistical analysis comparing the cell lines. **(C)** Cell viability Alamar Blue analysis at 24 hours timepoint. (n=4, ±SD, $p<0.5$ ANOVA and Sidak's post hoc test)

4.3.9 Response to VPS34-INI is reduced with increases in dose concentration in all breast cancer cell lines.

The breast cancer cell lines were last to be examined for their response to VPS34-INI. The treatment results were remarkable in that the observed responses were variable and not dose-dependent, with some cells responding at lower concentrations and not at all at the higher concentration. Figure 4-15 shows a decrease in cell viability at higher concentrations, although it never reached below 50% in any cell lines. The most significant decrease in cell viability was observed in the MDA-MB-231 compared to the real-time analysis. However, this response was not observed to be dose-dependent. The response was inconsistent, possibly due to that particular time or limited concentration range reflecting similar trends in the T47D cell line.

Conversely, the Hs578T cell line at the 24-hour timepoint showed a dose-response in cell viability, but beyond this time point, this cell line is more sensitive to the lower dose, suggesting that the drug activity rate is limited. For example, when the Alamar Blue data was analysed to determine the IC_{50} values, they were as follows T47D is $2.4X10^{-6}$ M, Hs578T is $9.72X10^{-6}$ M, and MDA-MB-231 is $1.05X10^{-6}$ M. The IC_{50} results in Figure 4-15B demonstrated that the sensitivity was highest in the MDA-MB-231 and T47D cell lines, and there was a decrease in the Hs578T cell line. In line with previous comments, the concentration range would benefit from being extended in future studies, and the range used for this study was based on the available literature [536]

A



B

Cell line	IC_{50} (M)	Comparison	P value
T47D	$2.4x10^{-6}$	Versus Hs578T Versus MDA-MB-231	<0.0001 NS
Hs578T	$9.72x10^{-6}$	Versus T47D Versus MDA-MB-231	<0.0001 <0.0001
MDA-MB-231	$1.05x10^{-6}$	Versus T47D Versus Hs578T	NS <0.0001

Figure 4-15 Limited dose-response to VPS34-INI treatment in breast cancer cell lines

(A) A study of the cell viability using the traditional Alamar Blue analysis at the 24 hours timepoint. Significance determined between groups. **(B)** The IC_{50} values of all cell lines as determined by prism software with a statistical analysis comparing the cell lines

These variations in cellular response prevented a confident IC_{50} from being determined by the Xcelligence. Alternatively, real-time analyse performed to examine the cellular response for the same period as the Alamar Blue assay to gain insight into the variability. As displayed in Figure 4-16, there is minimal impact on the cell index for the T4D and MDA-MB-231, which is in contrast to the viability data, and it may reflect the measurement difference of the experiments as the real-time is affected by cellular morphology and adherence whilst mitochondrial perturbations impact the Alamar Blue. However, the Hs578T did display a precise dose-related cell index, but it was not concentration dependant, which is curious.

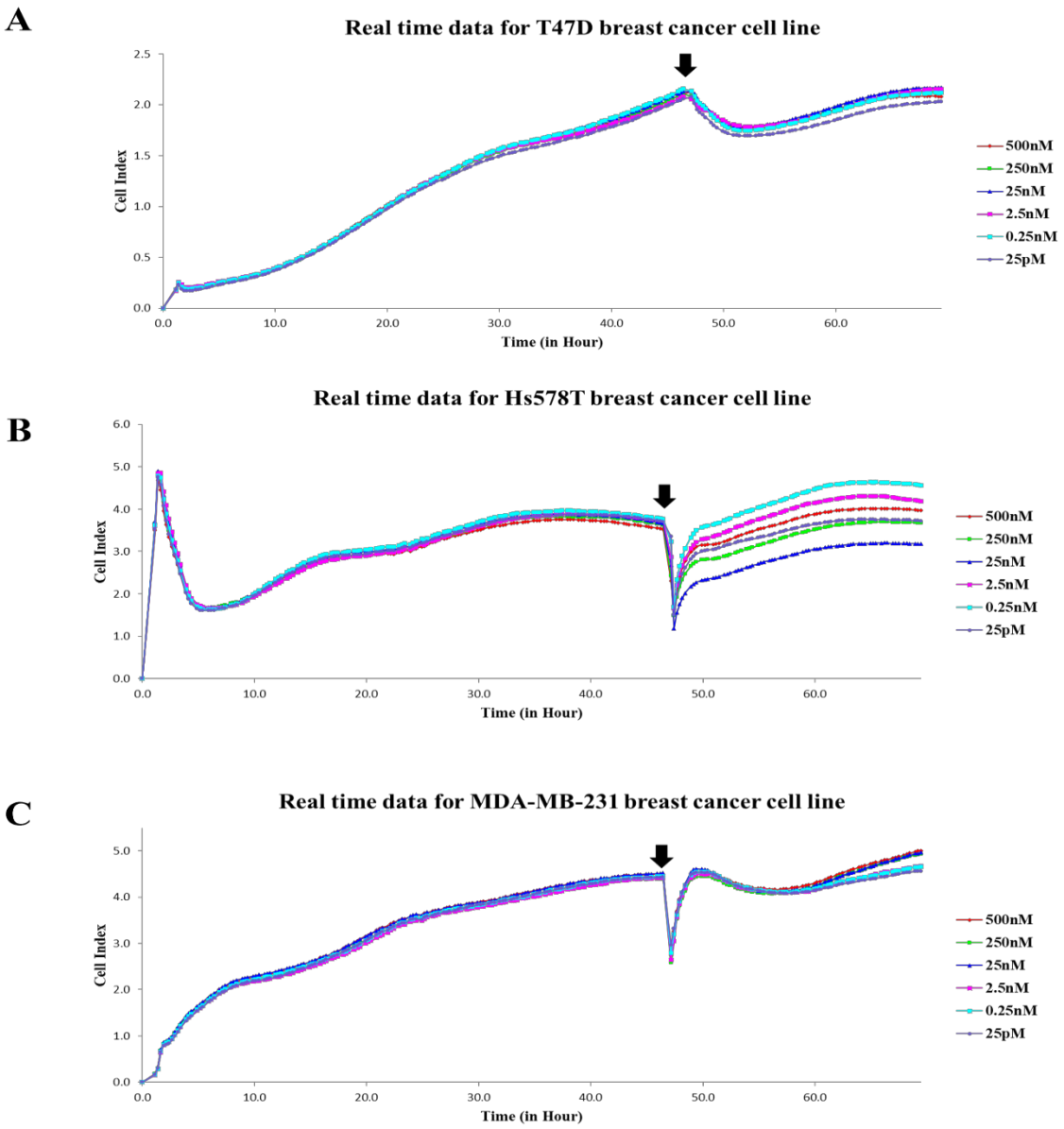


Figure 4-16 Real-time analysis demonstrates negligible response to VPS34-INI in breast cancer cell lines

The Xcelligence system was used to collect real-time analysis of breast cancer cell lines in response to VPS34-INI treatment **(A)** A representative data analysis of the T47D breast cancer cell line real-time data show no effect to cell index after VPS34-INI treatment (treatment addition indicated by the black arrow) **(B)** A representative image of Hs578T breast cancer cell over 72 hours (48 hour growth phase and 24 hour treatment) demonstrated dose dependant changes in cell index in response to VPS34-INI treatment for 24 hours of treatment **(C)** Representative data from the real time analysier for the MDA-MB-231 breast cancer cell line show no effect to cell index after VPS34-INI treatment. (n=4)

Collectively the results highlight the challenges of autophagic inhibition, at least at the initial stages, as shown in Table 4-2. The results were inconsistent between drugs; although they are all described as VPS34 inhibitors, these variations are proposed due to the difference in specificity and mechanism of action. Only the MDA-MB-231 showed increased sensitivity to VPS34 inhibition compared to mammary epithelial cell line MCF10A consistently across all the VPS34 inhibitors. The cell-permeable version of 3Ma-IV was the only drug that demonstrated a response expected from the observed autophagic activity in chapter 3, with a sensitivity increase within the more aggressive phenotypes. The results from SAR-405 indicate a loss of drug efficacy in the presence of the HRAS mutation but not KRAS. This differential response would be an important finding if this drug were used in a clinical setting. Finally, the response to VPS34-INI was the most intriguing because the increase in dose concentration abated its effects. These differences highlight the difficulty in cancer treatment as three drugs with the same target elicit three different responses, likely due to the individual differences in the cellular subtypes and the drug's mechanisms of action, or a combination of both

Table 4-2 Increased autophagic activity sensitises RAS active cells to VPS34 inhibition

Cell Line	3-Methyladenin (3Ma)	3-Methyladenine -IV (3Ma-IV)	Fold Change to MCF-10A	SAR-405	VPS34-INI
MCF-10A	**No Response**	**0.88M**		No Response	No Response
MCF-10A RAS^{V12}	**NT**	**0.0008M**	**1100**	**0.0001768M**	**$2.4x10^{-5}$ M**
MDA-MB-468	**NT**	**0.002M**	**440**	No Response	No Response
MDA-MB-468 +50ng/mL EGF	**NT**	**0.0005M**	**1760**	No Response	No Response
T47D	**NT**	**0.008M**	**110**	No Response	**$2.4x10^{-6}$ M**
Hs578T	**0.001668M**	**0.0006M**	**1466**	**0.0000112M**	**$9.72x10^{-6}$ M**
MDA-MB-231	**NT**	**0.0002M**	**4400**	No Response	**$1.05x10^{-6}$ M**

NT= Not Treated NA=Not Applicable

The previous experiments utilised drugs that targeted and inhibited VPS34 inhibition, a key player in the early stages of the autophagic process. Its inhibition demonstrated some significant responses and sensitivity, so it was considered that targeting later in the autophagic process may be promising. Therefore, the potential benefits of targeting the autophagic process at a later stage were examined using Bafilomycin A1 to compare and contrast previous results where the initiation complex was targeted. As depicted in Figure 4-17, Bafilomycin A1 inhibits lysosomal activity and fusion between the autophagosome and the lysosome to form the autolysosome.

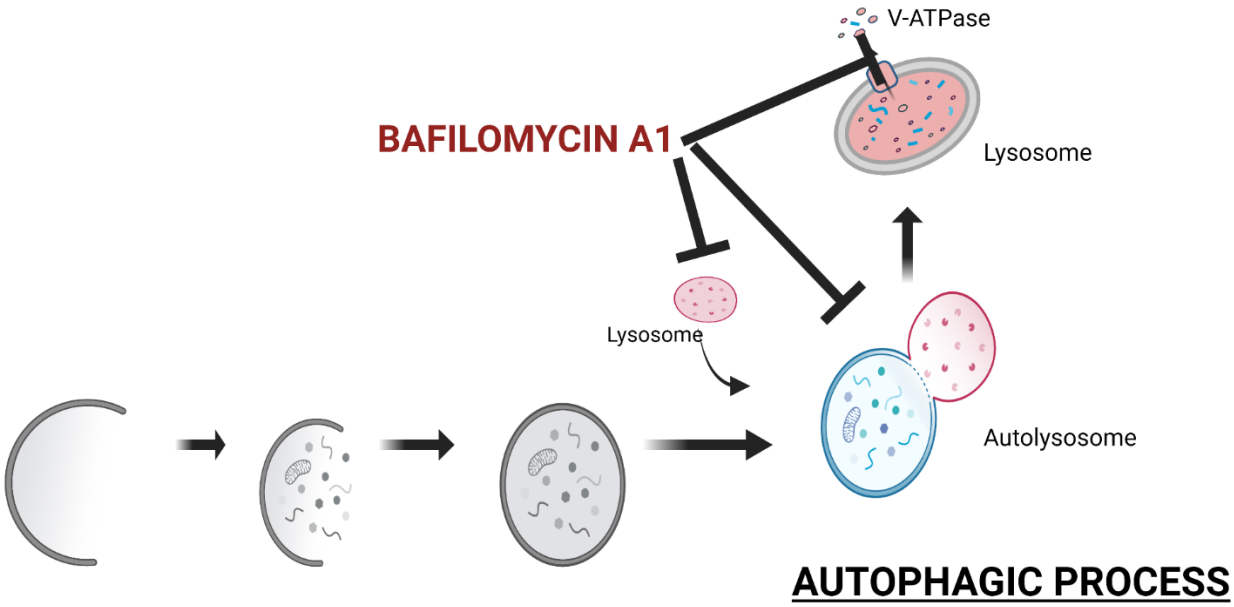


Figure 4-17 Schematic diagram of activity of Bafilomycin A1 on the autophagic process.

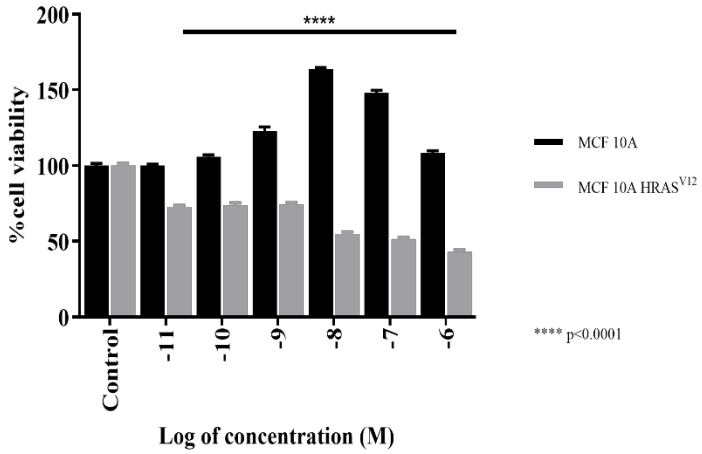
The diagram depicts where Bafilomycin A1 actively inhibits the autophagic process. The mechanism of action of Bafilomycin A1 is to inhibit the vacuolar H+ ATPase (V-ATPase). Consequently, this blocks proton influx, facilitating acidification within the lysosomal lumen and degradation of lysosomal content. Furthermore, the fusion of the autophagosome to the lysosome is also prevented.

Created with BioRender.com

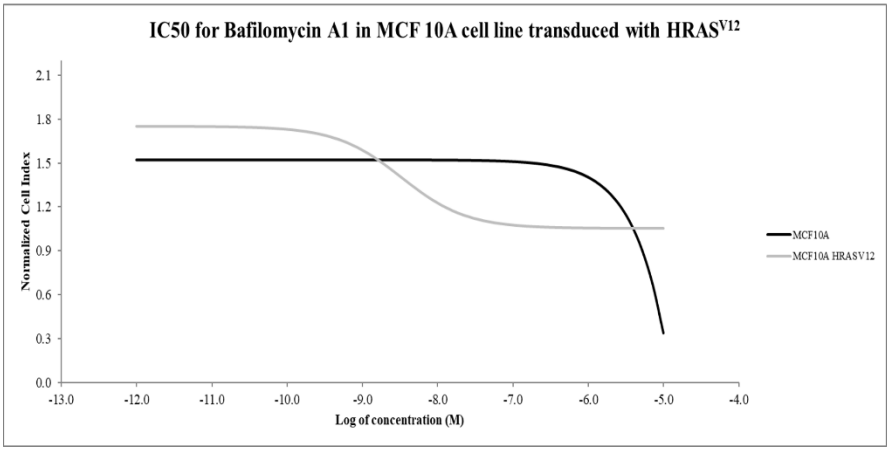
4.3.10 The presence of $HRAS^{V12}$ significantly increased sensitivity to vacuolar H+ ATPase (V-ATPase) inhibition with Bafilomycin A1 treatment.

The results in Figure 4-18 show that the recombinant expression of $HRAS^{V12}$ in the MCF10A cells significantly increased their sensitivity to Bafilomycin A1 treatment. The IC_{50} of Bafilomycin A1 was observed to have a 10^{8}-fold change in the IC_{50} compared to the control MCF10A cells. Consistent with these results, the Alamar Blue assay demonstrated a significant decrease in cell viability at the 24-hour timepoint. Surprisingly, the cell viability percentages increased with treatment in the MCF10A, suggesting an increase in cell number observed at all concentrations. The data also indicates that Bafilomycin A1 effects are observed quickly and at low concentrations in the context of oncogenic transformation and not observed in the immortalised "normal" counterpart. Further, these differences may reflect differences in the dependence of the cell type on the lysosome. Evidence suggests that transformed cells are more susceptible to lysosomotrophic agents as they induce cathepsin and TNF-dependent cell death pathways which may explain the variations observed here. [537]

A



B



C

Cell line	IC_{50} (M)	P value
MCF10A	2.45M	
MCF10A $HRAS^{V12}$	$3.30X10^{-9}M$	<0.0001

Figure 4-18 The presence of $HRAS^{V12}$ increases sensitivity to Bafilomycin A1

(A) An initial study of the cell viability using the traditional Alamar Blue analysis at the at 24 hours time point **(B)** Real-time analysis of MCF10A breast cell lines transduced with $HRAS^{V12}$ in the Xcelligence system was used to determine the IC_{50} for the treatment with vacuolar H^+ATPase (V-ATPase) inhibitor Bafilomycin A1.for 72 hours **(C)** The IC_{50} values of all cell lines as determined by RTCA software with a statistical analysis comparing the cell lines. (n=4, ±SD, $p<0.05$ ANOVA and Sidak's post hoc test)

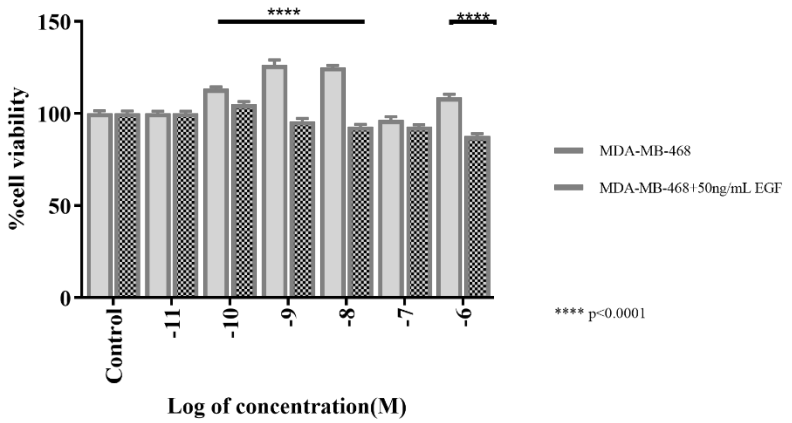
4.3.11 The presence of EGF with breast cancer cell line MDA-MB-468 did not change the sensitivity to treatment with vacuolar H+ ATPase (V-ATPase) inhibitor Bafilomycin A1.

The breast cancer cell line MDA-MB-468 were exposed to the EGF ligand to induce RAS activity to facilitate the epithelial to mesenchymal transition. In addition, this RAS active model was utilised to determine its response to later stage autophagic inhibition with the lysosomal inhibitor Bafilomycin A1. As depicted in Figure 4-19 denote a response to Bafilomycin A1 with or without EGF. The Xcelligence determined the IC_{50} to be similar between the MDA-MB-468 cell line and MDA-MB-468 +EGF cell line, with slightly higher sensitivity seen in the absence of EGF.

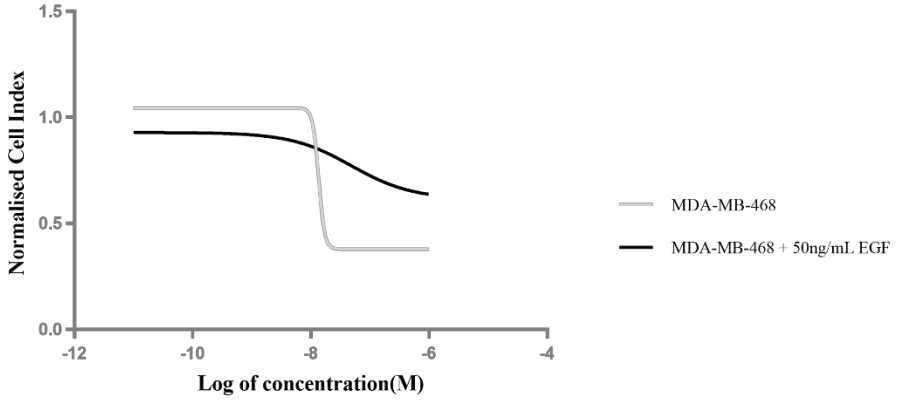
However, when we examine all the results from the Alamar Blue assay, it shows the MDA-MB-468 +EGF show an initial no change, even slight increase until above the 10^{-11} concentration, at which point there is a minimal decline in viability observed. In addition, the MDA-MB-468 cell line either maintained or increased cell number at all concentrations. This data suggests that significant responses to Bafilomycin A1 are observed beyond the 24-hour time point in the MDA-MB-468 cell lines with or without EGF.

The similarity between IC_{50} of the MDA-MB 468 with and without EGF exposure is a favourable indicator for the use of Bafilomycin A1 as it shows that its efficacy is not perturbed by the survival advantages and treatment resistance often EMT can provide.

A **Cell Viability of breast cancer cell MDA-MB-468 in the presence of EGF treated with BafilomycinA1**



B **IC50 for Bafilomycin A1 in MDA-MB-468 cell line in the presence of EGF**



C

Cell line	IC_{50} (M)	P value
MDA-MB-468	1.36X10 $^{-8}$M	N/A
MDA-MB-468+50ng/mL EGF	4.85X10 $^{-8}$M	N/A

Figure 4-19 The treatment with Bafilomycin A1 is as equally effective with or without the presence of EGF

(A) A preliminary study of the cell viability using the traditional Alamar Blue analysis at the at 24 hours timepoint **(B)** Real-time analysis of breast cancer cell lines MDA-MB-468 in the presence of 50ng/mL EGF seeded in the Xcelligence system to determine the IC_{50} for the treatment with vacuolar H+ ATPase (V-ATPase) inhibitor Bafilomycin A1.for 72 hours **(C)** The IC_{50} values of all cell lines as determined by RTCA software with statistical analysis comparing the cell lines. (n=4, ±SD, $p<0.05$ ANOVA and Sidak's post hoc test)

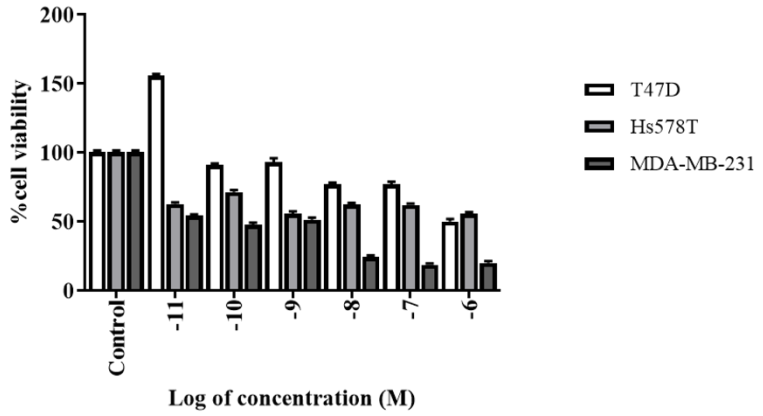
4.3.12 Lysosomal inhibition demonstrated efficacy in all breast cancer cell lines but significantly increased in the triple-negative subtype.

The increased efficacy of Bafilomycin A1 observed with the expression of $HRAS^{V12}$ was investigated further to determine if it would be translated to the breast cancer cell lines either with or without RAS mutation. The analysis from the Xcelligence demonstrates that treatment with Bafilomycin A1 is effective in all cell lines (Figure 4-20). The IC_{50} values show a significant difference between T47D and Hs578T breast cancer cell lines, but an even greater significance was observed between T47D and MDA-MB-231 breast cancer cell lines (Figure 4-20).

Furthermore, it implies that the sensitivity is predominantly RAS driven but potentially has other contributing factors. Notably, no significant differences in the type of RAS mutation as witnessed between the IC_{50}'s of Hs578T and MDA-MB-231 breast cancer cell lines. The Alamar Blue results are variable, with a consistent and robust response observed in the MDA-MB-231 cell line at all concentrations, indicating a dose-dependent response. The Hs578T cell line showed a decrease in cell viability, although the changes in viability between concentrations were variable and did not reflect a dose-dependency. This variability may reflect the 24-time points compared to the Xcelligence, continually examined over an extended 24-hour time course. For example, further decreases in viability might be observed at 48 hours and, as such, would not be seen in the Alamar Blue assay performed in Figure 4-16C. Similarly, the T47D cell line data from the Alamar Blue was unusual at the 10^{-11} M concentration of Bafilomycin A1, and the cell viability increases indicative of an increase in viable cells. However, subsequent doses resulted in a consistent decline in viability in all concentrations. When the cell viability between cell lines was compared, a significant difference was observed between all cell lines.

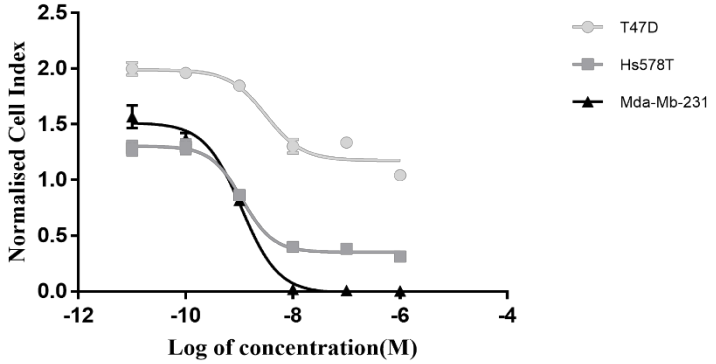
The data from Figure 4-18 and Figure 4-19 demonstrate a sensitivity of the breast cancer cells to the treatment of Bafilomycin A1, and this same efficacy was not witnessed in the immortalised normal cell line MCF10A. Interestingly, the results indicate a slight increase in sensitivity in the RAS mutant cell lines Hs578T and MDA-MB-231 compared RAS to wild-type cell line, T47D. A tremendous significance is observed between the normal cell line and all oncogenic cell lines.

A **Cell Viability of breast cancer cell lines treated with Bafilomycin A1**



T47D Vs Hs578T P<0.0001 T47D vs MDA-MB-231 P<0.0001 Hs578T vs MDA-MB-231 P<0.0001

B **Bafilomycin A1 treatment of breast cancer cell line T47D, Hs578T and MDA-MB-231**



C

Cell line	IC_{50} (M)	Comparison	P value
T47D	$3.32X10^{-9}M$	Versus Hs578T Versus MDA-MB-231	0.0486 0.0225
Hs578T	$1.15X10^{-9}M$	Versus T47D Versus MDA-MB-231	0.0486
MDA-MB-231	$1.02X10^{-9}M$	Versus T47D Versus Hs578T	0.0225

Figure 4-20 Bafilomycin A1 treatment efficacy is improved in the aggressive phenotype

(A) A pilot study of the cell viability using the traditional Alamar Blue analysis at the 24 hours timepoint. Significance determined significance T47D Vs Hs578T P<0.0001, T47D vs MDA-MB-231 P<0.0001 and Hs578T vs MDA-MB-231 P<0.0001 **(B)** Real-time analysis of breast cancer cell lines T47D, Hs578T and MDA-MB-231in the Xcelligence system was used to determine the IC50 for the treatment with vacuolar H+ ATPase (V-ATPase) inhibitor Bafilomycin A1.for 72 hours **(C)** The IC_{50} values of all cell lines as determined by RTCA software with a statistical analysis comparing the cell lines (n=4, ±SD, p<0.05 ANOVA and Sidak's post hoc test)

The investigation into the efficacy of autophagic inhibition with Bafilomycin A1 has shown significant efficacy *in vitro*. However, the results do not portray any significant influence of RAS activation on efficacy. When results from other figures (Figure 4-18 and Figure 4-20) are examined, there is a significant increase in the efficacy of treatment with Bafilomycin A1 in RAS mutant cell types, which include MCF10A $HRAS^{V12}$, Hs578T and MDA-MB-231 cell lines. Nevertheless, when all IC_{50} values are tabulated in Table 4-3, it demonstrates that although RAS mutation may increase sensitivity, oncogenesis is the most significant marker for efficacy in Bafilomycin A1. These results highlight the potential of a promising target for future breast cancer treatment.

Table 4-3 Increased autophagic activity sensitises RAS cells to lysosomal inhibition

Cell Line	BafilomycinA1	Fold Change to MCF-10A
MCF-10A	2.45M	
MCF-10A RAS^{V12}	$3.30X10^{-9}M$	$7.42X10^{8}$
MDA-MB-468	$1.36X10^{-8}M$	$1.80X10^{8}$
MDA-MB-468 +50ng/mL EGF	$4.85X10^{-8}M$	$5.05X10^{7}$
T47D	$3.32X10^{-9}M$	$7.38\ X10^{8}$
Hs578T	$1.15X10^{-9}M$	$2.13X10^{9}$
MDA-MB-231	$1.02X10^{-9}M$	$2.40X10^{9}$

4.4 DISCUSSION

It was established that the increased presence of autophagic activity could be correlated to a subset of cells, which all share a similar characteristic of either a RAS mutation or aberrant RAS activity, which, in turn, contributes to a more aggressive phenotype. These more aggressive phenotypes are identified clinically due to their limited treatment options and propensity to metastasise. Therefore, this study has focused on the feasibility of targeting the early autophagic process as a treatment plan for RAS mutant/activated highly advanced cell types in breast cancer. Although further examination is needed, the results point to the use of autophagy inhibitors as a potentially effective treatment, particularly in the most aggressive phenotypes, which are usually resistant to treatment and highly metastatic.

4.4.1 The VPS34 inhibitor's treatment efficacy was more influential in the transformed cells than normal counterparts.

To delineate the positive results of the VPS34 inhibitors observed in the transformed cell lines, the indirect or other aspects of VPS34 activity need to be considered. The literature has identified that VPS34 can form another complex called complex II, which excludes ATG14 in exchange for UVRAG. It is shown that this complex II has a regulator of endosomal trafficking [538]. Of interest, both complexes rely on the direct binding of VPS35 and VPS15, which is what all the VPS34 inhibitors prevent, which has been demonstrated in SAR-405 and VPS34-INI [538, 539]. Although there were effects for inhibition of the endosomal pathway by 3-Ma observed by Punnonen et al., there is no evidence to date that this occurs with its derivative 3Ma-IV [540]. It is plausible that the loss of this endosomal trafficking could result in the cytotoxicity observed, and interestingly, the blockade by Bafilomycin A1 also blocks this trafficking. Palinov et al. demonstrated an inhibitory effect on the endocytic pathway with SAR-405 at around 12.5μM [538]. This concentration was used in this study, and it is speculated that it may explain some disparities between the real-time analysis and cell viability with SAR-405 treatment. It is plausible that there were changes to cell shape and adherence at the higher

concentrations affecting the cell index as the endosomal pathway is known to have regulatory roles in membrane dynamics and enzyme activation [541].

It is accepted that the inhibition of VPS34 and its subsequent blockage of the canonical pathway does not render the cell incapable of autophagic processing. The non-canonical pathways could be utilised or suggested that CMA could fulfil some of the loss of autophagy role [542]. However, westerns have not been performed, so a lysosomal inhibitor later in this study allowed crosstalk between other autophagic processes such as CMA to be removed [543]. It is suggested that these alternate responses to VPS34 inhibition were utilised in the normal mammary epithelial cell line MCF10A hence why there was limited response to VPS34 inhibition. This has also been shown in VPS34 null mice that there was no toxicity to mammary epithelial, although it was observed in the heart and liver, which is worth noting from a clinical perspective [544, 545]. If this were proven correct, it would be interesting to ascertain why the transformed cell does not have such capabilities and reinforces the result from chapter 3 demonstrating a dependence on autophagy once the cell transforms, particularly with RAS mutation.

More recently, evidence suggests that VPS34 has another pivotal role not relating to autophagy or the endosomal pathways that may give further clarity on the observed effects and direction for future investigations for this study. It has been suggested that VPS34 has a significant role in tumour progression. Jiang et al., comparative study of breast cancer, suggested that VPS34 has a pivotal role in tumourigenesis through the regulation of P62 at a transcriptional level by binding Keap-1, causing the release of NRF-2, resulting in the transcriptional activation of oncogenes [546]. Furthermore, it showed that the binding of P62 and Protein kinase C-delta (PKCδ) results in the activation of the MEK-ERK pathway [546]. The study by Jiang et al. suggests that the accumulation of VPS34 is the catalyst for this tumourigenic activity. This accumulation of VSP34 needs to be examined in response to its inhibition, as it is not clear from the literature if this would occur and was beyond the scope of this study. It warrants investigation to determine whether the inhibitors accumulate VPS34 or degradation and prevent interactions with PKCδ or P62. If not, the combination of VPS34 inhibitor with MEK-ERK inhibitor may be advantageous.

These observed differences between treatment responses may be due to some of the findings discussed by other studies. All have highlighted molecular crosstalk with VPS34, which could explain some of the disparities observed between the cell lines. Although this

can only be postulated at this stage, further elucidation of the molecular mechanisms underpinning these variations in the cell lines is required.

4.4.2 VPS34 inhibition is an efficacious treatment to target the aggressive breast cancer phenotype.

The inhibition of autophagy has proven to be a complex target due to its dynamic nature; the challenge has been deciding at what point to target the process. This study has centred around the efficacy of inhibiting the earlier stages of the autophagic process, specifically the initiation complex. Several molecules exist within that initiation complex, but many current inhibitors target the VPS34 enzyme [547-549].

VPS34 role is to phosphorylate phosphatidylinositol to produce PtdIns3P. PtdIns3P recruits molecules and regulators of protein-sorting pathways, specifically the autophagic and endocytic pathways. VPS34 has recently been observed in two complexes: complexes I and II. Both complexes have the same core units but vary by one sub-unit. Complex I comprises VPS34, VPS15, Beclin 1, and ATG14L, whereas complex II replaces ATG14L with UVRAG [550-552]. The literature has shown that these complexes have functional similarities and differences, with both complexes involved in autophagy. The differences are observed within complex II, which has an active role in the endocytic pathway and localisation. Several existing and newly identified small molecules or drugs inhibit VPS34 [553].

The Hs578T cell line's sensitivity to most of these inhibitors except for SAR-405 may be related to the other functions of VPS34 previously identified in that it is a positive regulator of the MTORC1/S6K1 pathway. These are downstream components of the PI3K pathway of which the Hs578T cell line has a functional mutation of PIK3R1, resulting in an upregulation of p110α and PTEN, respectively, with a net increase in PI3K signalling [554-556]. These upregulations can further explain the high sensitivity of Hs578T to 3Ma-IV, although, as mentioned previously, this derivative should not affect PI3KC1. However, Chicote et al. observed changes to AKT activation with 3Ma-IV, but specifics of the type PI3KC1 isoforms were described, and the activity towards AKT was less than 3Ma [331, 557]. The parent drug 3Ma is known to have activity on PI3K class I, specifically p110Y, but interestingly has not been indicated to have any effect on p110α. Although these

findings suggest some interaction between 3Ma-VI with p110α but further investigations are needed to confirm this. These other roles of VPS34, related explicitly to PI3K signalling, may be why the VPS34 inhibitor 3Ma-IV was consistently efficacious in all cell lines, with nearly all having a gene mutation that correlates with the PI3K pathway. This observation includes the T47D cell line, which has a PI3KA mutation resulting in a constitutive active p110α again, though there is no evidence of activity of 3Ma-IV on this isoform, and the p110Ɣ is encoded by a different gene (PI3KCG). This gene that encodes for p110Ɣ is known to interact with RAS, particularly KRAS. At the very least, the potential for the VPS34 inhibitor, notably 3Ma-IV, offers promising potential on many fronts, not just its ability to block oncogenic autophagy but to target other dysregulated molecules such as mTOR, YAP and Src in many cancers. These aberrations are commonly observed in the MDA-MB-231 cell line.

Due to the NF2 deletion, YAP and Src have unregulated activity in tumorigenesis [558-560]. Notably, Src inhibitors are currently limited in the clinical setting due to the high homology amongst the Src family members, leading to the low specificity of the drugs. Consequently, an increase in off-target effects, including but not limited to cardiotoxicity, has limited its feasibility as a target within the clinical setting. So an alternate target such as VPS34 inhibition may be feasible to target these pathways without the adverse effects [561-564].

Inhibition of VPS34 may also constitute a potential treatment option with increased efficacy towards triple-negative subtypes B, which display a mesenchymal phenotype; these include Hs578T and MDA-MB-231. However, regarding SAR-405, there was sensitivity observed by the real-time analysis in the Hs578T cell line, similar to MCF10A $HRAS^{V12}$, indicating that SAR-405 has improved efficacy in only these cell lines and was not effective in the others and may be reflective of the fact that it was repurposed drug. Furthermore, the data suggest that the HRAS mutation may have a role in response to this treatment. Although contrary to the observed increase in real-time, there was a decrease in cell viability in these cell lines in response to treatment with SAR-405, so further experimentation to determine if there are morphological changes with treatment in these cell lines may explain these discrepancies. The data from the treatment with VPS34-INI displayed a response independent of concentration or not linear, suggesting that other downstream targets may be responsible. This may support Bago et al. [340] previous suggestion that the localisation of PtdIns(3)P generated by VPS34 at the endosome was not

wholly lost and recovered by PI3K class II. It warrants further investigation, which may include exploring glycogen synthase kinase 3 (GSK3) levels and has been indicated as a robust biomarker for VPS34 activity [340]. To delineate whether the effects observed were off target or an alternate pathway circumventing the need for the PI3KC3 initiation complex is yet to be elucidated. Alternatively, this ineffectiveness may point toward the study's limitations and could be resolved with further experimentation to screen a broader concentration range and include repeated dosing regimens.

4.4.3 VPS34 inhibitors as a potential dual-target for RAS and autophagy in breast cancer.

The increased efficacy was observed in the RAS mutant cell lines, particularly the HRAS, referring to Hs578T, MCF10A $HRAS^{V12}$ and MDA-MB-231cell lines. These cell lines were susceptible to 3Ma-IV, and this efficacy was observed in the other VPS34 inhibitors but not to the same degree, but all transformed cells responded significantly compared to the MCF10A. This improved efficacy may indicate that 3Ma-IV's other PI3K class activity is vital in this context. It is proposed to be related to RAS localisation. RAS can localise anywhere and is not exclusively on the plasma membrane, particularly HRAS; instead, it is trafficked via the exocytic pathway via the Golgi to the plasma membrane. Post-translation modifications are suggested to dictate the localisation. However, all isoforms start at the ER, where enzymes facilitate these post-translational modifications [565, 566]. It was also shown that RAS activation could occur whilst the molecule is located at E.R., Golgi and even during transport to the plasma membrane. It is suggested that VPS34 inhibition could interfere with this localisation process of RAS through its effects on PI3P and may be reflected in the sensitivity seen by cell lines with HRAS mutation [565, 567]

The finding of current literature has alluded that RAS activity is not limited to the plasma membrane, but there is much evidence that RAS activity against downstream targets is often conducted whilst it is being translocated. An example of this is HRAS which engages Raf-1 on the Golgi. Furthermore, it has also been identified that the palmitoylation of HRAS and NRAS directs its movement between ER and Golgi for CAAX processing. It was observed that they could be activated on the endosome

membrane. Interestingly, ER restricted RAS can activate JNK from the plasma membrane, and ER tethered RAS can activate and directly signal to MAPK from this location [568]. Further studies have shown that HRAS preferentially translocates from the Golgi rather than the ER, and it has been shown to alter its activation of the RAF pathway due to the lack of available RAF [569].

Chapter 3 demonstrated a linkage between autophagy and RAS; it is suggested that RAS activates autophagy to support its activity and then becomes reliant on it. Using VPS34 inhibitors in this RAS active model of breast cancer was not as straightforward as predicted, given there was a dose-dependent response to the treatment with 3Ma-IV with improved sensitivity in the presence of EGF. It would indicate that the effectiveness of 3Ma-IV is due to how it inhibits VPS34, or more likely, due to its off-target effects. Given the consistency of 3-Ma-IV throughout this study, it warrants further investigation. Regarding SAR-405, its loss in efficacy in particular cell types is of concern and should be examined as this is currently progressing into clinical trials. Finally, VPS34-INI was limited by this study design. It is feasible to consider that the increases in cell viability may be a transient response due to the time or drug concentration limitations. Alternatively, which was not examined here, is the potential of these VPS34 inhibitors being used in combination with current first-line chemotherapeutics to assess their viability in a clinical setting and should be the future direction of this study as their use in this context has not been assessed yet.

4.4.4 The lysosomal inhibitor showed improved efficacy in all subtypes compared to the control.

The data from this study has clearly shown that autophagic inhibition is a promising future target for breast cancer treatment. The initial finding relating to VPS34 inhibition were inconsistent, suggesting that the need for VPS34, at least in the context of breast cancer, could be circumvented, particularly in the least aggressive phenotypes. There is a potential for VPS34 inhibition with 3Ma-IV in the context of either mutation, as the evidence suggests this relates to an increase in significant efficacy. Bafilomycin A1 treatment yielded a robust response across all cancer cell lines displaying an expected cytotoxic profile. Although the effects in the cell lines did show a trend toward RAS

activity, there was increased sensitivity in the cell lines with RAS mutation, namely Hs578T and MDA-MB-231 cells. Importantly was the observed difference in sensitivity to Bafilomycin A1 in cancer cells compared to the normal cell, which has been observed in other studies of different cancer types [570-572]. It is worth noting that these results may reflect mitochondrial effects of the Bafilomycin A1 has been shown to cause mitochondrial swelling through its ability to act as potassium ionophore; this was observed at nanomolar concentrations [353]. It will warrant further investigation in the context of breast cancer and the RAS mutated cell lines to determine if the effects are related to autophagic inhibition, mitochondrial dysregulation, or, most probably, both.

The overall variability highlights the complexities of targeting autophagy; it is clear from chapters 3 and 4 that autophagy is vital in the context of breast cancer, particularly metastatic disease. However, focusing our target on macroautophagy will be challenging with potential positive and negative outcomes, and the ability to circumvent inhibition is problematic. Nevertheless, this increase and significant efficacy of Bafilomycin A1 has shown tremendous potential in focusing on the later stages of the autophagic process and the lysosome. Therefore, further investigation of the actions of Bafilomycin A1 has led this study to direct its attention to the more targeted type of autophagy located at the lysosome chaperone-mediated autophagy (CMA).

4.4.5 Bafilomycin A1 highlights the potential of lysosome inhibition for breast cancer treatment.

This research into inhibiting the lysosome via blockade of the vacuolar H+ ATPase (V-ATPase) with Bafilomycin A1 has shown a novel sensitivity in all breast cancer cell lines. These results are particularly encouraging when the response is not observed in the regular mammary epithelial cell line. Some studies suggest the role of the lysosome is altered in cancer [573, 574] and, as such, is more sensitive to inhibition. Furthermore, it directs attention to another specific and targeted autophagy that occurs at the lysosome known as chaperone-mediated autophagy (CMA), inhibited functionally by Bafilomycin A1 [575, 576]. Thus, it is postulated to have a role in maintaining the oncogenic phenotype, and due to lysosomal inhibition, it is no longer able to facilitate these changes.

The mechanisms underpinning the cytotoxic effects of Bafilomycin were recently described in a study by Fitzwalter et al. identified FOXO3A as regulated through autophagy. As a consequence of Bafilomycin A1 inhibition, there was an increase in PUMA, resulting in a concomitant upregulation in apoptosis [357]. This increase in PUMA in response to Bafilomycin A1 treatment was also shown to be the mechanism responsible for cytotoxicity in hepatocellular carcinoma cell lines in a study by Yan et al. [356]. Although the mechanism underpinning the results observed here was beyond this study's scope, it gives some support and rationale to the cell death observed in this study. It should be noted that the study suggests this lends itself to dual-target with an MDM2 inhibitor, and it did look at the MCF10A [357]. So it would be interesting to interrogate whether this regulatory axis between FOXO3A and PUMA is more sensitive in the triple-negative subtypes, and thus Bafilomycin A1 treatment alone has an impact and negates the need for an adjuvant.

The response of the triple-negative subtype to Bafilomycin A1 in this study is in line with a previous study by Morgan et al. that demonstrated that in bladder cancer, the metastatic phenotype was more sensitive to lysosome inhibition [577]. In agreement with this study's findings, it also went on to suggest that targeting the lysosome can offer a dual effect in inhibiting both autophagic and lysosomal dependency. The data as a whole suggests there may be the potential to combine VP34 inhibitors such as 3Ma-IV with Bafilomycin A1 as a more effective treatment strategy.

Finally, all transformed cells responded to treatment of Bafilomycin A1, with efficacy increased in the presence of a RAS mutation. This effect needs to be explored further to determine if the response is due to inhibition of autophagy or CMA. The result presents an increased sensitivity of advanced cancer cells to autophagy inhibition; however, the question that these results have highlighted is at what stage of the autophagic process is the most effective. Alternatively, is the treatment of multiple stages a better option that need to be resolved? To guide the development of future drugs to inhibit autophagy as it is a promising adjuvant treatment strategy for targeting the metastatic disease.

4.5 CONCLUSION

In summary, the use of VPS34 inhibitors was influential in the RAS mutant cell lines compared to the non-transformed counterpart. The result has indicated that autophagy is a viable target in the RAS transformed cell lines, particularly and consistently in the MDA-MB-231 breast cancer cell line. Although the results varied between drugs, it was demonstrated that the transformed cell is sensitive to autophagic inhibition at the very least. Furthermore, it was demonstrated that VPS34 inhibition had differing efficacy between the drugs, which is suggested due to the multiple targets of 3Ma-IV and indicates that using a pan inhibitor rather than a specific one is a more efficacious treatment strategy. Finally, Bafilomycin A1 has demonstrated itself to be a robust treatment strategy against all breast cancer subtypes with limited efficacy on normal mammary cells, highlighting the importance of the lysosome in the context of breast cancer. The lysosomes are the central hub for all autophagic processes, further empahsising the promising target option autophagy could offer in breast cancer treatment.

Chapter 5: THE ROLE OF CHAPERONE-MEDIATED AUTOPHAGY IN THE DEVELOPMENT AND PROGRESSION OF BREAST CANCER

5.1 INTRODUCTION

Chaperone-mediated autophagy (CMA) is a targeted form of autophagy in which proteins are recognised for degradation by the presence of a KFERQ motif [578]. HSC70 and its co-chaperones bind this KFERQ motif on the CMA substrate and deliver it to Lamp2A for translocation into the lysosome for degradation. Lamp2A is a lysosomal transmembrane protein containing a cytosolic tail, transmembrane domain and luminal tail. The HSC70 targeting complex binds to the cytosolic tail of Lamp2A, stimulating multimerisation of Lamp2A to facilitate translocation of the unfolded protein to within the lysosomal lumen for degradation. This protein translocation to the luminal side is aided by lysosomal HSP90 and HSC70 and other molecules, as detailed in chapter 1. After the target protein has been translocated, the Lamp2A returns to its monomeric state, either retained in the lysosomal membrane for further use or degraded (Figure 5-1) [259, 274, 579-581].

Dice et al. identified CMA as a targeted degradation process for maintaining cellular proteostasis, first reporting this approximately 25 years ago [259, 582]. Since then, much has been learned, albeit slowly, as experimental progress has been constrained by the fact that it is only conserved in mammalian systems and has only been reviewed in humans and mice. Nevertheless, research has progressed since CMA key effectors Lamp2A and HSC70 were described with the recognition of the targeting motif. Co-discoverer of CMA, Prof. Ana Maria Cuervo, has been proactive in CMA research and instrumental in developing many tools to aid further research and understanding of CMA. One such tool has been the publicly available KFERQ-finder platform to identify canonical KFERQ motifs and putative KFERQ-like motifs exposed as targets due to acetylation or phosphorylation [264].

This platform is helping researchers better understand how and why CMA is vital for many disease states and guide future treatment strategies. CMA has been implicated in ageing [1], neurodegenerative disorders [583], immunological development [584], and cancer [575, 585-587].

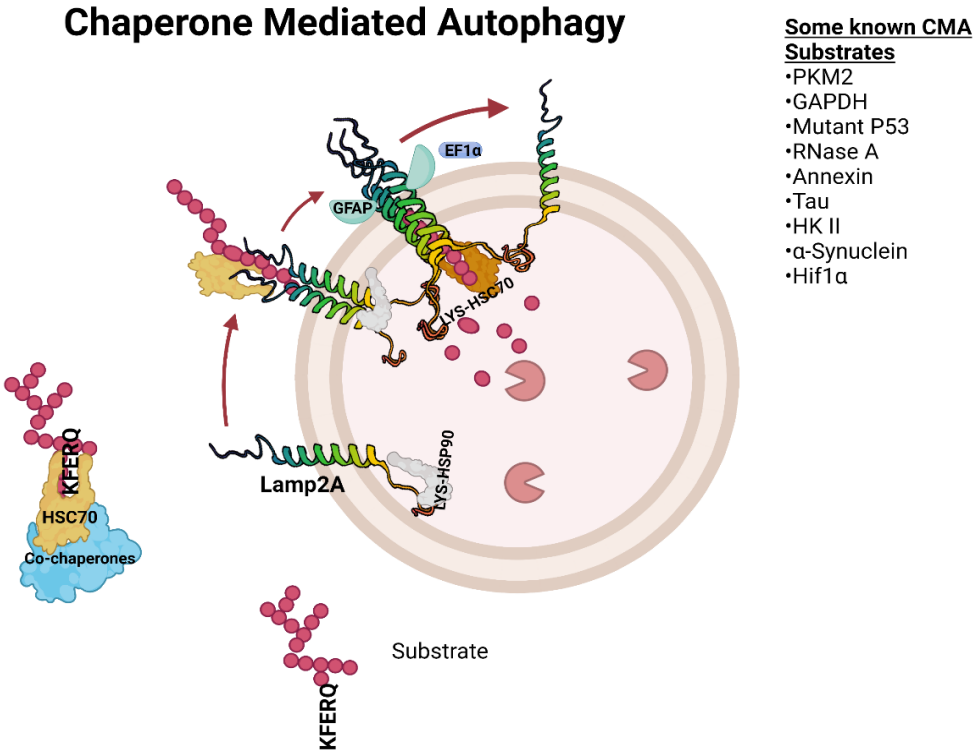


Figure 5-1 Schematic of substrate processing by chaperone-mediated autophagy

The process of CMA degradation involves recognising CMA-specific substrates with the presence of the KFERQ motif, which is bound by cytosolic HSC70. The HSC70 itself is further bound by co-chaperones such as the C-terminus of HSC70-interacting protein (CHIP), the heat shock protein 40 (HSP40) and the HSP70–HSP90 organising protein (HOP). The bound substrate is then translocated to the lysosomal membrane, where the HSC binds Lamp2A, facilitating protein unfolding. Whilst this is underway, the lysosomal HSP90 initiates multimerisation stabilised by GFAP. The Lamp2A multimer enables the unfolded protein to cross the lysosomal membrane for degradation aided by lysosomal HSC70. The Lamp2A multimer disassociates to monomeric forms available for further substrate binding and translocation. Alternatively, it is cleaved by cathepsin A and metalloproteinase to degrade it by the lysosomal hydrolase.

Regarding this study in the context of cancer, CMA key effectors are both upregulated or downregulated, suggesting it as a pro-tumorigenic and a tumour suppressor that appears to be both cell and context-specific [588, 589]. Therefore, this study seeks to gain an in-depth understanding of CMA in the role of breast cancer progression and contribute to understanding CMA in the context of breast cancer.

This study will examine the functional effects of CMA in the cellular context and will knock down the critical effector Lamp2A. First, note that the lentivirus was explicitly directed at Lamp2A as it is one of three transcript variants of Lamp2. The other variants include Lamp2B and Lamp2C. All Lamp2 variants conserve the same luminal region but differ in the transmembrane domain and the cytosolic tails. Thus, they are functionally independent, although theoretically, they could all share their luminal functions [581, 590, 591].

As described in chapters 3 and 4, the previous findings of this thesis have directed the focus of this chapter to be on CMA. This focus on CMA culminated after it was observed in the earlier chapters that macroautophagy was upregulated in breast cancer with mutated and or hyperactivated RAS. This finding leads to examining the feasibility of macroautophagy inhibition as a treatment option for breast cancer. The inhibitors utilised to examine this was VPS34 inhibitors that target the initiation complex, of which several inhibitors have varying specificity. As a comparison, the study also investigated the efficacy of a lysosomal inhibitor, and the results showed varying levels of efficacy with the VPS34 inhibitors but revealed a consistent and increased efficacy with the lysosomal inhibitor. Following these results, the more selective autophagic process CMA became of interest and warranted further investigation as research in this area is still somewhat limited. At the start of this study, there was minimal research into CMA concerning cancer [307], but it has evolved slowly since. Therefore, this chapter will focus on an initial screen for the presence of CMA's essential effector proteins Lamp2A and HSC70 within cell lysate and, more specifically, the lysosomal fraction to identify altered expression within these cell lines. Based on the expression levels of Lamp2A, several cell lines were chosen for further functional studies. Notably, no tetracycline-inducible Lamp2A vector was available at the beginning of this study, so one was developed as described in Chapter 2. Through the knockdown of Lamp2A, this study can ascertain the importance of CMA in cell biology [592]. These findings will add to and expand the current knowledge of CMA in breast cancer and may lead to promising future research into improving patient treatment options.

5.2 HYPOTHESIS AND AIMS

Hypothesis: "Chaperone-mediated autophagy key molecule Lamp2A is a key mediator of breast cancer cell growth and progression."

The aims of this chapter are:

-Identify the presence of Lamp2 and its transcript variants Lamp2A and Lamp2B in a progressive panel of breast cancer cell lines.

-To determine if Lamp2A levels change in the RAS progressive panel of active and mutated cell lines from the previous studies.

-Investigate the functional changes in breast and breast cancer cell lines from the basal subtype with an inducible Lamp2A knockdown.

-To examine the role of Lamp2A in the mesenchymal phenotype.

5.3 RESULTS

5.3.1 Lamp2A expression is increased in more aggressive breast cancer phenotypes.

An initial screen of a progressive panel of breast cancer cells was undertaken to observe the expression pattern of the CMA effector protein Lamp2A. In addition, the correlation between CMA and breast cancer cell phenotype was examined in a panel of breast cancer cell lines with the inclusion of a 'normal' breast cell line, as demonstrated in Figure 5-2. Finally, the numerous breast cancer cell lines were ordered from least to the most aggressive phenotype as a model of the breast cancer progression continuum.

The results from Figure 5-2 demonstrated a significantly higher expression of Lamp2A in the more aggressive breast cancer cell line, with the only exception being the MCF7 cell line. For CMA to be functionally active, it requires not only Lamp2A but also HSC70. Nevertheless, CMA is limited by Lamp2A and HSC70 equally; the expression of HSC70 was examined. It was highly expressed at a cytosolic level across the entire cell line panel; as expected, this is a highly expressed protein in the cytosol. Therefore, it needs to be examined at a lysosomal level to use its expression as an indicator of CMA activity. The other Lamp2 isoform, Lamp2B, was examined in Figure 5-2B. to confirm the specificity of the Lamp2A antibody and validate the previous Lamp2A results. Lamp2B expression differed from Lamp2A and was higher in the least aggressive phenotype, except the BT549 breast cancer cell line with high expression in both isoforms.

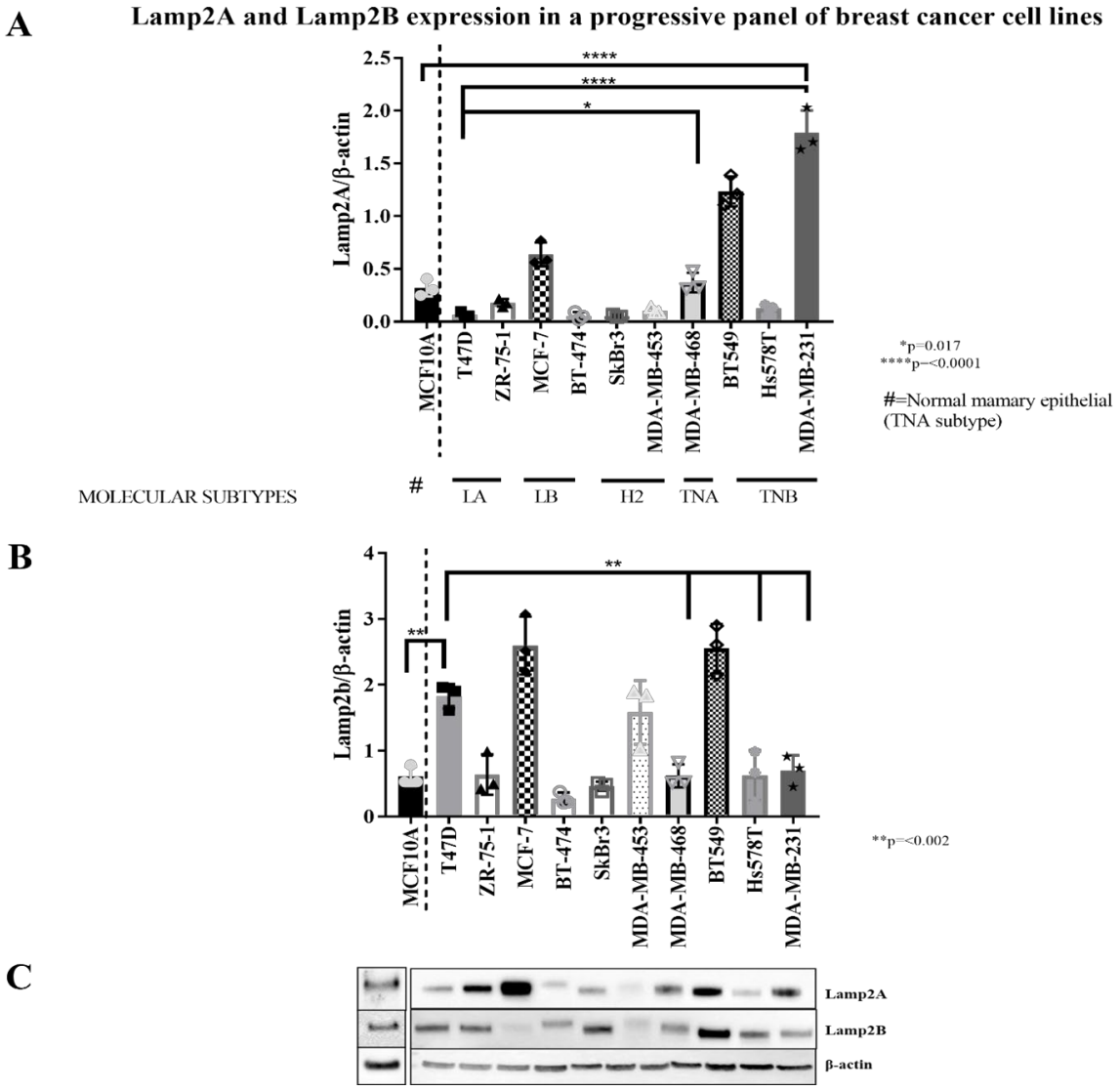


Figure 5-2 The expression of Lamp2A is increased in the aggressivephenotype where Lamp2B is differentially expressed in the breast cancer cell lines

(A) The densitometry analysis of Lamp2A demonstrated a significant difference between the molecular subtypes. **(B)** The densitometry analysis of Lamp2B displays the opposite of Lamp2A . There is distinct differences between the molecular subtypes(LA=luminal A, LB=luminal B, H2=HER2, TNA=triple negative-basal A and TNB=triple-negative-basal B**. (C)** Representative western blot of Lamp2 proteins demonstrates clear expression differences between the cell lines under basal conditions (n=3, ±SD, $p<0.05$ ANOVA and Tukey's post hoc test)

To further examine the trends in expression patterns reflected by the breast cells subtype, the data were re-analysed for the expression ratios of the Lamp2 isoforms Lamp2A to Lamp2B. Furthermore, the cell lines were grouped by molecular subtypes rather than progression. Cell lines were divided by molecular features rather than oncogenic progression based on these grouping criteria. Although the cell lines remain in the same order as in Figure 5-2, the MCF10A breast cell line would be deemed a basal subtype as shown here and by others [593] or, more specifically, basal A (TNA). As mentioned in greater detail in chapters 1 and 3, breast cells can be categorised based on their molecular features or lack thereof. However, as speculated and confirmed by Figure 5-3, there is a significant difference between the molecular subtypes. Lamp2A was expressed higher in the TNA and TNB subtypes, and this was increased as a ratio of Lamp2B, with significance observed between all cell lines and MDA-MB-231 (Figure 5-3). This expression ratio was further exemplified when Lamp2B to Lamp2A (Figure 5-3B), as represented on the graph as expected, was higher in the luminal subtypes, significantly so in the T47D breast cancer cell line.

The results from Figure 5-2 and Figure 5-3 have demonstrated a higher expression of CMA regulators, at least at a cytosolic level in the basal groups TNA and TNB subtypes, particularly significant in the MDA-MB-231 breast cancer cell line (refer to localisation images of Lamp2A in APPENDIX V). However, this does not confirm CMA, and these key regulators, Lamp2A and HSC70, need to examine within the lysosome to validate CMA activity.

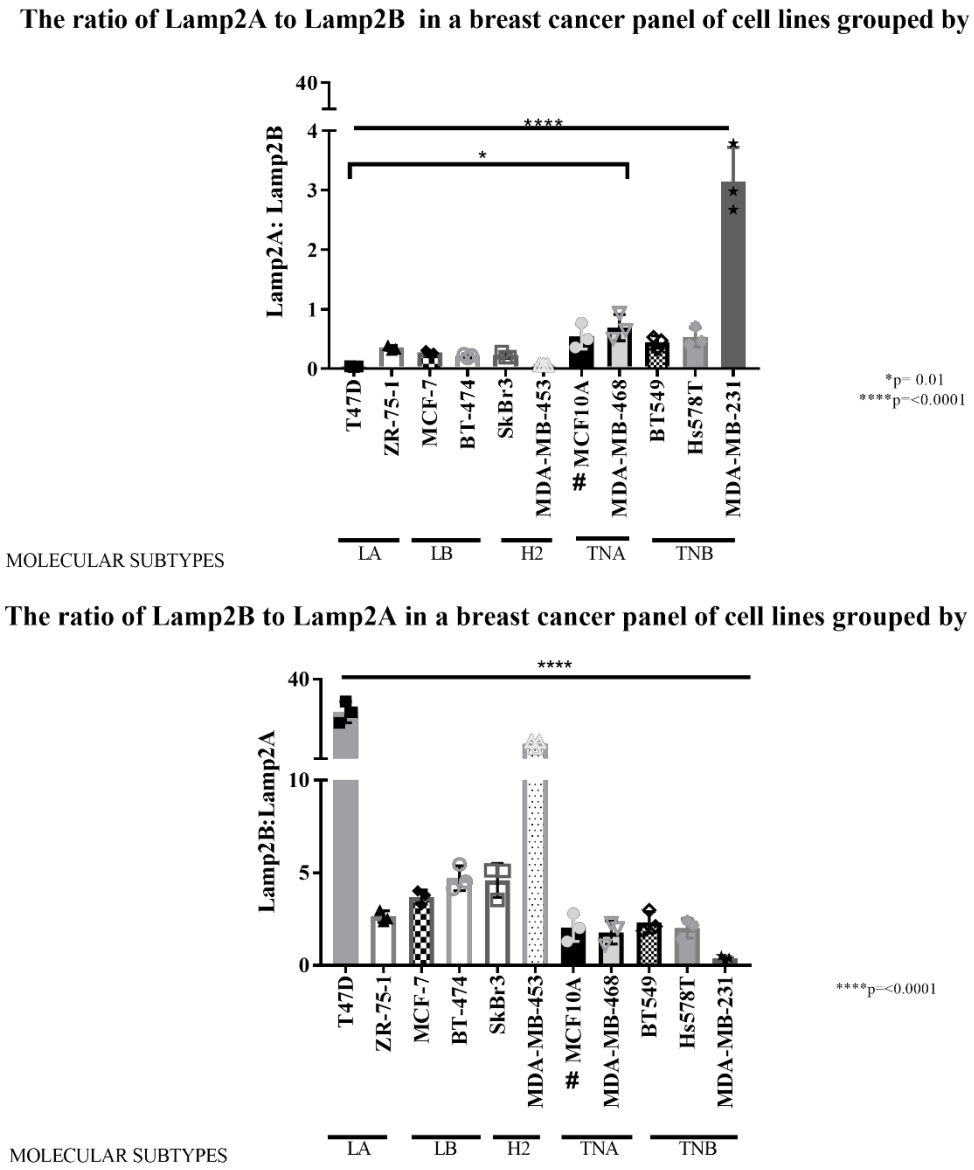


Figure 5-3 Lamp2A and Lamp2B are differential expressed in molecular subtypes

(A) The densitometry analysis of the Lamp2A to Lamp2B ratio demonstrated a significant difference between the molecular subtypes. **(B)** The densitometry analysis of the opposite ratio of Lamp2B to Lamp2A was examined to show distinct differences between the molecular subtypes(LA=luminal A, LB=luminal B, H2=HER2, TNA=triple negative-basal A and TNB=triple-negative-basal B and # =is "normal" mammary cell line (n=3, ±SD, $p<0.05$ ANOVA and Tukey's post hoc test)

The lysosome enrichment for this study was collected by the sucrose gradient fractionation method, as detailed in Chapter 2. In addition, the study narrowed its focus to the cell lines from the LA, TNA and TNB subtypes. The lysosomal enrichment can be defined as CMA active when there is the presence of both Lamp2A and HSC70. However, not all lysosomes are CMA active, and the presence of Lamp2A on its own would be deemed non-CMA active, as would HSC70 on its own. HSC70 has other lysosomal roles, including microautophagy. The role or purpose of Lamp2A on its own may be CMA active lysosomes that are defunct and require degradation; however, it has not been elucidated. Figure 5-4 results indicate that all lysosome enrichments contain Lamp2A and HSC70 and thus are deemed CMA active. Curiously, the MCF10A cell line had the least HSC70, and it is wondered if this could reflect the activity. Based on these findings, it is essential to determine the role of CMA and understand if the upregulated expression of Lamp2A is functionally relevant, and if so, does this functional importance changes during tumorigenesis?

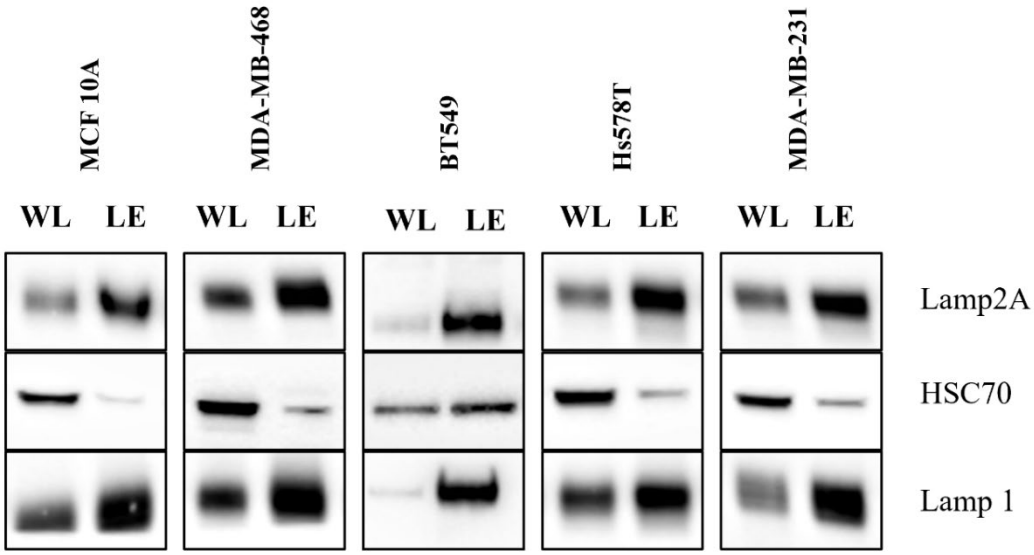


Figure 5-4 CMA regulators are expressed in the lysosomal enrichment of oncogenic subtypes.

The whole-cell lysate (WL) and the lysosomal enrichment (LE) from the same sample were collected with gradient fractionation. In addition, the samples were probed with western blot for key CMA regulators Lamp2A and HSC70 (n=4)

5.3.2 Lamp2A expression does not correlate with the presence of a RAS mutation.

To examine the probability of a correlation between CMA and RAS similarly to those indicated in chapter 3 with macroautophagy, the RAS progression panel utilised from the aforementioned chapter 3 was probed for the expression of the key CMA regulator Lamp2A. To determine if the observed changes in Lamp2A were specific to that transcript variant and not indicative of other transcript variants B or C. The level of Lamp2B variants was also included to confirm the specificity of the findings. Unfortunately, the Lamp2C variant could not be measured due to the lack of commercially available antibodies.

Briefly, the RAS panel includes the 'normal' breast cell line MCF10A and MCF10A cells oncogenic transformed with $HRAS^{V12}$ (MCF10A $HRAS^{V12}$), which represents the ectopic expression of the RAS mutation in a "normal" cell line (Figure 5-5A). The inclusion of MDA-MB-468, which expresses WT RAS, but due to the overexpression of EGFR and with the exogenous addition of its ligand EGF, results in an exponential activation of RAS to hyperactivation at 50ng/ml of EGF, resulting in the transition from epithelial to mesenchymal phenotype (Figure 5-5). The remainder of the panel includes breast cancer cell lines, T47D cell line with WT RAS and act as an oncogenic control to compare to the most aggressive mesenchymal cell lines, Hs578T and MDA-MB-231, which both have RAS mutations $HRAS^{G12}$ and $KRAS^{G13}$, respectively (Figure 5-5A). Cell lysates were collected at the basal level, with all cell lines being replenished with fresh media 4 hours prior to collection to prevent nutrient stress confounding results. The data in figure 5.2 show Lamp2A was significantly higher in the more advanced MDA-MB-468, Hs578T and MDA-MB-231 breast cancer cell lines compared to the T47D breast cancer cell line (Figure 5-5). The 'normal' MCF10A expressed similar Lamp2A levels to that of the T47D cells with no observable alteration in Lamp2A with the expression of $HRAS^{V12}$ in the transformed MCF10A $HRAS^{V12}$ cells (Figure 5-5). It was also noted that there were distinct differences in the expression patterns between the isoforms of Lamp2A and Lamp2B. Lamp2B expression was relatively lower than that of Lamp2A overall normalised to actin (Figure 5-5 C and D), and in contrast to the Lamp2A expression pattern, the highest level was observed in the T47D compared to all other cell lines.

Interestingly, in the MDA-MB-468 cell line, there was an increase in Lamp2A and Lamp2B in a dose-dependent response to EGF addition. Although the data do not indicate a

direct correlation with RAS, the expression analysis demonstrates an association of increased Lamp2A expression in more aggressive breast cell lines. Although the Lamp2B intensity is not as elevated in the most aggressive cell lines, it was present in all cell lines, and the result suggests that Lamp2B is upregulated in carcinogenesis. It may indicate that their roles are not shared but distinct or that there may be a preference for one variant over the other. The increased expression of Lamp2B may indicate an increase in autophagy as the literature suggests Lamp2B has a role in autophagosome to lysosome fusion [590]. This postulate would further support the previous finding of chapter 3 that autophagy was upregulated in the MDA-MB-468 model. The results have not indicated any clear correlation between mutant RAS and CMA. However, there does appear to be a response by CMA and or specifically in the expression of Lamp2A in the context of RAS activation. This upregulation of Lamp2A in response to EGF suggests that CMA may have a role in targeting proteins integral in the activity EGFR-RAS axis and would warrant further investigation.

The result from Figure 5-2 to Figure 5-5 collectively shows a significant upregulation in CMA and, more specifically, Lamp2A within the basal subtypes A and B (TNA and TNB). Therefore, the study will focus on these cell lines and examine the biological significance of the observed increase in CMA and its effector protein Lamp2A.

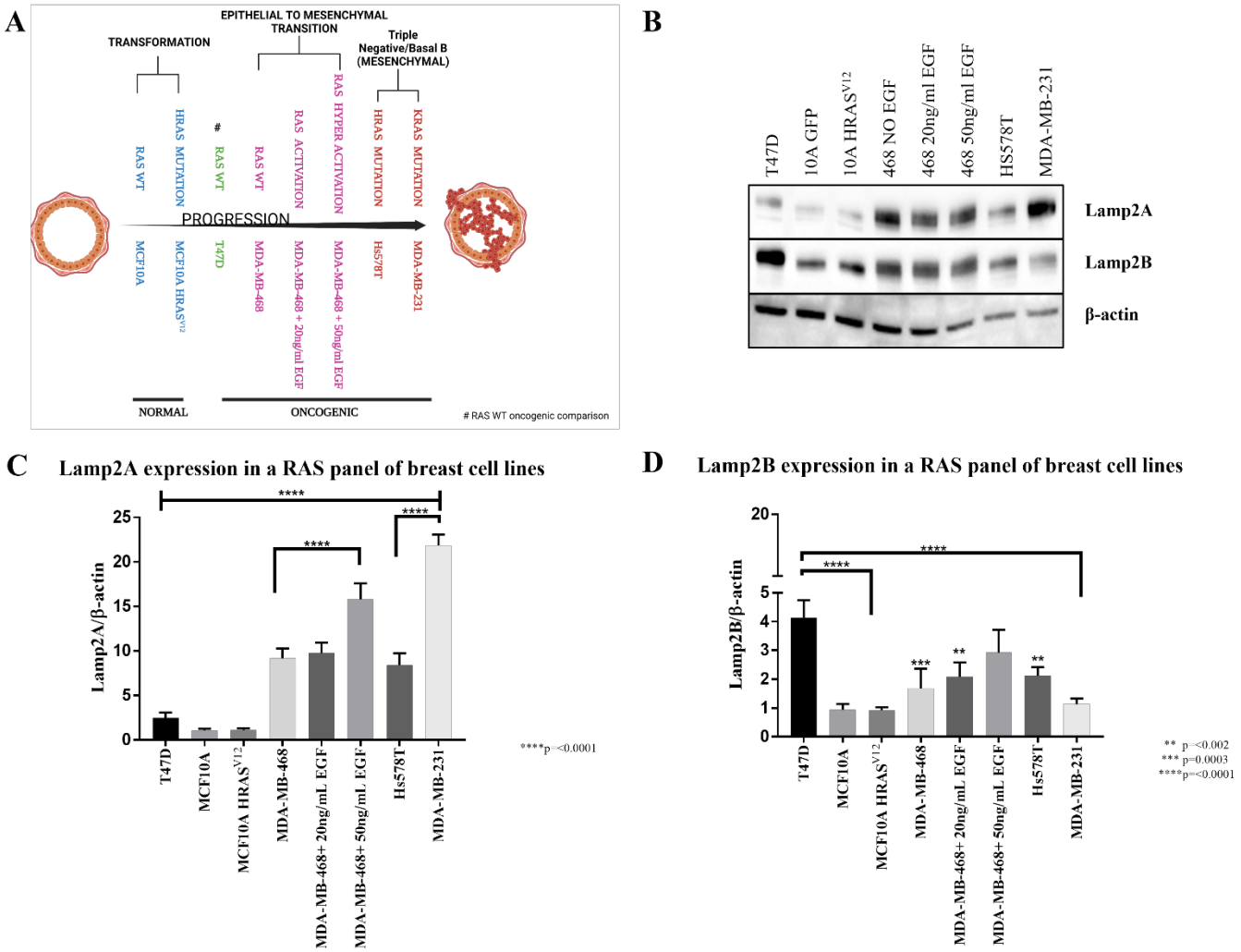


Figure 5-5 The expression of lamp 2A increased in the breast cancer cell line compared to breast cell lines

(A) The "RAS panel" has been represented schematically to show the different cell lines included due to their respective RAS presentation or lack in a RAS continuum. **(B)** Western blot of protein expression under the same conditions demonstrates differences between the RAS panel cell lines. **(C)** The densitometry analysis of Lamp2A expression intensity compared to loading control demonstrated that the difference between cell lines was significant **(D)** The densitometry analysis of Lamp2B expression intensity compared to loading control demonstrated a difference between cells lines note astrix denoting significance on columns is compared to T47D cell line. (n=3, ±SD, $p<0.05$ ANOVA and Tukey's post hoc test)

5.3.3 The loss of Lamp2A in breast cell line MCF10A confers no significant biological effect.

5.3.3.1 *Lamp2A knockdown validation*

The biological importance of CMA was examined through the genetic knockdown of Lamp2A in the basal group identified in the earlier data, specifically the TNA subtypes. The study's initial focus was to explore and establish a baseline of CMA in the "normal" breast cell line MCF10A, which itself is classified as a basal subtype. This study generated the Lamp2A shRNA-Mir and inserted it into the TRIPZ backbone, a tetracycline-inducible lentiviral knockdown system, as detailed in Chapter 2. The MCF10A cell line was selected with puromycin, and this study opted to omit Fluorescence-activated cell sorting (FACs) selection as it can lead to clonal selection and loss of heterogeneity. The result from Figure 5-6 reveals that Lamp2A was successfully knocked down in an inducible manner with the addition of doxycycline (Dox) added at a concentration of 1µg/mL for all cell lines and experiments.

Furthermore, the Lamp2A construct was controlled for any confounding influence of the viral transduction by including a non-targeting shRNA. The specificity of the construct was confirmed by probing for the other transcript variant, Lamp2B. The results for Lamp2B indicate it is still present and may even slightly increase its expression with the knockdown of Lamp2A (Figure 5-6 A-C). The lysosome enrichment and corresponding whole cell lysate were collected to examine the Lamp2A knockdown at its target site. The data shows that Lamp2A is knocked down by approximately 80% in the whole-cell compared to controls Lamp2AshRNA Dox and non-targeting-shRNA with and without Dox (Figure 5-6 D). This knockdown was also present in the lysosome enrichment, but not as much.

Furthermore, the lysosome enrichment with the non-targeting shRNA plus Dox increased the level of Lamp2A. It would be interesting to determine if CMA regulates proteins involved in Dox degradation; this may even explain the higher levels in the lysosome enrichment with Lamp2A knockdown. Lamp2A may be increased and shuttled to the lysosome in response to its need or be retained in the lysosome membrane for longer. To resolve this for future experiments, it may require the cells to be left exposed to Dox for

longer than 72 hours for this increased reduction of Lamp2A at the lysosome to be observed.

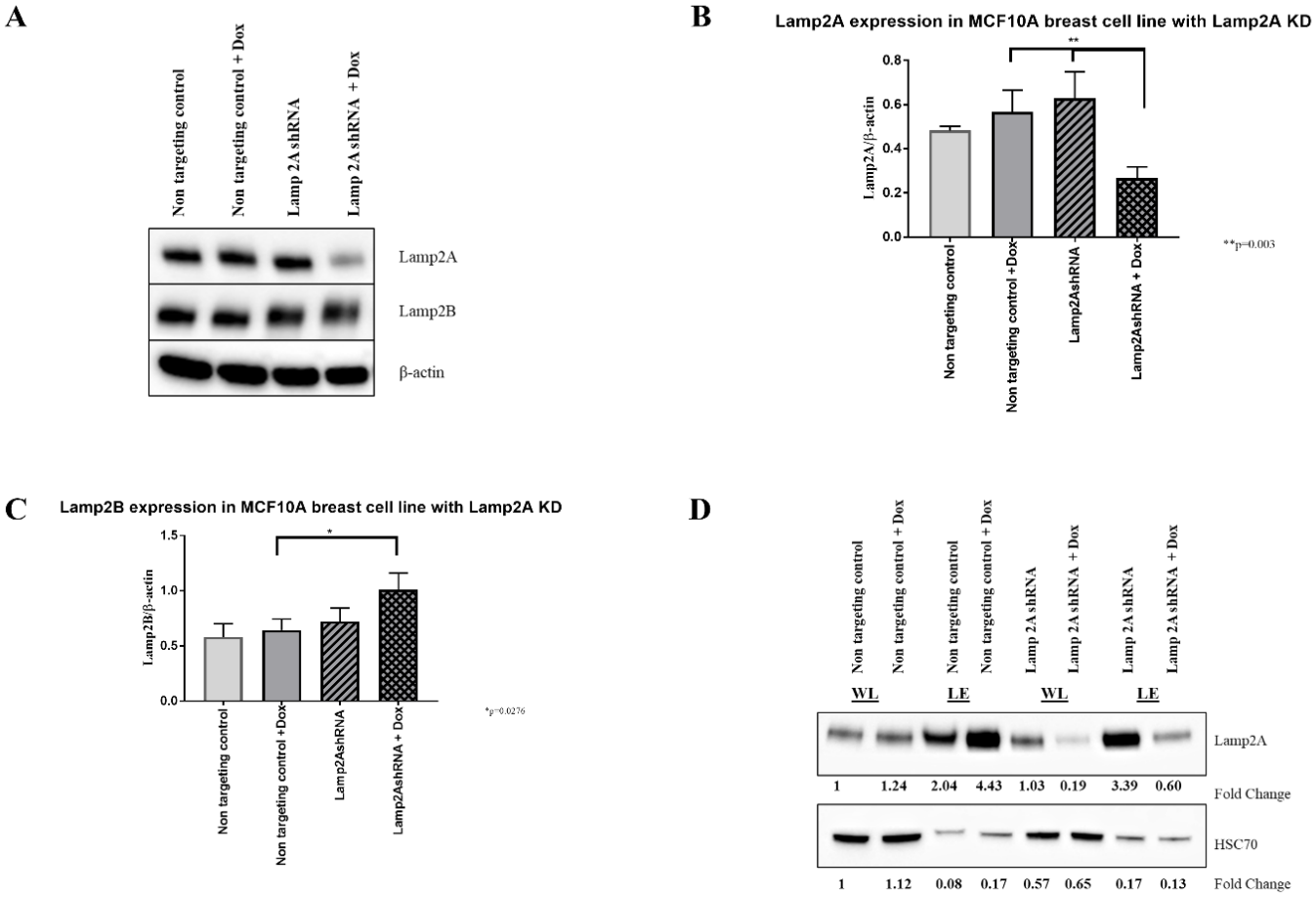


Figure 5-6 Lamp2A knockdown was observed in the MCF10A breast cell line

(A) Western blot representative image to confirm Lamp2A knockdown (KD) contrasted to other transcript variant Lamp2B. The MCF10A was transduced with Lamp2AshRNA or non-targeting shRNA (NT) as control, with all samples shown with or without Induction by Dox (1µg/mL). **(B)** Densitometry analysis of intensity compared to control of Lamp2A. **(C)** Densitometry analysis of intensity compared to control of Lamp2B. **(D)** Whole-cell lysate (WL) and lysosome enrichment (LE) of Lamp2A KD and control a representative western blot image with the calculated fold change compared to control without Dox (set at 1). (n=3, ±SD, $p<0.05$ ANOVA and Tukey's post hoc test)

To further validate the previous findings of Figure 5-6 above, the cells were visualised with a fluorescent filter (TRITC) to identify the presence of the turboRFP (tRFP) as represented in Figure 5-7. The tRFP is expressed when the TRE promotor is switched on in the presence of Dox and is an indicator of viral transduction and successful expression of the target shRNA as the tRFP is upstream of the shRNA. As expected, the cells with no Dox did not express tRFP, while the addition of Dox resulted in tRFP expression transduced with either Lamp2AshRNA or the non-targeting-shRNA, respectively. The images of the MCF10ALamp2AshRNA as presented in Figure 5-7 show no apparent differences in cellular morphology in response to knockdown of Lamp2A by the addition of Dox.

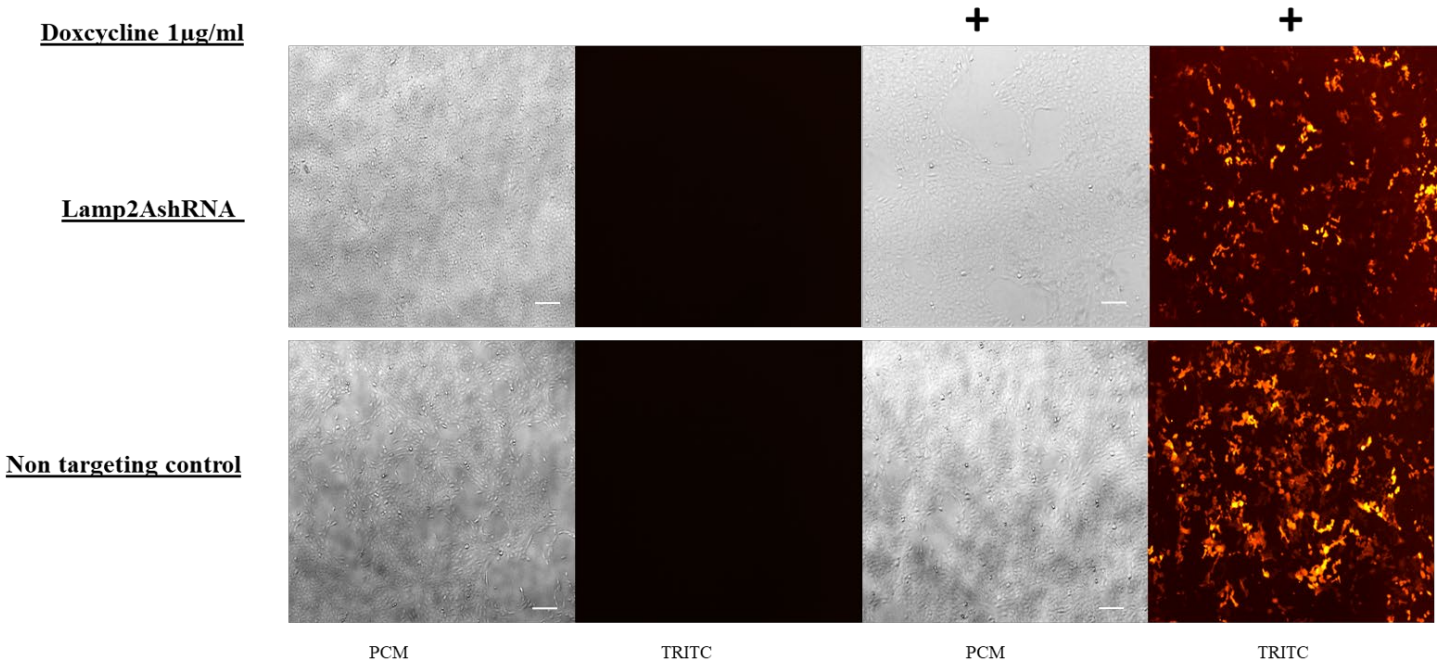


Figure 5-7 The MCF10A cellular morphology was unchanged by the knockdown of Lamp2A

Micrograph images of the MCF10A cell line transduced with Lamp2A or non-targeting with or without Dox were captured with phase-contrast microscopy (PCM) at 40 X magnification. In addition, images of tRFP were captured with a fluorescent filter (TRITC) at 100 X magnification to confirm activation of lentivirus with Dox addition. (n=3)(scale bar=200µm)

Confirming no morphological difference, additional images were taken at higher magnification. The cells were examined visually for any morphological changes in response to Lamp2A knockdown. The images were taken with the phase contrast filter, as displayed in Figure 5-8. The images indicate no observable changes of significance between the MCF10A Lamp2AshRNA cells with or without the presence of Dox.

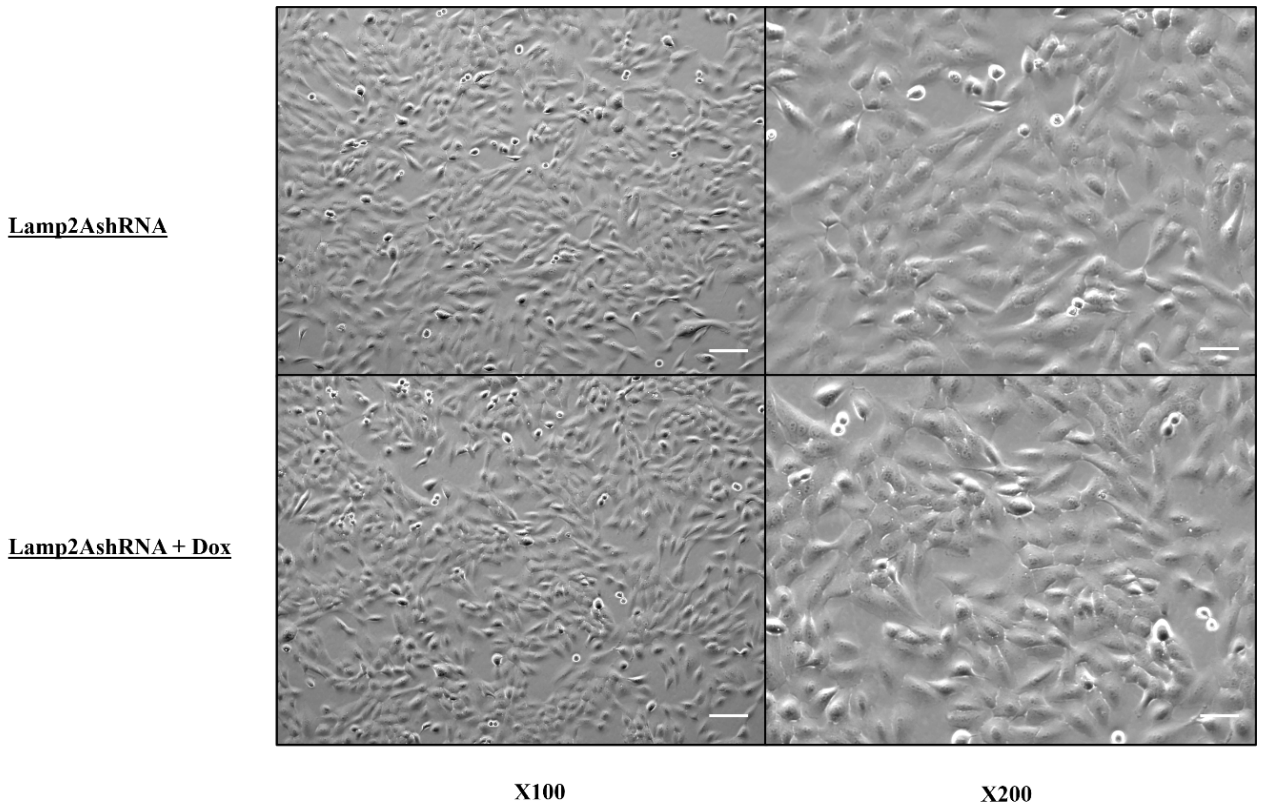


Figure 5-8 MCF10A morphology does not change with Lamp2A knockdown.

Micrograph images were taken with a phase-contrast filter of MCF10AshRNA cell lines with and without Dox (for 72 hours). Images captured at X100 (scale bar=100μm) and X200 (scale bar=50μm) magnification.

5.3.3.1 Lamp2A knockdown in lysosomal enrichment

CMA processing was examined in Figure 5-10 by collecting lysosome enrichment with the whole-cell counterpart in MCF10A with Lamp2A knockdown. The lysosome enrichment for this analysis was collected in 500µl fractions instead of a single 1ml volume, as pictured in Figure 5-6D. The fractions confirm that most of the lysosome enrichment is located within the first 1ml of the collection. The western blot for Figure 5-9 presents several findings; firstly, it was re-confirmed Lamp2A was lost in the lysosomal fraction, but not as much as the whole cell lysate as determined earlier, maybe due to retention of existing Lamp2A for reuse. On the other hand, the expression of Lamp2B was not lost with Lamp2A KD; from the results overall, there is a significant increase in the lysosomal fraction. HSC70 was examined for levels and appeared to decrease with the Lamp2A knockdown. This decrease in HSC70 may be due to loss at the lysosomal membrane, within the lysosomal lumen, or both. Finally, other confirmed CMA substrates were examined to identify any changes in response to the removal of Lamp2A in their degradation. There was a noticeable decline in the levels of GAPDH with the knockdown of Lamp2A, but interestingly there was faint to no PK1/2. Note that the PK1/2 antibody detects isoforms 1 and 2 of PKM, a known CMA substrate, found within the lysosome enrichment. However, this may be due to a high turnover rate as it is an essential molecule within the glycolytic pathway. Furthermore, its breakdown rate is either higher or lower and, as such, is not observed. In conclusion, future investigations with a lysosomal alkaliser that prevents acidification, such as Bafilomycin A1, need to be added to prevent lysosomal content degradation and to understand the changes observed in these substrates.

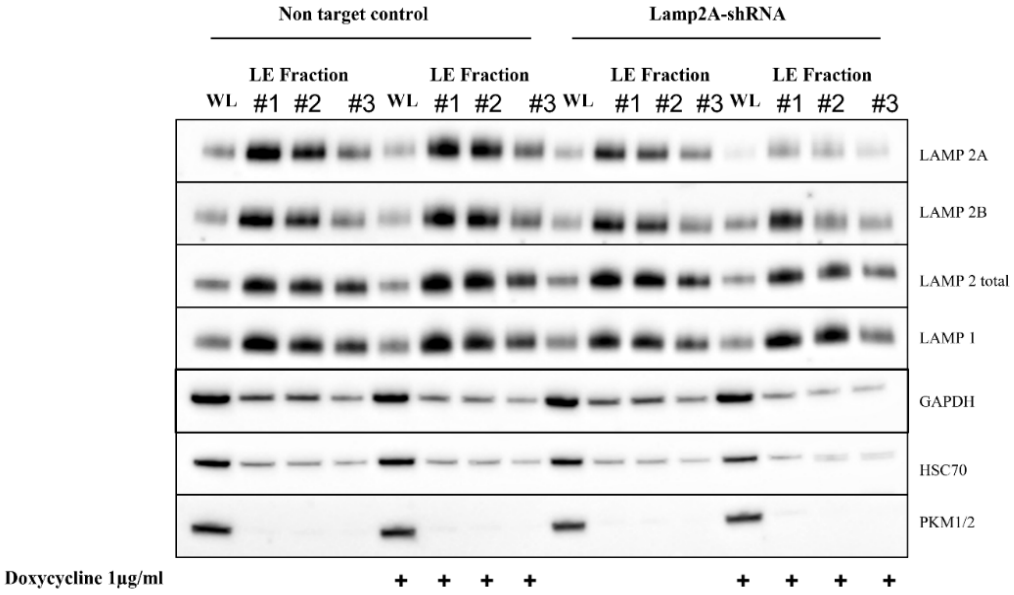


Figure 5-9 The lysosomal enrichment of MCF10A with Lamp2A KD shows differences in known CMA substrates

The representative western blot image of the lysosomal enrichment (LE) fractioned with comparative whole cell lysate (WL) for the Lamp2 isoforms, lamp1 and confirmed CMA substrates to examine the effect Lamp2A knockdown has on CMA processing. (n=3)

5.3.4 Knockdown of Lamp2A showed no functional importance to the MCF10A breast cell line

5.3.4.1 Cell viability with Lamp2A knockdown

The successful knockdown of Lamp2A was depicted in Figure 5-6. However, this data could not determine the biological consequences. Therefore, this study explored the biological changes in the MCF10A breast cell line with Lamp2A reduction with an initial experiment of cell viability using Alamar Blue as described in C

hapter 2. The cells were exposed to Dox for 72 hours to achieve maximal knockdown, and after another24 hours the Alamar Blue assay was performed. The findings in Figure 5-10 demonstrate that the removal of Lamp2A had a negligible impact on cell viability compared to control

5.3.4.2 Wound healing with Lamp2A knockdown

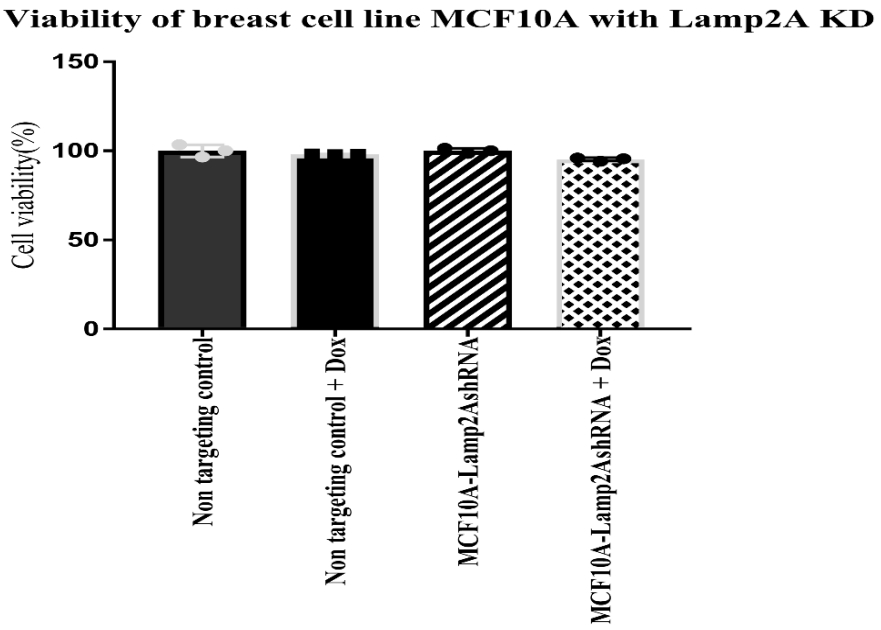


Figure 5-10 The cell viability of MCF10A cells did not change 24 hours after knockdown

Cell viability was measured with Alamar Blue assay (RFU) in the MCF10A breast cell lines with Lamp2AshRNA KD and non-targeting control with or without Dox (Dox). The percentage of cell viability was determined compared to control without Dox. The Alamar Blue assay was performed after 24 hours after maximum knockdown was reached (by 72 hours). (n=3, ±SD, $p<0.05$ ANOVA and Tukey's post hoc test)

Another aspect of cellular biology investigated was wound healing (scratch assay), as represented in Figure 5-11, which determines the cell's ability to migrate on a 2-D surface to close a gap or scratch. This wound healing assay not only examines the motility, it inherently captures the cellular response to changes in the cell-to-cell contacts, biochemical signals and molecular changes as a collective in a cellular population, rather than a single cell. In this study, the RTCA Xcelligence MP system was utilised. This system uses a 96-well plate, with each well having an electrode strip in the centre, as represented in Figure 5-11 B of the empty well. After cells are grown to confluence, a scratch tool removes the cells from the electrode region. The scratch can be confirmed from the RTCA reading in Figure 5-11 where impedance (cell index) is present; therefore, there is cellular adherence to this region, but it is lost after applying the scratch as there are no longer cells adhered to

generate a reading, but this returns as the cells move across and adhere over the electrode to close the wound.

It should be noted that mitomycin C1 was added to prevent proliferation, so wound closure indicated cellular migration. In addition, the cell lines were pretreated with Dox to ensure that the Lamp2A knockdown was maximal so its impacts biologically could be measured. Therefore, the data is interpreted as the rate of change of cell index over time, as indicated in the graph in Figure 5-11, where it is evident that the removal of Lamp2A had no impact on the rate at which the cells closed the wound as was the case with the non-targeting shRNA the presence of Dox (1μg/mL).

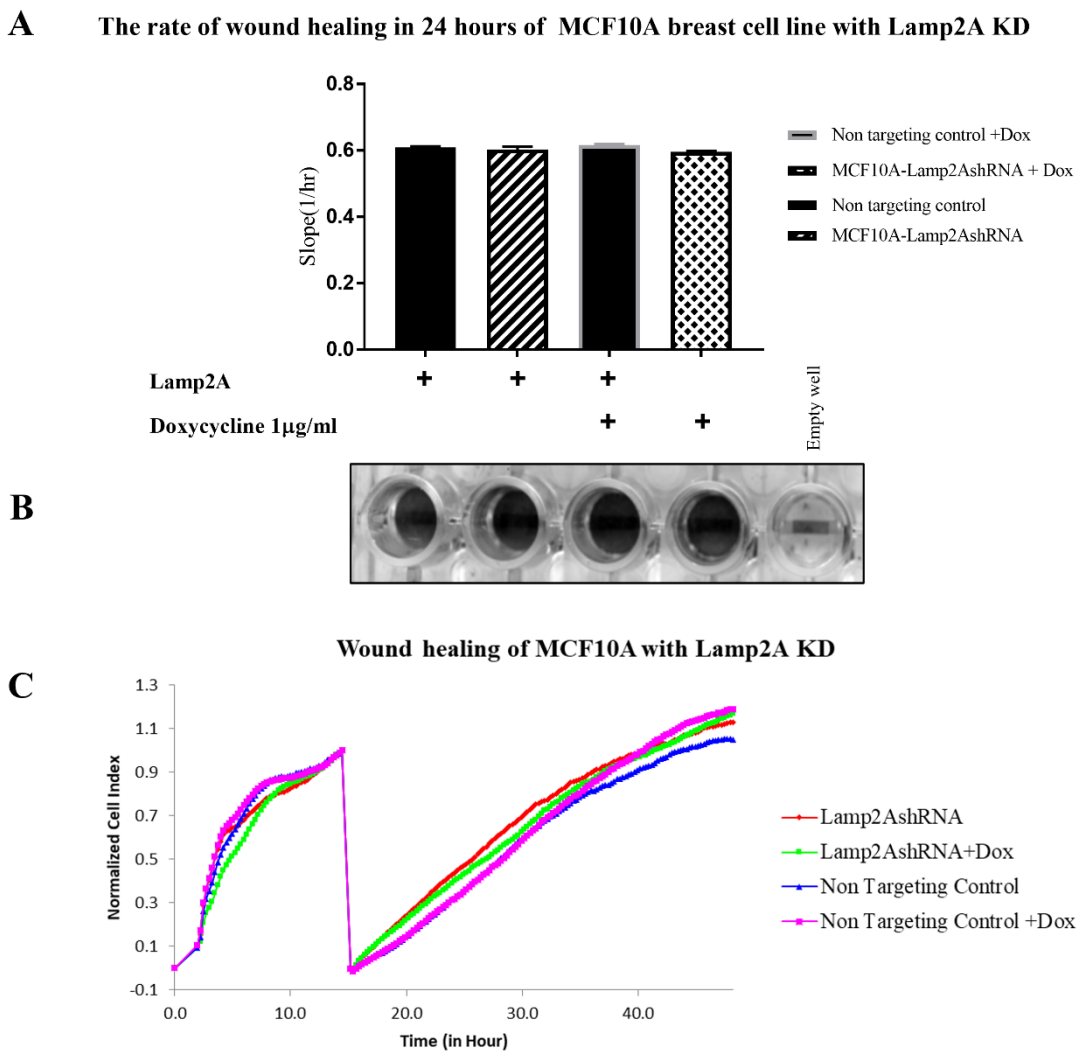


Figure 5-11 The wound healing capacity of MCF10A was unchanged by Lamp2A KD

(A) The rate of wound healing as determined by the RTCA software, the slope, represents the rate of change of the cell index as a function of time between wound scratch and 24 hours. **(B)** A representative image of the wound plates wells of the respective cell lines stained after completion of the assay and an empty well to visualise the scratch area where the electrode is located. **(C)** The plotted results from the RTCA Xcelligence MP system were used to measure the respective cell lines real-time wound healing closure note black arrow indicates when the wound was applied. (n=3, ±SD, $p<0.05$ ANOVA and Tukey's post hoc test)

5.3.4.3 Anchorage-dependant clonogenic survival and growth with Lamp2A knockdown

The next aspect of cell biology examined in the context of Lamp2A knockdown was anchorage-dependant growth, whereby cells are seeded at low density and allowed to form colonies on a solid surface. In this context, there were two questions to be answered: Did Lamp2A prevent colony formation, and after a colony has formed, does the knockdown of Lamp2A intervene with colony growth? (Figure 5-12) In Figure 5-13, the cells were induced with Dox before seeding to determine the impact of anchorage and colony formation concerning Lamp2A. As indicated by the results, there were no observable differences between the groups. Therefore, the study performed the assay again, but the cells were seeded and given time to adhere before the Dox was added to examine if the removal of Lamp2A would affect the colony's growth. As displayed in Figure 5-14 are to be compared, it is clear that the removal of lamp 2A pre or post-seeding resulted in no differences in the colony number as they were found to be similar between the experiments.

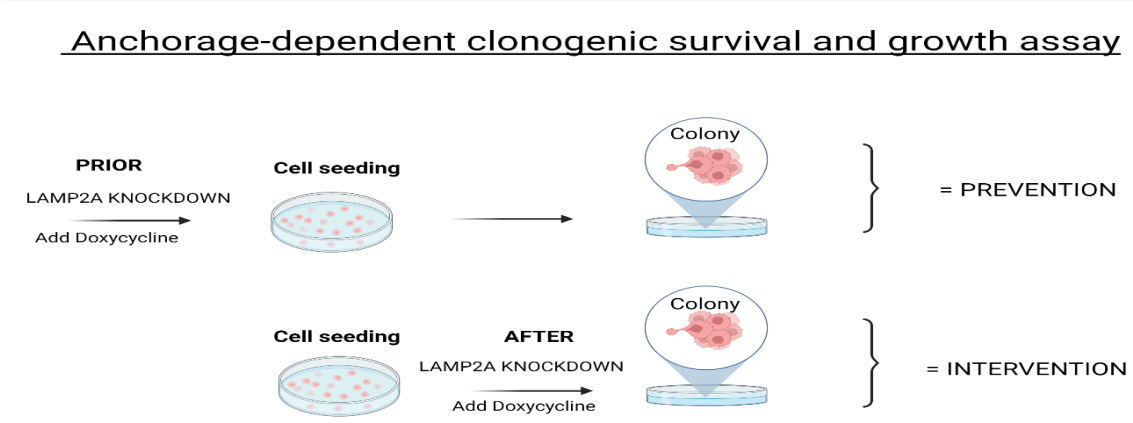


Figure 5-12 Schematic representation of the colony-forming experimental design

In the visual representation of the experimental design for colony-forming studies, cells treated with doxycycline to induce knockdown prior to cell seeding are termed as “intervention”. Alternatively, cells seeded and left for 24 hours and then treated with doxycycline to induce knockdown are termed “prevention”. Created with BioRender.com

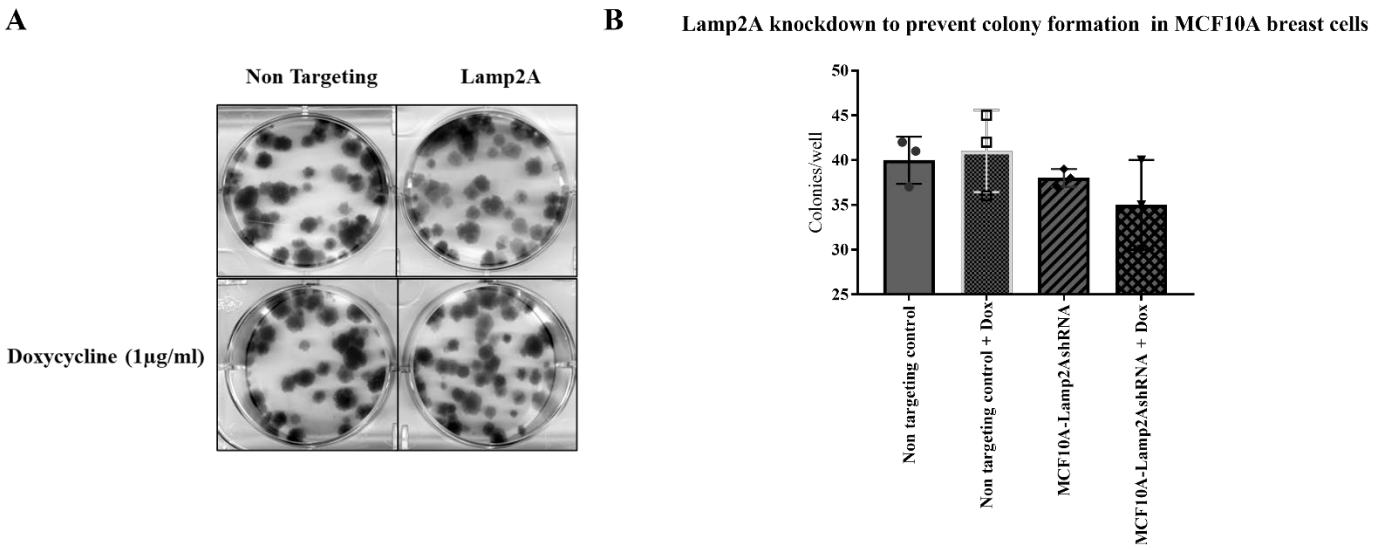


Figure 5-13 The removal of Lamp2A after colony formation did not affect growth.

(A) A representative image of fixed and stained colonies formed by MCF10A Lamp2AshRNA and control cell lines after the anchorage-dependent growth assay was completed. **(B)** Graph indicating the number of colonies counted per well with FIJI analysis software. (n=3, ±SD, $p<0.05$ ANOVA and Tukey's post hoc test)

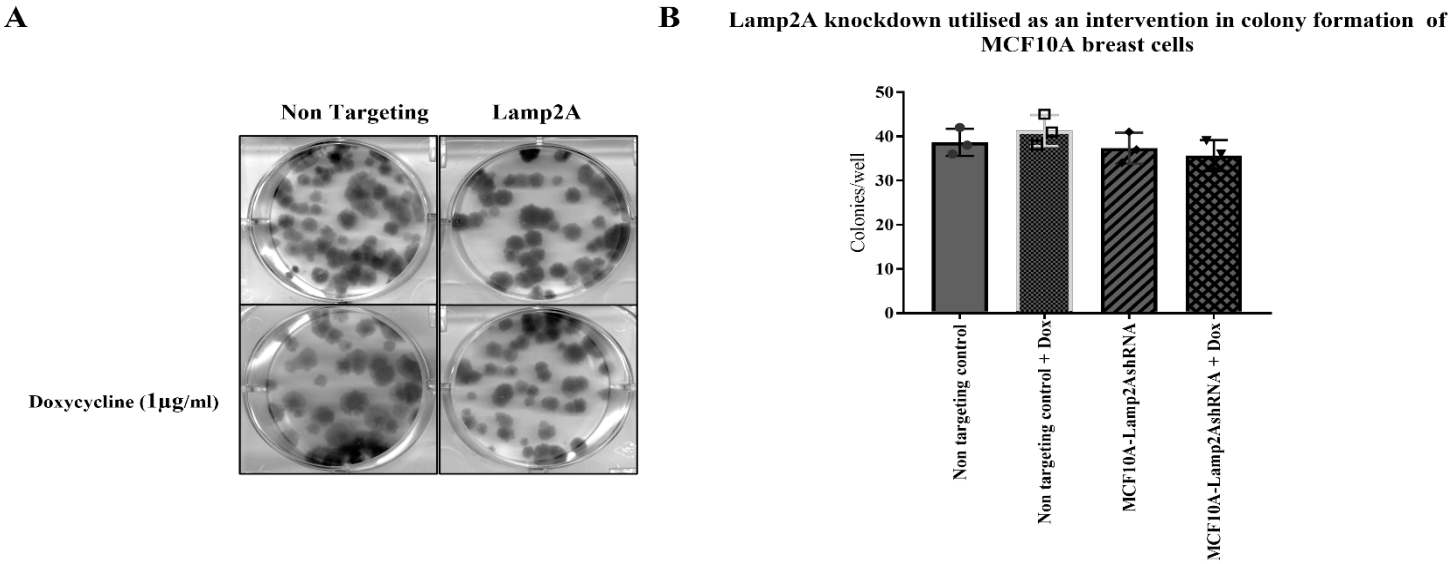


Figure 5-14 The knockdown of Lamp2A did not affect colony formation in the MCF10A breast cell line.

(A) A representative image of fixed and stained colonies formed by MCF10A Lamp2AshRNA and control cell lines after the anchorage-dependent growth assay was completed. **(B)** Graph indicating the number of colonies counted per well with FIJI analysis software. (n=3, ±SD, $p<0.05$ ANOVA and Tukey's post hoc test)

5.3.4.4 Acini formation with Lamp2A knockdown

The final functional experiment undertaken in this cellular context was 3D growth. The MCF10A cell line is seeded in a Geltrex suspension on a solidified Geltrex layer where the MCF10A's form spherical acini over time. The acini are replicative of those found in the mammary tissue, and as these structures, the acinus inner mass begins the process of apoptosis to form an inner lumen at approximately 12 days. The images in Figure 5-15 demonstrate no visible changes to the acini formation with Lamp2A knockdown compared to either non-targeting lines or Lamp2AshRNA in the absence of Dox. Furthermore, there were no observable changes consistently on days four and twelve.

In summary, the Lamp2A construct developed effectively induced Lamp2A knockdown in the MCF10A breast cell line. However, the functional studies have shown that removing Lamp2A does not affect cell viability, migration, colony formation, or 3D growth in the MCF10A breast cell line.

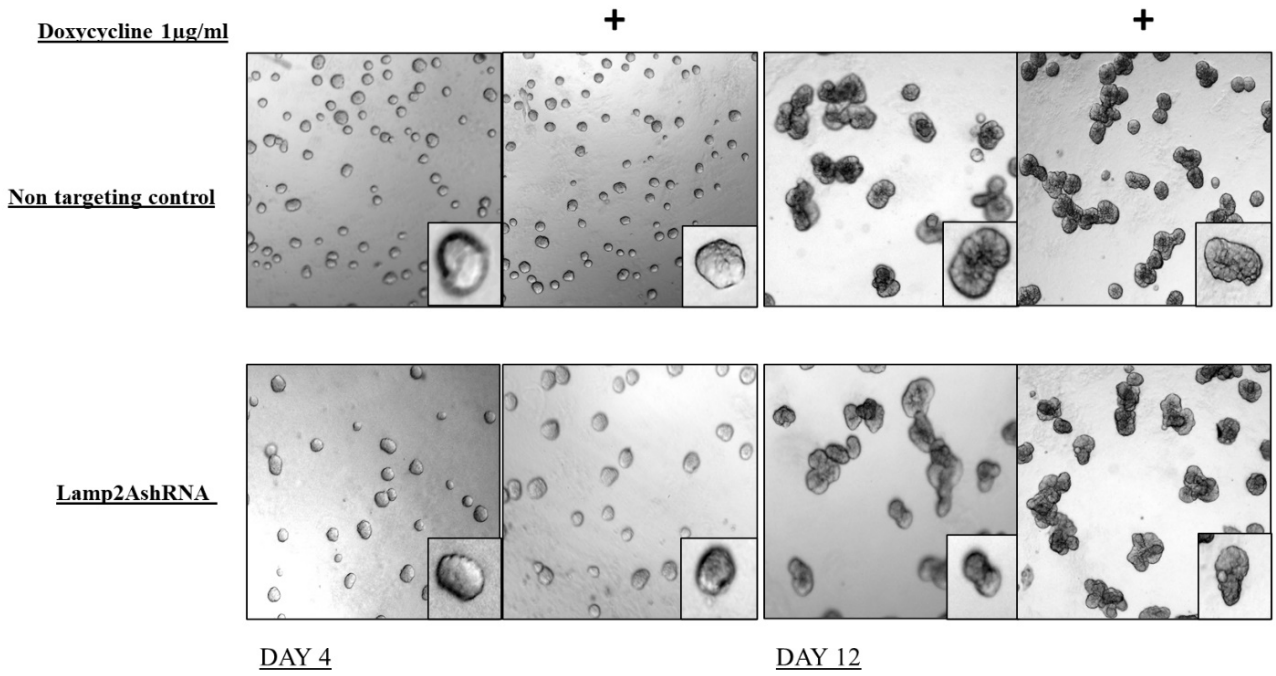


Figure 5-15 The knockdown of Lamp2A did not alter the MCF10A acini formation.

The acini formed by the MCF10A Lamp2AshRNA and non-targeting control cell lines with or without Dox were captured with phase-contrast microscopy at 100X magnification on days 4 and 12 days, respectively. (n=3)

5.3.5 The knockdown of Lamp2A in the basal breast cancer cell line MDA-MB-468 resulted in biological changes.

5.3.5.1 Lamp2A knockdown validation

The role of Lamp2A was investigated further, with the study turning its focus to a tumorigenic cell line from the TNA subtype. The cell line chosen was MDA-MB-468 which, further on from our initial findings from the earlier experiments, displayed upregulated CMA regulators Lamp2A and HSC70 in whole-cell lysate and lysosome enrichment (Figure 5-4). The MDA-MB-468 cell line was transduced with Lamp2AshRNA, and in parallel, another cell line was developed with a non-targeting shRNA control. The results in Figure 5-16 demonstrate that the expression of Lamp2A was reduced by approximately 70-80% compared to the control. It was also significantly reduced when compared to Lamp2AshRNA cell lysate without the presence of Dox. The Lamp2A knockdown was also verified to be specific to that variant and had no impact on Lamp2B, as seen in Figure 5-16C.

It was observed in this context not to increase the expression of Lamp2B as detected in the MCF10A cell line earlier. When this knockdown was examined within the lysosome enrichment, the reduction of Lamp2A compared to control was not as great as that observed in Lamp2AshRNA and no Dox control in the whole cell. As mentioned previously, this is potentially a caveat in the study, and future collection should be performed beyond the 72 hours to ensure the removal of residual Lamp2A at the lysosomal membrane, or at least to determine how long this reuse of Lamp2A can be maintained.

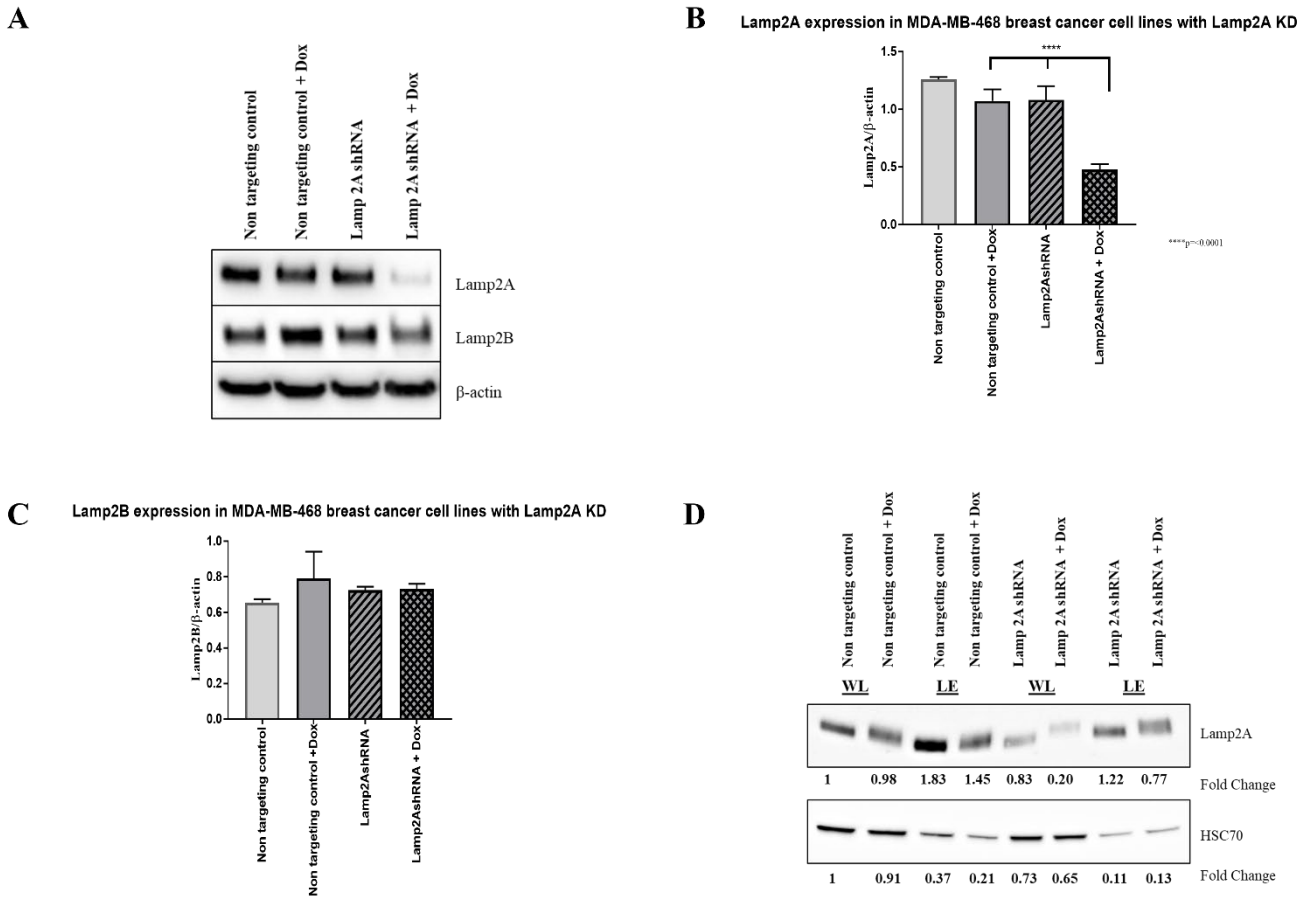


Figure 5-16 Lamp2A is knockdown in the MDA-MB-468 breast cancer cell line.

(A) Western blot representative image to confirm Lamp2A knockdown (KD) contrasted to other transcript variant Lamp2B. The MDA-MB-468 breast cancer cell line was transduced with Lamp2AshRNA or non-targeting sh-RNA (NT) as control, with all samples shown with or without Induction by Dox (1µg/mL). **(B)** Densitometry analysis of intensity compared to control of Lamp2A. **(C)** Densitometry analysis of intensity compared to control of Lamp2B. **(D)** Whole-cell lysate and lysosome enrichment of Lamp2A KD and control a representative western blot image with the calculated fold change compared to control without Dox (set at 1). (n=3, ±SD, $p<0.05$ ANOVA and Tukey's post hoc test)

The presence of tRFP was examined by microscopy and images captured in Figure 5-17. The images exhibited the expected tRFP cells only in the presence of Dox and were not visible in its absence. The phase-contrast images captured to examine the morphology show confluence differences or the high number of transient cells floating in the non-targeting and obscuring the view. However, there are differences between the groups with much lower confluence observed in the Lamp2A shRNA with or without Dox. Although this is a general observation, further viability studies were required to confirm this.

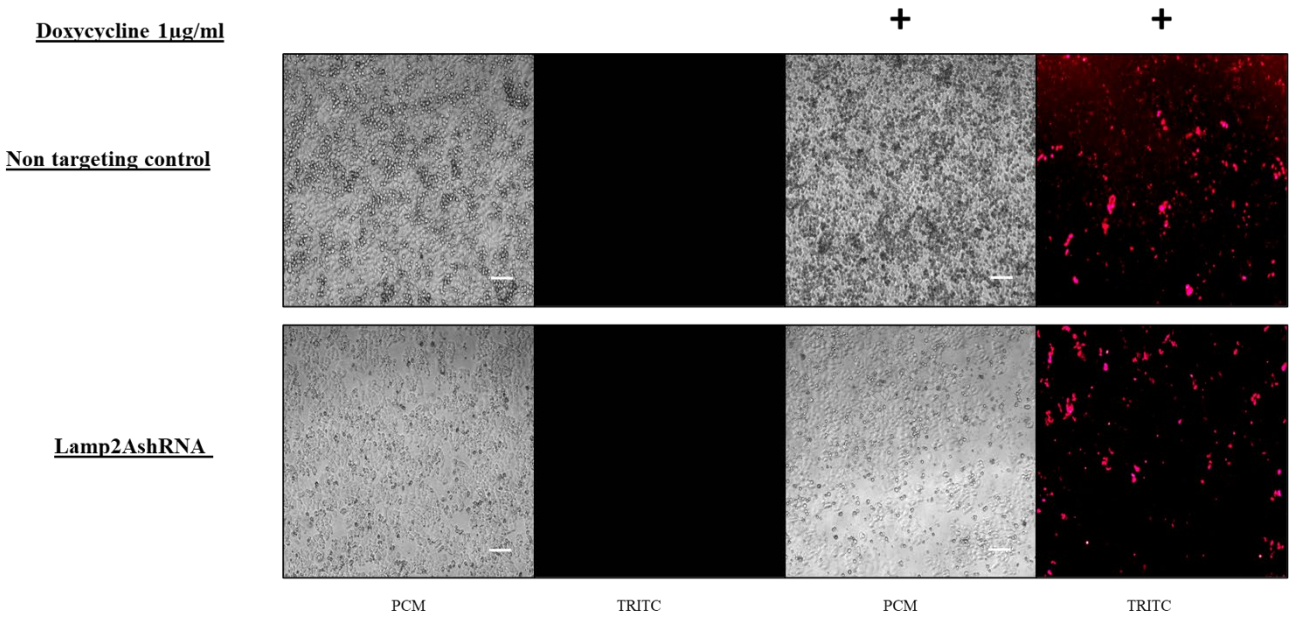


Figure 5-17 The breast cancer cell line MDA-MB-468 displays a reduction in cell numbers with Lamp2A KD.

Micrograph images of the MDA-MB-468 cell line transduced with Lamp2A or non-targeting with or without Dox were captured with phase-contrast microscopy (PCM) at 40 X magnification. In addition, images of tRFP were captured with a fluorescent filter (TRITC) at 40 X magnification to confirm activation of lentivirus with Dox addition. (n=3)(scale bar=200µm)

5.3.5.2 Lamp2A knockdown in lysosomal enrichment

The consequence of Lamp2A downregulation on CMA activity was examined, with the lysosomal enrichment being probed for known CMA substrates to observe any changes (Figure 5-18). Again, there was observed to be a reduction in Lamp2A. However, this amount of knockdown was not replicated to the same extent in the lysosome enrichment as the whole cell lysate. This observation might be due to the concentration of Lamp2A within the enrichment itself. The first two fractions contain most of the lysosomal content indicated by lamp1 expression. Although, to date, the expression of Lamp2B appears to be lower expressed in the Lamp2AshRNA lysosomal enrichment but is higher in the other groups and does not appear to be induced by the Dox as the same was not seen in the non-targeting shRNA with Dox, suggesting there may be some downstream effect of Lamp2A loss for Lamp2B. As for the CMA substrates, minor decreased pyruvate kinase M1 (PK1/2) levels within the lysosome enrichment and a slight decrease in HSC70 within the whole cell coinciding with the reduction of Lamp2A (Figure 5-18).

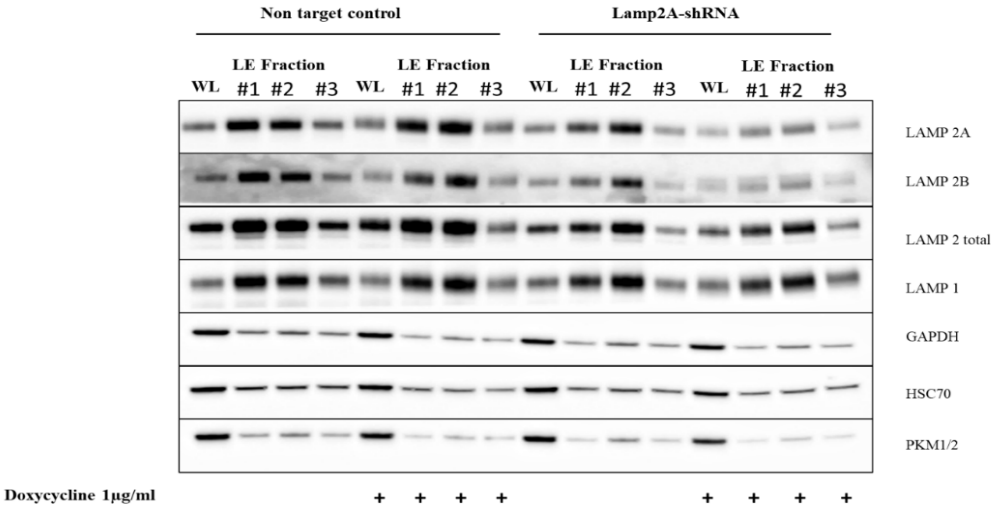


Figure 5-18 The MDA-MB-468 breast cancer cell line displays minimal differences with Lamp2A KD.

The representative western blot image of the lysosomal enrichment (LE) fractioned with comparative whole cell lysate (WL) for the Lamp2 isoforms, lamp1 and confirmed CMA substrates to examine the effect of Lamp2A knockdown has on CMA processing. (n=3)

5.3.5.3 Cell viability with Lamp2A knockdown

The MDA-MB-468 breast cancer cell line with the Lamp2AshRNA and the non-targeting shRNA control were grown with or without Dox and assessed for viability, as shown in Figure 5-19. The outcome of the Alamar Blue assay displayed a significant decrease in cell viability by approximately 40% compared to all the other groups. These results support the reduction in cells present in the images from Figure 5-17. However, the decrease in the Lamp2AshRNA without Dox may relate to a slight increase in the proliferation rate of the non-targeting control, as was seen with one of the replicates during the Alamar Blue assay.

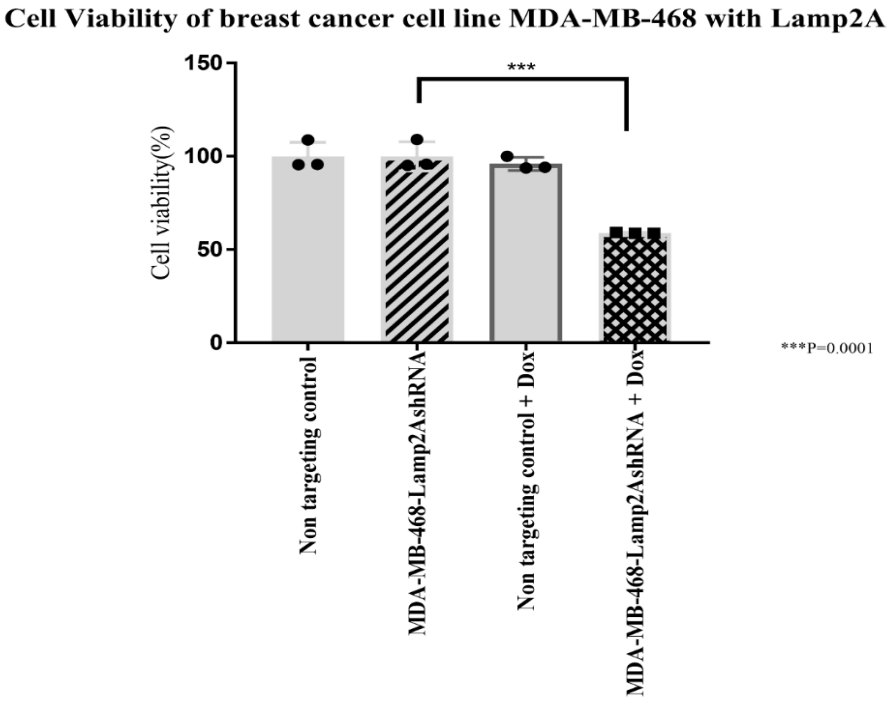
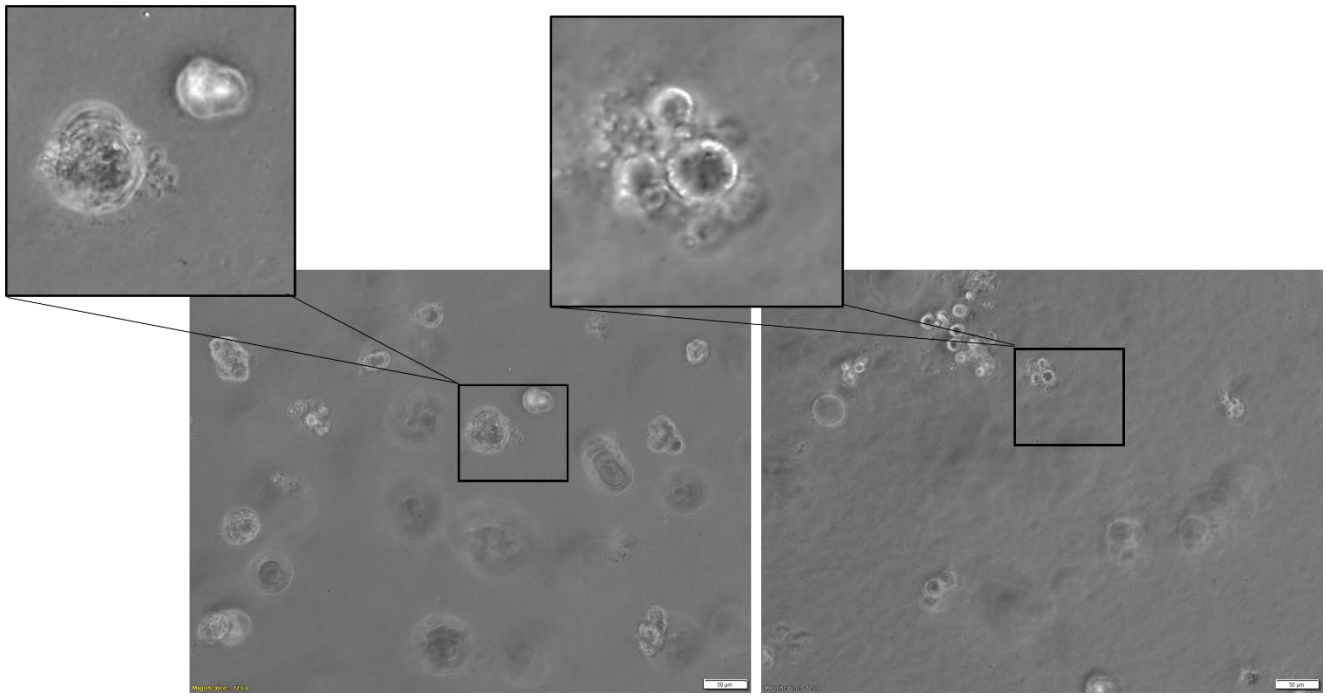


Figure 5-19 The knockdown of Lamp2A significantly decreases cell viability in the MDA-MB-468 breast cancer cell line.

The Alamar Blue assay (RFU) measured cell viability in the MDA-MB-468 breast cancer cell lines with either Lamp2AshRNA KD and non-targeting control with or without Dox (Dox). The percentage of cell viability was determined compared to control without Dox. The cell was grown for 72 hours in the presence of Dox to achieve maximal KD, and then after the following 24 hours, an Alamar Blue assay was performed. (n=3, ±SD, $p<0.05$ ANOVA and Tukey's post hoc test)

5.3.5.4 Invasion outgrowth with Lamp2A knockdown

The MDA-MB-468 breast cancer line with Lamp2AshRNA or non-targeting shRNA was grown in 3D culture (Refer to APPENDIX V for images of non-targeting shRNA). The cells were seeded in and on Geltrex, providing a semisolid extracellular matrix that the cell must invade to move and grow. This process involves the cell actively breaking down the matrix to enable it to migrate through it. As the representative images in Figure 5-20 show, with Lamp2A removal, the cellular colonisation is reduced, suggesting they do not survive in this environment compared to the control. In addition, the images in the inset display invasive growth without Lamp2A knockdown, but the cells where Dox has been added appear to be stressed and undergoing cellular death.



Lamp2A shRNA **Lamp2A shRNA + Dox (1µg/ml)**

Figure 5-20 The invasive potential of MDA-MB-468 breast cancer cell line by the reduction of Lamp2A

The MDA-MB-468 breast cancer cell line was seeded in Geltrex suspension on to solidified Geltrex basement layer. The cells were allowed time to grow with or without Dox, and the growth of the cell was captured at 100X magnification (scale bar 50µm)(n=3).

5.3.6 The addition of EGF in the MDA-MB-468 with Lamp2A knockdown enhances the biological effects observed.

5.3.6.1 Cell viability during EMT with Lamp2A knockdown

The MDA-MB-468 cell line is part of the TNA subtype, which has a distinct basal-like morphology which differs from the TNB with a mesenchymal morphology. The baseline results from Figure 5-2 to Figure 5-5 clearly show that the MDA-MB-231 cell lines had the highest expression of CMA markers compared to the TNA subtype. So to investigate the role these phenotypic differences have, the MDA-MB-468 cell line can be induced to mesenchymal phenotype with the addition of EGF as described previously. The viability of Figure 5-21 of the MDA-MB-468 with Lamp2A knockdown cell line in the presence of 50ng/ml EGF was approximately 30% compared to control. These results are compared to those observed in Figure 5-19, where the cell viability of MDA-MB-468 Lamp2AshRNA was approximately 60%. The addition of EGF decreased the viability by another 30% or half. To validate these findings, images of the MDA-MB-468 breast cancer cell were taken to visualise the effects of EGF in the context of Lamp2A knockdown.

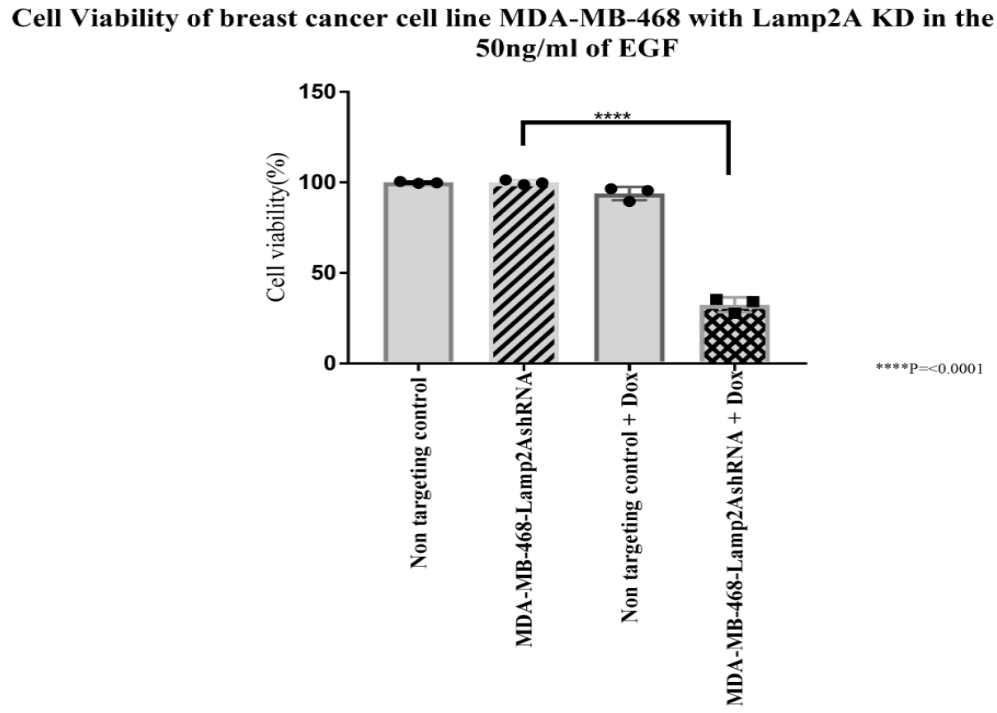


Figure 5-21 EGF does not prevent the decrease in cell viability with Lamp2A KD in the MDA-MB-468 breast cancer cell line.

Cell viability was measured with Alamar Blue assay (RFU) in the MDA-MB-468 breast cancer cell lines with either Lamp2AshRNA KD and non-targeting control with or without Dox (Dox) and all in the presence of EGF. The percentage of cell viability was determined compared to control without Dox. The cells were pretreated with EGF for 24 hours prior to Lamp2A KD for 72 hours, and then after the following 24 hours, an Alamar Blue assay was performed. . (n=3, ±SD, $p<0.05$ ANOVA and Tukey's post hoc test)

This decreased cell viability was witnessed in the micrograph images displayed in Figure 5-22. The images are of the MDA-MB-468 Lamp2AshRNA and non-targeting-shRNA with or without Dox, and all groups were grown in the presence of EGF. The MDA-MB-468 Lamp2AshRNA plus Dox show very few viable cells remaining, and the cells present are stressed and many rounding up a feature of cellular death. Also, the cell with Lamp2A knockdown appears larger than the non-targeting control plus Dox. Further studies would be of interest to examine the levels of Lamp2A and the presence of other morphological markers such as E-Cadherin and Vimentin in the cells remaining after lamp2A knockdown. The data from Figure 5-21 and Figure 5-22 suggest that adding EGF enhances the effects due to the reduction in Lamp2A.

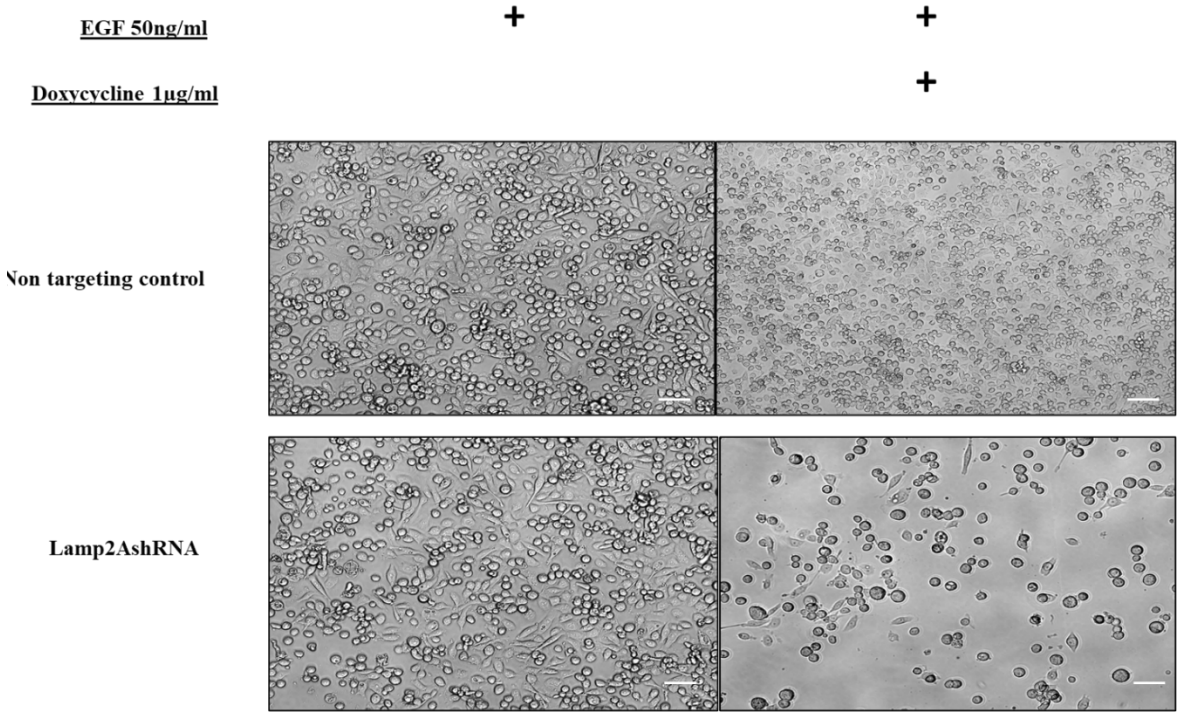


Figure 5-22 The addition of EGF with Lamp2A knockdown leads to increased cell death in the MDA-MB-468 cell line.

Micrograph images of the MDA-MB-468 cell line transduced with Lamp2A with or without Dox in the presence of EGF were captured with phase-contrast microscopy (PCM) at 100 X magnification. The cells were treated with EGF for 24 hours prior to Dox treatment for 72 hours for maximal Lamp2A KD, and images were taken the following 24 hours. (n=3) (scale bar=100µm)

5.3.6.2 Anchorage-dependent clonogenic survival and growth in EMT with Lamp2A knockdown

The final study considers the cell's ability to form colonies with this combination. The MDA-MB-468 Lamp2-shRNA cell line was pretreated with Dox, seeded, and allowed to adhere and form colonies before EGF was added. The data in Figure 5-23 demonstrates that colony formation is reduced by approximately 80% in MDA-MB-468 Lamp2AshRNA when EGF is added, compared to a reduction of approximately 40% in MDA-MB-468 Lamp2AshRNA in the absence of EGF. Figure 5-23 findings suggest that the EGF growth stimulating activity is suppressed in this context as the EGF is added to the media after Lamp2A knockdown. In Figure 5-21 and Figure 5-22, the EGF was added to cause a phenotypic change before Lamp2A knockdown was induced. So further studies into Lamp2A and EGF need to be undertaken to understand the relationship by changing the combination of EGF addition and Lamp2A knockdown. (refer to APPENDIX V for combined Figures 5-18 and 5-23 and Figures 5-20 and 5-22)

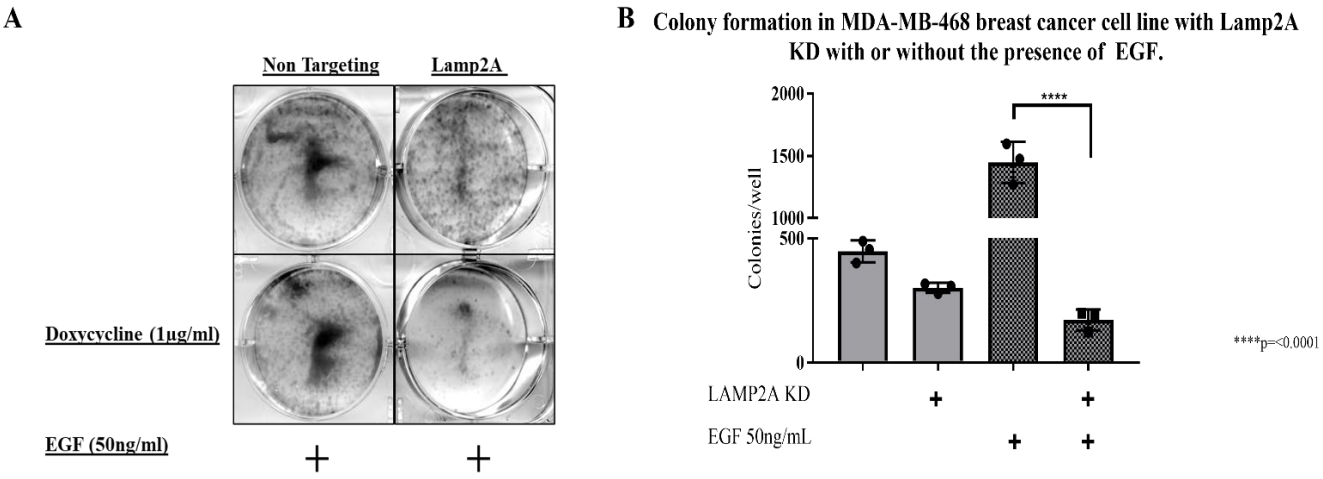


Figure 5-23 The presence of EGF further reduced colony formation in MDA-MB-468 with Lamp2A KD.

(A) Representative images of colonies formed by MDA-MB-468 with Lamp2A-shRNA with or without Dox and with or without EGF. The colonies formed by the cell lines were fixed and stained after the anchorage-dependent growth assay was completed. **(B)** Graph indicating the number of colonies counted per well with FIJI analysis software. (n=3, ±SD, $p<0.05$ ANOVA and Tukey's post hoc test)

5.3.7 The knockdown of Lamp2A in the breast cancer cell line Hs578T resulted in biological changes.

5.3.7.1 Lamp2A knockdown validation

The role of Lamp2A in the TNB subtype was investigated in the Hs578T breast cancer cell line, which has a mesenchymal phenotype and is one of the more aggressive breast cancer cell line utilised in this study. The study will focus on two cell lines from this subtype, the Hs578T and the MDA-MB-231 breast cancer cell line. First to be investigated was the Hs578T breast cancer cell line. As depicted in Figure 5-24, the Hs578T breast cancer cell line was successfully transduced with Lamp2AshRNA or non-targeting shRNA. The knockdown of Lamp2A in the Hs578T breast cancer cell line resulted in an approximate 90% reduction of Lamp2A expression, as shown in Figure 5-24 A and B. Although there was apparent variability between the groups, the expression of differences in Lamp2B was found to be non-significant. When levels of CMA markers were investigated within the lysosomal enrichment in response to Lamp2A knockdown, it was observed that Lamp2A was lost to a greater extent within the whole cell lysate than the lysosome enrichment. At this point of the study, it is becoming common that Lamp2A is residually maintained for at least 24 hours, as all Lamp2A knockdown has consistently reached its maximal in this study by 48 hours.

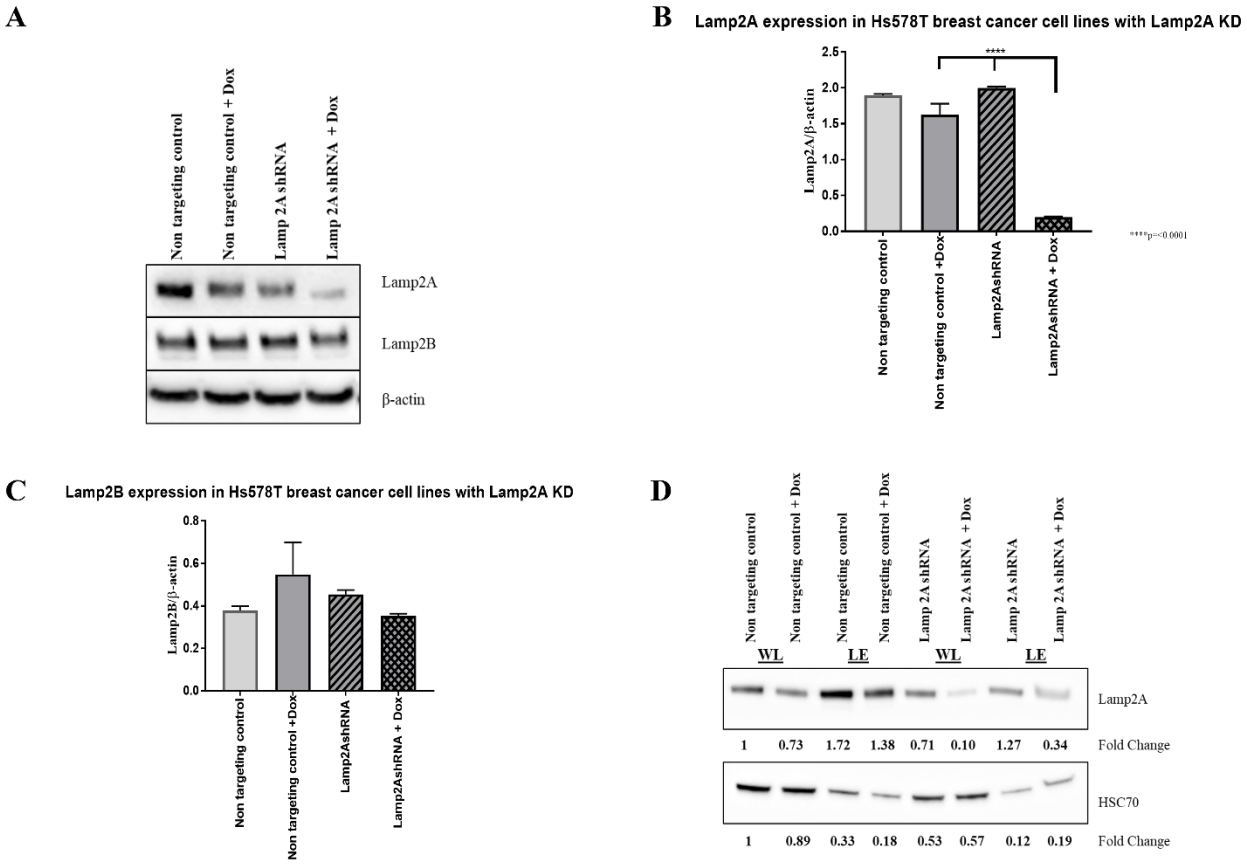


Figure 5-24 Lamp2A knockdown is confirmed in the Hs578T breast cancer cell line.

(A) Western blot representative image to confirm Lamp2A knockdown contrasted with another variant Lamp2B. The Hs578T breast cancer cell line was transduced with Lamp2A shRNA or non-targeting shRNA (NT) as control, with all samples shown with or without Induction by Dox (1µg/mL). **(B)** Densitometry analysis of intensity compared to control of Lamp2A **(C)** Densitometry analysis of intensity compared to the control of Lamp2B. **(D)** Whole-cell lysate and lysosome enrichment of Lamp2A knockdown and control a representative western blot image with the calculated fold change compared to control without Dox (set at 1). (n=3, ±SD, $p<0.05$ ANOVA and Tukey's post hoc test)

To determine the effectiveness of the knockdown through the visualisation of the tRFP. Figure 5-25 conforms to the expected results with tRFP present when Dox is added and not when it is absent. The phase-contrast images show similarities between all groups. There is what appears to be a senescent cell in the Lamp2AshRNA with Dox, and to support this further, this cell does not appear to have an RFP signal in the matching TRITC images for the PCM. When they reach high density, this cell line can have some round cells as seen in the other groups.

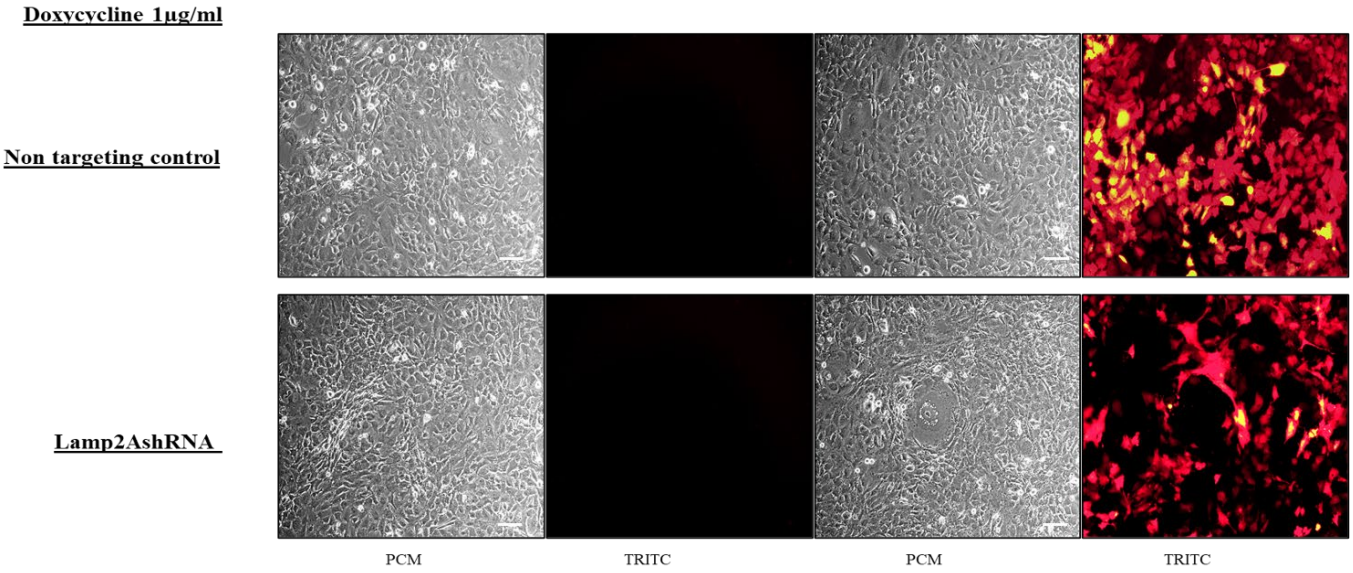


Figure 5-25 The breast cancer cell line Hs578T displays confirmation of Lamp2A KD.

Micrograph images of the Hs578T breast cancer cell line transduced with Lamp2A or non-targeting with or without Dox were captured with phase-contrast microscopy (PCM) at 100 X magnification. In addition, images of tRFP were captured with a fluorescent filter (TRITC) at 100 X magnification to confirm activation of lentivirus with Dox addition. (n=3)(scale bar=100µm)

5.3.7.2 Lamp2A knockdown in lysosomal enrichment

The Hs578T cell line transduced with Lamp2AshRNA or non-targeting-shRNA, with or without Dox, had lysosomal enrichment fractioned with the whole-cell lysate collected before for comparison. The data in Figure 5-26 shows Lamp2A knockdown in the whole cell lysate and the lysosomal enrichment, but as seen previously, not to the same extent. Thus, there does not appear to be any clear trend in the expression of CMA substrates. However, as mentioned previously, this may be a study design limitation. Future collections of all cell lines should be completed with a lysosomal inhibitor to prevent degradation of the lysosomal content and better understand the CMA substrates.

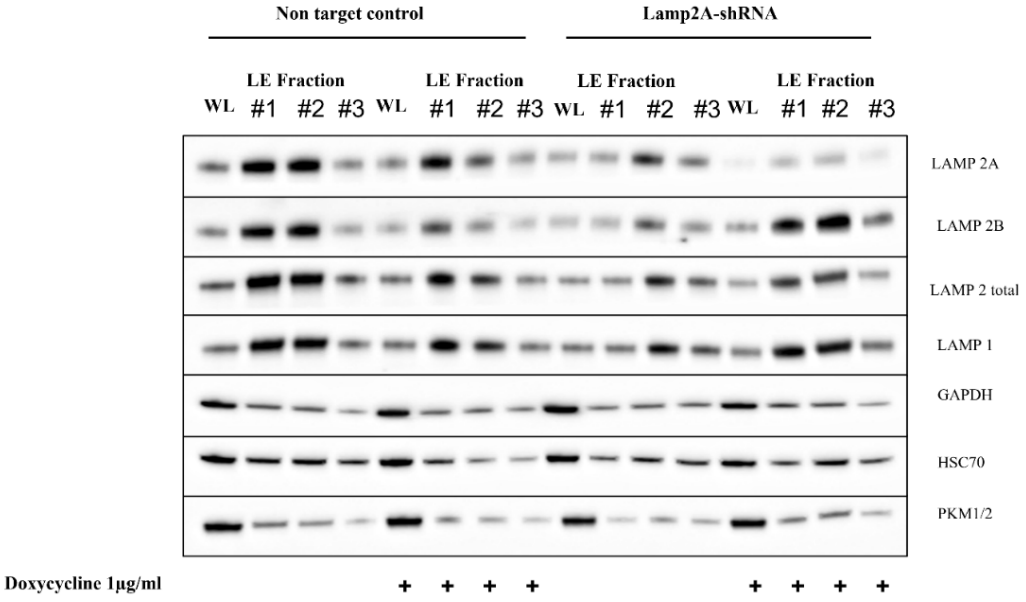


Figure 5-26 The Hs578T breast cancer cells display no changes to CMA substrates with Lamp2A knockdown.

The representative western blot image of the lysosomal enrichment (LE) fractioned with comparative whole cell lysate (WL) for the Lamp2 isoforms, lamp1 and confirmed CMA substrates to examine the effect of Lamp2A reduction has on CMA processing. (n=3)

Subsequently, the study determined the effect of Lamp2A knockdown in HS578T concerning cell viability. As depicted in Figure 5-27, the knockdown of Lamp2A resulted in a decrease in cell viability; in response to Lamp2A, there was a reduction of 40%. It is worth mentioning that the Dox is at 1ug/ml, which is a minimal amount to account for any off-target effects. It could be reduced further to 0.5ug/ml if further studies were carried out in this context.

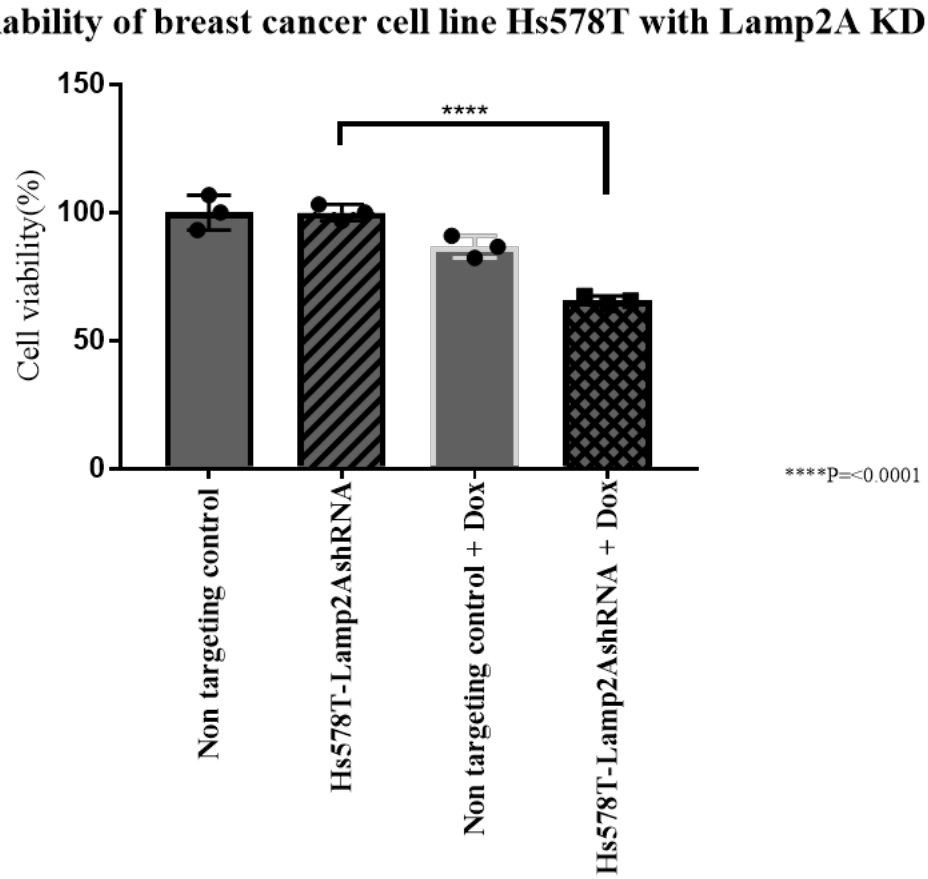


Figure 5-27 The knockdown of Lamp2A reduces cell viability in the Hs578T breast cancer cell line.

The Alamar Blue assay (RFU) measured cell viability in the Hs578T breast cancer cell lines with either Lamp2AshRNA knockdown and non-targeting control with or without Dox (Dox). The percentage of cell viability was determined compared to control without Dox. The cells were grown for 72 hours in the presence of Dox to achieve maximal knockdown, and then after the following 24 hours, an Alamar Blue assay was performed. (n=3, ±SD, $p<0.05$ ANOVA and Tukey's post hoc test)

5.3.7.3 Anchorage-dependent clonogenic survival and growth in Hs578T breast cancer cell line with Lamp2A knockdown

An anchorage-dependent assay was carried out to examine the effects of Lamp2A knockdown on the Hs578T breast cancer cell line. As with some of the previous cell lines, the assay was completed in two ways (Figure 5-12): with cells seeded before the induction of Lamp2A knockdown (Figure 5-28), or the cells were seeded after the knockdown of Lamp2A to recapitulate the use of Lamp2A as an intervention or prevention of colony formation respectively (Figure 5-29). As demonstrated in Figure 5-29, the knockdown of Lamp2A after seeding did not intervene with colony growth. Conversely, the knockdown of Lamp2A before seeding prevented colony formation by approximately 30%. It was noted that no differences were observed in the other groups with or without Dox.

These results collectively highlight Lamp2A as necessary in cell viability and colony formation in the Hs578T cell line. Notably, it was found that CMA substrates did not show any changes; whether this reflects the study limitations or whether the known substrates are altered in this oncogenic context is yet to be elucidated. Interestingly, the initial data (Figure 5-2) demonstrated that Lamp2A was not as highly expressed in the Hs578T cell line as its other TNB subtype counterpart, the MDA-MB-231 breast cell line. This will be of interest if this biological importance is increased in the MDA-MB-231 or not and will indicate whether the cytosolic expression of Lamp2A is an essential biomarker of CMA activity in this context.

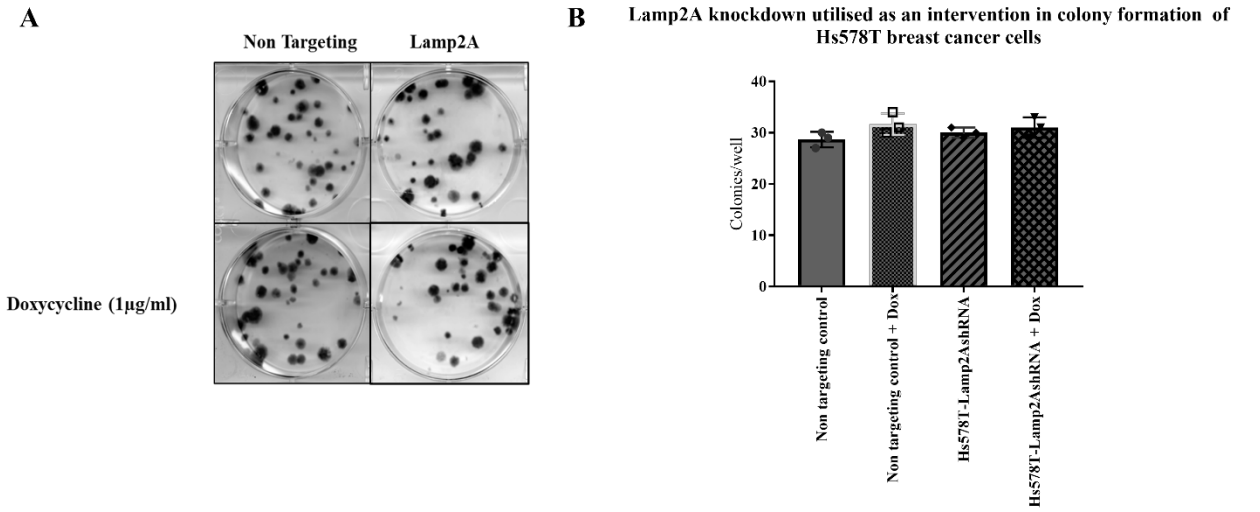


Figure 5-28 The Hs578T breast cancer cell lines colony growth was not altered by Lamp2A knockdown.

(A) Representative image of completed anchorage-dependent growth assay fixed and stained colonies. It was formed by Hs578T cells seeded before Lamp2-shRNA was induced and control cell lines. **(B)** Graph indicating the number of colonies counted per well with FIJI analysis software. (n=3, ±SD, $p<0.05$ ANOVA and Tukey's post hoc test)

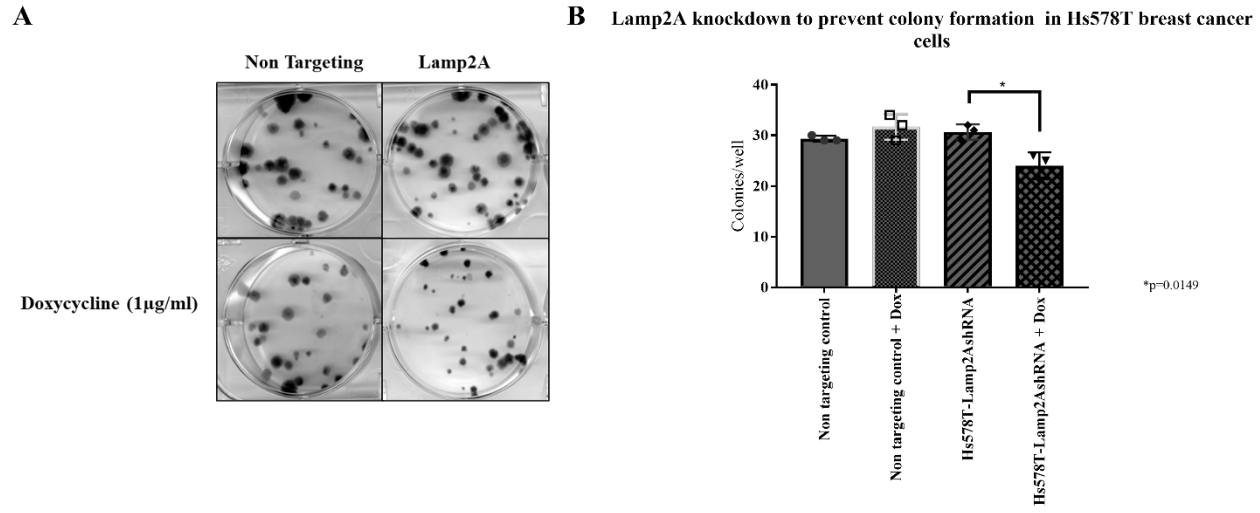


Figure 5-29 The knockdown of Lamp2A decreased the colony-forming capacity of the Hs578T breast cancer cell line.

(A) Representative image of completed anchorage-dependent growth assay fixed and stained colonies. It was formed by Hs578T cells seeded after Lamp2-shRNA was induced along with control cell lines. **(B)** Graph indicating the number of colonies counted per well with FIJI analysis software. (n=3, ±SD, $p<0.05$ ANOVA and Tukey's post hoc test)

5.3.8 The knockdown of Lamp2A in the MDA-MB-231 breast cancer cell line has a biological impact.

5.3.8.1 Lamp2A knockdown validation

To complete this study investigation of the role of CMA or, more specifically, Lamp2A in the breast cell molecular subtype, the triple-negative basal A (TNA) and basal B (TNB). The MDA-MB-231 breast cancer cell line was utilised in this part of the study. It should be highlighted that these cell lines had the highest expression of Lamp2A (Figure 5-2 to Figure 5-5) and are regarded as the most aggressive breast cancer cell line. The MDA-MB-231 breast cancer cell line was transduced with Lamp2AshRNA in parallel with the non-targeting-shRNA, with both shRNA constructs being Dox-inducible. The Lamp2AshRNA was observed to knock down Lamp2A by approximately 90% (Figure 5-30B). There was an increase in Lamp2B observed with the knockdown of Lamp2A, but it was not significant between the Lamp2AshRNA without Dox or non-targeting with Dox. However, there was a significant difference between non-targeting with Dox and Lamp2AshRNA with Dox ($p=0.0136$). The results from the lysosome enrichment and whole-cell samples (Figure 5-30C) demonstrated a reduction of Lamp2A in both, showing an increase of HSC70, respectively. There may be an accumulation of HSC70 occurring in response to the Lamp2A knockdown, and whether this is within the lysosomal lumen or the cytosolic face of the lysosomal membrane requires further elucidation. It is predicted that Lamp2A is utilised to deliver the Lys-HSC70 into the lysosome, and further studies with lysosomal inhibitor and the use of different lysate buffers to remove the cytosolic fraction of HSC70 to delineate this changer is required.

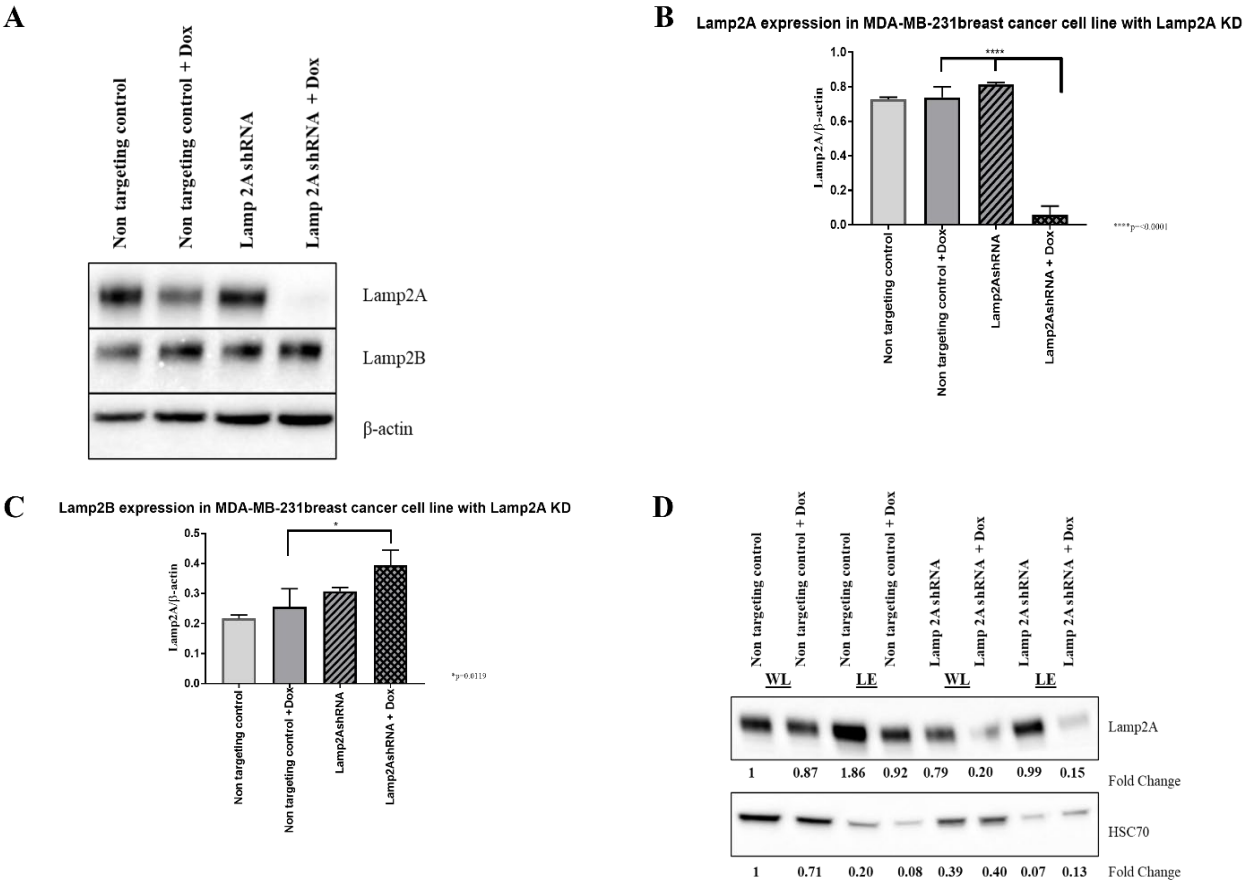


Figure 5-30 The MDA-MB-231 breast cancer cell line was successfully transduced with Lamp2A knockdown

(A) Western blot representative image to confirm Lamp2A knockdown contrasted with another variant Lamp2B. The MDA-MB-231 breast cancer cell line was transduced with Lamp2AshRNA or non-targeting sh-RNA (NT) as control, with all samples shown with or without Induction of Dox.(1µg/mL) **(B)** Densitometry analysis of intensity compared to control of Lamp2A. **(C)** Densitometry analysis of intensity compared to control of Lamp2B. **(D)** Whole-cell lysate and lysosome enrichment of Lamp2A knockdown and control a representative western blot image with the calculated fold change compared to control without Dox (set at 1). (n=3, ±SD, $p<0.05$ ANOVA and Tukey's post hoc test)

The Lamp2AshRNA and non-targeting-shRNA were present and actively expressed, as indicated in Figure 5-31. In addition, the cells demonstrate the presence of tRFP in the presence of Dox. From a morphological perspective, presented in the micrograph images presented in Figure 5-32 show the cell numbers decline in response to the reduction in the level of Lamp2A, and there is also a distinct increase in the presence of rounded cells indicating cellular death, but it was not significant

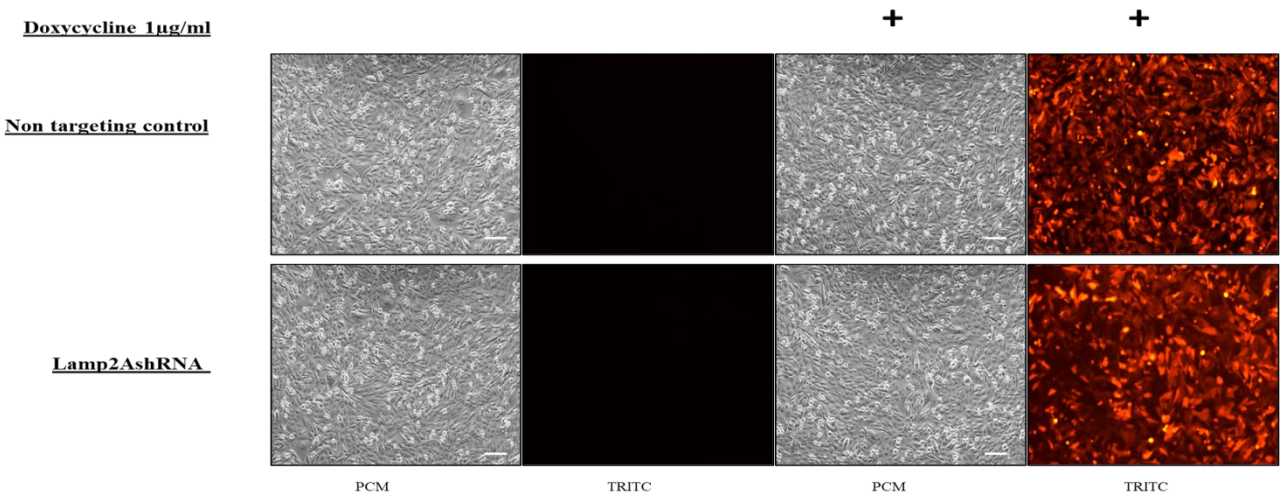


Figure 5-31 MDA-MB-231 breast cancer cell line high tRFP confirms Lamp2AshRNA expression.

Micrograph images of the MDA-MB-231 breast cancer cell line transduced with Lamp2A or non-targeting with or without Dox were captured with phase-contrast microscopy (PCM) at 100 X magnification. In addition, images of tRFP were captured with a fluorescent filter (TRITC) at 100 X magnification to confirm activation of lentivirus with Dox addition. (n=3)(scale bar= 100µm)

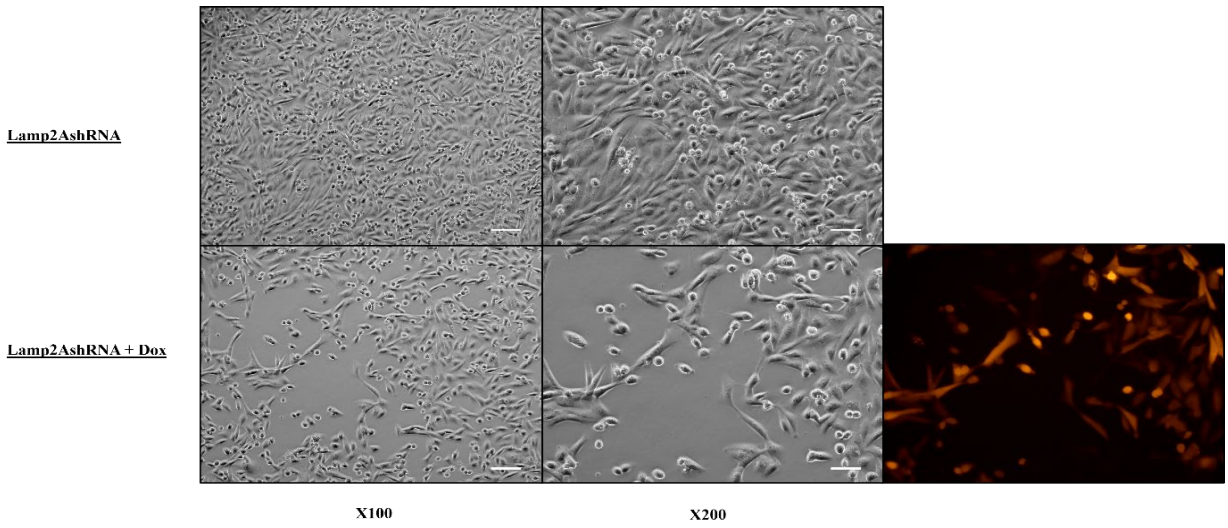


Figure 5-32 The knockdown of Lamp2A reduces MDA-MB-231 breast cancer cell numbers.

Micrograph images of MDA-MB-231 Lamp2AshRNA cell lines with and without Dox (after 72hours Dox treatment). Images taken with phase-contrast filter at X200 (scale bar=50µm) and X100 (scale bar=100µm) magnification. The TRITC (RED) image matches corresponding to Lamp2AshRNA+Dox at X200 magnification.

5.3.8.2 Lamp2A knockdown in lysosomal enrichment

The effects of Lamp2A knockdown were examined in the lysosomal component of the whole-cell lysate. Sucrose gradient fractionation was used to fraction the lysosome to collect a sample of lysosome enrichment for analysis. As illustrated in Figure 5-33, Lamp2A was lost in the whole-cell fraction and lysosomal enrichment, although not to a great extent. There are no apparent differences between the CMA substrates' levels of interest, though some inconsistencies between the groups warrant further investigation. Further investigations would require the potential CMA substrates to be interrogated further with a pulse-chase experiment or mass spectrometry on the lysosomal content.

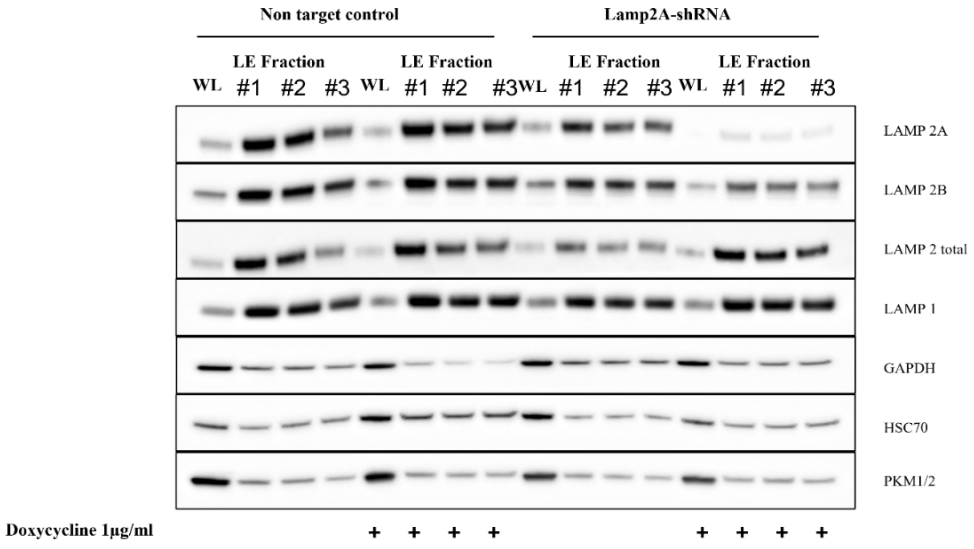


Figure 5-33 The removal of Lamp2A in the MDA-MB-231 breast cancer cell line does not affect CMA substrates.

The representative western blot image of the lysosomal enrichment (LE) fractioned with comparative whole cell lysate (WL) for the Lamp2 isoforms, lamp1 and confirmed CMA substrates to examine the effect of Lamp2A knockdown has on CMA processing. (n=3)

5.3.8.3 Cell viability with Lamp2A knockdown

The cell viability of the MDA-MB-231 was measured with Alamar Blue and is presented in Figure 5-34. The results indicate that the viability of the MDA-MB-231 breast cancer cell line is reduced by 40% compared to all other groups with the knockdown of Lamp2A. There was no significant difference in cell viability found between the other groups.

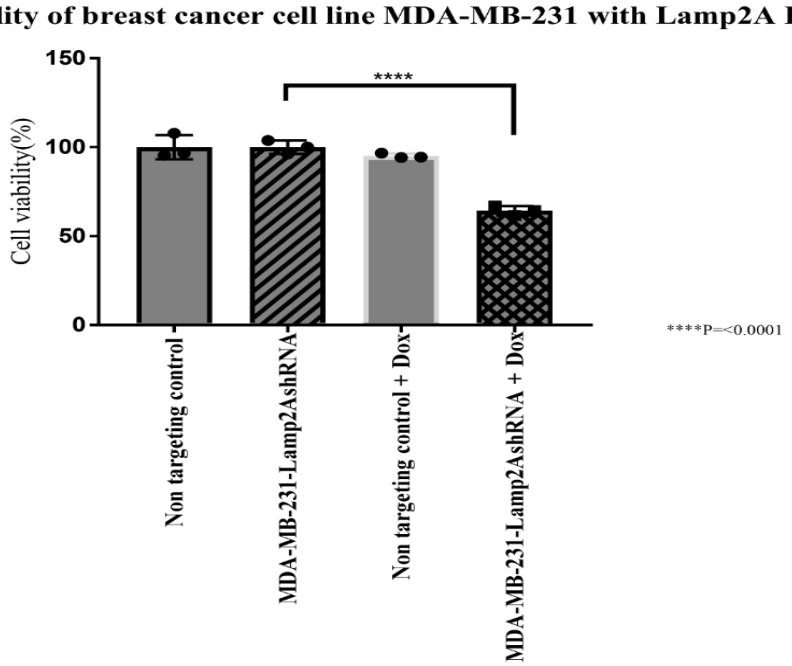


Figure 5-34 The knockdown of Lamp2A in the MDA-MB-231 breast cancer cell line resulted in a decrease in cell viability compared to the control

The Alamar Blue assay (RFU) measured cell viability in the MDA-MB-231breast cancer cell lines with either Lamp2AshRNA knockdown and non-targeting control with or without Dox. The percentage of cell viability was determined compared to control without Dox. The cells were grown for 72 hours in the presence of Dox to achieve maximal knockdown, and then after the following 24 hours, an Alamar Blue assay was performed. (n=3, ±SD, $p<0.05$ ANOVA and Tukey's post hoc test)

5.3.9 Removal of Lamp2A impaired the functional activity of the breast cancer cell line MDA-MB-231.

5.3.9.1 Wound healing with Lamp2A knockdown

This area of the experiment considered the functional capacity of the MDA-MB-231 breast cancer cell lines transduced with Lamp2AshRNA tetracycline-inducible knockdown. The first functional experiment undertaken was to determine the cells' ability to migrate as a functional group to close the gap between cells formed by a scratch (wound) being administered. For this experiment, the MDA-MB-231 Lamp2AshRNA and non-targeting-shRNA, both with and without Dox, were included. First, the cells were grown to confluence in the specialised wound healing plates for the Xcelligence RTCA MP system (as described in Chapter 2). Then the ACCU wound scratch tool (Agilent, California. USA) performed scratches in all 96 wells of the plate simultaneously. The real-time analyser then undertook continuous readings every 15 minutes, and this data was later analysed with RTCA software. The software determines the rate of change of cell index over time, referred to as 'the slope', as observed in Figure 5-35 A). The cell index, as mentioned previously, is an arbitrary measure of cellular impedance upon the electrode within the well. In the context of wound healing, the electrode is located as a strip down the centre of the well, as observed in the image of the empty well in Figure 5-35 B. The result of the rate of change was decreased with the reduction in Lamp2A significantly when compared to non-targeting ($p=0.0003$), non-targeting with Dox ($p=0.0002$) and Lamp2AshRNA without Dox ($p=<0.0001$). It should be noted that no significant difference was found between the other groups when compared against each other. The wells in which the cell undertook the experiment were fixed and stained at completion, as shown in Figure 5-35 B and the real-time analysis data was included in Figure 5-35 C.

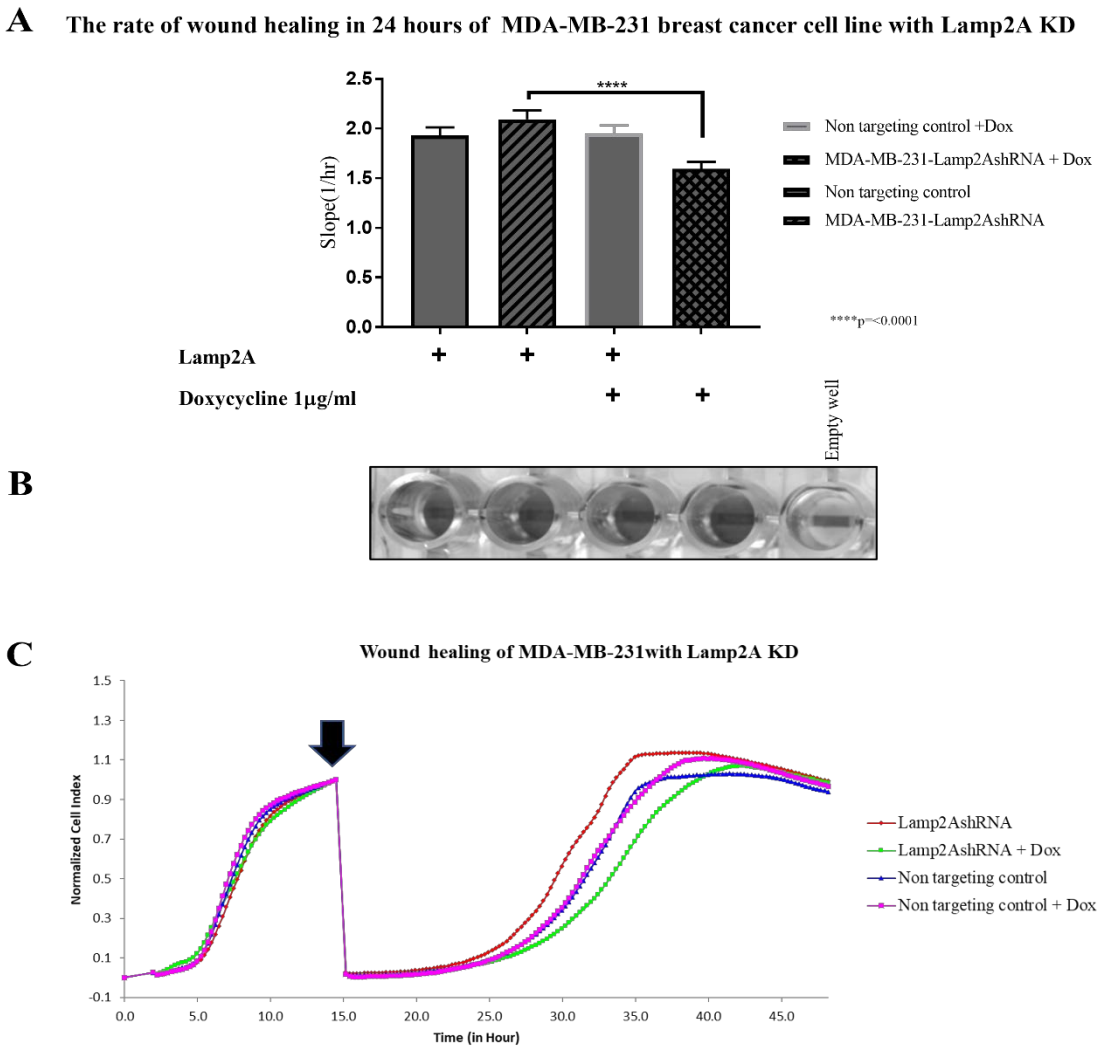


Figure 5-35 The MDA-MB-231 breast cancer cell line had a decreased rate of wound healing with Lamp2A knockdown.

(A) The rate of wound healing as determined by the RTCA software, the slope, represents the rate of change of the cell index as a function of time between wound scratch and 24 hours. **(B)** A representative image of the wells of the wound plate and stained after completion of the assay included an empty well to visualise the scratch area where the electrode is located. **(C)** The plotted results from the RTCA Xcelligence MP system were used to measure the respective cell line's in real-time wound healing closure black arrow indicates when the wound was applied. (n=3, ±SD, $p<0.05$ ANOVA and Tukey's post hoc test)

5.3.9.2 Microchemotaxis migration with Lamp2A knockdown

In addition to the wound healing experiment, MDA-MB-231 breast cancer cell lines with Lamp2AshRNA and non-targeting-shRNA were examined in a transwell migration assay, as detailed in Chapter 2. This experiment examines single-cell movement, whereas the wound healing assay examines population movement. The Xcelligence RTCA DP system was utilised with invasion and migration plates (CIM plates). Cells were seeded into the top chamber and were allowed to migrate through the membrane, adhering to the underside of the membrane, which contained electrodes that measured impendence. Thus, the cell index increased relative to the number of cells adhering and impeding the signal from the electrodes. The rate of change over 4 hours was used to determine the slope with wound healing. As depicted in Figure 5-36 A, the migration rate was significantly decreased in the MDA-MB-231 with Lamp2A knockdown compared to all other groups, with no significance determined between the other groups. Figure 5-36 B shows a data output from the Xcelligence over real-time with cell impendence measured continuously for over four hours. Figure 5-36 C is a fixed and stained image of the CIM plates between the electrodes (black circle); migrated cells can be observed in purple.

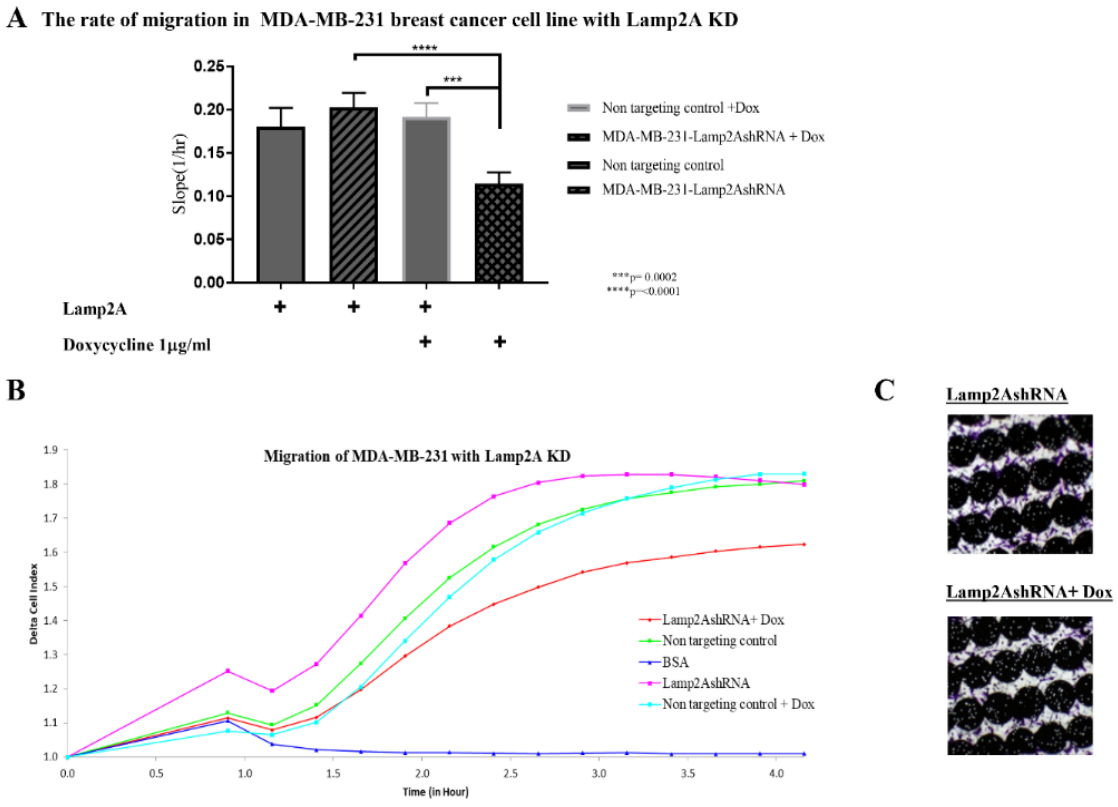


Figure 5-36 The knockdown of Lamp2A impeded migration in the MDA-MB-231 breast cancer cell line.

(A) The rate of migration as determined by the RTCA software, the slope, represents the rate of change of the cell index as a function of time between 0 hours and 4 hours. **(B)** The plotted results from the RTCA Xcelligence DP system were used to measure the respective cell lines real-time transwell migration. **(C)** A representative image of CIM plates wells of the respective cell lines stained after completion of the assay to visualise the cells migrated to the other side visible in between the well electrodes. (n=3, ±SD, $p<0.05$ ANOVA and Tukey's post hoc test)

5.3.9.3 Anchorage-dependent clonogenic survival and growth in MDA-MB-231 breast cancer cell line with Lamp2A knockdown

The following functional study focused on the cell's ability to form colonies and the growth of colonies in response to Lamp2A removal. As shown in Figure 5-37 A, the representative image shows that with Lamp2A knockdown, colonies are reduced. After all, replicates were counted and analysed, and it was determined that the removal of Lamp2A after seeding intervened with the growth of the colonies by approximately 50% (Figure 5-37B). This finding was significant compared to all groups, where no difference was found.

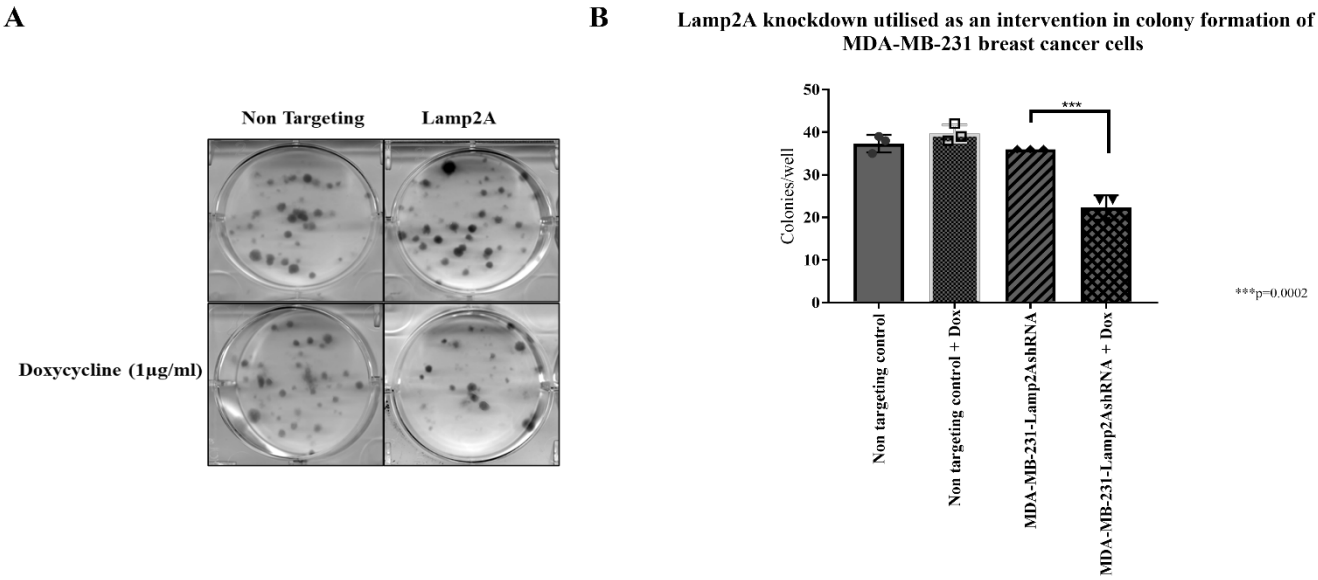


Figure 5-37 The colony growth was impaired by Lamp2A knockdown in MDA-MB-231 breast cancer cell lines.

(A) Representative image of completed anchorage-dependent growth assay fixed and stained colonies. It was formed by MDA-MB-231 breast cancer cells seeded before Lamp2-shRNA is induced to knockdown along with control cell lines. **(B)** Graph indicating the number of colonies counted per well with FIJI analysis software. (n=3, ±SD, $p<0.05$ ANOVA and Tukey's post hoc test)

To delineate the role of Lamp2A in growth as displayed in the figure above versus anchorage dependence. Another growth assay was performed to examine the preventative effects of Lamp2A knockdown in the cell's ability to attach and anchor to enable them to form colonies. The cells had Lamp2A knocked down before seeding to assess the effect on anchorage capabilities precisely. As displayed in Figure 5-38, the MDA-MB-231 breast cancer cell line with Lamp2AshRNA and non-targeting-shRNA with or without Dox were seeded after 72 hours of shRNA induction. Again, as demonstrated in Figure 5-38, there is nearly a complete loss of colony establishment and formation from the group with Lamp2A knockdown. When these colonies were counted for analysis, there was an approximate 97% loss of colonies with Lamp2A reduction, and no difference was found between the other groups. It indicates that it is important in colonisation but is pivotal in the attachment and establishment of the colony with Lamp2A decrease, rendering the cell incapable of colony-forming. It is speculated that the loss of colonies observed in Figure 5-37 above may be due to these same effects observed below and warrant the examination of cell adhesion molecules as possible CMA substrates to explain these findings further.

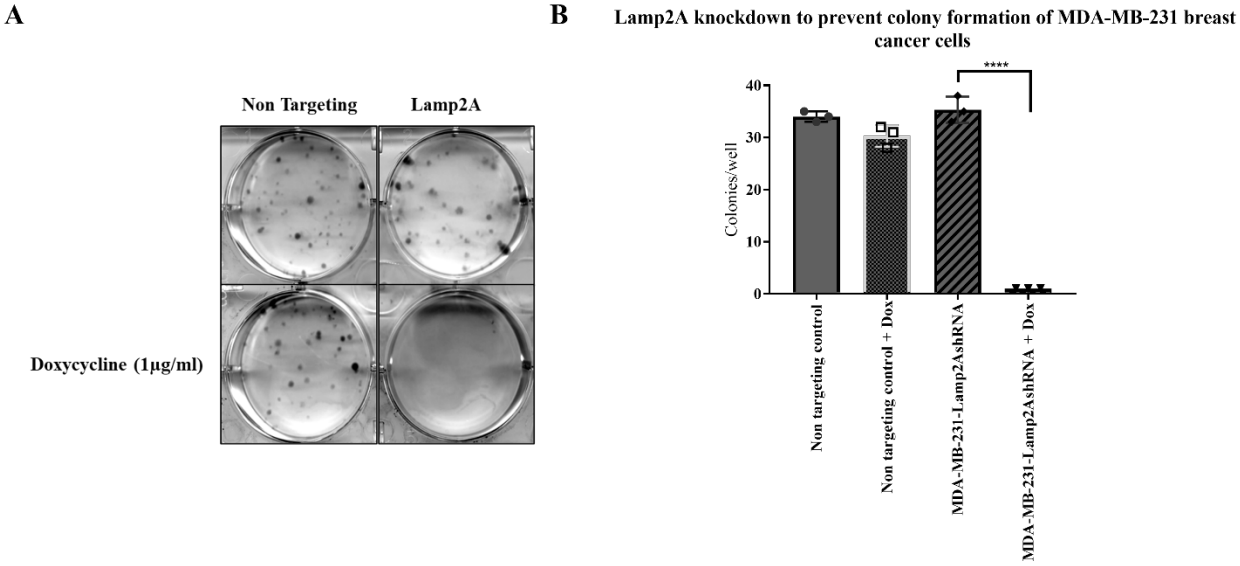


Figure 5-38 MDA-MB-231 breast cancer cells could not form colonies with the knockdown of Lamp2A.

(A) Representative image of completed anchorage-dependent growth assay fixed and stained colonies. It was formed by MDA-MB-231 breast cancer cells seeded after Lamp2-shRNA was knocked down through Dox treatment and control cell lines. **(B)** Graph indicating the number of colonies counted per well with FIJI analysis software(n=3, ±SD, $p<0.05$ ANOVA and Tukey's post hoc test)

5.3.9.4 Anchorage-dependent clonogenic survival and growth in MDA-MB-231 with Lamp2A knockdown in the presence of EGF

It was leading on from findings previously with the MDA-MB-468 (Figure 5-23), whereby the effects of Lamp2A knockdown were enhanced in the presence of EGF. This study investigated whether this response was specific to the MDA-MB-468 cell line or was the result of the reduction of Lamp2A causing EGF to become cytotoxic. In addition, a preliminary study was performed with another anchorage dependant growth assay undertaken in the presence of EGF with MDA-MB-231 breast cancer cell lines Lamp2AshRNA and non-targeting-shRNA with or without Dox. Figure 5-39 examines the effects of EGF in the context of the MDA-MB-231 breast cancer cell lines with Lamp2A knockdown. Although, as seen in Figure 5-37, the removal of Lamp2A still reduced the colony growth even in the growth-assisted environment of EGF, there was a net increase in colonies of 20% in the presence of EGF. Thus, the colony growth was significantly reduced by approximately 60 %. Interestingly, this is slightly higher than without EGF and suggests a need for further studies to elucidate these findings.

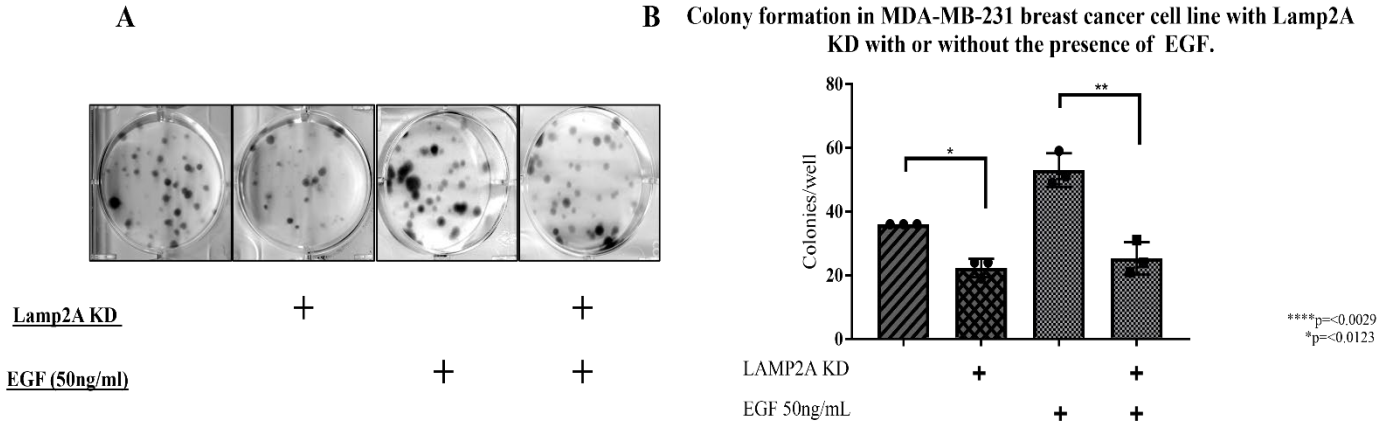


Figure 5-39 The addition of EGF does not reverse the colony growth inhibition observed in MDA-MB-231 with Lamp2A knockdown.

(A) Representative image of completed anchorage-dependent growth assay fixed and stained colonies. It was formed by MDA-MB-231 breast cancer cells seeded after EGF exposure but before Lamp2-shRNA is induced to knockdown was similarly undertaken in the control cell lines. **(B)** Graph indicating the number of colonies counted per well with FIJI analysis software. (n=3, ±SD, $p<0.05$ ANOVA and Tukey's post hoc test)

5.3.9.5 Invasion outgrowth with Lamp2A knockdown

Further functional studies were performed, including an invasion outgrowth experiment with knockdown of Lamp2A before seeding; however, this resulted in no cells surviving, which was not conducive to examining invasion. Therefore, the experiments shown in Figure 5-40 are qualitative images showing that the knockdown of Lamp2A displays more altered invasiveness than that of the non-targeting shRNA with Dox. In addition, the magnified insteps of the colonies demonstrate an altered invasion pattern in the presence of Lamp2A knockdown, and the cells appear to grow in larger clusters with a spherical appearance. In contrast, without Lamp2A knockdown, the cells display a distinct disorganised growth with defined invasive sprouts. It also appears that the addition of Dox potentially induces aggregation or regression to an acinus-like structure compared to the groups without Dox. Further Dox titration and staining studies are needed to investigate cadherins and other markers to determine whether the phenotype is more epithelial than control. Moreover, if there is a luminal component as observed in acini in these structures would be recommended.

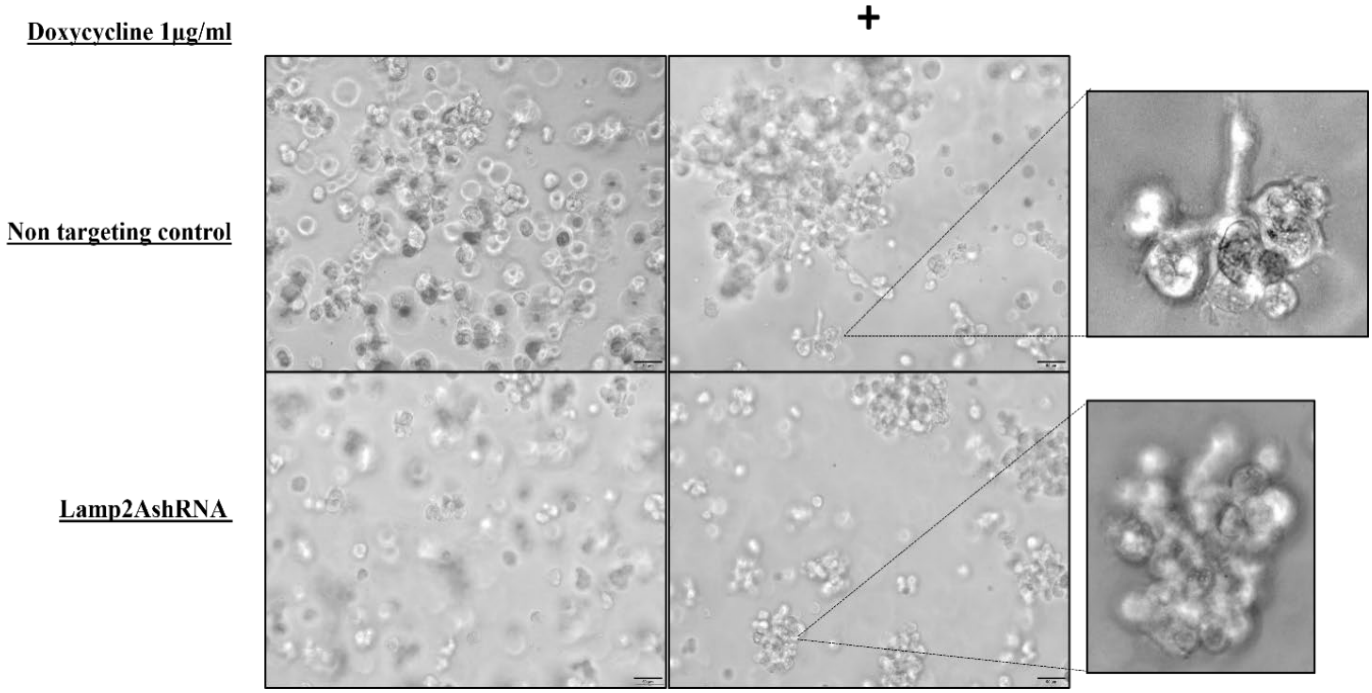


Figure 5-40 The MDA-MB-231 cell line displays altered invasive growth with the knockdown of Lamp2A.

The MDA-MB-231 breast cancer cell line was seeded in Geltrex suspension on to solidified Geltrex basement layer. The cells were grown with or without the presence of Dox during the assay, and the growth of the cell was captured Scale bar = 50µm .

Table 5-1 Summary of findings

			EFFECT of LAMP2A KNOCKDOWN					
Cell line	**Lamp2A knockdown (%)**		**Cell viability**	**Wound healing**	**Invasion/ 3D growth**	**Migration**	**Colony-forming (Intervention)**	**Colony-forming (Prevention)**
	WL	**LE**						
MCF10A	80	50	None	None	None	None	None	None
MDA-MB-468	80	50	*Reduced	N/A	*Reduced	N/A	*Reduced	N/A
MDA-MB-468 + EGF	N/A	N/A	*Reduced	N/A	N/A	N/A	*Reduced	N/A
HS578T	85	65	*Reduced	N/A	N/A	N/A	None	*Reduced
MDA-MB-231	90	80	*Reduced	*Reduced	Altered	*Reduced	*Reduced +EGF *Reduced	*Reduced (****)

* = effects were significance N/A= Experiment not performed WL= whole lysate LE= Lysosome enrichment

5.4 DISCUSSION

The earlier chapters (3&4) examined macroautophagy, whereas this chapter has focused on the more specific form of autophagy, CMA. This study has utilised a progressive breast cancer panel screening approach to guide the cell lines to be included in the functional studies of CMA or, more specifically, Lamp2A. It has been demonstrated that CMA is upregulated in the more aggressive phenotype. This increase was shown to be of biological significance to this breast cancer subtype. Interestingly this functional importance was not observed in the "normal" mammary epithelial cell line MCF10A. This study has highlighted the importance of CMA to the aggressive phenotype and petitions the need for further studies to determine what specifically CMA is targeting or regulating in this cellular context that makes it so important.

5.4.1 The breast cell subtype demonstrates a correlation with CMA but not mutant RAS

The study described in this chapter followed similar lines of enquiry as previous chapters and initially investigated whether CMA showed any expression pattern when examined in a progressive panel of breast cell lines. The results demonstrate the critical effector protein Lamp2A in the more aggressive subtype's triple-negative basal A and basal B. Interestingly, the opposite expression profile was observed in the Lamp2B transcript variant; another variant Lamp2C. However, there is currently no antibody available, explaining why it has not been examined in this study. (Figure 5-2 to Figure 5-4) There is less known regarding the Lamp2B and Lamp2C variants than that of Lamp2A, but they are described to have different functional roles. Currently, Lamp2A is the most well described, with its well-established role in CMA; however, there is still much that is not known and needs elucidation [274, 580, 581, 592, 594]. In addition, there is some information regarding Lamp2B relating to its association with Danon disease [595]; more recently, there have been studies relating to its role in exosomes [596], lysosomes and autophagosome fusion [590]. Regarding Lamp2C, there is currently very little knowledge, but some research shows that it is a facilitator of RNA degradation [591, 597]. It would be of interest to examine the role of particular Lamp2B in this context to determine if, as

shown by others to be related to autophagy and if so, its reduction in the more aggressive phenotypes related to the suppression in autophagic activity observed in these cell lines in chapter 3. A great deal of research is still required to investigate the LAMP2 transcripts to properly understand their independent and inter-dependent functions, mainly in the context of cancer but even at a normal physiological state

Leading on from this, the RAS progressive panel was further examined to determine if there was a correlation to the presence of RAS, particularly mutant RAS. This study initially focused on a panel of breast cell lines with varying RAS mutation and activation degrees to identify a correlation between CMA markers and activity, as depicted in Figure 5-5. The result shows no clear pattern or association with mutant or specifically mutant HRAS. On further investigation for studies to support these findings concerning CMA and oncogenic RAS, a causal relationship was mentioned due to change in energetic demand as a consequence of oncogenic RAS, but without any data to support this. Therefore, the recently developed KFERQ-like motif finder tool by Kirschner et al. was accessed to examine if RAS had a KFERQ-like motif, indicating that it could be a CMA substrate [264]. The RAS isoforms NRAS, HRAS and KRAS were all submitted into the KFERQ finder and results which have been included in APPENDIX VI demonstrate that all the RAS isoforms conserve a canonical KFERQ-like motif at position 101 of the sequence and a post-translation modification resulting in a KFERQ-like motif due to acetylation at location 161.

Furthermore, the acetylation causes a KFERQ-like motif of the sequence at 161, and the acetylation can substitute for glutamine. Interestingly the KRAS had the presence of a further three post-translational modifications that could result in the presence of KFERQ-like motifs at loctation165; the phosphorylation can result in the substitute for acidic amino acids of the KFERQ and at position 166, a possibility of two KERFQ-like motifs due to combination of acetylation and phosphorylation at this residue (refer to APPENDIX VII). This increase in KFERQ target sites in KRAS may explain the observed upregulation of Lamp2A in the MDA-MB-231 cell line, which has a KRAS mutation. Furthermore, it is worth noting that it has been recently identified that the KFERQ-like motif can also be targeted and utilised in endosomal microautophagy degradation pathways [598]. Concerning RAS mutations, there was no evidence to suggest that the HRAS alters Lamp2A expression. Although it may be naïve to assume that expression levels alone could indicate functional changes, the basal levels of Lamp2A in MCF10A HRAS and Hs578T

cell lines may be sufficient to meet any conferred changes with its expression. Without any previous literature to aid in these explanations, there is a need to focus more efforts on the functional activity of CMA. This aspect of real-time functionality limited this study. It could even be proposed that the increase of Lamp2A was observed similarly to those observed with increased LC3-II, as shown in chapter 3. Thus, the increase in Lamp2A expression may indicate dysfunction rather than increased function.

There is still much research to be undertaken to confirm RAS isoforms as bona fide CMA substrates, and it is warranted as this may identify a feasible target for treatment in RAS-driven cancers.

5.4.2 CMA inhibition was shown to have no functional implications in regular mammary epithelial compared to a carcinogenic counterpart.

The MCF10A cell line is representative of "normal" non-transformed mammary epithelial model cells, and although spontaneously immortalised, it has been used as such by us and others [375]. Therefore, MCF10A cells were examined to determine a baseline or what would be expected under normal conditions for CMA to compare these transformed MCF10A cells and other well-established oncogenic cell lines. The data revealed that Lamp2A was present at moderate levels in MCF10A cells, as Lamp2B was slightly higher, and all the other results demonstrated expected changes of CMA and its substrates with the knockdown Lamp2A. These findings were also noted and detailed by Han et al., who identified no impact of Lamp2A knockdown in the MCF-10A in a siRNA model [599]. Unlike this current study which developed the Lamp2AshRNA inducible system, it is more biologically relevant as it allows for controlled reduction of Lamp2A, and upon removal of Dox, Lamp2A returns. In addition, this inducible system reduces off-target effects and attenuates stress responses by the cell during transfection [600]. Overall, the study suggested that the knockdown of Lamp2A reduced ATG5-dependent macroautophagy.

Interestingly, these observations were not present in the normal mammary epithelial and appeared to be tumour specific. In concordance with this, Tang et al. results show the same expression of CMA effector Lamp2A and CMA substrates as this study. However, no biological assay was performed to evaluate the function and compare it to this study [601]. This study by Tang also showed that this data was similar in the Hela cells derived from

cervical tumours, thus does not discount the supposition that the role of CMA is altered from non-oncogenic to oncogenic mammary cells. The role of Lamp2A in the carcinogenic realm has recently come to the forefront in the study by Wang et al. it was suggested that Lamp2A has the potential as a prognostic biomarker for GBM [585]. There have been further reports that Lamp2 has the potential as a prognostic marker in other cancers such as prostate [602, 603], gastric[575], colorectal [586], breast [587, 604], lung [605, 606] and even tumour-associated macrophages (TAMs) [584] . These findings, along with others, demonstrate a change in the role of CMA in the context of cancer that results in its upregulation, as shown to have a significant role in the cell function that is not found in the non-oncogenic counterpart.

In other disease contexts, specifically neurodegenerative such as Parkinson's, the loss of CMA has been shown to contribute to the disease progression. However, the exact reasons cancer is dependent on CMA are yet to be fully understood and the mechanism underpinning them. This information could be pivotal in future treatment strategies, and given that CMA was not demonstrated to be essential in the normal cell through a Lamp2 knock out mice [607], particularly in the context of breast epithelia, this was not isoform-specific. It does, however, indicate that Lamp2A could make a promising target for treatment

5.4.3 CMA dependence increases as cells transition from basal to mesenchymal phenotype.

The results from the initial part of this study have found the expression of Lamp2A to increase in the mesenchymal cell lines compared to epithelial counterparts. This increase in the mesenchymal phenotype was examined more precisely in the EMT model; thus, the MDA-MB-468 breast cancer cell line exposed to EGF was found to have dose-dependent increases in Lamp2A. A study mentioned prior by Tang found that in the MCF10A cell line, EMT was suppressed by CMA through the degradation of p65. It is suggested that p65 accumulation during CMA inhibition activates EMT via snail, which was also observed in the Hela cell line [601]. Although this study looked at EMT, it used alternate activation methods including TNFα, TGFβ, hypoxia and exclusively in the MCF10A may explain the variation observed in this study with Tang's findings. However, concerning oncogenesis, it

was clear that CMA was a positive regulator in the breast cancer cell line, unlike that observed by Tang in the Hela cell line, suggesting that this may be a cell and context-specific behaviour. These findings by Tang were also observed by Zheng et al., study although there were a few notable differences [588]. Zheng et al. study focused on Hepatocellular carcinoma found that increases in Lamp2 inhibited EMT attributes such as motility and invasiveness. The study went on to show Lamp2 knockdown increased mesenchymal markers. The molecular mechanism underpinning this activity is suggested to be Lamp2 suppression of snail. A limitation of this study is that it examined for Lamp2 total and did not differentiate between the isoforms. It seems unlikely that this would be occurring in the context of the MDA-MB-231 breast cancer cell. A study by Paul et al. revealed that the MDA-MB-231 cells have shown that Protein Kinase C zeta (PKCζ) is involved in the NFκB-p65 signalling pathway responsible for invasiveness [608]. It is even suggested that PKCζ may be the link between EGF induction and activation of NFκB. When PKCζ was knockdown in the MDA-MB-231, it was found to cause the expression of E-cadherin and ZO-1, both epithelial markers. So based on this and these findings, it could be speculated that the reverse is true in this context and that Lamp2A knockdown is possible due to degradation changes in components of the NFκB-p65 signalling pathway resulting in MET and, as a consequence, cytotoxicity, loss of invasive and migratory potential similar to what was observed in this study. Leading on from this and what was of interest was that in the MD-MB-468 EMT with Lamp2A reduction, there was an observed attenuation of the growth stimulating properties of EGF, which also held true for the MDA-MB-231 breast cancer cell line. On further investigation, it was found with the KFERQ-finder that the EGFR receptor has 13 putative KFERQ-like motifs at numerous positions exposed for targeting by either or combination of phosphorylation, acetylation, or the replacement of the "Q" with asparagine as detailed in APPENDIX VII, interestingly there were no canonical motifs. So, it is proposed that CMA is used for EGFR recycling, and with the knockdown of Lamp2A, the EGFR receptors accumulate and perturb cellular function, even resulting in cell death as the reduction may affect not only the EGFR receptor but further downstream targets of the NFκB-p65 signalling pathway, reducing the cell's ability to maintain homeostasis. This aspect of the study warrants further investigation to elucidate the toxicity incurred by EGF in the context of Lamp2A knockdown, and the benefits of these findings would be significant.

5.4.4 EGFR activation sensitives cells to the knockdown of Lamp2A

Initially, the study observed an increase in Lamp2A with activation of the pathway by exogenous means through the addition of EGF. However, this was also observed with Lamp2B and could indicate upregulation in overall lysosomal numbers under these conditions. This upregulation in response to EGF may be due to several reasons: it is reflective of the increased changing metabolic needs of the MDA-MB-468 as they transition into the mesenchymal phenotype triggered by the addition of EGF. In addition, there may be a significant shift in the molecular environment, as observed by Chu et al. [609] initially and since supported by others [610]. Chu et al. found that the loss of E-cadherin resulted in a reduction in glycolysis, shown to be a consequence of the reduction in HIF-1α [609].

Interestingly, there is evidence by Ferreira et al. [611] and others [612] who have put forth evidence that CMA degrades HIF-1α, specifically during nutrient stress conditions [611, 613]. The observed increase in Lamp2A in response to EGF stimulation may be due to increased CMA substrate degradation of molecules such as HIF-1α but not limited to only HIF-1α. This postulation may flag Lamp2A as part of the molecular underpinnings of the concurrent loss of HIF-1α with loss of E-cadherin, as described in studies by Chu et al. [609] and Hugo et al. [433].

Another explanation for the increased expression of Lamp2A in response to EGF is that it stimulates NFAT, particularly NFAT-1, a transcription factor that regulates Lamp2 expression [281, 614]. Several studies have shown that the addition of the EGF ligand and resulting epithelial to mesenchymal transition is directed by calcium signalling [615]. NFAT is suggested to be regulated by calcium-calcineurin, and calcium calcineurin is induced by calcium which is increased in response to EGF and EGFR signalling. Therefore, an increase in calcium due to the EGF ligand increases NFAT, increasing Lamp2A. This postulate, to some extent, has been supported by this study as it has been that the addition of EGF ligand increases Lamp2A expression. Therefore, it is also plausible that an increase of Lamp2A in the EGF-induced conditions results in increases in calcium, which then releases NFAT to facilitate the transcription of Lamp2. However, some of the previous studies were in different cellular contexts, and this data suggests that it may hold in this cellular context and warrants further inquiry. There is a linear relationship between

Lamp2A expression and EGFR activation. It is yet to be determined if this is due to the RAS-RAF axis or PI3K-AKT axis, but both pathways require further support to correlate to this upregulation in Lamp2A in this setting confidently.

Further research into the changes in lysosomal content with the addition of EGF with and without Lamp2A would assist in determining why Lamp2A is increased. Furthermore, additional research could uncover the targeted substrates of that increase, which may identify the cause. The Lamp2 transcript variants show differential expression patterns in a breast cancer panel.

5.4.5 CMA reduction was demonstrated to impede the more aggressive phenotype's functionality significantly.

Kon et al. had similar findings to this current study in that there was a decrease in proliferation and colony formation with Lamp2A knockdown. However, that study utilised lung cancer cell lines A549 and H460 and recapitulated these findings in vivo resulting in regression of tumour growth and reduced metastasis noted in the lung xenografts [616]. In line with this study, Han et al. demonstrated that a loss of Lamp2A in MDA-MB-231 and MDA-MB-468 reduced the breast cancer cells invasion, migration, and proliferation capacity *in vitro* and *in vivo* [599]. Interestingly Han et al. observed concomitant changes in ATG-5 dependant macroautophagy, although, from the initial findings in this study, there was observed to be a decrease in LC3 levels in the MDA-MB-231 and the same antibody was utilised in both studies. It should be noted that Han's study utilised siRNA knockdown of Lamp2A, which may be where the difference is to be found. Although further investigation with nutrient deprivation and Bafilomycin may find similar results.

Nevertheless, at basal levels in this study, there was a reduction in LC3 expression in Lamp2A knockdown and similarly in the parental cell lines and non-targeting with the addition of Dox. Therefore, there would also need to be some examination of the levels of ATG 5, as this was described to be the modulator of these changes. In recognition of these findings, a search of the KFERQ finder found ATG 5 to have a canonical KFERQ motif at position 61. This finding is yet to be reviewed experimentally but lends itself to further elucidation and a further explanation of Han's findings.

A recent study by Tokarchuk et al. supports this current study, as do other studies that show that low levels of Lamp2A result in a decrease in cell proliferation. Notably, this study focused on HER2 negative cell lines T47D and MCF-7 breast cancer lines [589]. The study determined that the disease-free survival of HER 2 negative breast cancer patients was decreased with high levels of Lamp2A expression, conferring poorer patient prognosis. This study also utilised a lentiviral system, but it was not inducible, and to date, this study is the only one to have developed a tetracycline-inducible Lamp2A knockdown.

This chapter's results highlighted the importance of CMA in breast cancer; interestingly, many cell lines showed little change in known CMA substrates at a protein and lysosomal level with Lamp2A knockdown. Revealing an important avenue of enquiry, although, in research by Saha, it was shown that Lamp2A aids survival in breast cancer cells by reducing the oxidated protein from the cellular environment reducing cell death and, as a consequence, promoting survival [587]. This study also showed expected changes in bona fide CMA substrates GAPDH and PKM. However, that study included the luminal subtype and utilised the T47D and MCF7 cell lines. In contrast, a study by Peng et al. has shown the mesenchymal subtype, specifically the Hs578T and BT549 cell lines, to have increased oxidation levels, which results in metabolic reprogramming within the hypoxic environment facilitating invasive phenotype [617]. Therefore, it could be hypothesised that as the cell lines become more aggressive from the luminal through to the mesenchymal subtypes, CMA's or, more specifically, Lamp2A's role is modified from what is expected to something aberrant or even dysfunctional, as is the case for macroautophagy. The results in the MCF10A somewhat support this hypothesis as immortalised "normal" breast cell line that did present the expected changes in CMA substrates GAPDH and HSC70 but notably no changes in PKM. Alternatively, these differences may reflect CMA-targeted protein turnover rates in the different cellular contexts and highlight alterations in metabolism or other regulatory molecules that favour oncogenesis.

Further, a recent study by Hao et al. performed proteomics and bioinformatics experimentation of breast cancer cell line SUM159, and they found that translation initiating factors were a large portion of the content within the CMA-activated lysosome [301]. In particular, eukaryotic translation initiation factor 4A1 (EIF4A1), eukaryotic translation initiation factor 4H (EIF4H) and DEAD-box helicase 3 X-linked (DDX3X). Identifying translation regulators as CMA targets adds another layer of complexity to CMA. It may assist in explaining some of the observed functional changes as EIF4A1 and

EIF4H are associated with initiating transcription of proteins that favour oncogenic attributes such as proliferation and survival [618, 619]. These findings highlight the need for more research into identifying CMA targets and what factors result in these changes if these targets change. It could be hypothesised that CMA targets change in response to the cellular environment. Is there an upregulation of CMA substrates not found in the non-oncogenic environment, or are there variations to post-translational modifications and, as a result, exposes putative KFERQ like motifs? It may be one or more and likely a combination of all these factors, but probably what is more pressing about CMA is its importance. It is clear from the results in this study that the knockdown of CMA key effector Lamp2A has a significant impact on cell viability, migration, invasion and colony formation in all the breast cancer cell lines tested with the highest sensitivity to its reduction were observed in the MDA-MB-231.

Nevertheless, these observations or impacts of Lamp2A knockdown did not hold true for the standard counterpart MCF10A breast cell line. This data suggests that in the standard mammary cell, the requirement for Lamp2A or CMA is not essential, so, therefore, what happens to make the cell turn a non-essential pathway into one of dependence. Other degradation pathways could pick up the redundancy of Lamp2A knockdown, although, from the previous chapter, macroautophagy is defunct in many mesenchymal cell lines, particularly under stress; these other pathways may not compensate for this loss. These suggestions are plausible but do not help explain the dependence on CMA for many aspects of their biological function in the oncogenic phenotype. It proposes that CMA or at least Lamp2A has a regulatory role in migration, invasion, proliferation and colony formation, but the question yet to be answered is why and how.

5.4.6 Lamp2A roles beyond that of crucial effector molecule for CMA

Some suggest that Lamp2A has other roles than just a key effector for CMA. For example, Damaghi et al. showed that Lamp2 was redistributed to the cell membrane in acidic environments to protect the cell. In addition, this study demonstrated in-vitro and in vivo and patient samples that Lamp2 was increased with cancer stage and aggressiveness, which also aligns with increased acidity [620]. However, the study was limited because it

examined total Lamp2, so it cannot be determined which variant is responsible for this role. These findings were also recapitulated recently by Raschner et al. in the prostate cancer context, where Lamp2 was significantly increased in response to the acidic environment [621]. Further on from this, a recent paper by Savic et al. used Lamp2 as a histological marker for acidosis based on Damaghi's original findings and cross-referenced to the pH mapping [620, 622]. It was shown in this context that Lamp2 was induced in response to pH, specifically acidosis and more prominent in the chronic acidosis setting.

Nevertheless, this study found the BT549 cell line to have high levels of Lamp2B and Lamp2A, with B being higher than A and these cells are commonly found to create an acidic environment, thought to be a consequence of increased protein oxidation and metabolic reprogramming within the cell. Alternatively, Sameni et al. observed that the BT549 breast cancer cells utilised intracellular proteolysis of the ECM component through the lysosome, so maybe the significant increase in Lamp2B is directly correlated with more lysosomes [623]. However, it highlights an area worth further investigation in the future as this may help target bone metastasis as they require an acidic environment to seed.

It should be noted that many cancers show poor prognosis with high expression of Lamp2, but to date, all the Kaplan Meier plotters only allow for analysis of total Lamp2, and there is much to be learned if the variants were examined independently.

5.5 CONCLUSION

In conclusion, this study has demonstrated the importance of CMA or, more specifically, Lamp2A in breast cancer cell lines. It has been shown to have a significant role in cell viability and is fundamental in the metastatic potential of breast cancer cell lines. Its upregulation was associated with the more aggressive subtypes TNA and TNB, further increasing with EMT proposing a role specifically in the mesenchymal phenotype. The Lamp 2 isoforms A and B showed differential expression in breast cell lines, highlighting their independent roles. These findings have further justified the rationale to pursue an inhibitor of Lamp2A in the context of cancer, particularly metastasis.

Chapter 6: FINAL DISCUSSION

6.1 INTRODUCTION

The process of autophagy plays an integral role in preventing carcinogenesis by maintaining homeostasis and facilitating the degradation of protein aggregates and defunct organelles into recyclable molecules [624, 625]. However, in contradiction to this, autophagy also maintains and aids the development of the carcinogenic phenotype after transformation [393, 626, 627]. Therefore, to target autophagy therapeutically in the context of cancer, there needs to be a greater understanding of the molecular mechanisms underpinning its activity in the context of cancer. This study has shown a co-dependent relationship between RAS and autophagy, conserved between mutant RAS and hyperactivated RAS, with the latter more common in breast cancer. Furthermore, the flexibility of autophagy to function via numerous pathways demonstrated the complexity of its targetability. In addition, these findings identified CMA as an area of interest, and the study focused on the less researched area of CMA. Initially, there was limited research to guide this part of the thesis, and therefore, this study had to determine the functional role of CMA in different breast cancer cellular contexts. It was demonstrated that CMA has a significant role in the metastatic phenotype, and these findings point toward further potential research avenues within this area.

6.2 SUMMARY OF FINDINGS OF THIS STUDY

6.2.1 RAS is reliant on macroautophagy in breast cancer cell lines.

The relationship between RAS and autophagy has been somewhat demonstrated in the context of KRAS mutations, particularly in pancreatic cancer [65, 400, 402-404, 628, 629]. This study showed a relationship between RAS and autophagy in line with these findings. Based on the current knowledge of available literature, this study was the first to examine it in the context of breast cancer. The results from chapter three have demonstrated a significant upregulation in autophagy markers and function at a basal level where mutant RAS is present. Furthermore, Eckert et al. [72] have shown that RAS hyperactivation is commonly present in breast cancer compared to mutation. Therefore in this study, RAS hyperactivation was examined to determine if the autophagic activity was similar to that observed in the RAS mutant cell lines. This RAS hyperactivation model was the MDA-MB-468 breast cancer cell line that overexpresses EGFR, so they are sensitive to EGF, and its addition induces the epithelial to mesenchymal transition through activation of the RAS pathways, and this response is dose-dependent. This RAS activation model displayed a similar co-dependence between autophagy and RAS, as did the RAS mutant cell lines. Thus, these findings suggested that it was upregulated in both RAS mutation and hyperactivation, at least in the context of autophagic activity. These increases in autophagic components and regulators were witnessed at an mRNA and protein level in the MCF10A $HRAS^{V12}$ model. In addition, bioinformatic analysis of breast cancer survival with gene combinations further supported these findings in that patient prognosis significantly increased with the combination of RAS and LC3B specifically (APPENDIX IV).

Interestingly, RAS in isolation showed no significance for patient prognosis; however, LC3B was an independent prognostic marker for poorer patient outcomes, which increased further with the addition of RAS, thus suggesting a deleterious combinatorial relationship. This relationship highlights a potential biomarker for adjuvant treatment with an autophagic inhibitor or activator.

6.2.2 Inhibition of macroautophagy in RAS active breast cancer cell lines

Autophagy inhibition has been demonstrated to be a potential target for cancer treatment. Several studies have shown that current first-line treatment combined with an autophagic inhibitor is promising in the neoadjuvant and adjuvant regimen, particularly in pancreatic cancer [65, 630-635]. In addition, there are other contexts where the inhibition of autophagy would be beneficial, such as the observed presence of autophagic activity in response to chemotherapeutic treatment; this presence of autophagy is suggested to facilitate chemoresistance [636-640]. Although similar to these current findings, some studies have identified discrepancies between results of autophagic inhibition being efficacious in cancer treatment or, conversely, autophagic inhibition aiding cancer growth. These differences appear context-dependent on cell type and experimental conditions [631, 641, 642].

Nevertheless, the current study has clearly shown the significant efficacy of PI3K inhibitors in specific cellular settings reflected by the degree of effectiveness between the cell lines. The most consistent treatment was observed with 3-Ma, which was also demonstrated recently by Chicote et al., where 3-Ma was shown to cause cytotoxicity in numerous cell lines, and observed cytotoxicity was found to be related to DNA damage. Furthermore, Chicote et al. examined Bafilomycin A1, which was found to induce high levels of cytotoxicity compared to 3-Ma and SAR-405, showing results similar to the findings of this study. However, the former utilised genetically modified MEFs and HeLa cell lines and was not as comprehensive as this study, which has included up to 11 cell lines, of which all are mammary cells to be compared and contrasted [557].

The results from multiple PI3K inhibitors utilised for this thesis suggest that the treatment's inhibitory effects could be circumvented, proposing that numerous other pathways could activate the autophagic process, independent of PI3KC3, at least in the initial stage. The findings from earlier chapters also showed that autophagy did not utilise the canonical pathway preferentially. Therefore, some of the efficacy conferred by 3-Ma may be reflective of its PI3K class I activity. To attempt to resolve this latter stage of the process was targeted through lysosomal inhibition as this step can not be circumvented. The results showed high sensitivity to lysosomal inhibition with the lysosomal inhibitor Bafilomycin A1. They suggested that the latter stage of the autophagic process, or the lysosome, was a more sensitive and direct target than the earlier stages of autophagy. As

was observed in this study, Wu et al. showed Bafilomycin A1 as efficacious in colon cancer [643]. These findings were supported further by Morgan et al., who demonstrated that bladder cancer's metastatic capability was attenuated by lysosomal inhibition [577]. The results from this study have supported previous findings observed in other cancer types and added to knowledge regarding breast cancer, highlighting the complexity of autophagic inhibition and emphasising the need for improved autophagic inhibitors.

Table 6-1 Summary of findings for chapter 3 and chapter 4

Cell line	LC3-II turnover		Autophagic Flux		P62 turnover		RESPONSE TO AUTOPHAGIC INHIBITION				
CONDITION	BASAL	INDUCED	BASAL	INDUCED	BASAL	INDUCED	VPS34 INHIBITORS				BAFIL0MYCIN A1
							3Ma	3Ma-IV	SAR-405	VPS34-INI	
MCF10A	→	↑	N/A	N/A	↑	↓	No response	0.88M	No response	No response	2.45M
MCF10A HRAS^{V12}	↑	↑	N/A	N/A	↑	↓	N/A	0.0008M	0.0001768 M	2.5x10^{-5}M	3.30x10^{-9}M
MDA-MB-468	↑	→	N/A	N/A	↑	↓	N/A	0.002M	No response	No response	1.36x10^{-8}M
MDA-MB-468 + EGF	↑	↓	N/A	N/A	↑	↓	N/A	0.0005M	No response	No response	4.85x10^{-8}M
T47D	↑	↑	✚	✚	N/A	N/A	N/A	0.088M	No response	2.4x10^{-6}M	3.32x10^{-9}M
HS578T	↑	↓	✚	✖	N/A	N/A	0.001668M	0.0006M	0.0000112 M	9.72x10^{-6}M	1.15x10^{-9}M
MDA-MB-231	↑	↑	✚	✖	N/A	N/A	N/A	0.0002M	No response	1.05x10^{-6} M	1.02x10^{-9}M

LEGEND : ↑INCREASE ↓DECREASE →UNCHANGED ✚ POSITIVE FLUX ✖ BLOCKED/SURPRESSED FLUX

6.2.3 Chaperone-mediated autophagy in breast cancer cell progression

In this study, the lysosome was observed to be a location of sensitivity for breast cancer. The lysosome is related to macroautophagy and a targeted form of autophagy called chaperone-mediated autophagy (CMA). Therefore, the role of CMA was examined in breast cancer and was observed to be of functional importance, particularly within the metastatic phenotype. Others have supported these findings, and growing evidence suggests that CMA has a pivotal role in the aggressive phenotype in many tumour types, including breast, lung, gastric and colon [307, 586, 599, 644]. Furthermore, the study found that CMA dependence was conserved to the more aggressive basal subtypes with increased functional importance, particularly in the mesenchymal cell lines Bt549, Hs578T and MDA-MB-231 breast cancer cell lines. These results have supported study findings by Han et al. and Kon et al., where the knockdown of Lamp2A reduced cell survival, migration, invasion, and colonisation as a prevention and intervention model [307, 599]. Thus, this study has added fundamental research in breast cancer that advances the field. This study has shown, like others, that CMA has a vital role in cancer, yet there is still much to be elucidated. Such as the mechanisms underpinning its activity in cancer. Identifying the cancer-related CMA substrates raises questions: Are these different from those in the normal cell and, if so, why? Does the critical effector protein Lamp2A have other roles in the context of cancer? As the questions are answered, CMA may expose itself as a future treatment target, particularly metastatic disease.

Table 6-2 Summary of findings chapter 5

			EFFECT of LAMP2A KNOCKDOWN					
Cell line	**Lamp2A knockdown (%)**		**Cell viability**	**Wound healing**	**Invasion/ 3D growth**	**Migration**	**Colony-forming (Intervention)**	**Colony-forming (Prevention)**
	WL	**LE**						
MCF10A	80	50	None	None	None	None	None	None
MDA-MB-468	80	50	*Reduced	N/A	*Reduced	N/A	*Reduced	N/A
MDA-MB-468 + EGF	N/A	N/A	*Reduced	N/A	N/A	N/A	*Reduced	N/A
HS578T	85	65	*Reduced	N/A	N/A	N/A	None	*Reduced
MDA-MB-231	90	80	*Reduced	*Reduced	Altered	*Reduced	*Reduced +EGF *Reduced	*Reduced (****)

* = effects were significance N/A= Experiment not performed WL= whole lysate LE= Lysosome enrichment

6.3 TARGETABILITY OF AUTOPHAGY IN BREAST CANCER TREATMENT

This study has shown that macro or chaperone-mediated autophagy is upregulated in breast cancer. Furthermore, the role of autophagy as a whole was vital to cell survival, particularly in the more aggressive phenotype. Significantly, this observed dependence in the aggressive cancer phenotype, at least in the context of macroautophagy, was found to correlate with RAS mutation and activation. Although this was not as evident in CMA, it cannot be ruled out, and further studies would be required to determine if this as the presence of the KFERQ motif on RAS isoforms suggests that CMA may be a regulator of its degradation but is yet to be confirmed experimentally (APPENDIX VII).

These findings demonstrated that macroautophagy at a basal level was elevated to maximal capacity in the RAS mutant cell lines Hs578T and MDA-MB-231 breast cancer cell lines. Furthermore, it was determined that the "normal" inducers of autophagy, such as starvation, resulted in dysfunction, suggesting that given autophagy is a rate-limiting process, the maximum autophagic processing capacity is reached in this cellular context and as such cannot respond to further induction ques. Although beyond the scope of this study, it is postulated that the use of an autophagic activator may be just as advantageous as an inhibitor. It is reasonable that if the autophagic process is at capacity, then adding a chemical inducer such as rapamycin may cause dysfunction to the point of cell death. Luan et al. has shown rapamycin as a potential treatment for renal cancer and focused explicitly on mTOR inhibition. However, that study did not examine autophagic activity, which would be of interest [645]. Evidence suggests that rapamycin is a potential therapeutic agent against cancer alone or in combination in different cellular contexts [646, 647].

Curiously, autophagy is often identified as a resistance mechanism in cancer cells in response to certain chemotherapeutics. So, it is feasible that autophagic activation in chemoresistance may be valuable and an additional adjuvant where resistance is observed. Furthermore, Gremke et al. has recently shown that mTOR inhibition resistance with autophagic blockade exposes metabolic pathways for target, and chemosensitivity is regained [648]. These recent findings strengthen this hypothesis of autophagic inhibition as a treatment for chemoresistance.

In continuation, autophagy has significant potential as a neoadjuvant or even adjuvant depending on the context it is being used in cancer treatment, such as if it was used clinically to prevent primary tumour growth or whether it was for metastatic disease or even chemoresistance. However, as observed in this study and others, there are still limited autophagic inhibitors available. Currently, many of the inhibitors either lack specificity or have reduced solubility. Regarding PI3K inhibitors used in this study, there was evident variation between cell types and drug efficacy which, as discussed previously, may reflect the differing degrees of specificity between the drugs, study design or initiation circumvention and may even be a combination of all of these factors. Concerning the latter by-passing, the initiation complex for activation may represent a genuine obstacle. It is speculated that the process may be activated by alternate means and is still an area requiring further research. So, in acknowledgement of these findings, it is advised that alternate targets of the autophagy process may be more viable. Based on the results of this study, it is proposed that developing a small molecule to target LC3B specifically could have tremendous potential. This study and the patient data from many different patient database platforms have shown consistently that the LC3B isoform confers a poor prognosis. However, the LC3A and LC3C isoforms are correlated with better patient outcomes. Therefore, a drug developed against LC3B could be a promising solution to the common conundrum in drug development, weighing the adverse effects against cancer cell cytotoxicity. Theoretically, an inhibitor specifically targeted to LC3B would not completely inhibit autophagy, and the "pathologic" autophagy would be replaced with the "good" autophagy. However, there is no explanation for why the isoforms confer different patient outcomes. In this study, the LC3B isoform was preferentially expressed compared to the others.

Irrespective, LC3 would potentially be a better target than other molecules within the initiation complex as it is a fundamental molecule in the autophagic process. Although it has been suggested that autophagosome formation still occurs in the LC3$\beta^{-/-}$ mice through compensatory mechanisms, such as GABARAP, there was no increase noted, nor was LC3A upregulated in response to the loss of LC3β [649]. Another option relating to LC3 inhibition was recently described by Putryski et al. where preliminary data of LC3, Gabarap and P62 inhibitors peptides were developed and were found to be effective in sensitising AML to Cytarabine. Ultimately it was suggested that inhibition of all three in combination was a more effective treatment strategy [650]. Similar efficacy was observed

in a study by Gray et al. where peptides against LC3 were utilised in ovarian cancer combined with carboplatin, which resulted in tumour regression *in vivo* [651]. There is also some recent evidence by Gomes-da-Silva et al. that LC3 has a role in protecting the Golgi during damage which would add to its targetability [652]. Through the blockage of autophagy, mitochondrial quality control is lost due to deficiencies in mitophagy. Though it has been suggested that the mitochondria can facilitate their degradation via self-generated vesicles to remove defunct mitochondria to the lysosome in the absence of ATG7 or FIP200 precisely, but has not been shown in direct LC3 inhibition [653].

The high sensitivity to autophagic inhibition was observed with lysosomal inhibition with Bafilomycin A1 in all cancer cell lines compared to the normal breast cell counterpart was an area of particular interest in this thesis. Lysosomal fusion to the autophagosome is a critical step in the autophagic process and, as a consequence, is a robust target for autophagic inhibition [351, 654, 655]. These results were in line with findings by Yan et al., although his study was in hepatocellular carcinoma (HCC), he found increased sensitivity to treatment, but the sensitivity to Bafilomycin A1 was much higher in this study with IC_{50} within the lower nanomolar [356]. In addition, there have been several studies showing various pathway activations in response to Bafilomycin A1 [355, 577, 656, 657]. For example, studies by Graham et al. showed BCL2 Interacting Protein 3 (BNIP3) to be the means of cell death in breast cancer and, further, was reported to prevent cell survival mechanisms in the hypoxic environment [658].

In contrast, in HCC, Bafilomycin A1 induced cell death was observed to be related to PUMA, although both mechanisms are related to Bcl-2 [356]. Nevertheless, clinically Bafilomycin A1 has not yet been considered a treatment option because it has shown high toxicity and is limited as a viable treatment [659, 660]. More recently, Yuan et al. demonstrated in the paediatric xenograft model of leukaemia that Bafilomycin A1 at the nanomolar range had no off-target toxicity [355]. Similarly to Yuan et al., IC_{50} of Bafilomycin A1 was observed at the nanomolar range in the cancer cell lines, compared to mammary epithelial cell line in the molar range. In response to the limitations of Bafilomycin A1, the clinical focus has shifted to chloroquine and hydroxychloroquine. These two drugs were already approved to treat patients and work by inhibiting the lysosome, albeit by different mechanisms. As a net consequence, chloroquine and /hydroxychloroquine also inhibit the lysosome, preventing its functional capacity but mechanistically entering the lysosome and interfering with lysosomal pH compared to

inhibition of the V-ATPase pumps in the case of Bafilomycin A1. There have been several clinical trials with hydroxychloroquine as a neoadjuvant in numerous cancers, particularly in pancreatic cancer [641, 661-663].

A recent systematic review and meta-analysis by Xu et al. have shown that the inclusion of autophagic inhibitor chloroquine/hydroxychloroquine results in a better patient response than chemotherapy on its own [363]. However, there have been concerns regarding the off-target effects of these drugs; for example, recently, Fedele and Proud showed that both Bafilomycin and chloroquine over an extended period have an inhibitory effect mTORC1 signalling and, as a result, mimic lysosomal storage disorders [664]. Furthermore, Bafilomycin A1 and Chloroquine have been shown to replicate cellular features of neurodegenerative diseases [665] such as Parkinson's, suggesting that lysosomal dysfunction contributes to disease development [666].

It led the study to consider other autophagic pathways as they are all connected by the lysosome. On further review, it was indicated that autophagy and CMA are engaged in crosstalk [262]. Therefore, the scope of the study to broaden to include it to also focus on CMA, and there was some evidence to suggest it was upregulated in the context of cancer. In line with other studies, the results from this study have shown that the critical CMA effector molecule, Lamp2A, was observed to have a significant role in cancer survival and metastatic capacity [307, 310, 599, 667]. Based on these findings and others, developing an inhibitor of CMA or Lamp2A hold promise [592]. Because the targeting of CMA would not affect all lysosomes as not all lysosomes are CMA active, meaning some lysosomes do not have Lamp2A; thus, an inhibitor of Lamp2A would not inhibit all lysosomal function. Thus, this may limit the significant adverse effects with complete lysosomal inhibition, as noted earlier with its long-term use, particularly in neurons and cardiocytes. Therefore, all research relating to pharmacological agents for CMA has been on activators due to its identified loss of activity and role in neuronal degeneration. As mentioned for macroautophagy, accelerating to dysfunction may also be feasible in CMA, as it is a rate-limited process. Thus, a CMA activator may cause dysfunction and lethality, but similarly to macroautophagy, this proposition may only be helpful in the most aggressive cell lines where basal activity is already elevated. Recently, Endicott et al. has shown that CMA is activated in the lysosomes of rat livers in response to PI3K class I inhibitors pictilisib or buparlisib [319]. In addition, earlier findings presented by Finn et al. show the HSP90 inhibitor geldanamycin and the inhibitor of G6PDH (6-AN) activated

CMA activity, whereas its activity was inhibited by anisomycin and cycloheximide [668]. Further recent evidence suggests that CMA has a regulatory role in ferroptosis through HSP90 dependant mechanisms [669]. Furthermore, recent evidence suggest CMA's role may expand to include the targeted uptake of proteins into the exosome and was observed in the delivery of HIF-1α to normoxic cells under hypoxic conditions[670]. Notably, this is the first study to observe these findings, but it warrants further investigation and may elucidate much of the lamp2A increases observed in the context of cancer. However, there is still much to be understood about CMA in cancer and identifying targeted substrates will further the understanding of its importance, whether it be within the lysosome or exosome will also be of great interest.

Currently, the development of robust autophagic inhibitors is impeded due to fundamental deficiencies in the literature of the environmental and context differences in autophagic activity between cancers. These factors will be resolved as our understanding of the molecular mechanisms underpinning them in the context of cancer deepens. So will the ability to develop effective drugs and targets with limited adverse effects to the potential all the research has identified to date.

6.4 FUTURE DIRECTIONS

This thesis has broadened the knowledge and understanding of macroautophagy and chaperone-mediated autophagy concerning breast cancer progression. However, there remain many questions that need to be answered with the following future studies;

-The result from macroautophagy has highlighted a relationship between RAS and autophagy—study to knockdown LC3B and the consequence to the RAS models and sensitivity to treatments.

-The result from macroautophagy has exposed a dichotomous role of the LC3 isoforms—study to knockdown and overexpress the LC3 isoforms individually to elucidate these differences.

-The results from the 3Ma-IV and Bafilomycin A1 demonstrated significant results— further in vivo experimentation to determine efficacy and toxicity is warranted.

-It was a common theme amongst all pharmacological inhibitors that they have adverse off-target effects and or lack specificity—studies to continue or focus on developing novel inhibitors or small molecules screening to repurpose existing agents for future autophagic inhibitors.

-These studies have shown robust results in the importance of Lamp2A in breast cancer metastatic capabilities— a study with a mouse model of metastasis with the genetically modified cell from this thesis would support the *in vitro* findings in a complex system.

-The CMA process from the data has a pivotal role in the degradation of vital proteins—studies to examine if the lysosomal content changes in the non-oncogenic compared to the oncogenic cell would add valuable information.

6.5 CONCLUSION

In conclusion, this study has added to and supported the current literature on the importance of autophagy in cancer. It has added novel findings to the body of knowledge regarding breast cancer and metastatic disease. Most importantly, it has, as have many others, strengthened the support and need for further research into molecular mechanisms underpinning autophagic activity and the reasons why the autophagic process becomes pathologic in the context of cancer.

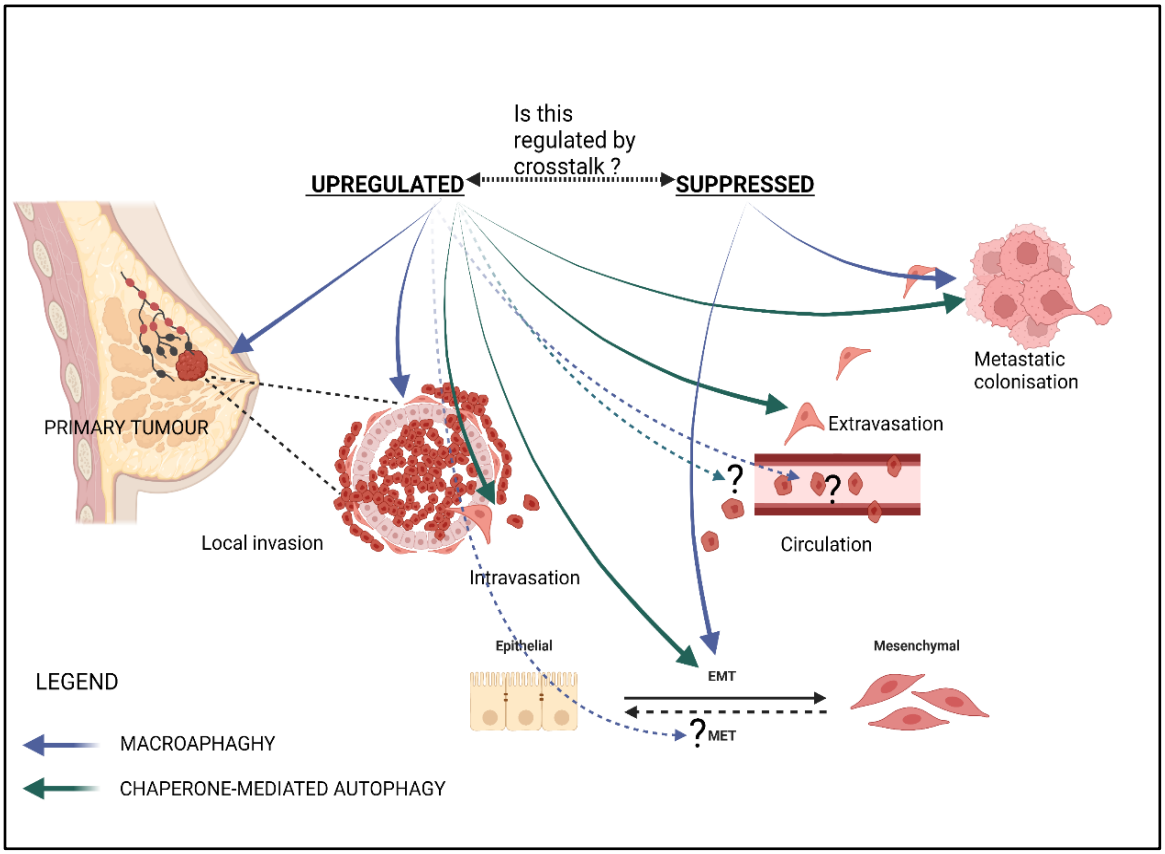


Figure 6-1 Autophagy in metastatic breast cancer.

Graphical representation of where autophagy (blue arrow) and CMA(green arrow) were found to be upregulated and suppressed, with proposed activities denoted by dashed lines and respective colours

Created with BioRender.com

REFERENCES

1. Health, A.I.o. and Welfare, *Cancer data in Australia*. 2021, AIHW: Canberra.

2. Health, A.I.o. and Welfare, *BreastScreen Australia monitoring report 2020*. 2020, AIHW: Canberra.

3. Lei, S., et al., *Global patterns of breast cancer incidence and mortality: A population-based cancer registry data analysis from 2000 to 2020.* Cancer Commun (Lond), 2021. **41**(11): p. 1183-1194.

4. Velazquez Berumen, A., et al., *Defining priority medical devices for cancer management: a WHO initiative.* Lancet Oncol, 2018. **19**(12): p. e709-e719.

5. Mutebi, M., et al., *Breast cancer treatment: A phased approach to implementation.* Cancer, 2020. **126 Suppl 10**: p. 2365-2378.

6. Ginsburg, O., et al., *Breast cancer early detection: A phased approach to implementation.* Cancer, 2020. **126 Suppl 10**(Suppl 10): p. 2379-2393.

7. Rositch, A.F., et al., *The role of dissemination and implementation science in global breast cancer control programs: Frameworks, methods, and examples.* Cancer, 2020. **126 Suppl 10**: p. 2394-2404.

8. McCormack, V., et al., *Breast cancer survival and survival gap apportionment in sub-Saharan Africa (ABC-DO): a prospective cohort study.* Lancet Glob Health, 2020. **8**(9): p. e1203-e1212.

9. Morrison, D.H., et al., *Tumour biomarker expression relative to age and molecular subtypes of invasive breast cancer.* British Journal of Cancer, 2012. **107**(2): p. 382-387.

10. Yancik, R., *Cancer burden in the aged: an epidemiologic and demographic overview.* Cancer, 1997. **80**(7): p. 1273-83.

11. Benz, C.C., *Impact of aging on the biology of breast cancer.* Critical reviews in oncology/hematology, 2008. **66**(1): p. 65-74.

12. Ly, D., et al., *An international comparison of male and female breast cancer incidence rates.* International journal of cancer, 2013. **132**(8): p. 1918-1926.

13. Brewer, H.R., et al., *Family history and risk of breast cancer: an analysis accounting for family structure.* Breast cancer research and treatment, 2017. **165**(1): p. 193-200.

14. Li, C.I., et al., *Reproductive factors and risk of estrogen receptor positive, triple-negative, and HER2-neu overexpressing breast cancer among women 20-44 years of age.* Breast Cancer Res Treat, 2013. **137**(2): p. 579-87.

15. Chung, S., et al., *Association between chronological change of reproductive factors and breast cancer risk defined by hormone receptor status: results from the Seoul Breast Cancer Study.* Breast Cancer Res Treat, 2013. **140**(3): p. 557-65.

16. Picon-Ruiz, M., et al., *Obesity and adverse breast cancer risk and outcome: Mechanistic insights and strategies for intervention.* CA: a cancer journal for clinicians, 2017. **67**(5): p. 378-397.

17. Meier-Abt, F., et al., *Parity induces differentiation and reduces Wnt/Notch signaling ratio and proliferation potential of basal stem/progenitor cells isolated from mouse mammary epithelium.* Breast Cancer Res, 2013. **15**(2): p. R36.

18. Kotsopoulos, J., et al., *Breastfeeding and the risk of breast cancer in BRCA1 and BRCA2 mutation carriers.* Breast Cancer Res, 2012. **14**(2): p. R42.

19. Shinde, S.S., et al., *Higher parity and shorter breastfeeding duration: association with triple-negative phenotype of breast cancer.* Cancer, 2010. **116**(21): p. 4933-43.

20. Moskowitz, C.S., et al., *Breast cancer after chest radiation therapy for childhood cancer.* Journal of clinical oncology : official journal of the American Society of Clinical Oncology, 2014. **32**(21): p. 2217-2223.

21. Marshall, L.M., et al., *Risk of breast cancer associated with atypical hyperplasia of lobular and ductal types.* Cancer Epidemiol Biomarkers Prev, 1997. **6**(5): p. 297-301.

22. Hartmann, L.C., et al., *Atypical hyperplasia of the breast--risk assessment and management options.* The New England journal of medicine, 2015. **372**(1): p. 78-89.

23. *Type and timing of menopausal hormone therapy and breast cancer risk: individual participant meta-analysis of the worldwide epidemiological evidence.* The Lancet, 2019. **394**(10204): p. 1159-1168.

24. Vinogradova, Y., C. Coupland, and J. Hippisley-Cox, *Use of hormone replacement therapy and risk of breast cancer: nested case-control studies using the QResearch and CPRD databases.* BMJ, 2020. **371**: p. m3873.

25. Rumgay, H., et al., *Global burden of cancer in 2020 attributable to alcohol consumption: a population-based study.* The Lancet Oncology, 2021. **22**(8): p. 1071-1080.

26. Shiovitz, S. and L.A. Korde, *Genetics of breast cancer: a topic in evolution.* Annals of oncology : official journal of the European Society for Medical Oncology, 2015. **26**(7): p. 1291-1299.

27. Beckmann, M.W., et al., *Multistep carcinogenesis of breast cancer and tumour heterogeneity.* J Mol Med (Berl), 1997. **75**(6): p. 429-39.

28. Feng, Y., et al., *Breast cancer development and progression: Risk factors, cancer stem cells, signaling pathways, genomics, and molecular pathogenesis.* Genes & Diseases, 2018. **5**(2): p. 77-106.

29. Makki, J., *Diversity of Breast Carcinoma: Histological Subtypes and Clinical Relevance.* Clinical medicine insights. Pathology, 2015. **8**: p. 23-31.

30. Nguyen, Q.H., et al., *Profiling human breast epithelial cells using single cell RNA sequencing identifies cell diversity.* Nature Communications, 2018. **9**(1): p. 2028.

31. Mao, Y., et al., *Stromal cells in tumor microenvironment and breast cancer.* Cancer metastasis reviews, 2013. **32**(1-2): p. 303-315.

32. Bussard, K.M., et al., *Tumor-associated stromal cells as key contributors to the tumor microenvironment.* Breast Cancer Research, 2016. **18**(1): p. 84.

33. Benson, J.R., *The TNM staging system and breast cancer.* The Lancet Oncology, 2003. **4**(1): p. 56-60.

34. Giuliano, A.E., et al., *Breast Cancer—Major changes in the American Joint Committee on Cancer eighth edition cancer staging manual.* CA: A Cancer Journal for Clinicians, 2017. **67**(4): p. 290-303.

35. Koh, J. and M.J. Kim, *Introduction of a New Staging System of Breast Cancer for Radiologists: An Emphasis on the Prognostic Stage.* Korean journal of radiology, 2019. **20**(1): p. 69-82.

36. Hanahan, D. and R.A. Weinberg, *Hallmarks of cancer: the next generation.* Cell, 2011. **144**(5): p. 646-74.

37. Amjad, E., et al., *Systems biology comprehensive analysis on breast cancer for identification of key gene modules and genes associated with TNM-based clinical stages.* Scientific Reports, 2020. **10**(1): p. 10816.

38. Perou, C.M., et al., *Molecular portraits of human breast tumours.* Nature, 2000. **406**(6797): p. 747-752.

39. Stephens, P.J., et al., *The landscape of cancer genes and mutational processes in breast cancer.* Nature, 2012. **486**(7403): p. 400-404.

40. van de Vijver, M.J., et al., *A Gene-Expression Signature as a Predictor of Survival in Breast Cancer.* New England Journal of Medicine, 2002. **347**(25): p. 1999-2009.

41. Sørlie, T., et al., *Gene expression patterns of breast carcinomas distinguish tumor subclasses with clinical implications.* Proceedings of the National Academy of Sciences, 2001. **98**(19): p. 10869.

42. Sørlie, T., et al., *Repeated observation of breast tumor subtypes in independent gene expression data sets.* Proceedings of the National Academy of Sciences, 2003. **100**(14): p. 8418.

43. Herschkowitz, J.I., et al., *Identification of conserved gene expression features between murine mammary carcinoma models and human breast tumors.* Genome Biol, 2007. **8**(5): p. R76.

44. Prat, A., et al., *Phenotypic and molecular characterization of the claudin-low intrinsic subtype of breast cancer.* Breast Cancer Research, 2010. **12**(5): p. R68.

45. Toss, A. and M. Cristofanilli, *Molecular characterization and targeted therapeutic approaches in breast cancer.* Breast Cancer Research, 2015. **17**(1): p. 60.

46. Lehmann, B.D., et al., *Identification of human triple-negative breast cancer subtypes and preclinical models for selection of targeted therapies.* The Journal of Clinical Investigation, 2011. **121**(7): p. 2750-2767.

47. Fougner, C., et al., *Re-definition of claudin-low as a breast cancer phenotype.* Nature Communications, 2020. **11**(1): p. 1787.

48. Burstein, M.D., et al., *Comprehensive genomic analysis identifies novel subtypes and targets of triple-negative breast cancer.* Clin Cancer Res, 2015. **21**(7): p. 1688-98.

49. Liu, Y.-R., et al., *Comprehensive transcriptome analysis identifies novel molecular subtypes and subtype-specific RNAs of triple-negative breast cancer.* Breast cancer research : BCR, 2016. **18**(1): p. 33-33.

50. Duffy, M.J., et al., *Clinical use of biomarkers in breast cancer: Updated guidelines from the European Group on Tumor Markers (EGTM).* Eur J Cancer, 2017. **75**: p. 284-298.

51. Wang, D.-Y., et al., *Molecular stratification within triple-negative breast cancer subtypes.* Scientific Reports, 2019. **9**(1): p. 19107.

52. Tseng, L.-M., et al., *A comparison of the molecular subtypes of triple-negative breast cancer among non-Asian and Taiwanese women.* Breast cancer research and treatment, 2017. **163**(2): p. 241-254.

53. Gadaleta, E., et al., *Characterization of four subtypes in morphologically normal tissue excised proximal and distal to breast cancer.* npj Breast Cancer, 2020. **6**(1): p. 38.

54. Li, J., et al., *Tumor Characterization in Breast Cancer Identifies Immune-Relevant Gene Signatures Associated With Prognosis.* Frontiers in Genetics, 2019. **10**(1119).

55. Neve, R.M., et al., *A collection of breast cancer cell lines for the study of functionally distinct cancer subtypes.* Cancer Cell, 2006. **10**(6): p. 515-527.

56. Huang, K.-l., et al., *Pathogenic Germline Variants in 10,389 Adult Cancers.* Cell, 2018. **173**(2): p. 355-370.e14.

57. Qing, T., et al., *Germline variant burden in cancer genes correlates with age at diagnosis and somatic mutation burden.* Nature Communications, 2020. **11**(1): p. 2438.

58. Southey, M.C., et al., *Morphological predictors of BRCA1 germline mutations in young women with breast cancer.* British Journal of Cancer, 2011. **104**(6): p. 903-909.

59. Perera, R.M. and N. Bardeesy, *On Oncogenes and Tumor Suppressor Genes in the Mammary Gland.* Cold Spring Harbor Perspectives in Biology, 2012. **4**(6).

60. Osborne, C., P. Wilson, and D. Tripathy, *Oncogenes and tumor suppressor genes in breast cancer: potential diagnostic and therapeutic applications.* Oncologist, 2004. **9**(4): p. 361-77.

61. Ren, X., et al., *Oncogene PRR14 promotes breast cancer through activation of PI3K signal pathway and inhibition of CHEK2 pathway.* Cell Death & Disease, 2020. **11**(6): p. 464.

62. Iranzo, J., I. Martincorena, and E.V. Koonin, *Cancer-mutation network and the number and specificity of driver mutations.* Proceedings of the National Academy of Sciences, 2018. **115**(26): p. E6010.

63. Riely, G.J. and H.A. Yu, *EGFR: The Paradigm of an Oncogene-Driven Lung Cancer.* Clinical cancer research : an official journal of the American Association for Cancer Research, 2015. **21**(10): p. 2221-2226.

64. Hobbs, G.A., C.J. Der, and K.L. Rossman, *RAS isoforms and mutations in cancer at a glance.* Journal of cell science, 2016. **129**(7): p. 1287-1292.

65. Kinsey, C.G., et al., *Protective autophagy elicited by RAF→MEK→ERK inhibition suggests a treatment strategy for RAS-driven cancers.* Nature medicine, 2019. **25**(4): p. 620-627.

66. Waters, A.M. and C.J. Der, *KRAS: The Critical Driver and Therapeutic Target for Pancreatic Cancer.* Cold Spring Harbor perspectives in medicine, 2018. **8**(9): p. a031435.

67. Zsákai, L., et al., *Targeted drug combination therapy design based on driver genes.* Oncotarget, 2019. **10**(51): p. 5255-5266.

68. Zehir, A., et al., *Mutational landscape of metastatic cancer revealed from prospective clinical sequencing of 10,000 patients.* Nature medicine, 2017. **23**(6): p. 703-713.

69. Sánchez-Muñoz, A., et al., *Lack of evidence for KRAS oncogenic mutations in triple-negative breast cancer.* BMC Cancer, 2010. **10**(1): p. 136.

70. Rädler, P.D., et al., *Highly metastatic claudin-low mammary cancers can originate from luminal epithelial cells.* Nature Communications, 2021. **12**(1): p. 3742.

71. Tokumaru, Y., et al. *KRAS signaling enriched triple negative breast cancer is associated with favorable tumor immune microenvironment and better survival*. American journal of cancer research, 2020. **10**, 897-907.

72. Eckert, L.B., et al., *Involvement of ras activation in human breast cancer cell signaling, invasion, and anoikis.* Cancer Research, 2004. **64**(13): p. 4585-4592.

73. Galiè, M., *RAS as Supporting Actor in Breast Cancer.* Frontiers in Oncology, 2019. **9**(1199).

74. Loboda, A., et al., *A gene expression signature of RAS pathway dependence predicts response to PI3K and RAS pathway inhibitors and expands the population of RAS pathway activated tumors.* BMC Medical Genomics, 2010. **3**(1): p. 26.

75. van Maaren, M.C., et al., *Ten-year recurrence rates for breast cancer subtypes in the Netherlands: A large population-based study.* International Journal of Cancer, 2019. **144**(2): p. 263-272.

76. Metzger-Filho, O., et al., *Patterns of Recurrence and Outcome According to Breast Cancer Subtypes in Lymph Node–Negative Disease: Results From International Breast Cancer Study Group Trials VIII and IX.* Journal of Clinical Oncology, 2013. **31**(25): p. 3083-3090.

77. Colleoni, M., et al., *Annual Hazard Rates of Recurrence for Breast Cancer During 24 Years of Follow-Up: Results From the International Breast Cancer Study Group Trials I to V.* J Clin Oncol, 2016. **34**(9): p. 927-35.

78. Perez, E.A., et al., *Trastuzumab plus adjuvant chemotherapy for human epidermal growth factor receptor 2-positive breast cancer: planned joint analysis of overall survival from NSABP B-31 and NCCTG N9831.* J Clin Oncol, 2014. **32**(33): p. 3744-52.

79. Wang, J. and B. Xu, *Targeted therapeutic options and future perspectives for HER2-positive breast cancer.* Signal Transduction and Targeted Therapy, 2019. **4**(1): p. 34.

80. Pinto, A.C., et al., *Trastuzumab for patients with HER2 positive breast cancer: delivery, duration and combination therapies.* Breast, 2013. **22 Suppl 2**: p. S152-5.

81. Valachis, A., et al., *Trastuzumab combined to neoadjuvant chemotherapy in patients with HER2-positive breast cancer: A systematic review and meta-analysis.* The Breast, 2011. **20**(6): p. 485-490.

82. Gallagher, C.M., et al., *Delay in initiation of adjuvant trastuzumab therapy leads to decreased overall survival and relapse-free survival in patients with HER2-positive non-metastatic breast cancer.* Breast cancer research and treatment, 2016. **157**(1): p. 145-156.

83. Heyde, A., et al., *Consecutive seeding and transfer of genetic diversity in metastasis.* Proceedings of the National Academy of Sciences, 2019. **116**(28): p. 14129.

84. Valastyan, S. and R.A. Weinberg, *Tumor metastasis: molecular insights and evolving paradigms.* Cell, 2011. **147**(2): p. 275-92.

85. Yan, M. and P. Jurasz, *The role of platelets in the tumor microenvironment: From solid tumors to leukemia.* Biochimica et Biophysica Acta (BBA) - Molecular Cell Research, 2016. **1863**(3): p. 392-400.

86. Pantel, K. and M.R. Speicher, *The biology of circulating tumor cells.* Oncogene, 2016. **35**(10): p. 1216-1224.

87. Müller, A., et al., *Involvement of chemokine receptors in breast cancer metastasis.* Nature, 2001. **410**(6824): p. 50-6.

88. Psaila, B. and D. Lyden, *The metastatic niche: adapting the foreign soil.* Nature Reviews Cancer, 2009. **9**(4): p. 285-293.

89. Hoshino, A., et al., *Tumour exosome integrins determine organotropic metastasis.* Nature, 2015. **527**(7578): p. 329-335.

90. Park, S.-Y. and J.-S. Nam, *The force awakens: metastatic dormant cancer cells.* Experimental & Molecular Medicine, 2020. **52**(4): p. 569-581.

91. Bushnell, G.G., et al., *Breast cancer dormancy: need for clinically relevant models to address current gaps in knowledge.* npj Breast Cancer, 2021. **7**(1): p. 66.

92. Welch, D.R. and D.R. Hurst, *Defining the Hallmarks of Metastasis.* Cancer Research, 2019. **79**(12): p. 3011.

93. Riggio, A.I., K.E. Varley, and A.L. Welm, *The lingering mysteries of metastatic recurrence in breast cancer.* British Journal of Cancer, 2021. **124**(1): p. 13-26.

94. Tohme, S., R.L. Simmons, and A. Tsung, *Surgery for Cancer: A Trigger for Metastases.* Cancer research, 2017. **77**(7): p. 1548-1552.

95. Alieva, M., J. van Rheenen, and M.L.D. Broekman, *Potential impact of invasive surgical procedures on primary tumor growth and metastasis.* Clinical & Experimental Metastasis, 2018. **35**(4): p. 319-331.

96. Karagiannis, G.S., J.S. Condeelis, and M.H. Oktay, *Chemotherapy-Induced Metastasis: Molecular Mechanisms, Clinical Manifestations, Therapeutic Interventions.* Cancer Research, 2019. **79**(18): p. 4567.

97. D'Alterio, C., et al., *Paradoxical effects of chemotherapy on tumor relapse and metastasis promotion.* Seminars in Cancer Biology, 2020. **60**: p. 351-361.

98. Lu, W. and Y. Kang, *Epithelial-Mesenchymal Plasticity in Cancer Progression and Metastasis.* Developmental Cell, 2019. **49**(3): p. 361-374.

99. Lourenco, A.R., et al., *Differential Contributions of Pre- and Post-EMT Tumor Cells in Breast Cancer Metastasis.* Cancer Research, 2020. **80**(2): p. 163.

100. Iuliani, M., et al., *Current and Emerging Biomarkers Predicting Bone Metastasis Development.* Frontiers in Oncology, 2020. **10**: p. 789.

101. Paul, M.R., et al., *Genomic landscape of metastatic breast cancer identifies preferentially dysregulated pathways and targets.* The Journal of Clinical Investigation, 2020. **130**(8): p. 4252-4265.

102. Kroemer, G., G. Marino, and B. Levine, *Autophagy and the integrated stress response.* Mol Cell, 2010. **40**(2): p. 280-93.

103. White, E., *Deconvoluting the context-dependent role for autophagy in cancer.* Nature Reviews. Cancer, 2012. **12**(6): p. 401-410.

104. Kimmelman, A.C., *The dynamic nature of autophagy in cancer.* Genes Dev, 2011. **25**(19): p. 1999-2010.

105. Sahu, R., et al., *Microautophagy of Cytosolic Proteins by Late Endosomes.* Developmental Cell, 2011. **20**(1): p. 131-139.

106. de Duve, C. and R. Wattiaux, *Functions of Lysosomes.* Annual Review of Physiology, 1966. **28**(1): p. 435-492.

107. Mijaljica, D., M. Prescott, and R.J. Devenish, *Microautophagy in mammalian cells: revisiting a 40-year-old conundrum.* Autophagy, 2011. **7**(7): p. 673-82.

108. Tekirdag, K. and A.M. Cuervo, *Chaperone-mediated autophagy and endosomal microautophagy: Joint by a chaperone.* The Journal of biological chemistry, 2018. **293**(15): p. 5414-5424.

109. Seki, T. and H. Katsuki, *Chapter 26 - Mammalian microautophagy: mechanism and roles in disease*, in *Autophagy in Health and Disease (Second Edition)*, B.A. Rothermel and A. Diwan, Editors. 2022, Academic Press. p. 385-397.

110. Sato, M., et al., *Fluorescent-based evaluation of chaperone-mediated autophagy and microautophagy activities in cultured cells.* Genes Cells, 2016. **21**(8): p. 861-73.

111. Mejlvang, J., et al., *Starvation induces rapid degradation of selective autophagy receptors by endosomal microautophagy.* The Journal of cell biology, 2018. **217**(10): p. 3640-3655.

112. Li, J., et al., *AMPK regulates ESCRT-dependent microautophagy of proteasomes concomitant with proteasome storage granule assembly during glucose starvation.* PLOS Genetics, 2019. **15**(11): p. e1008387.

113. Olsvik, H.L., et al., *Endosomal microautophagy is an integrated part of the autophagic response to amino acid starvation.* Autophagy, 2019. **15**(1): p. 182-183.

114. Yang, X., et al., *TORC1 regulates vacuole membrane composition through ubiquitin- and ESCRT-dependent microautophagy.* Journal of Cell Biology, 2020. **219**(3).

115. Chauhan, A.S., et al., *Trafficking of a multifunctional protein by endosomal microautophagy: linking two independent unconventional secretory pathways.* The FASEB Journal, 2019. **33**(4): p. 5626-5640.

116. Oshima, M., et al., *Reciprocal Regulation of Chaperone-Mediated Autophagy/Microautophagy and Exosome Release.* Biol Pharm Bull, 2019. **42**(8): p. 1394-1401.

117. Uytterhoeven, V., L. Deaulmerie, and P. Verstreken, *Increased endosomal microautophagy reduces Tau driven synaptic dysfunction.* Frontiers in Neuroscience, 2018. **12**.

118. Nixon, R.A., *The role of autophagy in neurodegenerative disease.* Nature Medicine, 2013. **19**(8): p. 983-997.

119. Menzies, F.M., et al., *Autophagy and Neurodegeneration: Pathogenic Mechanisms and Therapeutic Opportunities.* Neuron, 2017. **93**(5): p. 1015-1034.

120. Djajadikerta, A., et al., *Autophagy Induction as a Therapeutic Strategy for Neurodegenerative Diseases.* Journal of Molecular Biology, 2020. **432**(8): p. 2799-2821.

121. Kitada, M. and D. Koya, *Autophagy in metabolic disease and ageing.* Nature Reviews Endocrinology, 2021. **17**(11): p. 647-661.

122. Aman, Y., et al., *Autophagy in healthy aging and disease.* Nature Aging, 2021. **1**(8): p. 634-650.

123. Ravikumar, B., et al., *Regulation of Mammalian Autophagy in Physiology and Pathophysiology.* Physiological Reviews, 2010. **90**(4): p. 1383-1435.

124. Menikdiwela, K.R., et al., *Autophagy in metabolic syndrome: breaking the wheel by targeting the renin–angiotensin system.* Cell Death & Disease, 2020. **11**(2): p. 87.

125. Rabinowitz, J.D. and E. White, *Autophagy and metabolism.* Science (New York, N.Y.), 2010. **330**(6009): p. 1344-1348.

126. Xia, Q., et al., *The Role of Autophagy in Skeletal Muscle Diseases.* Frontiers in Physiology, 2021. **12**(291).

127. Margeta, M., *Autophagy Defects in Skeletal Myopathies.* Annual Review of Pathology: Mechanisms of Disease, 2020. **15**(1): p. 261-285.

128. Ghartey-Kwansah, G., et al., *Autophagy in the control and pathogenesis of parasitic infections.* Cell & Bioscience, 2020. **10**(1): p. 101.

129. Ahmad, L., S. Mostowy, and V. Sancho-Shimizu, *Autophagy-Virus Interplay: From Cell Biology to Human Disease.* Frontiers in Cell and Developmental Biology, 2018. **6**(155).

130. Orvedahl, A. and B. Levine, *Eating the enemy within: autophagy in infectious diseases.* Cell Death & Differentiation, 2009. **16**(1): p. 57-69.

131. Levine, B., N. Mizushima, and H.W. Virgin, *Autophagy in immunity and inflammation.* Nature, 2011. **469**(7330): p. 323-335.

132. Tao, S. and I. Drexler, *Targeting Autophagy in Innate Immune Cells: Angel or Demon During Infection and Vaccination?* Frontiers in Immunology, 2020. **11**(460).

133. Germic, N., et al., *Regulation of the innate immune system by autophagy: monocytes, macrophages, dendritic cells and antigen presentation.* Cell Death & Differentiation, 2019. **26**(4): p. 715-727.

134. Bravo-San Pedro, J.M., G. Kroemer, and L. Galluzzi, *Autophagy and Mitophagy in Cardiovascular Disease.* Circulation Research, 2017. **120**(11): p. 1812-1824.

135. Zech, A.T.L., et al., *Autophagy in cardiomyopathies.* Biochimica et Biophysica Acta (BBA) - Molecular Cell Research, 2020. **1867**(3): p. 118432.

136. Nakatogawa, H., *Mechanisms governing autophagosome biogenesis.* Nature Reviews Molecular Cell Biology, 2020. **21**(8): p. 439-458.

137. Ge, L., et al., *The ER–Golgi intermediate compartment is a key membrane source for the LC3 lipidation step of autophagosome biogenesis.* eLife, 2013. **2**: p. e00947.

138. Tan, D., et al., *The EM structure of the TRAPPIII complex leads to the identification of a requirement for COPII vesicles on the macroautophagy pathway.* Proceedings of the National Academy of Sciences of the United States of America, 2013. **110**(48): p. 19432-19437.

139. Ravikumar, B., et al., *Plasma membrane contributes to the formation of pre-autophagosomal structures.* Nat Cell Biol, 2010. **12**(8): p. 747-57.

140. Sanchez-Wandelmer, J., N.T. Ktistakis, and F. Reggiori, *ERES: sites for autophagosome biogenesis and maturation?* Journal of Cell Science, 2015. **128**(2): p. 185-192.

141. Hamasaki, M., et al., *Autophagosomes form at ER–mitochondria contact sites.* Nature, 2013. **495**(7441): p. 389-393.

142. Knævelsrud, H., et al., *Membrane remodeling by the PX-BAR protein SNX18 promotes autophagosome formation.* Journal of Cell Biology, 2013. **202**(2): p. 331-349.

143. Longatti, A., et al., *TBC1D14 regulates autophagosome formation via Rab11- and ULK1-positive recycling endosomes.* The Journal of cell biology, 2012. **197**(5): p. 659-675.

144. Puri, C., et al., *Diverse Autophagosome Membrane Sources Coalesce in Recycling Endosomes.* Cell, 2013. **154**(6): p. 1285-1299.

145. Kojima, W., et al., *Mammalian BCAS3 and C16orf70 associate with the phagophore assembly site in response to selective and non-selective autophagy.* Autophagy, 2021. **17**(8): p. 2011-2036.

146. Kim, J., et al., *AMPK and mTOR regulate autophagy through direct phosphorylation of Ulk1.* Nature Cell Biology, 2011. **13**(2): p. 132-141.

147. Hosokawa, N., et al., *Nutrient-dependent mTORC1 association with the ULK1-Atg13-FIP200 complex required for autophagy.* Molecular biology of the cell, 2009. **20**(7): p. 1981-1991.

148. Alers, S., et al., *Role of AMPK-mTOR-Ulk1/2 in the regulation of autophagy: cross talk, shortcuts, and feedbacks.* Molecular and cellular biology, 2012. **32**(1): p. 2-11.

149. Shi, X., et al., *The autophagy adaptor NDP52 and the FIP200 coiled-coil allosterically activate ULK1 complex membrane recruitment.* eLife, 2020. **9**: p. e59099.

150. Mailler, E., et al., *The autophagy protein ATG9A enables lipid mobilization from lipid droplets.* Nature Communications, 2021. **12**(1): p. 6750.

151. Orsi, A., et al., *Dynamic and transient interactions of Atg9 with autophagosomes, but not membrane integration, are required for autophagy.* Molecular biology of the cell, 2012. **23**(10): p. 1860-1873.

152. Guardia, C.M., et al., *Structure of Human ATG9A, the Only Transmembrane Protein of the Core Autophagy Machinery.* Cell Reports, 2020. **31**(13): p. 107837.

153. Karanasios, E., et al., *Autophagy initiation by ULK complex assembly on ER tubulovesicular regions marked by ATG9 vesicles.* Nat Commun, 2016. **7**: p. 12420.

154. Fujita, N., et al., *The Atg16L complex specifies the site of LC3 lipidation for membrane biogenesis in autophagy.* Molecular biology of the cell, 2008. **19**(5): p. 2092-2100.

155. Tanida, I., T. Ueno, and E. Kominami, *LC3 conjugation system in mammalian autophagy.* Int J Biochem Cell Biol, 2004. **36**(12): p. 2503-18.

156. Galluzzi, L., et al., *Molecular definitions of autophagy and related processes.* The EMBO Journal, 2017. **36**(13): p. 1811-1836.

157. Tremel, S., et al., *Structural basis for VPS34 kinase activation by Rab1 and Rab5 on membranes.* Nature Communications, 2021. **12**(1): p. 1564.

158. Xing, H., et al., *Crosstalk between exosomes and autophagy: A review of molecular mechanisms and therapies.* Journal of Cellular and Molecular Medicine, 2021. **25**(5): p. 2297-2308.

159. Yu, L., Y. Chen, and S.A. Tooze, *Autophagy pathway: Cellular and molecular mechanisms.* Autophagy, 2018. **14**(2): p. 207-215.

160. Gatica, D., et al., *Vac8 determines phagophore assembly site vacuolar localization during nitrogen starvation-induced autophagy.* Autophagy, 2021. **17**(7): p. 1636-1648.

161. Reggiori, F. and C. Ungermann, *Autophagosome Maturation and Fusion.* Journal of Molecular Biology, 2017. **429**(4): p. 486-496.

162. Shrestha, B.K., et al., *NIMA-related kinase 9-mediated phosphorylation of the microtubule-associated LC3B protein at Thr-50 suppresses selective autophagy of p62/sequestosome 1.* J Biol Chem, 2020. **295**(5): p. 1240-1260.

163. Nakamura, S. and T. Yoshimori, *New insights into autophagosome–lysosome fusion.* Journal of Cell Science, 2017. **130**(7): p. 1209-1216.

164. Noda, T., N. Fujita, and T. Yoshimori, *The late stages of autophagy: how does the end begin?* Cell Death & Differentiation, 2009. **16**(7): p. 984-990.

165. Chen, Y. and L. Yu, *Recent progress in autophagic lysosome reformation.* Traffic, 2017. **18**(6): p. 358-361.

166. Scarlatti, F., et al., *Role of non-canonical Beclin 1-independent autophagy in cell death induced by resveratrol in human breast cancer cells.* Cell Death & Differentiation, 2008. **15**(8): p. 1318-1329.

167. Tian, S., et al., *Beclin 1-independent autophagy induced by a Bcl-XL/Bcl-2 targeting compound, Z18.* Autophagy, 2010. **6**(8): p. 1032-1041.

168. Sun, L., et al., *Beclin-1-independent autophagy mediates programmed cancer cell death through interplays with endoplasmic reticulum and/or mitochondria in colbat chloride-induced hypoxia.* Am J Cancer Res, 2015. **5**(9): p. 2626-42.

169. Grishchuk, Y., et al., *Beclin 1-independent autophagy contributes to apoptosis in cortical neurons.* Autophagy, 2011. **7**(10): p. 1115-31.

170. Feng, Y., et al., *Unc-51-like kinase (ULK) complex-independent autophagy induced by hypoxia.* Protein & Cell, 2019. **10**(5): p. 376-381.

171. Tamura, N., et al., *Hyperosmotic Stress Induces Unconventional Autophagy Independent of the Ulk1 Complex.* Molecular and Cellular Biology. **39**(16): p. e00024-19.

172. Cheong, H., et al., *Ammonia-induced autophagy is independent of ULK1/ULK2 kinases.* Proceedings of the National Academy of Sciences, 2011. **108**(27): p. 11121.

173. Gammoh, N., et al., *Interaction between FIP200 and ATG16L1 distinguishes ULK1 complex–dependent and –independent autophagy.* Nature Structural & Molecular Biology, 2013. **20**(2): p. 144-149.

174. Nishida, Y., et al., *Discovery of Atg5/Atg7-independent alternative macroautophagy.* Nature, 2009. **461**(7264): p. 654-658.

175. Ma, T., et al., *Atg5-independent autophagy regulates mitochondrial clearance and is essential for iPSC reprogramming.* Nature Cell Biology, 2015. **17**(11): p. 1379-1387.

176. Goebel, T., et al., *Proteaphagy in Mammalian Cells Can Function Independent of ATG5/ATG7 **.* Molecular & Cellular Proteomics, 2020. **19**(7): p. 1120-1131.

177. Yeo, S.Y., et al., *Transglutaminase 2 contributes to a TP53-induced autophagy program to prevent oncogenic transformation.* eLife, 2016. **5**: p. e07101.

178. Kargapolova, Y., et al., *Overarching control of autophagy and DNA damage response by CHD6 revealed by modeling a rare human pathology.* Nature Communications, 2021. **12**(1): p. 3014.

179. Lin, W., et al., *Autophagy confers DNA damage repair pathways to protect the hematopoietic system from nuclear radiation injury.* Scientific Reports, 2015. **5**(1): p. 12362.

180. Yin, X., et al., *The Role of Autophagy in Sepsis: Protection and Injury to Organs.* Frontiers in Physiology, 2019. **10**: p. 1071.

181. Namkoong, S., et al., *Autophagy Dysregulation and Obesity-Associated Pathologies.* Mol Cells, 2018. **41**(1): p. 3-10.

182. He, L., et al., *Autophagy: The Last Defense against Cellular Nutritional Stress.* Advances in Nutrition, 2018. **9**(4): p. 493-504.

183. Sinha, R.A., B.K. Singh, and P.M. Yen, *Reciprocal Crosstalk Between Autophagic and Endocrine Signaling in Metabolic Homeostasis.* Endocrine Reviews, 2017. **38**(1): p. 69-102.

184. Jain, K., et al., *Autophagy in breast cancer and its implications for therapy.* Am J Cancer Res, 2013. **3**(3): p. 251-65.

185. Abedin, M.J., et al., *Autophagy delays apoptotic death in breast cancer cells following DNA damage.* Cell Death Differ, 2007. **14**(3): p. 500-10.

186. Carey, L., et al., *The triple negative paradox: primary tumor chemosensitivity of breast cancer subtypes.* Clin Cancer Res, 2007. **13**: p. 2329 - 2334.

187. Degenhardt, K., et al., *Autophagy promotes tumor cell survival and restricts necrosis, inflammation, and tumorigenesis.* Cancer Cell, 2006. **10**(1): p. 51-64.

188. Levine, B. and G. Kroemer, *Autophagy in the Pathogenesis of Disease.* Cell, 2008. **132**(1): p. 27-42.

189. Antonucci, L., et al., *Basal autophagy maintains pancreatic acinar cell homeostasis and protein synthesis and prevents ER stress.* Proc Natl Acad Sci U S A, 2015. **112**(45): p. E6166-74.

190. Lien, K., et al., *Low-dose metronomic chemotherapy: A systematic literature analysis.* European Journal of Cancer, 2013. **49**(16): p. 3387-3395.

191. Ueno, T., et al., *Differential Involvement of Autophagy and Apoptosis in Response to Chemoendocrine and Endocrine Therapy in Breast Cancer: JBCRG-07TR.* International journal of molecular sciences, 2019. **20**(4): p. 984.

192. He, Y., et al., *The prognostic value of autophagy-related markers beclin-1 and microtubule-associated protein light chain 3B in cancers: a systematic review and meta-analysis.* Tumor Biology, 2014. **35**(8): p. 7317-7326.

193. Tang, H., et al., *Decreased BECN1 mRNA Expression in Human Breast Cancer is Associated with Estrogen Receptor-Negative Subtypes and Poor Prognosis.* EBioMedicine, 2015. **2**(3): p. 255-263.

194. Delaney, J.R., et al., *Autophagy gene haploinsufficiency drives chromosome instability, increases migration, and promotes early ovarian tumors.* PLoS Genet, 2020. **16**(1): p. e1008558.

195. Wijshake, T., et al., *Tumor-suppressor function of Beclin 1 in breast cancer cells requires E-cadherin.* Proceedings of the National Academy of Sciences, 2021. **118**(5): p. e2020478118.

196. Wang, Z., et al., *MicroRNA-25 regulates chemoresistance-associated autophagy in breast cancer cells, a process modulated by the natural autophagy inducer isoliquiritigenin.* Oncotarget, 2014. **5**(16): p. 7013-7026.

197. Garbar, C., et al., *Chemotherapy treatment induces an increase of autophagy in the luminal breast cancer cell MCF7, but not in the triple-negative MDA-MB231.* Scientific Reports, 2017. **7**.

198. Tracey, N., et al., *HO-1 drives autophagy as a mechanism of resistance against HER2-targeted therapies.* Breast Cancer Research and Treatment, 2020. **179**(3): p. 543-555.

199. Liu, P., et al., *The role of autophagy in the cytotoxicity induced by trastuzumab emtansine (T-DM1) in HER2-positive breast cancer cells.* AMB Express, 2020. **10**(1): p. 107.

200. Desai, S., et al., *Heat shock factor 1 (HSF1) controls chemoresistance and autophagy through transcriptional regulation of autophagy-related protein 7 (ATG7).* J Biol Chem, 2013. **288**(13): p. 9165-76.

201. Bousquet, G., et al., *Targeting autophagic cancer stem-cells to reverse chemoresistance in human triple negative breast cancer.* Oncotarget; Vol 8, No 21, 2017.

202. Walcher, L., et al., *Cancer Stem Cells—Origins and Biomarkers: Perspectives for Targeted Personalized Therapies.* Frontiers in Immunology, 2020. **11**: p. 1280.

203. Reya, T., et al., *Stem cells, cancer, and cancer stem cells.* Nature, 2001. **414**(6859): p. 105-111.

204. Li, W., et al., *Unraveling the roles of CD44/CD24 and ALDH1 as cancer stem cell markers in tumorigenesis and metastasis.* Scientific Reports, 2017. **7**(1): p. 13856.

205. Goldstein, L.J., et al., *A window-of-opportunity trial of the CXCR1/2 inhibitor reparixin in operable HER-2-negative breast cancer.* Breast Cancer Research, 2020. **22**(1): p. 4.

206. Kaverina, N., et al., *Astrocytes promote progression of breast cancer metastases to the brain via a KISS1-mediated autophagy.* Autophagy, 2017. **13**(11): p. 1905-1923.

207. Maycotte, P., et al., *Autophagy Supports Breast Cancer Stem Cell Maintenance by Regulating IL6 Secretion.* Molecular Cancer Research, 2015. **13**(4): p. 651-658.

208. Gong, C., et al., *Beclin 1 and autophagy are required for the tumorigenicity of breast cancer stem-like/progenitor cells.* Oncogene, 2013. **32**(18): p. 2261-2272.

209. Yue, W., et al., *Inhibition of the autophagic flux by salinomycin in breast cancer stem-like/progenitor cells interferes with their maintenance.* Autophagy, 2013. **9**(5): p. 714-29.

210. Liao, M., et al., *Autophagy Blockade by Ai Du Qing Formula Promotes Chemosensitivity of Breast Cancer Stem Cells Via GRP78/β-Catenin/ABCG2 Axis.* Frontiers in Pharmacology, 2021. **12**(1336).

211. Wolf, J., et al., *A mammosphere formation RNAi screen reveals that ATG4A promotes a breast cancer stem-like phenotype.* Breast Cancer Res, 2013. **15**(6): p. R109.

212. Ye, Z.-q., et al., *Circular RNA CDR1as-induced autophagy regulates the proliferation and migration of CD44+/CD24- phenotype breast cancer stem cells in vitro.* All Life, 2021. **14**(1): p. 569-576.

213. Yeo, S.K., et al., *Autophagy Differentially Regulates Distinct Breast Cancer Stem-like Cells in Murine Models via EGFR/Stat3 and Tgfβ/Smad Signaling.* Cancer Research, 2016. **76**(11): p. 3397-3410.

214. Li, Y., et al., *Matrix Stiffness Regulates Chemosensitivity, Stemness Characteristics, and Autophagy in Breast Cancer Cells.* ACS Applied Bio Materials, 2020. **3**(7): p. 4474-4485.

215. Zhao, X.-L., et al., *High-mobility group box 1 released by autophagic cancer-associated fibroblasts maintains the stemness of luminal breast cancer cells.* The Journal of pathology, 2017. **243**(3): p. 376-389.

216. Sanchez, C.G., et al., *Activation of autophagy in mesenchymal stem cells provides tumor stromal support.* Carcinogenesis, 2011. **32**(7): p. 964-972.

217. Kumar, D., S. Shankar, and R.K. Srivastava, *Rottlerin-induced autophagy leads to the apoptosis in breast cancer stem cells: molecular mechanisms.* Mol Cancer, 2013. **12**(1): p. 171.

218. Fu, Y., et al., *Resveratrol Inhibits Breast Cancer Stem-Like Cells and Induces Autophagy via Suppressing Wnt/β-Catenin Signaling Pathway.* PLOS ONE, 2014. **9**(7): p. e102535.

219. Sosa, M.S., P. Bragado, and J.A. Aguirre-Ghiso, *Mechanisms of disseminated cancer cell dormancy: an awakening field.* Nature reviews. Cancer, 2014. **14**(9): p. 611-622.

220. Yeh, A.C. and S. Ramaswamy, *Mechanisms of Cancer Cell Dormancy—Another Hallmark of Cancer?* Cancer Research, 2015. **75**(23): p. 5014.

221. Summers, M.A., M.M. McDonald, and P.I. Croucher, *Cancer Cell Dormancy in Metastasis.* Cold Spring Harbor Perspectives in Medicine, 2020. **10**(4).

222. Vera-Ramirez, L., et al., *Autophagy promotes the survival of dormant breast cancer cells and metastatic tumour recurrence.* Nature Communications, 2018. **9**(1): p. 1944.

223. Liang, G., et al., *Autophagy-associated circRNA circCDYL augments autophagy and promotes breast cancer progression.* Molecular Cancer, 2020. **19**(1): p. 65.

224. Marsh, T., et al., *Autophagic Degradation of NBR1 Restricts Metastatic Outgrowth during Mammary Tumor Progression.* Developmental Cell, 2020. **52**(5): p. 591-604.e6.

225. Othman, A.H., M. Tandon, and J. Pratap, *Autophagy modulation in bone metastatic breast cancer: A potential therapeutic targeting strategy.* Journal of Clinical Oncology, 2015. **33**(15_suppl): p. e22009-e22009.

226. Akalay, I., et al., *Epithelial-to-Mesenchymal Transition and Autophagy Induction in Breast Carcinoma Promote Escape from T-cell–Mediated Lysis.* Cancer Research, 2013. **73**(8): p. 2418.

227. Qiang, L., et al., *Regulation of cell proliferation and migration by p62 through stabilization of Twist1.* Proceedings of the National Academy of Sciences, 2014. **111**(25): p. 9241.

228. Saxena, M., et al., *AMP-activated protein kinase promotes epithelial-mesenchymal transition in cancer cells through Twist1 upregulation.* Journal of Cell Science, 2018. **131**(14): p. jcs208314.

229. Tan, P., et al., *TRIM59 promotes breast cancer motility by suppressing p62-selective autophagic degradation of PDCD10.* PLoS Biol, 2018. **16**(11): p. e3000051.

230. Manent, J., et al., *Autophagy suppresses Ras-driven epithelial tumourigenesis by limiting the accumulation of reactive oxygen species.* Oncogene, 2017. **36**(40): p. 5576-5592.

231. Sung, S., J. Choi, and H. Cheong, *Catabolic pathways regulated by mTORC1 are pivotal for survival and growth of cancer cells expressing mutant Ras.* Oncotarget, 2015. **6**(38): p. 40405-17.

232. Lock, R., et al., *Autophagy-dependent production of secreted factors facilitates oncogenic RAS-driven invasion.* Cancer Discov, 2014. **4**(4): p. 466-79.

233. Abe, T., et al., *LZTR1 facilitates polyubiquitination and degradation of RAS-GTPases.* Cell Death Differ, 2020. **27**(3): p. 1023-1035.

234. Feng, F., et al., *The dual roles of autophagy in gliomagenesis and clinical therapy strategies based on autophagic regulation mechanisms.* Biomedicine & Pharmacotherapy, 2019. **120**: p. 109441.

235. Takai, T., et al., *Synthetic miR-143 Exhibited an Anti-Cancer Effect via the Downregulation of K-RAS Networks of Renal Cell Cancer Cells In Vitro and In Vivo.* Mol Ther, 2019. **27**(5): p. 1017-1027.

236. Liang, F., et al., *The crosstalk between STAT3 and p53/RAS signaling controls cancer cell metastasis and cisplatin resistance via the Slug/MAPK/PI3K/AKT-mediated regulation of EMT and autophagy.* Oncogenesis, 2019. **8**(10): p. 59.

237. Booth, L., et al., *The levels of mutant K-RAS and mutant N-RAS are rapidly reduced in a Beclin1 / ATG5 -dependent fashion by the irreversible ERBB1/2/4 inhibitor neratinib.* Cancer Biol Ther, 2018. **19**(2): p. 132-137.

238. Booth, L., et al., *Neratinib and entinostat combine to rapidly reduce the expression of K-RAS, N-RAS, Gα(q) and Gα(11) and kill uveal melanoma cells.* Cancer Biol Ther, 2019. **20**(5): p. 700-710.

239. Behrouj, H., et al., *Effect of casein kinase 1α inhibition on autophagy flux and the AKT/phospho-β-catenin (S552) axis in HCT116, a RAS-mutated colorectal cancer cell line.* Canadian Journal of Physiology and Pharmacology, 2021. **99**(3): p. 284-293.

240. Alves, S., et al., *Colorectal cancer-related mutant KRAS alleles function as positive regulators of autophagy.* Oncotarget, 2015. **6**(31): p. 30787-802.

241. Goulielmaki, M., et al., *BRAF associated autophagy exploitation: BRAF and autophagy inhibitors synergise to efficiently overcome resistance of BRAF mutant colorectal cancer cells.* Oncotarget, 2016. **7**(8): p. 9188-221.

242. Lee, C.S., et al., *MAP kinase and autophagy pathways cooperate to maintain RAS mutant cancer cell survival.* Proc Natl Acad Sci U S A, 2019. **116**(10): p. 4508-4517.

243. Guo, J.Y., et al., *Autophagy provides metabolic substrates to maintain energy charge and nucleotide pools in Ras-driven lung cancer cells.* Genes Dev, 2016. **30**(15): p. 1704-17.

244. Tsang, T., et al., *Copper is an essential regulator of the autophagic kinases ULK1/2 to drive lung adenocarcinoma.* Nat Cell Biol, 2020. **22**(4): p. 412-424.

245. Wang, W., et al., *DEPDC1 up-regulates RAS expression to inhibit autophagy in lung adenocarcinoma cells.* J Cell Mol Med, 2020. **24**(22): p. 13303-13313.

246. Qiu, J., et al., *Distinct subgroup of the Ras family member 3 (DIRAS3) expression impairs metastasis and induces autophagy of gastric cancer cells in mice.* J Cancer Res Clin Oncol, 2018. **144**(10): p. 1869-1886.

247. Sutton, M.N., et al., *RAS-related GTPases DIRAS1 and DIRAS2 induce autophagic cancer cell death and are required for autophagy in murine ovarian cancer cells.* Autophagy, 2018. **14**(4): p. 637-653.

248. Bildik, G., et al., *DIRAS3: An Imprinted tumor suppressor gene that regulates RAS and PI3K-driven cancer growth, motility, autophagy and tumor dormancy.* Mol Cancer Ther, 2021.

249. Zhong, C., et al., *Oncogenic Ras is downregulated by ARHI and induces autophagy by Ras/AKT/mTOR pathway in glioblastoma.* BMC Cancer, 2019. **19**(1): p. 441.

250. Hobbs, G.A., et al., *Atypical KRAS(G12R) Mutant Is Impaired in PI3K Signaling and Macropinocytosis in Pancreatic Cancer.* Cancer Discov, 2020. **10**(1): p. 104-123.

251. Ropolo, A., et al., *A Novel E2F1-EP300-VMP1 Pathway Mediates Gemcitabine-Induced Autophagy in Pancreatic Cancer Cells Carrying Oncogenic KRAS.* Front Endocrinol (Lausanne), 2020. **11**: p. 411.

252. Yue, P., et al., *Development of an autophagy-related signature in pancreatic adenocarcinoma.* Biomed Pharmacother, 2020. **126**: p. 110080.

253. Sanduja, S., et al., *AMPK promotes tolerance to Ras pathway inhibition by activating autophagy.* Oncogene, 2016. **35**(40): p. 5295-5303.

254. Bryant, K.L., et al., *Combination of ERK and autophagy inhibition as a treatment approach for pancreatic cancer.* Nat Med, 2019. **25**(4): p. 628-640.

255. Karasic, T.B., et al., *Effect of Gemcitabine and nab-Paclitaxel With or Without Hydroxychloroquine on Patients With Advanced Pancreatic Cancer: A Phase 2 Randomized Clinical Trial.* JAMA Oncol, 2019. **5**(7): p. 993-998.

256. Wang, P., Y. Du, and J. Wang, *Indentification of breast cancer subtypes sensitive to HCQ-induced autophagy inhibition.* Pathology - Research and Practice, 2019. **215**(10): p. 152609.

257. Gao, L., et al., *Histone deacetylase inhibitor trichostatin A and autophagy inhibitor chloroquine synergistically exert anti-tumor activity in H-ras transformed breast epithelial cells.* Mol Med Rep, 2018. **17**(3): p. 4345-4350.

258. Tekirdag, K. and A.M. Cuervo, *Chaperone-mediated autophagy and endosomal microautophagy: Jointed by a chaperone.* Journal of Biological Chemistry, 2018. **293**(15): p. 5414-5424.

259. Cuervo, A.M. and J.F. Dice, *A receptor for the selective uptake and degradation of proteins by lysosomes.* Science, 1996. **273**(5274): p. 501-3.

260. Cuervo, A.M. and J.F. Dice, *Unique properties of lamp2a compared to other lamp2 isoforms.* Journal of Cell Science, 2000. **113**(24): p. 4441-4450.

261. Kaushik, S., et al., *Chaperone-mediated autophagy at a glance.* J Cell Sci, 2011. **124**(Pt 4): p. 495-9.

262. Cuervo, A.M. and E. Wong, *Chaperone-mediated autophagy: roles in disease and aging.* Cell Res, 2014. **24**(1): p. 92-104.

263. Cuervo, A.M. and E. Wong, *Chaperone-mediated autophagy: roles in disease and aging.* Cell Research, 2014. **24**(1): p. 92-104.

264. Kirchner, P., et al., *Proteome-wide analysis of chaperone-mediated autophagy targeting motifs.* PLOS Biology, 2019. **17**(5): p. e3000301.

265. Majeski, A.E. and J. Fred Dice, *Mechanisms of chaperone-mediated autophagy.* The International Journal of Biochemistry & Cell Biology, 2004. **36**(12): p. 2435-2444.

266. Chiang, H.-L., et al., *A Role for a 70-Kilodalton Heat Shock Protein in Lysosomal Degradation of Intracellular Proteins.* Science, 1989. **246**(4928): p. 382-385.

267. Bandyopadhyay, U., et al., *The Chaperone-Mediated Autophagy Receptor Organizes in Dynamic Protein Complexes at the Lysosomal Membrane.* Molecular and Cellular Biology, 2008. **28**(18): p. 5747-5763.

268. Wu, Z., et al., *Chaperone-mediated autophagy is involved in the execution of ferroptosis.* Proceedings of the National Academy of Sciences, 2019. **116**(8): p. 2996.

269. Gong, Z., et al., *Humanin is an endogenous activator of chaperone-mediated autophagy.* Journal of Cell Biology, 2017. **217**(2): p. 635-647.

270. Salvador, N., et al., *Import of a cytosolic protein into lysosomes by chaperone-mediated autophagy depends on its folding state.* J Biol Chem, 2000. **275**(35): p. 27447-56.

271. Agarraberes, F.A. and J.F. Dice, *A molecular chaperone complex at the lysosomal membrane is required for protein translocation.* J Cell Sci, 2001. **114**(Pt 13): p. 2491-9.

272. Orenstein, S.J. and A.M. Cuervo, *Chaperone-mediated autophagy: molecular mechanisms and physiological relevance.* Seminars in cell & developmental biology, 2010. **21**(7): p. 719-726.

273. Arias, E., et al., *Lysosomal mTORC2/PHLPP1/Akt Regulate Chaperone-Mediated Autophagy.* Mol Cell, 2015. **59**(2): p. 270-84.

274. Bandyopadhyay, U., et al., *The Chaperone-Mediated Autophagy Receptor Organizes in Dynamic Protein Complexes at the Lysosomal Membrane.* Molecular and Cellular Biology, 2008. **28**(18): p. 5747-5763.

275. Kaushik, S., A.C. Massey, and A.M. Cuervo, *Lysosome membrane lipid microdomains: novel regulators of chaperone-mediated autophagy.* Embo j, 2006. **25**(17): p. 3921-33.

276. Cuervo, A.M. and J.F. Dice, *Regulation of lamp2a levels in the lysosomal membrane.* Traffic, 2000. **1**(7): p. 570-83.

277. Zhang, J., et al., *Cystinosin, the small GTPase Rab11, and the Rab7 effector RILP regulate intracellular trafficking of the chaperone-mediated autophagy receptor LAMP2A.* J Biol Chem, 2017. **292**(25): p. 10328-10346.

278. Napolitano, G., et al., *Impairment of chaperone-mediated autophagy leads to selective lysosomal degradation defects in the lysosomal storage disease cystinosis.* EMBO Mol Med, 2015. **7**(2): p. 158-74.

279. Anguiano, J., et al., *Chemical modulation of chaperone-mediated autophagy by retinoic acid derivatives.* Nat Chem Biol, 2013. **9**(6): p. 374-82.

280. Valdor, R., et al., *Chaperone-mediated autophagy regulates T cell responses through targeted degradation of negative regulators of T cell activation.* Nat Immunol, 2014. **15**(11): p. 1046-54.

281. Pajares, M., et al., *Transcription factor NFE2L2/NRF2 modulates chaperone-mediated autophagy through the regulation of LAMP2A.* Autophagy, 2018. **14**(8): p. 1310-1322.

282. Aydin, Y., et al., *Chaperone-Mediated Autophagy Promotes Beclin1 Degradation in Persistently Infected Hepatitis C Virus Cell Culture.* Am J Pathol, 2018. **188**(10): p. 2339-2355.

283. Massey, A.C., et al., *Consequences of the selective blockage of chaperone-mediated autophagy.* Proc Natl Acad Sci U S A, 2006. **103**(15): p. 5805-10.

284. Ali, D.M., et al., *Optineurin downregulation induces endoplasmic reticulum stress, chaperone-mediated autophagy, and apoptosis in pancreatic cancer cells.* Cell Death Discovery, 2019. **5**(1): p. 128.

285. Vakifahmetoglu-Norberg, H., et al., *Chaperone-mediated autophagy degrades mutant p53.* Genes Dev, 2013. **27**(15): p. 1718-30.

286. Wang, C., et al., *Phosphorylation of ULK1 affects autophagosome fusion and links chaperone-mediated autophagy to macroautophagy.* Nat Commun, 2018. **9**(1): p. 3492.

287. Nascimbeni, A.C., et al., *Autophagy dysregulation in Danon disease.* Cell Death & Disease, 2018. **8**(1): p. e2565-e2565.

288. Cuervo, A.M. and J.F. Dice, *Age-related decline in chaperone-mediated autophagy.* J Biol Chem, 2000. **275**(40): p. 31505-13.

289. Boya, P., R. Gomez Sintes, and A.M. Cuervo, *Chaperone-mediated autophagy is a cytoprotective response of photoreceptors during aging and retinal diseases.* Investigative Ophthalmology & Visual Science, 2019. **60**(9): p. 1669-1669.

290. Cuervo, A.M., et al., *Direct lysosomal uptake of alpha 2-microglobulin contributes to chemically induced nephropathy.* Kidney Int, 1999. **55**(2): p. 529-45.

291. Sooparb, S., et al., *Suppression of chaperone-mediated autophagy in the renal cortex during acute diabetes mellitus.* Kidney International, 2004. **65**(6): p. 2135-2144.

292. Xu, X., et al., *Metformin activates chaperone-mediated autophagy and improves disease pathologies in an Alzheimer disease mouse model.* Protein & Cell, 2021. **12**(10): p. 769-787.

293. Caballero, B., et al., *Acetylated tau inhibits chaperone-mediated autophagy and promotes tau pathology propagation in mice.* Nature Communications, 2021. **12**(1): p. 2238.

294. Alvarez-Erviti, L., et al., *Chaperone-Mediated Autophagy Markers in Parkinson Disease Brains.* Archives of Neurology, 2010. **67**(12): p. 1464-1472.

295. Koga, H., et al., *Constitutive Upregulation of Chaperone-Mediated Autophagy in Huntington's Disease.* The Journal of Neuroscience, 2011. **31**(50): p. 18492.

296. Xu, Y., et al., *Chaperone-mediated autophagy regulates the pluripotency of embryonic stem cells.* Science, 2020. **369**(6502): p. 397-403.

297. Dong, S., et al., *Monitoring spatiotemporal changes in chaperone-mediated autophagy in vivo.* Nat Commun, 2020. **11**(1): p. 645.

298. Gomes, L.R., C.F.M. Menck, and A.M. Cuervo, *Chaperone-mediated autophagy prevents cellular transformation by regulating MYC proteasomal degradation.* Autophagy, 2017. **13**(5): p. 928-940.

299. Yang, F., et al., *Stabilization of MORC2 by estrogen and antiestrogens through GPER1- PRKACA-CMA pathway contributes to estrogen-induced proliferation*

and endocrine resistance of breast cancer cells. Autophagy, 2020. **16**(6): p. 1061-1076.

300. Park, C., Y. Suh, and A.M. Cuervo, *Regulated degradation of Chk1 by chaperone-mediated autophagy in response to DNA damage.* Nat Commun, 2015. **6**: p. 6823.

301. Hao, Y., et al., *Targetome analysis of chaperone-mediated autophagy in cancer cells.* Autophagy, 2019. **15**(9): p. 1558-1571.

302. Xie, W., et al., *Chaperone-mediated autophagy prevents apoptosis by degrading BBC3/PUMA.* Autophagy, 2015. **11**(9): p. 1623-1635.

303. Bonhoure, A., et al., *Acetylation of translationally controlled tumor protein promotes its degradation through chaperone-mediated autophagy.* European Journal of Cell Biology, 2017. **96**(2): p. 83-98.

304. Li, L., et al., *Deacetylation of tumor-suppressor MST1 in Hippo pathway induces its degradation through HBXIP-elevated HDAC6 in promotion of breast cancer growth.* Oncogene, 2016. **35**(31): p. 4048-57.

305. Peng, J.-q., et al., *Chaperone-mediated autophagy regulates apoptosis and the proliferation of colon carcinoma cells.* Biochemical and Biophysical Research Communications, 2020. **522**(2): p. 348-354.

306. Ichikawa, A., et al., *Chaperone-mediated autophagy receptor modulates tumor growth and chemoresistance in non-small cell lung cancer.* Cancer Sci, 2020. **111**(11): p. 4154-4165.

307. Kon, M., et al., *Chaperone-mediated autophagy is required for tumor growth.* Sci Transl Med, 2011. **3**(109): p. 109ra117.

308. Cao, D., et al., *Chaperone-mediated autophagy affects tumor cell proliferation and cisplatin resistance in esophageal squamous cell carcinoma.* Thorac Cancer, 2021. **12**(7): p. 1048-1057.

309. Zhou, J., et al., *Chaperone-mediated autophagy regulates proliferation by targeting RND3 in gastric cancer.* Autophagy, 2016. **12**(3): p. 515-28.

310. Saha, T., *LAMP2A overexpression in breast tumors promotes cancer cell survival via chaperone-mediated autophagy.* Autophagy, 2012. **8**(11): p. 1643-56.

311. Han, Q., et al., *Downregulation of ATG5-dependent macroautophagy by chaperone-mediated autophagy promotes breast cancer cell metastasis.* Sci Rep, 2017. **7**(1): p. 4759.

312. Valdor, R., et al., *Glioblastoma ablates pericytes antitumor immune function through aberrant up-regulation of chaperone-mediated autophagy.* Proceedings of the National Academy of Sciences, 2019. **116**(41): p. 20655.

313. Lv, L., et al., *Acetylation Targets the M2 Isoform of Pyruvate Kinase for Degradation through Chaperone-Mediated Autophagy and Promotes Tumor Growth.* Molecular Cell, 2011. **42**(6): p. 719-730.

314. Xia, H.-g., et al., *Degradation of HK2 by chaperone-mediated autophagy promotes metabolic catastrophe and cell death.* Journal of Cell Biology, 2015. **210**(5): p. 705-716.

315. Yang, T., et al., *PIM2-mediated phosphorylation of hexokinase 2 is critical for tumor growth and paclitaxel resistance in breast cancer.* Oncogene, 2018. **37**(45): p. 5997-6009.

316. Klionsky, D.J., et al., *Guidelines for the use and interpretation of assays for monitoring autophagy (4th edition)1.* Autophagy, 2021. **17**(1): p. 1-382.

317. Pursiheimo, J.P., et al., *Hypoxia-activated autophagy accelerates degradation of SQSTM1/p62.* Oncogene, 2009. **28**(3): p. 334-344.

318. Hubbi, M.E., et al., *Chaperone-mediated Autophagy Targets Hypoxia-inducible Factor-1α (HIF-1α) for Lysosomal Degradation*.* Journal of Biological Chemistry, 2013. **288**(15): p. 10703-10714.

319. Endicott, S.J., et al., *Inhibition of class I PI3K enhances chaperone-mediated autophagy.* J Cell Biol, 2020. **219**(12).

320. Li, J., S.G. Kim, and J. Blenis, *Rapamycin: one drug, many effects.* Cell metabolism, 2014. **19**(3): p. 373-379.

321. Roskoski, R., *Properties of FDA-approved small molecule protein kinase inhibitors.* Pharmacological Research, 2019. **144**: p. 19-50.

322. Hua, H., et al., *Targeting mTOR for cancer therapy.* Journal of Hematology & Oncology, 2019. **12**(1): p. 71.

323. Nyfeler, B., et al., *Relieving Autophagy and 4EBP1 from Rapamycin Resistance.* Molecular and Cellular Biology, 2011. **31**(14): p. 2867-2876.

324. Liu, T., et al., *Combination of an Autophagy Inducer and an Autophagy Inhibitor: A Smarter Strategy Emerging in Cancer Therapy.* Frontiers in Pharmacology, 2020. **11**: p. 408.

325. Liu, P., et al., *Targeting the phosphoinositide 3-kinase pathway in cancer.* Nature reviews. Drug discovery, 2009. **8**(8): p. 627-644.

326. Yang, J., et al., *Targeting PI3K in cancer: mechanisms and advances in clinical trials.* Molecular Cancer, 2019. **18**(1): p. 26.

327. Miller, S., et al., *Finding a fitting shoe for Cinderella: searching for an autophagy inhibitor.* Autophagy, 2010. **6**(6): p. 805-807.

328. Pei, Y., et al., *Quassinoid analogs with enhanced efficacy for treatment of hematologic malignancies target the PI3Kγ isoform.* Communications biology, 2020. **3**(1): p. 267-267.

329. Wu, Y.-T., et al., *Dual role of 3-methyladenine in modulation of autophagy via different temporal patterns of inhibition on class I and III phosphoinositide 3-kinase.* The Journal of biological chemistry, 2010. **285**(14): p. 10850-10861.

330. Fan, S., et al., *Silibinin induced-autophagic and apoptotic death is associated with an increase in reactive oxygen and nitrogen species in HeLa cells.* Free Radic Res, 2011. **45**(11-12): p. 1307-24.

331. Wu, Y., et al., *Synthesis and screening of 3-MA derivatives for autophagy inhibitors.* Autophagy, 2013. **9**(4): p. 595-603.

332. Dong, Y., et al., *Inhibition of autophagy by 3-MA promotes hypoxia-induced apoptosis in human colorectal cancer cells.* Eur Rev Med Pharmacol Sci, 2019. **23**(3): p. 1047-1054.

333. Shin, D., et al., *RITA plus 3-MA overcomes chemoresistance of head and neck cancer cells via dual inhibition of autophagy and antioxidant systems.* Redox Biology, 2017. **13**: p. 219-227.

334. Chicote, J., et al., *Cell Death Triggered by the Autophagy Inhibitory Drug 3-Methyladenine in Growing Conditions Proceeds With DNA Damage.* Frontiers in pharmacology, 2020. **11**: p. 580343-580343.

335. Bago, R., et al., *The hVps34-SGK3 pathway alleviates sustained PI3K/Akt inhibition by stimulating mTORC1 and tumour growth.* The EMBO Journal, 2016. **35**(17): p. 1902-1922.

336. Pasquier, B., *SAR405, a PIK3C3/Vps34 inhibitor that prevents autophagy and synergizes with MTOR inhibition in tumor cells.* Autophagy, 2015. **11**(4): p. 725-726.

337. Ronan, B., et al., *A highly potent and selective Vps34 inhibitor alters vesicle trafficking and autophagy.* Nature Chemical Biology, 2014. **10**(12): p. 1013-1019.

338. Noman Muhammad, Z., et al., *Inhibition of Vps34 reprograms cold into hot inflamed tumors and improves anti–PD-1/PD-L1 immunotherapy.* Science Advances. **6**(18): p. eaax7881.

339. Lee, Y.S., et al., *Mitophagy Induction by ROS-PINK1 Signaling Protects Head and Neck Cancer From Radiotherapy.* International Journal of Radiation Oncology, Biology, Physics, 2021. **111**(3): p. S56.

340. Bago, R., et al., *Characterization of VPS34-IN1, a selective inhibitor of Vps34, reveals that the phosphatidylinositol 3-phosphate-binding SGK3 protein kinase is a downstream target of class III phosphoinositide 3-kinase.* The Biochemical journal, 2014. **463**(3): p. 413-427.

341. Schläfli, A.M., et al., *ALK inhibition activates LC3B-independent, protective autophagy in EML4-ALK positive lung cancer cells.* Scientific Reports, 2021. **11**(1): p. 9011.

342. Meunier, G., et al., *Antileukemic activity of the VPS34-IN1 inhibitor in acute myeloid leukemia.* Oncogenesis, 2020. **9**(10): p. 94.

343. Lawrence, R.E. and R. Zoncu, *The lysosome as a cellular centre for signalling, metabolism and quality control.* Nature Cell Biology, 2019. **21**(2): p. 133-142.

344. Davidson, S.M. and M.G. Vander Heiden, *Critical Functions of the Lysosome in Cancer Biology.* Annual Review of Pharmacology and Toxicology, 2017. **57**(1): p. 481-507.

345. Shin, H.R. and R. Zoncu, *The Lysosome at the Intersection of Cellular Growth and Destruction.* Developmental Cell, 2020. **54**(2): p. 226-238.

346. Parenti, G., D.L. Medina, and A. Ballabio, *The rapidly evolving view of lysosomal storage diseases.* EMBO Molecular Medicine, 2021. **13**(2): p. e12836.

347. Morgan, M.J., et al., *Metastatic cells are preferentially vulnerable to lysosomal inhibition.* Proceedings of the National Academy of Sciences, 2018. **115**(36): p. E8479.

348. Song, Y., et al., *One Stone, Three Birds: pH Triggered Transformation of Aminopyronine and Iminopyronine Based Lysosome Targeting Viscosity Probe for Cancer Visualization.* Analytical Chemistry, 2021. **93**(3): p. 1786-1791.

349. Hansen, M.B., et al., *Identification of lysosome-targeting drugs with anti-inflammatory activity as potential invasion inhibitors of treatment resistant HER2 positive cancers.* Cellular Oncology, 2021. **44**(4): p. 805-820.

350. Fassl, A., et al., *Increased lysosomal biomass is responsible for the resistance of triple-negative breast cancers to CDK4/6 inhibition.* Science Advances. **6**(25): p. eabb2210.

351. Wang, R., et al., *Molecular basis of V-ATPase inhibition by bafilomycin A1.* Nature Communications, 2021. **12**(1): p. 1782.

352. Mauvezin, C. and T.P. Neufeld, *Bafilomycin A1 disrupts autophagic flux by inhibiting both V-ATPase-dependent acidification and Ca-P60A/SERCA-dependent autophagosome-lysosome fusion.* Autophagy, 2015. **11**(8): p. 1437-1438.

353. Teplova, V.V., et al., *Bafilomycin A1 is a potassium ionophore that impairs mitochondrial functions.* Journal of Bioenergetics and Biomembranes, 2007. **39**(4): p. 321.

354. Li, X., et al., *Bafilomycin A1 targets patient-derived CD34+CD19+ leukemia stem cells.* Haematologica, 2020. **105**(1): p. e17-e21.

355. Yuan, N., et al., *Bafilomycin A1 targets both autophagy and apoptosis pathways in pediatric B-cell acute lymphoblastic leukemia.* Haematologica, 2015. **100**(3): p. 345-356.

356. Yan, Y., et al., *Bafilomycin A1 induces caspase-independent cell death in hepatocellular carcinoma cells via targeting of autophagy and MAPK pathways.* Scientific Reports, 2016. **6**(1): p. 37052.

357. Fitzwalter, B.E., et al., *Autophagy Inhibition Mediates Apoptosis Sensitization in Cancer Therapy by Relieving FOXO3a Turnover.* Dev Cell, 2018. **44**(5): p. 555-565.e3.

358. Sullivan, D.J., et al., *On the molecular mechanism of chloroquine's antimalarial action.* Proceedings of the National Academy of Sciences, 1996. **93**(21): p. 11865.

359. Schrezenmeier, E. and T. Dörner, *Mechanisms of action of hydroxychloroquine and chloroquine: implications for rheumatology.* Nature Reviews Rheumatology, 2020. **16**(3): p. 155-166.

360. Fox, R.I., *Mechanism of action of hydroxychloroquine as an antirheumatic drug.* Semin Arthritis Rheum, 1993. **23**(2 Suppl 1): p. 82-91.

361. Al-Bari, M.A.A., *Chloroquine analogues in drug discovery: new directions of uses, mechanisms of actions and toxic manifestations from malaria to multifarious diseases.* Journal of Antimicrobial Chemotherapy, 2015. **70**(6): p. 1608-1621.

362. Mauthe, M., et al., *Chloroquine inhibits autophagic flux by decreasing autophagosome-lysosome fusion.* Autophagy, 2018. **14**(8): p. 1435-1455.

363. Xu, R., et al., *The clinical value of using chloroquine or hydroxychloroquine as autophagy inhibitors in the treatment of cancers: A systematic review and meta-analysis.* Medicine, 2018. **97**(46): p. e12912-e12912.

364. Liu, J., et al., *An Improved Method of Preparing High Efficiency Transformation Escherichia coli with Both Plasmids and Larger DNA Fragments.* Indian journal of microbiology, 2018. **58**(4): p. 448-456.

365. Nakata, Y., X. Tang, and K.K. Yokoyama, *Preparation of competent cells for high-efficiency plasmid transformation of Escherichia coli.* Methods Mol Biol, 1997. **69**: p. 129-37.

366. Zhang, S. and M.D. Cahalan, *Purifying plasmid DNA from bacterial colonies using the QIAGEN Miniprep Kit.* J Vis Exp, 2007(6): p. 247.

367. Jia, F.-J., et al., *A strategy for constructing and verifying short hairpin RNA expression vectors.* Journal of RNAi and gene silencing : an international journal of RNA and gene targeting research, 2007. **3**(1): p. 248-253.

368. Paddison, P.J., et al., *Cloning of short hairpin RNAs for gene knockdown in mammalian cells.* Nat Methods, 2004. **1**(2): p. 163-7.

369. Chang, K., et al., *Creating an miR30-Based shRNA Vector.* Cold Spring Harbor Protocols, 2013. **2013**(7): p. pdb.prot075853.

370. Dickins, R.A., et al., *Probing tumor phenotypes using stable and regulated synthetic microRNA precursors.* Nat Genet, 2005. **37**(11): p. 1289-95.

371. Vert, J.-P., et al., *An accurate and interpretable model for siRNA efficacy prediction.* BMC Bioinformatics, 2006. **7**(1): p. 520.

372. Hannon, G.J. and J.J. Rossi, *Unlocking the potential of the human genome with RNA interference.* Nature, 2004. **431**(7006): p. 371-8.

373. Hannon, G.J., *RNA interference.* Nature, 2002. **418**(6894): p. 244-51.

374. Dow, L.E., et al., *Loss of human Scribble cooperates with H-Ras to promote cell invasion through deregulation of MAPK signalling.* Oncogene, 2008. **27**(46): p. 5988-6001.

375. Nguyen, C.H., et al., *Heat-shock factor 1 both positively and negatively affects cellular clonogenic growth depending on p53 status.* Biochem J, 2013. **452**(2): p. 321-9.

376. Debnath, J., S.K. Muthuswamy, and J.S. Brugge, *Morphogenesis and oncogenesis of MCF-10A mammary epithelial acini grown in three-dimensional basement membrane cultures.* Methods, 2003. **30**(3): p. 256-68.

377. Kho, D., et al., *Application of xCELLigence RTCA Biosensor Technology for Revealing the Profile and Window of Drug Responsiveness in Real Time.* Biosensors, 2015. **5**(2): p. 199-222.

378. Chiu, C.-H., et al., *Comparison between xCELLigence biosensor technology and conventional cell culture system for real-time monitoring human tenocytes proliferation and drugs cytotoxicity screening.* Journal of Orthopaedic Surgery and Research, 2017. **12**(1): p. 149.

379. Junka, A., et al., *Use of the Real Time xCelligence System for Purposes of Medical Microbiology.* Polish journal of microbiology / Polskie Towarzystwo Mikrobiologów = The Polish Society of Microbiologists, 2012. **61**: p. 191-197.

380. Ke, N., et al., *The xCELLigence system for real-time and label-free monitoring of cell viability.* Methods Mol Biol, 2011. **740**: p. 33-43.

381. Lo, H.W., et al., *Epidermal growth factor receptor cooperates with signal transducer and activator of transcription 3 to induce epithelial-mesenchymal transition in cancer cells via up-regulation of TWIST gene expression.* Cancer Res, 2007. **67**(19): p. 9066-76.

382. Ackland, M.L., et al., *Epidermal Growth Factor-Induced Epithelio-Mesenchymal Transition in Human Breast Carcinoma Cells.* Laboratory Investigation, 2003. **83**(3): p. 435-448.

383. Kattan, Z., et al., *Role of manganese superoxide dismutase on growth and invasive properties of human estrogen-independent breast cancer cells.* Breast Cancer Res Treat, 2008. **108**(2): p. 203-15.

384. Bird, C. and S. Kirstein, *Real-time, label-free monitoring of cellular invasion and migration with the xCELLigence system.* Nature Methods, 2009. **6**(8): p. v-vi.

385. Limame, R., et al., *Expression profiling of migrated and invaded breast cancer cells predicts early metastatic relapse and reveals Krüppel-like factor 9 as a potential suppressor of invasive growth in breast cancer.* Oncoscience, 2014. **1**(1): p. 69-81.

386. Kouspou, M.M. and J.T. Price, *Analysis of cellular migration using a two-chamber methodology.* Methods Mol Biol, 2011. **787**: p. 303-17.

387. Price, J.T. and E.W. Thompson, *Models for studying cellular invasion of basement membranes.* Methods Mol Biol, 1999. **129**: p. 231-49.

388. Schindelin, J., et al., *Fiji: an open-source platform for biological-image analysis.* Nature Methods, 2012. **9**(7): p. 676-682.

389. Schmidt, H., et al., *Enrichment and analysis of secretory lysosomes from lymphocyte populations.* BMC Immunology, 2009. **10**(1): p. 41.

390. Graham, J.M., *Isolation of Lysosomes from Tissues and Cells by Differential and Density Gradient Centrifugation.* Current Protocols in Cell Biology, 2000. **7**(1): p. 3.6.1-3.6.21.

391. Levine, B. and D.J. Klionsky, *Autophagy wins the 2016 Nobel Prize in Physiology or Medicine: Breakthroughs in baker's yeast fuel advances in biomedical research.* Proceedings of the National Academy of Sciences, 2017. **114**(2): p. 201.

392. Nassour, J., et al., *Autophagic cell death restricts chromosomal instability during replicative crisis.* Nature, 2019. **565**(7741): p. 659-663.

393. Galluzzi, L., et al., *Autophagy in malignant transformation and cancer progression.* The EMBO Journal, 2015. **34**(7): p. 856-880.

394. Li, S., A. Balmain, and C.M. Counter, *A model for RAS mutation patterns in cancers: finding the sweet spot.* Nat Rev Cancer, 2018. **18**(12): p. 767-777.

395. Castellano, E. and E. Santos, *Functional specificity of ras isoforms: so similar but so different.* Genes & cancer, 2011. **2**(3): p. 216-231.

396. Olsen, S.N., et al., *Loss of RasGAP Tumor Suppressors Underlies the Aggressive Nature of Luminal B Breast Cancers.* Cancer Discovery, 2017. **7**(2): p. 202.

397. Sears, R. and J.W. Gray, *Epigenomic Inactivation of RasGAPs Activates RAS Signaling in a Subset of Luminal B Breast Cancers.* Cancer Discov, 2017. **7**(2): p. 131-133.

398. Kim, M.S., et al., *p38 kinase is a key signaling molecule for H-Ras-induced cell motility and invasive phenotype in human breast epithelial cells.* Cancer Res, 2003. **63**(17): p. 5454-61.

399. Kinsey, C.G., et al., *Protective autophagy elicited by RAF-->MEK-->ERK inhibition suggests a treatment strategy for RAS-driven cancers.* Nat Med, 2019. **25**(4): p. 620-627.

400. Wang, Y., et al., *Autophagy inhibition specifically promotes epithelial-mesenchymal transition and invasion in RAS-mutated cancer cells.* Autophagy, 2019. **15**(5): p. 886-899.

401. Kim, M.J., et al., *Involvement of autophagy in oncogenic K-Ras-induced malignant cell transformation.* J Biol Chem, 2011. **286**(15): p. 12924-32.

402. Poillet-Perez, L., et al., *Autophagy maintains tumour growth through circulating arginine.* Nature, 2018. **563**(7732): p. 569-573.

403. Lock, R., et al., *Autophagy facilitates glycolysis during Ras-mediated oncogenic transformation.* Molecular biology of the cell, 2011. **22**(2): p. 165-178.

404. Guo, J.Y., et al., *Activated Ras requires autophagy to maintain oxidative metabolism and tumorigenesis.* Genes Dev, 2011. **25**(5): p. 460-70.

405. Goodspeed, A., et al., *Tumor-Derived Cell Lines as Molecular Models of Cancer Pharmacogenomics.* Molecular Cancer Research, 2016. **14**(1): p. 3.

406. Goodspeed, A., et al., *Tumor-Derived Cell Lines as Molecular Models of Cancer Pharmacogenomics.* Molecular Cancer Research, 2016. **14**(1): p. 3-13.

407. Cowell, J.K., et al., *Molecular characterization of the t(3;9) associated with immortalization in the MCF10A cell line.* Cancer Genet Cytogenet, 2005. **163**(1): p. 23-9.

408. Kadota, M., et al., *Delineating Genetic Alterations for Tumor Progression in the MCF10A Series of Breast Cancer Cell Lines.* PLOS ONE, 2010. **5**(2): p. e9201.

409. Dow, L.E., et al., *Loss of human Scribble cooperates with H-Ras to promote cell invasion through deregulation of MAPK signalling.* Oncogene, 2008. **27**: p. 5988.

410. Wee, P. and Z. Wang, *Epidermal Growth Factor Receptor Cell Proliferation Signaling Pathways.* Cancers (Basel), 2017. **9**(5).

411. Pinilla-Macua, I., et al., *EGF receptor signaling, phosphorylation, ubiquitylation and endocytosis in tumors in vivo.* eLife, 2017. **6**: p. e31993.

412. Högnason, T., et al., *Epidermal growth factor receptor induced apoptosis: potentiation by inhibition of Ras signaling.* FEBS Letters, 2001. **491**(1): p. 9-15.

413. Gugnoni, M., et al., *Autophagy and epithelial–mesenchymal transition: an intricate interplay in cancer.* Cell Death and Disease, 2016. **7**: p. e2520.

414. Chavez, K.J., S.V. Garimella, and S. Lipkowitz, *Triple negative breast cancer cell lines: one tool in the search for better treatment of triple negative breast cancer.* Breast disease, 2010. **32**(1-2): p. 35-48.

415. Kraus, M.H., Y. Yuasa, and S.A. Aaronson, *A position 12-activated H-ras oncogene in all HS578T mammary carcinosarcoma cells but not normal mammary cells of the same patient.* Proc Natl Acad Sci U S A, 1984. **81**(17): p. 5384-8.

416. Dai, X., et al., *Breast Cancer Cell Line Classification and Its Relevance with Breast Tumor Subtyping.* Journal of Cancer, 2017. **8**(16): p. 3131-3141.

417. Dai, X., et al., *Cancer Hallmarks, Biomarkers and Breast Cancer Molecular Subtypes.* Journal of Cancer, 2016. **7**(10): p. 1281-1294.

418. Yin, L., et al., *Triple-negative breast cancer molecular subtyping and treatment progress.* Breast Cancer Research, 2020. **22**(1): p. 61.

419. Bertucci, F., P. Finetti, and D. Birnbaum, *Basal breast cancer: a complex and deadly molecular subtype.* Current molecular medicine, 2012. **12**(1): p. 96-110.

420. Elenbaas, B., et al., *Human breast cancer cells generated by oncogenic transformation of primary mammary epithelial cells.* Genes & development, 2001. **15**(1): p. 50-65.

421. Kimura, S., T. Noda, and T. Yoshimori, *Dissection of the autophagosome maturation process by a novel reporter protein, tandem fluorescent-tagged LC3.* Autophagy, 2007. **3**(5): p. 452-460.

422. Ganley, I.G., et al., *Distinct autophagosomal-lysosomal fusion mechanism revealed by thapsigargin-induced autophagy arrest.* Molecular cell, 2011. **42**(6): p. 731-743.

423. Yoshii, S.R. and N. Mizushima, *Monitoring and Measuring Autophagy.* International journal of molecular sciences, 2017. **18**(9): p. 1865.

424. Klionsky, D.J., et al., *Guidelines for the use and interpretation of assays for monitoring autophagy.* Autophagy, 2012. **8**(4): p. 445-544.

425. Inami, Y., et al., *Persistent activation of Nrf2 through p62 in hepatocellular carcinoma cells.* Journal of Cell Biology, 2011. **193**(2): p. 275-284.

426. Komatsu, M., et al., *The selective autophagy substrate p62 activates the stress responsive transcription factor Nrf2 through inactivation of Keap1.* Nature Cell Biology, 2010. **12**(3): p. 213-223.

427. Ichimura, Y., et al., *Phosphorylation of p62 Activates the Keap1-Nrf2 Pathway during Selective Autophagy.* Molecular Cell, 2013. **51**(5): p. 618-631.

428. El Guerrab, A., et al., *Anti-EGFR monoclonal antibodies and EGFR tyrosine kinase inhibitors as combination therapy for triple-negative breast cancer.* Oncotarget, 2016. **7**(45): p. 73618-73637.

429. Olayioye, M.A., et al., *The ErbB signaling network: receptor heterodimerization in development and cancer.* Embo j, 2000. **19**(13): p. 3159-67.

430. Yarden, Y. and M.X. Sliwkowski, *Untangling the ErbB signalling network.* Nat Rev Mol Cell Biol, 2001. **2**(2): p. 127-37.

431. Kalluri, R. and R.A. Weinberg, *The basics of epithelial-mesenchymal transition.* The Journal of clinical investigation, 2009. **119**(6): p. 1420-1428.

432. Christiansen, J.J. and A.K. Rajasekaran, *Reassessing epithelial to mesenchymal transition as a prerequisite for carcinoma invasion and metastasis.* Cancer Res, 2006. **66**(17): p. 8319-26.

433. Hugo, H., et al., *Epithelial requirement for in vitro proliferation and xenograft growth and metastasis of MDA-MB-468 human breast cancer cells: Oncogenic rather than tumor-suppressive role of E-cadherin.* Breast Cancer Research, 2017. **19**.

434. Azimi, I., et al., *Altered purinergic receptor-Ca2+ signaling associated with hypoxia-induced epithelial-mesenchymal transition in breast cancer cells.* Molecular Oncology, 2016. **10**(1): p. 166-178.

435. Chowdhury, S., et al., *Insights into autophagosome biogenesis from structural and biochemical analyses of the ATG2A-WIPI4 complex.* Proceedings of the National Academy of Sciences of the United States of America, 2018. **115**(42): p. E9792-E9801.

436. Koukourakis, M.I., et al., *Autophagosome Proteins LC3A, LC3B and LC3C Have Distinct Subcellular Distribution Kinetics and Expression in Cancer Cell Lines.* PloS one, 2015. **10**(9): p. e0137675-e0137675.

437. Ladoire, S., et al., *Immunohistochemical detection of cytoplasmic LC3 puncta in human cancer specimens.* Autophagy, 2012. **8**(8): p. 1175-1184.

438. Chan, L.L., et al., *A novel image-based cytometry method for autophagy detection in living cells.* Autophagy, 2012. **8**(9): p. 1371-82.

439. Runwal, G., et al., *LC3-positive structures are prominent in autophagy-deficient cells.* Scientific Reports, 2019. **9**(1): p. 10147.

440. Győrffy, B., et al., *An online survival analysis tool to rapidly assess the effect of 22,277 genes on breast cancer prognosis using microarray data of 1,809 patients.* Breast Cancer Res Treat, 2010. **123**(3): p. 725-31.

441. Nagy, Á., et al., *Validation of miRNA prognostic power in hepatocellular carcinoma using expression data of independent datasets.* Scientific Reports, 2018. **8**(1): p. 9227.

442. Yeo, S.Y., et al., *Transglutaminase 2 contributes to a TP53-induced autophagy program to prevent oncogenic transformation.* eLife, 2016. **5**: p. e07101-e07101.

443. Zhang, H. and N. McCarty, *Tampering with cancer chemoresistance by targeting the TGM2-IL6-autophagy regulatory network.* Autophagy, 2017. **13**(3): p. 627-628.

444. Junkins, R.D., C. McCormick, and T.-J. Lin, *The emerging potential of autophagy-based therapies in the treatment of cystic fibrosis lung infections.* Autophagy, 2014. **10**(3): p. 538-547.

445. Rabouille, C., *COPII vesicles and the expansion of the phagophore.* eLife, 2019. **8**: p. e44944.

446. Ge, L., L. Wilz, and R. Schekman, *Biogenesis of autophagosomal precursors for LC3 lipidation from the ER-Golgi intermediate compartment.* Autophagy, 2015. **11**(12): p. 2372-2374.

447. Dong, H., et al., *IFNg-induced Irgm1 promotes tumorigenesis of melanoma via dual regulation of apoptosis and Bif-1-dependent autophagy.* Oncogene, 2015. **34**(42): p. 5363-5371.

448. Chauhan, S., M.A. Mandell, and V. Deretic, *IRGM governs the core autophagy machinery to conduct antimicrobial defense.* Mol Cell, 2015. **58**(3): p. 507-21.

449. Davis, S., et al., *Sec24 phosphorylation regulates autophagosome abundance during nutrient deprivation.* Elife, 2016. **5**.

450. Cui, Y., et al., *A COPII subunit acts with an autophagy receptor to target endoplasmic reticulum for degradation.* Science (New York, N.Y.), 2019. **365**(6448): p. 53-60.

451. Pacheco, C.D., R. Kunkel, and A.P. Lieberman, *Autophagy in Niemann–Pick C disease is dependent upon Beclin-1 and responsive to lipid trafficking defects.* Human Molecular Genetics, 2007. **16**(12): p. 1495-1503.

452. Schultz, M.L., et al., *Coordinate regulation of mutant NPC1 degradation by selective ER autophagy and MARCH6-dependent ERAD.* Nature Communications, 2018. **9**(1): p. 3671.

453. Sarkar, S., et al., *Impaired Autophagy in the Lipid-Storage Disorder Niemann-Pick Type C1 Disease.* Cell Reports, 2013. **5**(5): p. 1302-1315.

454. Kuzu, O.F., et al., *Modulating cancer cell survival by targeting intracellular cholesterol transport.* British Journal of Cancer, 2017. **117**(4): p. 513-524.

455. Moussay, E., et al., *The acquisition of resistance to TNFα in breast cancer cells is associated with constitutive activation of autophagy as revealed by a transcriptome analysis using a custom microarray.* Autophagy, 2011. **7**(7): p. 760-70.

456. Kiyono, K., et al., *Autophagy is activated by TGF-beta and potentiates TGF-beta-mediated growth inhibition in human hepatocellular carcinoma cells.* Cancer Res, 2009. **69**(23): p. 8844-52.

457. Hu, J., et al., *MARCH5 RNA promotes autophagy, migration, and invasion of ovarian cancer cells.* Autophagy, 2017. **13**(2): p. 333-344.

458. Liang, C., et al., *TGFB1-induced autophagy affects the pattern of pancreatic cancer progression in distinct ways depending on SMAD4 status.* Autophagy, 2020. **16**(3): p. 486-500.

459. Nüchel, J., et al., *TGFB1 is secreted through an unconventional pathway dependent on the autophagic machinery and cytoskeletal regulators.* Autophagy, 2018. **14**(3): p. 465-486.

460. Nicoli, E.R., et al., *Determination of autophagy gene ATG16L1 polymorphism in human colorectal cancer.* Rom J Morphol Embryol, 2014. **55**(1): p. 57-62.

461. Fujita, N., et al., *The Atg16L complex specifies the site of LC3 lipidation for membrane biogenesis in autophagy.* Mol Biol Cell, 2008. **19**(5): p. 2092-100.

462. Walczak, M. and S. Martens, *Dissecting the role of the Atg12-Atg5-Atg16 complex during autophagosome formation.* Autophagy, 2013. **9**(3): p. 424-5.

463. Kabeya, Y., et al., *LC3, a mammalian homologue of yeast Apg8p, is localized in autophagosome membranes after processing.* EMBO J, 2000. **19**: p. 5720 - 5728.

464. Tanida, I., T. Ueno, and E. Kominami, *LC3 and Autophagy.* Methods Mol Biol, 2008. **445**: p. 77-88.

465. Mauthe, M. and F. Reggiori, *ATG proteins: Are we always looking at autophagy?* Autophagy, 2016. **12**(12): p. 2502-2503.

466. Mizushima, N., T. Yoshimori, and Y. Ohsumi, *The role of Atg proteins in autophagosome formation.* Annu Rev Cell Dev Biol, 2011. **27**: p. 107-32.

467. Gammoh, N., et al., *Interaction between FIP200 and ATG16L1 distinguishes ULK1 complex-dependent and -independent autophagy.* Nature structural & molecular biology, 2013. **20**(2): p. 144-149.

468. Alsaadi, R.M., et al., *ULK1-mediated phosphorylation of ATG16L1 promotes xenophagy, but destabilizes the ATG16L1 Crohn's mutant.* EMBO Rep, 2019.

469. Lystad, A.H., et al., *Distinct functions of ATG16L1 isoforms in membrane binding and LC3B lipidation in autophagy-related processes.* Nature cell biology, 2019. **21**(3): p. 372-383.

470. Li, S.S., et al., *p62/SQSTM1 interacts with vimentin to enhance breast cancer metastasis.* Carcinogenesis, 2017. **38**(11): p. 1092-1103.

471. Li, S.-S., et al., *p62/SQSTM1 interacts with vimentin to enhance breast cancer metastasis.* Carcinogenesis, 2017. **38**(11): p. 1092-1103.

472. Ellis, M.J. and C.M. Perou, *The Genomic Landscape of Breast Cancer as a Therapeutic Roadmap.* Cancer Discovery, 2013. **3**(1): p. 27.

473. Stephens, P.J., et al., *The landscape of cancer genes and mutational processes in breast cancer.* Nature, 2012. **486**(7403): p. 400-4.

474. Zardavas, D., W.A. Phillips, and S. Loi, *PIK3CA mutations in breast cancer: reconciling findings from preclinical and clinical data.* Breast Cancer Research, 2014. **16**(1): p. 201.

475. Yu, M., et al., *A developmentally regulated inducer of EMT, LBX1, contributes to breast cancer progression.* Genes Dev, 2009. **23**(15): p. 1737-42.

476. Mathew, R., et al., *Autophagy Suppresses Tumorigenesis through Elimination of p62.* Cell, 2009. **137**(6): p. 1062-1075.

477. Pankiv, S., et al., *p62/SQSTM1 binds directly to Atg8/LC3 to facilitate degradation of ubiquitinated protein aggregates by autophagy.* J Biol Chem, 2007. **282**(33): p. 24131-45.

478. Gatica, D., V. Lahiri, and D.J. Klionsky, *Cargo recognition and degradation by selective autophagy.* Nature cell biology, 2018. **20**(3): p. 233-242.

479. Rusten, T.E. and H. Stenmark, *p62, an autophagy hero or culprit?* Nature Cell Biology, 2010. **12**(3): p. 207-209.

480. Cohen-Kaplan, V., et al., *p62- and ubiquitin-dependent stress-induced autophagy of the mammalian 26S proteasome.* Proceedings of the National Academy of Sciences, 2016. **113**(47): p. E7490.

481. Kageyama, S., et al., *Proteasome dysfunction activates autophagy and the Keap1-Nrf2 pathway.* J Biol Chem, 2014. **289**(36): p. 24944-55.

482. Katsuragi, Y., Y. Ichimura, and M. Komatsu, *Regulation of the Keap1–Nrf2 pathway by p62/SQSTM1.* Current Opinion in Toxicology, 2016. **1**: p. 54-61.

483. Lisek, K., et al., *Mutant p53 tunes the NRF2-dependent antioxidant response to support survival of cancer cells.* Oncotarget, 2018. **9**(29): p. 20508-20523.

484. Jiang, X., et al., *VPS34 stimulation of p62 phosphorylation for cancer progression.* Oncogene, 2017. **36**: p. 6850.

485. Wang, L., X. Ye, and T. Zhao, *The physiological roles of autophagy in the mammalian life cycle.* Biological Reviews, 2019. **94**(2): p. 503-516.

486. Dunphy, F.R., et al., *Treatment of estrogen receptor-negative or hormonally refractory breast cancer with double high-dose chemotherapy intensification and bone marrow support.* Journal of Clinical Oncology, 1990. **8**(7): p. 1207-1216.

487. Blackwell, K.L., et al., *Randomized Study of Lapatinib Alone or in Combination With Trastuzumab in Women With ErbB2-Positive, Trastuzumab-Refractory Metastatic Breast Cancer.* Journal of Clinical Oncology, 2010. **28**(7): p. 1124-1130.

488. Karantza, V. and E. White, *Role of Autophagy in Breast Cancer.* Autophagy, 2007. **3**(6): p. 610-613.

489. Klionsky, D.J., et al., *Guidelines for the use and interpretation of assays for monitoring autophagy (3rd edition).* Autophagy, 2016. **12**(1): p. 1-222.

490. Chang, C.-H., et al., *A novel orally available seleno-purine molecule suppresses triple-negative breast cancer cell proliferation and progression to metastasis by inducing cytostatic autophagy.* Autophagy, 2019. **15**(8): p. 1376-1390.

491. Du, W.W., et al., *A circular RNA circ-DNMT1 enhances breast cancer progression by activating autophagy.* Oncogene, 2018. **37**(44): p. 5829-5842.

492. Zhang, H., et al., *Epigenetic Regulation of NAMPT by NAMPT-AS Drives Metastatic Progression in Triple-Negative Breast Cancer.* Cancer Research, 2019. **79**(13): p. 3347.

493. Carchman, E.H., et al., *Dysregulation of Autophagy Contributes to Anal Carcinogenesis.* PLOS ONE, 2016. **11**(10): p. e0164273.

494. Seranova, E., et al., *Dysregulation of autophagy as a common mechanism in lysosomal storage diseases.* Essays in biochemistry, 2017. **61**(6): p. 733-749.

495. Wu, W., et al., *The autophagic paradox in cancer therapy.* Oncogene, 2011. **31**: p. 939-53.

496. Limpert, A.S., et al., *Autophagy in Cancer: Regulation by Small Molecules.* Trends in pharmacological sciences, 2018. **39**(12): p. 1021-1032.

497. Cichowski, K. and T. Jacks, *NF1 Tumor Suppressor Gene Function: Narrowing the GAP.* Cell, 2001. **104**(4): p. 593-604.

498. Ogata, H., et al., *Human breast cancer MDA-MB-231 cells fail to express the neurofibromin protein, lack its type I mRNA isoform and show accumulation of P-MAPK and activated Ras.* Cancer Lett, 2001. **172**(2): p. 159-64.

499. Sears, R. and J.W. Gray, *Epigenomic Inactivation of RasGAPs Activates RAS Signaling in a Subset of Luminal B Breast Cancers.* Cancer Discovery, 2017. **7**(2): p. 131.

500. Stephen, A.G., et al., *Dragging ras back in the ring.* Cancer Cell, 2014. **25**(3): p. 272-81.

501. Maertens, O. and K. Cichowski, *An expanding role for RAS GTPase activating proteins (RAS GAPs) in cancer.* Adv Biol Regul, 2014. **55**: p. 1-14.

502. Kiuru, M. and K.J. Busam, *The NF1 gene in tumor syndromes and melanoma.* Laboratory Investigation, 2017. **97**(2): p. 146-157.

503. Davis, F.M., et al., *Induction of epithelial-mesenchymal transition (EMT) in breast cancer cells is calcium signal dependent.* Oncogene, 2014. **33**(18): p. 2307-2316.

504. Liu, Y.-L., et al., *Assessing metastatic potential of breast cancer cells based on EGFR dynamics.* Scientific reports, 2019. **9**(1): p. 3395-3395.

505. Lo, H.-W., et al., *Epidermal Growth Factor Receptor Cooperates with Signal Transducer and Activator of Transcription 3 to Induce Epithelial-Mesenchymal Transition in Cancer Cells via Up-regulation of TWIST Gene Expression.* Cancer Research, 2007. **67**(19): p. 9066.

506. Davis, F.M., et al., *Assessment of gene expression of intracellular calcium channels, pumps and exchangers with epidermal growth factor-induced epithelial-mesenchymal transition in a breast cancer cell line.* Cancer Cell Int, 2013. **13**(1): p. 76.

507. Verma, N., et al., *PYK2 sustains endosomal-derived receptor signalling and enhances epithelial-to-mesenchymal transition.* Nature Communications, 2015. **6**(1): p. 6064.

508. Hugo, H.J., et al., *Epithelial requirement for in vitro proliferation and xenograft growth and metastasis of MDA-MB-468 human breast cancer cells: oncogenic rather than tumor-suppressive role of E-cadherin.* Breast Cancer Research, 2017. **19**(1): p. 86.

509. Ichimura, Y., et al., *Structural Basis for Sorting Mechanism of p62 in Selective Autophagy.* Journal of Biological Chemistry, 2008. **283**(33): p. 22847-22857.

510. Sanchez-Garrido, J., V. Sancho-Shimizu, and A.R. Shenoy, *Regulated proteolysis of p62/SQSTM1 enables differential control of autophagy and nutrient sensing.* Science Signaling, 2018. **11**(559): p. eaat6903.

511. Walker, A., et al., *Nrf2 signaling and autophagy are complementary in protecting breast cancer cells during glucose deprivation.* Free radical biology & medicine, 2018. **120**: p. 407-413.

512. Villar, V.H., et al., *mTORC1 inhibition in cancer cells protects from glutaminolysis-mediated apoptosis during nutrient limitation.* Nature communications, 2017. **8**: p. 14124-14124.

513. Weidberg, H., et al., *LC3 and GATE-16/GABARAP subfamilies are both essential yet act differently in autophagosome biogenesis.* The EMBO journal, 2010. **29**(11): p. 1792-1802.

514. Berthier, A., et al., *High expression of gabarapl1 is associated with a better outcome for patients with lymph node-positive breast cancer.* British journal of cancer, 2010. **102**(6): p. 1024-1031.

515. Boyer-Guittaut, M., et al., *The role of GABARAPL1/GEC1 in autophagic flux and mitochondrial quality control in MDA-MB-436 breast cancer cells.* Autophagy, 2014. **10**(6): p. 986-1003.

516. Eng, C.H., et al., *Macroautophagy is dispensable for growth of KRAS mutant tumors and chloroquine efficacy.* Proceedings of the National Academy of Sciences, 2016. **113**(1): p. 182-187.

517. Nyfeler, B. and C.H. Eng, *Revisiting autophagy addiction of tumor cells.* Autophagy, 2016. **12**(7): p. 1206-1207.

518. Bishop, E. and T.D. Bradshaw, *Autophagy modulation: a prudent approach in cancer treatment?* Cancer Chemotherapy and Pharmacology, 2018. **82**(6): p. 913-922.

519. Guo, J.Y., et al., *Autophagy suppresses progression of K-ras-induced lung tumors to oncocytomas and maintains lipid homeostasis.* Genes & development, 2013. **27**(13): p. 1447-1461.

520. Endo, S., et al., *Autophagy Is Required for Activation of Pancreatic Stellate Cells, Associated With Pancreatic Cancer Progression and Promotes Growth of Pancreatic Tumors in Mice.* Gastroenterology, 2017. **152**(6): p. 1492-1506.e24.

521. Yang, A., et al., *Autophagy is critical for pancreatic tumor growth and progression in tumors with p53 alterations.* Cancer discovery, 2014. **4**(8): p. 905-913.

522. Zhan, Z., et al., *Autophagy facilitates TLR4- and TLR3-triggered migration and invasion of lung cancer cells through the promotion of TRAF6 ubiquitination.* Autophagy, 2014. **10**(2): p. 257-268.

523. Lauzier, A., et al., *Colorectal cancer cells respond differentially to autophagy inhibition in vivo.* Scientific Reports, 2019. **9**(1): p. 11316.

524. Yang, A., et al., *Autophagy Sustains Pancreatic Cancer Growth through Both Cell-Autonomous and Nonautonomous Mechanisms.* Cancer Discovery, 2018. **8**(3): p. 276.

525. Wu, Y.T., et al., *Dual role of 3-methyladenine in modulation of autophagy via different temporal patterns of inhibition on class I and III phosphoinositide 3-kinase.* J Biol Chem, 2010. **285**(14): p. 10850-61.

526. Yang, L., et al., *BH3 mimetic ABT-737 sensitizes colorectal cancer cells to ixazomib through MCL-1 downregulation and autophagy inhibition.* Am J Cancer Res, 2016. **6**(6): p. 1345-57.

527. Feng, Y., et al., *Autophagy Inhibitor (LY294002) and 5-fluorouracil (5-FU) Combination-Based Nanoliposome for Enhanced Efficacy Against Esophageal Squamous Cell Carcinoma.* Nanoscale Res Lett, 2018. **13**(1): p. 325.

528. Martin, K.R., et al., *A Potent and Selective ULK1 Inhibitor Suppresses Autophagy and Sensitizes Cancer Cells to Nutrient Stress.* iScience, 2018. **8**: p. 74-84.

529. Liu, X., et al., *Inhibition of Autophagy by Chloroquine Enhances the Antitumor Efficacy of Sorafenib in Glioblastoma.* Cell Mol Neurobiol, 2016. **36**(7): p. 1197-208.

530. Foster, F.M., et al., *The phosphoinositide (PI) 3-kinase family.* Journal of Cell Science, 2003. **116**(15): p. 3037.

531. Fruman, D.A. and C. Rommel, *PI3K and cancer: lessons, challenges and opportunities.* Nature reviews. Drug discovery, 2014. **13**(2): p. 140-156.

532. Ronan, B., et al., *A highly potent and selective Vps34 inhibitor alters vesicle trafficking and autophagy.* Nature Chemical Biology, 2014. **10**: p. 1013.

533. Heckmann, B.L., et al., *The autophagic inhibitor 3-methyladenine potently stimulates PKA-dependent lipolysis in adipocytes.* British journal of pharmacology, 2013. **168**(1): p. 163-171.

534. Shenoy, N., et al., *Drugs with anti-oxidant properties can interfere with cell viability measurements by assays that rely on the reducing property of viable cells.* Laboratory Investigation, 2017. **97**(5): p. 494-497.

535. Pasquier, B., et al., *Discovery of (2S)-8-[(3R)-3-methylmorpholin-4-yl]-1-(3-methyl-2-oxobutyl)-2-(trifluoromethyl)-3,4-dihydro-2H-pyrimido[1,2-a]pyrimidin-6-one: a novel potent and selective inhibitor of Vps34 for the treatment of solid tumors.* J Med Chem, 2015. **58**(1): p. 376-400.

536. Onorati, A.V., et al., *Targeting autophagy in cancer.* Cancer, 2018. **124**(16): p. 3307-3318.

537. Guicciardi, M.E., M. Leist, and G.J. Gores, *Lysosomes in cell death.* Oncogene, 2004. **23**(16): p. 2881-2890.

538. Pavlinov, I., M. Salkovski, and L.N. Aldrich, *Beclin 1–ATG14L Protein–Protein Interaction Inhibitor Selectively Inhibits Autophagy through Disruption of VPS34 Complex I.* Journal of the American Chemical Society, 2020. **142**(18): p. 8174-8182.

539. Stjepanovic, G., et al., *Unveiling the role of VPS34 kinase domain dynamics in regulation of the autophagic PI3K complex.* Molecular & Cellular Oncology, 2017. **4**(6): p. e1367873.

540. Punnonen, E.L., V.S. Marjomäki, and H. Reunanen, *3-Methyladenine inhibits transport from late endosomes to lysosomes in cultured rat and mouse fibroblasts.* Eur J Cell Biol, 1994. **65**(1): p. 14-25.

541. Carpentier, S., et al., *Class III Phosphoinositide 3-Kinase/VPS34 and Dynamin are Critical for Apical Endocytic Recycling.* Traffic, 2013. **14**(8): p. 933-948.

542. Codogno, P., M. Mehrpour, and T. Proikas-Cezanne, *Canonical and non-canonical autophagy: variations on a common theme of self-eating?* Nat Rev Mol Cell Biol, 2011. **13**(1): p. 7-12.

543. Kaushik, S., et al., *Constitutive activation of chaperone-mediated autophagy in cells with impaired macroautophagy.* Molecular biology of the cell, 2008. **19**(5): p. 2179-2192.

544. Jaber, N. and W.X. Zong, *Class III PI3K Vps34: essential roles in autophagy, endocytosis, and heart and liver function.* Ann N Y Acad Sci, 2013. **1280**: p. 48-51.

545. Jaber, N., et al., *Class III PI3K Vps34 plays an essential role in autophagy and in heart and liver function.* Proc Natl Acad Sci U S A, 2012. **109**(6): p. 2003-8.

546. Jiang, X., et al., *VPS34 stimulation of p62 phosphorylation for cancer progression.* Oncogene, 2017. **36**(50): p. 6850-6862.

547. Noman, M.Z., et al., *Inhibition of Vps34 reprograms cold into hot inflamed tumors and improves anti–PD-1/PD-L1 immunotherapy.* Science Advances, 2020. **6**(18): p. eaax7881.

548. Dyczynski, M., et al., *Targeting autophagy by small molecule inhibitors of vacuolar protein sorting 34 (Vps34) improves the sensitivity of breast cancer cells to Sunitinib.* Cancer Lett, 2018. **435**: p. 32-43.

549. Ohashi, Y., S. Tremel, and R.L. Williams, *VPS34 complexes from a structural perspective.* Journal of lipid research, 2019. **60**(2): p. 229-241.

550. Baskaran, S., et al., *Architecture and dynamics of the autophagic phosphatidylinositol 3-kinase complex.* eLife, 2014. **3**: p. e05115.

551. Stjepanovic, G., et al., *Vps34 Kinase Domain Dynamics Regulate the Autophagic PI 3-Kinase Complex.* Molecular cell, 2017. **67**(3): p. 528-534.e3.

552. Ohashi, Y., et al., *Membrane characteristics tune activities of endosomal and autophagic human VPS34 complexes.* eLife, 2020. **9**: p. e58281.

553. Dyczynski, M., et al., *Targeting autophagy by small molecule inhibitors of vacuolar protein sorting 34 (Vps34) improves the sensitivity of breast cancer cells to Sunitinib.* Cancer Letters, 2018. **435**: p. 32-43.

554. Turturro, S.B., et al., *Somatic loss of PIK3R1 may sensitize breast cancer to inhibitors of the MAPK pathway.* Breast Cancer Res Treat, 2019. **177**(2): p. 325-333.

555. Chen, L., et al., *Characterization of PIK3CA and PIK3R1 somatic mutations in Chinese breast cancer patients.* Nature Communications, 2018. **9**(1): p. 1357.

556. Cheung, L.W.T., et al., *Naturally occurring neomorphic PIK3R1 mutations activate the MAPK pathway, dictating therapeutic response to MAPK pathway inhibitors.* Cancer cell, 2014. **26**(4): p. 479-494.

557. Chicote, J., et al., *Cell Death Triggered by the Autophagy Inhibitory Drug 3-Methyladenine in Growing Conditions Proceeds With DNA Damage.* Frontiers in Pharmacology, 2020. **11**: p. 1632.

558. Quinn, H.M., et al., *YAP and β-Catenin Cooperate to Drive Oncogenesis in Basal Breast Cancer.* Cancer Res, 2021. **81**(8): p. 2116-2127.

559. Aragona, M., et al., *A mechanical checkpoint controls multicellular growth through YAP/TAZ regulation by actin-processing factors.* Cell, 2013. **154**(5): p. 1047-1059.

560. Petrilli, A.M. and C. Fernández-Valle, *Role of Merlin/NF2 inactivation in tumor biology.* Oncogene, 2016. **35**(5): p. 537-548.

561. Hirsch, D.S., et al., *pp60^{c-Src} Phosphorylates and Activates Vacuolar Protein Sorting 34 to Mediate Cellular Transformation.* Cancer Research, 2010. **70**(14): p. 5974.

562. Cai, H., et al., *Differential transformation capacity of Src family kinases during the initiation of prostate cancer.* Proc Natl Acad Sci U S A, 2011. **108**(16): p. 6579-84.

563. Whitesell, L., et al., *Inhibition of heat shock protein HSP90-pp60v-src heteroprotein complex formation by benzoquinone ansamycins: essential role for stress proteins in oncogenic transformation.* Proc Natl Acad Sci U S A, 1994. **91**(18): p. 8324-8.

564. Gilani, R.A., et al., *UM-164: A Potent c-Src/p38 Kinase Inhibitor with In Vivo Activity against Triple-Negative Breast Cancer.* Clin Cancer Res, 2016. **22**(20): p. 5087-5096.

565. Ahearn, I.M., et al., *Regulating the regulator: post-translational modification of RAS.* Nature Reviews Molecular Cell Biology, 2012. **13**(1): p. 39-51.

566. Nussinov, R., C.-J. Tsai, and H. Jang, *Oncogenic Ras Isoforms Signaling Specificity at the Membrane.* Cancer Research, 2018. **78**(3): p. 593.

567. Nussinov, R., C.J. Tsai, and H. Jang, *Oncogenic Ras Isoforms Signaling Specificity at the Membrane.* Cancer Res, 2018. **78**(3): p. 593-602.

568. Chiu, V.K., et al., *Ras signalling on the endoplasmic reticulum and the Golgi.* Nature Cell Biology, 2002. **4**(5): p. 343-350.

569. Apolloni, A., et al., *H-ras but not K-ras traffics to the plasma membrane through the exocytic pathway.* Molecular and cellular biology, 2000. **20**(7): p. 2475-2487.

570. Na, Y., et al., *Bafilomycin A1 targets both autophagy and apoptosis pathways in pediatric B-cell acute lymphoblastic leukemia.* Haematologica, 2015. **100**(3): p. 345-356.

571. Li, L.Q., et al., *Inhibition of autophagy by bafilomycin A1 promotes chemosensitivity of gastric cancer cells.* Tumour Biol, 2016. **37**(1): p. 653-9.

572. Wu, Y.C., et al., *Inhibition of macroautophagy by bafilomycin A{sub 1} lowers proliferation and induces apoptosis in colon cancer cells.* 2009.

573. Hämälistö, S. and M. Jäättelä, *Lysosomes in cancer-living on the edge (of the cell).* Current opinion in cell biology, 2016. **39**: p. 69-76.

574. Petersen, N.H., et al., *Transformation-associated changes in sphingolipid metabolism sensitize cells to lysosomal cell death induced by inhibitors of acid sphingomyelinase.* Cancer Cell, 2013. **24**(3): p. 379-93.

575. Zhou, J., et al., *Chaperone-mediated autophagy regulates proliferation by targeting RND3 in gastric cancer.* Autophagy, 2016. **12**(3): p. 515-528.

576. Han, Q., et al., *Downregulation of ATG5-dependent macroautophagy by chaperone-mediated autophagy promotes breast cancer cell metastasis.* Scientific Reports, 2017. **7**(1): p. 4759.

577. Morgan, M.J., et al., *Metastatic cells are preferentially vulnerable to lysosomal inhibition.* Proc Natl Acad Sci U S A, 2018. **115**(36): p. E8479-e8488.

578. Kaushik, S. and A.M. Cuervo, *Proteostasis and aging.* Nature Medicine, 2015. **21**(12): p. 1406-1415.

579. Kaushik, S. and A.M. Cuervo, *The coming of age of chaperone-mediated autophagy.* Nature Reviews Molecular Cell Biology, 2018. **19**(6): p. 365-381.

580. Dong, S., et al., *Monitoring spatiotemporal changes in chaperone-mediated autophagy in vivo.* Nature Communications, 2020. **11**(1): p. 645.

581. Cuervo, A.M. and J.F. Dice, *Unique properties of lamp2a compared to other lamp2 isoforms.* J Cell Sci, 2000. **113 Pt 24**: p. 4441-50.

582. Cuervo, A.M., J.F. Dice, and E. Knecht, *A population of rat liver lysosomes responsible for the selective uptake and degradation of cytosolic proteins.* J Biol Chem, 1997. **272**(9): p. 5606-15.

583. Li, W., et al., *Phosphorylation of LAMP2A by p38 MAPK couples ER stress to chaperone-mediated autophagy.* Nature Communications, 2017. **8**(1): p. 1763.

584. Wang, R., et al., *Tumor cells induce LAMP2a expression in tumor-associated macrophage for cancer progression.* EBioMedicine, 2019. **40**: p. 118-134.

585. Wang, Y., et al., *Discovery of LAMP-2A as potential biomarkers for glioblastoma development by modulating apoptosis through N-CoR degradation.* Cell Communication and Signaling, 2021. **19**(1): p. 40.

586. Xuan, Y., et al., *Inhibition of chaperone-mediated autophagy reduces tumor growth and metastasis and promotes drug sensitivity in colorectal cancer.* Mol Med Rep, 2021. **23**(5): p. 360.

587. Saha, T., *LAMP2A overexpression in breast tumors promotes cancer cell survival via chaperone-mediated autophagy.* Autophagy, 2012. **8**(11): p. 1643-1656.

588. Zheng, H., et al., *Lamp2 inhibits epithelial-mesenchymal transition by suppressing Snail expression in HCC.* Oncotarget, 2018. **9**(54): p. 30240-30252.

589. Tokarchuk, I., et al., *Increased LAMP2A levels correlate with a shorter disease-free survival of HER2 negative breast cancer patients and increased breast cancer cell viability.* Biochemical and Biophysical Research Communications, 2021. **569**: p. 47-53.

590. Chi, C., et al., *LAMP-2B regulates human cardiomyocyte function by mediating autophagosome–lysosome fusion.* Proceedings of the National Academy of Sciences, 2019. **116**(2): p. 556.

591. Fujiwara, Y., et al., *An RNautophagy/DNautophagy receptor, LAMP2C, possesses an arginine-rich motif that mediates RNA/DNA-binding.* Biochem Biophys Res Commun, 2015. **460**(2): p. 281-6.

592. Massey, A.C., et al., *Consequences of the selective blockage of chaperone-mediated autophagy.* Proceedings of the National Academy of Sciences, 2006. **103**(15): p. 5805.

593. Charafe-Jauffret, E., et al., *Gene expression profiling of breast cell lines identifies potential new basal markers.* Oncogene, 2006. **25**(15): p. 2273-2284.

594. Bandyopadhyay, U., et al., *Identification of regulators of chaperone-mediated autophagy.* Mol Cell, 2010. **39**(4): p. 535-47.

595. Nishino, I., et al., *Primary LAMP-2 deficiency causes X-linked vacuolar cardiomyopathy and myopathy (Danon disease).* Nature, 2000. **406**(6798): p. 906-10.

596. Li, Z., et al., *Fusion protein engineered exosomes for targeted degradation of specific RNAs in lysosomes: a proof-of-concept study.* Journal of Extracellular Vesicles, 2020. **9**(1): p. 1816710.

597. Fujiwara, Y., et al., *Discovery of a novel type of autophagy targeting RNA.* Autophagy, 2013. **9**(3): p. 403-409.

598. Sahu, R., et al., *Microautophagy of cytosolic proteins by late endosomes.* Dev Cell, 2011. **20**(1): p. 131-9.

599. Han, Q., et al., *Downregulation of ATG5-dependent macroautophagy by chaperone-mediated autophagy promotes breast cancer cell metastasis.* Scientific Reports, 2017. **7**.

600. Zhang, J., et al., *A more efficient RNAi inducible system for tight regulation of gene expression in mammalian cells and xenograft animals.* RNA (New York, N.Y.), 2007. **13**(8): p. 1375-1383.

601. Tang, J., et al., *Impaired p65 degradation by decreased chaperone-mediated autophagy activity facilitates epithelial-to-mesenchymal transition.* Oncogenesis, 2017. **6**(10): p. e387-e387.

602. Morell, C., et al., *Up-Regulated Expression of LAMP2 and Autophagy Activity during Neuroendocrine Differentiation of Prostate Cancer LNCaP Cells.* PLOS ONE, 2016. **11**(9): p. e0162977.

603. Hahm, E.-R., et al., *The Role of Lysosome-associated Membrane Protein 2 in Prostate Cancer Chemopreventive Mechanisms of Sulforaphane.* Cancer Prevention Research, 2020. **13**(8): p. 661.

604. Tokarchuk, I., et al., *Increased LAMP2A levels correlate with a shorter disease-free survival of HER2 negative breast cancer patients and increased breast cancer cell viability.* Biochem Biophys Res Commun, 2021. **569**: p. 47-53.

605. Ichikawa, A., et al., *Chaperone-Mediated Autophagy-Dependent Chemoresistance in Non-Small Cell Lung Cancer.* European Respiratory Journal, 2019. **54**(suppl 63): p. OA1605.

606. Losmanová, T., et al., *Chaperone-Mediated Autophagy Markers LAMP2A and HSC70 Are Independent Adverse Prognostic Markers in Primary Resected Squamous Cell Carcinomas of the Lung.* Oxid Med Cell Longev, 2020. **2020**: p. 8506572.

607. Rothaug, M., et al., *LAMP-2 deficiency leads to hippocampal dysfunction but normal clearance of neuronal substrates of chaperone-mediated autophagy in a mouse model for Danon disease.* Acta Neuropathologica Communications, 2015. **3**(1): p. 6.

608. Paul, A., et al., *PKCζ Promotes Breast Cancer Invasion by Regulating Expression of E-cadherin and Zonula Occludens-1 (ZO-1) via NFκB-p65.* Scientific reports, 2015. **5**: p. 12520-12520.

609. Chu, K., et al., *The paradox of E-cadherin: role in response to hypoxia in the tumor microenvironment and regulation of energy metabolism.* Oncotarget, 2013. **4**(3): p. 446-62.

610. Hugo, H.J., et al., *Epithelial requirement for in vitro proliferation and xenograft growth and metastasis of MDA-MB-468 human breast cancer cells: oncogenic rather than tumor-suppressive role of E-cadherin.* Breast Cancer Res, 2017. **19**(1): p. 86.

611. Ferreira, J.V., et al., *STUB1/CHIP is required for HIF1A degradation by chaperone-mediated autophagy.* Autophagy, 2013. **9**(9): p. 1349-1366.

612. Hubbi, M.E., et al., *Chaperone-mediated autophagy targets hypoxia-inducible factor-1α (HIF-1α) for lysosomal degradation.* J Biol Chem, 2013. **288**(15): p. 10703-14.

613. Hubbi, M.E., et al., *Chaperone-mediated Autophagy Targets Hypoxia-inducible Factor-1α (HIF-1α) for Lysosomal Degradation* *. Journal of Biological Chemistry, 2013. **288**(15): p. 10703-10714.

614. Zhang, J., et al., *Inflammation-induced inhibition of chaperone-mediated autophagy maintains the immunosuppressive function of murine mesenchymal stromal cells.* Cellular & Molecular Immunology, 2021. **18**(6): p. 1476-1488.

615. Davis, F.M., et al., *Induction of epithelial–mesenchymal transition (EMT) in breast cancer cells is calcium signal dependent.* Oncogene, 2014. **33**(18): p. 2307-2316.

616. Kon, M., et al., *Chaperone-mediated autophagy is required for tumor growth.* Science translational medicine, 2011. **3**(109): p. 109ra117-109ra117.

617. Peng, M., et al., *Intracellular citrate accumulation by oxidized ATM-mediated metabolism reprogramming via PFKP and CS enhances hypoxic breast cancer cell invasion and metastasis.* Cell Death & Disease, 2019. **10**(3): p. 228.

618. Nasr, Z., et al., *eIF4F suppression in breast cancer affects maintenance and progression.* Oncogene, 2013. **32**(7): p. 861-871.

619. Rubio, C.A., et al., *Transcriptome-wide characterization of the eIF4A signature highlights plasticity in translation regulation.* Genome Biology, 2014. **15**(10): p. 476.

620. Damaghi, M., et al., *Chronic acidosis in the tumour microenvironment selects for overexpression of LAMP2 in the plasma membrane.* Nature Communications, 2015. **6**: p. 8752.

621. Rauschner, M., et al., *Impact of the acidic environment on gene expression and functional parameters of tumors in vitro and in vivo.* Journal of Experimental & Clinical Cancer Research, 2021. **40**(1): p. 10.

622. Savic, L.J., et al., *Molecular Imaging of Extracellular Tumor pH to Reveal Effects of Locoregional Therapy on Liver Cancer Microenvironment.* Clin Cancer Res, 2020. **26**(2): p. 428-438.

623. Sameni, M., K. Moin, and B. Sloane, *Imaging Proteolysis by Living Human Breast Cancer Cells.* Neoplasia (New York, N.Y.), 2000. **2**: p. 496-504.

624. Feng, Y., et al., *The machinery of macroautophagy.* Cell Research, 2014. **24**(1): p. 24-41.

625. Amaravadi, R., A. Kimmelman, and E. White, *Recent insights into the function of autophagy in cancer.* Genes & Development, 2016. **30**: p. 1913-1930.

626. Kondo, Y., et al., *The role of autophagy in cancer development and response to therapy.* Nature Reviews Cancer, 2005. **5**(9): p. 726-734.

627. Bustos, S.O., et al., *Emerging Autophagy Functions Shape the Tumor Microenvironment and Play a Role in Cancer Progression - Implications for Cancer Therapy.* Frontiers in Oncology, 2020. **10**(2549).

628. Kim, M.-J., et al., *Involvement of autophagy in oncogenic K-Ras-induced malignant cell transformation.* The Journal of biological chemistry, 2011. **286**(15): p. 12924-12932.

629. Eng, C.H., et al., *Macroautophagy is dispensable for growth of KRAS mutant tumors and chloroquine efficacy.* Proceedings of the National Academy of Sciences, 2016. **113**(1): p. 182.

630. Bryant, K.L., et al., *Combination of ERK and autophagy inhibition as a treatment approach for pancreatic cancer.* Nature medicine, 2019. **25**(4): p. 628-640.

631. Wolpin, B.M., et al., *Phase II and pharmacodynamic study of autophagy inhibition using hydroxychloroquine in patients with metastatic pancreatic adenocarcinoma.* The oncologist, 2014. **19**(6): p. 637-638.

632. Zeh, H.J., et al., *A Randomized Phase II Preoperative Study of Autophagy Inhibition with High-Dose Hydroxychloroquine and Gemcitabine/Nab-Paclitaxel in Pancreatic Cancer Patients.* Clin Cancer Res, 2020. **26**(13): p. 3126-3134.

633. AlMasri, S.S., et al., *Encouraging long-term survival following autophagy inhibition using neoadjuvant hydroxychloroquine and gemcitabine for high-risk patients with resectable pancreatic carcinoma.* Cancer Medicine, 2021. **10**(20): p. 7233-7241.

634. Xu, R., et al., *The clinical value of using chloroquine or hydroxychloroquine as autophagy inhibitors in the treatment of cancers: A systematic review and meta-analysis.* Medicine, 2018. **97**(46).

635. Mukhopadhyay, S., et al., *Autophagy is required for proper cysteine homeostasis in pancreatic cancer through regulation of SLC7A11.* Proceedings of the National Academy of Sciences, 2021. **118**(6): p. e2021475118.

636. Qadir, M.A., et al., *Macroautophagy inhibition sensitizes tamoxifen-resistant breast cancer cells and enhances mitochondrial depolarization.* Breast Cancer Res Treat, 2008. **112**(3): p. 389-403.

637. Pagotto, A., et al., *Autophagy inhibition reduces chemoresistance and tumorigenic potential of human ovarian cancer stem cells.* Cell Death & Disease, 2017. **8**(7): p. e2943-e2943.

638. Sun, C., et al., *miR-34a mediates oxaliplatin resistance of colorectal cancer cells by inhibiting macroautophagy via transforming growth factor-β/Smad4 pathway.* World journal of gastroenterology, 2017. **23**(10): p. 1816-1827.

639. Lee, K.-H., et al., *Proteasome Inhibitor-Induced IκB/NF-κB Activation is Mediated by Nrf2-Dependent Light Chain 3B Induction in Lung Cancer Cells.* Molecules and cells, 2018. **41**(12): p. 1008-1015.

640. Bousquet, G., et al., *Targeting autophagic cancer stem-cells to reverse chemoresistance in human triple negative breast cancer.* Oncotarget, 2017. **8**(21): p. 35205-35221.

641. Karasic, T.B., et al., *Effect of Gemcitabine and nab-Paclitaxel With or Without Hydroxychloroquine on Patients With Advanced Pancreatic Cancer: A Phase 2 Randomized Clinical Trial.* JAMA Oncology, 2019. **5**(7): p. 993-998.

642. Hong, T.S., et al., *Long Term Follow-up of a Phase II Study of Autophagy Inhibition with Hydroxychloroquine (HCQ) and Preoperative (Preop) Short Course Chemoradiation (SCRT) Followed by Early Surgery for Resectable Ductal Adenocarcinoma of the Head of Pancreas (PDAC).* International Journal of Radiation Oncology, Biology, Physics, 2020. **108**(3): p. S151.

643. Wu, Y.C., et al., *Inhibition of macroautophagy by bafilomycin A1 lowers proliferation and induces apoptosis in colon cancer cells.* Biochemical and Biophysical Research Communications, 2009. **382**(2): p. 451-456.

644. He, K., et al., *Phase II Clinical Trial Evaluating Complete Metastasis Ablation After Progression on Checkpoint Inhibition.* International Journal of Radiation Oncology*Biology*Physics, 2021. **111**(3, Supplement): p. e471-e472.

645. Luan, F.L., et al., *Rapamycin is an effective inhibitor of human renal cancer metastasis11See Editorial by Sukhatme and Strom, p. 1160.* Kidney International, 2003. **63**(3): p. 917-926.

646. Alayev, A., et al., *The combination of rapamycin and resveratrol blocks autophagy and induces apoptosis in breast cancer cells.* Journal of cellular biochemistry, 2015. **116**(3): p. 450-457.

647. Rezazadeh, D., et al., *Rapamycin Reduces Cervical Cancer Cells Viability in Hypoxic Condition: Investigation of the Role of Autophagy and Apoptosis.* OncoTargets and therapy, 2020. **13**: p. 4239-4247.

648. Gremke, N., et al., *mTOR-mediated cancer drug resistance suppresses autophagy and generates a druggable metabolic vulnerability.* Nature Communications, 2020. **11**(1): p. 4684.

649. Cann, G.M., et al., *Developmental expression of LC3alpha and beta: absence of fibronectin or autophagy phenotype in LC3beta knockout mice.* Dev Dyn, 2008. **237**(1): p. 187-95.

650. Putyrski, M., et al., *Disrupting the LC3 Interaction Region (LIR) Binding of Selective Autophagy Receptors Sensitizes AML Cell Lines to Cytarabine.* Frontiers in Cell and Developmental Biology, 2020. **8**: p. 208.

651. Gray, J.P., et al., *Directed evolution of cyclic peptides for inhibition of autophagy.* Chemical Science, 2021. **12**(10): p. 3526-3543.

652. Gomes-da-Silva, L.C., et al., *Recruitment of LC3 to damaged Golgi apparatus.* Cell Death & Differentiation, 2019. **26**(8): p. 1467-1484.

653. Towers, C.G., et al., *Mitochondrial-derived vesicles compensate for loss of LC3-mediated mitophagy.* Developmental Cell, 2021. **56**(14): p. 2029-2042.e5.

654. Yamamoto, A., et al., *Bafilomycin A1 prevents maturation of autophagic vacuoles by inhibiting fusion between autophagosomes and lysosomes in rat hepatoma cell line, H-4-II-E cells.* Cell Struct Funct, 1998. **23**(1): p. 33-42.

655. Klionsky, D.J., et al., *Does bafilomycin A1 block the fusion of autophagosomes with lysosomes?* Autophagy, 2008. **4**(7): p. 849-850.

656. Li, L.-q., et al., *Inhibition of autophagy by bafilomycin A1 promotes chemosensitivity of gastric cancer cells.* Tumor Biology, 2016. **37**(1): p. 653-659.

657. Lu, X., et al., *Bafilomycin A1 inhibits the growth and metastatic potential of the BEL-7402 liver cancer and HO-8910 ovarian cancer cell lines and induces alterations in their microRNA expression.* Experimental and therapeutic medicine, 2015. **10**(5): p. 1829-1834.

658. Graham, R., J. Thompson, and K. Webster, *Inhibition of the vacuolar ATPase induces Bnip3-dependent death of cancer cells and a reduction in tumor burden and metastasis.* Oncotarget, 2013. **5**.

659. Li, Z., et al., *Complete elucidation of the late steps of bafilomycin biosynthesis in Streptomyces lohii.* The Journal of biological chemistry, 2017. **292**(17): p. 7095-7104.

660. Dröse, S. and K. Altendorf, *Bafilomycins and Concanamycins as inhibitors of V-ATPases and P-ATPases.* The Journal of experimental biology, 1997. **200**: p. 1-8.

661. Goldberg, S.B., et al., *A Phase I Study of Erlotinib and Hydroxychloroquine in Advanced Non–Small-Cell Lung Cancer.* Journal of Thoracic Oncology, 2012. **7**(10): p. 1602-1608.

662. Li, Y., et al., *Hydroxychloroquine induced lung cancer suppression by enhancing chemo-sensitization and promoting the transition of M2-TAMs to M1-like macrophages.* Journal of Experimental & Clinical Cancer Research, 2018. **37**(1): p. 259.

663. O'Hara, M.H., et al., *Phase II trial of the autophagy inhibitor hydroxychloroquine with FOLFOX and bevacizumab in front line treatment of metastatic colorectal cancer.* Journal of Clinical Oncology, 2017. **35**(15_suppl): p. 3545-3545.

664. Fedele, A.O. and C.G. Proud, *Chloroquine and bafilomycin A mimic lysosomal storage disorders and impair mTORC1 signalling.* Bioscience reports, 2020. **40**(4): p. BSR20200905.

665. Klucken, J., et al., *Alpha-synuclein aggregation involves a bafilomycin A 1-sensitive autophagy pathway.* Autophagy, 2012. **8**(5): p. 754-766.

666. Guiney, S.J., et al., *Fibrillar α-synuclein toxicity depends on functional lysosomes.* Journal of Biological Chemistry, 2020. **295**(51): p. 17497-17513.

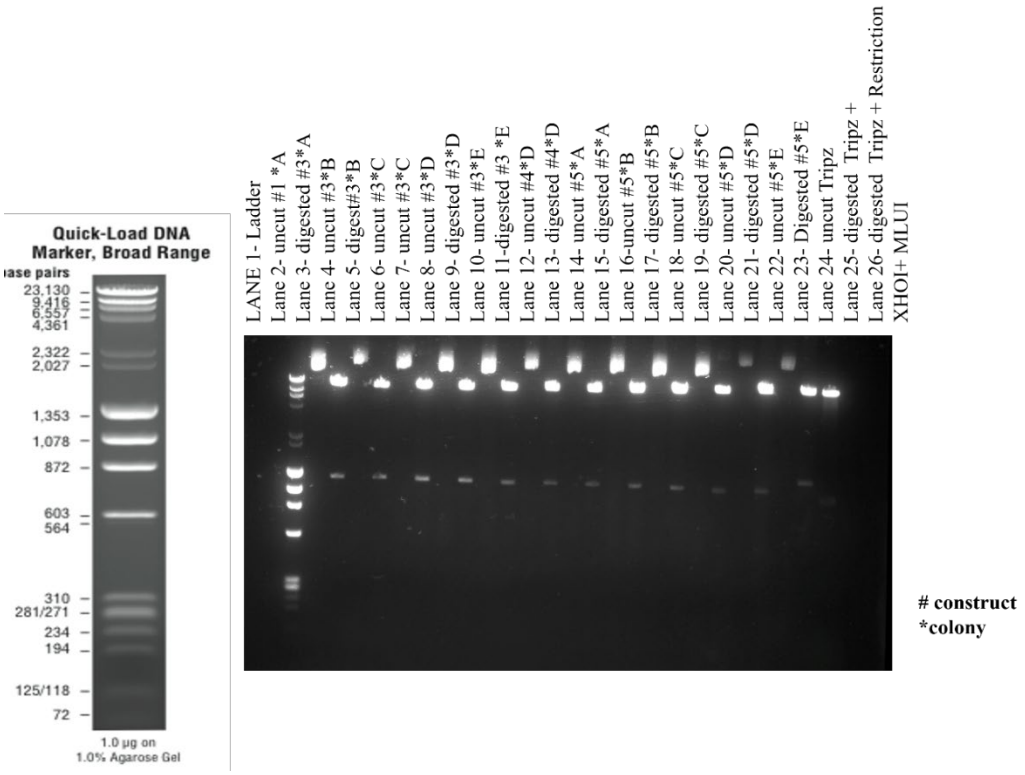
667. Zhou, H., et al., *Chaperone-mediated Autophagy Governs Progression of Papillary Thyroid Carcinoma via PPARγ-SDF1/CXCR4 Signaling.* The Journal of Clinical Endocrinology & Metabolism, 2020. **105**(10): p. 3308-3323.

668. Finn, P.F., et al., *Effects of small molecules on chaperone-mediated autophagy.* Autophagy, 2005. **1**(3): p. 141-5.

669. Wu, Z., et al., *Chaperone-mediated autophagy is involved in the execution of ferroptosis.* Proceedings of the National Academy of Sciences of the United States of America, 2019. **116**(8): p. 2996-3005.

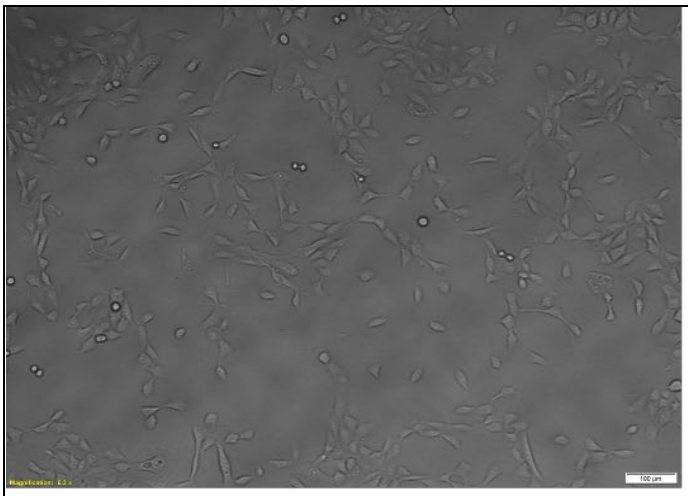
670. Ferreira, J.V., et al., *LAMP2A regulates the loading of proteins into exosomes.* Science Advances. **8**(12): p. eabm1140.

APPENDIX I

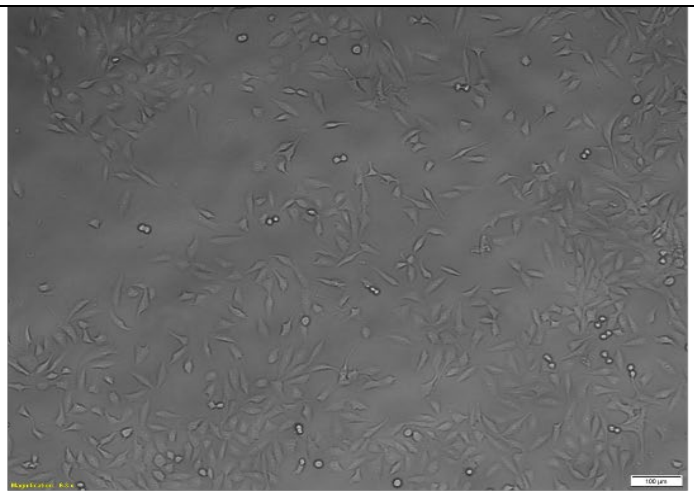


Representative TRIPZ Inducible shRNA clones with Lamp2A constructs were grown for 18 hours at 37 °C, and the plasmid was isolated. Clones were then digested with XHOI and MLUI run on an agarose gel. The expected band sizes are 14000bp 1200 bp. No recombinant products are visible.

APPENDIX II

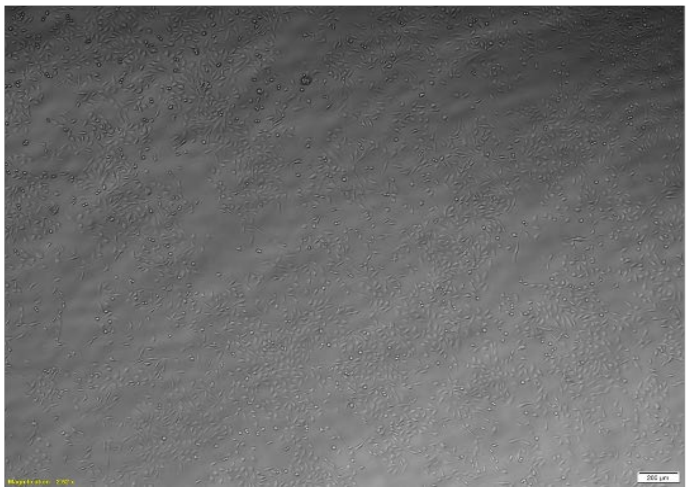


MCF10A

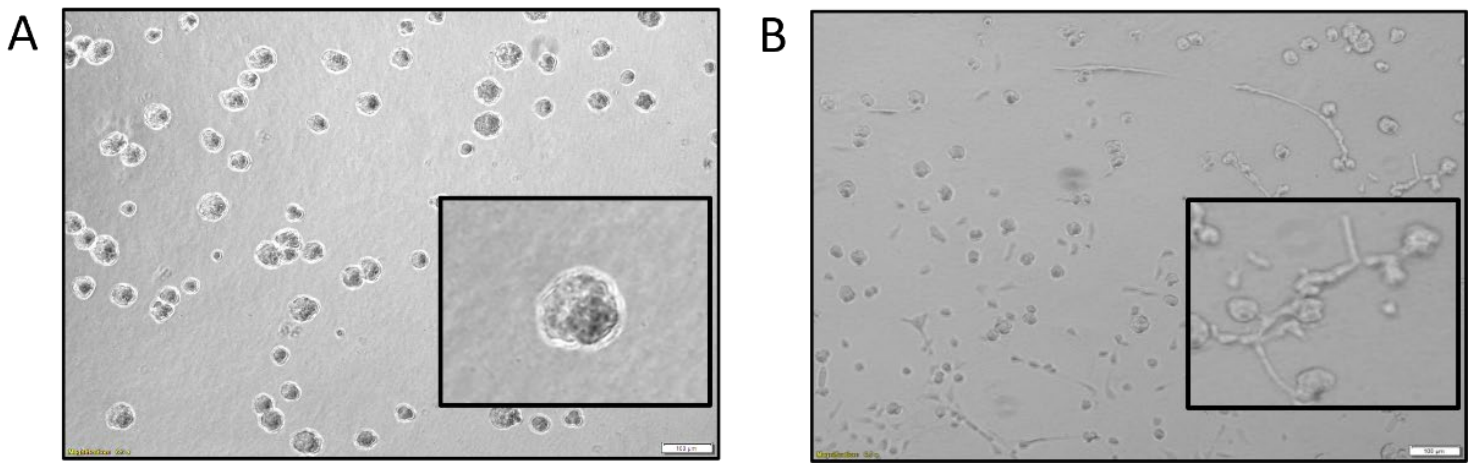


MCF10A HRAS^{V12}

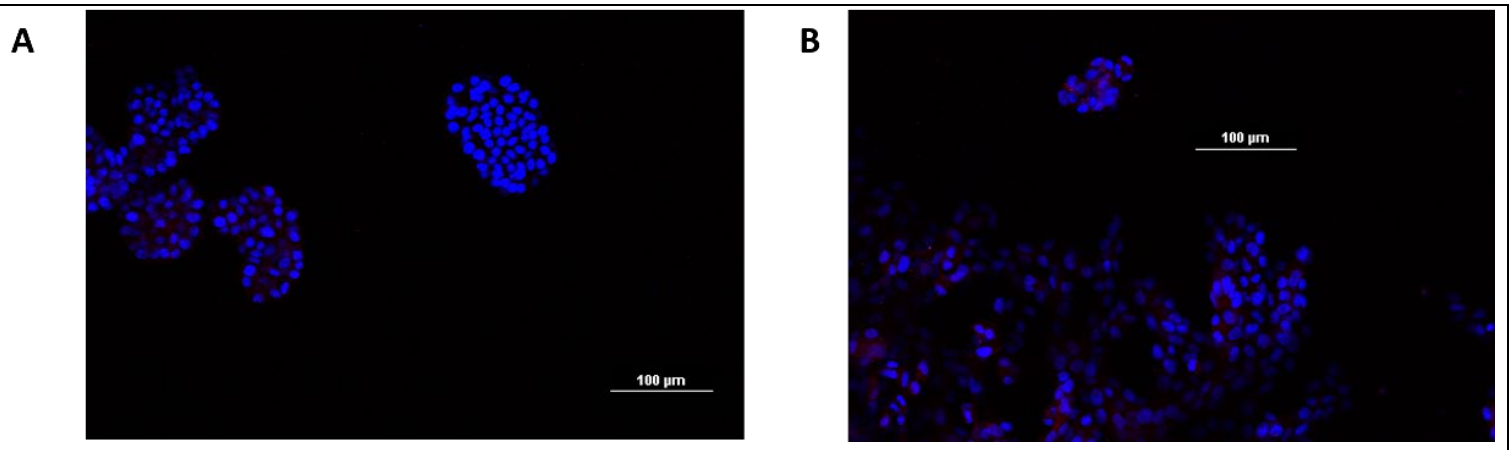




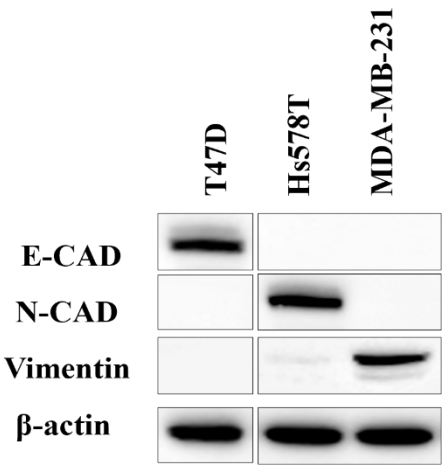
Micrograph images of MCF10A and MCF10A HRAS^{V12} at high (scale bar = 100µm) and low magnification (scale bar = 200µm)



Images of acini formation (scale bar = 100µm) by MCF10A (A) and MCF10A HRAS^{V12} include a close-up of one representative acinus from the image as indicated by the black box.

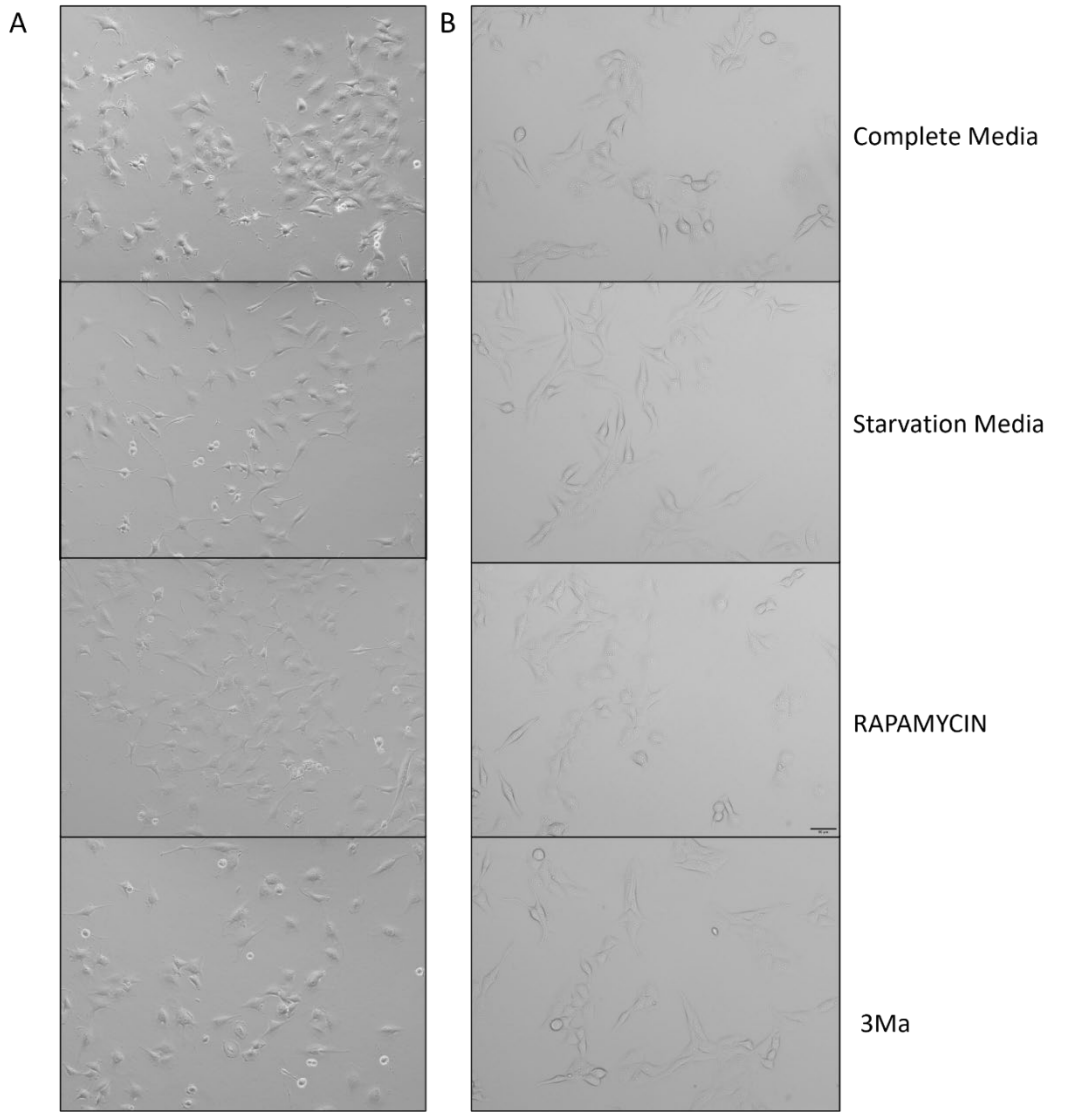


Representative images of acini formation at X100 magnification of MCF10A (A) andMCF10A HRAS^{V12} stained with Hoechst 3342 (living cells)



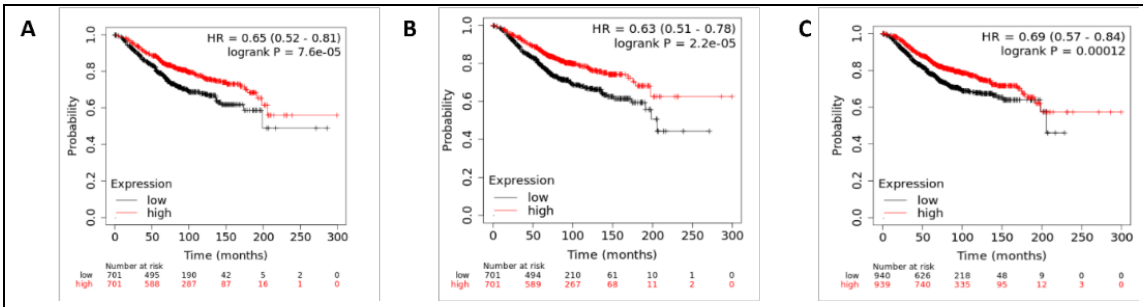
Representative western blot of the epithelial marker E-cadherin in T47D cell compared to mesenchymal markers N-cadherin and vimentin in Hs578T and MDA-MB-231 breast cancer cell lines.

APPENDIX III

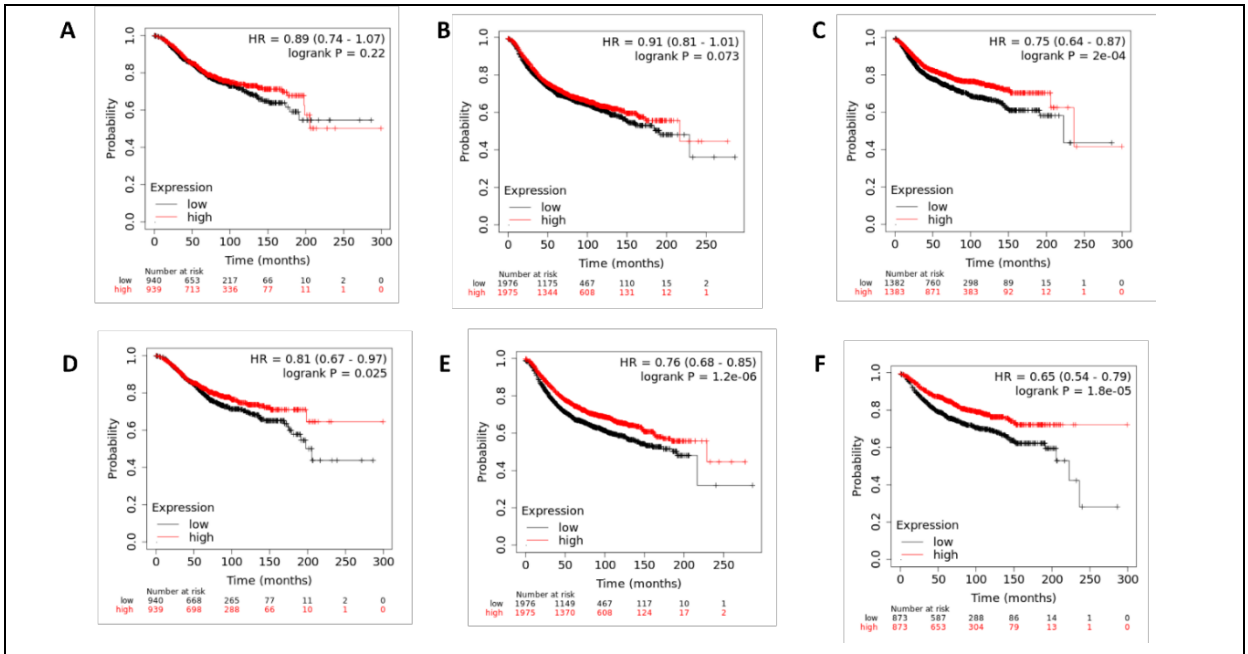


Morphological images of Hs578T (A) and MDA-MB-231 (B) breast cancer cell lines after 24 hours of the indicated treatments (scale bar 50μM)

APPENDIX IV

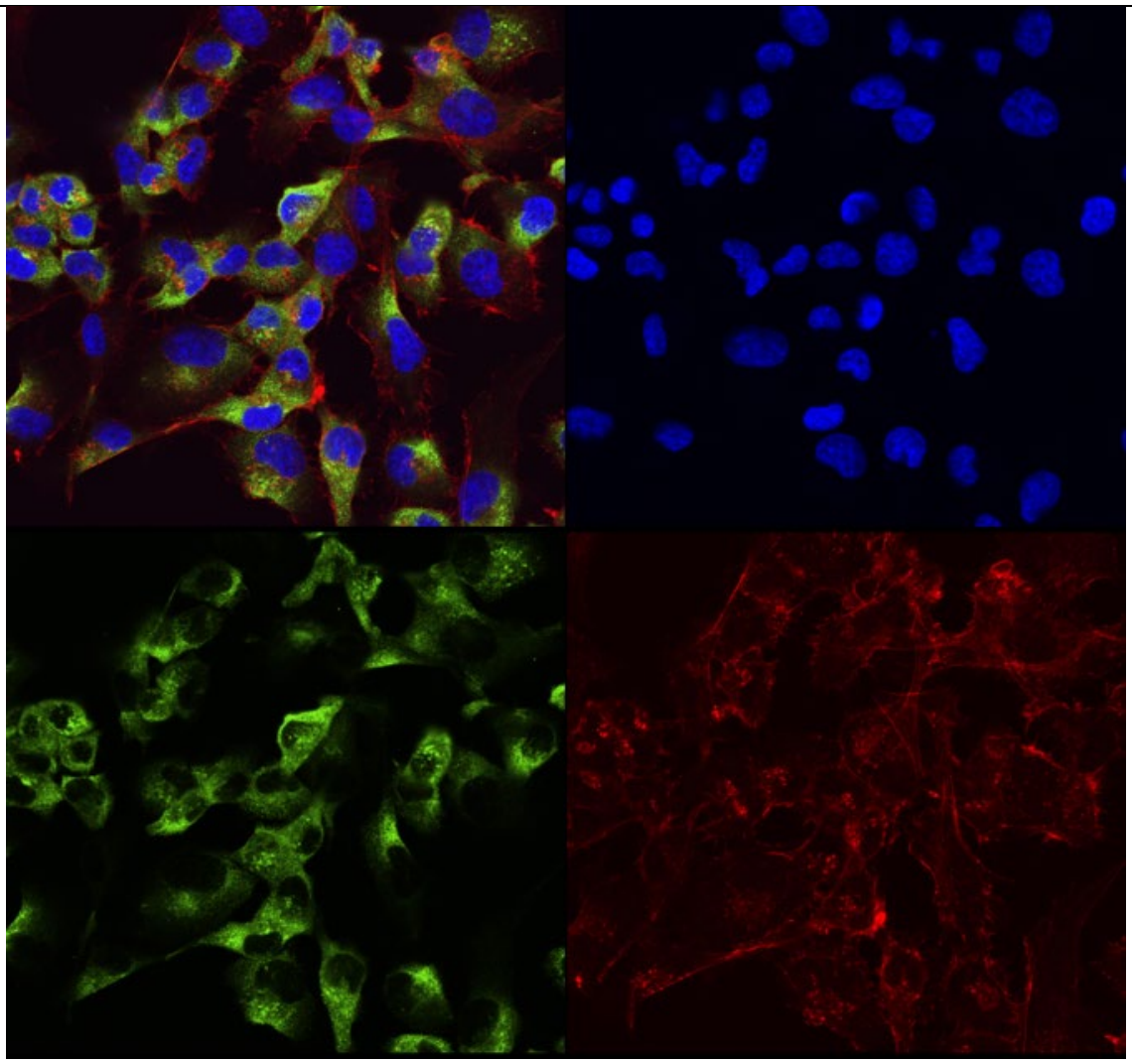


The Kaplan-Meier Plotter data for the prognosis probability of breast cancer patients' overall survival(OS) was examined. With the presence of gene ratios of the LC3 orthologues Gabarap(A), GabarapL1(B) and GabarapL2(C) as a ratio to LC3B.

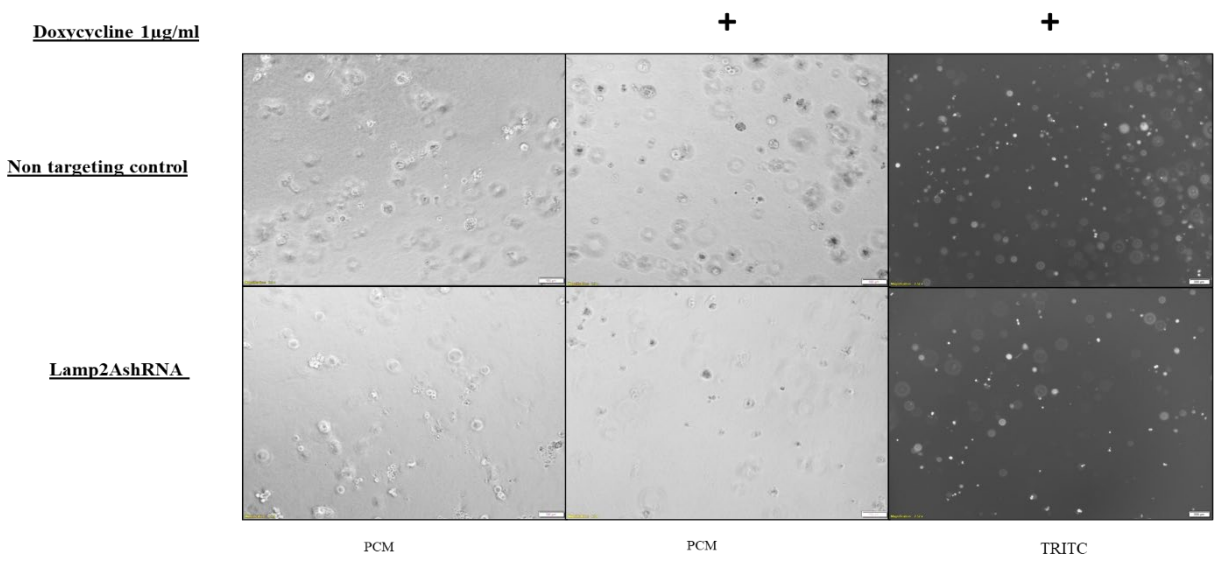


The Kaplan-Meier Plotter data for breast cancer patients with gene ratios of HRAS to LC3B; OS (A), RFS (B) and DMFS (C). The gene ratio of KRAS to LC3B; OS (D), RFS (E) and DMFS (F).

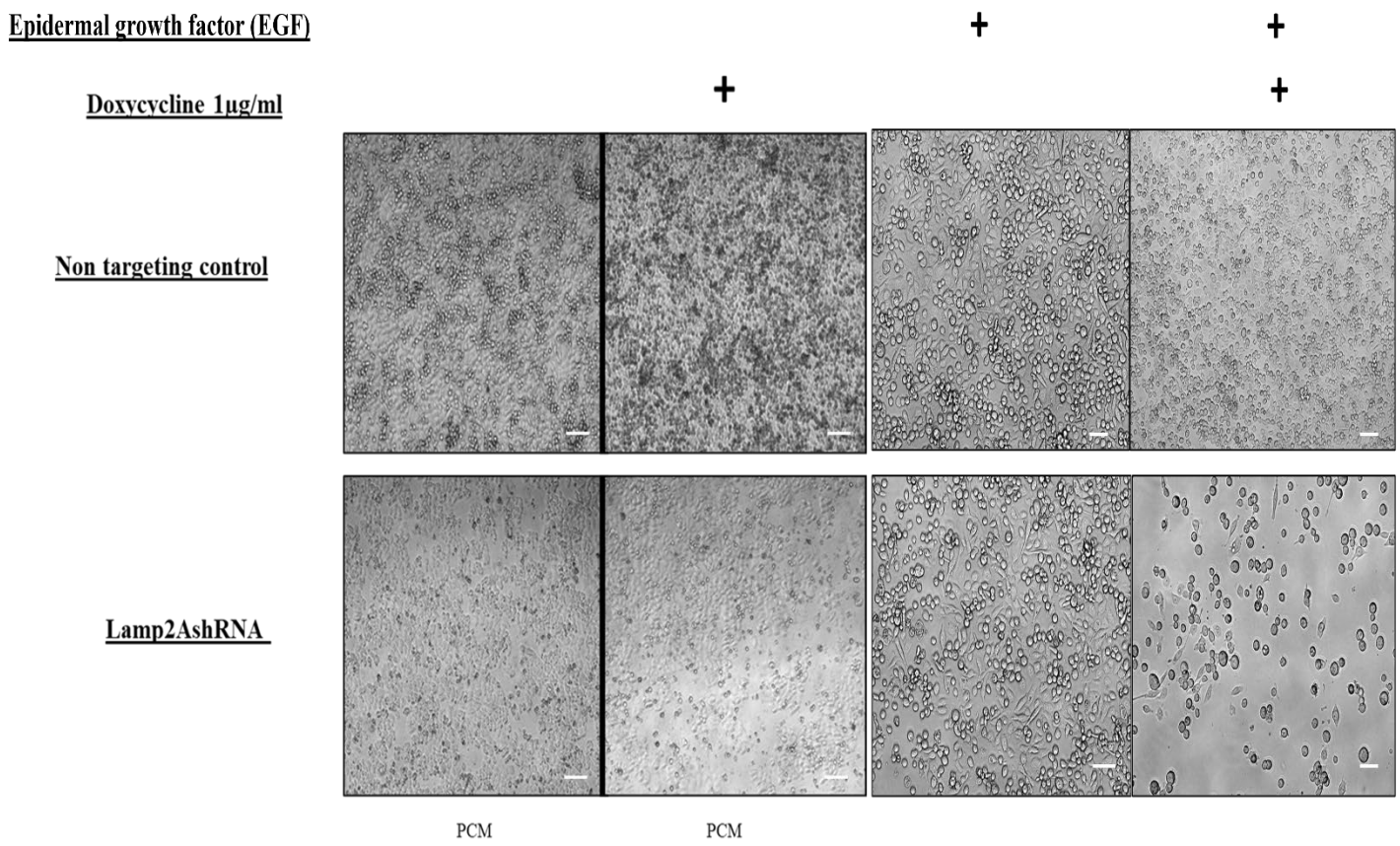
APPENDIX V



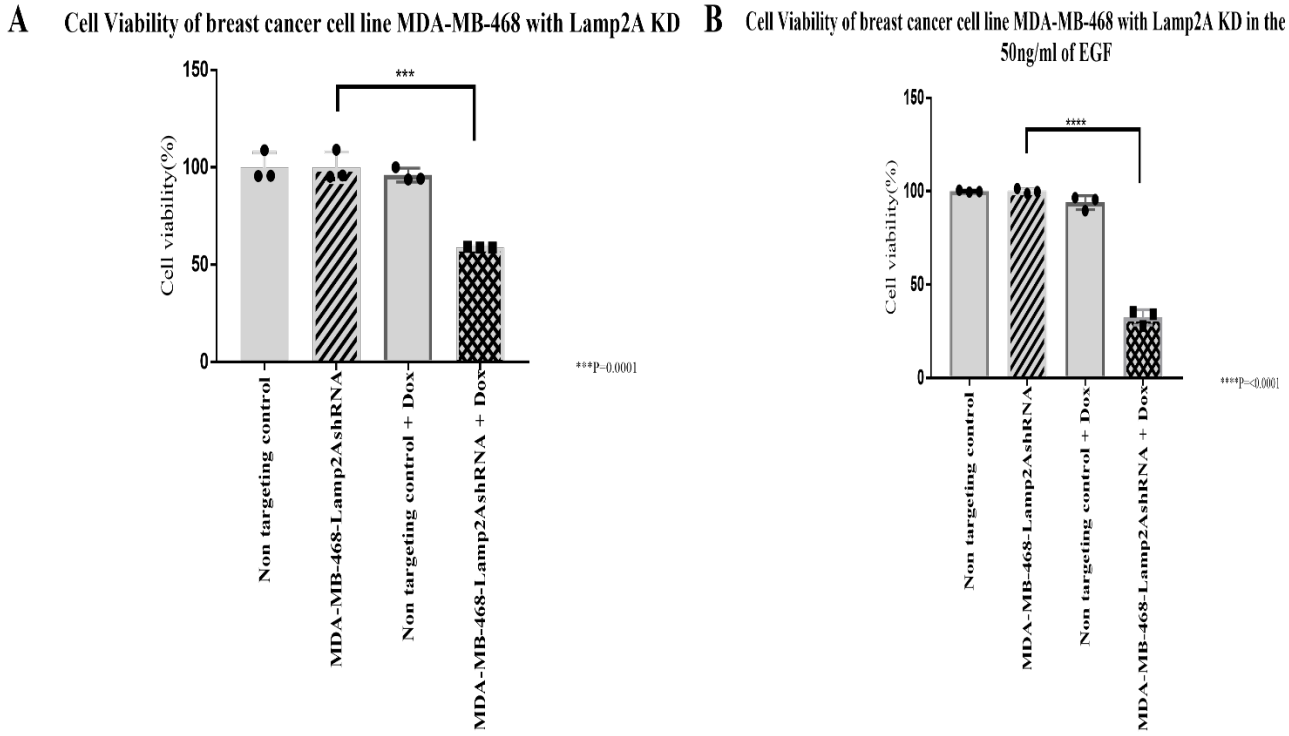
MDA-MB-231 breast cancer cell line stained with Lamp2A (FITC), Nucleus (DAPI) and Phalloidin (TRITC) at 400X magnification



Representative micrograph images of MDA-MB-468 transduced with Lamp2AshRNA or non-targeting shRNA with or without doxycycline. The cells were grown in 3D culture with Matrigel as the basement membrane, and images were captured at low magnification (X10) with phase contrast and TRITC to capture RFP fluorescence in response to doxycycline exposure. Scale bar for phase contrast microscopy (PCM) is 100µm and for images with a TRITC filter is 100µm.



Micrograph images of the MDA-MB-468 breast cancer cells from figures 5-18 and 5-23 put together so the effects of EGF can be directly compared. (scale bar without EGF= 200 µm with EGF =100µm)



Cell viability graphs of MDA-MB-468 breast cancer cell lines from figures 5.20 (A) and 5.22 (B) have been combined such that a direct comparison can be made of the effect of EGF.

APPENDIX VI

UniProt ID: P01112 **protein names:** GTPase HRAS (H-RAS-1)

MTEYKLVVVGAGGVGKSALTIQLIQNHFVDEYDPTIEDSYRKQVVIDGETCLLDI
LDTAGQEEYSAMRDQYMRTGEGFLCVFAINNTKSFEDIHQYREQIKRVKDSDDV
PMVLVGNKCDLAARTVESRQAQDLARSYGIPYIETSAKTRQGVEDAFYTLVREIR
QHKLRKLNPPDESGPGCMSCKCVLS

entry	status	protein_names	gene_names	length	motif	motif_start	motif_type	ubi.inactivated
P01112	reviewed	GTPase HRas	HRAS HRAS1	189	KRVKD	101	acetyl. act.	TRUE
P01112	reviewed	GTPase HRas	HRAS HRAS1	189	REIRQ	161	canonical	FALSE

UniProt ID: P01116 **protein names:** GTPase KRAS (K-RAS 2)

MTEYKLVVVGAGGVGKSALTIQLIQNHFVDEYDPTIEDSYRKQVVIDGETCLLDI
LDTAGQEEYSAMRDQYMRTGEGFLCVFAINNTKSFEDIHHYREQIKRVKDSEDV
PMVLVGNKCDLPSRTVDTKQAQDLARSYGIPFIETSAKTRQRVEDAFYTLVREIR
QYRLKKISKEEKTPGCVKIKKCIIM

entry	status	protein_names	gene_names	length	motif	motif_start	motif_type	ubi.inactivated
P01116	reviewed	GTPase KRas (K-Ras 2) (Ki-Ras) (c-K-ras)	KRAS KRAS2 RASK2	189	KRVKD	101	acetyl. act.	TRUE
P01116	reviewed	GTPase KRas (K-Ras 2) (Ki-Ras) (c-K-ras)	KRAS KRAS2 RASK2	189	REIRQ	161	canonical	FALSE
P01116	reviewed	GTPase KRas (K-Ras 2) (Ki-Ras) (c-K-ras)	KRAS KRAS2 RASK2	189	QYRLK	165	phos. act.	TRUE
P01116	reviewed	GTPase KRas (K-Ras 2) (Ki-Ras) (c-K-ras)	KRAS KRAS2 RASK2	189	YRLKK	166	acetyl. and phos	TRUE
P01116	reviewed	GTPase KRas (K-Ras 2) (Ki-Ras) (c-K-ras)	KRAS KRAS2 RASK2	189	KKISK	169	acetyl. and phos	TRUE

UniProtID: P01111 **protein names:** GTPaseNRAS

MTEYKLVVVGAGGVGKSALTIQLIQNHFVDEYDPTIEDSYRKQVVIDGETCLLDI
LDTAGQEEYSAMRDQYMRTGEGFLCVFAINNSKSFADINLYREQIKRVKDSDDV
PMVLVGNKCDLPTRTVDTKQAHELAKSYGIPFIETSAKTRQGVEDAFYTLVREIR
QYRMKKLNSSDDGTQGCMGLPCVVM

entry	status	protein_names	gene_names	length	motif	motif_start	motif_type	ubi.inactivated
P01111	reviewed	GTPase NRas	NRAS HRAS	189	KRVKD	101	acetyl. act.	TRUE
P01111	reviewed	GTPase NRas	NRAS HRAS	189	REIRQ	161	canonical	FALSE

APPENDIX VII

UniProt ID: P00533 **protein names:** Epidermal growth factor receptor (EC 2.7.10.1) (Proto-oncogene c-ErbB-1) (Receptor tyrosine-protein kinase erbB-1)
MRPSGTAGAALLALLAALCPASRALEEKKVCQGTSNKLTQLGTFEDHFLSLQRMFNNCEVVLGNL
EITYVQRNYDLSFLKTIQEVAGYVLIALNTVERIPLENLQIIRGNMYYENSYALAVLSNYDANKTGL
KELPMRNLQEILHGAVRFSNNPALCNVESIQWRDIVSSDFLSNMSMDFQNHLGSCQKCDPSCPNGS
CWGAGEENCQKLTKIICAQQCSGRCRGKSPSDCCHNQCAAGCTGPRESDCLVCRKFRDEATCKDT
CPPLMLYNPTTYQMDVNPEGKYSFGATCVKKCPRNYVVTDHGSCVRACGADSYEMEEDGVRKC
KKCEGPCRKVCNGIGIGEFKDSLSINATNIKHFKNCTSISGDLHILPVAFRGDSFTHTPPLDPQELDIL
KTVKEITGFLLIQAWPENRTDLHAFENLEIIRGRTKQHGQFSLAVVSLNITSLGLRSLKEISDGDVIIS
GNKNLCYANTINWKKLFGTSGQKTKIISNRGENSCKATGQVCHALCSPEGCWGPEPRDCVSCRNV
SRGRECVDKCNLLEGEPREFVENSECIQCHPECLPQAMNITCTGRGPDNCIQCAHYIDGPHCVKTCP
AGVMGENNTLVWKYADAGHVCHLCHPNCTYGCTGPGLEGCPTNGPKIPSIATGMVGALLLLLVV
ALGIGLFMRRRHIVRKRTLRRLLQERELVEPLTPSGEAPNQALLRILKETEFKKIKVLGSGAFGTVY
KGLWIPEGEKVKIPVAIKELREATSPKANKEILDEAYVMASVDNPHVCRLLGICLTSTVQLITQLMP
FGCLLDYVREHKDNIGSQYLLNWCVQIAKGMNYLEDRRLVHRDLAARNVLVKTPQHVKITDFGL
AKLLGAEEKEYHAEGGKVPIKWMALESILHRIYTHQSDVWSYGVTVWELMTFGSKPYDGIPASEIS
SILEKGERLPQPPICTIDVYMIMVKCWMIDADSRPKFRELIIEFSKMARDPQRYLVIQGDERMHLPSP
TDSNFYRALMDEEDMDDVVDADEYLIPQQGFFSSPSTSRTPLLSSLSATSNNSTVACIDRNGLQSCPI
KEDSFLQRYSSDPTGALTEDSIDDTFLPVPEYINQSVPKRPAGSVQNPVYHNQPLNPAPSRDPHYQD
PHSTAVGNPEYLNTVQPTCVNSTFDSPAHWAQKGSHQISLDNPDYQQDFFPKEAKPNGIFKGSTAE
NAEYLRVAPQSSEFIGA

entry	status	protein_names	gene_names	length	motif	motif_sta	motif_type	ubi.inacti
P00533	reviewed	Epidermal growth factor receptor	EGFR ERBB	1210	LKTIQ	79	phos. act.	TRUE
P00533	reviewed	Epidermal growth factor receptor	EGFR ERBB	1210	VRFSN	148	asparagine and phos. act.	FALSE
P00533	reviewed	Epidermal growth factor receptor	EGFR ERBB	1210	QKLTK	208	phos. act.	TRUE
P00533	reviewed	Epidermal growth factor receptor	EGFR ERBB	1210	KLTKI	209	acetyl. and phos. act.	TRUE
P00533	reviewed	Epidermal growth factor receptor	EGFR ERBB	1210	LKTVK	395	acetyl. and phos. act.	TRUE
P00533	reviewed	Epidermal growth factor receptor	EGFR ERBB	1210	LRSLK	450	acetyl. and phos. act.	TRUE
P00533	reviewed	Epidermal growth factor receptor	EGFR ERBB	1210	QKTKI	486	phos. act.	TRUE
P00533	reviewed	Epidermal growth factor receptor	EGFR ERBB	1210	KTKII	487	acetyl. and phos. act.	TRUE
P00533	reviewed	Epidermal growth factor receptor	EGFR ERBB	1210	KIISN	489	asparagine and phos. act.	TRUE
P00533	reviewed	Epidermal growth factor receptor	EGFR ERBB	1210	KRTLR	676	acetyl. and phos. act.	TRUE
P00533	reviewed	Epidermal growth factor receptor	EGFR ERBB	1210	NKEIL	756	asparagine	TRUE
P00533	reviewed	Epidermal growth factor receptor	EGFR ERBB	1210	KFREL	960	acetyl. act.	TRUE
P00533	reviewed	Epidermal growth factor receptor	EGFR ERBB	1210	QRYLV	976	phos. act.	FALSE